BRIDGE PILE BENT P-DELTA CURVES IN TRANSVERSE DIRECTION USING

FB-PIER AND GTSTRUDL PUSHOVER ANALYSIS PROCEDURES

Except where reference is made to the work of others, the work described in this thesis is my own or was done in collaboration with my advisory committee. This thesis does not include proprietary or classified information.

Douglas Grant Hughes

Certificate of Approval:

G. Ed Ramey
Professor
Civil Engineering

Robert W. Barnes
Assistant Professor
Civil Engineering

Chai H. Yoo
Professor
Civil Engineering

Stephen L. McFarland
Dean
Graduate School

BRIDGE PILE BENT P-DELTA CURVES IN TRANSVERSE DIRECTION USING FB-PIER AND GTSTRUDL PUSHOVER ANALYSIS PROCEDURES

Douglas Grant Hughes

A Thesis

Submitted to

the Graduate Faculty of

Auburn University

in Partial Fulfillment of the

Requirements for the

Degree of

Master of Science

Auburn, Alabama
August 8, 2005

BRIDGE PILE BENT P-DELTA CURVES IN TRANSVERSE DIRECTION USING

FB-PIER AND GTSTRUDL PUSHOVER ANALYSIS PROCEDURES

Douglas Grant Hughes

Signature of Author

6/13/2005
Date

Copy sent to:

Name Date

VITA

Douglas Grant Hughes, son of Reginald and Deborah (Wilson) Hughes, was born January 6, 1981 in Nashville, Tennessee. He graduated McGavock High School as a distinguished scholar in 1999 and enrolled in the College of Engineering at Auburn University in Auburn, Alabama in September 1999. He graduated magna cum laude with a Bachelor of Civil Engineering degree in December 2003. After completing his undergraduate coursework he entered the Graduate School at Auburn University in January 2004.

THESIS ABSTRACT

BRIDGE PILE BENT P-DELTA CURVES IN TRANSVERSE DIRECTION USING FB-PIER AND GTSTRUDL PUSHOVER ANALYSIS PROCEDURES

Douglas Grant Hughes

Master of Science, August 8, 2005
(B.C.E., Auburn University, 2003)

352 Typed Pages

Directed by G. Ed Ramey

Extreme flood events may create large transverse water loads that cause piles of a bent to bend about their weak axes in addition to causing scour. A comparison of the nonlinear pushover analysis procedures and resulting p-delta curves for bridge bents using GTSTRUDL and FB-Pier is presented in this thesis to determine which program most accurately models the pushover behavior of bents during these extreme flooding events. The buckling and pushover capacities of typical standard ALDOT non X-braced and X-braced bents are evaluated for various levels of scour. Stability of the non X-braced bents in the transverse direction is assessed to determine if the end battered piles provide sufficient lateral bracing to prevent sidesway. Several bent parameters were varied to examine sensitivities to flexural stiffness of the piles/bent including soil stiffness modulus, degree of end pile battering, and flexural stiffness of the bent cap. Special consideration was also given to the connections of the piles to the ground and bent cap. It was estimated that these connections would be most accurately modeled with 50% rotational fixities, but neither GTSTRUDL nor FB-Pier have the ability to model partial fixities. Thus, alternate modelings were examined to develop bent models which are believed to behave similarly to those in the field. Conclusions and recommendations are then made based on which computer program models, FB-Pier or GTSTRUDL, provides the most appropriate pushover analysis modeling for in-situ bents.

ACKNOWLEDGMENTS

This report was prepared as part of a research project under cooperative agreement between the Alabama Department of Transportation (ALDOT) and the Highway Research Center (HRC) at Auburn University. The author is grateful to the ALDOT and HRC for their sponsorship and support of this work. Special thanks is also due to Dr. Ramey for his guidance and family members for their continued support during the course of this research.

STYLE MANUAL AND SOFTWARE USED

Style Manual Used:

Chicago Manual of Style

Computer Software Used:

FB-Pier V3

GTSTRUDL release 27

Microsoft Excel

TABLE OF CONTENTS

LIST OF TABLES

LIST OF FIGURES

CHAPTER 1: INTRODUCTION

1.1 Statement of Problem

Alabama has hundreds of highway bridges that were designed and constructed prior to 1990 and therefore not designed for scour. In addition, there are hundreds of county bridges constructed using standardized designs for which scour analysis is not part of the foundation design. The Alabama Department of Transportation (ALDOT) is currently performing an assessment of scour susceptibility of its bridges, and a part of this assessment requires an evaluation of the structural stability of these bridges for an estimated scour event. It appears that buckling of the pile bents in the transverse direction governs the bridge failure load from a structural stability viewpoint. During extreme flooding events, debris tends to gather around the end piles of bents to create a debris raft. Water currents acting on these debris rafts may impose large transverse forces on the bents causing the piles to fail by buckling about their weak axes.

The computer program FB-Pier allows a rather sophisticated modeling of the pile-soil system of a pile bent and appears to be widely used by state highway agencies. However, its modeling of nonlinear behavior appears to leave much to be desired. The pushover analysis procedure in the computer program GTSTRUDL does not allow sophisticated modeling of soil settings, but appears to handle nonlinear behavior quite nicely. H. Granholm developed an analytical solution and equations for piles embedded in soils and found that buckling capacities of such piles were quite insensitive to the properties of the soil setting. Thus, it appears that the GTSTRUDL modeling and pushover analysis procedure has the potential of providing an easier modeling and more accurate failure load estimation than does FB-Pier for those pile bent cases requiring closer examination in ALDOT's bridge bent adequacy "screening tool" evaluation process. Checking this via comparative modeling and analyses is one of the impetuses and purposes of this research.

Though ALDOT pile bent standards show the pile bents X-braced in the transverse direction, in some cases, the X-bracing may be omitted and replaced with a concrete encasement of the pile from 3 feet below the ground line to the underside of the bent cap. When this is done, the steel H-pile and encasement are not interlocked via shear lugs to act compositely, and only a very light steel spiral (No. 2 bar at 12 in. pitch) is used in the encasement. Thus, if a major scour event occurs, the non X-braced bent must essentially rely on the end batter piles to provide sufficient lateral support to prevent sidesway bucking in the transverse direction. Analytically/numerically assessing whether these bents can achieve this is the second impetus and purpose of this research.

1.2 Objective

The objectives of this investigation are two fold and as follows:

1. Compare the relative modeling ease and accuracy of predicted transverse bucking/failure loads of typical bridge pile bents using FB-Pier and GTSTRUDL pushover analyses, and make a recommendation on which software/procedure should be used in pile bent cases requiring closer examination in extreme scour events.
2. Analytically/numerically assess the adequacy of the bent end batter piles in providing sufficient lateral support to prevent a sidesway mode of bent bucking.

1.3 Work Plan

The work plan to accomplish the above objectives is briefly outlined below.

1. Review and select a few typical ALDOT bridge pile bents to serve as case studies in the modeling/analysis comparisons.
2. Review the FB-Pier Users Manual and practice modeling and analyses of pile bents using FB-Pier.
3. Review GTSTRUDL modeling and pushover analysis procedure and practice modeling and analyses of pile bents using GTSTRUDL Pushover Analysis.

4. Perform FB-Pier modeling and failure load analysis of the typical bridge pile bents identified in (1) above.
5. Perform GTSTRUDL pushover analysis of the typical bridge pile bents identified in (1) above to determine the failure loads.
6. Compare the modeling work/effort and failure loads in (2) - (5) above, and also with results from analytical analyses using Granholm's equation.
7. Perform analytical and GTSTRUDL analyses of pile bents with a range of end pile batters from 0-2 in. in 12 in. and for a range of scour levels/heights of bent cap above ground line to assess the bents lateral stiffness and propensity to buckle in the lateral/transverse direction.
8. Draw appropriate conclusions and recommendations regarding the modeling work effort required and the failure load predictions of the FB-Pier and GTSTRUDL Pushover analysis procedures.
9. Draw appropriate conclusions and recommendations regarding the behavior and bucking capacity of non X-braced and X-braced pile bents and their adequacy in a major scour event.
10. Prepare a final report on the research work.

1.4 SCOPE

This investigation was limited to a review of the user manuals for FB-Pier and GTSTRUDL pushover analysis and applications of these software packages in analyzing the transverse bucking capacities of some typical ALDOT bridge pile bents. Comparisons of results from theses two software packages were made to assess their relative merits. Also, analytical and computer analyses of non X-braced pile bents were made to assess the transverse stiffness and bucking capacity of these bents to determine their adequacy during a major scour event. No laboratory or field tests were conducted to verify or refute the results of the numerical analyses.

CHAPTER 2: BACKGROUND AND LITERATURE REVIEW

2.1 Background

A common design/construction procedure for highway bridges in Alabama that are over marshes, low-lands, small creeks and shallow bodies of water is to have the bridge superstructure supported on pile bents. Some typical such bents are shown in Figures 2.1-2.3. During major flood events, the volume and velocity of flood waters flowing past these bents can cause considerable scouring to occur at the bents. Since the elastic buckling capacity and stability of these bents vary inversely with the square of the bent height, a scour of 15 feet at a bent that was originally 15 feet in height will reduce its elastic buckling load capacity by a factor of four. In turn this could result in a stability failure of the bent and thus collapse of the bridge.

In most pile bent supported bridges, the governing mode of failure in a major scour event is probably a buckling failure of the piles in the transverse direction or an undercutting of the piles and vertical plunging or tipping over of the bent. Analysis of pile bent buckling failures of the pile in the transverse direction due to scour using various modeling of the bents and various software packages is the purpose of this investigation. Thus, identification of the major parameters affecting transverse buckling of bridge pile bents, and determining the easiest means to quantify the effects of these parameters on bent load capacities is the focus of this literature review.

2.2 Literature Review

Column/Pile Buckling

Bridge bent piles are slender columns and subject to a possible stability or buckling failure. Perfect column/pile P-Δ and $P_{failure}$ curves are shown in Figures 2.4 and 2.5 respectively. As indicated in Figure 2.4, the perfect pile would exhibit no lateral deflection prior to reaching the

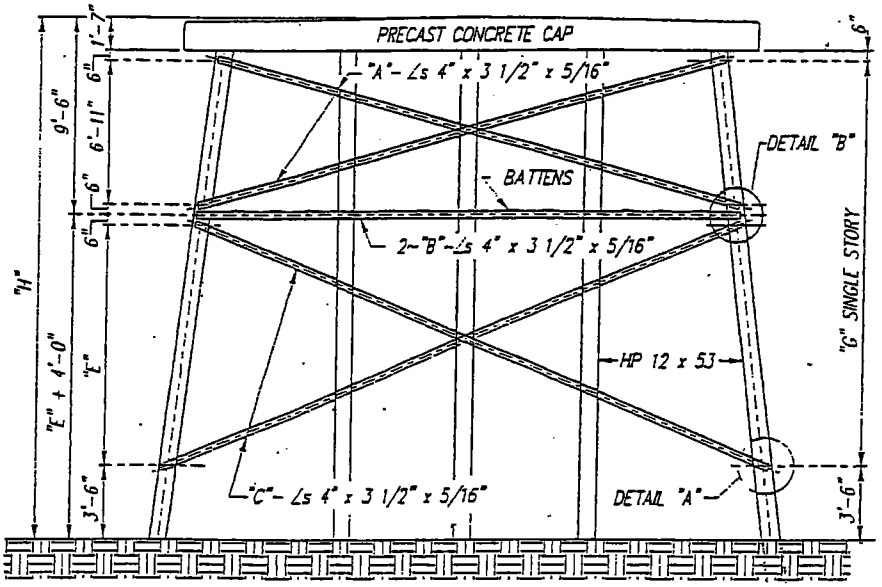

SWAYBRACING DETAILS

N.T.S.

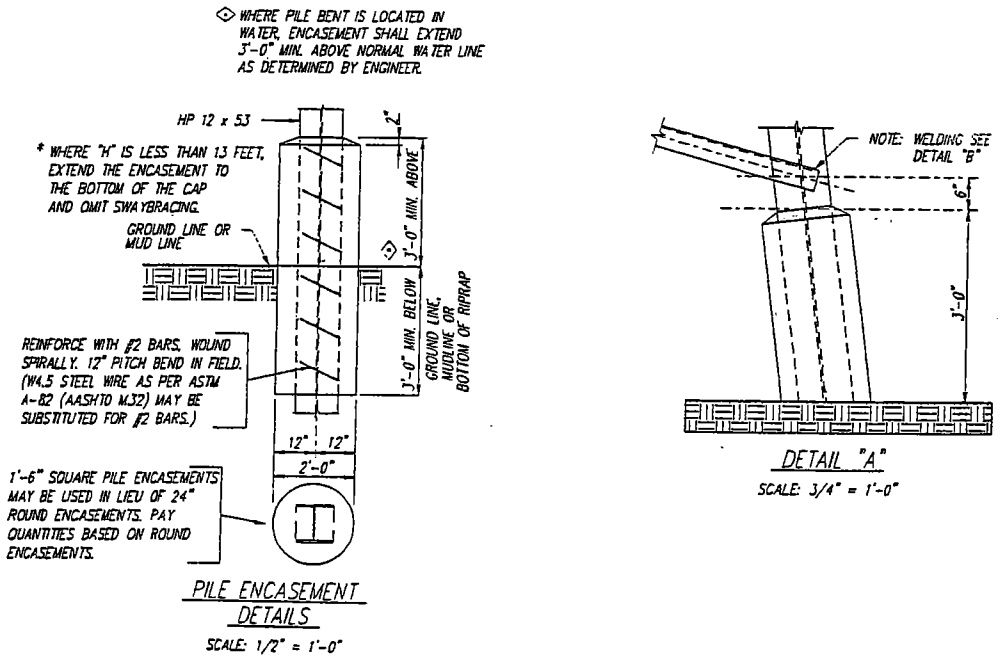

PILE ENCASEMENT DETAILS

SCALE: 1/2" = 1'-0"

DETAIL "A"

SCALE: 3/4" = 1'-0"

Figure 2.1. Typical ALDOT Bridge Pile Bent (2)

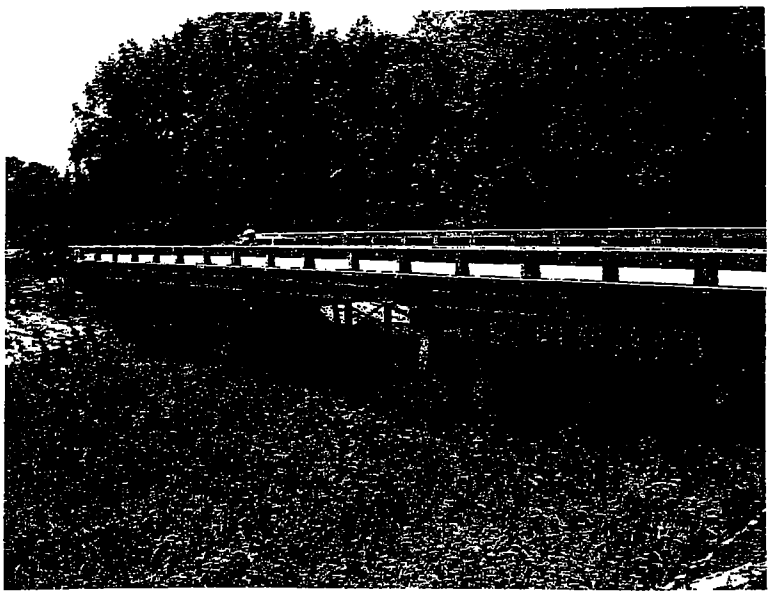

Figure 2.2. Pile Bent Supported Bridge Over Small Creek

Figure 2.3. Underside of Pile Bent Supported Bridge

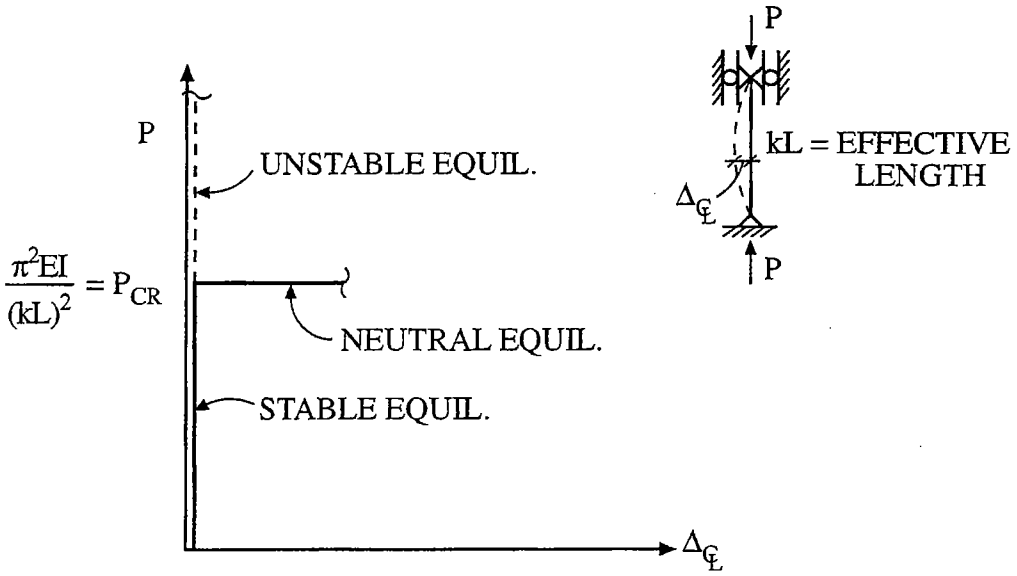

Figure 2.4. Perfect Pile P- Δ_{ℓ} Curve (3)

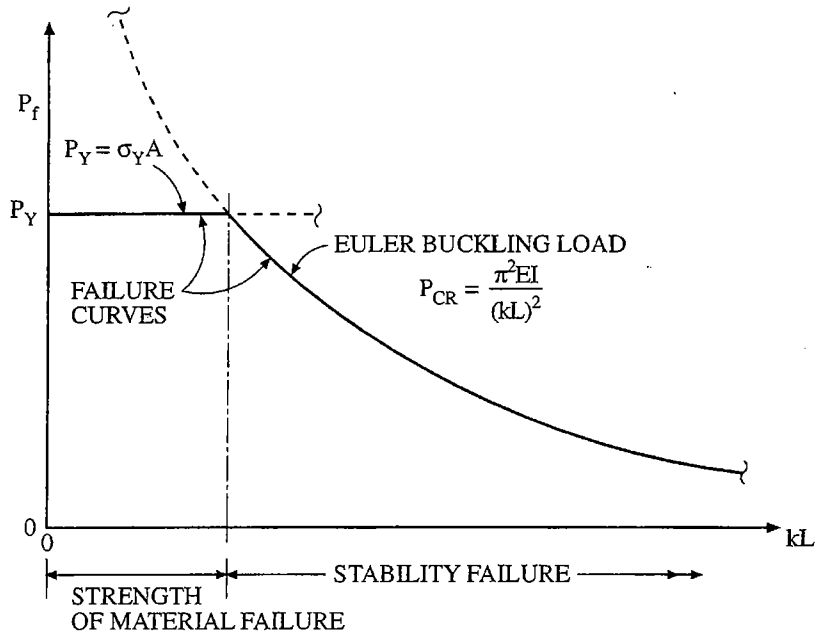

Figure 2.5. Perfect Pile P_f vs. kL Failure Curves (3)

buckling (P_{CR}) load. Figure 2.5 illustrates that a perfect pile may fail due to insufficient yield strength (P_y) or due to buckling (P_{CR}) depending on the pile effective length (kL). Piles (columns) in pile bents are never perfectly straight or subject to perfect concentric loading, and the effects of these imperfect conditions are reviewed below.

Imperfect columns are generally considered to be those which are not initially straight or those in which the load is applied with some eccentricity. Consider the case of an initially bent pin-ended column as show in Figure 2.6. Let the initial deformations of the column be given by y_o and the additional deformations due to bending by y as shown. The solution of this problem in the form of a load-deflection curve is given in Figure 2.7 for two values of initial imperfection. The effects of an imperfect axial loading on column behavior can be determined by considering the initially straight but eccentrically loaded column shown in Figure 2.8. For this column, the solution in the form of a load-center deflection curve for the two different values of load eccentricity/imperfection is given in Figure 2.9. Figures 2.7 and 2.9 reflect several important points about the behavior of imperfect columns, i.e.,

1. Imperfect columns begin to bend and deflect as soon as any axial load is applied.
2. The Euler load is a good approximation of the maximum load that a real imperfect column can support, provided that the magnitude of the imperfection is not excessive and the intensity of the loading does not cause yielding of the material.
3. The behavior of imperfect columns provides an alternate method of stability analysis, i.e., "The critical load is the load at which the deformation of a slightly imperfect system increases without bound. To apply this criterion, one gives the structural member or system to be investigated a small initial deformation and then determines the load at which the deformation becomes unbounded (7)."
4. The behavior of an imperfect system can be assessed by giving the system some initial crookedness or by applying the load eccentrically.

Due to residual and bending stresses, points within a pile cross-section will reach their yield stress long before the nominal P/A stress reaches the yield point. Thus, the σ vs. ℓ failure curve should be modified to account for this. The modification commonly taken is to assume a

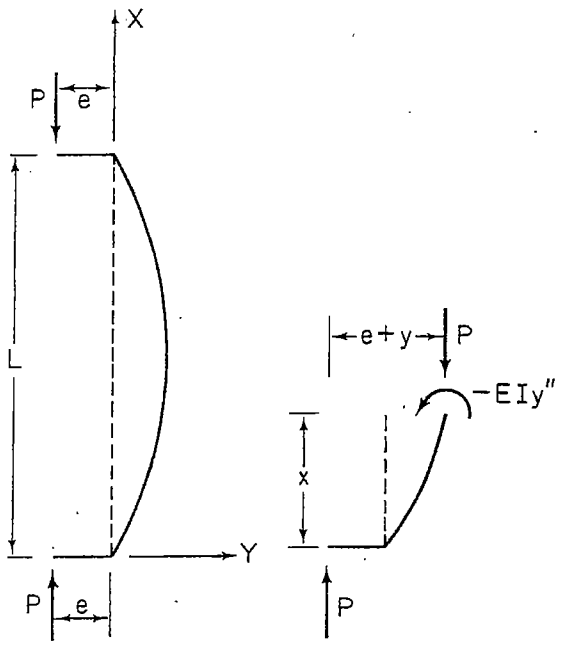

Figure 2.6. Initially Bent Column (7)

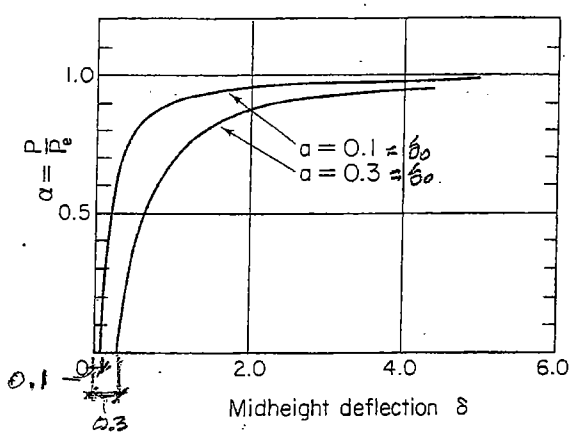

$$y = \frac{P/P_e}{1-P/P_e}\delta_0 \sin\frac{\pi x}{L}$$

At Mid Ht., $x = L/2$

$$\Leftarrow \delta = y_{mh} = \frac{P/P_e}{1-P/P_e}\delta_0$$

Figure 2.7. Load-Deflection Curves of Initially Bent Columns (7)

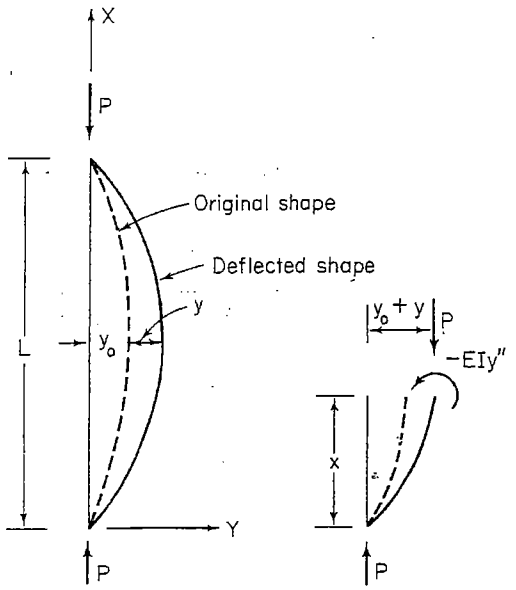

Figure 2.8. Eccentrically Loaded Column (7)

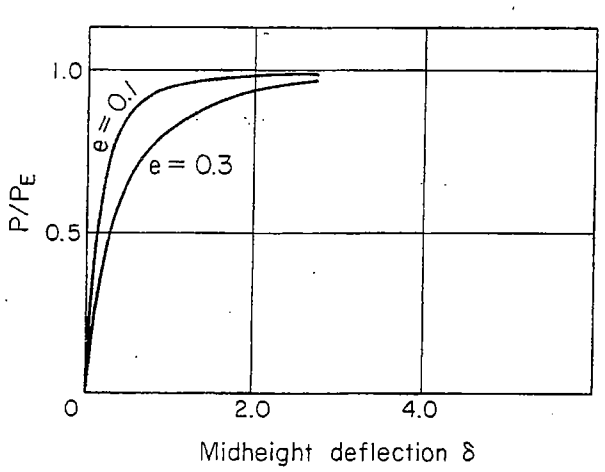

Figure 2.9. Load-Deflection Curves of Eccentrically Loaded Columns (7)

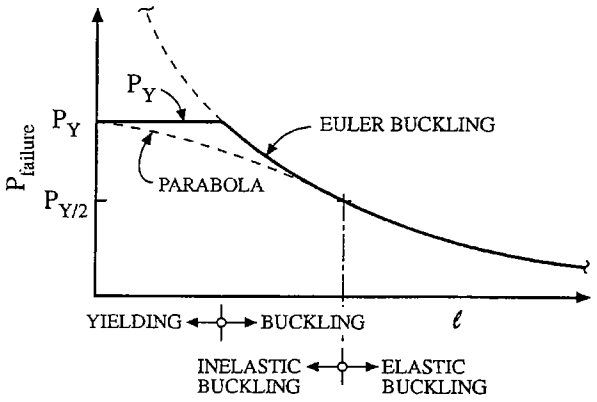

Figure 2.10. Column $P_{failure}$ vs. ℓ Curve (3)

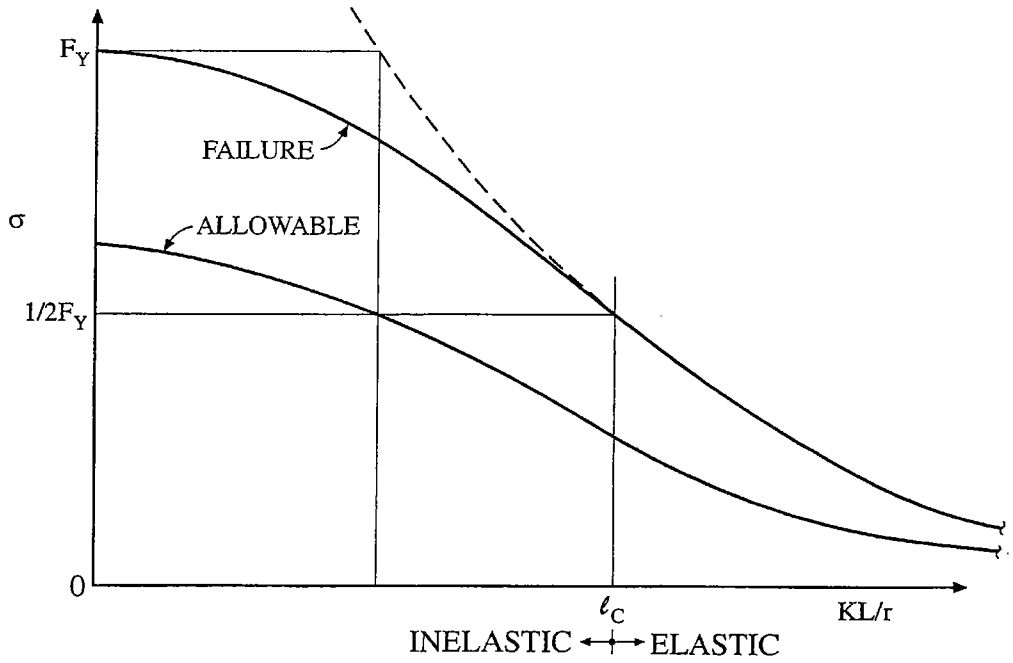

Figure 2.11. Elastic and Inelastic Buckling Regions (3)

parabolic curve from stress levels of σ_y to $\sigma_y/2$ or from P_y to $P_y/2$ as indicated in Figure 2.10. Alternatively, in stability problems the effect of member inelasticity on the buckling solution can be reasonably approximated by using the tangent modulus stiffness E_T instead of the elastic modulus, E. This is reflected in Figure 2.11. The inelastic stiffness is $E_T = \tau E$ where τ is the inelastic stiffness reduction factor. In this formulation,

$$P_{CR} = \frac{\pi^2 E_T I}{(kL)^2} \quad \text{or} \quad P_{CR} = \frac{\pi^2 \tau E I}{(kL)^2} \tag{2.1}$$

and, the elastic range is defined by the axial stress in the member, not the slenderness ratio. Inelastic stiffness E_T can also be determined directly as the slope of the stress-strain curve where yielding occurs.

Pile Bracing

Pile bracing is used to reduce the effective length of a pile and thus enhance its stability. In general, braces must have both stiffness and strength, and the requirements and guidelines for these are (2):

- Stiffness
  - Use brace stiffness at least twice the ideal value
  - Connection details can be detrimental to brace stiffness
- Strength
  - Brace forces are directly related to the magnitude of initial out-of-straightness or load eccentricities of the column/pile
  - Design the brace and its connections for 0.4%-1% of the column/pile compressive force

A system's ideal bracing stiffness can best be illustrated with a rigid bar stability problem as show in Figure 2.12. As evident in Figure 2.12, the stability of the rigid bar is directly related to bracing conditions at the top of the bar, i.e., the stiffness of the top spring. Note from this that if a column is perfectly straight and concentrically loaded, the bracing only needs stiffness, i.e., there is no force developed in the brace prior to buckling. However, if the column conditions are not

ideal, e.g., if the load is applied with an eccentricity Δ_o or the column is out-of-plumb, then the brace needs both stiffness and strength.

Lateral bracing of structural components and systems can be divided into four categories, i.e.,

- relative bracing system
- discrete bracing system
- continuous bracing system
- lean-on bracing system

These are illustrated in Figure 2.13.

Most engineers are familiar with the first three bracing categories (a-c) in Figure 2.13 (3). However, the fourth category, i.e., lean-on bracing, is not as familiar. In pile bents individual piles and whole pile bents have greater load capacity because of lean-on bracing. When compression members lean-on adjacent members for stability support (bracing), the ΣP concept (2) can be used to design the members. The ΣP concept can be explained using the problem shown in Figures 2.14, in which column A has a load P with three connecting beams attached between columns A and B. There are two principal buckling modes for this structure, the non sway and the sway modes. If column B is sufficiently slender, the system will buckle in the sway mode, shown by the dot-dash line in Figure 2.14a. In the sway mode the buckling strength involves the sum (ΣP_{CR}) of the buckling capacity of each column that sways. It should be noted that there can be axial load on all of the columns in the system. The system is stable in the sway mode if the sum of the applied loads (ΣP) is less than ΣP_{CR}. This assumes all the columns have the same height. If column B is sufficiently stiff, the buckling mode does not involve the lean-on bracing concept. Both modes must be checked.

Note in Figure 2.14b, as I_B is increased, the buckling load increases linearly until the ideal brace situation ($(I_B/I_A)_{ideal}$=15.3, or $I_B^{ideal} = 15.3\ I_A$) is reached where buckling occurs between the bracing or connection members. The response shown in Figure 2.14b indicates that the buckled shape is always a half sine curve until the full bracing is achieved when I_B is called I_B^{ideal} and is

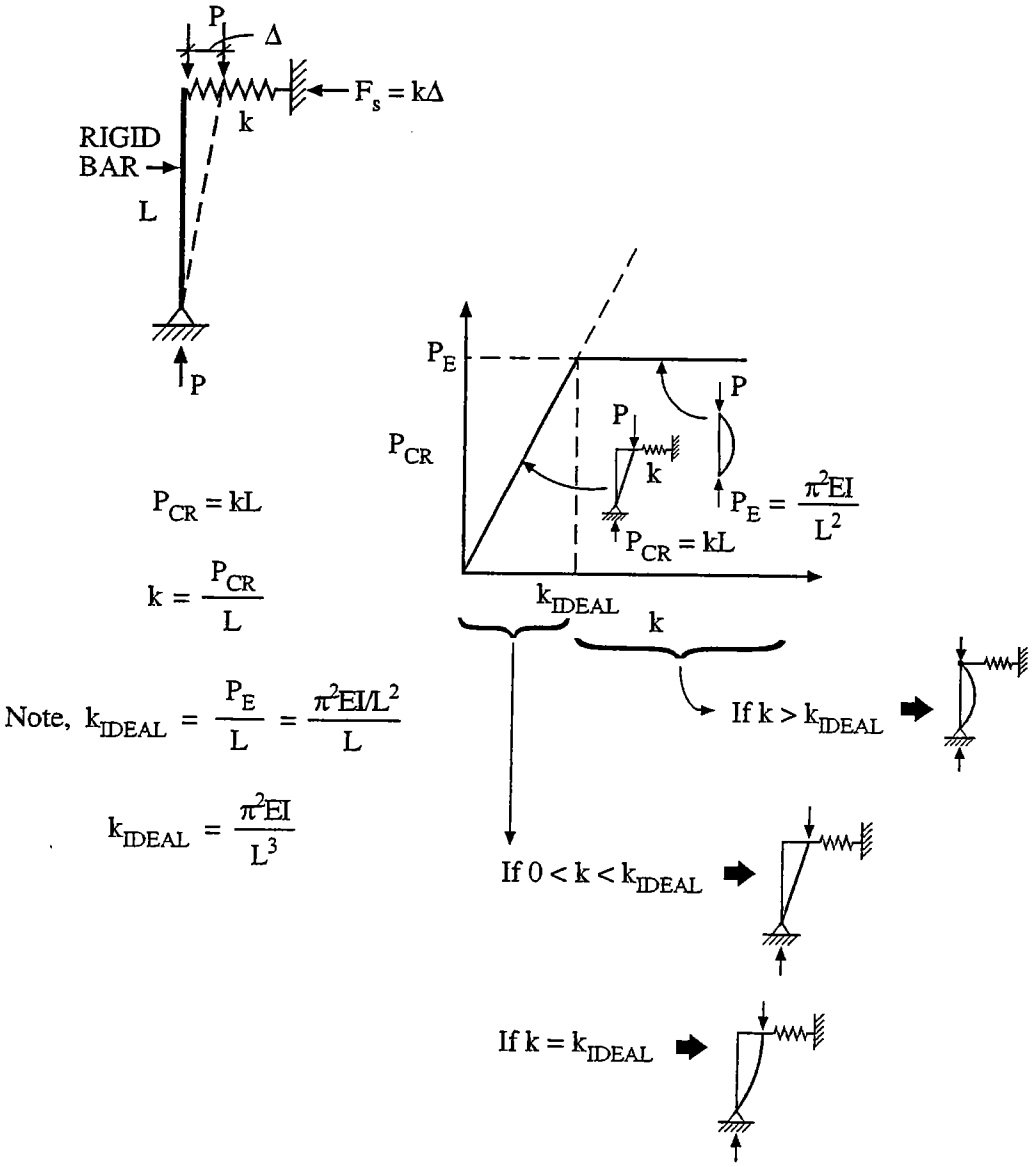

Figure 2.12. Ideal Bracing for a Rigid Bar Stability Case (3)

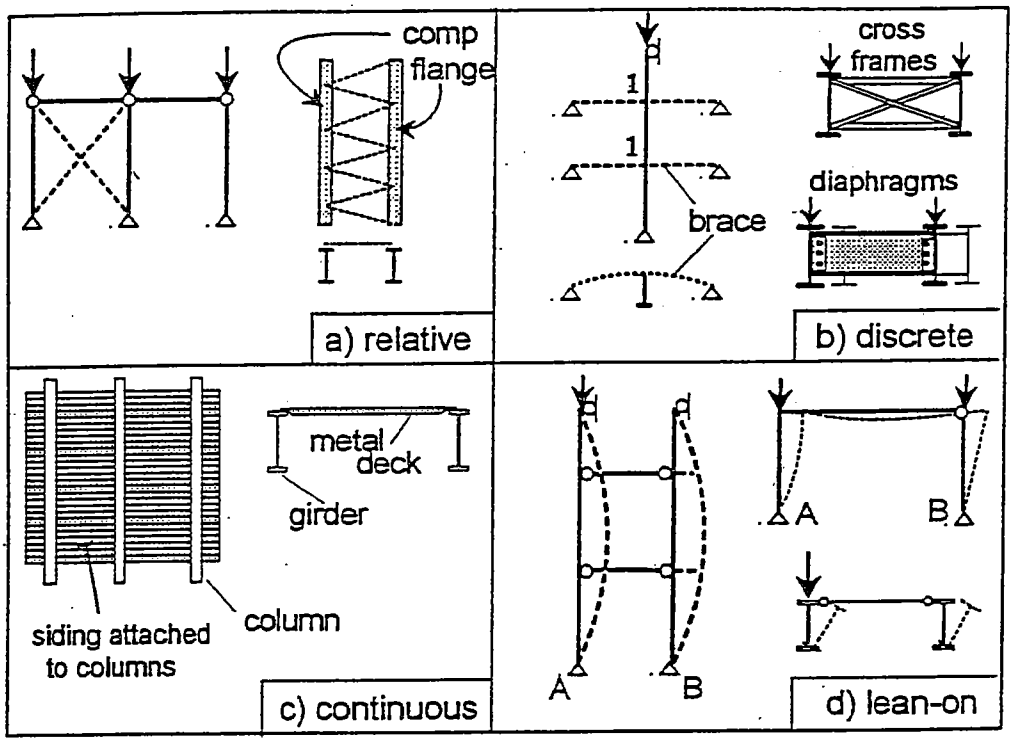

Figure 2.13. Types of Bracing Systems (2)

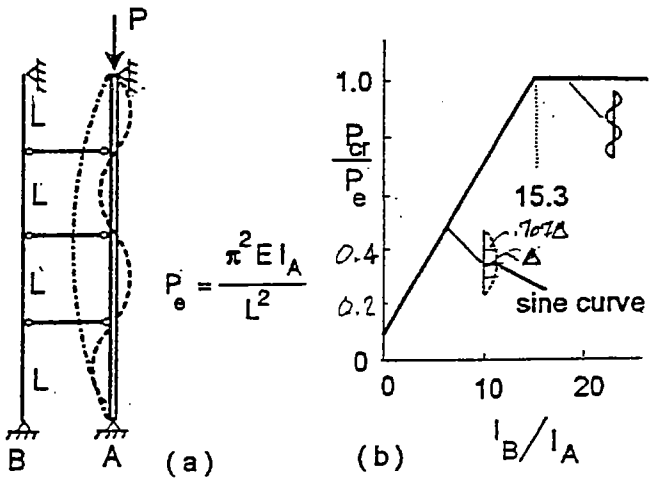

Figure 2.14. Lean-On Bracing (2)

analogous to k_{ideal}. There is no switching from one shape to the next higher mode as occurs for single point bracing, i.e., lean-on bracing is not the same as single point bracing. A lean-on system is one in which the "bracing" member must have the same shape as the "buckling" member. Such systems can be designed using the ΣP concept. Thus, a lean-on system relies on the lateral buckling strength of lightly loaded adjacent piles (or pile bents) to laterally support a more heavily loaded pile (or pile bent) when all of the piles (or pile bents) are horizontally tied together. In a lean-on system all piles must buckle simultaneously in a sway mode of buckling.

A typical bridge pile bent used by ALDOT is shown in Figure 2.1. Note in Figs 4.1 and 4.2 that bent piling has continuous bracing, i.e. the soil, below the ground line to prevent buckling about any axis. For buckling in the plane of the bents, i.e., in the transverse direction (about the pile's weak axis) the steel angle sway bracing provides relative bracing for the piling. Also, adjacent piling in the bent provide lean-on bracing (in the transverse direction) to the most heavily loaded pile in the bent. Lastly, adjacent bents could provide lean-on bracing for a sidesway mode of buckling in the longitudinal direction (about the pile's strong axis). However, after some longitudinal translation the expansion joints close and the bridge abutments at each end of the bridge prohibit a sidesway mode of buckling in the longitudinal direction (about the pile's strong axis).

Effect of Soil Subgrade Modulus on Pile Bucking Load

H. Granholm (1) developed an analytical solution for a pile partially embedded in a soil supporting medium as indicated in Figure 2.15. His solution allows one to evaluate the effect of soil subgrade modulus on pile buckling loads. The differential equation for the lower part of Granholm's pile elastic curve in Figure 2.15 is

$$EI\frac{d^4y}{dx^4} + P^2\frac{d^2y}{dx^2} + cy = 0 \qquad (2.2a)$$

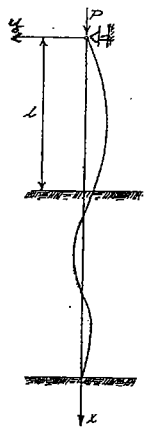

Figure 2.15. Partially Embedded Pile (1)

This equation indicates that the load intensity perpendicular to the axis of the pile is equal to the sum of the soil reaction pressure cy and an additional amount $P\frac{d^2y}{dx^2}$ due to the axial load and curvature of the pile. If we divide through by EI, Eq (2.2a) takes the form:

$$\frac{d^4y}{dx^4} + k^2\frac{d^2y}{dx^2} + a^4y = 0 \qquad (2.2b)$$

Where $k^2 = \frac{P}{EI}$ and $a^4 = \frac{c}{EI}$ and c = soil modulus (lb/ft^2). The differential equation for the upper part of the pile elastic curve is obtained from this equation by taking c = 0 and thus $a^4 = 0$, and,

$$\frac{d^4y}{dx^4} + k^2\frac{d^2y}{dx^2} = 0 \qquad (2.3)$$

By integrating these two equation and observing that the terminal conditions are satisfied, Granholm obtained the system characteristic equation as

$$\tan kl = kl\frac{1-\left(\frac{kl}{al}\right)^2 - \frac{1}{al}\left(\frac{kl}{al}\right)^2\sqrt{2-\left(\frac{kl}{al}\right)^2}}{1+\left(\frac{kl}{al}\right)^2 - \left(\frac{kl}{al}\right)^4 + al\left(\frac{kl}{al}\right)^2\sqrt{2-\left(\frac{kl}{al}\right)}} \qquad (2.4)$$

Note that Eqn. (2.4) is similar to the equation obtained when analyzing Euler's fixed-pinned column, i.e.,

$$\tan kl = kl$$

If one assumes al to be infinitely great, i.e., if the medium is assumed to be absolutely rigid, Eqn. (2.4) becomes Euler's equation for a fixed-pinned column which is thus obtained as a special case. A well-known graphical construction was applied for the solution of Euler's equation which consisted of determining the points of intersection between the curve y = tan kl and the straight line y=kl. This graphical construction suggests a similar procedure for solving Eqn. (2.4). The simplest way to find its roots for various values of al is to determine the point of intersection

between y = tan kl and the curve that is represented by the right hand member of the equation as indicated in Figure 2.16.

After thus determining the roots of the equation for a series of values of al one can graphically represent kl as a function of al. For kl, Granholm introduces the name "factor of buckling". Note that the "factor of buckling" is dimensionless. In Figure 2.17 the relation between the "factor of buckling" and al is shown graphically. With knowledge of the "factor of buckling", one can determine the critical load P from the relation

$$P_{CR} = (kl)^2 \frac{EI}{l^2} \qquad (2.5a)$$

Note, by definition that

$$(kl)^2 = \frac{P_{CR}}{EI} l^2 \qquad (2.5b)$$

For increasing values of al, the "factor of buckling", kl, approaches asymptotically the value 4.49 (approximately = $\pi\sqrt{2}$), which means that the critical load for increasing length of the pile or for increasing rigidity of the medium asymptotically approaches the critical load for Euler's fixed-pinned case. At the origin the function has the tangent kl = $al \cdot \sqrt{2}$. The value al = 0 thus corresponds to the load $P = 2a^2EI$, or, if one introduces the coefficient of lateral displacement c, instead of $P = 2a^2EI$, one obtains

$$P = 2\sqrt{cEI}$$

This value of P corresponds to the minimum buckling load when a pile is fully embedded ($l = 0$) in the soil, i.e.,

$$P_{min}^{\text{fully embedded}} = 2\sqrt{cEI_{min}}$$

Granholm also determined the characteristic equation for the case where the top of the pile in Figure 2.15 is fixed (rather than pinned), and his results for that condition are also shown in Figure 2.17. The support conditions for a bent pile buckling in the longitudinal direction, i.e., about its strong axis, are approximately those of a pile hinged at the top in Figure 2.17. For the same pile buckling in the transverse direction, i.e., about its weak axis, its top is between a

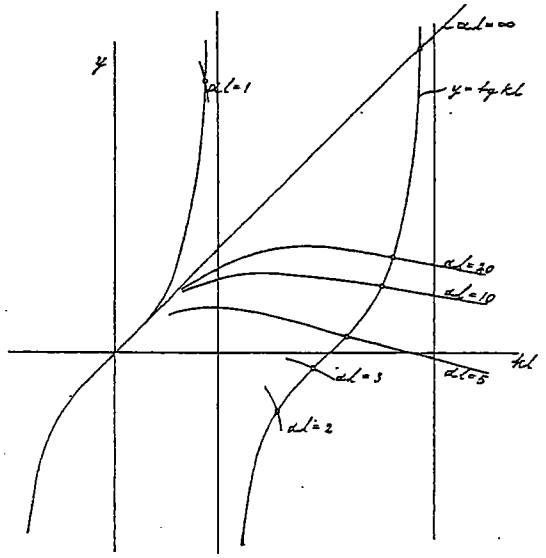

Figure 2.16. Graphical Solution of Eqn. 2.4 (1)

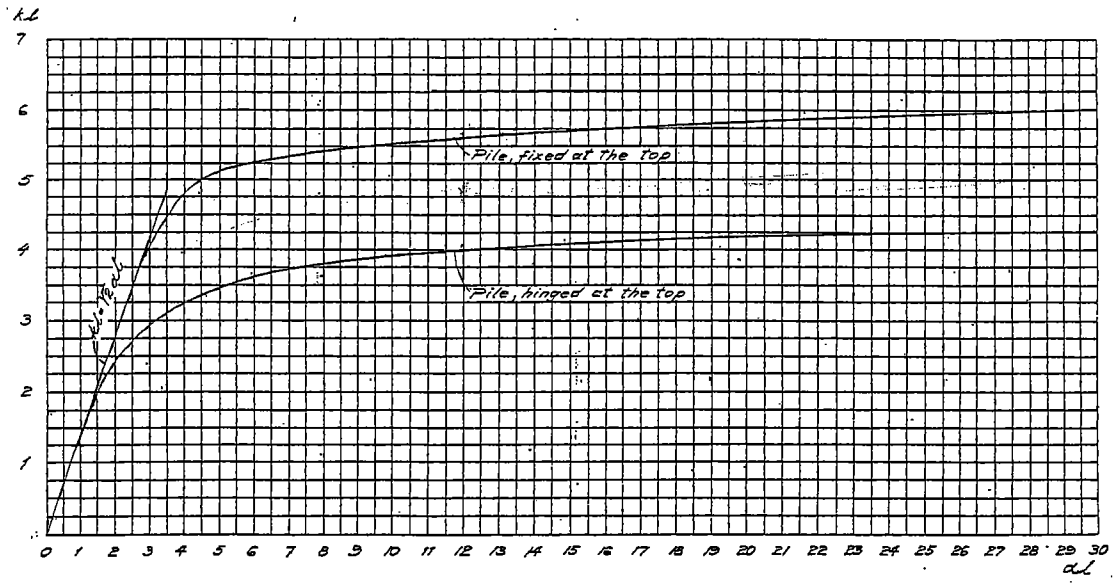

Figure 2.17. Relation Between al and kl for Pile Hinged and Fixed at Top (1)

pinned and a fixed condition. For this case, values of kl for both the pinned and fixed top could be extracted and the average of these used to estimate P_{CR}.

Pushover Analysis

Pushover analysis is a nonlinear analysis procedure that was born in the seismic analysis community. The technique is based on the conventional displacement method of analysis. Standard elastic and geometric stiffness matrices for the structure elements/members are progressively modified to account for geometric and/or material nonlinearity under constant gravity loads and incrementally increasing lateral loads or vice versa.

In GTSTRUDL, a Newton-Raphson solution technique based on the tangent stiffness method is used to solve the nonlinear equations resulting from the geometric and material nonlinearities. This solution technique is illustrated in Figure 2.18 (4). Load incrementation is particularly valuable for the nonlinear analysis of structures which exhibit dramatic changes in stiffness during the course of load application. Typical examples include cable structures, which demonstrate stress-stiffening behavior, and frame structures, which exhibit instability behavior (e.g. buckling). Stress stiffening behavior is characterized by rapidly increasing stiffness for small changes in strain, typically during the early stages of loading (see Figure 2.19a) (4). Frame structure instability is characterized by rapidly decreasing stiffness for small changes in deformation during the late stages of loading when the collapse load is approached (see Figure 2.19b) (4). In situations such as these, the nonlinear analysis may not converge if the total loading is applied as a single increment of sufficient magnitude to encompass the regions where the load-displacement response exhibits rapid stiffness change. Breaking the total loading into a smaller number of increments, particularly in the regions of rapid stiffness change, can significantly improve the success of the convergence and subsequent analysis.

Pushover analysis is described in GTSTRUDL Reference Manual, Vol. 3 (4) as an automated incremental load analysis which also contains a procedure that automatically searches for the load level at which structural instability or collapse occurs. In GTSTRUDL, the Pushover Analysis Data and Perform Pushover Analysis commands are used together to perform a

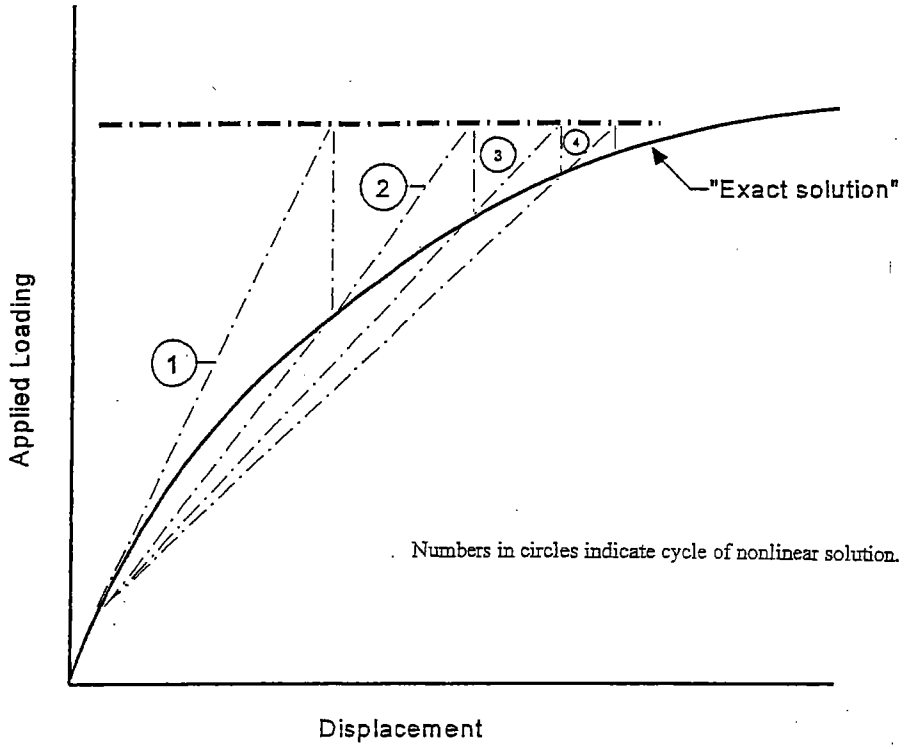

Figure 2.18. Direct Iteration Solution Procedure (4)

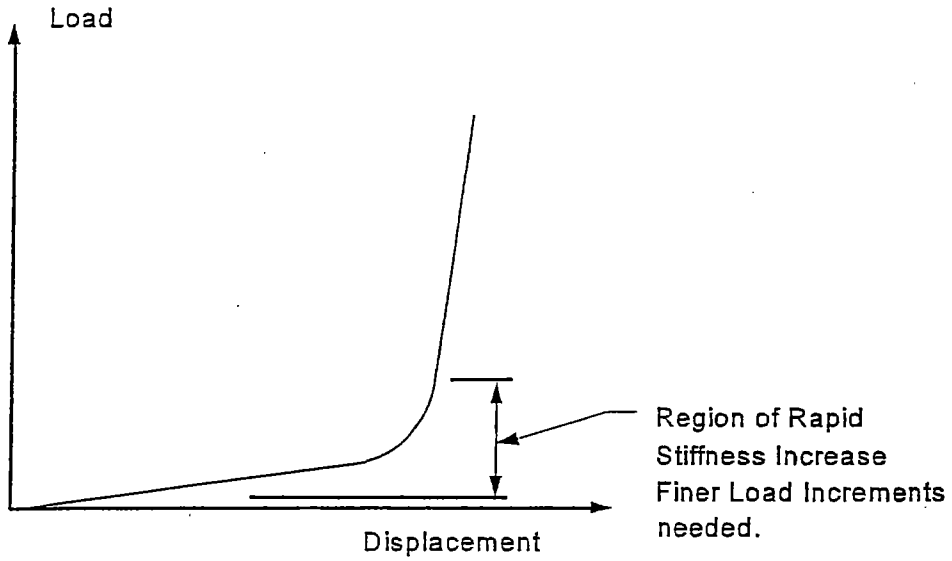

a) Typical Stress-Stiffening Response

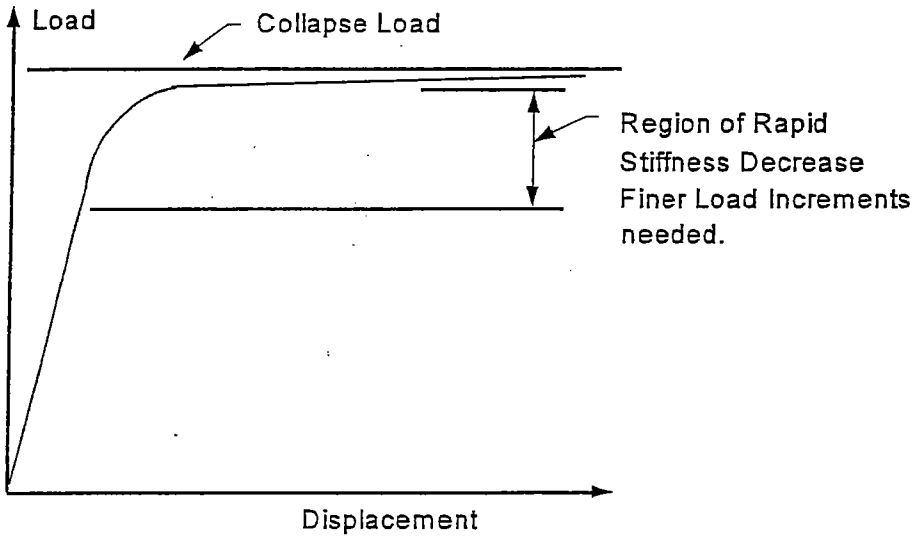

b) Typical Instability Response

Figure 2.19. Examples of Nonlinear Responses Requiring Load Incrementation (4)

pushover analysis. The Pushover Analysis Data command is used to specify the values for a series of parameters that control the pushover analysis procedure and must be given first. The Perform Pushover Analysis command follows and is used to execute the pushover analysis procedure. A Print Pushover Analysis Data command is used to verify the parameter values specified by the Pushover Analysis Data command.

FB-Pier recently added a pushover analysis capability to its software which can now perform a nonlinear pushover analysis of a pile or pile bent in a soil setting. As in the GTSTRUDL procedure, in the FB-Pier analysis procedure, two loads cases are required – one for permanently applied loads and one for loads to be incremented. FB-Pier's pushover analysis solution technique is not as sophisticated as GTSTRUDL's in that once the iteration process fails to converge it does not calculate reduced loading rates in order to converge to the exact solution. Therefore, smaller loading increments must be used to produce more accurate p-delta curves.

Structural Analysis in FB-Pier may be performed with linear or nonlinear pile behavior which are further explained by the FB-Pier help manual documentation (6) as follows:

Linear Behavior:

- Assumes the behavior is purely linear elastic.
- Deflections do not cause secondary moments; no P-delta moments (moments of the axial force times the displacements of one end of element to another).

Nonlinear Behavior:

- Uses input or default stress strain curves which are integrated over the cross-section of the piles.
- Uses P-delta moments (moments of the axial force times the displacements of one end of element to another). Furthermore, since the user subdivides the pile into a number of sub-elements, the P-y moments (moments of axial force times internal displacements within members due to bending) are also modeled.

The solution procedure for FB-Pier consists of two parts, the determination of the member strength criteria from the formation of interaction diagrams and the actual analysis of the structure (8). For nonlinear analysis the program first applies loads to the structure and determines the

resulting displacements of the members. Member strains are then determined from these displacements and the corresponding stresses are determined from either the default or user defined stress-strain curves. The program performs an integration over the cross section to get the forces from the stresses. Equilibrium is then checked to verify that the external loads are balanced by the internal stresses. If these loads are not balanced, the program iterates until the equilibrium is achieved (8).

When this solution procedure is performed for pushover analysis, the load at failure is determined by the failure ratio which is defined for each member and load increment as demand vs. capacity. The failure ratio is calculated from the interaction diagram for each cross-section of the structure and is an estimate of the percentage of the cross sections' capacity that has been reached for a given loading. To compute the failure ratio the length of the vector for the current load state is divided by the length of the vector when it pierces the failure surface as shown in the 3-D interaction diagram of Figure 2.20. This method assumes that the axial load will remain constant, which for indeterminate structures is not very realistic (6). In indeterminate structures all forces interact and in order for the moments to increase, the axial load must also increase (6).

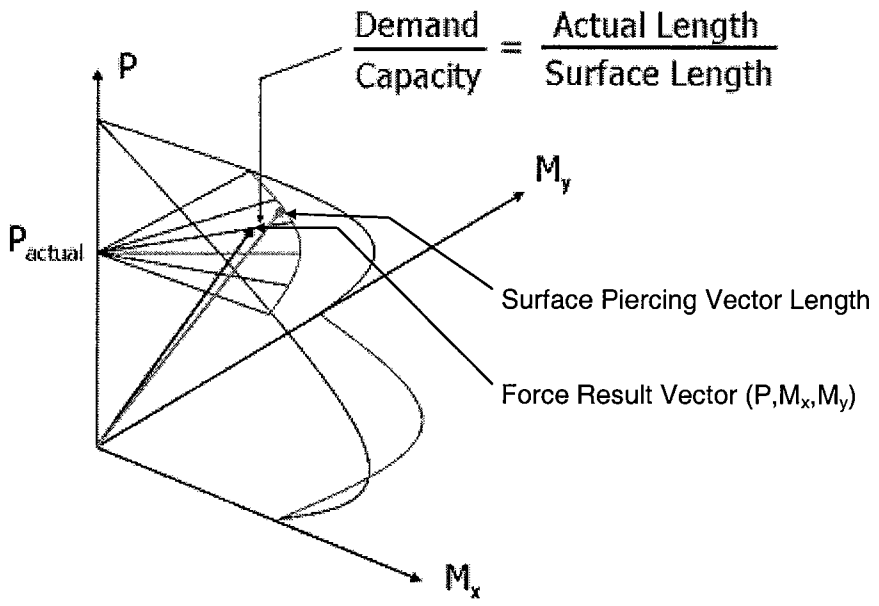

Figure 2.20. FB-Pier 3-D Interaction Diagram Showing Failure Ratio Calculation (8)

CHAPTER 3: THEORETICAL CONSIDERATIONS

3.1 General

Bridge bent piles are slender columns and subject to a possible stability or buckling failure. In investigating this failure mode, the first question to address is if the pile or bent can buckle in a sidesway mode. For existing bridges, this mode is probably not possible in the longitudinal direction. In an earlier report, Ramey and Brown (3) indicate that in the longitudinal direction of the bridge the end abutments will prevent a sidesway mode of buckling. They note that a sidesway mode could occur for small longitudinal movements (until the superstructure expansion joints are closed), after which the top support condition of the piles/bents would change to a pin condition with fixed translation and the associated elastic buckling load increases by a factor of eight. In the transverse direction, the bent X-bracing will prevent a sidesway mode of buckling. However, the sway bracing is often omitted for bent heights, H, $\leq$13ft and the effect of this will be discussed in this chapter.

Where sway bracing is employed, the largest value of effective length for a bent pile in the transverse direction will be the pile length from the bent cap to the ground line. Smaller values of effective length may be in order, depending on the pile end boundary conditions and bracing conditions, and this will also be discussed in this chapter.

3.2 Bent Pile Buckling in Transverse Direction

X-braced pile bents of the type used by the ALDOT cannot way in the transverse direction due to

- diagonal angle iron swaybracing
- batter piles on each end of the bent
- lateral support from continuous superstructures (when applicable)

(see Figure 2.1). Therefore, buckling of the bent piles in the transverse direction will be a nonsway mode with partial rotational fixity at the top due to the bent cap (assume 50% fixity), and partial fixity at the bottom due to the ground stiffness modulus (assume 50% fixity) as indicated in Figure 3.1a. The assumption of 50% rotational fixity at the pile top, i.e., at the bent cap, seems quite reasonable since the piles are typically embedded 1 ft into the cap as indicated in Figure 3.2 or connected by weldment to anchor plates embedded in the cap as indicated in Figure 3.3 (3). If one assumes that the swaybracing does not buckle, then for the case of a 5-pile bent (shown in Figure 3.4) with H=25ft (the largest value) and S=20ft (the largest probable value), the approximate buckling load for each of the piles in the bent would be as follows:

$$\ell_{mp} = \frac{\text{"E" or "G"}}{2} + 3.5' + S = \frac{11.5}{2} + 3.5 + 20 = 29.25'$$

where ℓ_{mp} = buckled loop-length of the middle pile and "E" or "G" is defined in the table at the top of Figure 3.4.

$$P_e^{mp} \approx \frac{1.5\pi^2 EI_y}{\ell_{mp}^2} = \frac{1.5\pi^2(29{,}000)(71.1)}{(29.25^2)(144)} = 250^k$$ (assume 50% fixity at bottom)

$$\ell_{ep} = 3.5' + S = 3.5' + 20 = 23.5'$$

where ℓ_{ep} = buckled loop-length of an end pile

$$P_e^{ep} \approx \frac{1.5\pi^2 EI_y}{\ell_{ep}^2} = \frac{1.5\pi^2(29{,}000)(71.1)}{(23.5^2)(144)} = 387^k$$

$$\ell_{ip} = \frac{\text{"E" or "G"}}{4} + 3.5' + S = \frac{11.5}{4} + 3.5 + 20 = 26.4'$$

where ℓ_{ip} = buckled loop-length of an intermediate pile

$$P_e^{ip} \approx \frac{1.5\pi^2(29{,}000)(71.1)}{(26.4^2)(144)} = 307^k$$

Due to "lean-on" bracing provided by adjacent piles and the bent cap,

$$P_e^{bent} = \sum P_{CR}^{piles} = 250^k + 2(307) + 2(387) = 1638^k$$

$$P_Y^{bent} = 5\,P_Y^{bent} = 5(446^k) = 2230^k$$

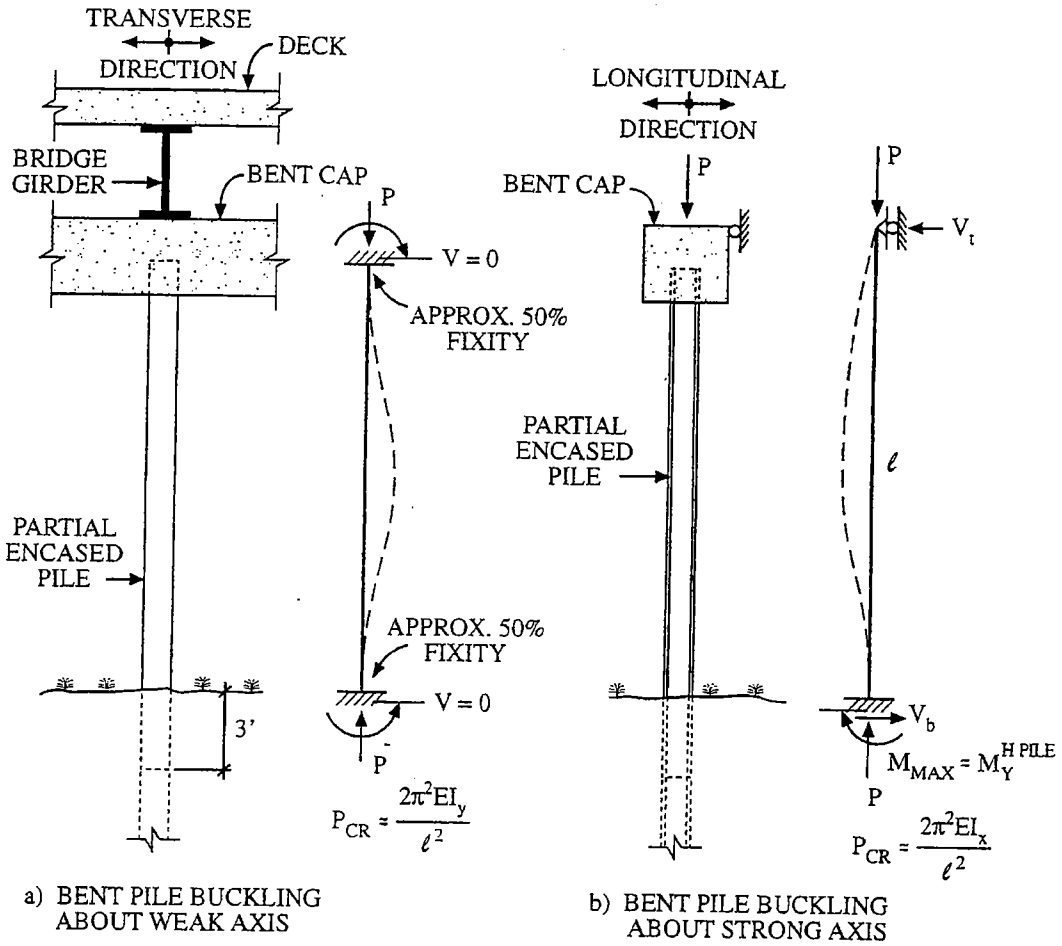

Figure 3.1. Partial Encased Bent Pile Buckling in a Non Sidesway Mode About its Weak and Strong Axes (3)

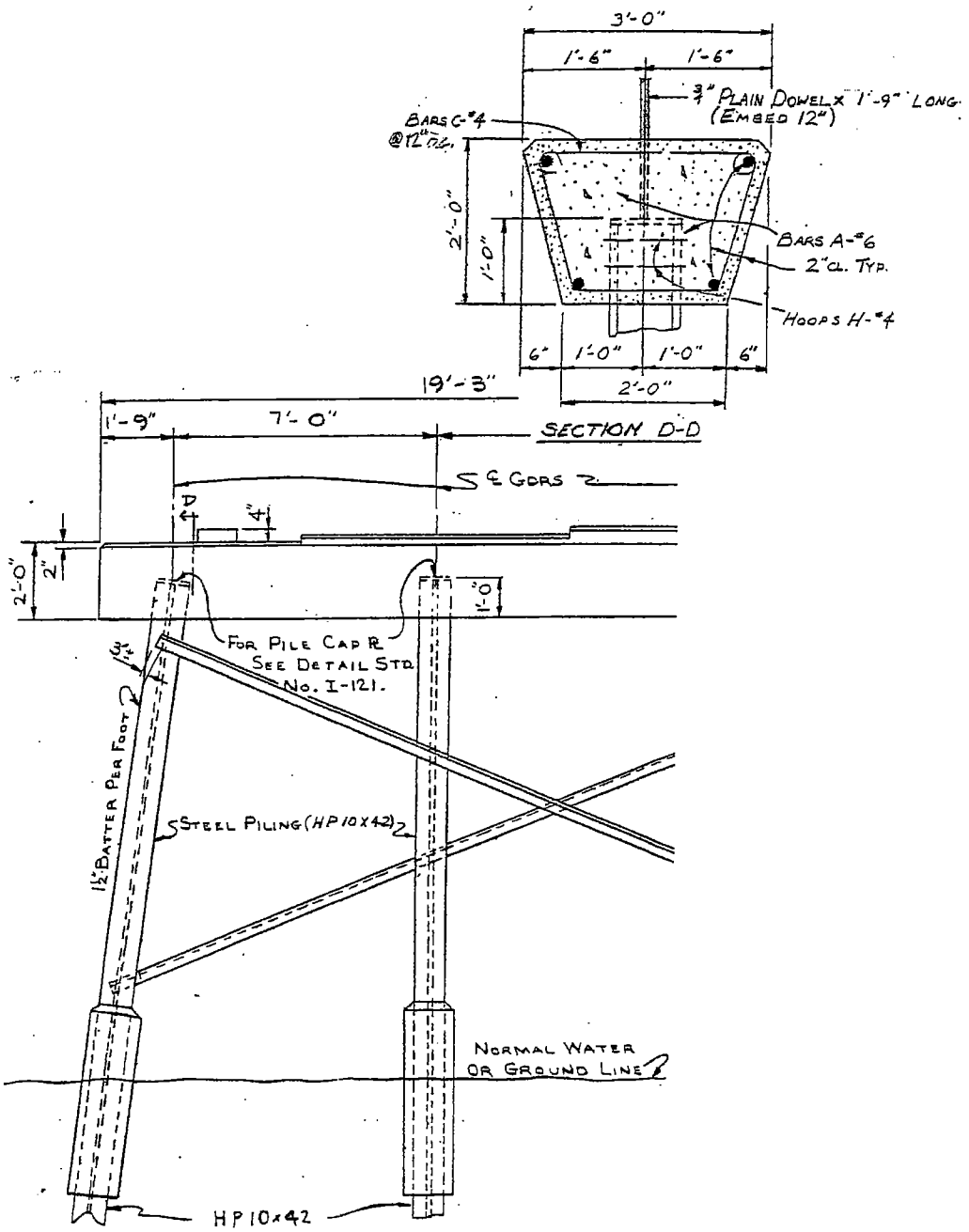

Figure 3.2. Pile Connections/Embedment to Bent Cap (3)

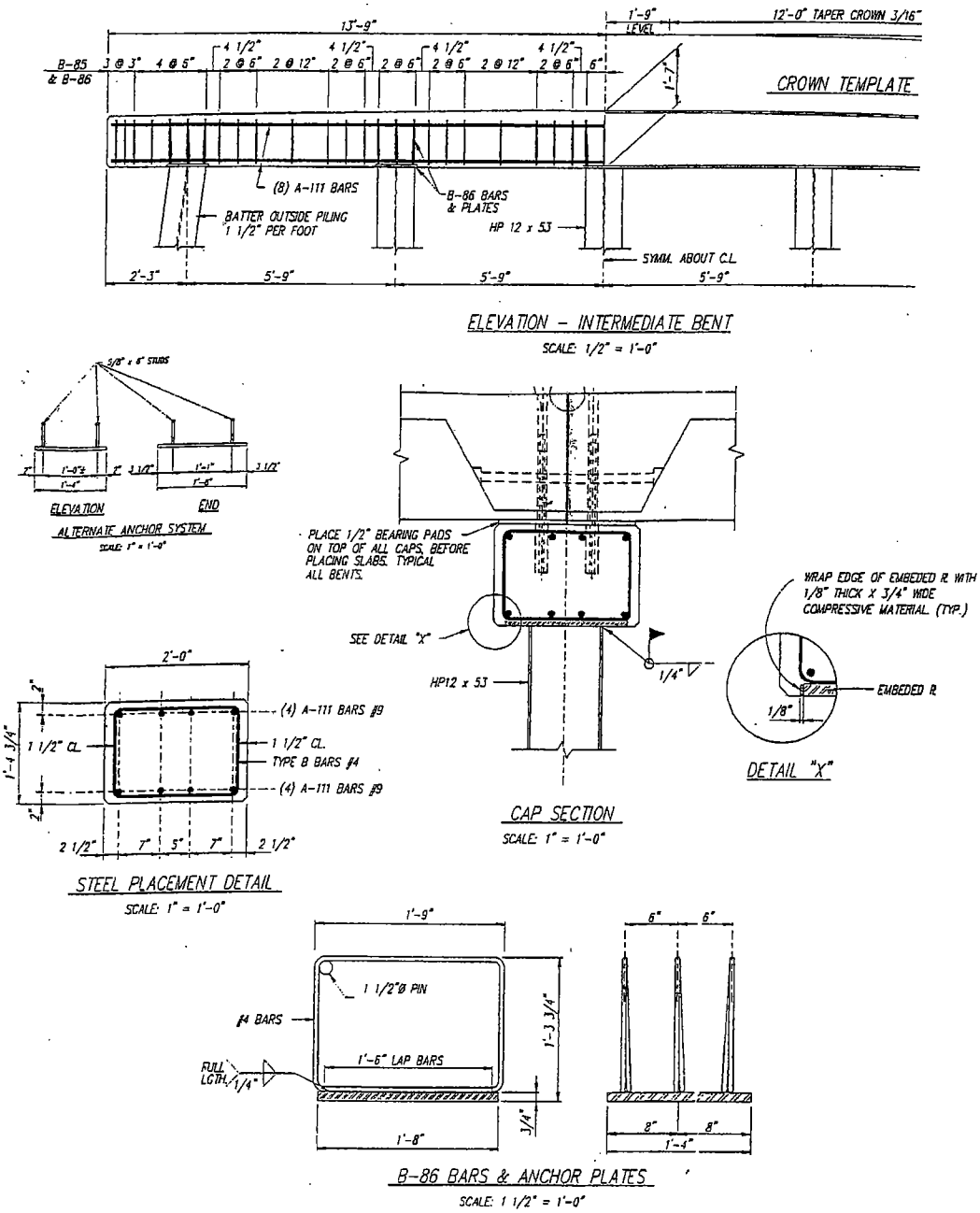

Figure 3.3. Pile Connections by Anchor Plates to Bent Cap (3)

TWO STORY BENT SWAYBRACING TABLES					
"H"	"E"	"A"	"B"	"C"	WT. LBS.
20'-0"	6'-6"	25'-6"	25'-6"	27'-3"	1205
21'-0"	7'-6"	25'-6"	25'-6"	27'-7"	1209
22'-0"	8'-6"	25'-6"	25'-6"	28'-0"	1216
23'-0"	9'-6"	25'-6"	25'-6"	28'-5"	1223
24'-0"	10'-6"	25'-6"	25'-6"	28'-11"	1230
25'-0"	11'-6"	25'-6"	25'-6"	29'-5"	1238

Largest → "H" Value

BATTEN WEIGHT TO BE ADDED TO ABOVE TABLES. 10-BATTENS REQ'D, 5/16" X 7 1/2" X 1'-6 1/4" @ 12.1# EACH.

NOTE: WEIGHT GIVEN IS TOTAL FOR TWO PIECES OF EACH LENGTH OF SWAYBRACING SHOWN IN BOTH TABLES

SINGLE STORY BENT SWAYBRACING TABLES			
"H"	"G"	"D"	WT. LBS.
13'-0"	7'-5"	25'-8"	395
14'-0"	8'-5"	26'-1"	401
15'-0"	9'-5"	26'-7"	409
16'-0"	10'-5"	27'-1"	417
17'-0"	11'-5"	27'-7"	425
18'-0"	12'-5"	28'-1"	432
19'-0"	13'-5"	28'-8"	441

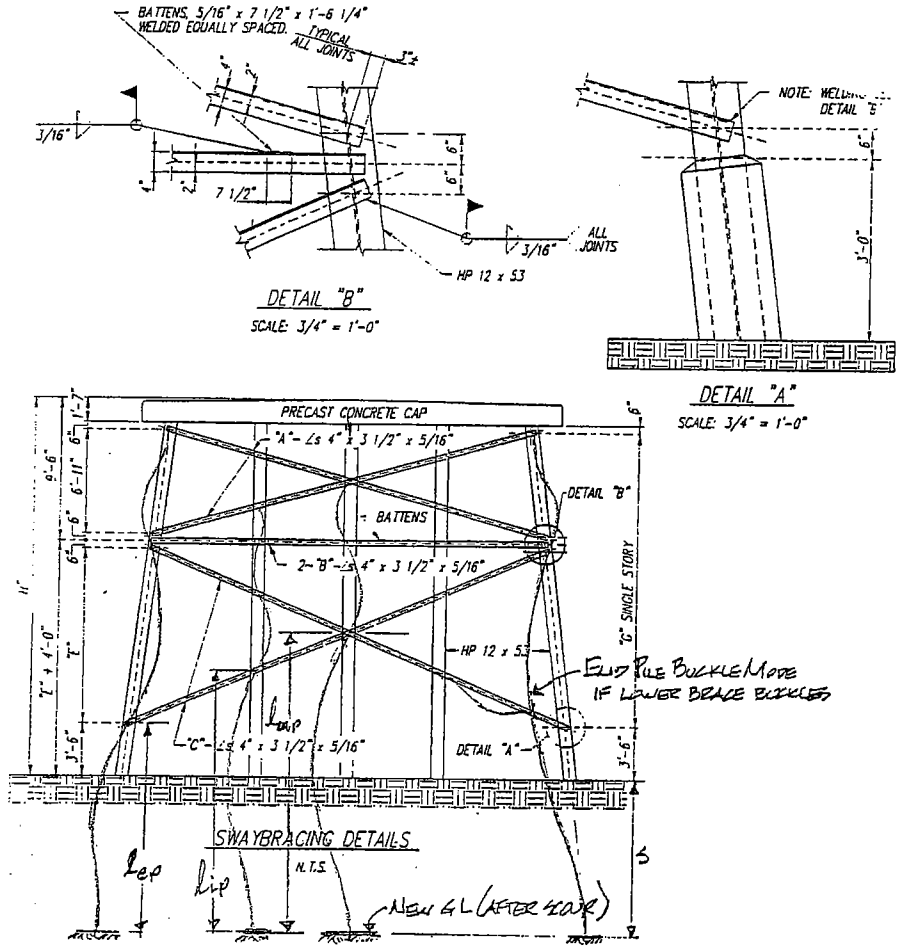

Figure 3.4. Bent Transverse Buckling (3)

Note, however, that the swaybracing members (see Figure 3.2) are relatively small angle iron and whereas they would prevent swaying of the bent, they will probably buckle themselves rather than prevent buckling of the individual piles (see right end pile in Figure 3.4). Therefore, it will be assumed that the swaybracing and batter piles will prevent transverse sidesway buckling of the bent, but that the individual bent piles will buckle in the transverse direction from the bent cap (assume 50% fixity) to the new ground line after scour (assume 50% fixity). Since 50% rotational fixities will be assumed at each end of the piles, the buckling loads per pile are reduced from

$P_e = \frac{4\pi^2 E I_w}{\ell^2}$ (for a pile with fully fixed ends) to

$$P_e \approx \frac{2\pi^2 E I_w}{\ell^2} \qquad (3.1)$$

Where

$I_w = I_{weak\ axis} = I_y$

ℓ = "H" (on pile bent standards) + S = height from new ground line to top of bent cap

Due to "lean-on" bracing from adjacent piles via the pile cap,

$$P_{CR} = \sum P_{CR}^{pile}$$

Using Eqn. (3.1) yields the elastic values of P_{CR} shown in Table 3.1 for ℓ values ranging from 15'-40' for HP 10x42 and 12x53 piles. These failure loads are presented graphically in the form of P_{CR} vs. ℓ curves in Figure 3.5. As indicated in Chapter 2, for $P_{CR} > P_y/2$, inelastic buckling loads should be used.

Using the parameters indicated in Figure 2.10 and $P_e \approx \frac{2\pi^2 E I_w}{\ell^2}$ for transverse pile buckling, we can determine the pile length above ground which separates inelastic and elastic buckling. This length is

$$\frac{2\pi^2 E I_w}{\ell^2} = \frac{P_y}{2} \longrightarrow \ell^2 = \frac{2\pi^2 E I_w}{P_y/2} \longrightarrow \ell = \sqrt{\frac{2\pi^2 E I_w}{P_y/2}}$$

or for A36 steel,

ℓ = 35.74' (for HP 10x42 pile)

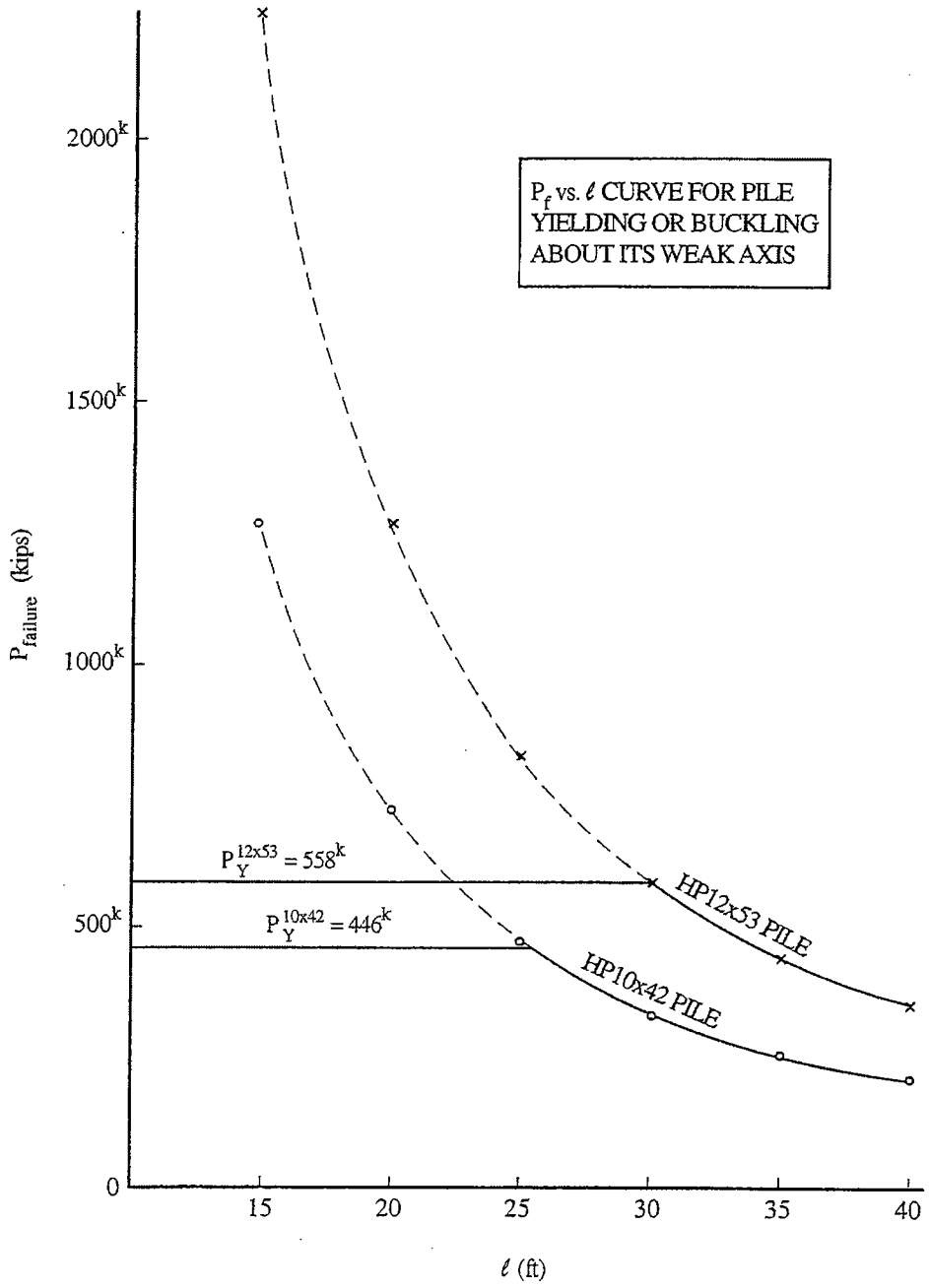

Figure 3.5. Elastic Transverse/Weak Axis Buckling of a Single Bent Pile for a Given Length (ℓ) above Ground Line after Scour (3)

ℓ = 42.54' (for HP 12x53 pile)

The inelastic buckling loads are approximated by a parabola extending between $\ell = 0$ and the above lengths. The following derivation was made to compute inelastic buckling loads.

The equation of the parabola is $P_{CR} = a + b\ell + c\ell^2$.

At $\ell = 0$, $P_{CR} = P_y$, and thus $a = P_y$

$$\frac{dP_{CR}}{d\ell} = 0 = b + 2c\ell$$

$$\therefore b = 0$$

$$\therefore P_{CR} = P_y + c\ell^2 \qquad (3.2)$$

Substituting the above pile lengths that divide elastic and inelastic buckling into Eqn. (3.2) yields,

$$P_y/2 = P_y + C(35.74)^2$$

$$C = -\frac{P_y}{2(35.74)^2} = -0.175 k/ft^2 \text{ (for HP10x42 pile)}$$

$$C = -\frac{P_y}{2(42.54)^2} = -0.154 k/ft^2 \text{ (for HP12x53 pile)}$$

Therefore, the inelastic buckling values in the range $P_y \geq P_{\text{inelastic buckling}} \geq P_y/2$ are approximated from the following equations,

$$P_{CR} = 446 - 0.175\,\ell^2 \text{ (for A36 steel HP10x42 pile)} \qquad (3.3)$$

$$P_{CR} = 558 - 0.175\,\ell^2 \text{ (for A36 steel HP12x53 pile)} \qquad (3.4)$$

These along with elastic buckling loads are given in Table 3.2 and plotted in Figure 3.6 over a range of $0 \leq \ell \leq 50$ ft.

Table 3.1. Pile Elastic Buckling Loads, P_e, vs. ℓ for HP 10x42 and 12x53 Piles

ℓ (ft)	*P_e (kips)	
	HP10x42	HP12x53
15	1267	2244
20	713	1263
25	456	808
30	317	561
35	233	413
40	178	316

*Based on Buckling in Transverse Direction as given by Eqn. (3.1)

$P_y^{HP10x42} = 12.4 \times 36 = 446^k$ (for A36 steel)

$P_y^{HP10x42} = 15.5 \times 36 = 558^k$ (for A36 steel)

Table 3.2. Transverse Inelastic and Elastic Buckling Loads vs. ℓ for HP10x42 and HP12x53 Piles of A36 Steel

ℓ = "H" + S (ft)	P_{CR} (kips)	
	HP10x42	HP12x53
0	446	558
5	442	554
10	429	543
15	407	523
20	376	496
25	337	462
30	289	419
35	232	369
35.74	223	-
40	178	312
42.54	-	312
45	141	249
50	114	202

* Shaded Values are $P_{elastic}$ Buckling

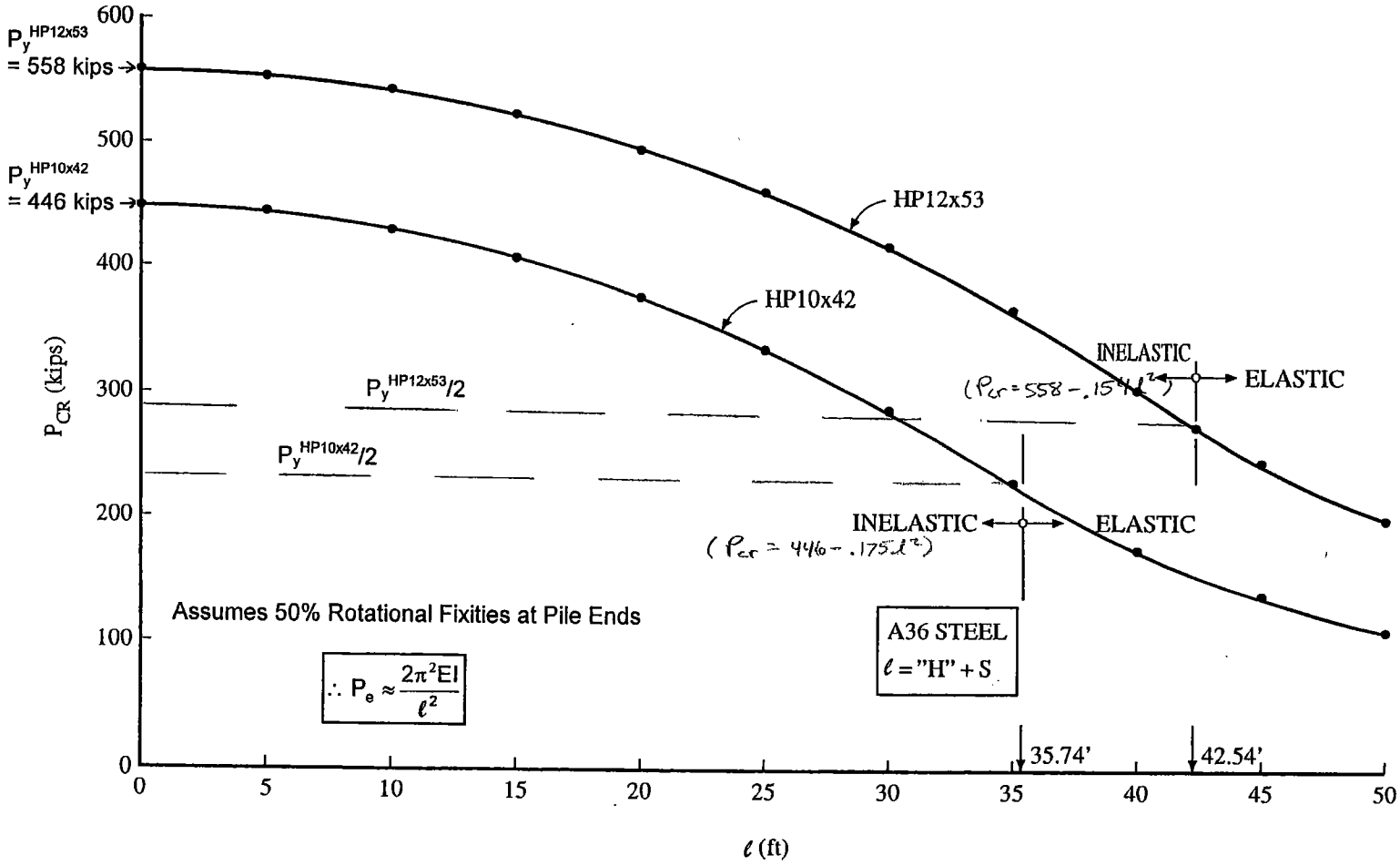

Figure 3.6. Transverse Inelastic and Elastic P_{CR} vs. ℓ for HP10x42 and HP12x53 Piles

3.3 Ideal Bracing Stiffness

In general, column/pile bracing requirements are

- Stiffness – to hold the braced point in place
- Strength – brace force and strength required are directly related to the initial out-of-straightness and/or load eccentricity.

For an ideal column pinned at its base the ideal top brace requirement (as shown in Figure 2.12) is

$$k_{ideal}^{pile} = \frac{P_e^{pile}}{\ell} = \frac{\pi^2 EI}{\ell^3} \text{ (Stiffness Requirement)}$$

$F_{brace} = 0$ (Strength Requirement)

These same results are also shown in Figure 3.7 except that β = brace stiffness rather then k.

The ideal brace stiffness of an entire pinned base pile bent model which consists of 5 piles is

$$k_{ideal}^{bent} = \frac{\sum^{\#piles} P_e^{pile}}{\ell} = \frac{5P_e^{pile}}{\ell}$$

Values of k_{ideal}^{bent} are summarized in Table 3.3 for HP 10x42 and HP 12x53 steel piles with pinned bases and appropriate modifications for inelastic buckling. For smaller length piles the pile failure mode will be one of inelastic buckling at loads well below the elastic buckling loads. Therefore, in more general terms, the ideal brace stiffness of an individual pile with a pinned base is

$$k_{ideal}^{pile} \approx \frac{P_{CR}^{pile}}{\ell}$$

and the ideal brace stiffness of the entire pinned base bent is

$$k_{ideal}^{bent} \approx \frac{\sum^{\#piles} P_{CR}^{pile}}{\ell}$$

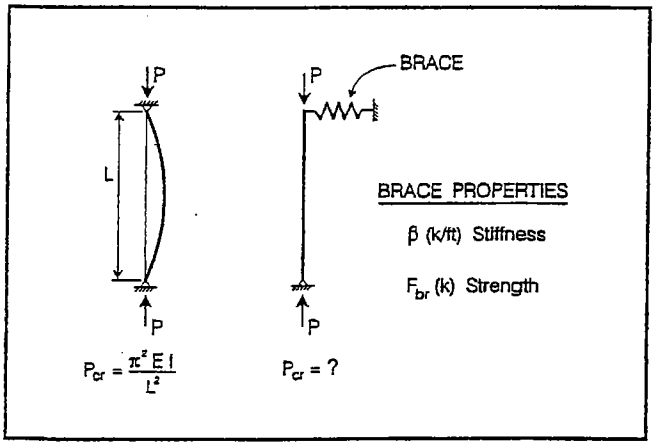

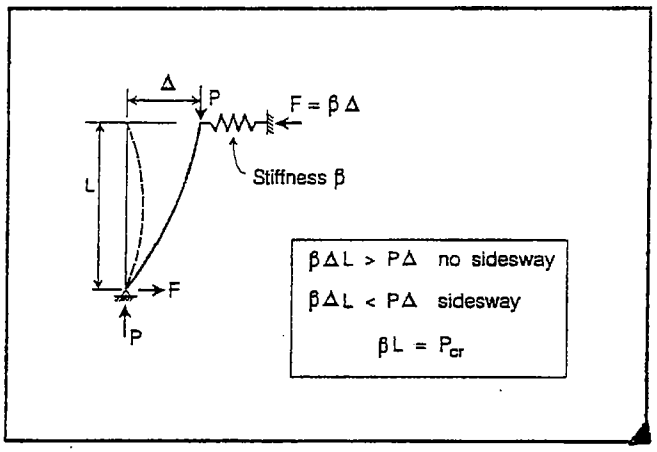

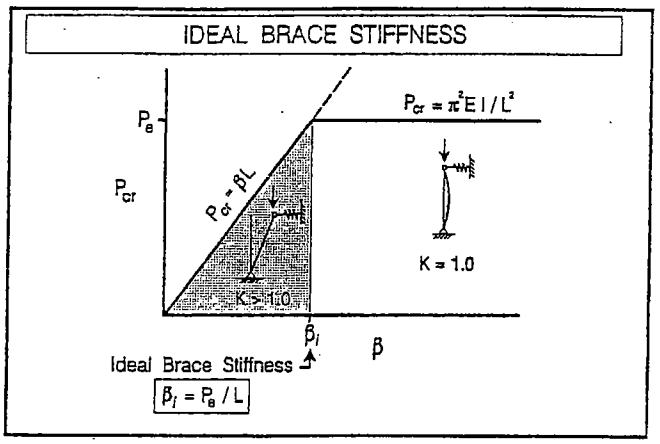

Figure 3.7. Ideal Brace Stiffness (2)

Table 3.3. Elastic and Inelastic Buckling Loads and k_{ideal}^{bent} Values for Pinned Base 5-Pile Bents with HP10x42 and HP12x53 Piles

ℓ = "H" + S (ft)	Pile Buckling Capacity, P_{CR} (kips) $P_e = \frac{\pi^2 E I_y}{\ell^2}$		$^{**}k_{ideal}^{bent} \approx \frac{5P_{CR}}{\ell}$ (k/in)	
	HP10x42	HP12x53	HP10x42	HP12x53
13	387	506	12.40	16.22
15	366	487	10.17	13.53
20	305	433	6.35	9.02
25	228	366	3.80	6.10
30	158	280	2.19	3.89
35	116	206	1.38	2.45
40	89	158	0.93	1.65

* Shaded Values are $P_{elastic}$ Buckling
** Values shown are for a 5-pile bent

The ideal brace stiffness for a pile with a fixed base is determined by multiplying the stiffness of the ideal brace with a pinned base (shown in Figure 3.7) by a factor of five to achieve 95% of the fully braced P_{CR} (3). This condition is shown in Figure 3.8. The K=0.7 condition shown in Figure 3.8 (where K is an effective length factor) is approximately the condition of ALDOT's bents in the transverse direction if they are prevented from sidesway. Therefore, for an individual pile in fixed base bents,

$$k_{ideal}^{pile} \approx \frac{5P_{CR}}{\ell}$$

Thus for the entire fixed base bent,

$$k_{ideal}^{bent} \approx \frac{\sum^{\#piles} 5P_{CR}}{\ell}$$

The ideal bent stiffness values of the fixed base pile bent can be determined by multiplying the k_{ideal}^{bent} values of the pinned base 5-pile bent (listed in Table 3.3) by 5. The resulting k_{ideal}^{bent} values for a fixed base pile bent are summarized in Table 3.4 for HP 10x42 and HP 12x53 steel piles.

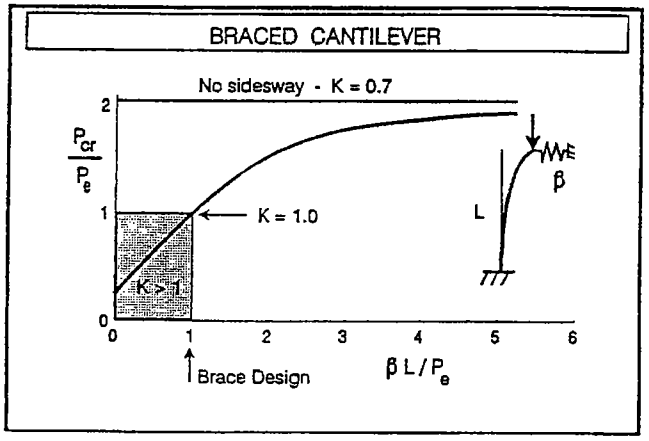

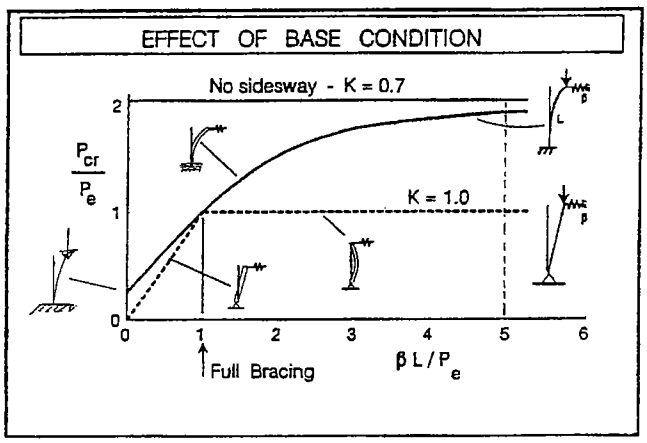

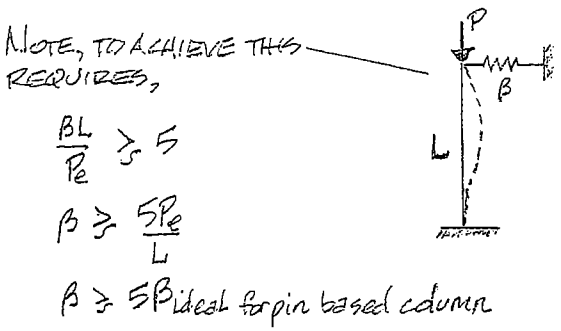

Figure 3.8. Brace Stiffness Required for Fixed Base Condition (2)

Table 3.4. Elastic and Inelastic Buckling Loads and k_{ideal}^{bent} Values for Fixed Base 5-Pile Bents with HP10x42 and HP12x53 Piles

L = "H" + S (ft)	Pile Buckling Capacity, P_{CR} (kips) $P_e = \frac{\pi^2 E I_y}{\ell^2}$		$^{**}k_{ideal}^{bent} \approx \frac{\sum_{\#piles} 5P_{cr}}{\ell}$ (k/in)	
	HP10x42	HP12x53	HP10x42	HP12x53
13	387	506	62.0	81.1
15	366	487	50.8	67.6
20	305	433	31.8	45.1
25	228	366	19.0	30.5
30	158	280	11.0	19.4
35	116	206	6.90	12.3
40	89	158	4.64	8.23

* Shaded Values are $P_{elastic}$ Buckling
** Values shown are for a 5-pile bent

Sidesway will occur if the pile bent fails as a result of insufficient lateral bracing. To determine if the lateral bracing is adequate, a comparison must be made between the ideal bent stiffness and the actual bent stiffness of the computer model. Most structures can be modeled by a series of spring elements which may be reduced to a single spring stiffness. The resulting elastic stiffness of the structure is defined as its equivalent stiffness, or k_{eq}. By comparing k_{eq} and k_{ideal}^{bent} it can be determined whether the piles will fail by sidesway or non sidesway buckling. If $k_{eq} > k_{ideal}$, the ideal brace stiffness requirement is exceeded and no sidesway occurs. In other words, the lateral stiffness required to hold the top of the pile in place as the axial load approaches P_{CR} is provided. Therefore, the bent cap is restrained from lateral translations and the pile bent fails by non sidesway buckling. Alternatively, when $k_{eq} < k_{ideal}$, the stiffness required to hold the top of the piles in place is not provided and sidesway will take place. Thus, the bent will fail by sidesway buckling and the buckling capacities will be significantly reduced. Values of bent k_{ideal} and k_{eq} may be conveniently plotted to compare k_{eq} and k_{ideal} values.

3.4. Simple Idealized Modeling of Bent for Estimating k_{eq}

Bridge pile bents are sometimes used without X-bracing but with a concrete pile encasement extending from 3 feet below ground line to the underside of the bent cap. However, because of the light steel spiral employed in the encasement and the vibratory nature of bridge and bent loads due to truck traffic, the concrete encasement could be lost with time (though ALDOT engineers report no such losses). Thus, let us examine the case of a bent without X-bracing and without pile encasement, but with batter piles at each end of the bent to see if the batter piles will provide sufficient lateral bracing to prevent sidesway buckling in the lateral or transverse direction. To simplify the analysis, Ramey and Brown (3), in their preliminary analysis, worked with the simple idealized bent model shown in Figure 3.9.

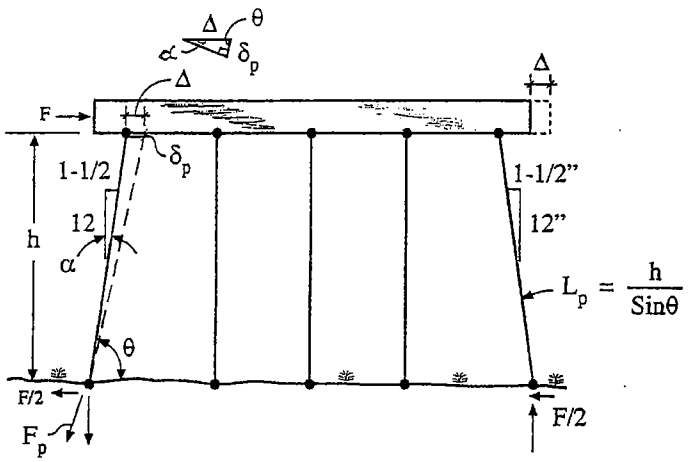

Figure 3.9. Simplified Bent Model (3)

For this simplified model,

$$\tan \alpha = \frac{1.5}{12} = 0.125$$

$$\alpha = 7.125^{\circ}$$

$$\therefore \theta = 90^{\circ} - \alpha = 82.875^{\circ}$$

$$\cos \theta = \frac{F/2}{F_p}$$

$$F_p = \frac{F/2}{\cos \theta}$$

$$\delta_p = \frac{F_p L_p}{A_p E_p} = \frac{\frac{F}{2\cos\theta} \times \frac{h}{\sin\theta}}{A_p E_p} = \frac{Fh}{2A_p E_p \cos\theta \sin\theta}$$

$$\cos \theta = \frac{\delta_p}{\Delta}$$

$$\Delta = \frac{\delta_p}{\cos \theta} = \frac{Fh}{2A_p E_p \cos^2 \theta \sin\theta}$$

$$F = \underbrace{\frac{2A_p E_p \cos^2 \theta \sin\theta}{h}}_{k_{eq}} \Delta$$

Therefore, for an idealized HP 10x42 pile bent ($A = 12.4\ in^2$),

$$k_{eq} = \frac{2 \times 12.4 in^2 \times 29{,}000\ ksi \times \cos^2 82.875 \times \sin 82.875}{h} = \frac{10{,}980^{k}}{h}$$

For an idealized HP 12x53 pile bent ($A=15.5\ in^2$),

$$k_{eq} = \frac{13{,}725}{h}$$

Thus, k_{eq} for various values of h are as shown in Table 3.5 and in Figure 3.10.

Table 3.5. Bent k_{eq} Values for Simple Idealized Model in Figure 3.9

Bent Height, h (ft)	k_{eq} (kip/in)	
	HP10x42	HP12x53
13	70.4	88.0
15	61.0	76.3
20	45.8	57.2
25	36.6	45.8
30	30.5	38.1
35	26.1	32.7
40	22.9	28.6

For an ideal column pinned at its base the ideal bracing requirements would be as indicated in Figure 3.7, i.e.,

$$k_{ideal} = \frac{P_e}{h}$$

For the simplified bent model shown in Figure 3.9,

$$k_{ideal}^{pile} = \frac{P_e^{pile}}{h}$$

And

$$k_{ideal}^{bent} = \frac{\Sigma P_e^{pile}}{h} = \frac{5P_e}{h}$$

Values of k_{ideal}^{bent} for the simplified bent in Figure 3.9 are given in Table 3.3 for HP10x42 and HP12x53 piles. These values of k_{ideal}^{bent} for pinned base bents are plotted in Figure 3.10 for convenience in comparing them with k_{eq} values from Table 3.5. As previously mentioned, since each $k_{eq} > k_{ideal}$ in Figure 3.10 sidesway buckling is not expected to occur based on the simplified analysis. The k_{ideal}^{bent} values for fixed base bents are given in Table 3.4 for HP10x42 and HP12x53 piles. These k-values are plotted in Figure 3.11 to compare with the k_{eq} values in Table 3.5. Note that Figure 3.11 also indicates that the batter piles should provide sufficient lateral support to prevent sidesway buckling of the pile bent, i.e.,

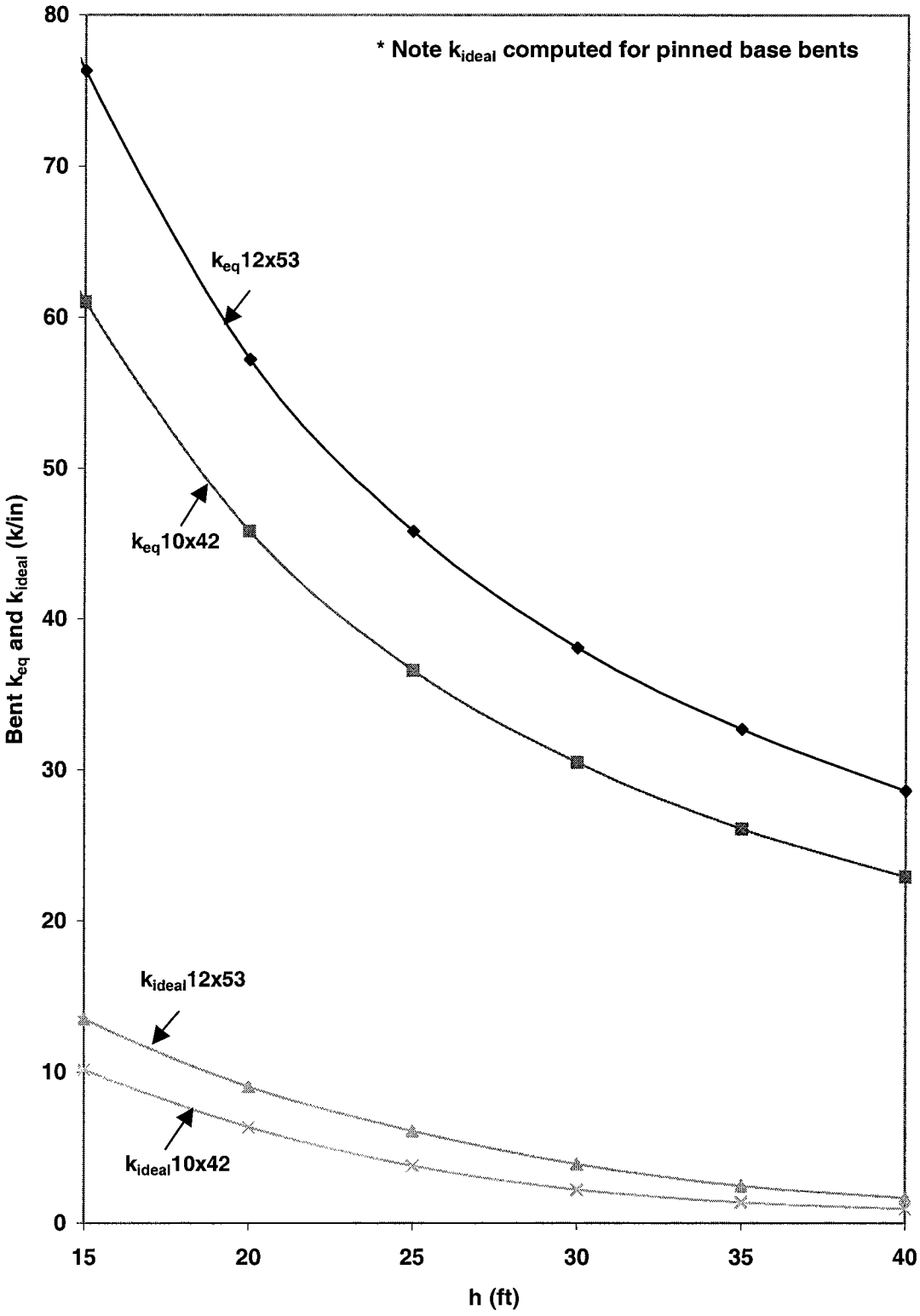

Figure 3.10. Bent k_{eq} and k_{ideal} vs h for Simplified Bent Model with HP10x42 and HP12x53 Piles

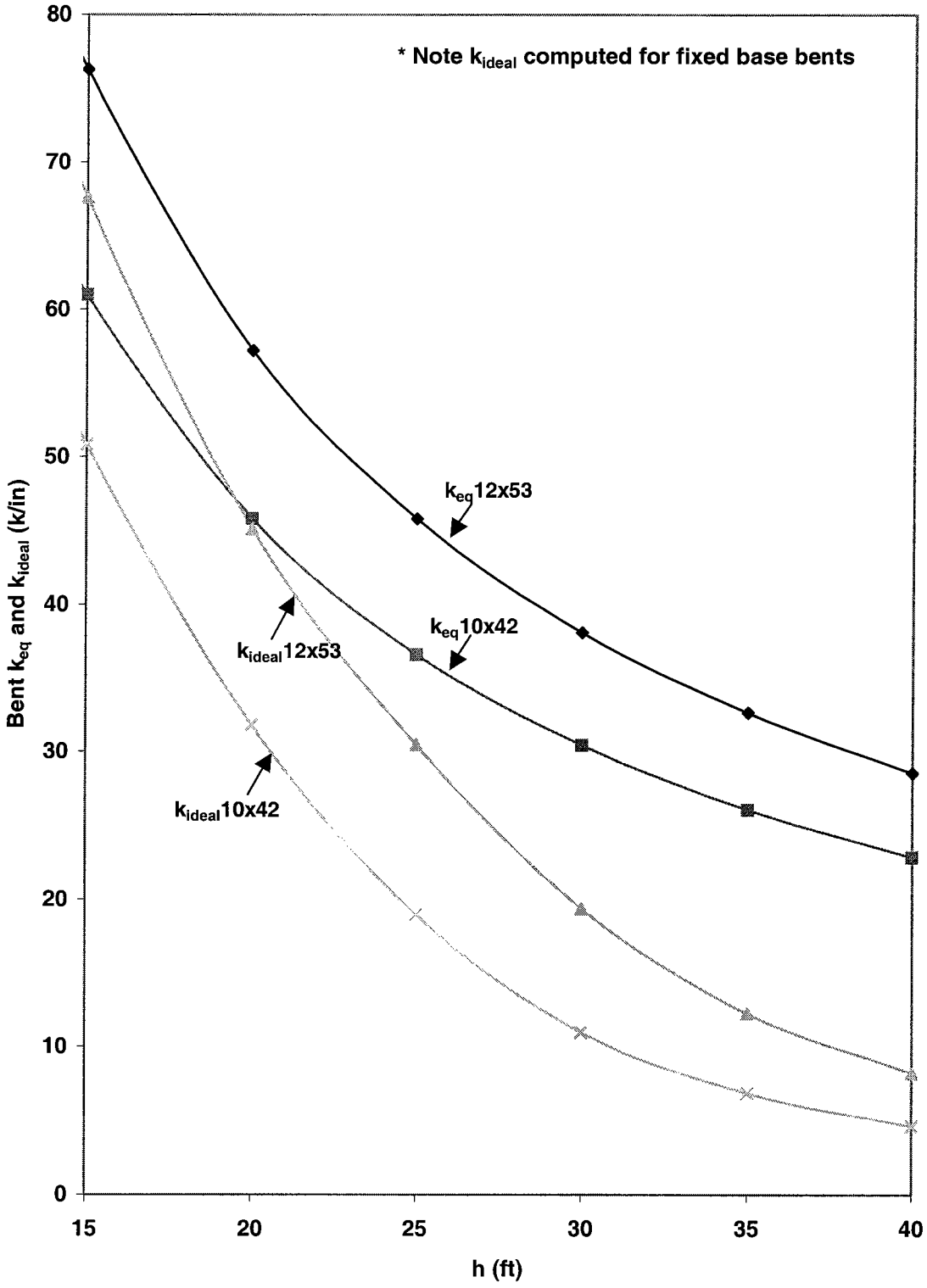

Figure 3.11. Bent k_{eq} and k_{ideal} vs h for Simplified Bent Model with HP10x42 and HP12x53 Piles

$k_{eq}^{bent} > k_{ideal}^{bent}$. For h values below 20 ft the approximate k_{eq}^{bent} values from the simplified analysis and k_{ideal}^{bent} are quite close, and the bents should probably be X-braced in addition to having the batter piles.

However, upon closer examination and study during the Phase II work, it is recognized that lateral bracing employing the axial stiffness of members as in the idealized frame of Figure 3.9 is much stiffer than bracing that employs the flexural stiffness of members as in the computer models. If actual bridge pile bents were as shown in Figure 3.9 with the piles pinned to the cap and foundation and the cap treated as a rigid member, they would have to resist lateral loads via the axial stiffness of the two end batter piles. However, this is not the case. A typical 5-pile bent (as shown in Figure 3.12) has some degree of fixity at the end of the piles.

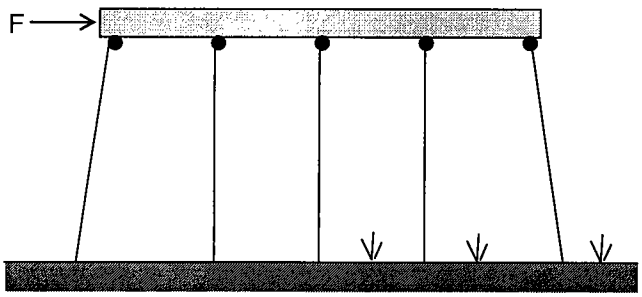

Figure 3.12. Typical 5-Pile Bridge Bent

Note for this bent, the end batter piles contribute some resistance to lateral loads via their axial stiffness; however, these same end piles can flex laterally and thus their lateral stiffness will be controlled by this lateral flexing.

If the bent were constructed with battered members that could only develop axial forces, such as that shown in Figure 3.13, then the lateral stiffness of such a bent would be controlled by the stiffer pin-ended/axially loaded end members, and would have much greater lateral stiffness than the bent of Figure 3.12.

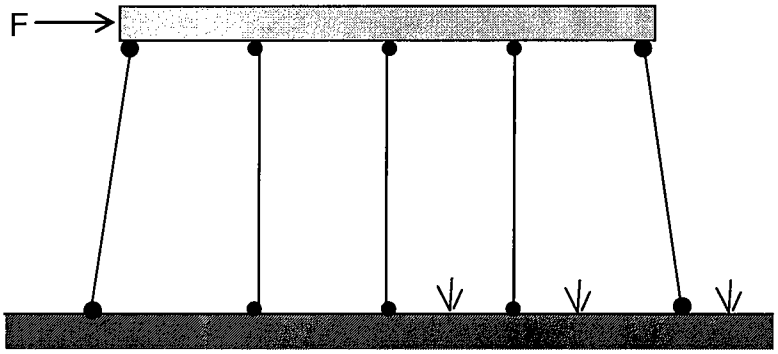

Figure 3.13. Hypothetical Bent with Pin-Pin End Members

Further simplified idealized bent models illustrate the significant difference in lateral stiffness afforded by the members developing bending moment (and relying on flexural stiffness). These models are shown in Figure 3.14.

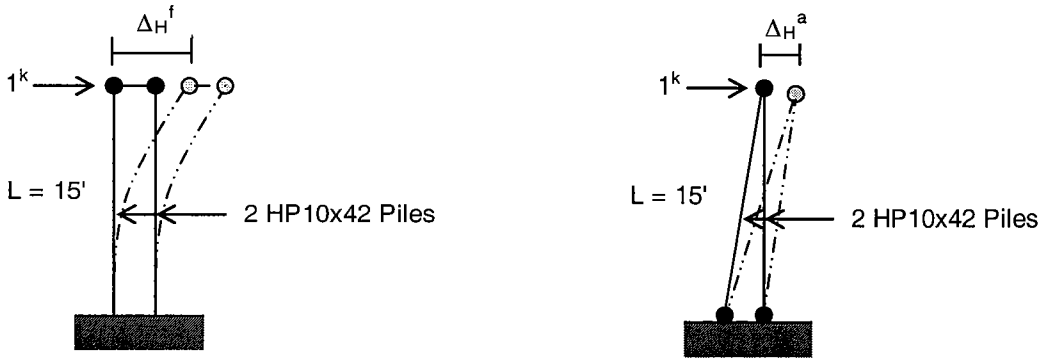

a) Bent Relying on Member Flexural Stiffness

b) Bent Relying on Member Axial Stiffness

Figure 3.14. Idealized Bent Lateral Stiffness

For the idealized bent resisting lateral loading via flexure as in Figure 3.14a,

$$\Delta_H^f = \frac{QL^3}{3EI} = \frac{0.5^k \times 15^3 \times 12^3}{3 \times 29{,}000 \times 71.7} = 0.4675 \text{ in/k}$$

$$\therefore k_f = \frac{1}{0.4675} = 2.14 \text{ k/in}$$

For the idealized bent resisting lateral loading via axial stiffness or truss action as in Figure 3.14b, the member forces, deformations, and Δ_H due to the 1 kip horizontal load shown in Figure 3.14b are shown in Figure 3.15. Therefore,

$$\Delta_H^a = 0.0648 \text{ in/k}$$

$$\therefore k_a = \frac{1}{0.0648} = 15.43 \text{ k/in}$$

Therefore,

$$\frac{k_a}{k_f} = \frac{15.43}{2.14} = 7.21$$

This reflects the much greater lateral stiffness of a system employing members in axial force to provide the lateral stiffness as opposed to those relying primarily on member flexural stiffness. Therefore the idealized bent in Figure 3.9 provides bent k_{eq} curves, shown in Figures 3.10 and 3.11, which are unconservatively high. Thus, bent lateral force, F, vs. Δ_{horz} curves with and without vertical bent cap loading should be developed for pile bents without X-bracing via stiffness analyses using GTSTRUDL and/or FB Pier to determine appropriate bent k_{eq} and k_{ideal} curves to replace those shown in Figures 3.10 and 3.11 (which were developed for the idealized bent shown in Figure 3.9). This is done in Chapters 5 and 6, and the resulting curves are presented and discussed in those chapters.

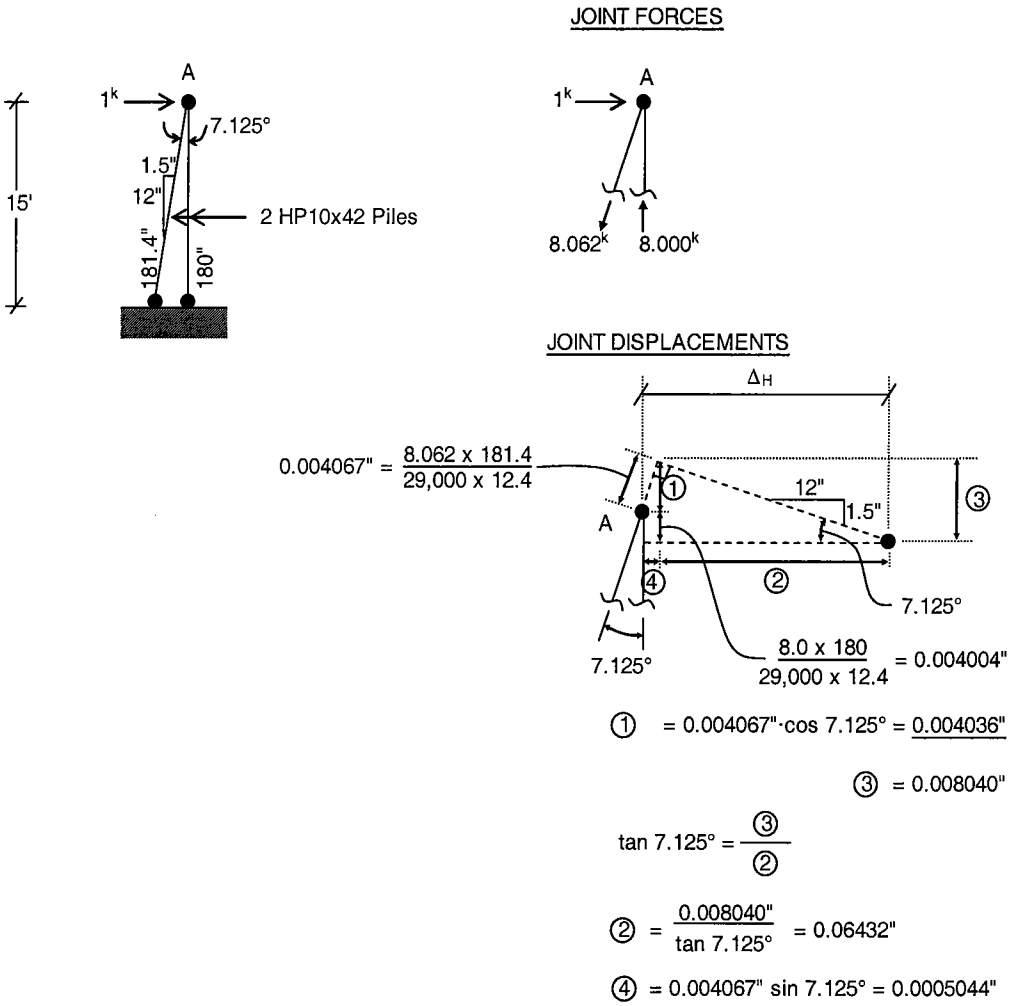

Figure 3.15. Idealized Truss Behavior Bent

3.5 Bent Cap Strength and Stiffness

As indicated in the Phase I report by Ramey and Brown (3), failure of the pile bent cap is unlikely due to the superstructure girders sitting directly above the piles. Significant relative vertical displacement between piles could cause failure of the cap in cases where the cap is lightly reinforced (as some are). Let us examine the forces set up in the cap in the event of a pile plunging or buckling failure.

From an examination of numerous pile bent standards, many pile cap geometries and pile spacings appear to be as shown in Figure 3.16 (see Table 4.1). For the pile cap indicated in this figure, for the pile to plunge or buckle, the P_{load} would have to exceed 87.1^{k} $+P_{plunging}$ or $P_{buckling}$ of the pile as can be seen in Figure 3.16. The P_{load} will never be this large and thus the failure indicated in Figure 3.16 will not occur.

Many bent caps, however, are only lightly reinforced such as the one shown in Figure 3.17 and are very susceptible to cap flexural failures as indicated. They provide very little reserve strength for resisting an applied P_{load} if the pile capacity P_{pile} is exceeded. For the pile cap indicated in Figure 3.17, pile plunging or buckling would occur if the P_{load} exceeded 34.8^{k} $+P_{plunging}$ or $P_{buckling}$ of the pile as can be seen from FBD(a) in Figure 3.17. However, even in this case, due to transverse continuity of the bridge superstructure, there would be a redistribution of loads across the width of the bridge (via the deck slab and diaphragms) if at a given pile location, $P_{load}>P_{pile}$.

The previous simplified bent model of Figure 3.9 assumes a completely rigid cap. However, the actual flexural stiffness of the cap may significantly reduce k_{eq}^{bent} values. Therefore, k_{eq}^{bent} values should be determined for various degrees of cap flexural stiffness, I. The sensitivity of k_{eq} to the bending strength of the cap should be evaluated by assigning various magnitudes of I for the cap in the computer models. These values include I for a completely rigid cap designated by I_{rigid}, a cap with flexural stiffness based on the gross cross section designated by I_{gross}, and finally a cap with flexural stiffness of the cracked section (concrete is cracked to the neutral axis) designated by I_{cr}. The effective stiffness of the cap under service loads, I_e, will lie

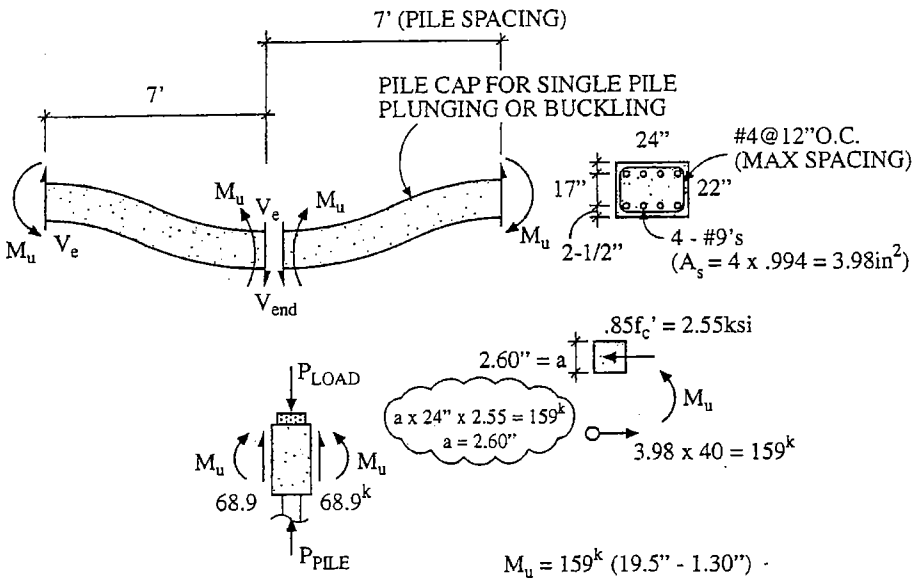

FBD (a)

$M_u = 159^k (19.5" - 1.30")$

$= 241^{1k}$

$$V_{end} = \frac{2M_u}{7'} \quad \frac{2x241^{1k}}{7} = 68.9^k$$

$2V_{end} = 137.8^k$

CHECK SHEAR CAPACITY

$V_u = \phi V_c + \phi V_s$ (0)

$= \phi(2\sqrt{fc'}\, b_w d) + \phi(\frac{A_v f_y d}{S})$

$= 0.85(2\sqrt{3000} \times 24 \times 19.5)$

$= 43.56^k$ ← Controls

Note: stirrup spacing exceeds max d/2 and $V_s = 0$

∴ IF $P_{LOAD} \geq 87.1^K + P_{CR\text{ - PILE (BUCKLING OR PLUNGING)}}$
THE PILE CAP WILL FAIL AS INDICATED ABOVE

Figure 3.16. Examination of Pile Cap Flexural Failure for Case of Well Reinforced Cap (3)

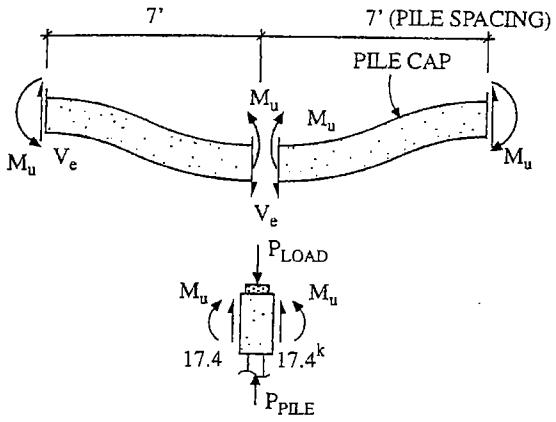

FBD (a)

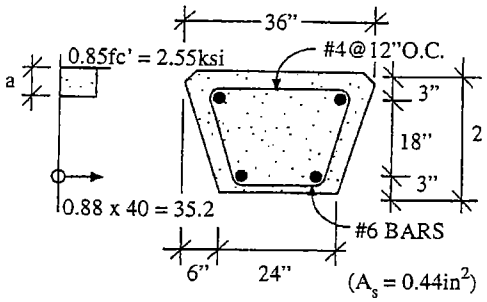

a x 2.55 x 36" = 35.2

a = 0.384"

$M_u = 139^k (19.5" - 1.30")$

$= 732^{11k} = 61^{1k}$

$$V_{end} = \frac{2M_u}{7'} \quad \frac{2x61^{1k}}{7} = 17.4^k$$

$2V_{end} = 34.8^k$ ← Controls

∴ IF $P_{LOAD} \geq 34.8^k + P_{CR\text{-}PILE\ (BUCKLING\ OR\ PLUNGING)}$

THE PILE CAP WILL TRY TO FAIL AS INDICATED ABOVE. HOWEVER IF THIS CONDITION IS EVER REACHED, THERE WILL BE A REDISTRIBUTION OF LOAD ACROSS THE WIDTH OF THE BRIDGE (VIA THE DECK SLAB AND DIAPHRAGMS)

CHECK SHEAR CAPACITY

$V_u = \phi V_c + \phi V_s$

$= \phi(2\sqrt{fc'}\, b_w d) + \phi(\frac{A_v f_y d}{S})$ → 0

$= 0.85(2\sqrt{3000} \times 30 \times 21)$

$= 58.7^k$

CAP HAS SUFFICIENT SHEAR CAPACITY TO DEVELOP FULL END M_u'S.

Note: stirrup spacing exceeds max d/2 and $V_s = 0$

Figure 3.17. Examination of Pile Cap Flexural Failure for Case of Lightly Reinforced Cap (3)

somewhere between I_{gross} and I_{cr} since small cracks on the tensile surface of the cap will reduce the gross section. According to ACI 318-02, the effective moment of inertia may be approximated as $0.35I_g$ for beams.

For the simplified bent cap cross-section of Figure 3.18 the following calculations were used to determine values for I corresponding to I_{rigid}, I_{gross}, I_e, and I_{cr}. The rigid cap was given an excessively large moment of inertia, i.e., $I_{rigid}=10{,}000{,}000in^4$.

Calculation of I_{gross}:

$$I_{gross} = \frac{1}{12} \cdot 36in \cdot (24in)^3 = 41{,}472in^4$$

Calculation of I_e:

$$I_e = 0.35I_{gross} = 14{,}515in^4$$

Calculation of I_{cr}:

$$\bar{y} = \frac{\sum(Ay)}{\sum A} = \frac{(b\bar{y})\frac{\bar{y}}{2} + nA_s d_1 + nA_s d_2}{b\bar{y} + nA_s + nA_s}$$

$$(b\bar{y})\frac{\bar{y}}{2} - nA_s d_1 - nA_s d_2 + nA_s \bar{y} + nA_s \bar{y} = 0$$

$E_s = 29{,}000{,}000psi \quad E_c = 57{,}000\sqrt{4000} = 3{,}605{,}000psi; \quad n = 8.06$

$$(36\bar{y})\frac{\bar{y}}{2} - 8.06(.88)(3) - 8.06(.88)(21) + 8.06(.88)\bar{y} + 8.06(.88)\bar{y} = 0$$

$$\bar{y} = 2.7in$$

$$I_{cr} = \frac{1}{3}b(\bar{y})^3 + nA_s(d_1 - \bar{y})^2 + nA_s(d_2 - \bar{y})^2$$

$$I_{cr} = \frac{1}{3}36(2.7)^3 + 7.09(3 - 2.7)^2 + 7.09(21 - 2.7)^2 = 2{,}612in^4$$

Note that these values of

$I_{rigid} = 10{,}000{,}000\ in^4$

$I_{gross} = 41{,}472\ in^4$

$I_{cr} = 2{,}612\ in^4$

give a huge range of I values and I ratios as follows:

$$\frac{I_{rigid}}{I_{gross}} = 241$$

$$\frac{I_{gross}}{I_{cr}} = 15.9$$

$$\frac{I_{rigid}}{I_{cr}} = 3{,}828$$

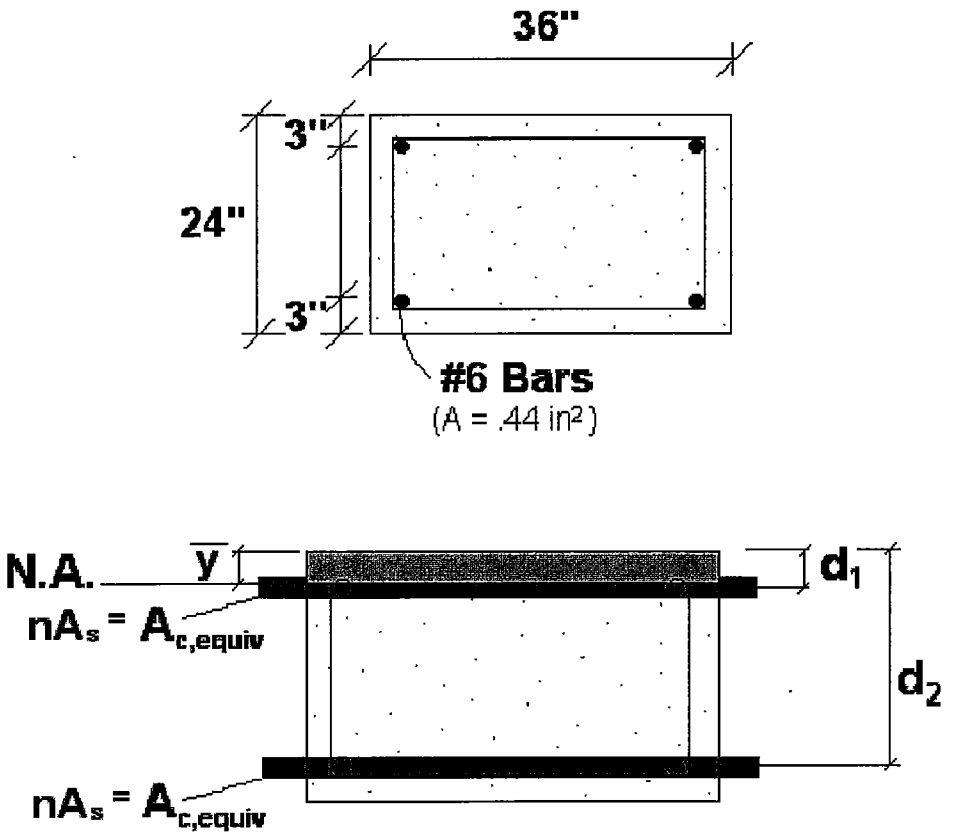

Figure 3.18. Simplified Bent Cap Cross Section For Determination of I_{gross} and I_{cr}

3.6 Effect of Soil Subgrade Modulus on Pile Buckling Load

As discussed in Chapter 2, H. Granholm (1) developed an analytical solution for pile buckling when partially embedded in a soil supporting medium as shown in Figure 2.15. To gain a feel for the sensitivity of pile and bent buckling capacity to soil subgrade modulus (k_o) and coefficient of lateral displacement (C) values, let us use Granholm's Equation to determine the buckling load about each axis for two of ALDOT's most widely used bent piles, i.e.,

HP 10x42 ($I_x = 210$ in^4, $I_y = 71.7$ in^4, $A = 12.4$ in^2)

HP 12x53 ($I_x = 393$ in^4, $I_y = 127$ in^4, $A = 15.5$ in^2)

Buckling in the longitudinal direction (about pile x-x axis) is considered because the end conditions that Granholm used were for the top of the pile being pinned which is the appropriate boundary condition for buckling in the longitudinal direction. Buckling in the transverse direction (about pile y-y axis) is considered because that is probably the controlling direction of bent buckling.

In this sensitivity analysis, we will assume the conditions shown in Figure 3.19. It should be noted that Earth Tech, Inc. used soil subgrade modulus values of

$k_o = 28.94, 43.4, 57.9, 86.8, 115.7, 289.4$ lb/in^3

in their earlier analysis with FB-Pier. Thus, we have expanded their range of k_o values at both the low and high ends to provide a range where the high value of k_o (578.8 lb/in^3) is more than 100 times larger than the lower value used.

Recall in Granholm's Eqn. (2.4) for the pile top being pinned that

$$k = \sqrt{\frac{P}{EI}}$$

$$a = \sqrt[4]{\frac{C}{EI}}$$

C = soil coefficient of lateral displacement (lb/in^2)

$C = k_o b$

k_o = soil subgrade modulus (lb/in^3)

b = pile width (in)

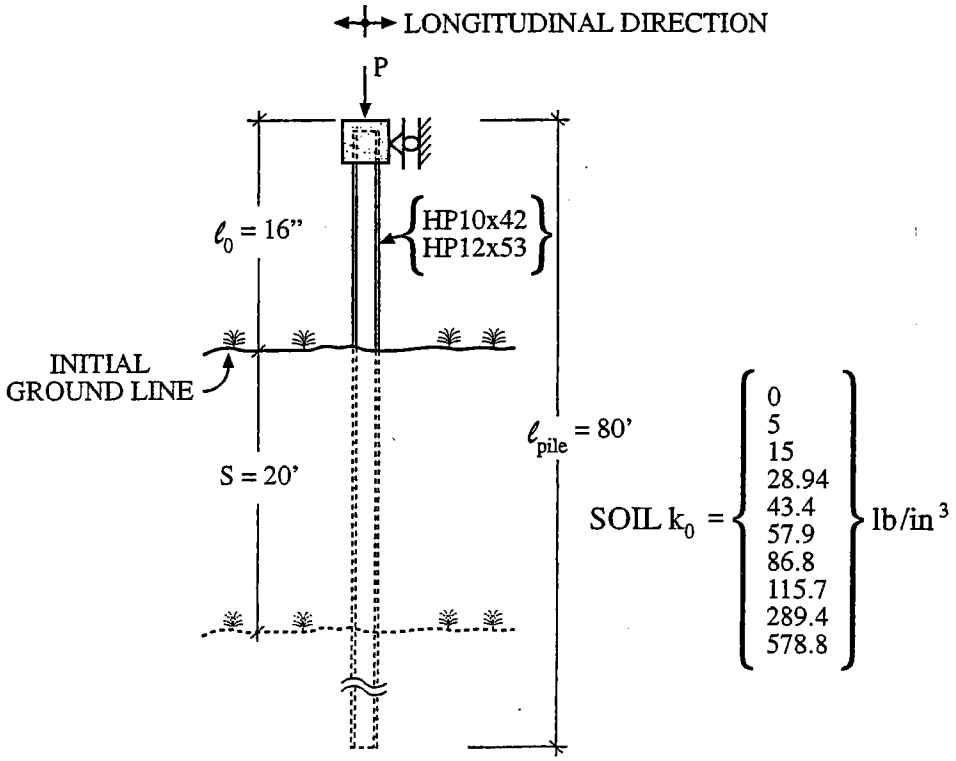

Figure 3.19. Pile Conditions for Sensitivity Analysis Using Granholm's Equations (3)

Using the above equations for k_o values, pile sizes, and lengths above ground shown in Figure 3.19, al values can be calculated. The al values are then used with Figure 2.17 to determine the kl values corresponding to buckling and from this the buckling load, P_{CR}. The P_{CR} values for each of the two pile sizes are shown in Tables 3.6 and 3.7 for buckling about the strong axes and Tables 3.8 and 3.9 for buckling about the weak axes. The corresponding plots of P_{CR} vs k_o are shown in Figures 3.20-3.23.

Note in Tables 3.6 and 3.7 for buckling in the longitudinal direction (about the piles' strong axis) that for $k_o = 0$, the pile would be a pin-pin column with $\ell = 80$ft and $P_{CR} = 65^k$ and 122^k for HP10x42 and HP12x53 piles respectively. Upper bound values of the buckling load (P_{CR}^{UB}) for $\ell = 16$ft and $\ell = 36$ft are given in the footnotes of Tables 3.6 and 3.7 as those for a pin-fixed column. In Tables 3.8 and 3.9 for buckling in the transverse direction (about the pile's weak axis) when $k_o = 0$, the pile would be partially fixed at the top by the bent cap (50% fixity was assumed) and pinned at the bottom. Thus, when $\ell = 80$ft, $P_{CR} = 33.4^k$ and 59^k for HP10x42 and HP12x53 piles respectively. P_{CR} values for assumed 50% fixities at each end of the pile when $\ell = 16$ft and 80ft are given in the footnotes of Tables 3.8 and 3.9.

Note in Figures 3.20 – 3.23 the rather insensitivity of the pile buckling load, P_{CR}, to the soil subgrade modulus value, k_o. This insensitivity becomes quite extreme as the scour level increases from S = 0 to S = 20ft as evident from the figures. Note that for a scour level of S =20 ft, i.e. $\ell = 36$ft, if $k_o > 30$ lb/in^3 (53k/ft^3) then P_{CR} becomes almost totally independent of k_o. As can be seen in Table 3.10 from Bowles (5), a k_o value this low is for a very soft soil setting. Thus for most pile settings, P_{CR} of the pile will be almost independent of the soil setting.

Table 3.6. P_{CR} vs. k_o for HP10x42 Pile Buckling in Longitudinal Direction or About Strong Axis (3)

k_0 (lb/in^3)	$C=k_0b$ (lb/in^2)	$C^{1/4}$	$(EI)^{1/4}$	$a = \sqrt[4]{C/EI_s}$ (per in.)	al		kl (pin at top)		$P_{CR}=(kl)^2 EI_s/l^2$ (kips)	
					l = 16'	l = 36'	l = 16'	l = 36'	l = 16'	l = 36'
0	0	0	279.4	0	0	0			65*	65*
5	50	2.659	279.4	0.00952	1.83	4.11	2.30	3.25	874	345
15	150	3.500	279.4	0.01253	2.41	5.41	2.65	3.52	1160	405
28.94	289	4.123	279.4	0.01476	2.83	6.38	2.87	3.67	1361	440
43.4	434	4.564	279.4	0.01634	3.14	7.06	2.97	3.73	1457	455
57.9	579	4.905	279.4	0.01756	3.37	7.59	3.05	3.77	1536	464
86.8	868	5.428	279.4	0.01943	3.73	8.39	3.18	3.82	1671	477
115.7	1157	5.832	279.4	0.02087	4.01	9.02	3.25	3.87	1745	489
289.4	2894	7.335	279.4	0.02625	5.04	11.34	3.45	3.96	1967	512
578.8	5788	8.722	279.4	0.03122	5.99	13.49	3.62	4.05	2164	536

$(EI)^{1/4} = (29{,}000{,}000 \times 210)^{1/4} = 279.4$

* For $k_0 = 0 \rightarrow \ell = 80', P_{CR} = \frac{\pi^2 EI_s}{80^2 \times 12^2} = \frac{\pi^2 \times 29{,}000 \times 210}{6400 \times 144} = 65^k$

$P_{CR}^{U.B.} = \frac{20.2 EI_s}{\ell^2} = \frac{20.2 \times 29{,}000 \times 210}{192^2} = 3337^k \rightarrow P_{CR}^{UB} = \frac{20.2 \times 29{,}000 \times 210}{432^2} = 659^k$

$P_y = A\sigma_y = 12.4 \times 36 = 446^k$

Table 3.7. P_{CR} vs. k_o for HP12x53 Pile Buckling in Longitudinal Direction or About Strong Axis (3)

k_o	$C=k_ob$	$C^{1/4}$	$(EI)^{1/4}$	$a=\sqrt[4]{C/EI_s}$	al		kl (pin at top)		$P_{CR}=(kl)^2 EI_s/l^2$ (kips)	
(lb/in^3)	(lb/in^2)			(per in.)	l = 16'	l = 36'	l = 16'	l = 36'	l = 16'	l = 36'
0	0	0	326.7	0	0	0			122*	122*
5	60	2.783	326.7	0.00852	1.64	3.68	2.15	3.15	1429	606
15	180	3.663	326.7	0.01121	2.15	4.84	2.50	3.43	1933	719
28.94	347	4.316	326.7	0.01321	2.54	5.71	2.73	3.60	2305	792
43.4	521	4.777	326.7	0.01462	2.81	6.32	2.87	3.65	2548	814
57.9	695	5.134	326.7	0.01571	3.02	6.79	2.95	3.71	2692	841
86.8	1042	5.682	326.7	0.01739	3.34	7.51	3.05	3.76	2877	864
115.7	1388	6.104	326.7	0.01868	3.59	8.07	3.13	3.80	3031	882
289.4	3473	7.677	326.7	0.02350	4.51	10.15	3.37	3.90	3513	929
578.8	6946	9.129	326.7	0.02794	5.36	12.07	3.50	4.00	3789	977

$(EI)^{1/4} = (29{,}000{,}000 \times 393)^{1/4} = 326.7$

$$^{*}\text{For } k_0 = 0 \rightarrow \ell = 80', P_{CR} = \frac{\pi^2 EI_s}{80^2 \times 12^2} = \frac{\pi^2 \times 29{,}000 \times 393}{6400 \times 144} = 122^k$$

$$P_{CR}^{UB} = \frac{20.2\,EI_s}{\ell^2} = \frac{20.2 \times 29{,}000 \times 393}{192^2} = 6245^k \rightarrow P_{CR}^{UB} = \frac{20.2 \times 29{,}000 \times 393}{432^2} = 123$$

$$P_y = A\sigma_y = 15.5 \times 36 = 558^k$$

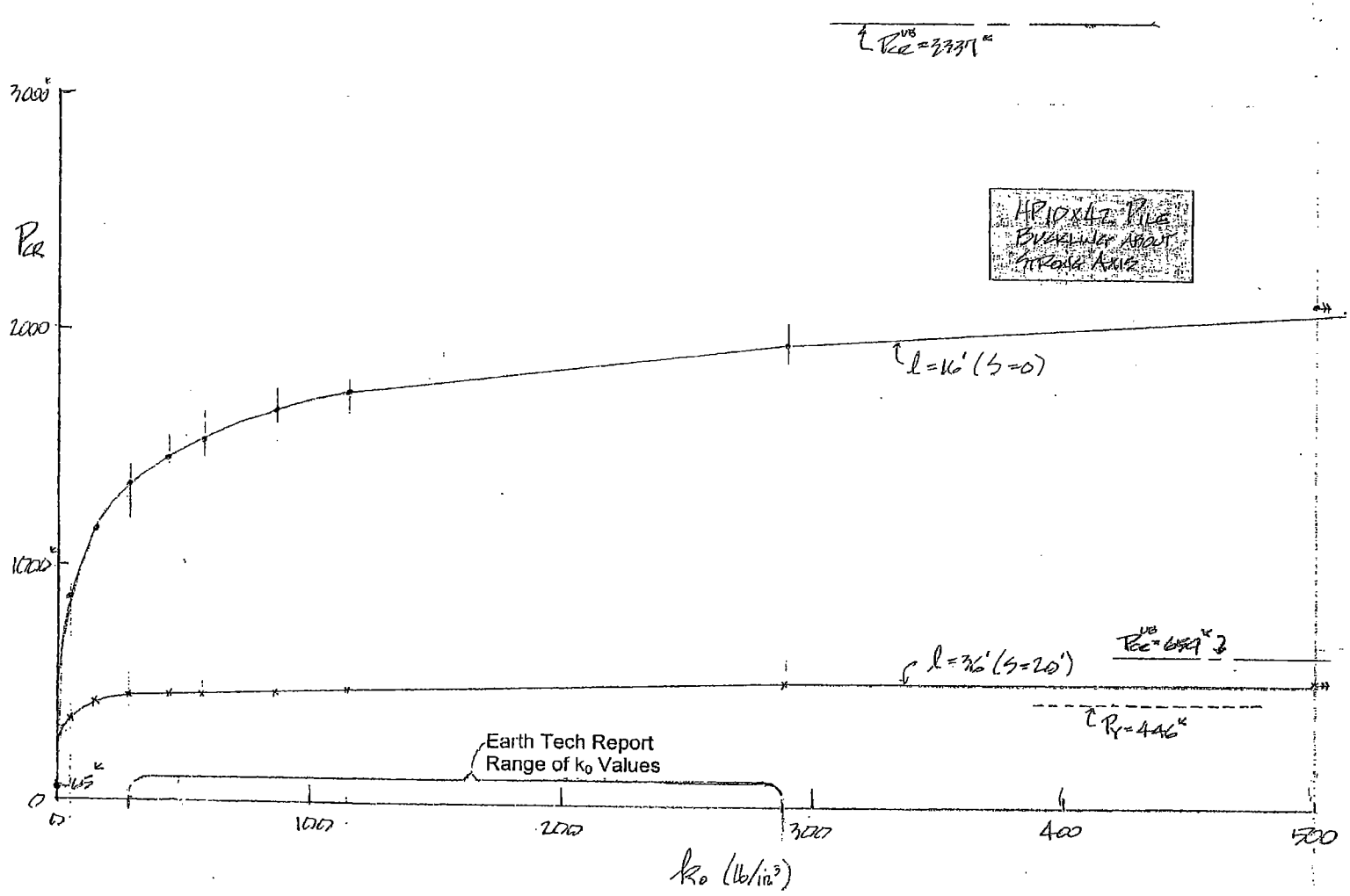

Figure 3.20. P_{CR} vs. k_o for HP10x42 Bent Pile Buckling About Strong Axis (3)

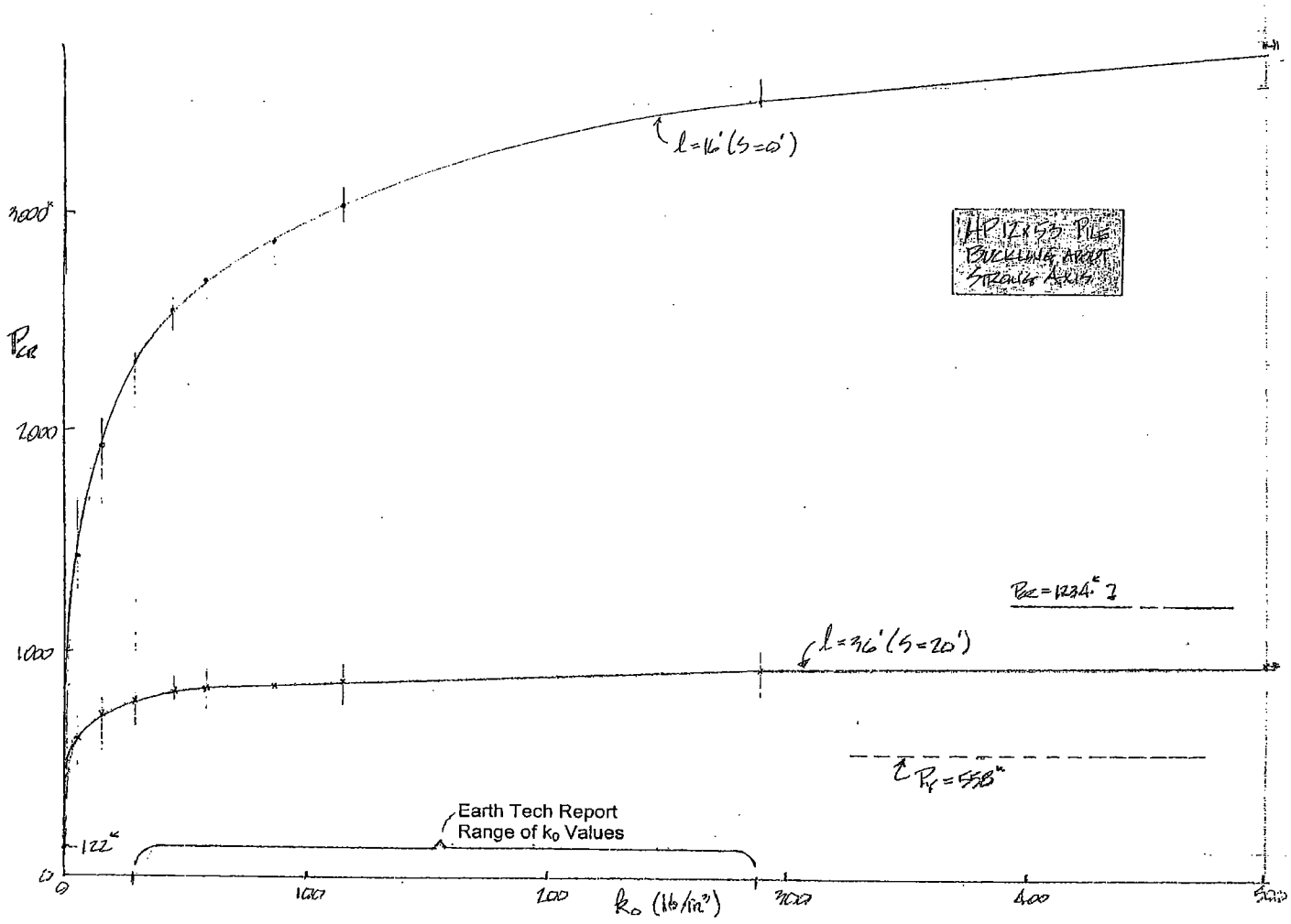

Figure 3.21. P_{CR} vs. k_o for HP12x53 Bent Pile Buckling About Strong Axis (3)

Table 3.8. P_{CR} vs. k_o for HP10x42 Pile Buckling in Transverse Direction or About Weak Axis (3)

k_0 (lb/in^3)	$C = k_0 b$ (lb/in^2)	$C^{1/4}$	$(EI)^{1/4}$	$a = \sqrt[4]{C/EI_w}$ (per in.)	al		kl (top pinned)		kl (top fixed)		$P_{CR}=(kl)_{ag}^2 EIw/l^2$ (kips)	
					l = 16'	l = 36'	l = 16'	l = 36'	l = 16'	l = 36'	l = 16'	l = 36'
0	0	0	213.54	0	0	0					33*	33*
5	50	2.659	213.54	0.01245	2.39	5.38	2.52	3.52	3.30	5.19	478	211
15	150	3.500	213.54	0.01639	3.15	7.08	2.97	3.74	4.12	5.37	709	231
28.94	289	4.123	213.54	0.01931	3.71	8.34	3.15	3.82	4.65	5.45	858	239
43.4	434	4.564	213.54	0.02137	4.10	9.23	3.25	3.87	4.85	5.50	925	245
57.9	579	4.905	213.54	0.02297	4.41	9.92	3.32	3.92	4.97	5.53	969	249
86.8	868	5.428	213.54	0.02542	4.88	10.98	3.45	3.96	5.12	5.58	1036	254
115.7	1157	5.832	213.54	0.02731	5.24	11.80	3.50	4.00	5.17	5.62	1060	258
289.4	2894	7.335	213.54	0.03435	6.60	14.84	3.70	4.08	5.31	5.72	1145	268
578.8	5788	8.722	213.54	0.04084	7.84	17.64	3.80	4.16	5.40	5.78	1194	275

$(EI)^{1/4} = (29{,}000{,}000 \times 71.7)^{1/4} = 213.54$

$$* \text{ For } k_0 = 0 \rightarrow l = 80', P_{CR} = \frac{1.5\pi^2 EI_w}{80^2 x 12^2} = \frac{1.5 x \pi^2 x 29{,}000 x 71.7}{6400 x 144} = 33.4^k$$

$$P_{CR}^{50\% \text{fixity each end}} \approx \frac{2\pi^2 EI_w}{\ell^2} = \frac{2\pi^2 x 29{,}000 x 71.7}{192^2} = 1114^k \rightarrow P_{CR}^{50\% \text{fix each end}} = \frac{2\pi^2 x 29{,}000 x 71.7}{432^2} = 220^k$$

$$P_y = \sigma_y A = 446^k$$

Table 3.9. P_{CR} vs. k_o for HP12x53 Pile Buckling in Transverse Direction or About Weak Axis (3)

k_0 (lb/in^3)	$C = k_0 b$ (lb/in^2)	$C^{1/4}$	$(EI)^{1/4}$	$a = \sqrt[4]{C/EI_w}$ (per in.)	al		kl (top pinned)		kl (top fixed)		$P_{CR}=(k\ell)^2{}_{avg}EIw/l^2$ (kips)	
					l = 16'	l = 36'	l = 16'	l = 36'	l = 16'	l = 36'	l = 16'	l = 36'
0	0	0	246.35	0	0	0					59*	59*
5	60	2.783	246.35	0.01130	2.17	4.88	2.53	3.45	3.00	5.12	764	362
15	180	3.663	246.35	0.01487	2.86	6.42	2.87	3.67	3.90	5.31	1145	398
28.94	347	4.316	246.35	0.01752	3.36	7.57	3.07	3.76	4.37	5.42	1383	416
43.4	521	4.777	246.35	0.01939	3.72	8.38	3.17	3.84	4.64	5.46	1523	427
57.9	695	5.134	246.35	0.02084	4.00	9.00	3.24	3.87	4.80	5.50	1615	433
86.8	1042	5.682	246.35	0.02306	4.43	9.96	3.34	3.91	4.98	5.53	1729	440
115.7	1388	6.104	246.35	0.02478	4.76	10.70	3.40	3.94	5.15	5.56	1826	445
289.4	3473	7.677	246.35	0.03116	5.98	13.46	3.62	4.04	5.26	5.68	1970	466
578.8	6946	9.129	246.35	0.03706	7.12	16.01	3.74	4.12	5.37	5.75	2073	481

$(EI)^{1/4} = (29{,}000{,}000 \times 127)^{1/4} = 246.35$

$$*\text{For } k_0 = 0 \rightarrow \ell = 80', P_{CR} = \frac{1.5\pi^2 EI_w}{80^2 \times 12^2} = \frac{1.5\pi^2 \times 29{,}000 \times 127}{6400 \times 144} = 59^k$$

$P_{CR}^{50\% \text{ Fix End}} \approx \frac{2\pi^2 EI_w}{\ell^2} = \frac{2\pi^2 \times 29{,}000 \times 127}{192^2} = 197^k \Rightarrow P_{CR}^{50\% \text{ Fix End}} = \frac{2\pi^2 \times 29{,}000 \times 127}{432^2} = 398^k$

$P_Y = 558^k$

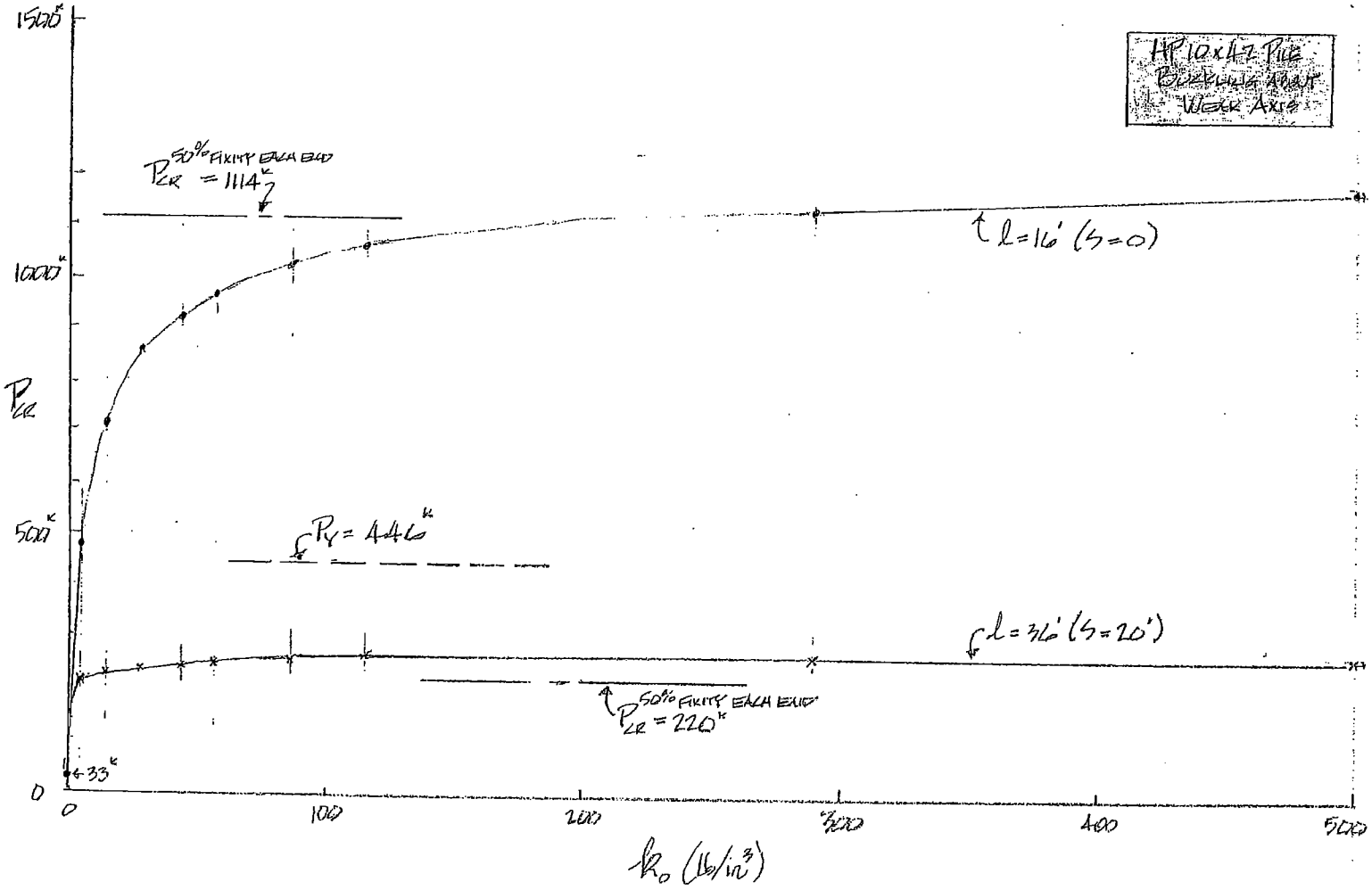

Figure 3.22. P_{CR} vs. k_o for HP10x42 Bent Pile Buckling About Weak Axis (3)

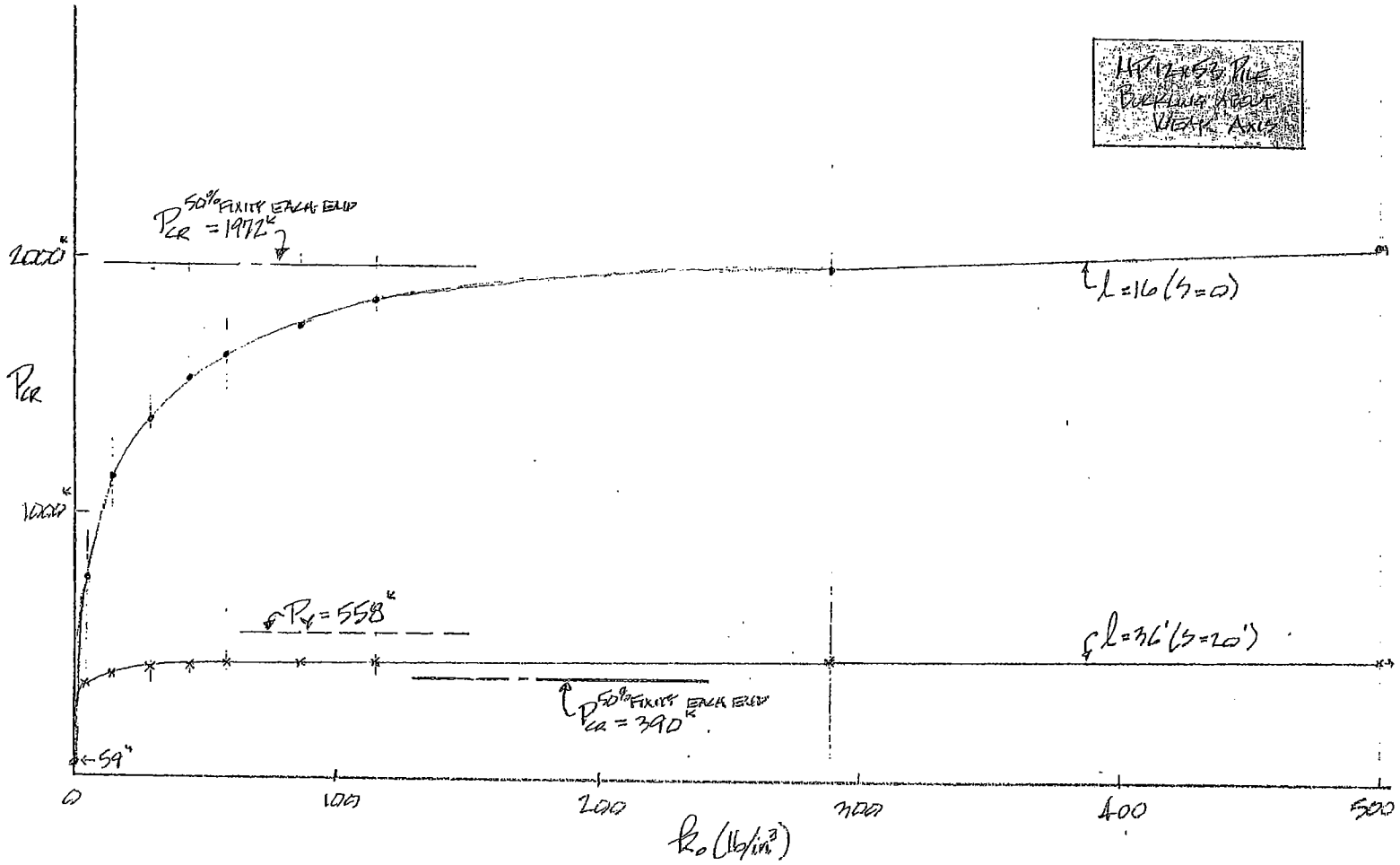

Figure 3.23. P_{CR} vs. k_o for HP12x53 Bent Pile Buckling About Weak Axis (3)

Table 3.10. Representative Range of Values of Lateral Modulus of Subgrade Reaction

(value of As in the equation ks = As +Bz) (5)

Soil*	k_s, MN/m^3	k_s, kcf	k/ft^3	lb/in^3
Dense sandy gravel	220-400	1400-2500	2000	1157
Medium dense coarse sand	157-300	1000-2000	1500	868
Medium sand	110-280	700-1800	1250	723
Fine or silty, fine sand	80-200	500-1200	850	492
Stiff clay (wet)	60-220	350-1400	900	521
Stiff clay (saturated)	30-110	175-700	450	260
Medium clay (wet)	39-140	250-900	600	347
Medium clay (saturated)	10-80	75-500	300	174
Soft clay	2-40	10-250	156	87

* Either wet or dry unless otherwise indicated.

Approximate Median Values

CHAPTER 4: TYPICAL ALDOT BRIDGE PILE BENT AND BRACING

4.1 General

A typical bridge pile bent used by the ALDOT is shown in Figure 4.1. The complete ALDOT Standard for the 5-pile bent shown in Figure 4.1 is shown in Figure 4.2. These figures show a precast concrete bent cap. However, the cap may be cast in place (CIP). Also note in the figures the range of bent height "H" values and the heights of single story and two story bents.

4.2 Summary of Common Pile Bent Parameter Values

In an earlier investigation by Ramey and Brown (3), A total of thirty-one ALDOT Bridge Pile Bent Standards were examined and the primary bent parameter values for these thirty-one Standards are summarized in Table 4.1. With bent bracing in mind, an examination of Table 4.1 reflects the following breakdowns:

a. Bent Pile Type
- 14" x 14" Prestressed Concrete – 2
- Steel HP – 29
  - HP 10 x 42 – 18
  - HP 12 x 53 – 11

  31 Bents

b. No. of Piles in Bents
- 3 Piles – 2
- 4 Piles – 10
- 5 Piles – 8
- 6 Piles – 10
- 7 Piles – 1

  31 Bents

c. End Pile Batter – 1 ½ in. per foot – 31 bents

d. Bent Sway Bracing
- None -- 2 (the two 14" x 14" Concrete Pile Bents)
- Single or two story X bracing with a L 4 x 3 ½ x 5/16 with 4" leg welded to pile. Omit sway bracing if pile is encased to cap -- 23 (Bent Standard dates were 1951-1982)
- Single or two story X bracing with a L 4 x 3 ½ x 5/16 with 4" leg welded to pile. -- 6 (Bent Standard dates were 1990-2001)

31 Bents

It appears that sometime between 1982 -1990 that the ALDOT may have stopped omitting the sway bracing for piles encased up to the cap, and/or stopped allowing piles to be encased up to the cap. Prior to 1980, a note was on the Bent Standards allowing this encasement, and Standards reviewed with a date of 1990 to the present time did not have this note. No Standards were reviewed with a date between 1980 -1992. Whatever the reason and change was, if they stopped omitting the sway bracing, it was a change that enhanced the transverse stability of the bents.

Note in Figs 4.1 and 4.2 that bent piling has continuous bracing, i.e. the soil, below the ground line to prevent buckling about any axis. For buckling in the plane of the bents, i.e., in the transverse direction (about the pile's weak axis) the steel angle swaybracing provides relative bracing for the piling. Also, adjacent piling in the bent provide lean-on bracing (in the transverse direction) to the most heavily loaded pile in the bent, Lastly, adjacent bent could provide lean-on bracing for a sidesway mode of buckling in the longitudinal direction (about the pile's strong axis). However, the bridge abutments at each end of the bridge generally prohibit a sidesway mode of buckling in the longitudinal direction.

Also note that an assumption of 50% fixity at the pile top, i.e., at the bent cap, for buckling in the transverse direction seems quite reasonable since the piles are typically embedded 1 ft. into the cap as indicated in Figure 4.3 for cast-in-place caps, or connected by weldment to anchor plates in the cap as indicated in Figure 4.4 for precast caps.

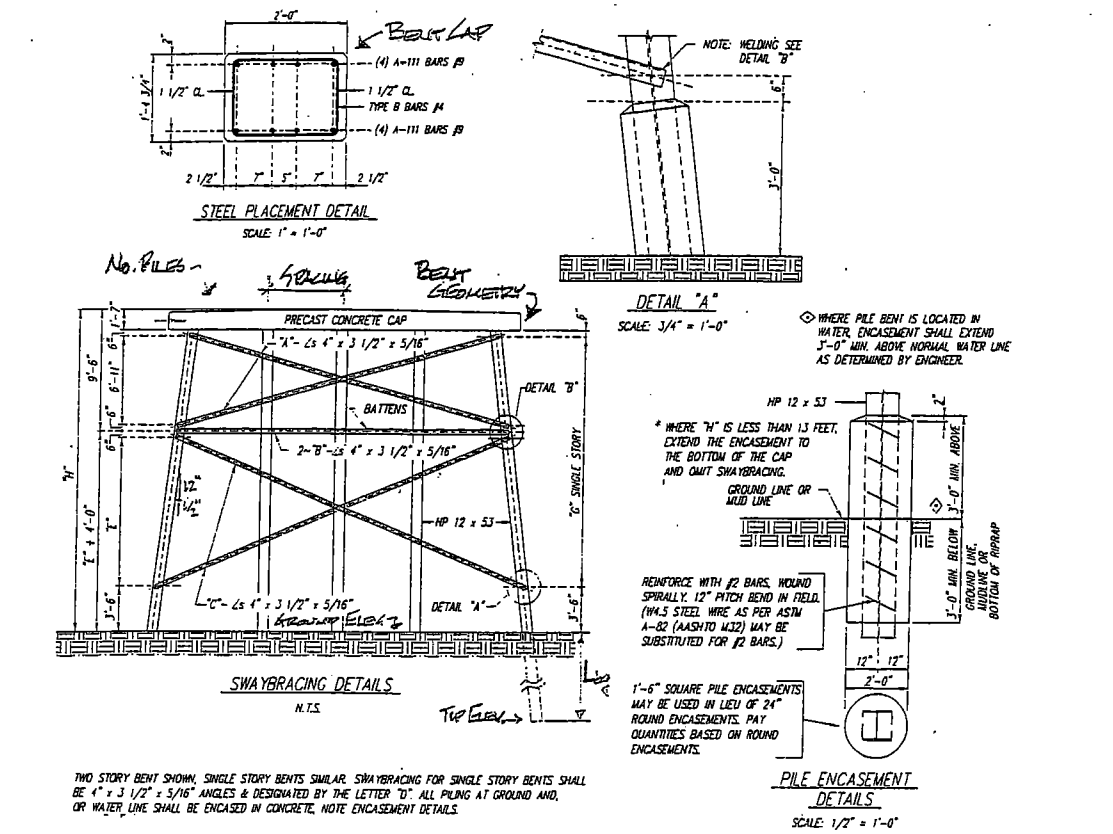

TWO STORY BENT
SWAYBRACING TABLES

"H"	"E"	"A"	"B"	"C"	WT. LBS.
20'-0"	6'-6"	25'-6"	25'-6"	27'-3"	1205
21'-0"	7'-6"	25'-6"	25'-6"	27'-7"	1209
22'-0"	8'-6"	25'-6"	25'-6"	28'-0"	1216
23'-0"	9'-6"	25'-6"	25'-6"	28'-5"	1223
24'-0"	10'-6"	25'-6"	25'-6"	28'-11"	1230
25'-0"	11'-6"	25'-6"	25'-6"	29'-5"	1238

BATTEN WEIGHT TO BE ADDED TO ABOVE TABLES. 10-BATTENS REQ'D, 5/16" X 7 1/2" X 1'-6 1/4" @ 12.1# EACH.

NOTE: WEIGHT GIVEN IS TOTAL FOR TWO PIECES OF EACH LENGTH OF SWAYBRACING SHOWN IN BOTH TABLES.

SINGLE STORY BENT
SWAYBRACING TABLES

"H"	"G"	"D"	WT. LBS.
13'-0"	7'-5"	25'-8"	395
14'-0"	8'-5"	26'-1"	401
15'-0"	9'-5"	26'-7"	409
16'-0"	10'-5"	27'-1"	417
17'-0"	11'-5"	27'-7"	425
18'-0"	12'-5"	28'-1"	432
19'-0"	13'-5"	28'-8"	441

Figure 4.1. Typical Pile Bent Geometry and Information

Table 4.1. ALDOT Bridge Pile Bent Standards (Subset)

Standard Dwg. No.	Standard Description	Date	Design Loading	Pile (No. Piles)	Pile Spacing	Outside Pile Batter	Cap	Bent Sway Bracing
PCB-2434	Precast concrete bent cap for use with steel piling and precast concrete bridge slabs 24' & 34' Spans 24' & 24 ½' Clear Roadway	1990	H15-44 HS20-44	HP 12x53 (5)	5'-9"	1 ½" per ft.	2' wide 1'-4 ¾"- 1'-7" deep 27'-6" long 4 # 9 Bars Top & Bot.	Single or two story X bracing with L 4 x 3 ½ x 5/16 with 4" leg welded to pile.
PCB-2832-30	Precast concrete bent cap for use with steel piling and precast concrete bridge slabs, 32' Span 28' Clear Roadway, 30º Skew	1994	H15-44 HS20-44	HP 12x53 (6)	6'-9"	1 ½" per ft.	2' wide 1'- 9 ½" - 2' 0 ½" deep 36'- 8 ½" long 4 # 9 Bars Top & Bot.	Single or two story X bracing with L 4 x 3 ½ x 5/16 with 4" leg welded to pile.
PCB-2834	Precast concrete bent cap for use with steel piling and precast concrete bridge slabs, 24' & 34' Spans 28' Clear Roadway	1990	H15-44 HS20-44	HP 12x53 (5)	6'-10 ½"	1 ½" per ft.	2' wide 1'- 9 1/16" - 2'-0 deep 31'-6" long 4 # 9 Bars Top & Bot.	Single or two story X bracing with L 4 x 3 ½ x 5/16 with 4" leg welded to pile.
PCB-2834-C	Precast concrete bent cap for use with steel piling and precast concrete bridge slabs for a curved bridge 34' Span 28' Clear Roadway	1993	H15-44 HS20-44	HP 12x53 (5)	6'-10 ½"	1 ½" per ft.	2'-9" wide 1'-9 1/16" deep 31'-6" long 4 # 9 Bars Top & Bot.	Single or two story X bracing with L 4 x 3 ½ x 5/16 with 4" leg welded to pile.
PCB-2840	Precast concrete bent cap for use with steel piling and precast concrete bridge slabs 40' Span 28' Clear Roadway	2001	HS20-44	HP 12x53 (5)	6'-10 ½"	1 ½" per ft.	2' wide 1'-9 1/16" - 2' deep 31'-6" long 4 # 8 Bars Top & Bot.	Single or two story X bracing with L 4 x 3 ½ x 5/16 with 4" leg welded to pile.
PCB-2840-CP	Precast concrete bent cap for use with 14' x 14' concrete piling and 24', 34', or 40' precast concrete bridge slabs 28' Clear Roadway	2001	HS20-44	14" x 14" PC (5)	6'-10 ½"	1 ½" per ft.	2'-3" wide 1'-5 1/16" - 1'-8" deep 31'-6" long 4 # 8 Bars Top 2 # 11 Bars Bot.	None
PCB-3540-30	Precast concrete split bent cap for use with steel piling and 32' or 40' prestress concrete bridge slabs 35' Clear Roadway 30º Skew	2001	HS20-44	HP 12x53 (7)	6'-10 ½"	1 ½" per ft.	2' wide 1/-9 1/16" - 2/-1 5/16" deep 45'-6" long 4 # 8 Bars Top & Bot.	Single or two story X bracing with L 4 x 3 ½ x 5/16 with 4" leg welded to pile.
PB-2834	Steel Pile Intermediate Bents 24'-34' Spans	1968	HS20-44	HP 10x42 (4)	8'-0"	1 ½" per ft.	3' wide @ top 2'-0" - 2'-4" deep 27'-2" long 2 # 6 Bars Top & Bot.	Single or two story X bracing with L 4 x 3 ½ x 5/16 with 4" leg welded to pile. Omit sway bracing if pile is encased to cap.
B-3411P	Steel Pile Intermediate Bent (for use with Type I Girders) 34' Roadway	1982	HS20-44	HP 12x53 (5)	7'-6"	1 ½" per ft.	3' wide @ top 2'-0" - 2'-2 ¾" deep 33'-6" long 2 # 6 Bars Top & Bot.	Single or two story X bracing with L 4 x 3 ½ x 5/16 with 4" leg welded to pile. Omit sway bracing if pile is encased to cap.
B-4011P	Steel Pile Intermediate Bent (for use with Type I Girders) 40' Roadway	1979	HS20-44	HP 12x53 (6)	7'-0"	1 ½" per ft.	3' wide @ top 2'-0" - 2'-2 15/16" deep 33'-6" long 2 # 6 Bars Top & Bot.	Single or two story X bracing with L 4 x 3 ½ x 5/16 with 4" leg welded to pile. Omit sway bracing if pile is encased to cap.

Standard Dwg. No.	Standard Description	Date	Design Loading	Pile (No. Piles)	Pile Spacing	Outside Pile Batter	Cap	Bent Sway Bracing
PB 2802	Steel Pile Intermediate Bents 24'-34' Spans 28' Roadway	1952	HS20-44	HP 10x42 (4)	8'-0"	1 ½" per ft.	3' wide @ top 2'-0" deep 27'-2" long 2 # 6 Bars Top & Bot.	Single or two story X bracing with ∟ 4 x 3 ½ x 5/16 with 4" leg welded to pile. Omit sway bracing if pile is encased to cap.
PB 2802-45 (45' Skew)	Concrete & Steel Pile Intermediate Bent - 4 Pile 24'-34' Spans 28' Roadway (with 1'-6" Safety Curbs)	1957	HS20-s16-44	HP 10x42 (4)	11'-4"	1 ½" per ft.	3' wide @ top 2'-0" deep 40'-8" long 2 # 6 Bars Top & Bot.	Single or two story X bracing with ∟ 4 x 3 ½ x 5/16 with 4" leg welded to pile. Omit sway bracing if pile is encased to cap.
PB 2803	Steel Pile Intermediate Bents 32'-38' Spans 28' Roadway (with 1'-6" Safety Curbs)	1952	HS20-s16-44	HP 10x42 (5)	6'-6"	1 ½" per ft.	3' wide @ top 2'-0" deep 29'-0" long 2 # 6 Bars Top & Bot.	Single or two story X bracing with ∟ 4 x 3 ½ x 5/16 with 4" leg welded to pile. Omit sway bracing if pile is encased to cap.
PB-4034 (1)	Steel Pile Intermediate Bents 34' Spans 40' Roadway	1980	HS20-44	HP 12x53 (5)	9'-0"	1 ½" per ft.	3' wide @ top 2'-0" - 2'-3 ¼" deep 39'-6" long 2 # 6 Bars Top & Bot.	Single or two story X bracing with ∟ 4 x 3 ½ x 5/16 with 4" leg welded to pile. Omit sway bracing if pile is encased to cap.
PCPB-4041	Prestressed Concrete Pile Intermediate Bent 34'-41' Spans 40' Roadway	1975	HS20-44	14" x 14" PC (Std. PSCP-1) (6)	7'-0"	1 ½" per ft.	3' wide @ top 2'-0" - 2'-3 1/16" deep 38'-6" long 4 # 6 Bars Top 2 # 6 Bars Bot.	None
B-4411P	Steel Pile Intermediate Bents (for use with Type I Girders) 44' Roadway		HS20-44	HP 12x53 (6)	8'-0"	1 ½" per ft.	3' wide @ top 2'-0" - 2'-4 11/16" deep 43'-6" long 2 # 6 Bars Top & Bot.	Single or two story X bracing with ∟ 4 x 3 ½ x 5/16 with 4" leg welded to pile. Omit sway bracing if pile is encased to cap.
PB-4434 PS	Steel Pile Intermediate Bents 34' Spans with Type I Girders 44' Roadway	1979	HS20-44	HP 12x53 (6)	8'-0"	1 ½" per ft.	3' wide @ top 2'-0" - 2'-4 11/16" deep 43'-6" long 2 # 6 Bars Top & Bot.	Single or two story X bracing with ∟ 4 x 3 ½ x 5/16 with 4" leg welded to pile. Omit sway bracing if pile is encased to cap.
PB-3934	Steel Pile Intermediate Bents 24'-34' Spans 39'-3" Roadway	1967	HS20-44	HP 10x42 (6)	8'-0"	1 ½" per ft.	3' wide @ top 2'-0" - 2'-5" deep 38'-6" long 2 # 6 Bars Top & Bot.	Single or two story X bracing with ∟ 4 x 3 ½ x 5/16 with 4" leg welded to pile. Omit sway bracing if pile is encased to cap.
PB 4034	Steel Pile Intermediate Bents 34' Spans 40' Roadway	1975	HS20-44	HP 10x42 (6)	7'-0"	1 ½" per ft.	3' wide @ top 2'-0" - 2'-4" deep 38'-6" long 2 # 6 Bars Top & Bot.	Single or two story X bracing with ∟ 4 x 3 ½ x 5/16 with 4" leg welded to pile. Omit sway bracing if pile is encased to cap.

Standard Dwg. No.	Standard Description	Date	Design Loading	Pile (No. Piles)	Pile Spacing	Outside Pile Batter	Cap	Bent Sway Bracing
PB-2200	Steel Pile Intermediate Bents 24'-34' Spans 22' Roadway (with 8" curbs)	1951	HS15-44	HP 10x42 (3)	8'-6"	1 ½" per ft.	3' wide @ top 2'-0" deep 20'-0" long 4 # 7 Bars Top & Bot.	Single or two story X bracing with ∟ 4 x 3 ½ x 5/16 with 4" leg welded to pile. Omit sway bracing if pile is encased to cap.
PB-2200-45 (45º skew)	Steel Pile Intermediate Bents Steel Beams and/or RCDG Spans 22' Roadway (with 8" curbs)	1962	HS15-44	HP 10x42 (3)	12'-0 ¼"	1 ½" per ft.	3' wide @ top 2'-0" deep 30'-6" long 3 # 6 Bars Top 2 # 6 Bars Bot.	Single or two story X bracing with ∟ 4 x 3 ½ x 5/16 with 4" leg welded to pile. Omit sway bracing if pile is encased to cap.
PB-2202-30 (30º skew)	Steel Pile Intermediate Bents Steel Beams and/or RCDG Spans 22' Roadway (with 8" curbs)	1961	HS15-44	HP 10x42 (4)	7'-1 7/16"	1 ½" per ft.	3' wide @ top 2'-2" deep 24'-8" long 4 # 7 Bars Top & Bot.	Single or two story X bracing with ∟ 4 x 3 ½ x 5/16 with 4" leg welded to pile. Omit sway bracing if pile is encased to cap.
PB-2202-45 (45º skew)	Steel Pile Intermediate Bents Steel Beams and/or RCDG Spans 22' Roadway (with 8" curbs)		HS15-44	HP 10x42 (4)	8'-8 11/16"	1 ½" per ft.	3' wide @ top 2'-0" deep 30'-8" long 4 # 7 Bars Top & Bot.	Single or two story X bracing with ∟ 4 x 3 ½ x 5/16 with 4" leg welded to pile. Omit sway bracing if pile is encased to cap.
PB 2400	Steel Pile Intermediate Bents 24'-42' Spans 24' Roadway (with 1'-6" Safety Curbs)	1952	HS15-44 HS20-44	HP 10x42 (4)	6'-8"	1 ½" per ft.	2' wide @ top 2'-0" deep 23'-0" long 2 # 6 Bars Top & Bot.	Single or two story X bracing with ∟ 4 x 3 ½ x 5/16 with 4" leg welded to pile. Omit sway bracing if pile is encased to cap.
PB-2400-30 (30º skew)	Steel Pile Intermediate Bents 24'-42' Spans 24' Roadway (with 1'-6" Safety Curbs)	1955	HS15-44 HS20-44	HP 10x42 (4)	7'-8 ½"	1 ½" per ft.	3' wide @ top 2'-0" deep 28'-0" long 2 # 6 Bars Top & Bot.	Single or two story X bracing with ∟ 4 x 3 ½ x 5/16 with 4" leg welded to pile. Omit sway bracing if pile is encased to cap.
PB-2434	Steel Pile Intermediate Bents 32'-38' Spans 24' Roadway	1973	HS20-44	HP 10x42 (4)	6'-8"	1 ½" per ft.	3' wide @ top 2'-0" - 2'-2" deep 23'-6" long 4 # 5 Bars Top & Bot.	Single or two story X bracing with ∟ 4 x 3 ½ x 5/16 with 4" leg welded to pile. Omit sway bracing if pile is encased to cap.
PB-2800	Steel Pile Intermediate Bents 24'-34' Spans 28' Roadway (with 1'-6" Safety Curbs)	1952	HS20-44	HP 10x42 (4)	8'-0"	1 ½" per ft.	3' wide @ top 2'-0" deep 27'-0" long 2 # 6 Bars Top & Bot.	Single or two story X bracing with ∟ 4 x 3 ½ x 5/16 with 4" leg welded to pile. Omit sway bracing if pile is encased to cap.
PB-2800-30 (30º skew)	Concrete Steel Pile Intermediate Bents - 4 Pile 24'-34' Spans 28' Roadway (with 1'-6" Safety Curbs)	1952	HS20-44	HP 10x42 (4)	9'-3"	1 ½" per ft.	3' wide @ top 2'-0" deep 32'-6" long 2 # 6 Bars Top & Bot.	Single or two story X bracing with ∟ 4 x 3 ½ x 5/16 with 4" leg welded to pile. Omit sway bracing if pile is encased to cap.

Standard Dwg. No.	Standard Description	Date	Design Loading	Pile (No. Piles)	Pile Spacing	Outside Pile Batter	Cap	Bent Sway Bracing
PB-4434	Steel Pile Intermediate Bents 32'-38' Spans 44' Roadway	1967	HS20-44	HP 10x42 (6)	8'-0"	1 ½" per ft.	3' wide @ top 2'-0" - 2'-4 11/16" deep 43'-6" long 2 # 6 Bars Top & Bot.	Single or two story X bracing with ∟ 4 x 3 ½ x 5/16 with 4" leg welded to pile. Omit sway bracing if pile is encased to cap.
PB-4434-30 (30º Skew)	Steel Pile Intermediate Bents 32'-38' Spans 44' Roadway	1967	HS20-44	HP 10x42 (6)	9'-3"	1 ½" per ft.	3' wide @ top 2'-0" - 2'-8" deep 51'-6" long 2 # 6 Bars Top & Bot.	Single or two story X bracing with ∟ 4 x 3 ½ x 5/16 with 4" leg welded to pile. Omit sway bracing if pile is encased to cap.
PB-4434-45 (45º Skew)	Steel Pile Intermediate Bents 32'-38' Spans 44' Roadway	1968	HS20-44	HP 10x42 (6)	11'-3 ¾"	1 ½" per ft.	3' wide @ top 2'-0" - 2'-4" deep 62'-6" long 2 # 6 Bars Top & Bot.	Single or two story X bracing with ∟ 4 x 3 ½ x 5/16 with 4" leg welded to pile. Omit sway bracing if pile is encased to cap.

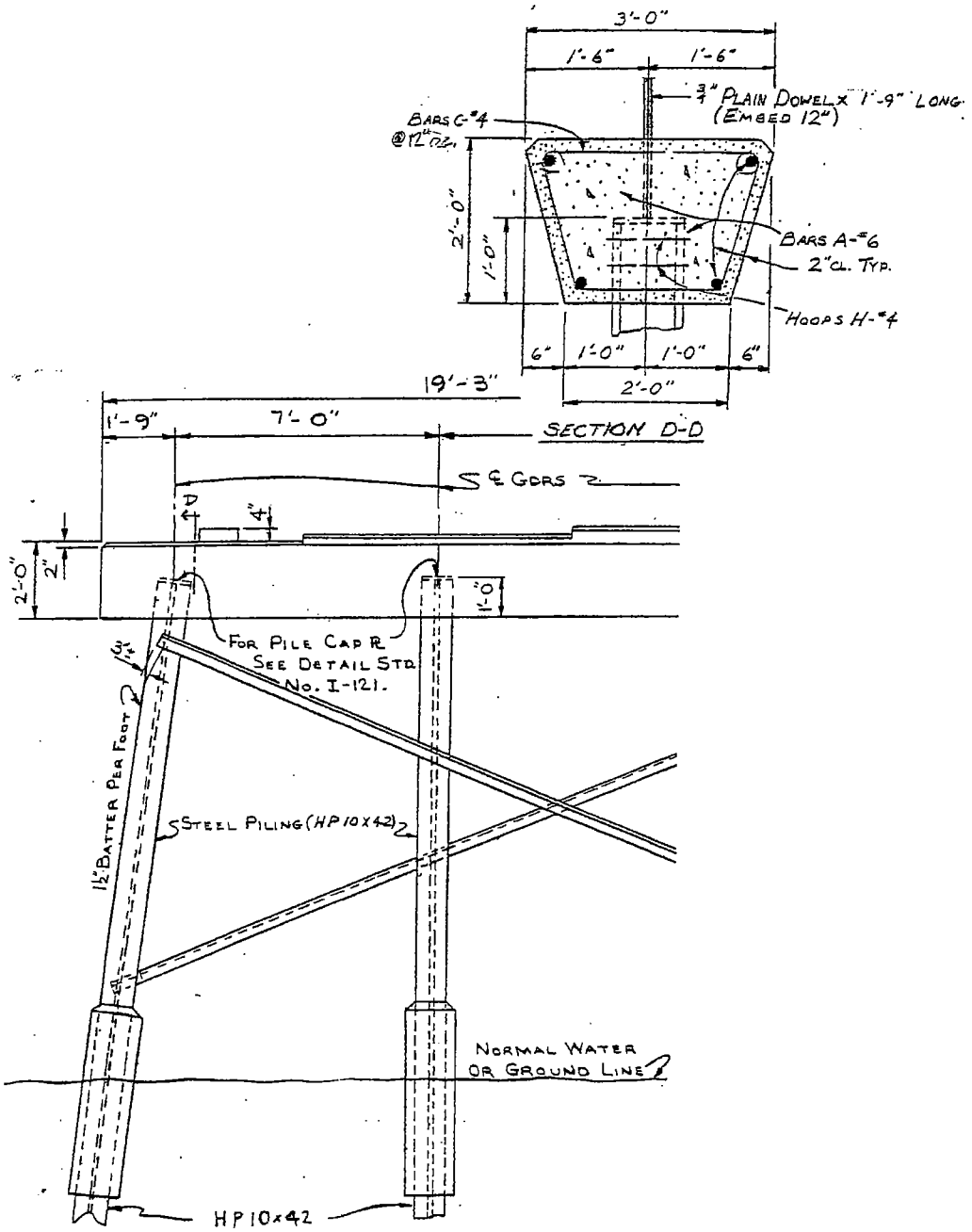

Figure 4.3. Pile Connections/Embedment to CIP Concrete Bent Cap

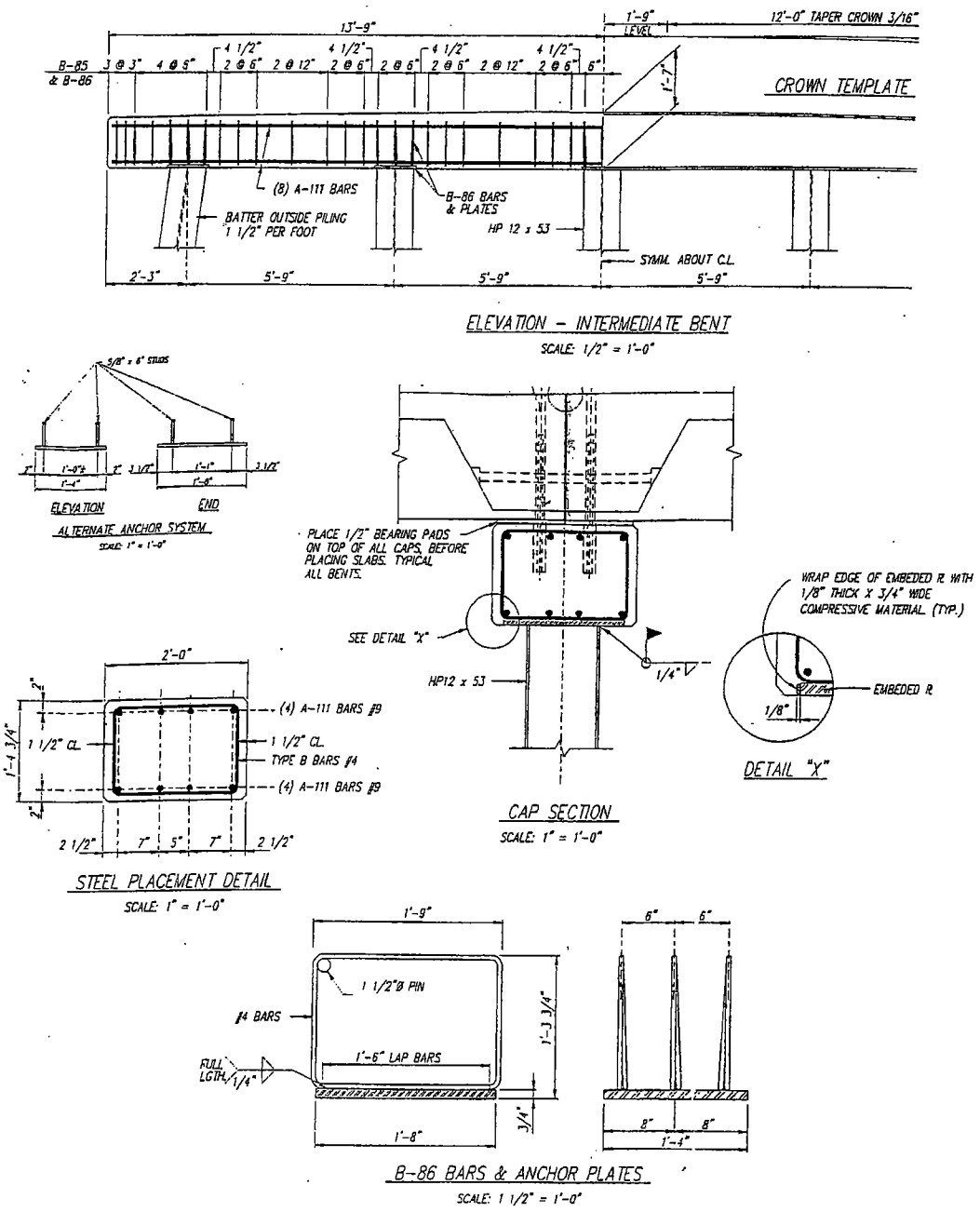

Figure 4.4. Pile Connections by Anchor Plates to Precast Concrete Bent Cap

CHAPTER 5: FB-PIER MODELINGS AND RESULTS

5.1 Methods for Estimating Pile Buckling Capacity

The method used thus far to determine the buckling load capacity of individual pile bents is based on the assumption that a 50% rotational fixity should be placed at the top and bottom of the piles. As mentioned previously (Section 3.2), this assumption seems reasonable since the bottom of the piles are supported by the soil stiffness modulus and the top of the piles are either embedded 1ft into the cap or connected by weldment to anchor plates embedded in the cap. The result of placing these partial fixities at pile ends gives the approximate elastic buckling equation

$$P_e \approx \frac{2\pi^2 EI}{L^2}$$

where L is the length between the existing ground line and the cap (see Fig.5.1a) and the coefficient represents n^2 where n is the number of half-sine waves of the buckled pile. For a pile fully fixed at both ends n=2 and for a pile pinned at each end n =1. Therefore, for the case of 50% rotational fixities at each end the approximate value of n is $\sqrt{2}$ or 1.414.

It appears that State Transportation Departments use various methods for determining the buckling load capacity of piles. Rather than to assume 50% fixities at the top and bottom of a pile, an alternate method is to place a 50% rotational fixity at the top of the pile only and estimate a new effective length where the bottom of the pile is assumed to be fully fixed. This method for calculating the elastic buckling load of piles is based on the approximate equation

$$P_e \approx \frac{3\pi^2 EI}{\ell^2}$$

where ℓ is the length between the point of full fixity below the ground line and the cap (see Figure 5.1b) and the coefficient represents the square of the number of half-sine waves of the buckled pile. For the case with a 50% rotational fixity at the top of the pile and full fixity at the bottom, n is

approximately $\sqrt{3}$ (the median of n=2 for fully fixed ends and n= $\sqrt{2}$ for 50% rotational fixities at both ends).

Thus, it is the purpose of this section to model pile bents and individual piles in various soil settings using FB-Pier to determine if the soil subgrade modulus greatly affects pile deflections, to locate the depths at which full fixity of the piles may be assumed, and to compare the ultimate buckling loads of the piles to the above approximate Euler buckling equations. The buckling capacity derived from Granholm's equation will also be compared with the approximate elastic buckling values.

5.2 Sensitivity of k_{eq} to Soil Subgrade Modulus

To take advantage of FB-Pier's soil modeling capabilities a study was performed to examine the effects that various soil modulus values, K_o, have on bent displacements. For this study a constant load of 1 kip was applied to the centerline of the bent cap for an HP10x42 5-pile non X-braced bent to determine the resulting displacements along the pile lengths. Soil modulus values pertaining to a large group of soils were considered for this analysis. Table 3.8 lists the representative ranges in soil modulus values for several soil types from dense sandy gravel to soft clay and will serve as a guide in determining the range of values which should be considered for this study. This table also gives median values of K_o for each range of soil modulus values. These median values were converted from kcf units to lb/in^3 since this conversion is required for input in FB-Pier.

In the initial analysis, soils having stiffness moduli ranging from 5 lb/in^3 to 2000 lb/in^3 were considered, but upon inspection of the resulting pile displacements it was determined that K_o values of 5 lb/in^3, 50 lb/in^3, 100 lb/in^3, and 500 lb/in^3 would be sufficient. For these K_o values the horizontal nodal displacements along the pile lengths were plotted in order to determine if increasing the soil modulus would significantly decrease bent displacements as well as to establish the depth at which the piles were assumed to have fixed bases. The results of this study are shown in Figures 5.2-5.5 for pile bents having pinned connections to the cap with a

similar analysis for pile bents having fixed connections to the cap in Figures 5.6-5.8. It appears from the graphs, that variations of the soil modulus does not greatly affect the pile displacements unless the modulus is extremely small, i.e. $K_o \leq 5$ lb/in^3. Additionally, the figures show that for each pile length, full fixity is usually achieved at 5ft below the ground (except where $K_o = 5$ lb/in^3).

5.3 Single Pile Buckling Loads and Deflections

In order to determine the buckling load of individual HP10x42 piles, the pushover analysis capability of FB-Pier was utilized to find the load just before collapse of the pile. Since two loads are required for this procedure, a constant horizontal force of 1 kip was applied to the pile near the center of the exposed length to simulate a small initial crookedness of the pile and an incremented axial load was placed at the top of the pile as shown in Figures 5.9-5.16. Since it was determined from Section 5.2 that the pile deflections are not very sensitive to different values of K_o, the soil modulus for this study was kept constant at $K_o = 100$ lb/in^3. The initial axial force on the pile of 100 kips was incremented by 10 kips using the automated pushover analysis procedure until convergence could no longer be reached. Where $P_{CR} > P_y/2 = 223^K$, the resulting axial load at failure of the pile is assumed to be the inelastic buckling load (P_{CR}) since the piles were analyzed with nonlinear (material) section behavior.

The results of this analysis are shown in Figures 5.9-5.16 for individual piles pinned at the top. The buckling loads (P_{CR}) for these piles were 410 kips, 380 kips, 310 kips, and 280 kips for pile lengths of 10ft, 15ft, 20ft, and 25ft respectively (see Table 5.2). The buckling analysis results for piles fixed at the top are shown in Figures 5.13-5.16. The buckling loads for these piles were 430kips, 420kips, 410kips, and 380k for pile lengths of 10ft, 15ft, 20ft, and 25ft respectively (see Table 5.2). As observed in Section 5.2, it can be seen from the buckled shape of the piles that full fixity is achieved approximately 5ft below the ground line regardless of the fixity condition at the top of the pile. Therefore, this additional 5ft to fixity has been included in the approximate elastic buckling equation which assumes a 50% rotational fixity at the top of the pile and full fixity below the ground. A comparison of the buckling values produced by FB-Pier to the elastic buckling equations of Section 5.1 shows that $P_{CR} < P_e$ for each pile length considered

(L=10ft –40ft) and $P_{CR} > P_y/2$ for $L \leq 30$ft. Thus, where $L \leq 30$ft the piles are expected to buckle inelastically.

Figure 5.17 provides a comparison of the HP10x42 pile buckling loads (P_{CR}) produced by FB-Pier (for piles with a fixed and pinned top) to those plotted in Figure 3.6 which were derived from the approximate buckling equation for piles with partial fixities ($P_e \approx \frac{2\pi^2 EI}{L^2}$). This figure shows that the P_{CR} values derived from the buckling equation for 50% rotational fixities at each end lie directly between those for piles with fixed and pinned tops from FB-Pier. This is true even for the case of inelastic buckling where the buckling loads were approximated with parabolic curve equations based on the elastic buckling equation. The FB-Pier P_{CR} values for piles pinned at the top lie slightly below the P_{CR} values of Figure 3.6, while the FB-Pier P_{CR} values for piles fixed at the top lie just above those of Figure 3.6. This comparison confirms that the elastic buckling loads as well as the parabolic approximation of inelastic P_{CR}, determined from the buckling equation $P_e \approx \frac{2\pi^2 EI}{L^2}$ for 50% rotational fixities in Section 3.2, is a reasonable assumption for non sidesway buckling. The inelastic buckling loads produced from this approximate buckling equation (as shown in Figure 3.6) do not lie exactly in the middle of the P_{CR} values from FB-Pier and this may also be the result of second order affects which are included in FB-Pier's nonlinear pushover analysis procedure. Second order effects occur as the pile undergoes flexural displacements which create additional stresses within the extreme fibers of the cross-section. These additional bending stresses were not accounted for in the first order derivation of Table 3.2.

5.4 Pile Buckling Loads Using Granholm's Equation

As mentioned in the Literature Review, H. Granholm developed an analytical solution to determine the buckling load for a pile partially embedded in a soil supporting medium. The buckling capacities (P_e) of individual piles using Granholm's equation assume that elastic buckling will occur. The buckling loads produced from Granholm's equation can be directly

compared to the buckling loads of the approximate elastic buckling equations previously discussed. Additionally, the elastic buckling loads predicted by Granholm can be compared to the P_{CR} buckling loads calculated from FB-Pier's pushover analysis. From this comparison the significance of nonlinear effects during pushover (buckling) can be seen. Since the top of the pile is prevented from translation in this study, the nonlinear effects only include the material nonlinearity expressed by the stress-strain curve of the steel HP piles and geometric nonlinearity from second order effects due to bending of the pile along its axis (because translation is not allowed at the top of the pile, geometric nonlinearity from the p-delta effect is omitted here). In a typical pushover analysis for an entire bent, however, geometric nonlinearity of the members also considers second order p-delta effects, or moments that result from lateral translation of one end of an axial loaded member with respect to the other end.

The process for determining P_{CR} using Granholm's equation first requires calculation of the coefficient "a" where $a^4 = c/EI_w$. In this equation "c" represents the soil stiffness modulus (lb/in^2), i.e., $c = K_o \cdot b$, where K_o is the soil modulus (lb/in^3) and b is the bearing width of the pile on the soil (the width of the wide flange = 10in for HP 10x42 piles). In Section 5.2 it was found that increasing the soil modulus did not have a significant affect on pile bent displacement for soil moduli values exceeding 5 lb/in^3. This conclusion can also be drawn from Figures 3.23 and 3.24 which show the relative insensitivity of P_{CR} to K_o for piles buckling about their weak axis. Therefore, in the analysis of P_{CR} from Granholm's equation the soil modulus, K_o, was given a constant value of $150lb/in^3$. The value "a" multiplied by the pile length, *l*, results in the term "a*l*," and this term is then used in Figure 2.17 to find the factor of buckling "k*l*" for the corresponding fixity condition at the top of the pile. Finally, the factor of buckling "k*l*" is placed into Granholm's equation for P_e, where $P_e = (kl)^2 \frac{EI}{l^2}$.

Table 5.1 lists several key parameters used in calculating Granholm's buckling capacity for pile lengths ranging from 10ft to 33ft (the largest probable unbraced length for typical levels of scour) and includes the factor of buckling terms (k*l*) extracted from Figure 2.17. Using Granholm's equation to calculate P_e values for piles with pinned connections at the top gives

buckling values ranging from 1388 kips to 210 kips for L=10ft to L=33ft respectively. With a fixed condition at the top of the pile Granholm's equation gives P_e values of 2898 kips to 416 kips for L=10ft to 33ft respectively. Table 5.2 lists these P_e values as well as the buckling loads predicted by the other methods discussed previously in this chapter. For the two pile end conditions, the P_e values from Granholm's equation can be averaged and compared with the P_e values in columns 1 and 2 of Table 5.2 which account for partial fixities at the ends of the pile.

5.5 Comparison of Alternate Methods for Estimating Pile Buckling Capacity

A comparison of the alternate methods previously described in Sections 5.1, 5.3, and 5.4 to predict the buckling capacity of individual piles is provided in Table 5.2. The two methods used to represent partial fixities at the pile ends, i.e., the first two columns in Table 5.2 give reasonably similar buckling capacities except for the case of very short bent heights of L $\leq$ 10ft. However, the piles will buckle inelastically when $P_{CR} > P_y/2$, or 223kips for an A36 steel HP10x42 pile. When elastic buckling does occur, i.e. $P_{CR} < P_y/2$, it appears that the modeling with 50% rotational fixities at both ends ($P_e \approx \frac{2\pi^2 EI}{L^2}$) will give a more conservative buckling capacity in comparison to the modeling with a 50% fixity at the top and an additional length to fixity ($P_e = \frac{3\pi^2 EI}{\ell^2}$). These results coupled with the belief that it is simpler to model the bent using its actual height, we will henceforth model the bent as shown in Figure 5.1a in order to determine the elastic buckling loads using the approximate equation $P_e \approx \frac{2\pi^2 EI}{L^2}$.

The average P_{CR} values from Granholm's elastic buckling equation for individual piles with fixed and pinned tops are less conservative than the P_{CR} values from the approximate buckling equations where elastic buckling controls, i.e. $P_{CR\text{-}AVG} < P_y/2$ (see Table 5.2). Since it does not appear that the soil modulus greatly affects the pile buckling capacity, the approximate buckling equation corresponding to 50% rotational fixities at each end of the pile is therefore favored for its simplicity and conservatism over the other elastic buckling methods. According to

the non sidesway P_{CR} values from Granholm's equation and realistic unbraced pile lengths of 10ft-33ft, P_{CR} values will be controlled by inelastic buckling since the elastic buckling capacities for these lengths exceed $P_y/2$. However, it is unlikely that the load applied to a pile will exceed $P_y/2$ (or 223 kips for an A36 HP10x42 pile) since typical pile loads are in the range of 100 – 160 kips. Therefore, bent piles which buckle inelastically should have sufficient buckling capacity and inelastic buckling of piles is not expected to occur.

The P_{CR} buckling loads produced by the nonlinear FB-Pier pushover (buckling) analysis (shown in Table 5.2) reveal that the geometric nonlinear p-y effects which occur due to bending during pushover (buckling) analysis are fairly significant. This is evident by a comparison of the average FB-Pier buckling capacity, $P_{CR\text{-}AVG}$, (for piles pinned and fixed at the top) to the alternate methods when elastic buckling controls and $P_{CR} < P_y/2$. For the elastic buckling pile length, L=40ft, the average FB-Pier buckling load (for piles pinned and fixed at the top) is smaller than those of the other elastic buckling methods which do not account for second order p-y effects due to geometric nonlinearity from displacements that occur due to bending along the axis of the member.

An additional comparison can be made in Table 5.3 between the buckling loads (P_{CR}^{pile}) of the alternate methods for estimating buckling capacity and FB-Pier's pushover (buckling) analysis of a 5-pile non X-braced bent (as shown in Section 7.2 with incremented vertical gravity loads over each pile). For the FB-Pier analysis in Section 7.2 two forms of geometric nonlinearity of the piles are considered (p-delta and p-y), where p-delta second order effects account for the additional moments which occur due to lateral displacement of the ends of an axial loaded member with respect to each other. Theoretically, the buckling loads for each method should be similar if elastic buckling controls and geometric nonlinearity is not considered. In Table 5.3, the approximate elastic buckling equations and Granholm's equation give much larger pile buckling capacities than FB-Pier's analysis of the non X-braced 5-pile bent even for pile lengths where elastic buckling (for an A36 steel HP10x42 pile) should control, i.e. $P_{CR} < 223^K$. This is probably

due to the occurrence of sidesway buckling of the non X-braced bent piles in FB-Pier which would lower the buckling capacity.

By comparing the FB-Pier pile buckling loads from Table 5.2 to those in Table 5.3, the effects of geometric nonlinearity due to lateral translation of the top of the pile (which is allowed only for the piles/bent in Table 5.3) can been seen. Although different pile lengths are considered in each table, it is apparent that geometric nonlinearity from the lateral displacement of the cap reduces the buckling loads of the piles in a non X-braced bent. This also supports the idea that material and geometric nonlinearity (both of which are incorporated in pushover analysis) are critical in the determination of pile and/or pile bent buckling loads. Furthermore, when geometric nonlinearity includes secondary effects due to bending displacements along the pile's axis (p-y) as well as secondary effects created from translation at one end of an axial loaded member with respect to the other end (p-delta), the pile buckling loads are further reduced.

Table 5.1. P_e vs. Pile Length for HP10x42 Pile Buckling in Transverse Direction or About Weak Axis Using Granholm's Equation, K_o = 150lb/in^3

Pile Length, *l* (ft)	**$a = (c/EI_w)^{1/4}$** $(in)^{-1}$	***al***	**Pinned at Cap**		**Fixed at Cap**	
			kl **Figure 2.17**	**P_e** **(kips)**	***kl*** **Figure 2.17**	**P_e** **(kips)**
10	0.0291436	3.50	3.10	1388	4.48	2898
13	0.0291436	4.55	3.35	959	5.00	2136
15	0.0291436	5.25	3.50	786	5.17	1722
18	0.0291436	6.30	3.68	604	5.30	1252
20	0.0291436	6.99	3.72	500	5.35	1033
23	0.0291436	8.04	3.80	394	5.42	802
25	0.0291436	8.74	3.85	342	5.48	694
28	0.0291436	9.79	3.90	280	5.52	561
33	0.0291436	11.54	3.98	210	5.60	416

Table 5.2. Comparison of Methods Used to Estimate Pile Buckling Loads for an Individual HP10x42 Pile about Weak Axis

50% fixity at both pile ends $P_e = \frac{2\pi^2 EI}{L^2}$		**50% fixity at top/ full fixity 5ft below ground line** $P_e = \frac{3\pi^2 EI}{\ell^2}$		**Granholm's Equation**		**FB-Pier Pushover (Buckling) Analysis**	
				Pinned at Top	Fixed at Top	Pinned at Top	Fixed at Top
L (ft)	P_e	ℓ (ft)	P_e	P_e	P_e	P_{CR}	P_{CR}
10	2850	*15*	1900	1388	2898	410	430
15	1267	*20*	1069	786	1722	380	420
20	713	*25*	684	500	1033	310	410
25	456	*30*	475	342	694	240	380
30	317	*35*	349	250	494	180	320
35	233	*40*	267	190	372	140	270
40	178	*45*	211	149	291	110	220

* Note: Elastic buckling is expected for shaded values ($P_{CR}<P_y/2=223^K$)

Use averages to compare with 50% fixity eqns.

Table 5.3. Comparison of Methods Used to Estimate Pile Buckling Loads for a 5-Pile Bent with HP10x42 Piles

50% fixity at both pile ends $P_e = \frac{2\pi^2 EI}{L^2}$		**50% fixity at top/ full fixity 5ft below ground line** $P_e = \frac{3\pi^2 EI}{\ell^2}$		**Granholm's Equation**		**FB-Pier Pushover (Buckling) Analysis Of Piles in a 5-Pile Bent**	
				Pinned at Top	Fixed at Top	Pinned at Top (Figures 7.2-7.6)	Fixed at Top (Figures 7.12-7.16)
L (ft)	P_e	ℓ (ft)	P_e	P_e	P_e	P_{CR}	P_{CR}
13	1687	*18*	1320	959	2136	160	380
18	880	*23*	808	604	1252	140	280
23	539	*28*	545	394	802	130	240
28	364	*33*	393	280	561	120	200
33	262	*38*	296	210	416	110	180
40	178	*45*	211	149	291	**100	**145

* Note: Elastic buckling is expected for shaded values ($P_{CR}<P_y/2=223^K$)

** Values obtained from an individual study and are not shown in Chapter 7

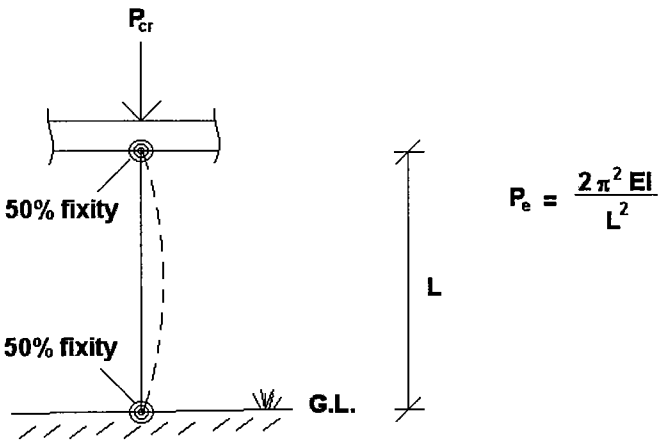

a) Partial Fixity at Top and Bottom of Pile (effective length = L)

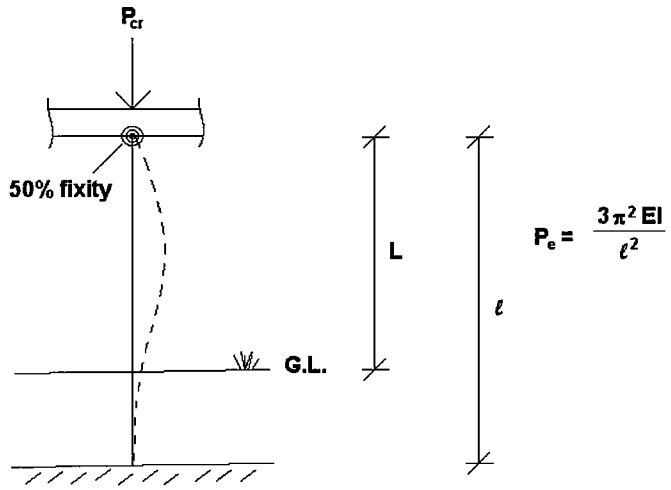

b) Partial Fixity at Top of Pile/ Full Fixity at Bottom (effective length = 1)

Figure 5.1. Alternate Models for Evaluating Elastic Buckling Loads of Individual Piles

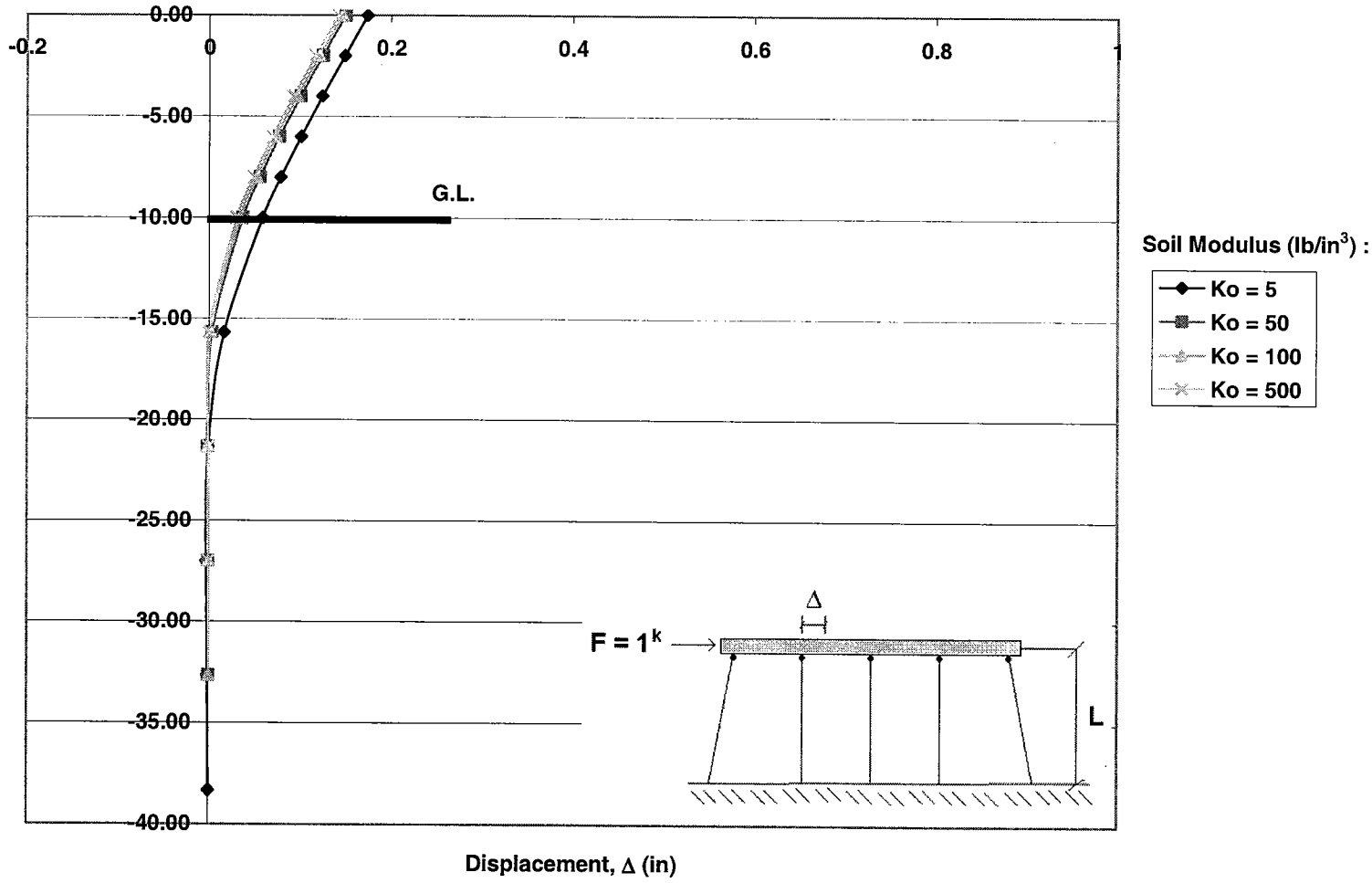

Figure 5.2. Pile No. 2 Horizontal Displacements, Δ, for k_{eq} Loading with Various Soil Moduli, Piles Pinned at Cap, L = 10 ft

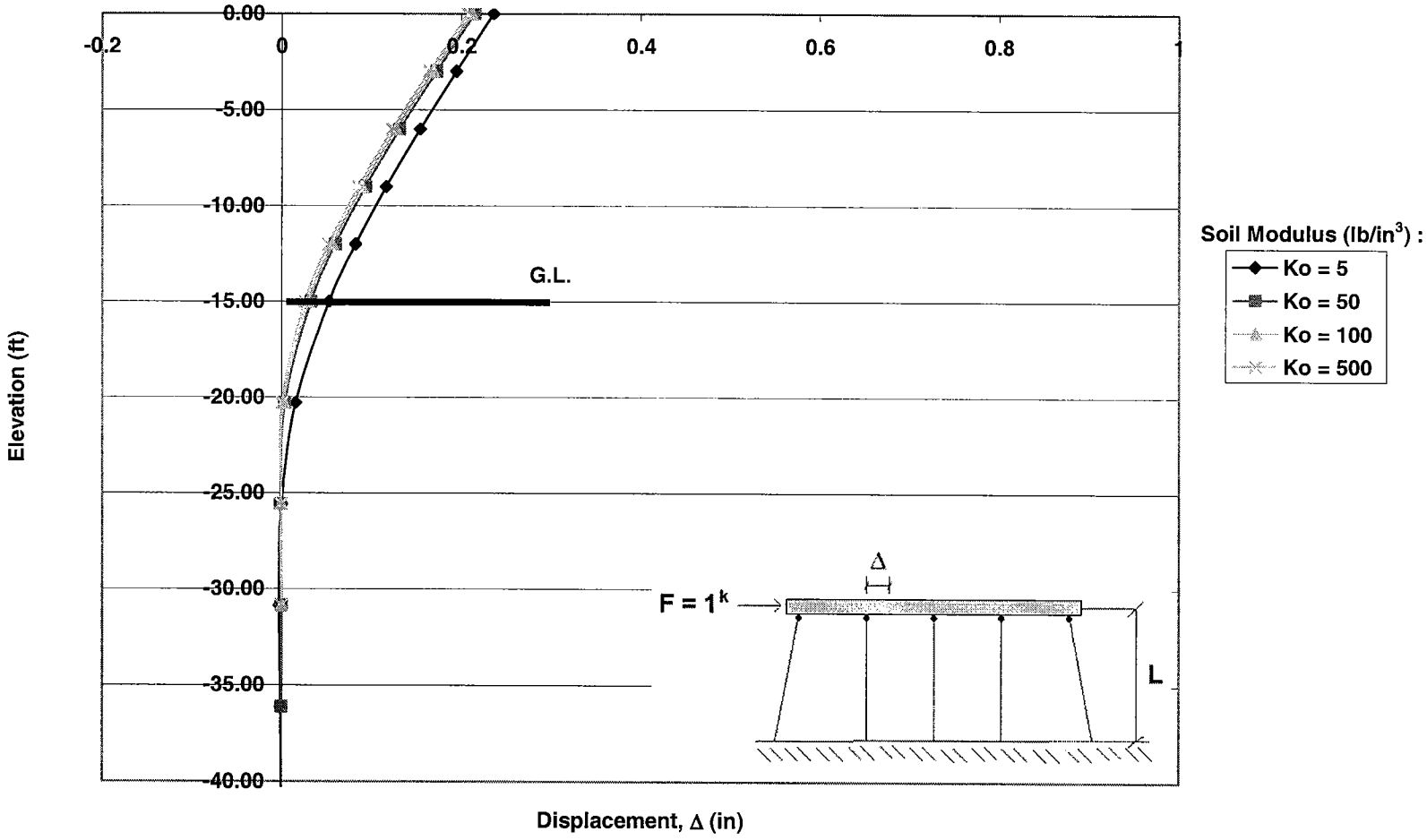

Figure 5.3. Pile No. 2 Horizontal Displacements, Δ, for k_{eq} Loading with Various Soil Moduli, Piles Pinned at Cap, L = 15 ft

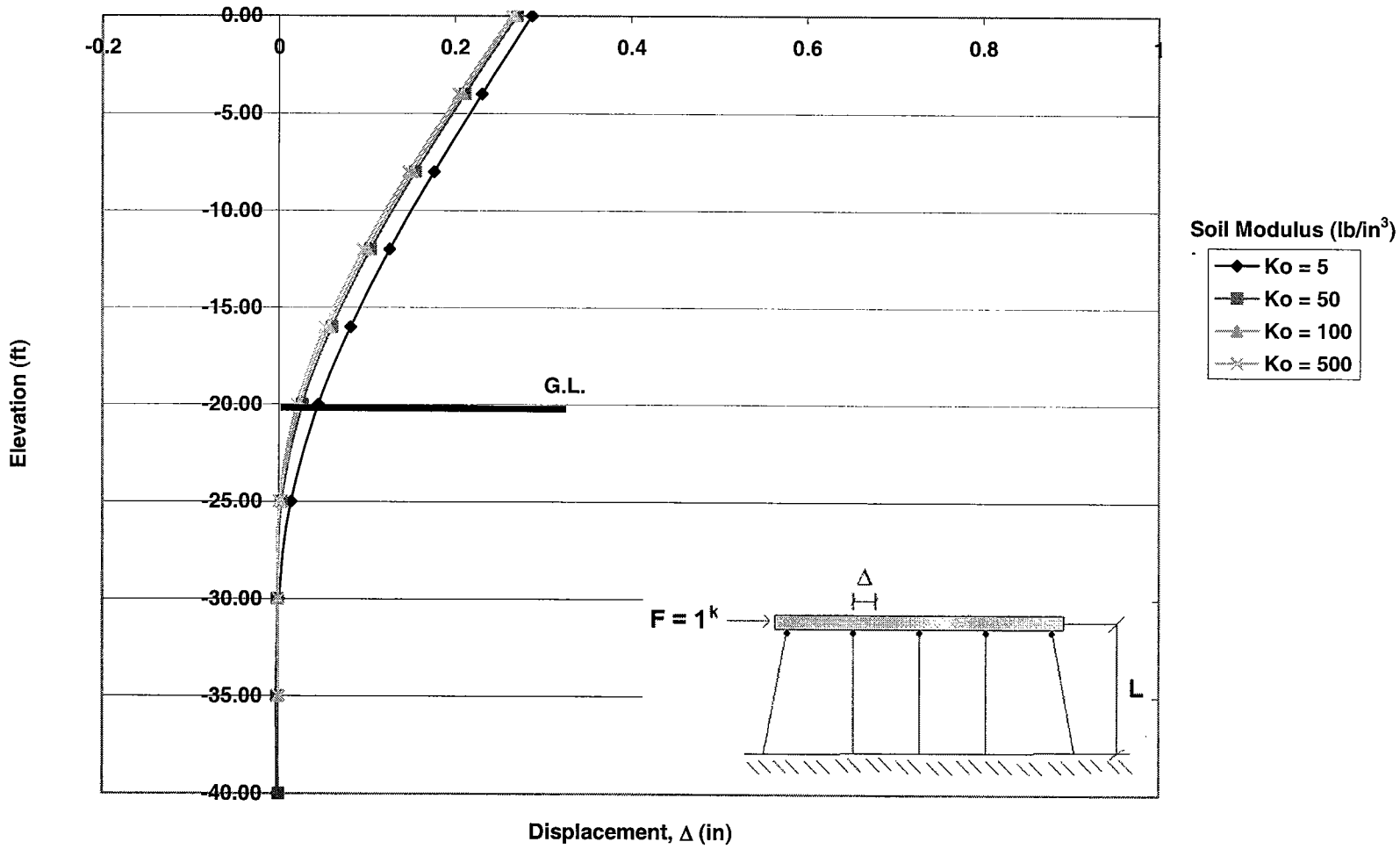

Figure 5.4. Pile No. 2 Horizontal Displacements, Δ, for k_{eq} Loading with Various Soil Moduli, Piles Pinned at Cap, L = 20 ft

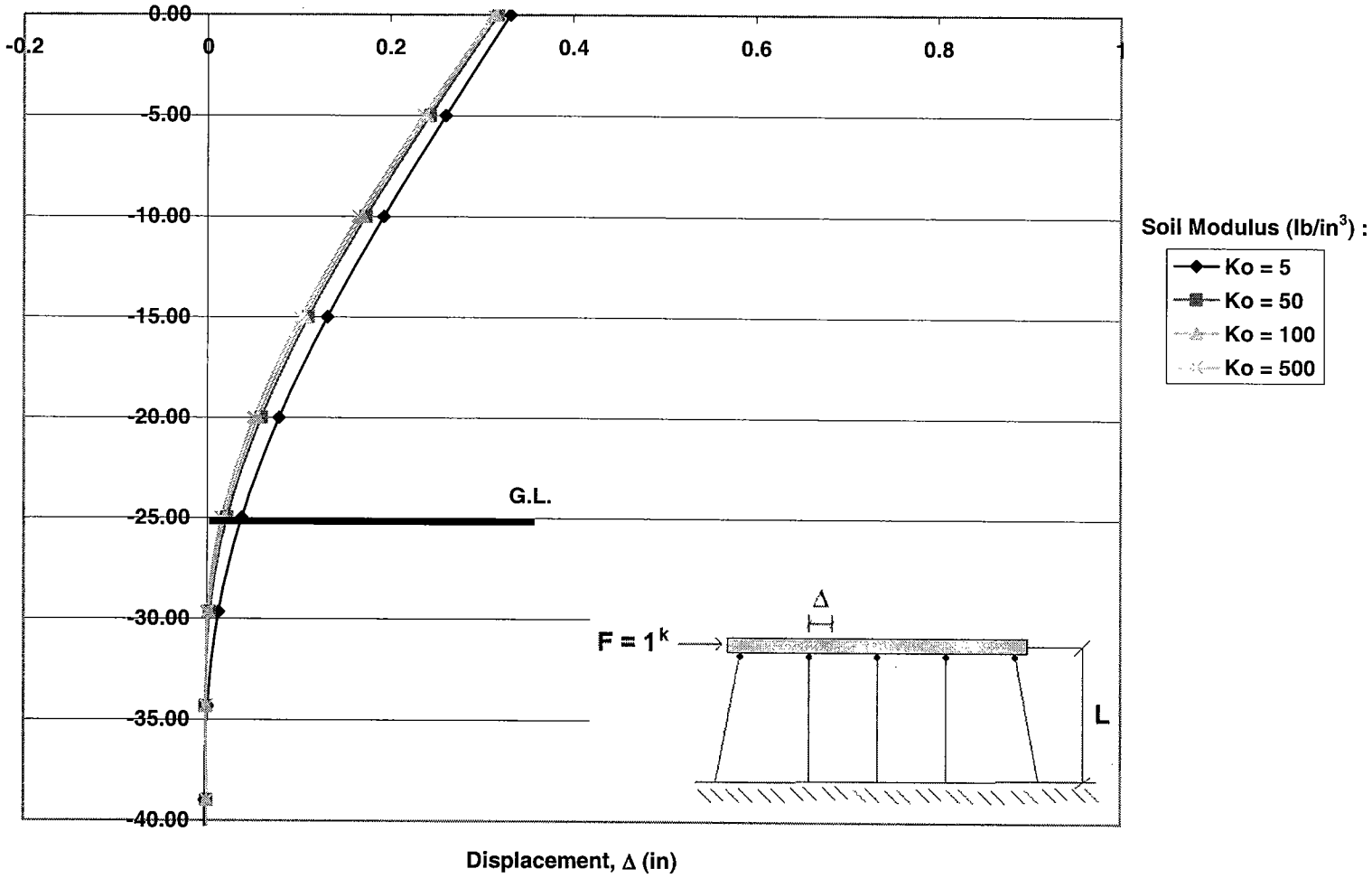

Figure 5.5. Pile No. 2 Horizontal Displacements, Δ, for k_{eq} Loading with Various Soil Moduli, Piles Pinned at Cap, L = 25 ft

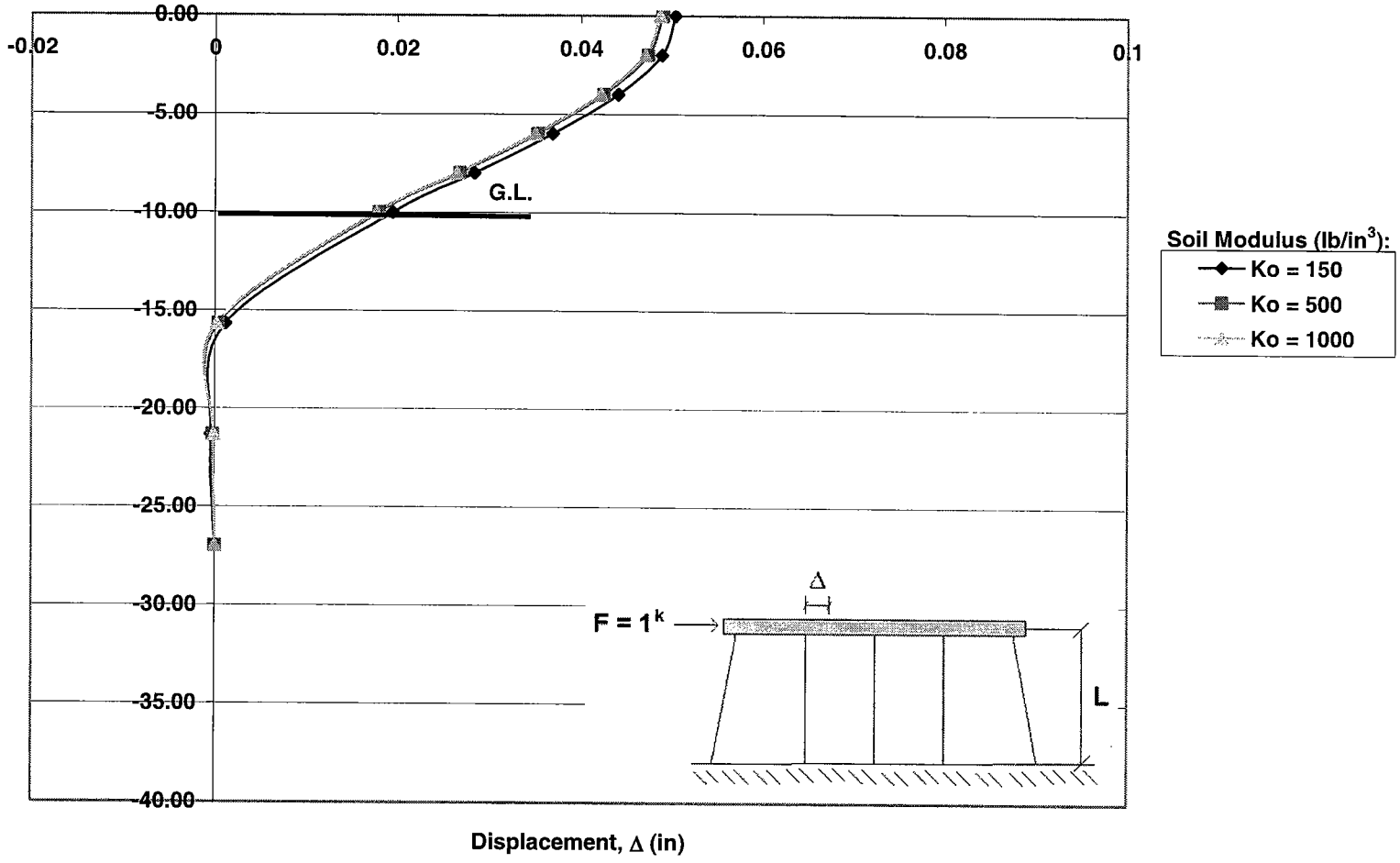

Fig 5.6. Pile No. 2 Horizontal Displacements, Δ, for k_{eq} Loading with Various Soil Moduli, Piles Fixed at Cap, L=10ft

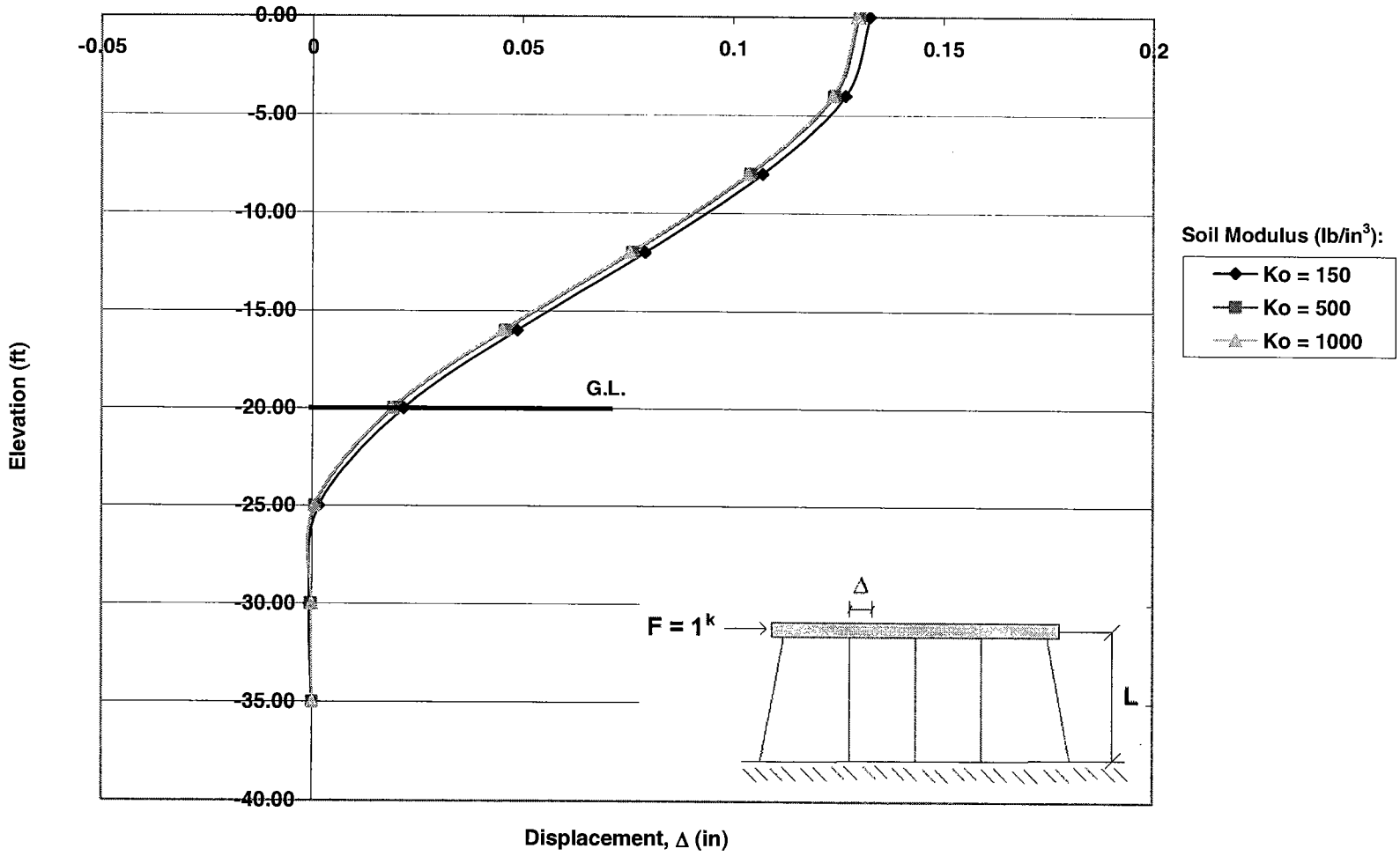

Fig 5.7. Pile No. 2 Horizontal Displacements, Δ, for k_{eq} Loading with Various Soil Moduli, Piles Fixed at Cap, L = 20ft

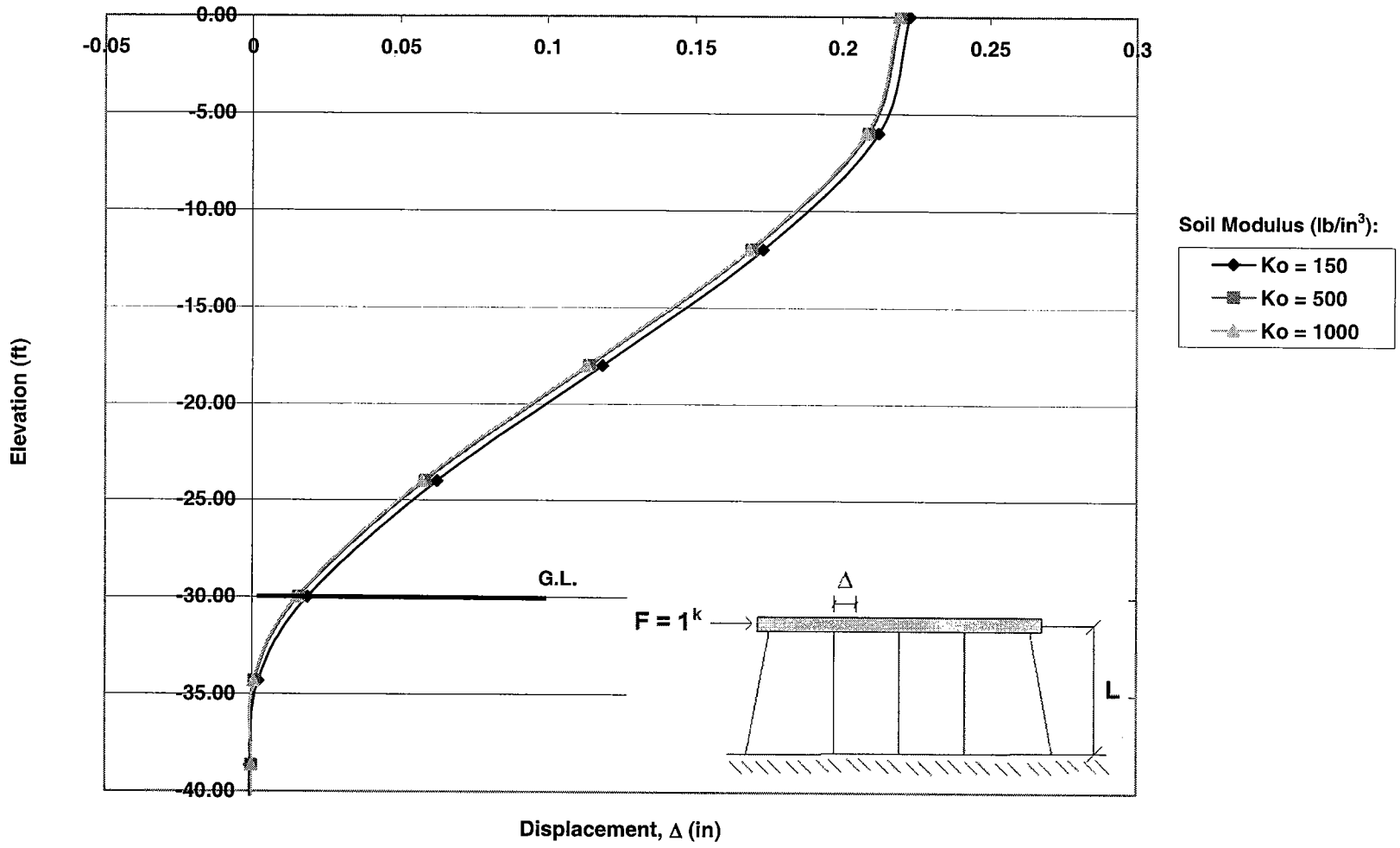

Fig 5.8. Pile No. 2 Horizontal Displacements, Δ, for k_{eq} Loading with Various Soil Moduli, Piles Fixed at Cap, L = 30ft

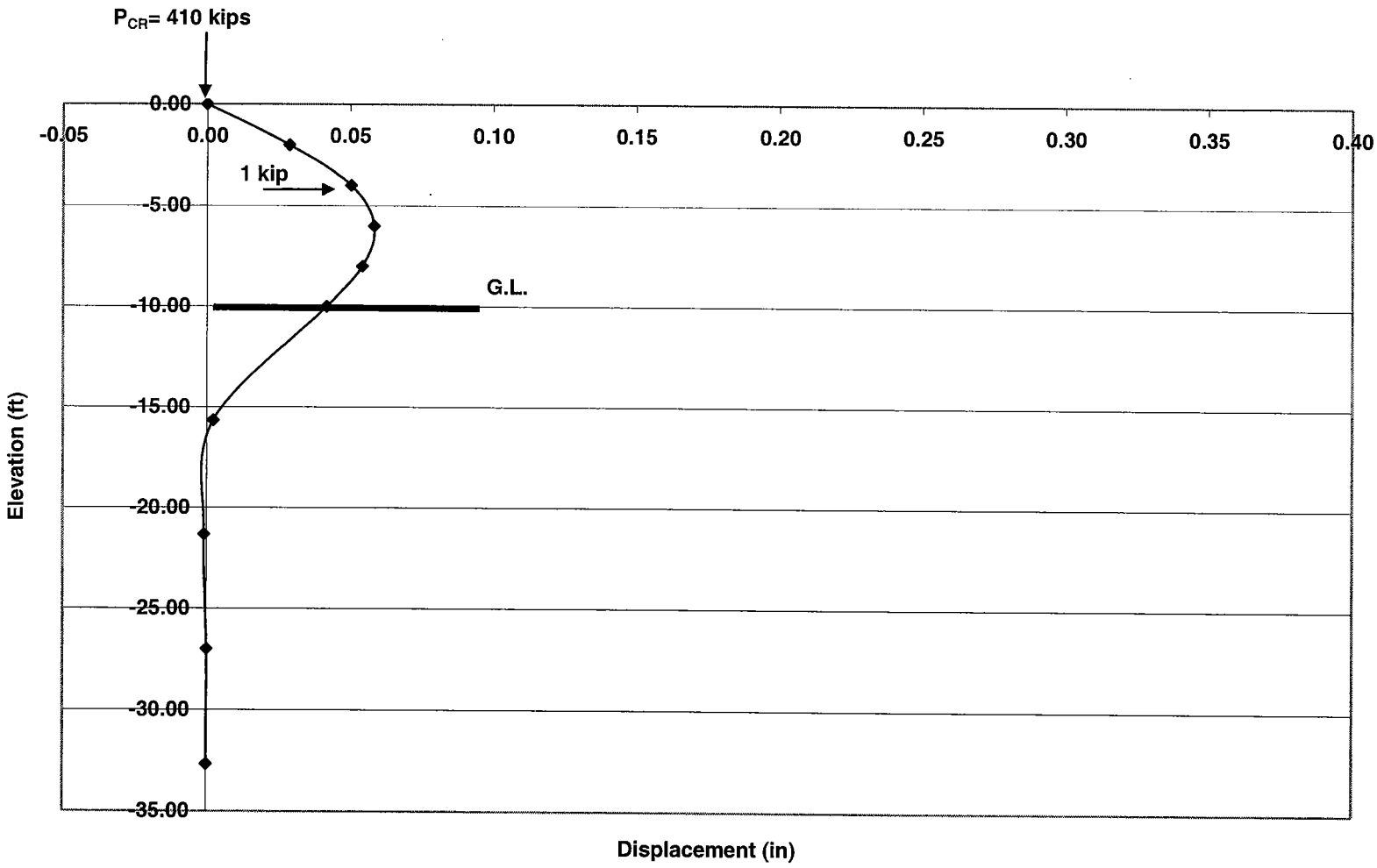

Figure 5.9. Single Pile Deflection at FB-Pier Buckling Load (P_{CR}) for an HP10x42 Pile Pinned at Top, Soil K_o = 100 lb/in^3, and Pile Length Above Groundline L = 10 ft

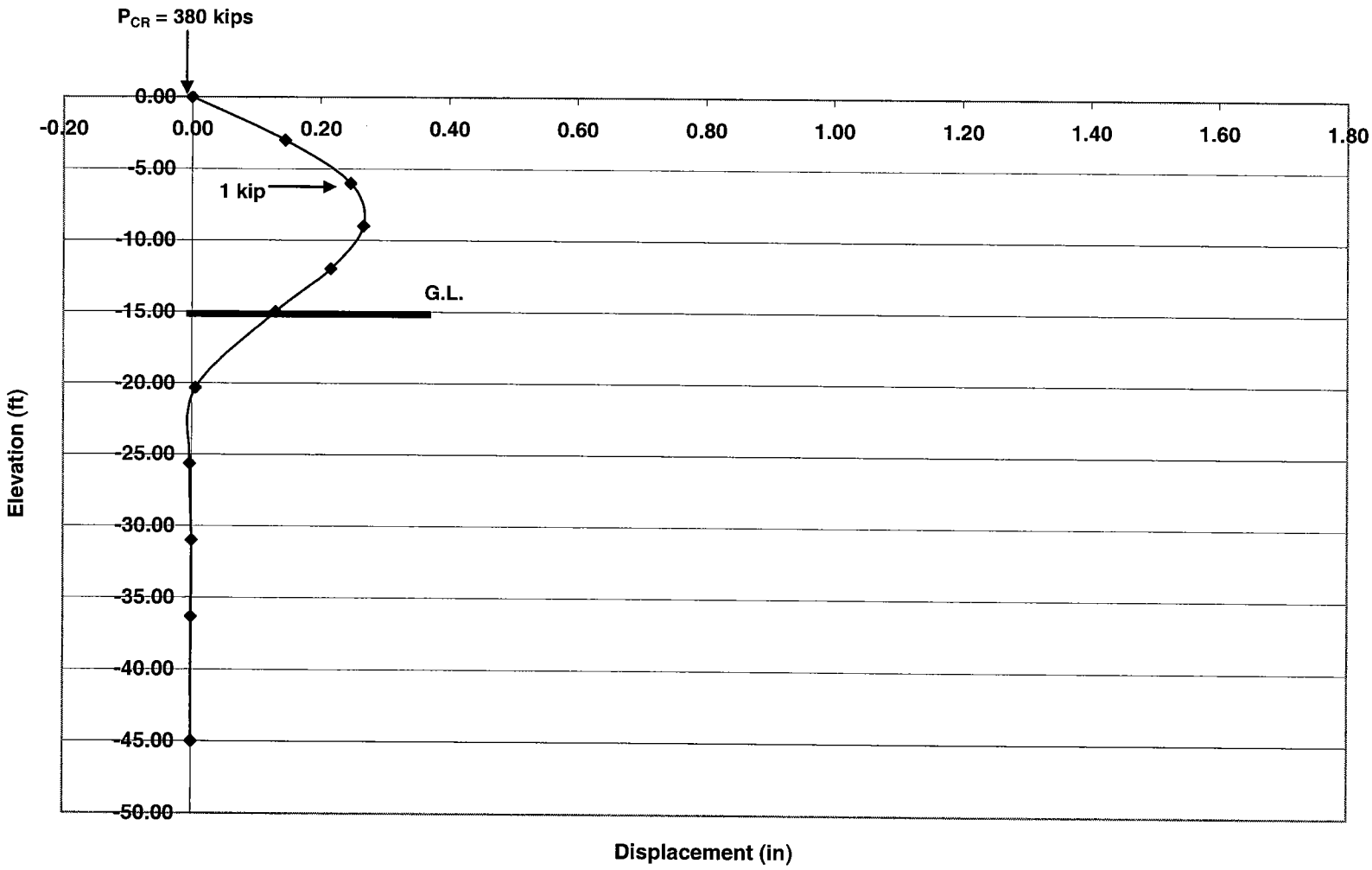

Figure 5.10. Single Pile Deflection at FB-Pier Buckling Load (P_{CR}) for an HP10x42 Pile Pinned at Top, Soil K_o = 100 lb/in^3, and Pile Length Above Groundline L = 15 ft

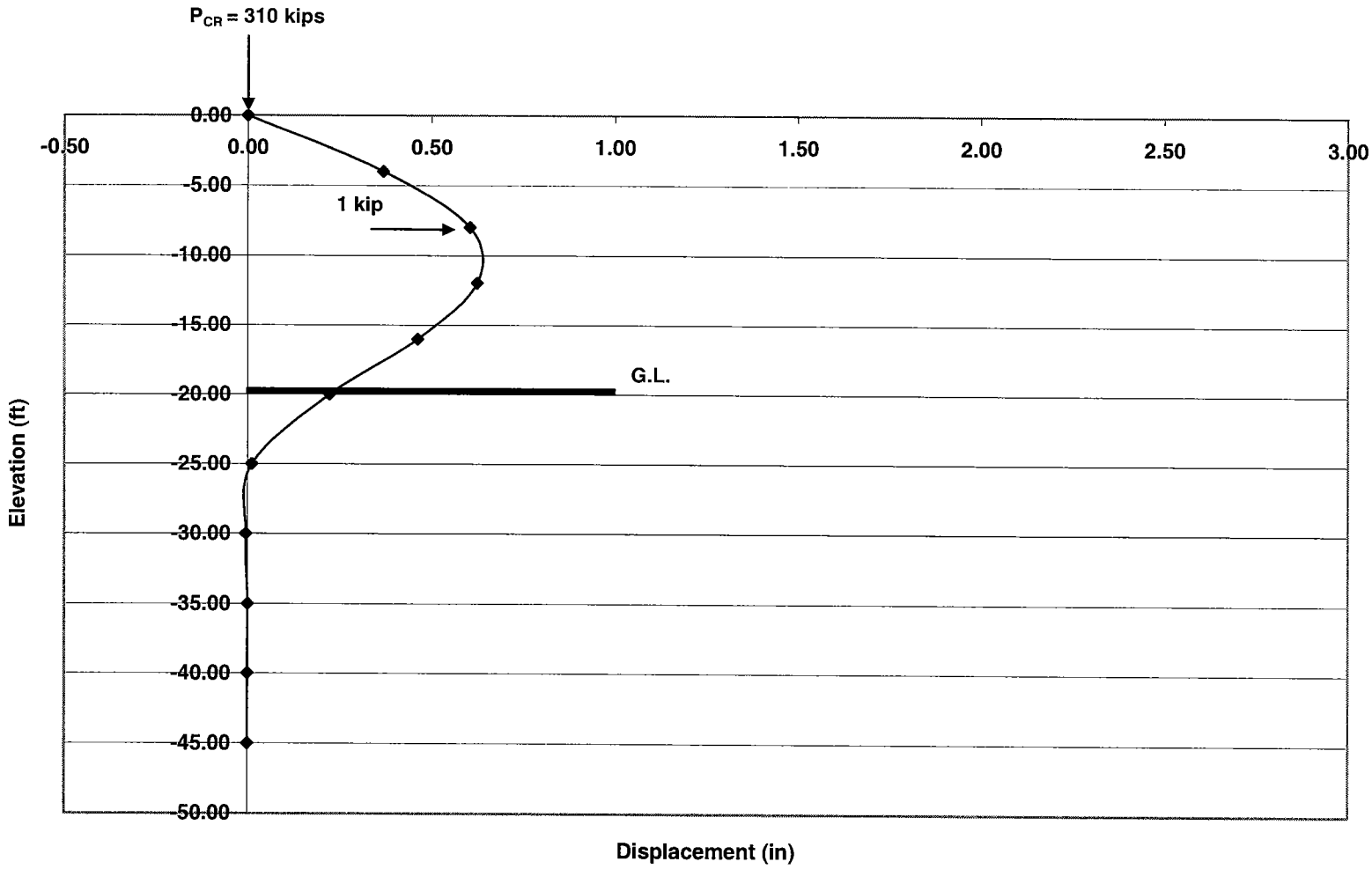

Figure 5.11. Single Pile Deflection at FB-Pier Buckling Load (P_{CR}) for an HP10x42 Pile Pinned at Top, Soil K_o = 100 lb/in^3, and Pile Length Above Groundline L = 20ft

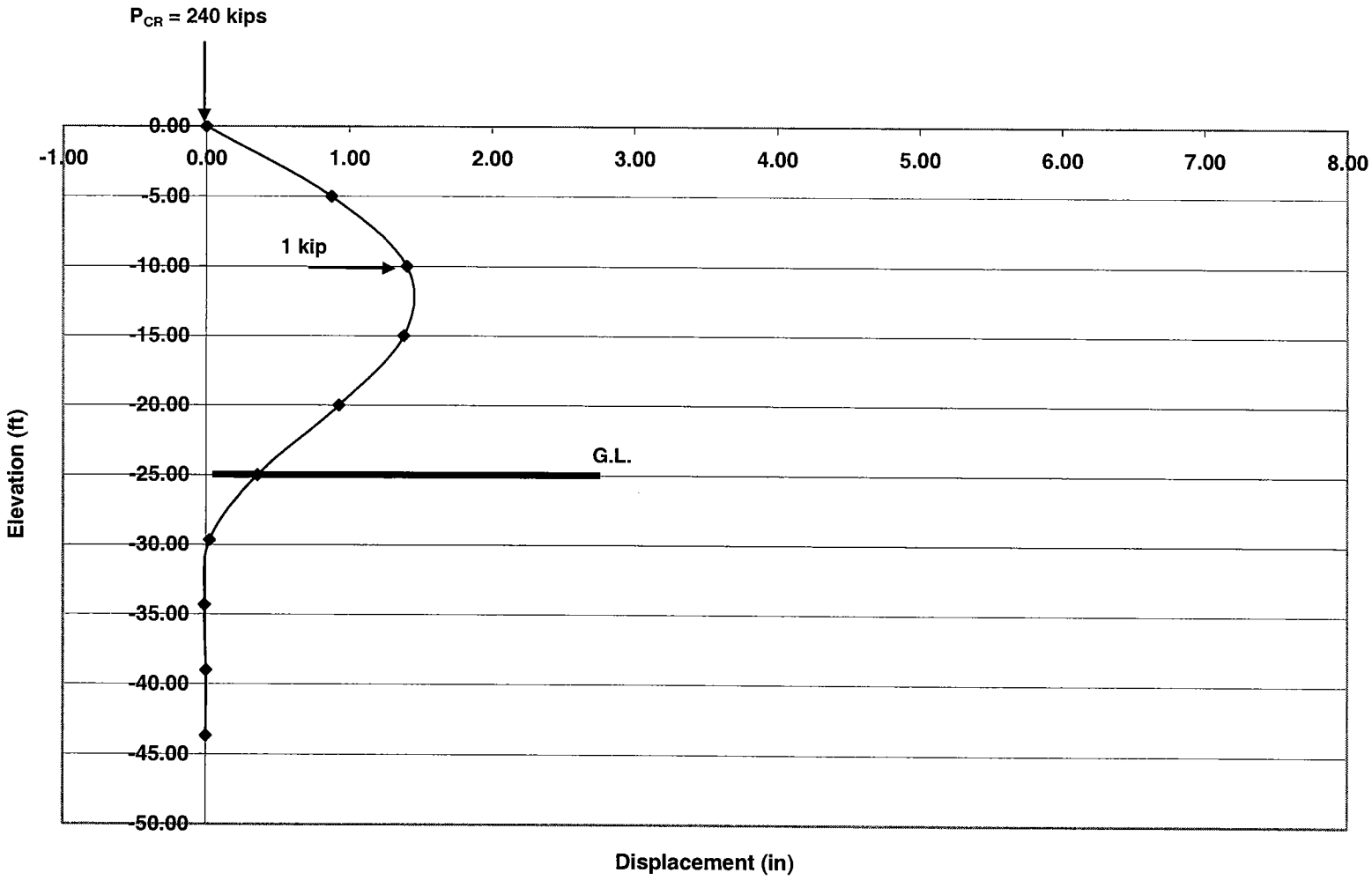

Figure 5.12. Single Pile Deflection at FB-Pier Buckling Load (P_{CR}) for an HP10x42 Pile Pinned at Top, Soil K_o = 100 lb/in^3, and Pile Length Above Groundline L = 25 ft

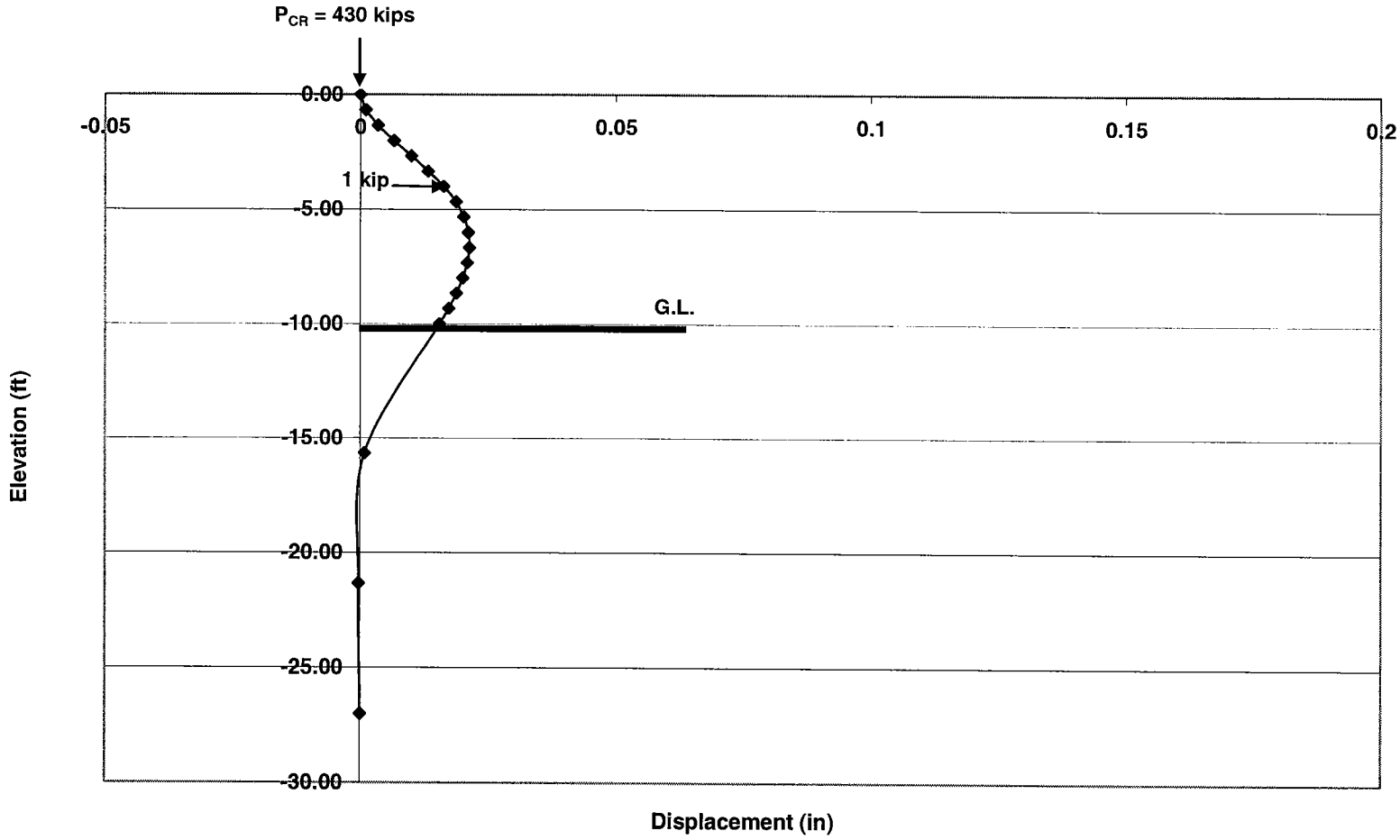

Figure 5.13. Single Pile Deflection at FB-Pier Buckling Load (P_{CR}) for an HP10x42 Pile Fixed at Top, Soil K_o = 100 lb/in^3, and Pile Length Above Groundline L = 10 ft

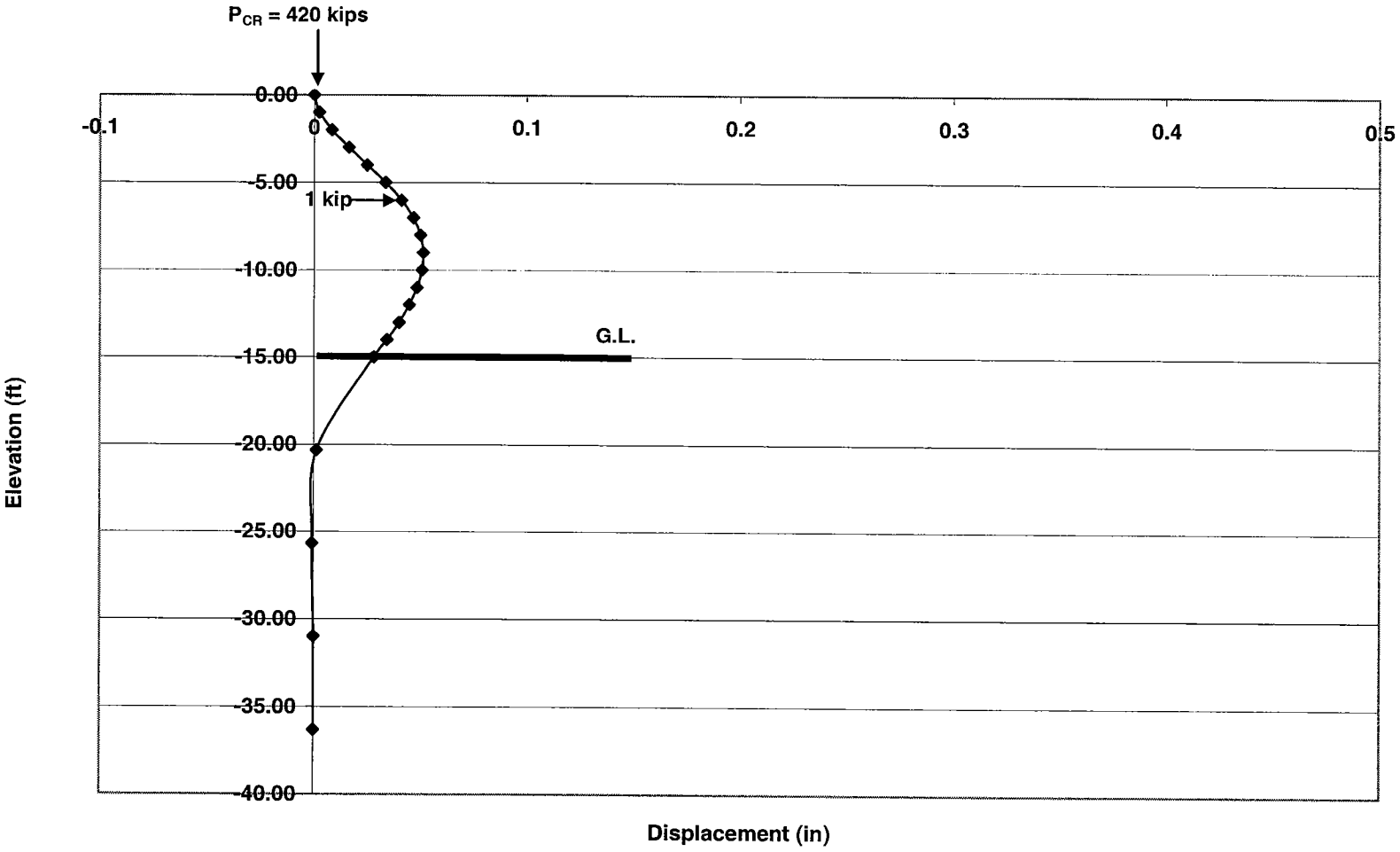

Figure 5.14. Single Pile Deflection at FB-Pier Buckling Load (P_{CR}) for an HP10x42 Pile Fixed at Top, Soil K_o = 100 lb/in^3, and Pile Length Above Groundline L = 15 ft

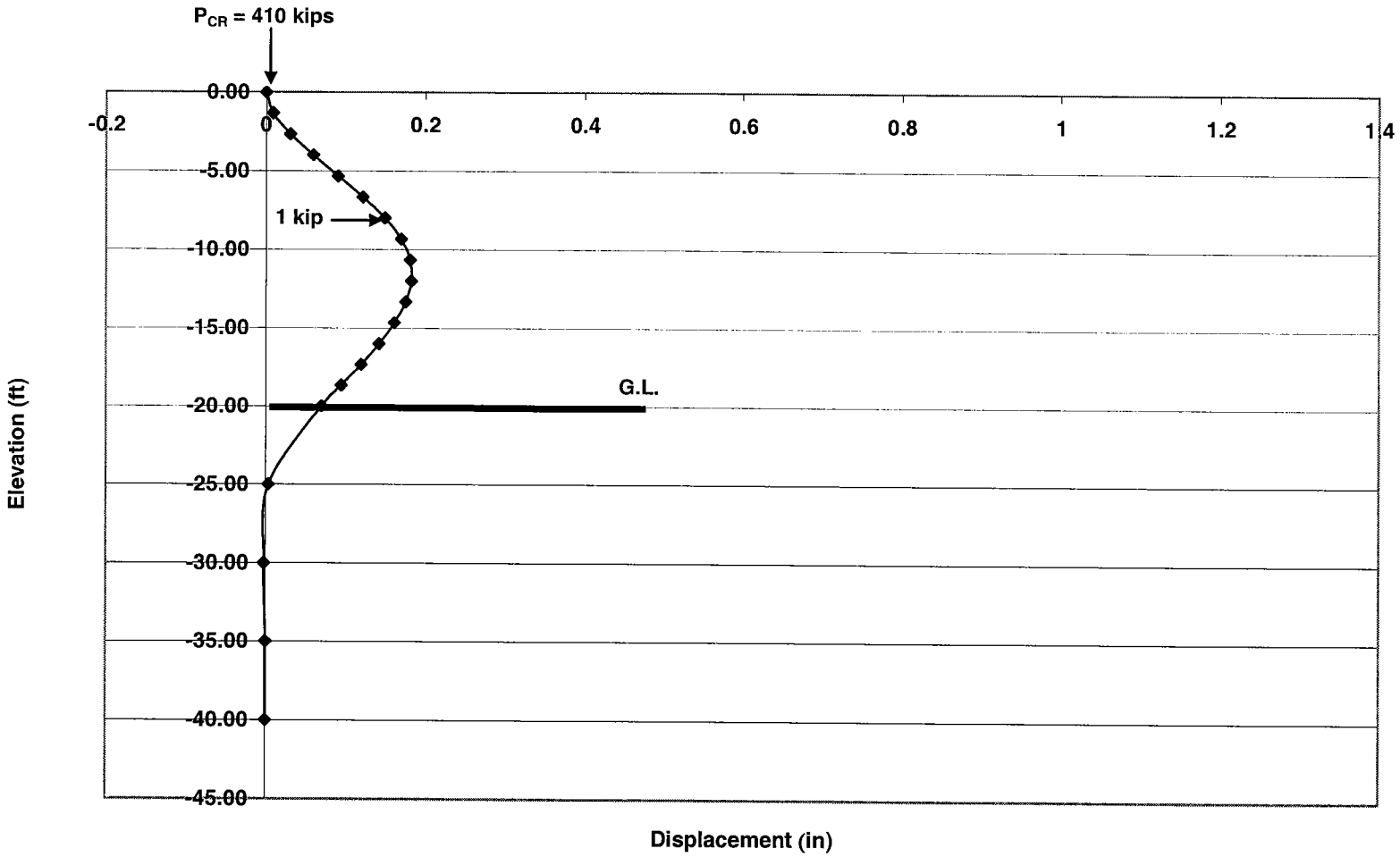

Figure 5.15. Single Pile Deflection at FB-Pier Buckling Load (P_{CR}) for an HP10x42 Pile Fixed at Top, Soil K_o = 100 lb/in^3, and Pile Length Above Groundline L = 20 ft

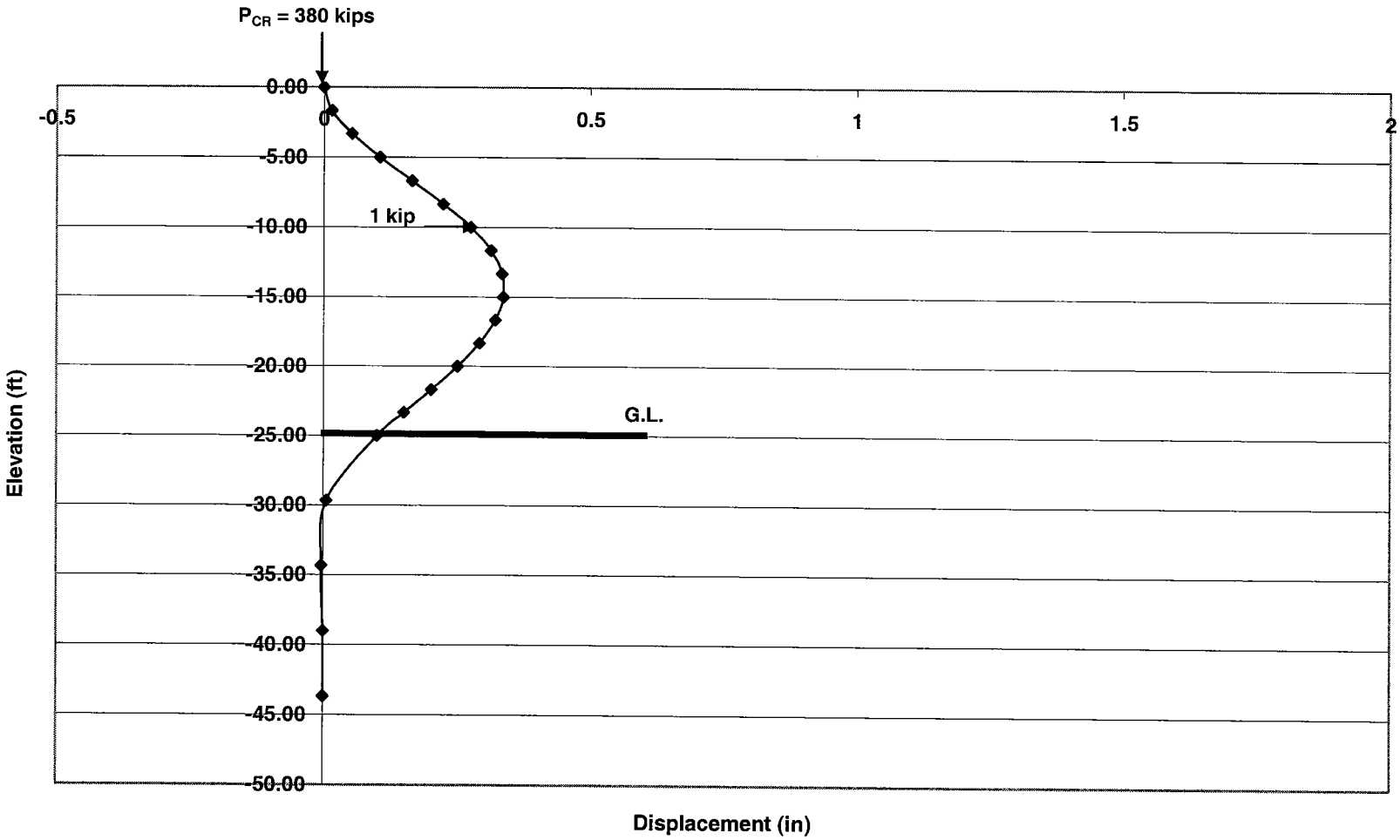

Figure 5.16. Single Pile Deflection at FB-Pier Buckling Load (P_{CR}) for an HP10x42 Pile Fixed at Top, Soil K_o = 100 lb/in^3, and Pile Length Above Groundline L = 25 ft

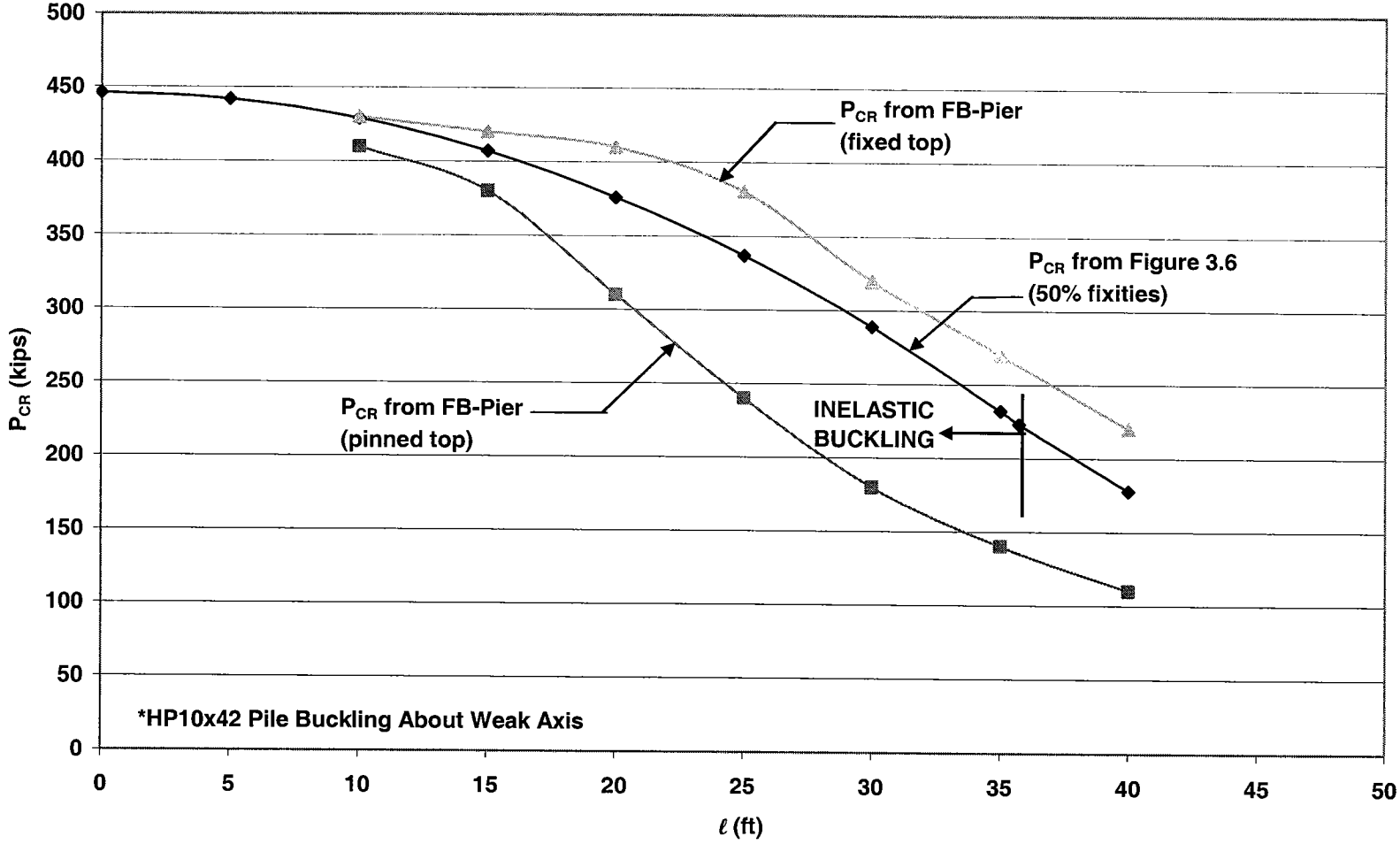

Figure 5.17. Comparison of HP10x42 Inelastic Pile Buckling Values from FB-Pier and Figure 3.6

CHAPTER 6: GTSTRUDL MODELINGS AND RESULTS

6.1 General

Several GTSTRUDL computer models were analyzed in the development of a bent model that behaves similarly to the expected behavior of those in the field. In particular, since partial fixities cannot be modeled by GTSTRUDL, the pile connections to the ground and cap were modeled as either fully pinned or fully fixed to provide a range of possible horizontal bent deflections when a transverse unit load of 1 kip is applied at the cap. From these deflections the equivalent transverse stiffness, k_{eq}, of the bents can be calculated to see if the battered piles provide sufficient bracing for non X-braced bents. This is checked by comparing the ideal bent transverse stiffness (k_{ideal}) to the equivalent stiffness of the model (k_{eq}). If $k_{eq} > k_{ideal}$, sufficient bracing is provided and the bent piles will buckle without sidesway. If sidesway buckling of the piles is prevented, the buckling equation is approximated as $P_e \approx \frac{2\pi^2 EI}{L^2}$ which accounts for 50% rotational fixities at the pile ends. If it is found that sidesway buckling does occur, the approximate buckling equation becomes $P_e \approx \frac{0.5\pi^2 EI}{L^2}$ which also accounts for the 50% rotational fixities at the pile ends. Each non X-braced bent model analyzed in this research consists of unencased steel H-piles. This assumption is believed to be valid since non X-braced bents do not have shear studs along the piles to maintain composite action between the steel and concrete encasement.

Initially, it was assumed that non X-braced bents may be modeled as the simplified bent shown in Figure 3.9. However, before comparing the equivalent stiffness of this simplified modeling to the ideal stiffness, a computer model should be developed to justify or reject the simplified model. In the course of developing an accurate computer model, several bent

parameters were varied to determine if k_{eq} is sensitive to the bending stiffness of the cap, the connection between the piles and ground, and the degree of end pile battering. Although all of ALDOT's standard bents are constructed using an end pile batter of 1.5" in 12", varying the end pile batter provides insight into stiffness gains resulting from larger pile batters. This may influence the use of larger pile batters in the construction of future bents (provided the non X-braced bents are highly susceptible to sidesway).

Additional sections of this chapter include a buckling analysis of standard ALDOT non X-braced bents as well as example GTSTRUDL input files which may serve as guides for future pushover analysis in the event that a site specific evaluation is required. A brief description of key analysis parameters are also provided. These example files include 5-pile bents that are non X-braced (H=13ft), one story X-braced (H=13ft), and two story X-braced (H=25ft).

6.2 Sidesway Analysis of Pinned/Pinned Pile Bents

The first GTSTRUDL non X-braced bent model to be examined in the analysis of sidesway susceptibility has piles pinned to the cap and ground. From this model, a direct comparison can be made to the original simplified bent model of Figure 3.9 which is also pinned at each end of the piles and has a 1 kip horizontal force applied at the cap to measure its stiffness. After performing a static analysis of the structure and viewing the deformed shape, it is apparent that the entire cap experiences a slight rotation and flexure near the end piles. This finding contests the original modeling of Figure 3.9 which bases its determination of k_{eq} on the assumption that no rotation or flexure of the cap occurs. Because of this rotation and flexure, the battered piles undergo less axial deformation than predicted in the simplified model and much lower values for k_{eq} are observed than previously calculated in Table 3.5.

The GTSTRUDL results of k_{eq} for pinned/pinned bents with various pile lengths are plotted in Figures 6.1-6.3 for end pile batters of 1" in 12", 1.5" in 12", and 2.0" in 12" respectively. These k_{eq} values can be compared with the k_{ideal} values also plotted in the figures to determine if sidesway buckling would occur before the piles reach their buckling capacity. The values of k_{ideal} for 5-pile bents pinned at the cap and ground are taken from Table 3.3. When $k_{eq} < k_{ideal}$ the

lateral bracing provided by the battered piles is not sufficient to hold the top of the piles in place at their non sidesway buckling capacities and the bent will experience sidesway buckling of the piles. Since the effective stiffness, I_e, of the cap is closest to the actual flexural stiffness of the cap under service loads, the heights at which sidesway buckling will occur are found to the left of the intersection of k_{ideal} and the k_{eq} value associated with cap $I=I_e$. The derivations of I_e as well as I_{rigid}, I_{gross}, and I_{cr} are given in Chapter 3.

As shown in Figure 6.1 for an end pile batter of 1" in 12", sidesway buckling of the piles will control when the bent height $\leq$ 43 ft (where the bent height is the length of the piles after scour, i.e. bent height = H + S). Similarly, in Figure 6.2 for an end pile batter of 1.5" in 12", sidesway buckling will occur when the bent height $\leq$ 31 ft. From Figure 6.3 with end pile battering of 2" in 12", sidesway buckling occurs when the bent height $\leq$ 25 ft. When the cap $I=I_e$, k_{eq} shows no significant sensitivity to the bent height. For each level of battering the decrease in k_{eq} is nearly linear and relatively small when the flexural stiffness of the cap equals I_e.

6.3. Sidesway Analysis of Pinned/Fixed Pile Bents

For the second sidesway analysis bent model the connection between the piles and bent cap remain pinned, but the connection to the ground is given a full fixity. This model is being analyzed to compare k_{eq} values with the previous pinned/pinned bent model and to determine the sensitivity of k_{eq} to the type of connection between the ground and piles. Ideally a 50% rotational fixity would be placed at each end of the piles to account for the predicted partial fixities. However, GTSTRUDL currently only has the capability to fully restrain or release a particular degree of freedom and, therefore, a fully fixed connection was used at the base of the piles.

For various pile lengths k_{eq} values for the pinned/fixed bent models are plotted in Figures 6.4-6.6 for end pile batters of 1" in 12", 1.5" in 12", and 2.0" in 12" respectively. The corresponding k_{ideal} values for this model were taken from Table 3.4. As mentioned previously, when $k_{eq} < k_{ideal}$ the lateral bracing provided by the battered piles is not sufficient to hold the top of the piles in place at their non sidesway buckling capacities and the bent will undergo sidesway buckling. Since I_e of the cap is closest to the actual flexural stiffness of the cap under service

loads, the heights at which sidesway buckling will occur are found to the left of the intersection of k_{ideal} and the k_{eq} value associated with I_e.

As shown in Figure 6.4 for an end pile batter of 1" in 12", sidesway buckling will occur for all pile lengths before and after scour. In Figure 6.5 for an end pile batter of 1.5" in 12", sidesway buckling will also occur for all pile lengths considered. From Figure 6.6 with end pile battering of 2" in 12", sidesway buckling occurs when the height $\leq$ 45 ft. Unlike the previous pinned/pinned bent model, k_{eq} for the pinned/fixed model appears to be slightly more sensitive to the bent height as observed for the smaller pile lengths. However, when the bent height > 25 ft and the cap $I=I_e$, the decrease in k_{eq} values becomes almost linear as in the previous pinned/pinned model.

6.4 Effects of End Pile Battering on Sidesway

To determine the sensitivity of k_{eq} to battering of the end piles, the previous bent models were analyzed for end pile batters of 1" in 12", 1.5" in 12", and 2.0" in 12". The main objectives for increasing the end pile battering were to observe the respective stiffness increases, reveal whether sidesway buckling is prevented or reduced, and determine if bents constructed in the future should incorporate larger batters. To provide a better comparison of the stiffness gains which result from increasing the degree of end pile battering, k_{eq} vs. H has been plotted in Figures 6.7 and 6.8 for the pinned/pinned and pinned/fixed models (with the cap $I = I_e$) and all three end pile batters. I_e was chosen since it is assumed to be closest to the actual flexural stiffness of the bent cap under service loads.

According to Figures 6.7 for the pinned/pinned model, increasing the battering by 0.5" in 12" nearly doubles k_{eq}. Aside from the expected increase in stiffness, increasing the batter reveals no major sensitivities. The increases in k_{eq} are nearly identical for each bent height. Figure 6.7 also shows that sidesway buckling is less likely to occur when the batter equals 2" in 12". Sidesway buckling occurs for bent heights $\leq$ 31 ft when the batter is 1.5", whereas sidesway buckling occurs for heights $\leq$ 26 ft when the batter is 2". For the pinned/fixed modeling shown in Figure 6.8, increasing the battering by 0.5" in 12" increases k_{eq} by a factor of approximately 1.5 for most bent heights considered. For this modeling sidesway buckling occurs for bent

heights ≤ 45 ft for each of the end pile batters 0" – 2". The latter pinned/fixed modeling is probably more representative of actual bents and sidesway for this model occurs even for maximum levels of scour whether the end pile batter is 1.5" or 2.0". Therefore, it does not appear that increasing the end pile batter provides significant stiffness advantages for typical non X-braced bent heights (L=H+S ≤ 33 ft), i.e. maximum bent height of 13ft and maximum scour of 20 ft.

6.5 Sidesway Analysis Conclusions

As shown from the previous sidesway study, most non X-braced bents are susceptible to sidesway buckling since $k_{eq}<k_{ideal}$ for bent heights corresponding to typical levels of scour (L=H+S=33ft). In Figures 6.1-6.6 it can be seen that k_{eq} is most sensitive to the flexural stiffness, I, of the cap at bent heights<30ft. Increasing I by adding reinforcement or other strengthening measures would not increase the stiffness of the bent enough to prevent sidesway. Additionally, it is expected that $I_{cr}<I_{actual}< I_{gross}$, since small stress cracks on the tensile surface of the cap reduce the gross cross-sectional area that carries stress. Therefore, the region of most interest on the graphs lies between I_{gross} and I_{cr} (where I_{cr} represents the fully cracked section), since the effective flexural stiffness of the cap lies between these two upper and lower stiffness bounds. This assumption is useful in that the range of heights at which the actual bent is susceptible to sidesway will slightly larger than the length given by the intersection of k_{ideal} and the k_{eq} value associated with cap $I=I_{gross}$, but slightly smaller than the length given by the intersection of k_{ideal} and the k_{eq} value associated with cap $I=I_{cr}$. Although k_{eq} values for cap $I=I_e$ are shown in the figures the effective stiffness of the cap may vary somewhat under service loads. ACI 318-02 permits the effective stiffness of beams to be derived from $I_e=0.35I_{gross}$, however, this is only an approximation to the actual stiffness.

To form a more complete study of the sidesway analysis of non X-braced bents, k_{eq} values were also determined for pinned/fixed bents having 3, 4, 5, and 6 piles. Plots of k_{eq} vs. pile length are shown in Figures 6.9-6.12 for bents with HP10x42 piles and Figures 6.13-6.16 for bents with HP12x53 piles. In these figures pile lengths range from 13ft (the tallest non X-braced

bent height) to 33ft (corresponding to the maximum expected scour of 20ft). Values for k_{ideal} are also shown for comparison and were calculated in a manner similar to those in Table 3.4 for the correct number of piles. With the cap I represented by the upper bound, I_{gross}, it can be seen that $k_{eq} < k_{ideal}$ for each bent and pile length considered. Thus, sidesway buckling of each non X-braced bent is expected and the pile buckling loads are governed by the approximate equation $P_e \approx \frac{0.5\pi^2 EI}{L^2}$ which has been reduced by half to account for 50% rotational fixities at the pile ends.

After performing the pushover analyses in the succeeding chapters, it was determined that modeling bents with fixed connections at the cap and pinned at the ground seems to provide slightly more realistic behavior of bents in the field and is the predominate model used in the pushover analysis procedures in subsequent chapters. Therefore, an abbreviated study was performed to compare k_{eq} values of pinned/fixed bents to k_{eq} values for the preferred fixed/pinned models. It should be noted that the pinned/fixed (fixed to the ground) bent modeling provides k_{eq} values that are nearly identical to the fixed/pinned (pinned to the ground) models. However, the k_{ideal} values were established from Figure 3.8 for pinned/pinned or pinned/fixed piles and the two previous models (pinned/pinned and pinned/fixed) provide the most appropriate modelings to compare k_{eq} with k_{ideal}. Since the k_{eq} values for the pinned/fixed and fixed/pinned models are nearly identical, the results of the pinned/fixed modeling shown in Figures 6.8-6.16 are acceptable even though the fixed/pinned model is preferred.

6.6 Buckling Analysis of Standard ALDOT Bents

After determining that most non X-braced bents are susceptible to failure by sidesway buckling, an additional study was considered to verify that these as well as standard X-braced bents can safely support typical gravity loads during and after an extreme scour event. GTSTRUDL's pushover analysis procedure can be used to perform a buckling analysis and make sure that standard bents have adequate buckling capacity. This check can be performed in two ways. The first method can be used to determine if a bent will provide adequate buckling capacity "during" the extreme flooding event which places large transverse water loads on the

bent. For this method, typical gravity loads may be assumed and placed above each pile of the bents. Realistic values for the maximum gravity loads applied to a pile ($P^{pile}_{max\ applied}$) are 100 kips, 120 kips, 140 kips, and 160 kips depending largely on span length between bents. Even though the gravity loads for this model are constant they create compression in the piles which can significantly reduce their lateral stiffness and cause a corresponding reduction in pushover capacity. The horizontal force for this model is created from water loads and is incremented until failure is reached. If the actual pushover force ($F_{t\ max\ applied}$) is less than the capacity predicted by the pushover analysis ($F_{t\ pushover\ load}$), the bent should have adequate load carrying capacity. If the GTSTRUDL pushover analysis fails to provide a solution even for small lateral forces, the gravity forces have reduced the lateral stiffness of the piles enough to cause instability. For the purposes of this research gravity loads were kept constant at 100kips per pile. Verification of the stability of bents under a range of constant gravity loads is not provided here, but will be presented in future research and the final "screening tool". The second method to determine bent buckling capacity also uses GTSTRUDL's pushover analysis procedure, but calculates the buckling capacity of bents "after" the extreme scour event has occurred. This method increments the vertical loads above each pile to determine the buckling capacity (P^{pile}_{max}) of the piles/bent when only a very small lateral load is applied, i.e. 0.1 kip. The small 0.1 kip force was used to introduce a very small lateral deflection of the piles which will be magnified by the p-delta effects as the pile loads are incremented. This latter method is presented in the following study to verify sufficient buckling capacity after an extreme scour event.

The buckling analysis was performed on standard bents with 3, 4, 5, and 6 piles to verify that each bent has sufficient buckling capacity for scour levels of S=0ft, 5ft, 10ft, 15ft, and 20ft. For this study, each bent has an end pile batter of 1.5" in 12", fixed connections between the piles and cap, and pinned connections between the piles and ground. The constant horizontal force of 0.1 kip was placed at the cap and the gravity loads above each pile were incremented. Even though the horizontal force and initial deflection are very small, the incremented gravity loads

reduce lateral stiffness of the piles and greatly amplify the lateral deflection as the buckling capacity of the piles is reached.

The buckling analysis results are shown in Figures 6.17a-6.20a for 3, 4, 5, and 6-pile non X-braced HP10x42 bents with H=13ft and S=0ft-20ft. Similarly, the buckling analysis results for the non X-braced HP12x53 bents are shown in Figures 6.17b-6.20b. These results are summarized in Table 6.1. It was previously mentioned that typical gravity loads ($P^{pile}_{max\ applied}$) range from 100kips to 160kips. As shown in the tables, the pile buckling capacity of the HP10x42 3-pile bent falls within or below the assumed range of gravity loads when $S \geq 10$ ft. The pile buckling capacities of the HP10x42 4-pile, 5-pile, and 6-pile bents on the other hand exceed the expected gravity loads which are assumed to act above each pile. For the HP12x53 pile bents, the pile buckling capacity of the 3-pile bent, falls within or below the assumed range in gravity loads when $S \geq 15$ft. The buckling capacities of the 4-pile, 5-pile, and 6-pile bents also exceed the expected gravity loads which act above each pile.

In general, buckling capacities determined from the pushover analysis are larger than those calculated from the proposed approximate elastic pile buckling equation $P_e \approx \frac{0.5\pi^2 EI}{L^2}$ which accounts for sidesway buckling as well as 50% rotational fixities at the pile ends. Reasons for the larger than expected buckling capacities of the 4, 5, and 6-pile non X-braced bents where elastic buckling should control are not quite clear but may be due to the redistribution of forces during pushover of the highly indeterminate bent structures. The slight counter-clockwise rotation of the bent cap caused the axial forces in some piles to be larger than others and allowed lean-on bracing of the piles to occur.

The buckling analysis results for the one story X-braced bents with HP10x42 piles are shown in Figures 6.21a-6.25a for 3, 4, 5, and 6-pile bents with H=13ft and S=0ft-20ft. Similarly, the buckling analysis results for bents with HP12x53 piles are shown in Figures 6.21b-6.25b. These results are summarized in Table 6.2. As shown in the tables, the pile buckling capacity of the HP10x42 3-pile bent falls within or below the typical gravity load of 100 kips when $S \geq 15$ft. The pile buckling capacities of the HP10x42 4-pile, 5-pile, and 6-pile bents, on the other hand

exceed the expected gravity loads above each pile. For the HP12x53 pile bents, the pile buckling capacity of the 3-pile bent, falls within or below the assumed range in gravity loads when $S \geq 20$ft. The pile buckling capacities of the HP12x53 4-pile, 5-pile, and 6-pile bents also exceed the typical range of gravity loads (100-160 kips) above each pile.

For the one story X-braced bents the proposed approximate elastic pile buckling equation is $P_e \approx \frac{2\pi^2 EI}{L^2}$ which assumes sidesway is prevented and pile ends have 50% rotational fixities. As shown in Table 6.2a and 6.2b, the buckling capacities determined from the pushover analysis of the one story X-braced bents with H=13ft are much smaller than the respective elastic buckling values. This is reasonable since the piles in each of these bents are expected to buckle inelastically, i.e. $P_e > P_y/2$.

Buckling analysis results for the two story X-braced bents with HP10x42 piles are shown in Figures 6.26a-6.30a for bents with 3, 4, 5, and 6 piles and H=25ft. The buckling analysis results for the two story X-braced bents with HP12x53 piles are shown in Figures 6.26b-6.30b. These results are summarized in Table 6.3. Where elastic buckling controls, i.e. $P_e > P_y/2 = 223$ kips for HP10x42 piles or $P_e > P_y/2 = 279$ kips for HP12x53 piles, GTSTRUDL's pushover analysis gives an average buckling load that is reasonably close to the approximate equation $P_e \approx \frac{2\pi^2 EI}{L^2}$ for the 4, 5, and 6-pile bents. Additionally, the buckling capacities of these bents remain within or above the assumed range of typical gravity loads (100 – 160 kips) which act above each pile. However, P_{CR} for the two story 3-pile bent becomes much lower than the elastic buckling load for larger levels of scour. Similar results can be seen in Table 6.3b for the two story X-braced bents with HP12x53 piles. It is not directly evident why the buckling capacity of the 3-pile bents becomes much smaller than the elastic buckling value for large levels of scour. However, some discrepancies in the buckling capacities where elastic buckling is expected may occur if the structure becomes unstable due to external loading before the elastic load of the pile is reached.

After observing the buckling capacities produced from GTSTRUDL's pushover analysis it appears that all 3-pile bents may require additional support near the foundation to prevent the occurrence of large levels of scour and keep buckling capacities above the expected gravity loads. Although there are some discrepancies between the approximate elastic buckling equations and the buckling capacities from the GTSTRUDL models, the approximate equations are thought to provide reasonable pile buckling values for the 4, 5, and 6-pile bents. This is supported by the fact that the pile capacities for these bents are above the range of typical bridge pile loads (100kips – 160kips) when the elastic buckling equations predict inelastic buckling (i.e. P_{CR}<160kips when P_e>P_y/2). Additionally, when the elastic buckling equations predict elastic buckling, i.e. P_e<P_y/2, the bent pile capacities are either very similar to the elastic buckling equations (for the X-braced bents) or conservative (for the non X-braced bents).

It should be recalled that this buckling analysis was performed with only a very small lateral load (i.e. 0.1kips) to simulate an initial imperfection in the piles which may be present in the form of load eccentricities or initial crookedness of the piles, however, in the presence of debris rafts and water currents these greater lateral forces may reduce the load carrying capacity of pile bents. Therefore, it is recommended that an additional examination be considered to determine if the bents have adequate buckling capacity during the extreme flood event. As stated at the beginning of this section, this study may be accomplished by placing various constant gravity loads above the piles in a bent and incrementing the horizontal force. If the pushover analysis fails to obtain a solution even for small transverse forces, the gravity loads above each pile may be too large. Thus adequate buckling capacity is not achieved by the bent and it is considered unstable. The results of this study will be provided in future research.

6.7 GTSTRUDL Pushover Analysis Modeling

GTSTRUDL's pushover analysis procedure can be used to determine the lateral forces that will cause a bent to fail for various levels of scour. This is particularly useful, since water currents acting on bents during an extreme flooding event can create rather large transverse loads. The goal of this section is to allow bridge engineers to become more familiar with the

GTSTRUDL input files used in this research for pushover analysis. The following input files may serve as a guide for creating non X-braced and X-braced bent input files in the event that future pushover analysis is required for a specific bent not analyzed in this research.

When creating models in GTSTRUDL, the user may opt to use the Model Wizard, GT MENU, or the Command Mode. Both GT MENU and the Command Mode allow the user to create structures with more complex geometries than the Model Wizard. If unfamiliar with the code or order of data required to create an input file, GT MENU offers a graphical interface to create and model structures. Once a model is completed using GT MENU, a text input file can be created, saved as a text file (with extension .txt), and edited using a basic text editing program such as Windows Notepad. Note that if pushover analysis is desired for various levels of scour, only the coordinates of the joints connected to the ground need editing. After the necessary editing has been performed the text file can then be opened in GTSTRUDL and the desired analysis can be performed. The following subsections (6.7.1-6.7.3) include example input files for 5-pile bents that are non X-braced (H=13ft), one story X-braced (H=13ft), and two story X-braced (H=25ft). A brief summary of key input parameters is provided with their descriptions given in the order of occurrence in the respective input files.

6.7.1 Non X-braced Bent Input File

The input file for each bent begins with the joint coordinates to define the model geometry. All joints are placed along the centerline of member axes as noted by joints 6-10 for the bent caps in the figures associated with each of the following example input files. Member incidences define which end of a member is specified as the start and which is the end. This becomes important when defining the location of member loads and plastic hinges. For standard shapes such as HP10x42 and HP12x53 piles, cross sectional properties are defined within GTSTRUDL tables. If the section dimensions are unique as in the case of the bent cap, these parameters may be specified under MEMBER PROPERTIES. When the command STATUS SUPPORT is used, all degrees of freedom associated with a joint are restrained. This allows the user to release key degrees of freedom later on using the JOINT RELEASES command and may

speed the solution of more complicated structures. Since the piles are modeled with pin connections at the ground, moments in the X, Y, and Z directions have been released for joints 1-5. The beta constant is used to define the orientation angle of the member in the global coordinate system. By using a beta value of 90 degrees for the piles they become oriented so that they buckle about their weak axis for transverse bent loads. The material constants are listed next and include the modulus of elasticity, density, poison's ratio, and coefficient of thermal expansion for each member. Following the material constants is the load data. The loading conditions for pushover are as shown in the respective figures. The horizontal force, "incr", is given an initial value of 1 kip at joint 6 whereas the vertical forces, "const", are given constant values of 100 kips at each joint 6-10. The nonlinear effects cannot be added to the model from GT MENU and, therefore, these parameters must be input by creating and/or editing the text input file. The nonlinear parameters included in typical pushover analysis include geometric nonlinearity as well as plastic hinges to account for material nonlinearity. When the plastic hinge parameter is included, a plastic hinge is placed at both the start and end of the member unless a specific end is specified. The first line of parameters associated with plastic hinges defines the hinge geometry and length. The number of divisions through/across the web and flange are listed and a grid is generated to compute fiber stresses throughout the member cross-section. This also allows the percentage of plastic hinge formation to be viewed after the analysis. The second line of plastic hinge parameters defines the stress strain relationship and is discussed further in Chapter 7. The plastic hinges in the following input file exhibit elastic-perfectly plastic stress strain behavior, since the ultimate stress at failure, FSU, is nearly equal to the yield stress, FY.

Example Non X-braced Bent GTSTRUDL Input File

```
STRUDL ' '
$$
$$    This  GTSTRUDL file created from GTMenu on  1/11/2005
$$
$$
UNITS  INCH  KIPS  DEG   FAH
$$
$$
JOINT COORDINATES GLOBAL
```

```
   1          0.0000000E+00  0.0000000E+00  0.0000000E+00
   2          1.1400000E+02  0.0000000E+00  0.0000000E+00
   3          2.1000000E+02  0.0000000E+00  0.0000000E+00
   4          3.0600000E+02  0.0000000E+00  0.0000000E+00
   5          4.2000000E+02  0.0000000E+00  0.0000000E+00
   6          1.8000000E+01  1.4400000E+02  0.0000000E+00
   7          1.1400000E+02  1.4400000E+02  0.0000000E+00
   8          2.1000000E+02  1.4400000E+02  0.0000000E+00
   9          3.0600000E+02  1.4400000E+02  0.0000000E+00
   10         4.0200000E+02  1.4400000E+02  0.0000000E+00
$$
$$
UNITS INCH KIPS DEG  FAH
$$
$$
$$
TYPE SPACE FRAME
MEMBER INCIDENCES
  1        1        6
  2        2        7
  3        3        8
  4        4        9
  5        5        10
  6        6        7
  7        7        8
  8        8        9
  9        9        10
$$
$$
UNITS INCH KIPS DEG  FAH
$$
MEMBER PROPERTIES   TABLE 'M/S/HP9 '  'HP10x42              '
  1        2        3        4        5
$$
MEMBER PROPERTIES  PRISMATIC  AX 8.6400000E+02  IX 1.0000000E+07  -
IY 1.0000000E+07  IZ 4.1472000E+04
  6        7        8        9
$$
STATUS SUPPORT -
  1        2        3        4        5      -
  6        7        8        9        10
$$
$$
UNITS INCH KIPS DEG  FAH
$$
JOINT RELEASES
  6        7        8        9        10     -
    FOR X  Y MOM Z
$$
  1        2        3        4        5      -
    MOM X  Y  Z
$$
$$
UNITS INCH KIPS DEG  FAH
$$
CONSTANTS
   BETA 0.0  ALL
   BETA 9.0000000E+01 -
  1        2        3        4        5
$$
UNITS INCH KIPS DEG  FAH
$$
CONSTANTS
   E   2.9000014E+04 ALL
   G   1.1000007E+04 ALL
   POI 3.0000001E-01 ALL
   DEN 2.8330021E-04 ALL
   CTE 6.4999999E-06 ALL
   E   3.6000017E+03 -
```

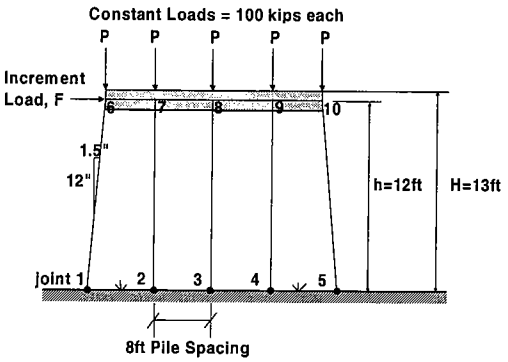

```
   6        7        8        9
    G   1.4400009E+03  -
   6        7        8        9
    POI 1.7000000E-01  -
   6        7        8        9
    DEN 8.6800042E-05  -
   6        7        8        9
    CTE 5.5000000E-06  -
   6        7        8        9
$$
UNITS  INCH  KIPS  DEG   FAH
$$
LOADING 'incr'
$$
 JOINT LOADS FOR X 1.0000000E+00
   6
$$
UNITS  INCH  KIPS  DEG   FAH
$$
LOADING 'const'
$$
 JOINT LOADS FOR  Y  -1.0000000E+02
   6        7        8        9        10
$$
NONLINEAR EFFECTS
$$
  GEOMETRY ALL MEMBERS
$$
  PLASTIC HINGE -
     FIBER GEOMETRY NTF 1 NTW 1 NBF 8 ND 8 LH 3.0 -
     STEEL FY 36.0 ESH .124 ESU .2 FSU 36.001 ALPHA 0.0 MEMBER 1 2 3 4 5
```

6.7.2 One Story X-braced Bent Input File

The one story X-braced bent input files were created with GTSTRUDL's graphical interface, GT MENU, so that the joint coordinates could be easily determined where the X-members intersect the piles. These locations are required so that pinned connections between the X-bracing and intermediate piles may be formed. Much of the one story X-braced bent input file is repeated from the non X-braced bent input file whose parameters were previously discussed in Subsection 6.7.1. An additional MEMBER PROPERTY group is added for X-members which are modeled using C4x7.25 channel members rather than the standard 4"x3 ½ "x 5/16" angle members. The reason for this substitution is explained in Section 8.4. The MEMBER RELEASES command is also unique to the X-braced bent models and must be specified for the X-members so they will not carry bending moments. Because these members do not carry moments, axial plastic hinges are inserted in the compression X-members so they fail (buckle) at their Euler buckling load of 34.3 kips (see Section 8.3). When the 34.3 kip buckling load is divided by the area of the C4x7.25 channel X-members, the corresponding axial stress at failure

is 16.1kips. Since the plastic hinges for the X-members have different properties from the plastic hinges in the H-piles, they must be kept separate. Thus, the plastic hinges in the compression X-members are represented by the second PLASTIC HINGE command. As shown, these hinges also exhibit elastic-perfectly plastic stress strain behavior. Plastic hinges were not inserted into the tension X-members since the axial forces in these members did not exceed the yield load of the member.

Example One Story X-braced Bent GTSTRUDL Input File

```
STRUDL ' '
$$
$$    This  GTSTRUDL file created from GTMenu on 10/28/2004
$$
$$
UNITS  FEET  KIPS  DEG   FAH
$$
$$
JOINT COORDINATES GLOBAL
   1          0.0000000E+00  0.0000000E+00  0.0000000E+00
   2          9.5000000E+00  0.0000000E+00  0.0000000E+00
   3          1.7500000E+01  0.0000000E+00  0.0000000E+00
   4          2.5500000E+01  0.0000000E+00  0.0000000E+00
   5          3.5000000E+01  0.0000000E+00  0.0000000E+00
   6          1.5000000E+00  1.2000000E+01  0.0000000E+00
   7          9.5000000E+00  1.2000000E+01  0.0000000E+00
   8          1.7500000E+01  1.2000000E+01  0.0000000E+00
   9          2.5500000E+01  1.2000000E+01  0.0000000E+00
   10         3.3500000E+01  1.2000000E+01  0.0000000E+00
   11          1.3125000E+00  1.0500000E+01  0.0000000E+00
   12          3.3687500E+01  1.0500000E+01  0.0000000E+00
   13          4.3750000E-01  3.5000000E+00  0.0000000E+00
   14          3.4562500E+01  3.5000000E+00  0.0000000E+00
   15          9.5000000E+00  8.7763157E+00  0.0000000E+00
   16          1.7500000E+01  7.0921054E+00  0.0000000E+00
   17          2.5500000E+01  8.7763157E+00  0.0000000E+00
   18          9.5000000E+00  5.4078951E+00  0.0000000E+00
   19          2.5500000E+01  5.4078951E+00  0.0000000E+00
$$
$$
UNITS  FEET  KIPS  DEG   FAH
$$
$$
TYPE  SPACE FRAME
MEMBER INCIDENCES
   1        6        7
   2        7        8
   3        8        9
   4        9        10
   5        1        13
   6        13       11
   7        11       6
   11       5        14
   12       14       12
   13       12       10
   16       2        18
   17       18       15
   18       15       7
   19       3        16
```

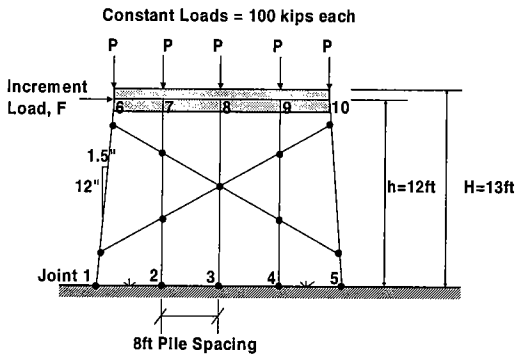

```
  20       16       8
  21       4        19
  22       19       17
  23       17       9
  24       11       15
  25       15       16
  26       16       19
  27       19       14
  28       13       18
  29       18       16
  30       16       17
  31       17       12
$$
$$
UNITS INCH KIPS DEG  FAH
$$
MEMBER PROPERTIES   TABLE 'M/S/HP9 '  'HP10x42            '
  5        6        7        11       12     -
  13       16       17       18       19     -
  20       21       22       23
$$
MEMBER PROPERTIES  PRISMATIC  AX 8.6400024E+02  IX 1.0000008E+07  -
IY 1.0000008E+07  IZ 4.1472023E+04
  1        2        3        4
$$
MEMBER PROPERTIES   TABLE 'CHANNEL9 '  'C4x7.25           '
  24       25       26       27       28     -
  29       30       31
STATUS SUPPORT -
  1        2        3        4        5      -
  6        7        8        9        10
$$
$$
UNITS INCH KIPS DEG  FAH
$$
JOINT RELEASES
  1        2        3        4        5      -
    MOM X  Y  Z
$$
  6        7        8        9        10     -
    FOR X  Y MOM Z
$$
$$
UNITS INCH KIPS DEG  FAH
$$
CONSTANTS
   BETA 0.0  ALL
   BETA 9.0000000E+01 -
  5        6        7        11       12     -
  13       16       17       18       19     -
  20       21       22       23
$$
MEMBER RELEASES
$$
  24       25       26       27       28     -
  29       30       31       -
STA MOM  Y  Z END MOM  Y  Z
$$
UNITS INCH KIPS DEG  FAH
$$
CONSTANTS
   E   2.9000002E+04 ALL
   G   1.1000001E+04 ALL
   POI 3.0000001E-01 ALL
   DEN 2.8330003E-04 ALL
   CTE 6.4999999E-06 ALL
   E   3.6000022E+03 -
  1        2        3        4
   G   1.4400011E+03 -
```

```
   1        2        3        4
    POI  1.7000000E-01  -
   1        2        3        4
    DEN  8.6800042E-05  -
   1        2        3        4
    CTE  5.5000000E-06  -
   1        2        3        4
$$
$$
UNITS  INCH  KIPS  DEG   FAH
$$
LOADING 'incr'
$$
 JOINT LOADS FOR  X   1.0000000E+00
   6
$$
UNITS  INCH  KIPS  DEG   FAH
$$
LOADING 'const'
$$
 JOINT LOADS FOR  Y  -1.0000000E+02
   6        7        8        9        10
$$
$$
 NONLINEAR EFFECTS
$$
  GEOMETRY ALL MEMBERS
$$
  PLASTIC HINGE -
     FIBER GEOMETRY NTF 1 NTW 1 NBF 8 ND 8 LH 3.0 -
     STEEL FY 36.0 ESH .124 ESU .2 FSU 36.001 ALPHA 0.0 MEMBER 5 TO 23
$$
  PLASTIC HINGE -
     FIBER GEOMETRY NTF 1 NTW 1 NBF 8 ND 8 LH 3.0 -
     STEEL FY 16.1 ESH .124 ESU .2 FSU 16.101 ALPHA 0.0 MEMBER 24 TO 27
```

6.7.3 Two Story X-braced Bent Input File

All parameters used in the two story X-braced GTSTRUDL input files are also seen in the one story X-braced input files. The only significant difference between the one and two story X-braced files, is the more complex geometry associated with the two story bent. The complex geometry greatly increases the number of members and joints and also calls for the use of GT MENU to locate the precise joint coordinates of X-member and pile intersections. As seen in the one story input file, the first set of plastic hinge parameters correspond to the H-piles whereas the second PLASTIC HINGE command represents those hinges used in the compression X-members. The X-bracing for the two story bent contains a horizontal strut which divides the upper and lower story and is modeled without axial plastic hinges. Plastic hinges are not required for the strut because only small axial loads are expected in this member and any compression

forces that may develop are not expected to reach its buckling capacity, since it is composed of two angle members welded together with battens to prevent buckling.

Example Two Story X-braced Bent GTSTRUDL Input File

```
STRUDL ' '
$$
$$    This  GTSTRUDL file created from GTMenu on 11/21/2004
$$
$$
UNITS  FEET  KIPS  DEG   FAH
$$
$$
JOINT COORDINATES GLOBAL
   1          0.0000000E+00  0.0000000E+00  0.0000000E+00
   2          1.1000000E+01  0.0000000E+00  0.0000000E+00
   3          1.9000000E+01  0.0000000E+00  0.0000000E+00
   4          2.7000000E+01  0.0000000E+00  0.0000000E+00
   5          3.8000000E+01  0.0000000E+00  0.0000000E+00
   6          3.0000000E+00  2.4000000E+01  0.0000000E+00
   7          1.1000000E+01  2.4000000E+01  0.0000000E+00
   8          1.9000000E+01  2.4000000E+01  0.0000000E+00
   9          2.7000000E+01  2.4000000E+01  0.0000000E+00
   10         3.5000000E+01  2.4000000E+01  0.0000000E+00
   11         2.8125000E+00  2.2500000E+01  0.0000000E+00
   12         3.5187500E+01  2.2500000E+01  0.0000000E+00
   13         2.0000000E+00  1.6000000E+01  0.0000000E+00
   14         3.6000000E+01  1.6000000E+01  0.0000000E+00
   15         1.9375000E+00  1.5500000E+01  0.0000000E+00
   16         3.6062500E+01  1.5500000E+01  0.0000000E+00
   17         1.8750000E+00  1.5000000E+01  0.0000000E+00
   18         3.6125000E+01  1.5000000E+01  0.0000000E+00
   19          4.3750000E-01  3.5000000E+00  0.0000000E+00
   20         3.7562500E+01  3.5000000E+00  0.0000000E+00
   21         1.1000000E+01  2.0896423E+01  0.0000000E+00
   22         1.9000000E+01  1.9329567E+01  0.0000000E+00
   23         2.7000000E+01  2.0896423E+01  0.0000000E+00
   24         1.1000000E+01  1.7762712E+01  0.0000000E+00
   25         2.7000000E+01  1.7762712E+01  0.0000000E+00
   26         1.1000000E+01  1.5500000E+01  0.0000000E+00
   27         1.9000000E+01  1.5500000E+01  0.0000000E+00
   28         2.7000000E+01  1.5500000E+01  0.0000000E+00
   29         1.1000000E+01  1.2059546E+01  0.0000000E+00
   30         1.9000000E+01  9.4816122E+00  0.0000000E+00
   31         2.7000000E+01  1.2059546E+01  0.0000000E+00
   32         1.1000000E+01  6.9036779E+00  0.0000000E+00
   33         2.7000000E+01  6.9036779E+00  0.0000000E+00
$$
$$
UNITS  INCH  KIPS  DEG   FAH
$$
$$
$$
TYPE  SPACE FRAME
MEMBER INCIDENCES
  1        6        7
  2        7        8
  3        8        9
  4        9        10
  5        1        19
  6        19       17
  7        17       15
  8        15       13
  9        13       11
```

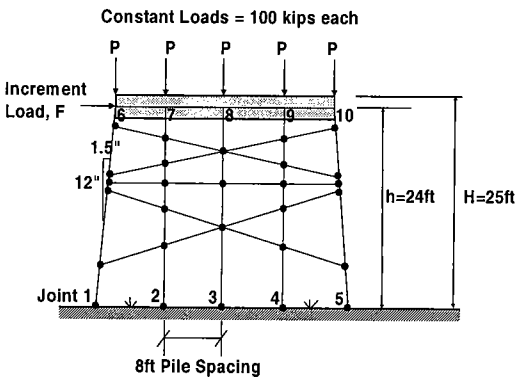

```
  10      11      6
  14      5       20
  15      20      18
  16      18      16
  17      16      14
  18      14      12
  19      12      10
  25      2       32
  26      32      29
  27      29      26
  28      26      24
  29      24      21
  30      21      7
  31      3       30
  32      30      27
  33      27      22
  34      22      8
  35      4       33
  36      33      31
  37      31      28
  38      28      25
  39      25      23
  40      23      9
  41      11      21
  42      21      22
  43      22      25
  44      25      14
  45      13      24
  46      24      22
  47      22      23
  48      23      12
  49      15      26
  50      26      27
  51      27      28
  52      28      16
  53      17      29
  54      29      30
  55      30      33
  56      33      20
  57      19      32
  58      32      30
  59      30      31
  60      31      18
$$
$$
UNITS  INCH  KIPS  DEG   FAH
$$
MEMBER PROPERTIES   TABLE 'M/S/HP9 '  'HP10x42              '
  5       6       7       8       9       -
  10      14      15      16      17      -
  18      19      25      26      27      -
  28      29      30      31      32      -
  33      34      35      36      37      -
  38      39      40
$$
MEMBER PROPERTIES  PRISMATIC  AX 8.6400006E+02  IX 1.0000002E+07   -
IY 1.0000002E+07  IZ 4.1472004E+04
  1       2       3       4
$$
MEMBER PROPERTIES   TABLE 'CHANNEL9'  'C4x7.25              '
  41      42      43      44      45      -
  46      47      48      49      50      -
  51      52      53      54      55      -
  56      57      58      59      60
$$
STATUS SUPPORT -
  1       2       3       4       5       -
  6       7       8       9       10
$$
```

```
$$
UNITS INCH KIPS DEG FAH
$$
JOINT RELEASES
  1      2      3      4      5      -
    MOM X Y Z
$$
  6      7      8      9      10     -
    FOR X Y MOM Z
$$
$$
UNITS INCH KIPS DEG FAH
$$
CONSTANTS
   BETA 0.0 ALL
   BETA 9.0000000E+01 -
  5      6      7      8      9      -
  10     14     15     16     17     -
  18     19     25     26     27     -
  28     29     30     31     32
   BETA 9.0000000E+01 -
  33     34     35     36     37     -
  38     39     40
$$
MEMBER RELEASES
$$
  41     42     43     44     45     -
  46     47     48     49     50     -
  51     52     53     54     55     -
  56     57     58     59     60     -
STA MOM Y Z END MOM Y Z
$$
UNITS INCH KIPS DEG FAH
$$
CONSTANTS
   E  2.9000004E+04 ALL
   G  1.1000002E+04 ALL
   POI 3.0000001E-01 ALL
   DEN 2.8330006E-04 ALL
   CTE 6.4999999E-06 ALL
   E  3.6000017E+03 -
  1      2      3      4
   G  1.4400009E+03 -
  1      2      3      4
   POI 1.7000000E-01 -
  1      2      3      4
   DEN 8.6800042E-05 -
  1      2      3      4
   CTE 5.5000000E-06 -
  1      2      3      4
$$
$$
UNITS INCH KIPS DEG FAH
$$
LOADING 'incr'
$$
 JOINT LOADS FOR X  1.00000000E+00
  6
$$
UNITS INCH KIPS DEG FAH
$$
LOADING 'const'
$$
 JOINT LOADS FOR Y -1.0000000E+02
  6      7      8      9      10
$$
$$
 NONLINEAR EFFECTS
$$
```

```
  GEOMETRY ALL MEMBERS

$$
  PLASTIC HINGE -
     FIBER GEOMETRY NTF 1 NTW 1 NBF 8 ND 8 LH 3.0 -
     STEEL FY 36.0 ESH .124 ESU .2 FSU 36.001 ALPHA 0.0 MEMBER 5 to 40
$$
  PLASTIC HINGE -
     FIBER GEOMETRY NTF 1 NTW 1 NBF 8 ND 8 LH 3.0 -
     STEEL FY 16.1 ESH .124 ESU .2 FSU 16.101 ALPHA 0.0 MEMBER 41 TO 44 53 to 56
```

Table 6.1 Comparison of Non X-braced Bent Buckling Capacities using $P_e \approx \frac{0.5\pi^2 EI}{L^2}$ and GTSTRDUL Pushover Analysis Procedure

Scour, S (ft) Original H=13ft	$P_e \approx \frac{0.5\pi^2 EI}{L^2}$	P_{CR} from GTSTRUDL Pushover Analysis (Buckling) Procedure			
		3-Pile Bent	4-Pile Bent	5-Pile Bent	6-Pile Bent
0	421.6	320	405	400	380
5	219.9	180	300	300	280
10	134.7	120	255	255	240
15	90.9	85	220	240	220
20	65.4	65	200	220	210

* Note Elastic Buckling is Expected for Shaded Values Only Since $P_e < P_y/2$

a) HP 10x42 Pile Bents

Scour, S (ft) Original H=13ft	$P_e \approx \frac{0.5\pi^2 EI}{L^2}$	P_{CR} from GTSTRUDL Pushover Analysis (Buckling) Procedure			
		3-Pile Bent	4-Pile Bent	5-Pile Bent	6-Pile Bent
0	746.8	519	550	550	546
5	389.6	315	435	420	390
10	238.6	210	345	353	315
15	161.0	150	300	315	285
20	115.9	110	270	300	260

* Note Elastic Buckling is Expected for Shaded Values Only Since $P_e < P_y/2$

b) HP 12x53 Pile Bents

Table 6.2 Comparison of One Story X-braced Bent Buckling Capacities using $P_e \approx \frac{2\pi^2 EI}{L^2}$ and GTSTRDUL Pushover Analysis Procedure

Scour, S (ft) Original H=13ft	$P_e \approx \frac{2\pi^2 EI}{L^2}$	P_{CR} from GTSTRUDL Pushover Analysis (Buckling) Procedure				
		3-Pile Bent	4-Pile Bent	5-Pile Bent	6-Pile Bent single X-braced	6-Pile Bent double X-braced
0	1686.5	453	441	442	442	445
5	879.7	320	360	345	330	360
10	538.8	173	248	255	240	242
15	363.6	110	200	218	203	210
20	261.7	76	178	205	190	200

*Note Inelastic Buckling Controls for Each Bent Since $P_e > P_y/2$

a) HP 10x42 Pile Bents

Scour, S (ft) Original H=13ft	$P_e \approx \frac{2\pi^2 EI}{L^2}$	P_{CR} from GTSTRUDL Pushover Analysis (Buckling) Procedure				
		3-Pile Bent	4-Pile Bent	5-Pile Bent	6-Pile Bent single X-braced	6-Pile Bent double X-braced
0	2987.3	551	554	554	553	555
5	1558.2	527	532	520	480	534
10	954.4	300	370	370	331	360
15	644.0	191	293	315	285	300
20	463.6	136	255	280	253	270

*Note Inelastic Buckling Controls for Each Bent Since $P_e > P_y/2$

b) HP 12x53 Pile Bents

Table 6.3 Comparison of Two Story X-braced Bent Buckling Capacities using $P_e \approx \frac{2\pi^2 EI}{L^2}$ and GTSTRDUL Pushover Analysis Procedure

Scour, S (ft) Original H=25ft	$P_e \approx \frac{2\pi^2 EI}{L^2}$	P_{CR} from GTSTRUDL Pushover Analysis (Buckling) Procedure				
		3-Pile Bent	4-Pile Bent	5-Pile Bent	6-Pile Bent single X-braced	6-Pile Bent double X-braced
0	456.0	437	436	439	439	443
5	316.7	245	265	270	255	315
10	232.7	143	180	195	195	225
15	178.1	90	150	170	165	190
20	140.8	65	130	160	160	180

*Note Elastic Buckling is Expected for Shaded Values Only Since $P_e < P_y/2$

a) HP 10x42 Pile Bents

Scour, S (ft) Original H=25ft	$P_e \approx \frac{2\pi^2 EI}{L^2}$	P_{CR} from GTSTRUDL Pushover Analysis (Buckling) Procedure				
		3-Pile Bent	4-Pile Bent	5-Pile Bent	6-Pile Bent single X-braced	6-Pile Bent double X-braced
0	807.8	549	552	554	554	554
5	561.0	425	440	423	400	492
10	412.1	240	285	300	285	320
15	315.5	158	225	248	240	270
20	249.3	115	190	220	210	240

*Note Elastic Buckling is Expected for Shaded Values Only Since $P_e < P_y/2$

b) HP 12x53 Pile Bents

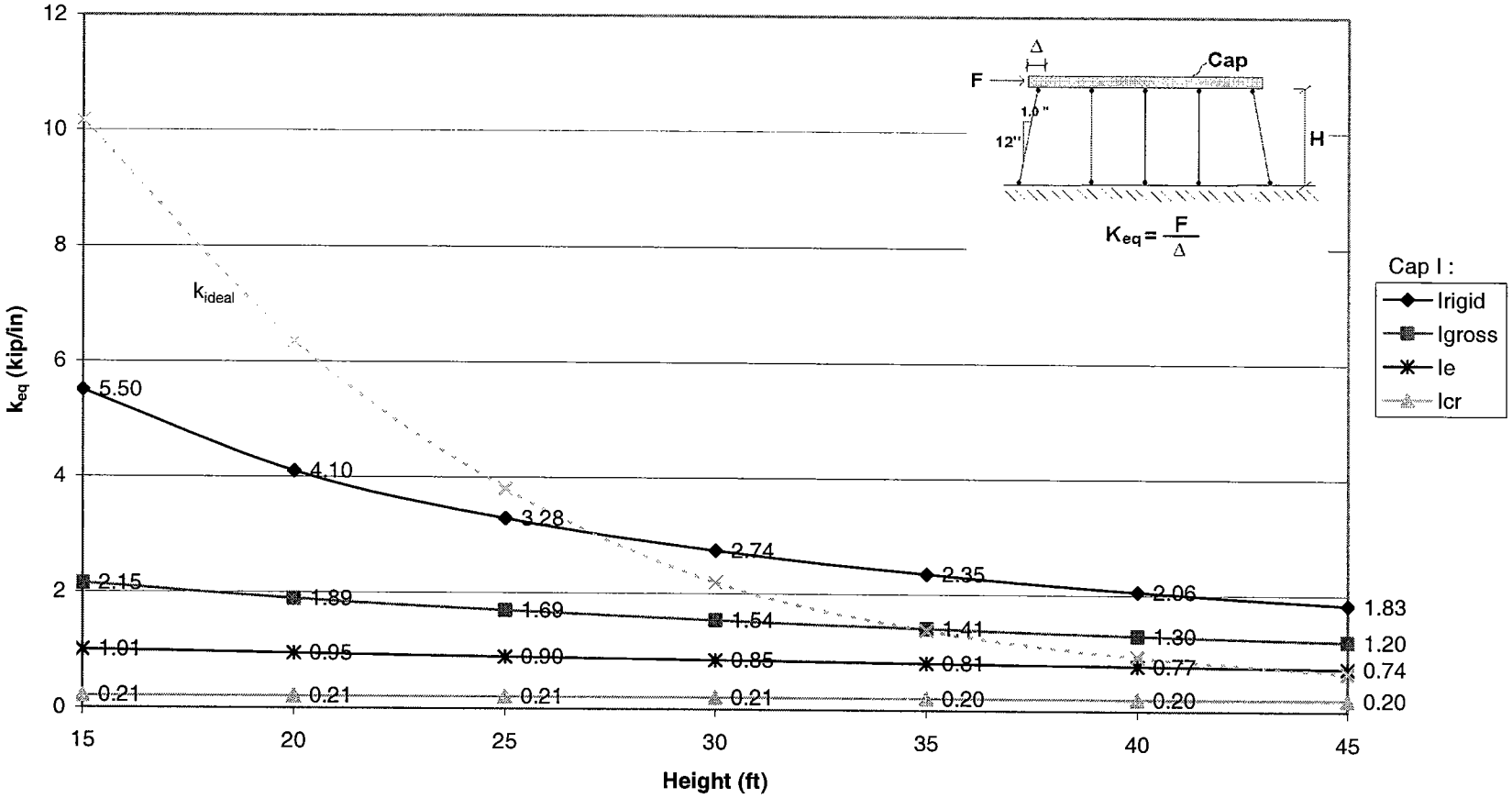

Figure 6.1. GTSTRUDL k_{eq} vs Bent Height for 5-Pile Bent with HP10x42 Piles (1.0" Batter) Piles Pinned to Cap/ Pinned at Ground

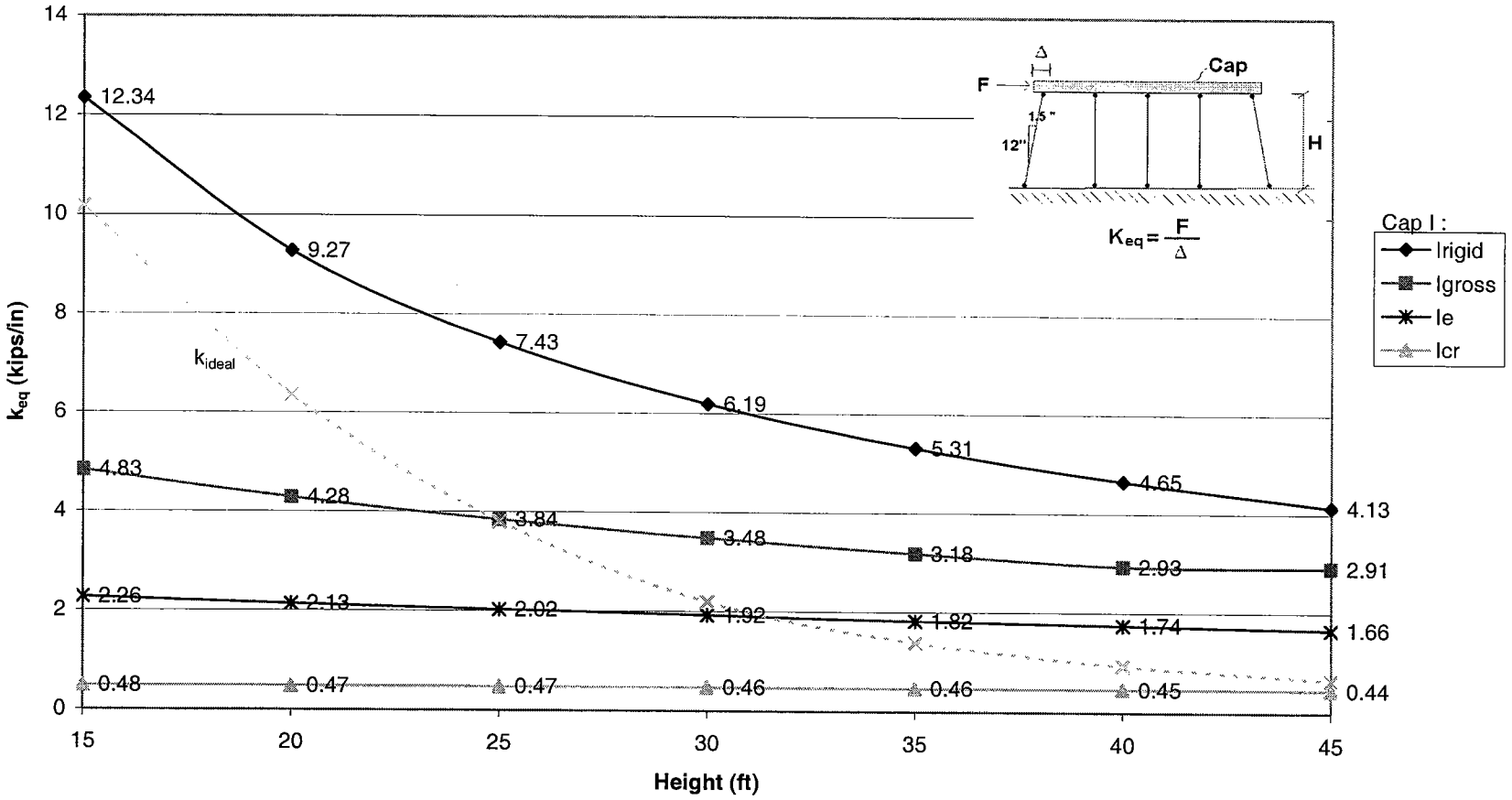

Figure 6.2. GTSTRUDL k_{eq} vs Bent Height for 5-Pile Bent with HP10x42 Piles (1.5" Batter) Pinned Connections to Cap/ Pinned at Ground

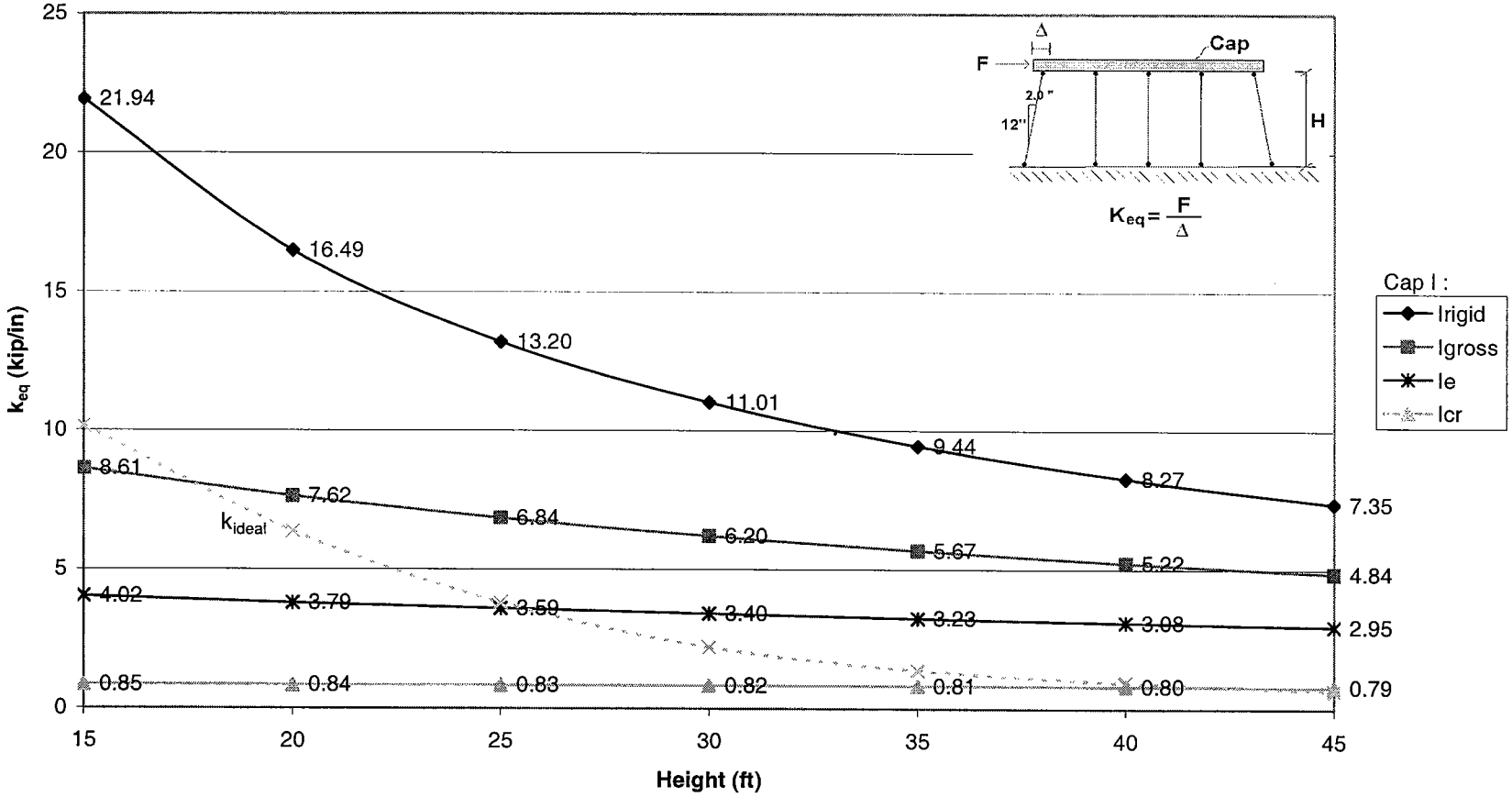

Figure 6.3. GTSTRUDL k_{eq} vs Bent Height for 5-Pile Bent with HP10x42 Piles (2.0in Batter) Pinned Connections to Cap/ Pinned at Ground

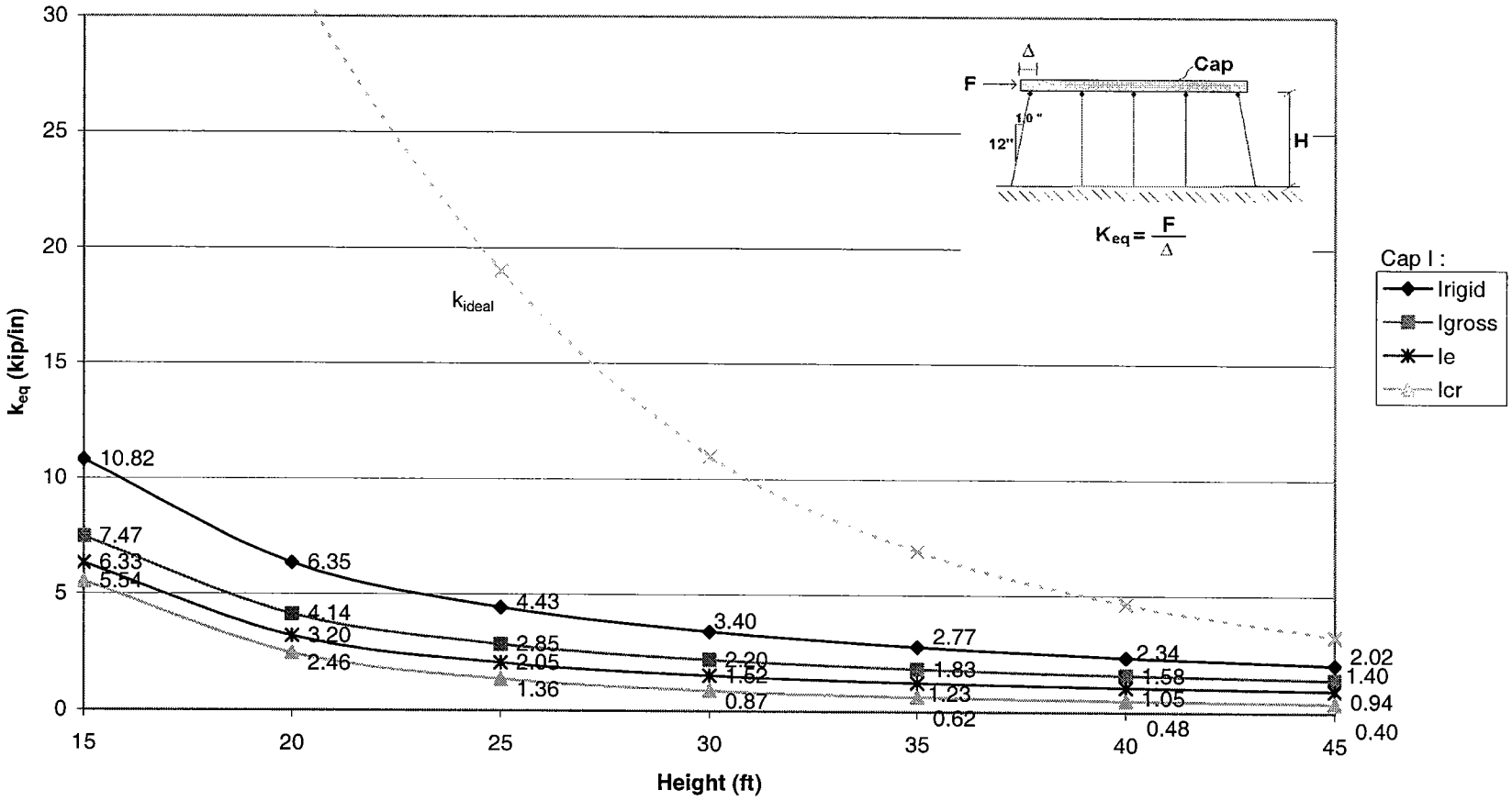

Figure 6.4. GTSTRUDL k_{eq} vs Bent Height for 5-Pile Bent with HP10x42 Piles (1.0" Batter) Pinned Connections to Cap/ Fixed at Ground

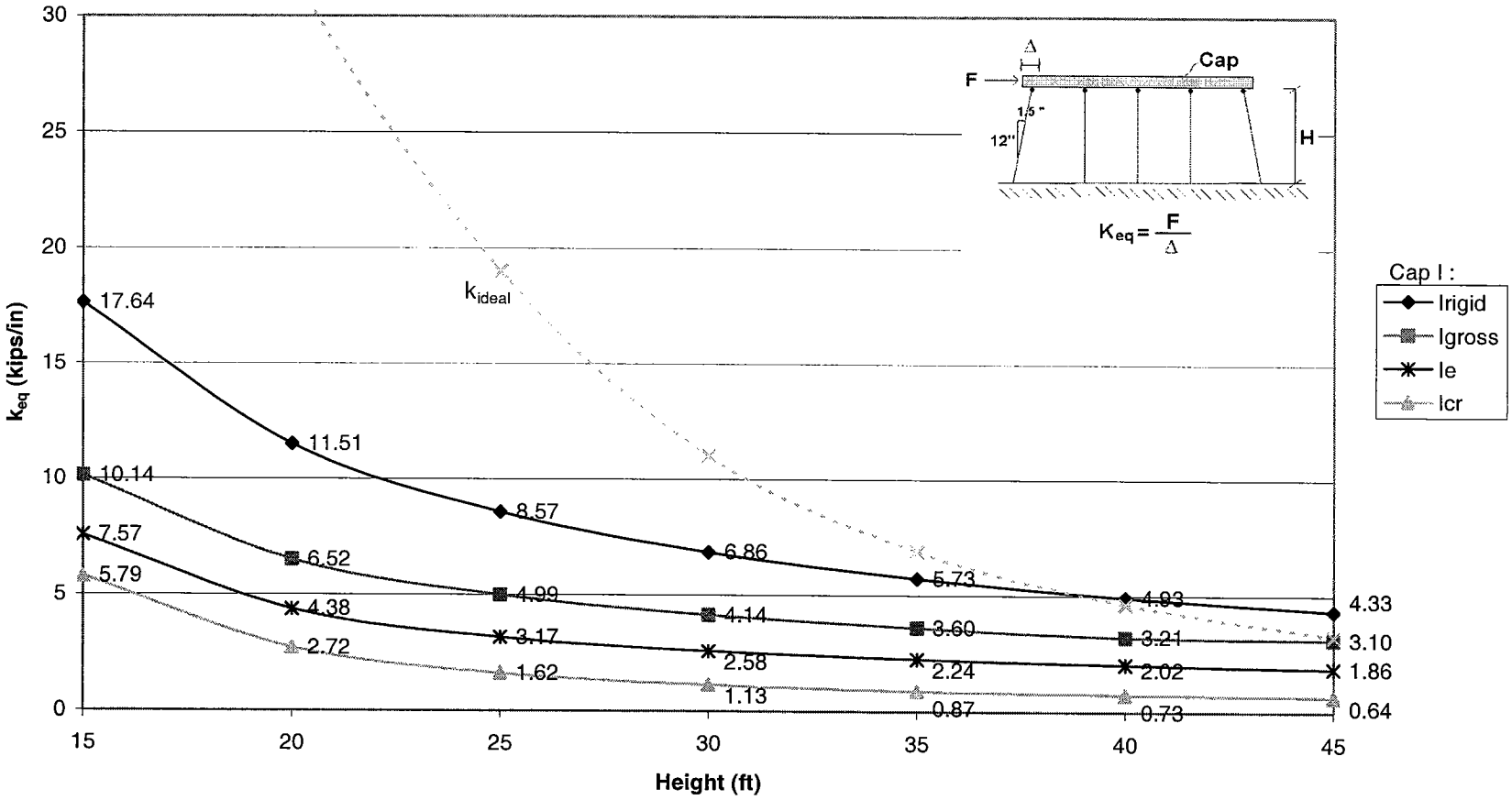

Figure 6.5. GTSTRUDL k_{eq} vs Bent Height for 5-Pile Bent with HP10x42 Piles (1.5" Batter) Pinned Connections to Cap/ Fixed at Ground

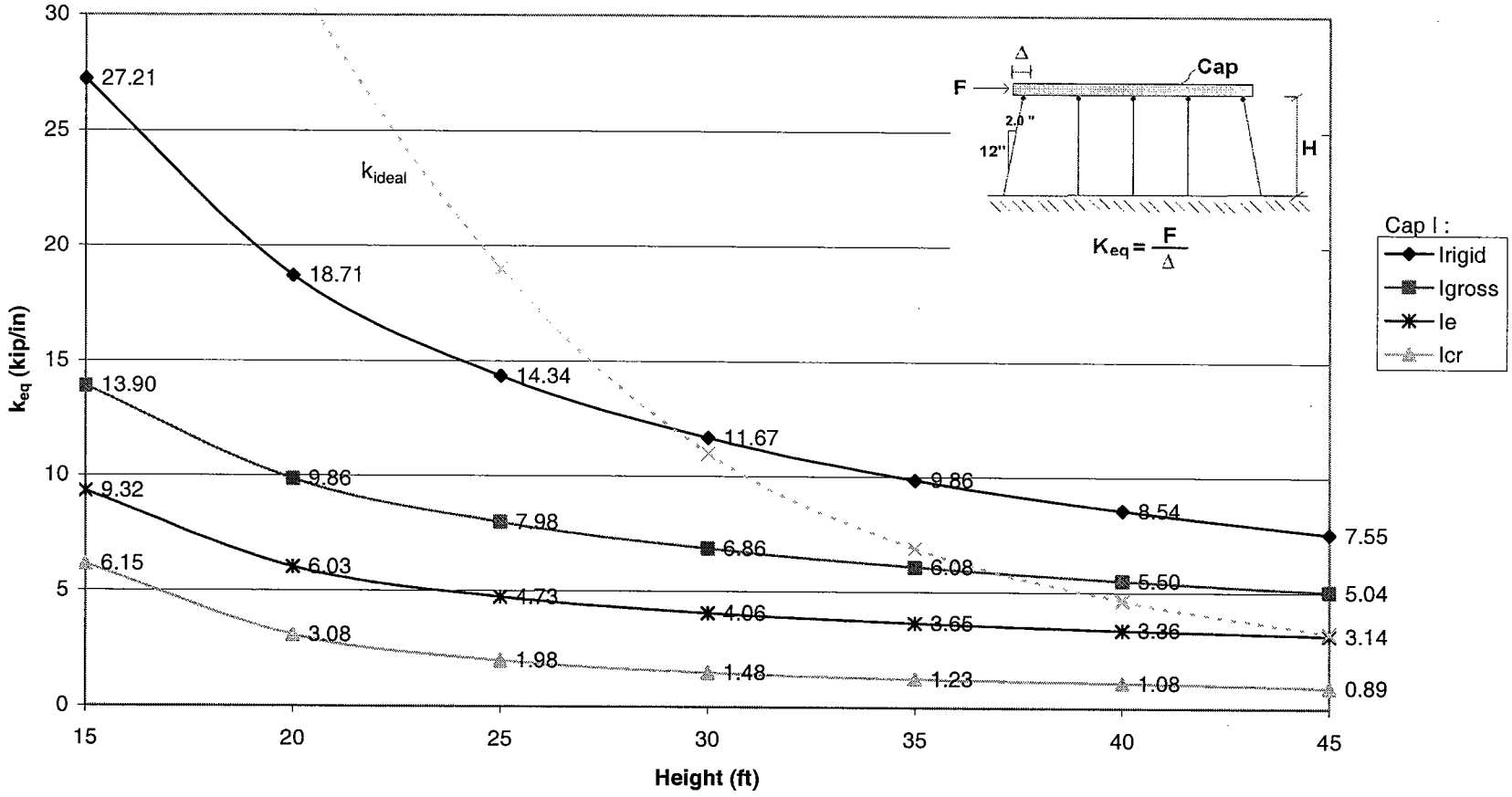

Figure 6.6. GTSTRUDL k_{eq} vs Bent Height for 5-Pile Bent with HP10x42 Piles (2.0" Batter) Pinned Connections to Cap/ Fixed at Ground

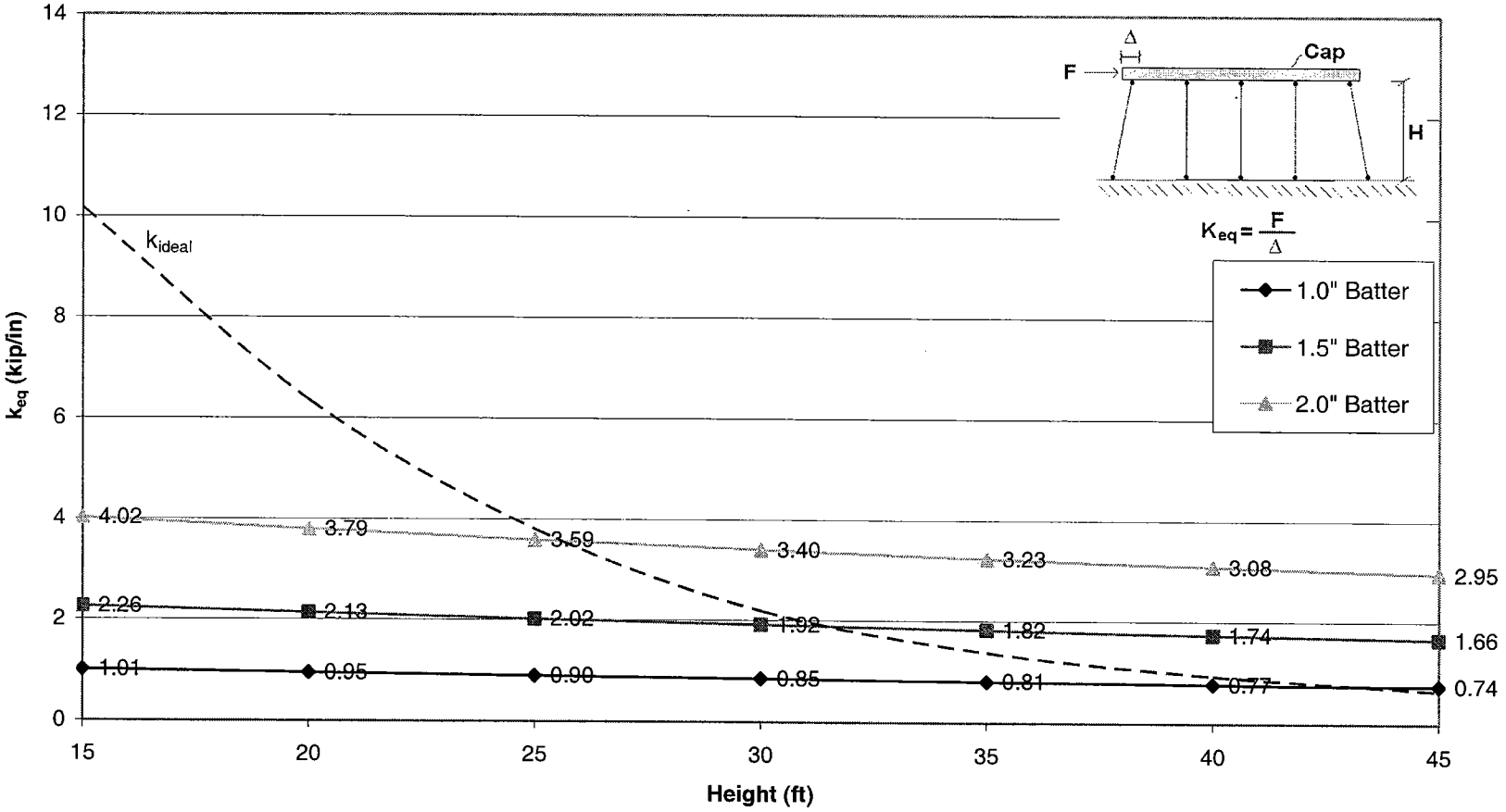

Figure 6.7. Effects of End Pile Battering and Bent Height on k_{eq} for 5-Pile Bent with HP10x42 Piles, Cap I = I_e, Pinned Connections at Cap/ Pinned at Ground

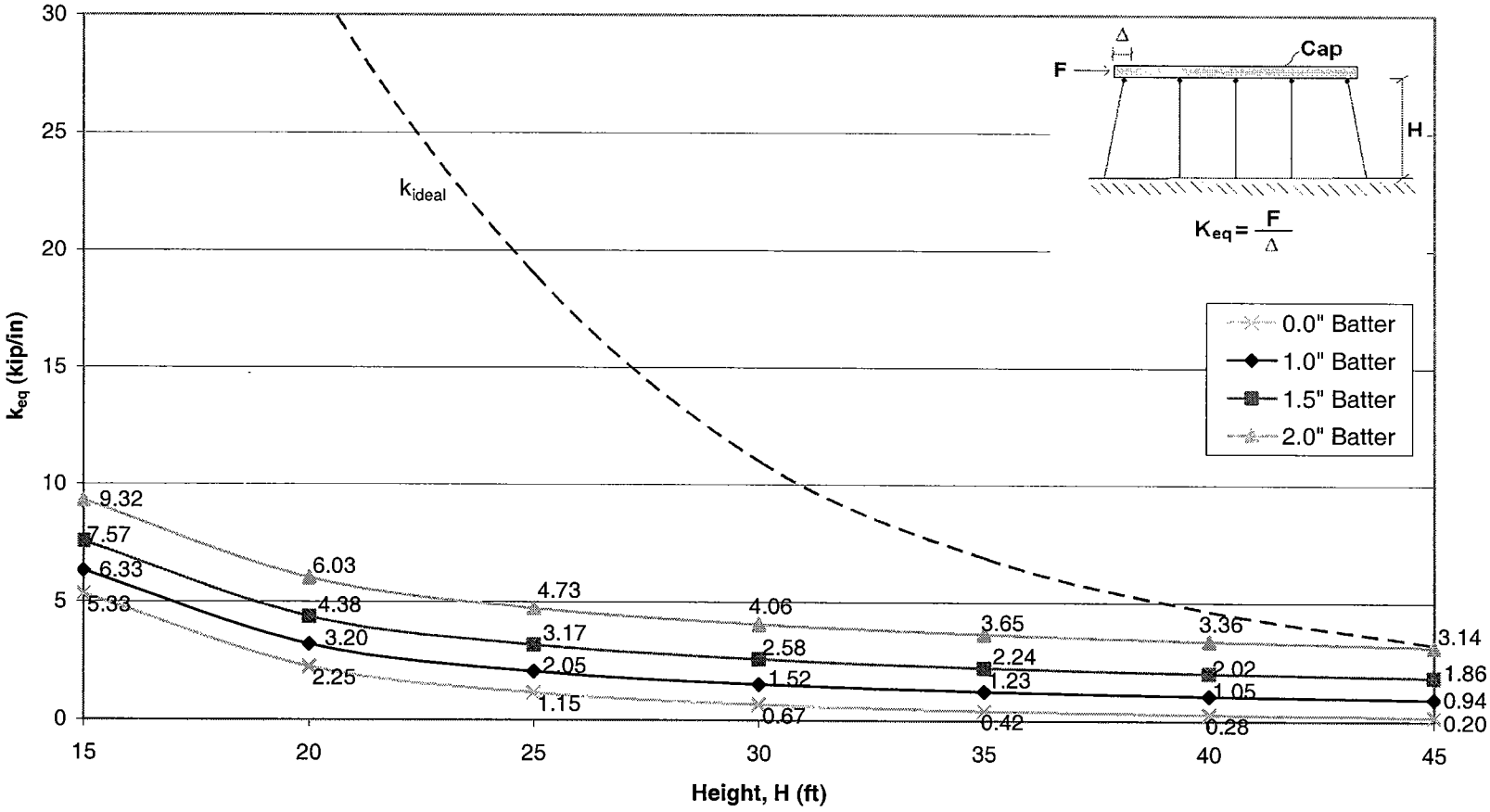

Figure 6.8. Effects of End Pile Battering and Bent Height on k_{eq} for 5-Pile Bent with HP10x42 Piles, Cap I = I_e, Pinned Connections at Cap/ Fixed at Ground

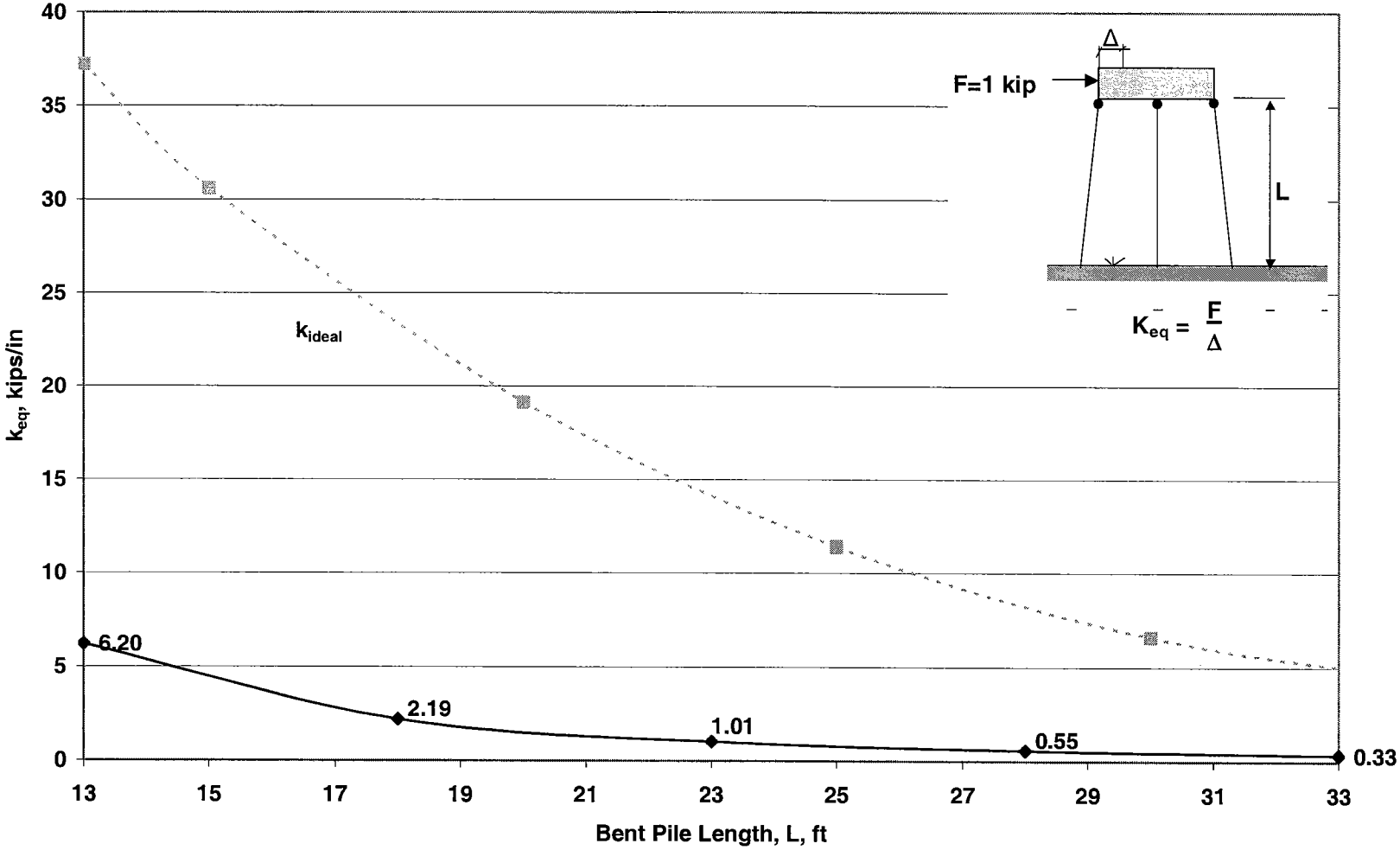

Figure 6.9. GTSTRUDL k_{eq} vs L for HP10x42 3-Pile Bent (1.5in Batter), Cap $I=I_{gross}$, Pinned to Cap/ Fixed at Ground

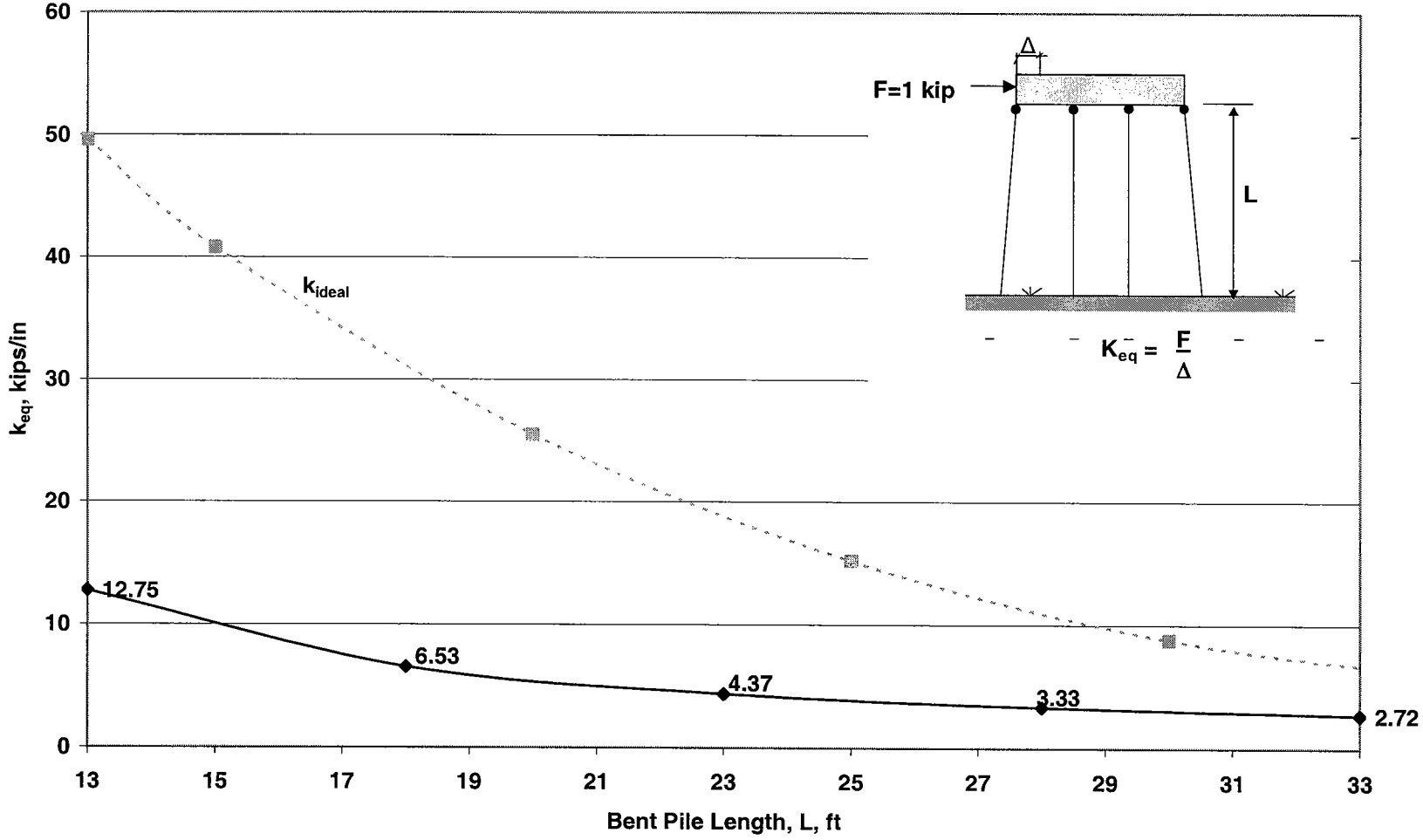

Figure 6.10. GTSTRUDL k_{eq} vs L for HP10x42 4-Pile Bent (1.5in Batter), Cap I=I_{gross}, Pinned to Cap/ Fixed at Ground

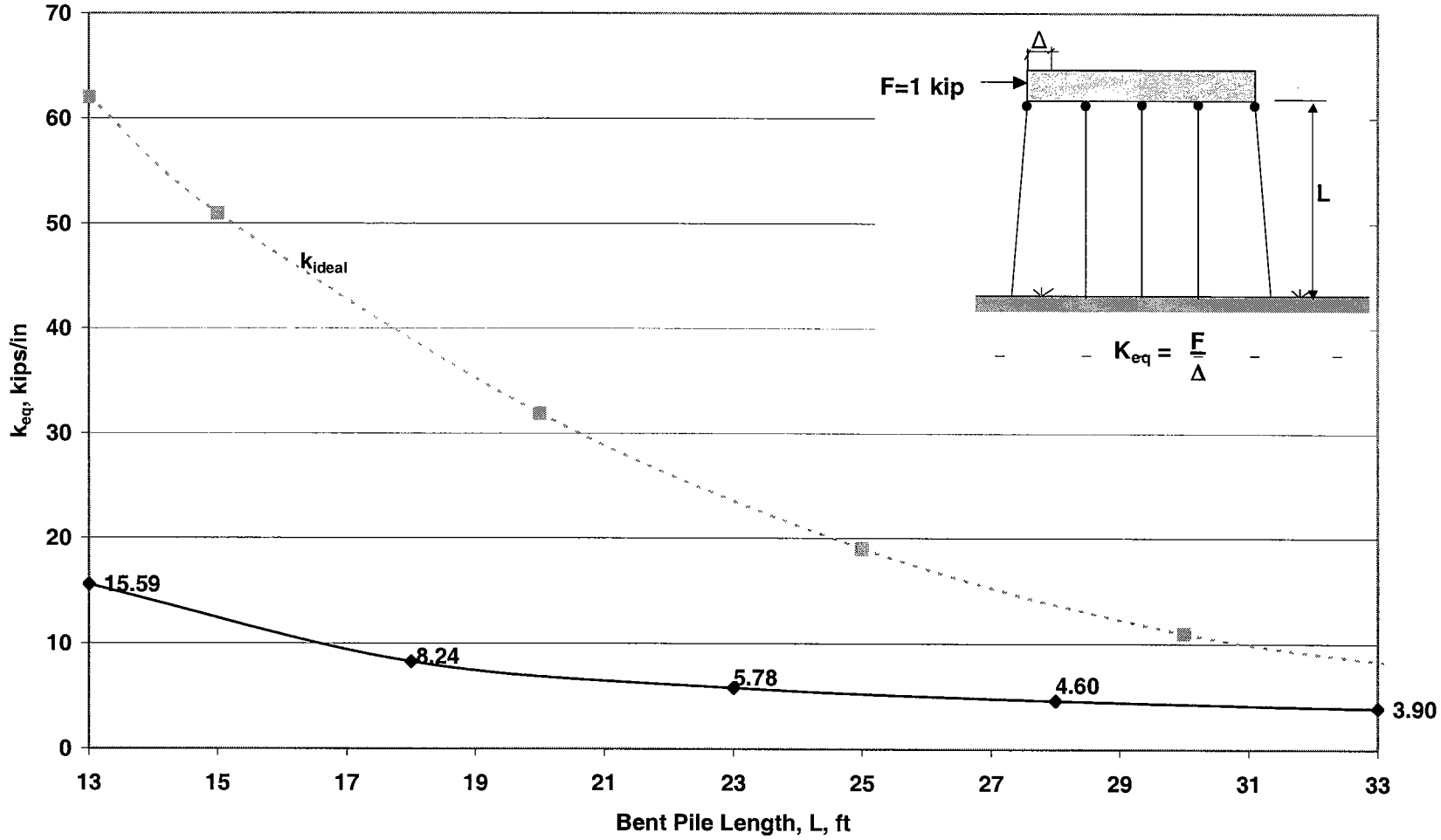

Figure 6.11. GTSTRUDL k_{eq} vs L for HP10x42 5-Pile Bent (1.5in Batter), Cap I=I_{gross}, Pinned to Cap/ Fixed at Ground

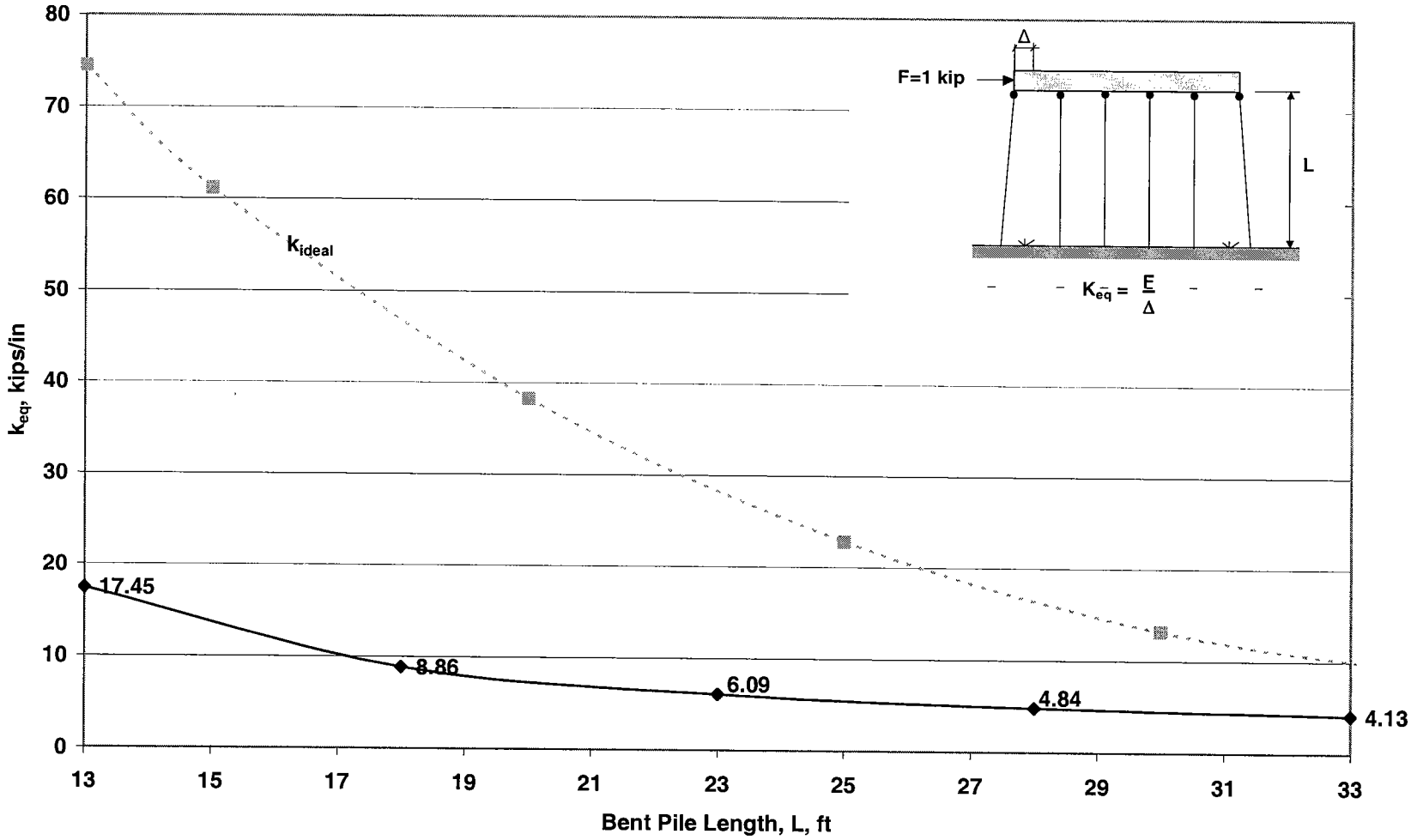

Figure 6.12. GTSTRUDL k_{eq} vs L for HP10x42 6-Pile Bent (1.5in Batter), Cap $I=I_{gross}$, Pinned to Cap/ Fixed at Ground

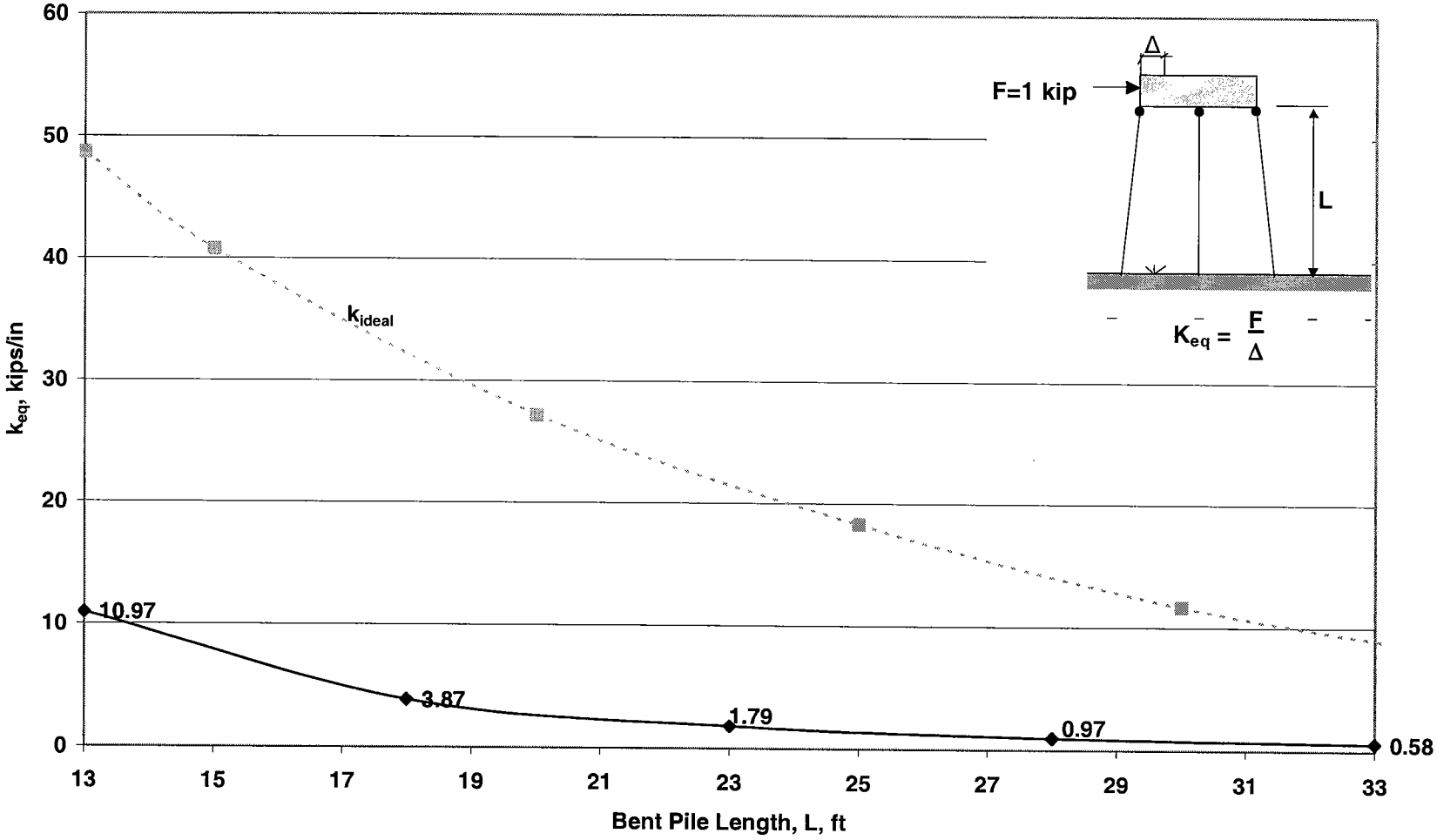

Figure 6.13. GTSTRUDL k_{eq} vs L for HP12x53 3-Pile Bent (1.5in Batter), Cap $I=I_{gross}$, Pinned to Cap/ Fixed at Ground

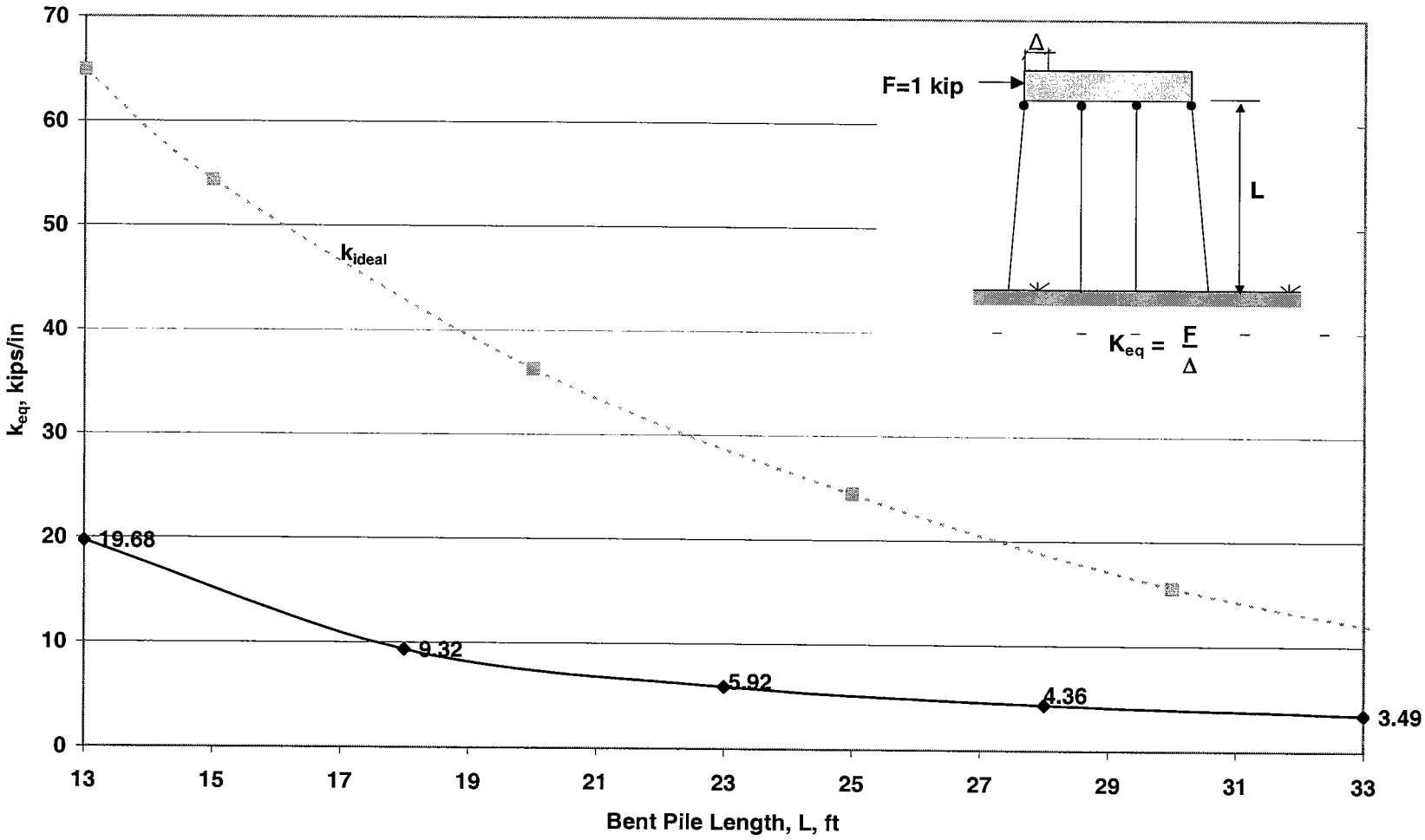

Figure 6.14. GTSTRUDL k_{eq} vs L for HP12x53 4-Pile Bent (1.5in Batter), Cap $I=I_{gross}$, Pinned to Cap/ Fixed at Ground

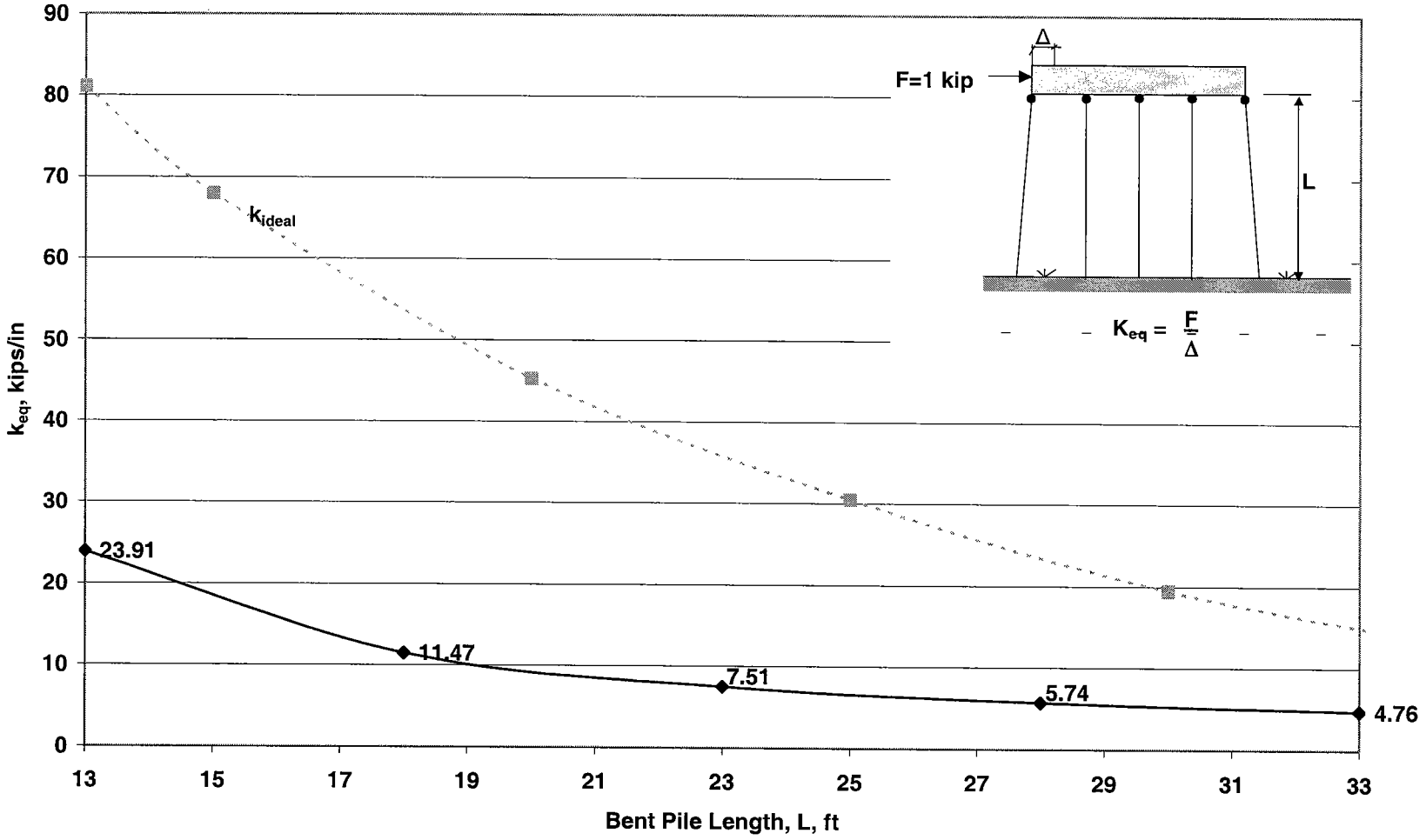

Figure 6.15. GTSTRUDL k_{eq} vs L for HP12x53 5-Pile Bent (1.5in Batter), Cap I=I_{gross}, Pinned to Cap/ Fixed at Ground

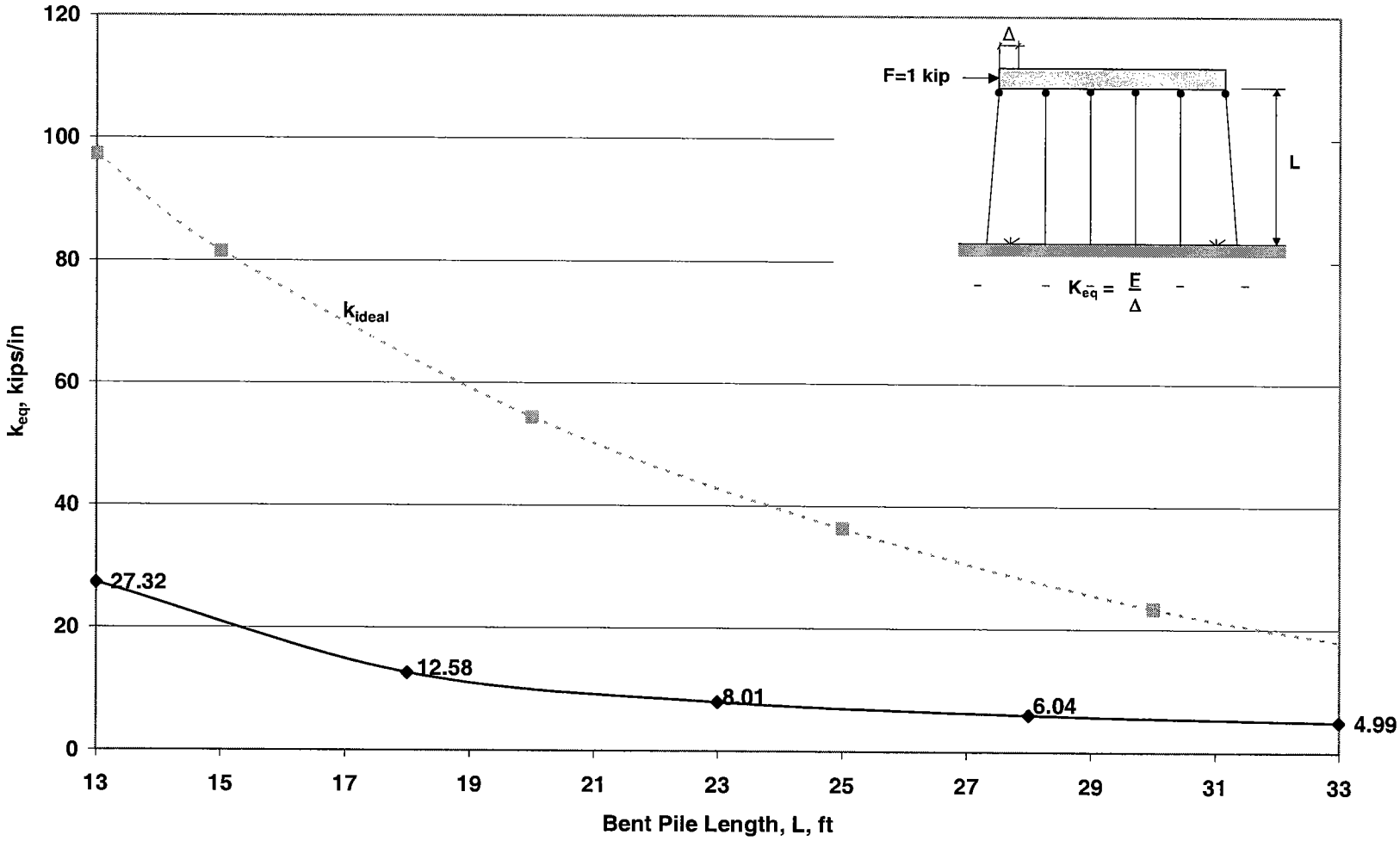

Figure 6.16. GTSTRUDL k_{eq} vs L for HP12x53 6-Pile Bent (1.5in Batter), Cap I=I_{gross}, Pinned to Cap/ Fixed at Ground

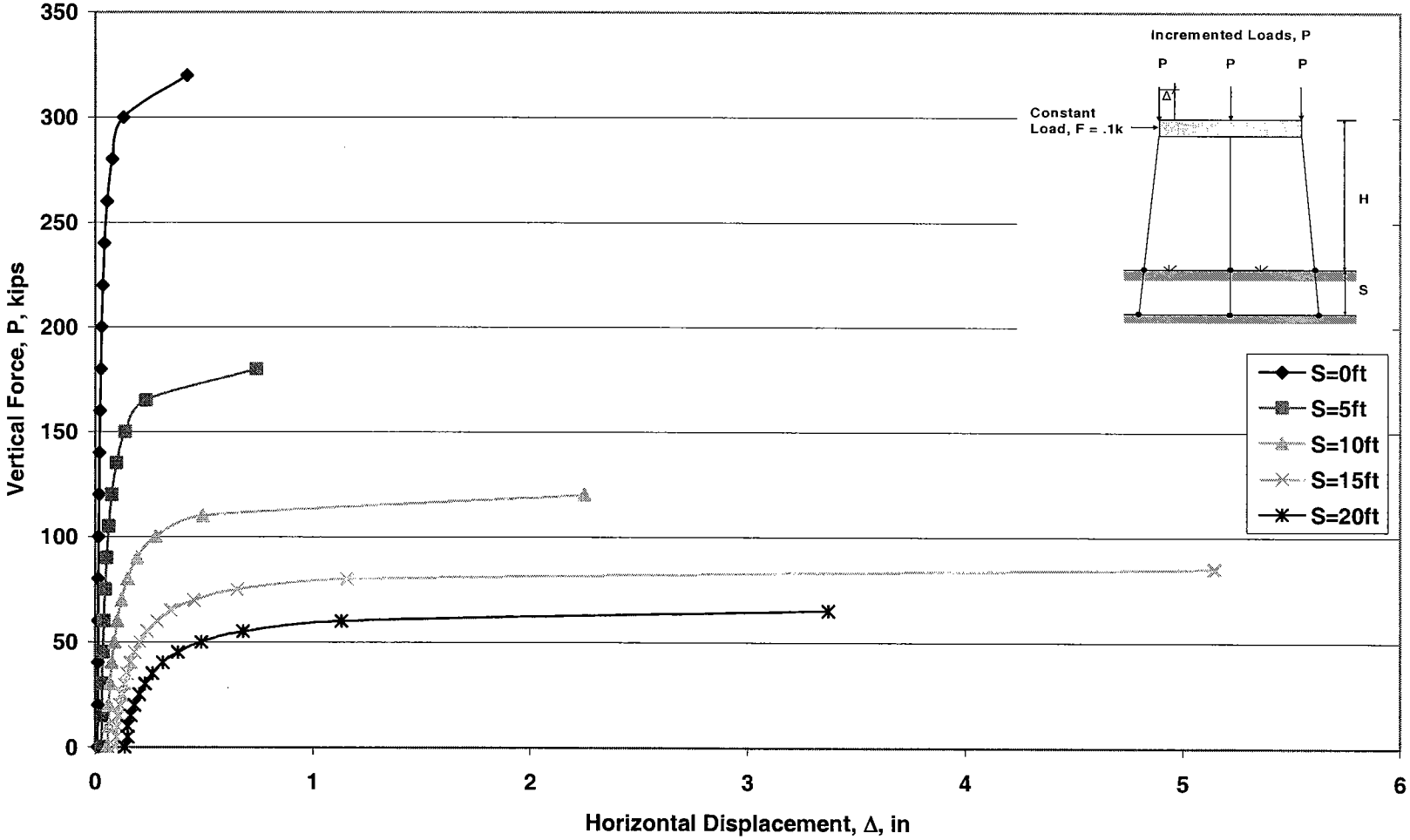

Figure 6.17a. GTSTRUDL Buckling Analysis of HP10x42 3-Pile Bent Subjected to Scour, H=13ft

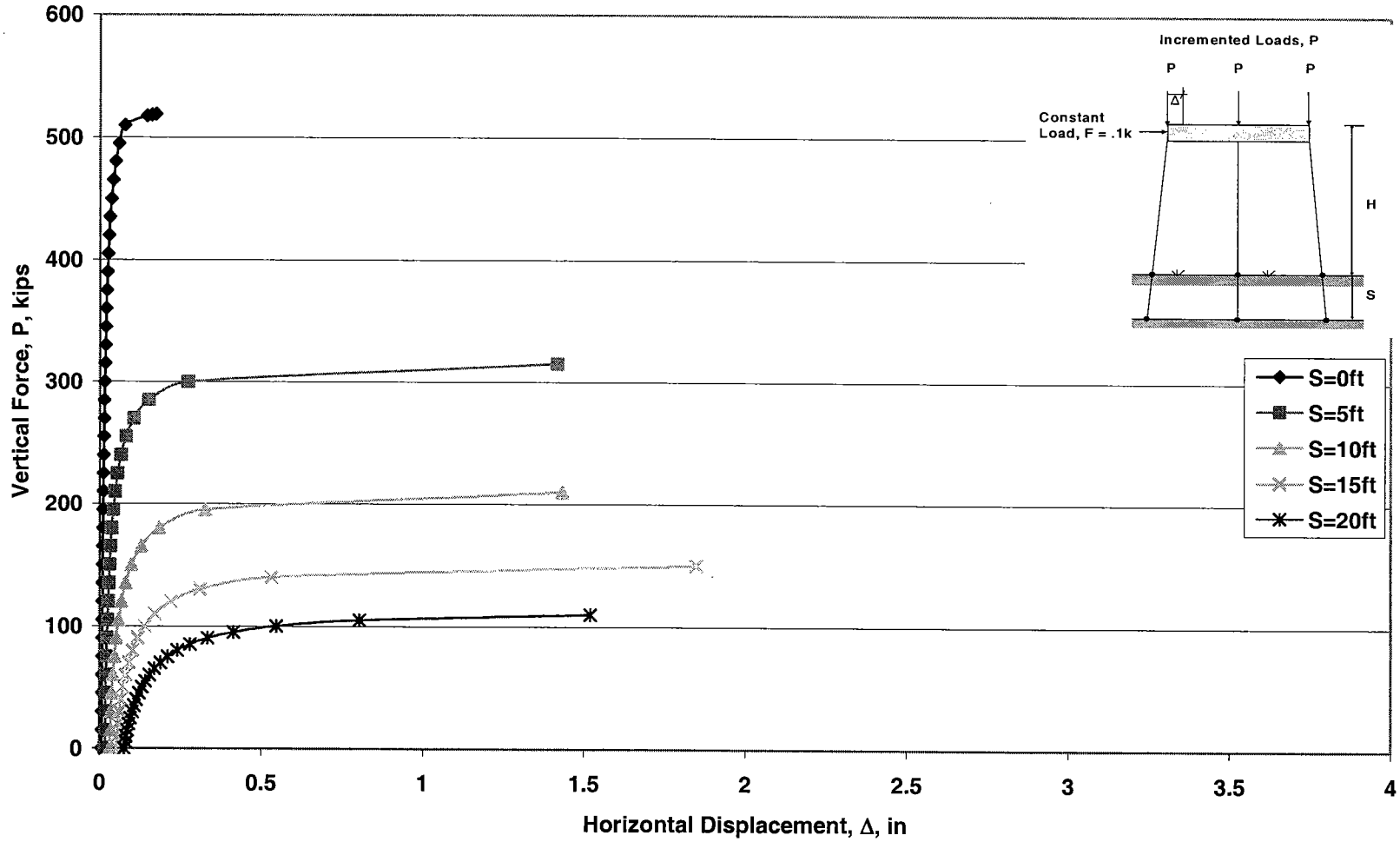

Figure 6.17b. GTSTRUDL Buckling Analysis of HP12x53 3-Pile Bent Subjected to Scour, H=13ft

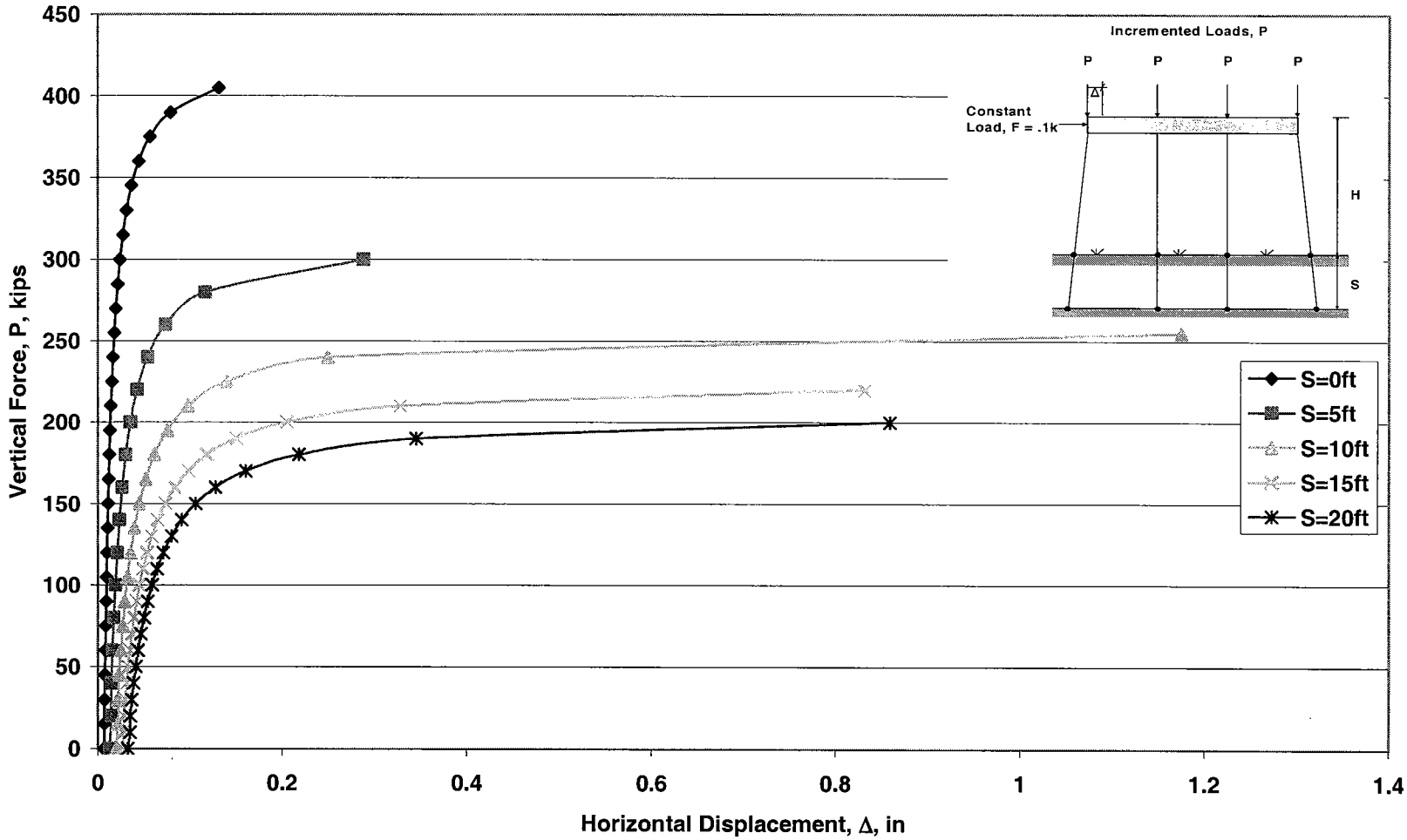

Figure 6.18a. GTSTRUDL Buckling Analysis of HP10x42 4-Pile Bent Subjected to Scour, H=13ft

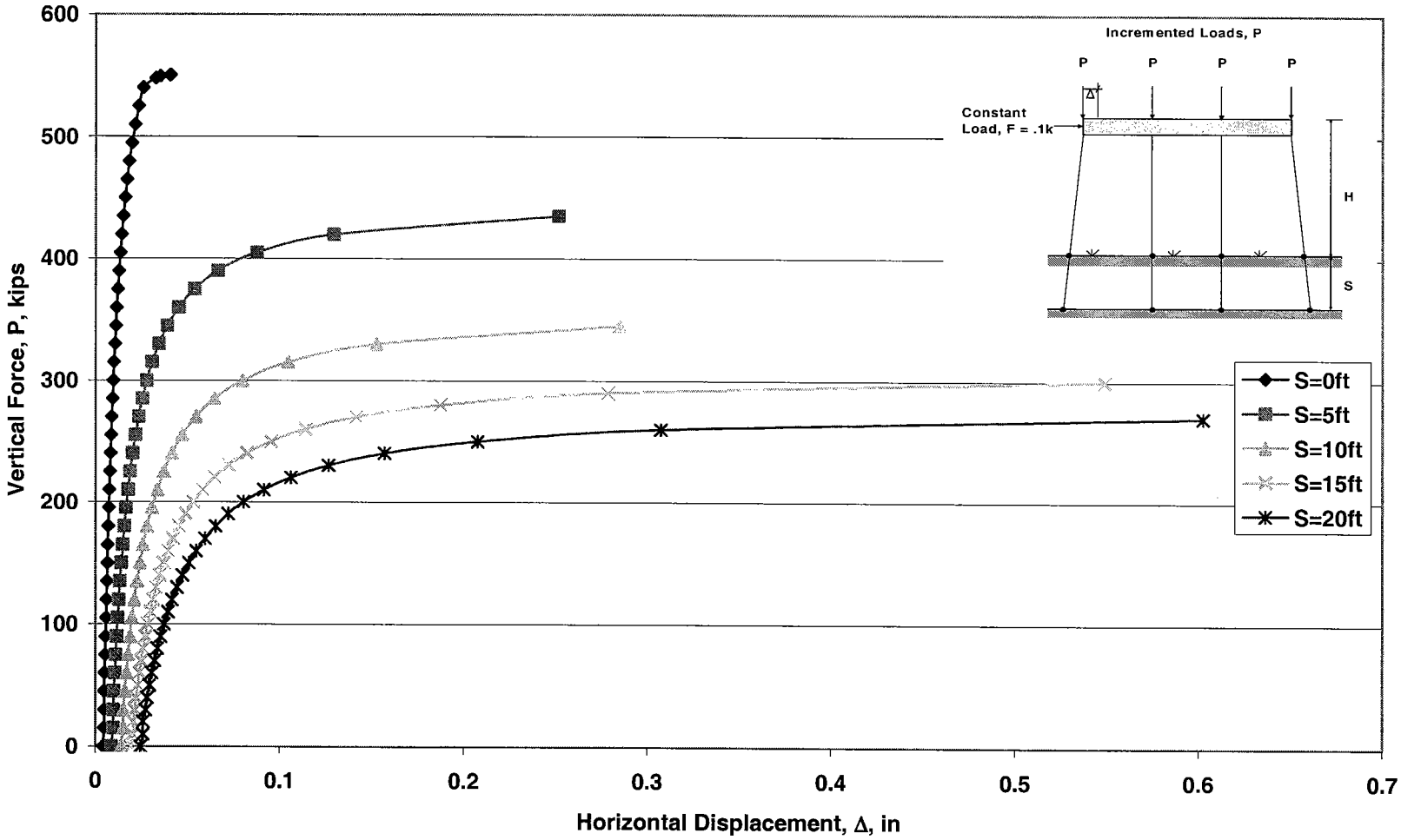

Figure 6.18b. GTSTRUDL Buckling Analysis of HP12x53 4-Pile Bent Subjected to Scour, H=13ft

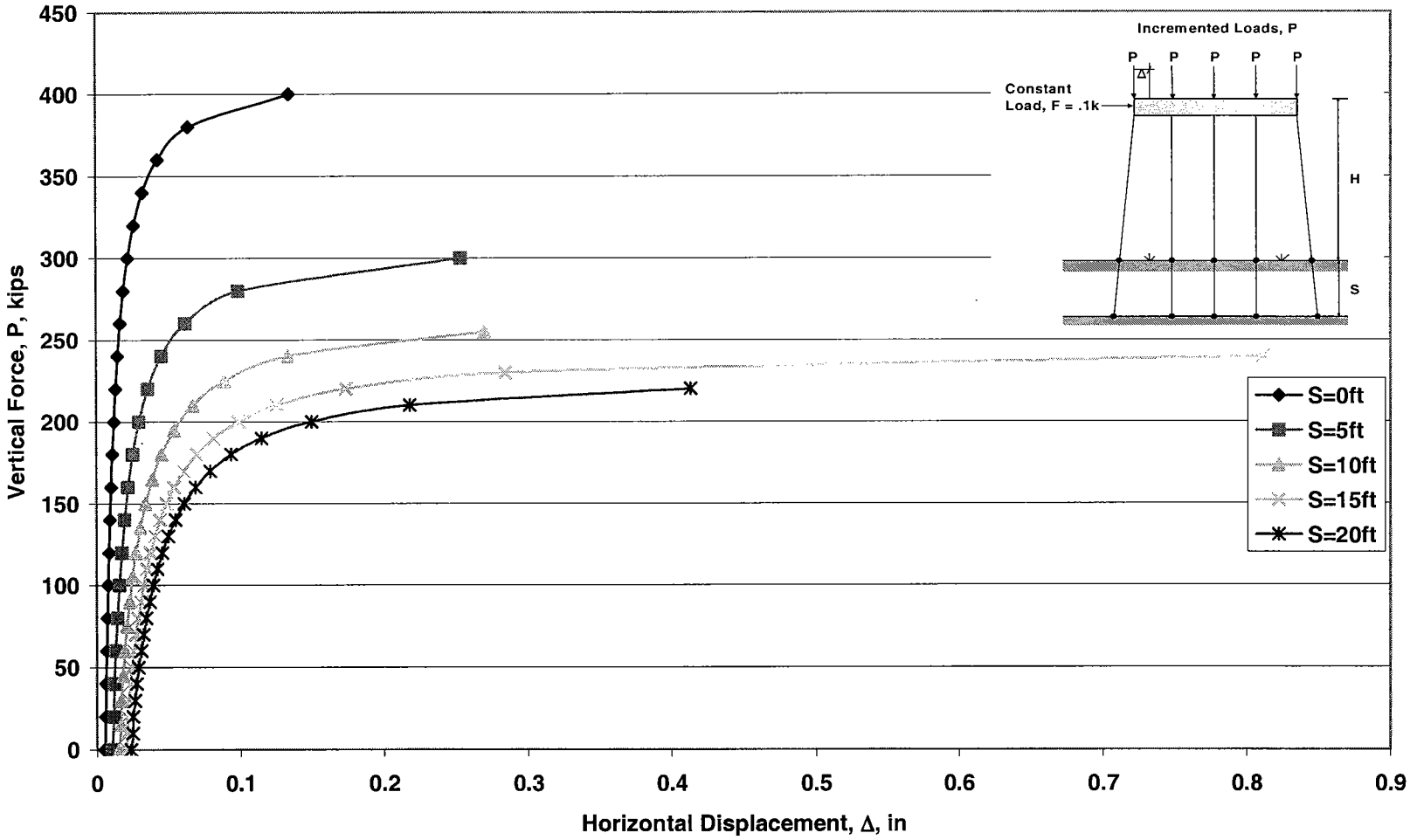

Figure 6.19a. GTSTRUDL Buckling Analysis of HP10x42 5-Pile Bent Subjected to Scour, H=13ft

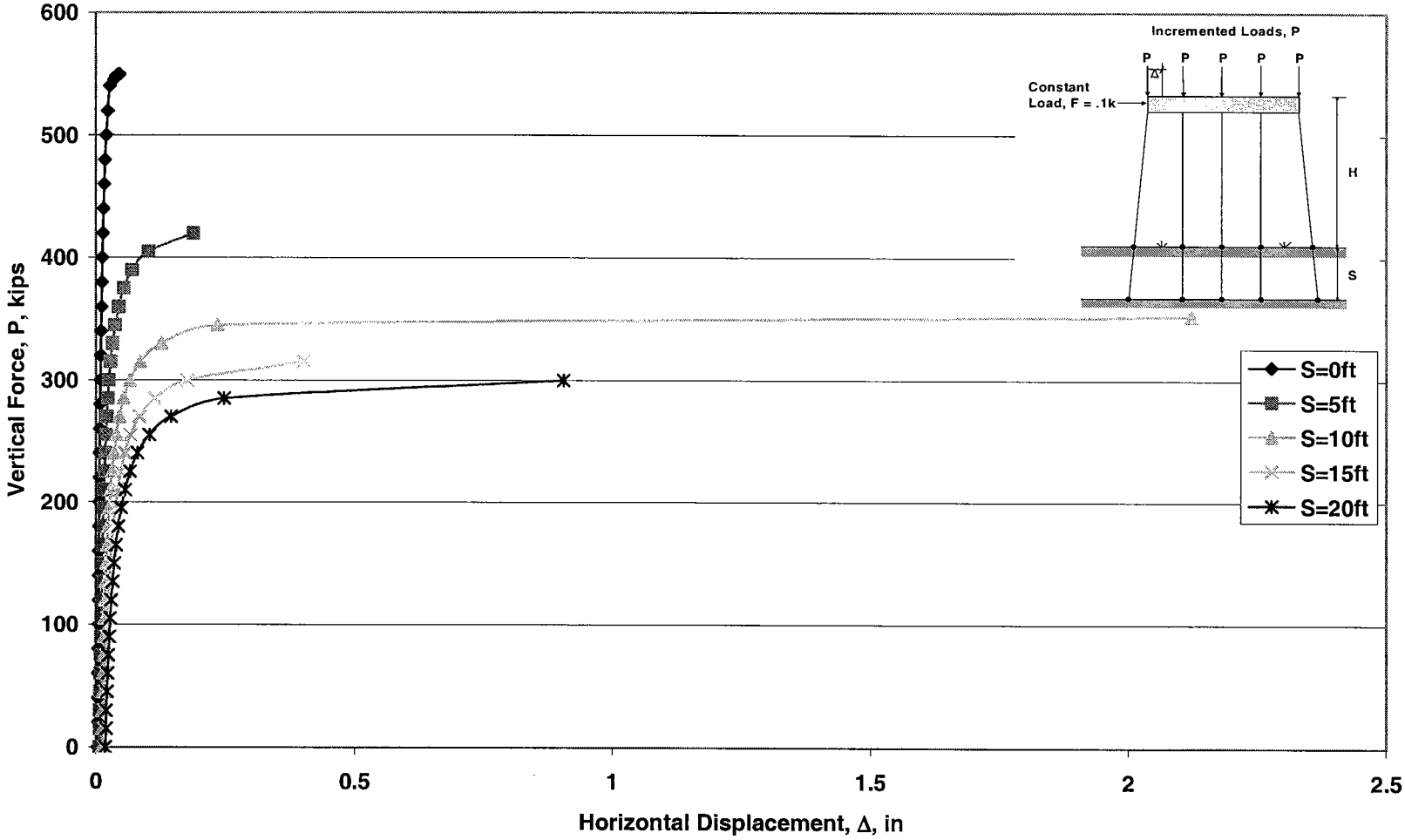

Figure 6.19b. GTSTRUDL Buckling Analysis of HP12x53 5-Pile Bent Subjected to Scour, H=13ft

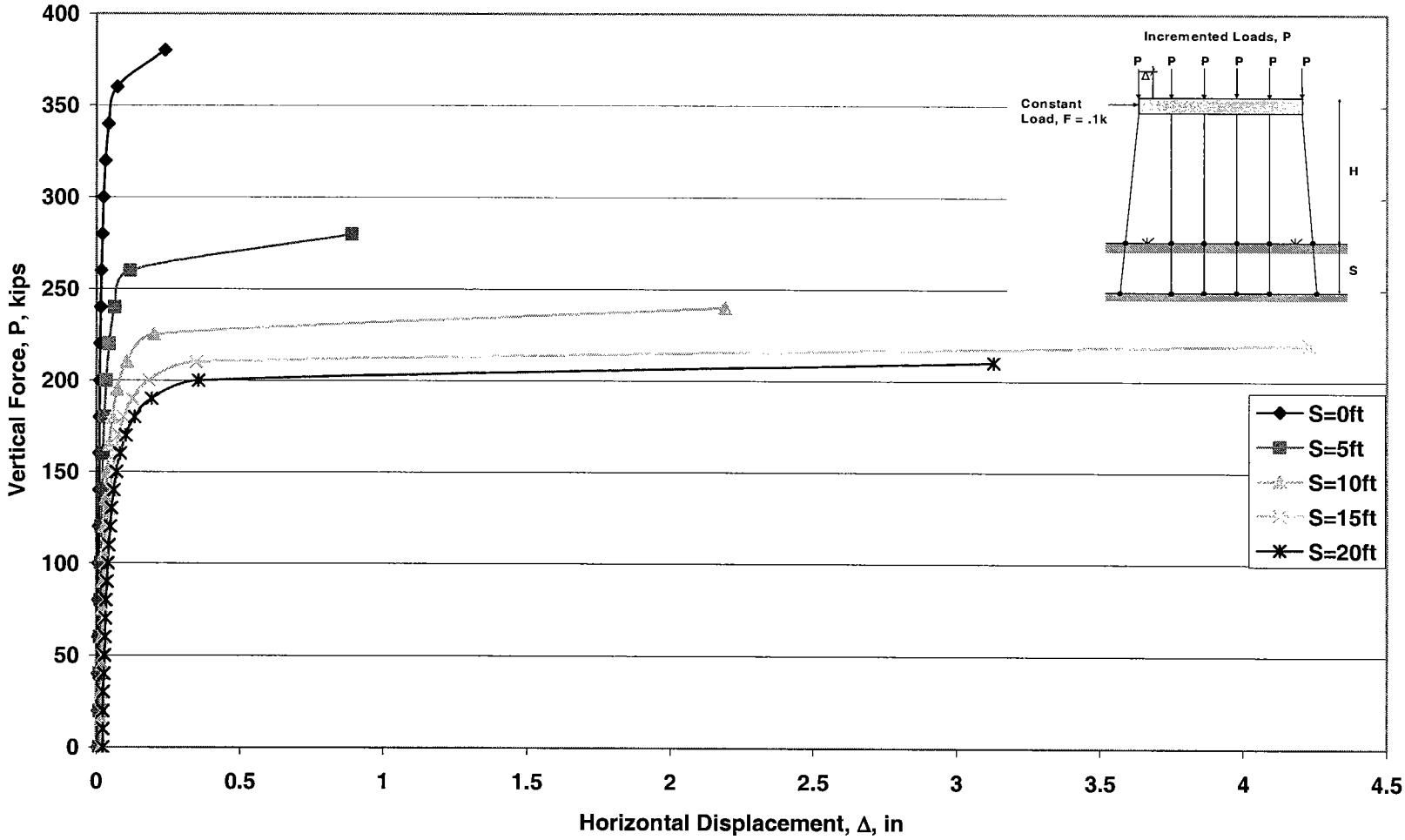

Figure 6.20a. GTSTRUDL Buckling Analysis of HP 10x42 6-Pile Bent Subjected to Scour, H=13ft

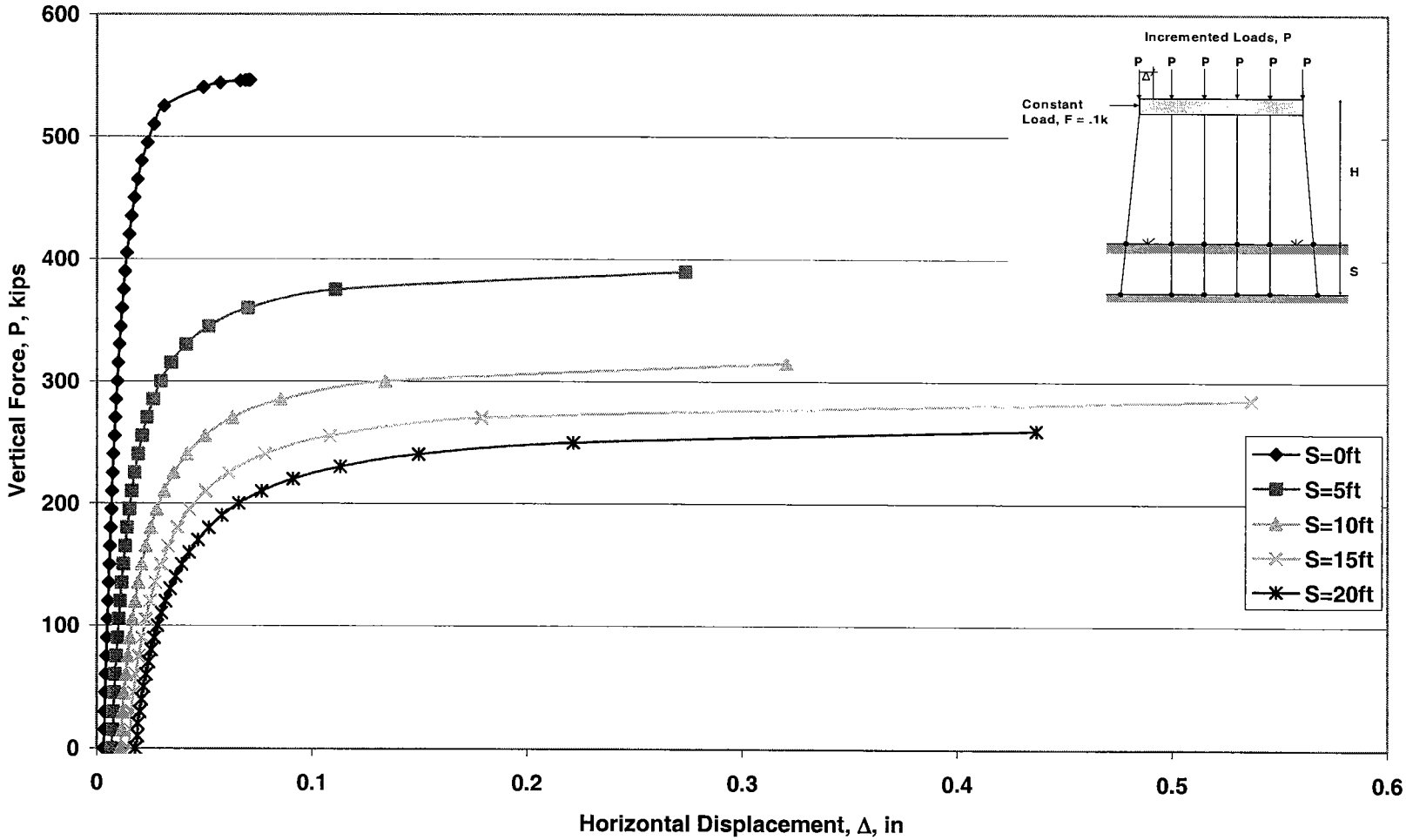

Figure 6.20b. GTSTRUDL Buckling Analysis of HP12x53 6-Pile Bent Subjected to Scour, H=13ft

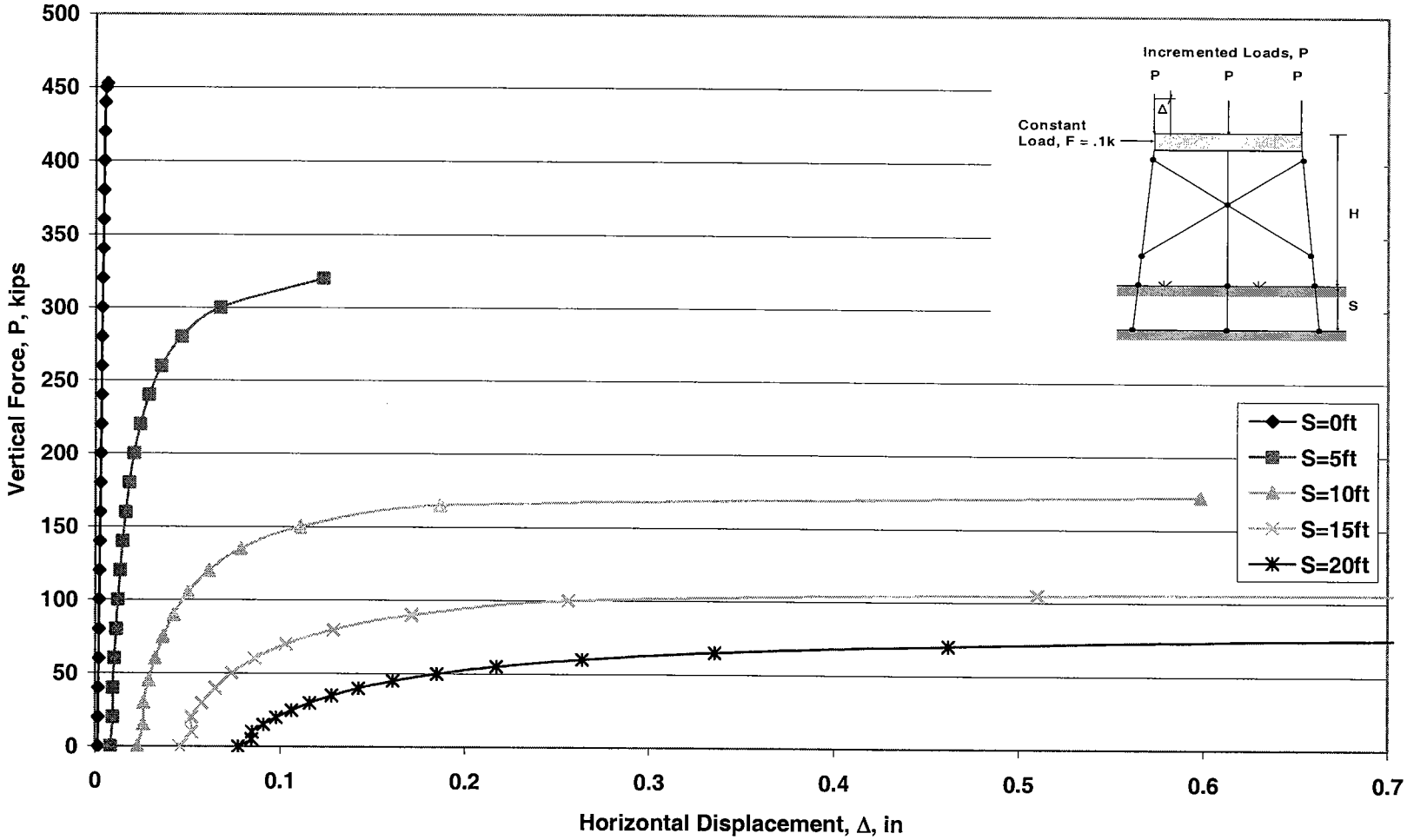

Figure 6.21a. GTSTRUDL Buckling Analysis of One Story X-braced HP10x42 3-Pile Bent Subjected to Scour, H=13ft

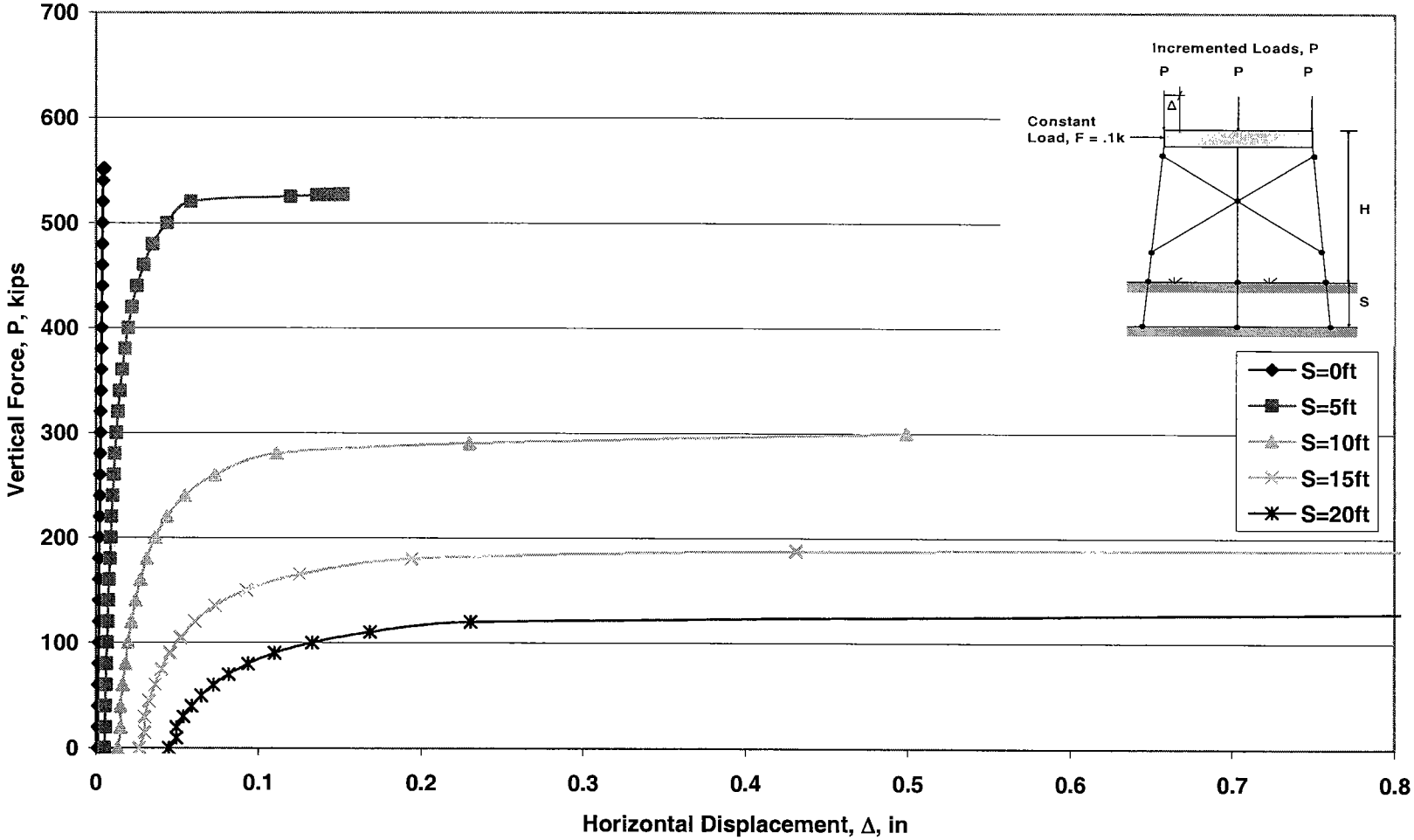

Figure 6.21b. GTSTRUDL Buckling Analysis of One Story X-braced HP12x53 3-Pile Bent Subjected to Scour, H=13ft

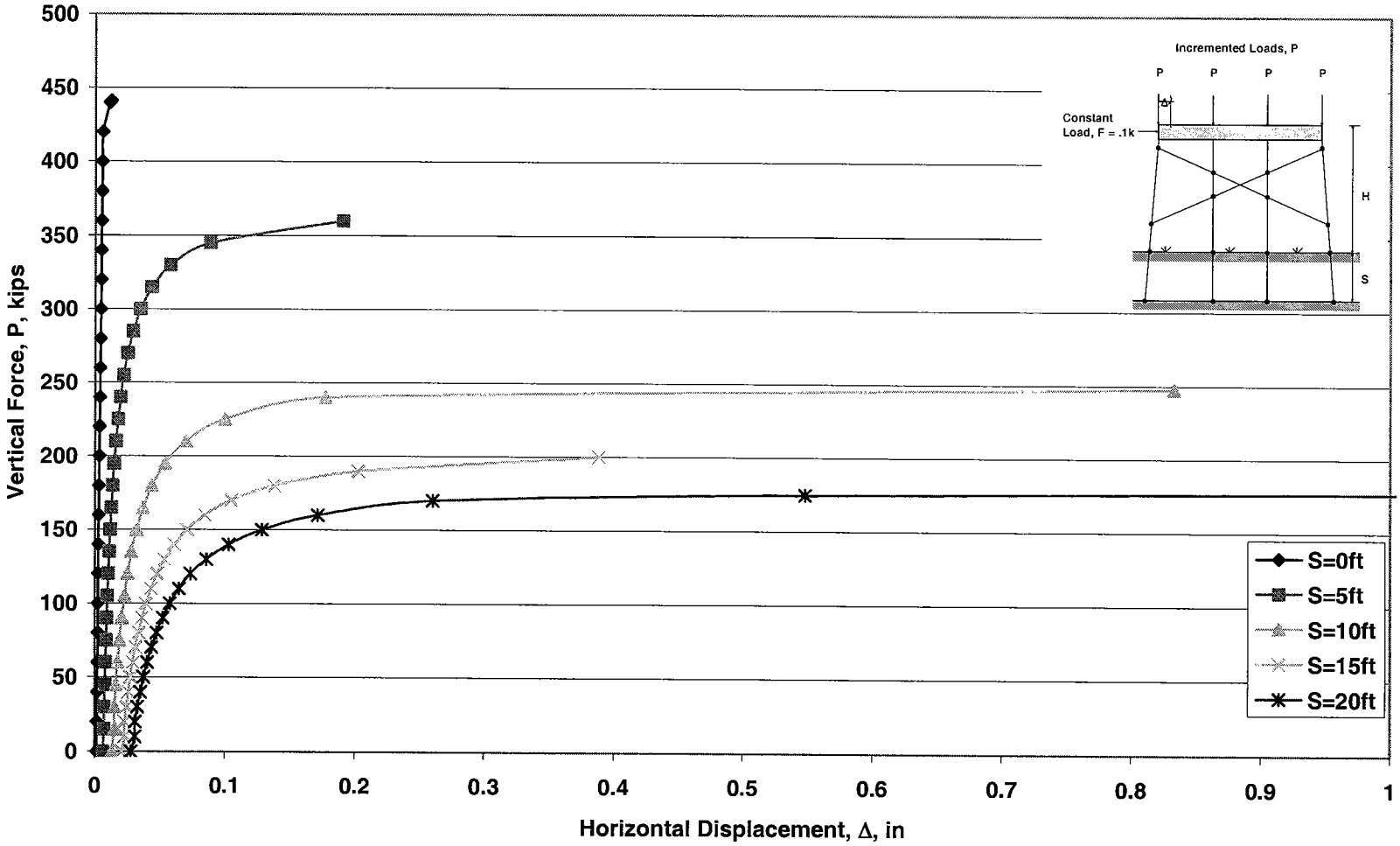

Figure 6.22a. GTSTRUDL Buckling Analysis of One Story X-braced HP10x42 4-Pile Bent Subjected to Scour, H=13ft

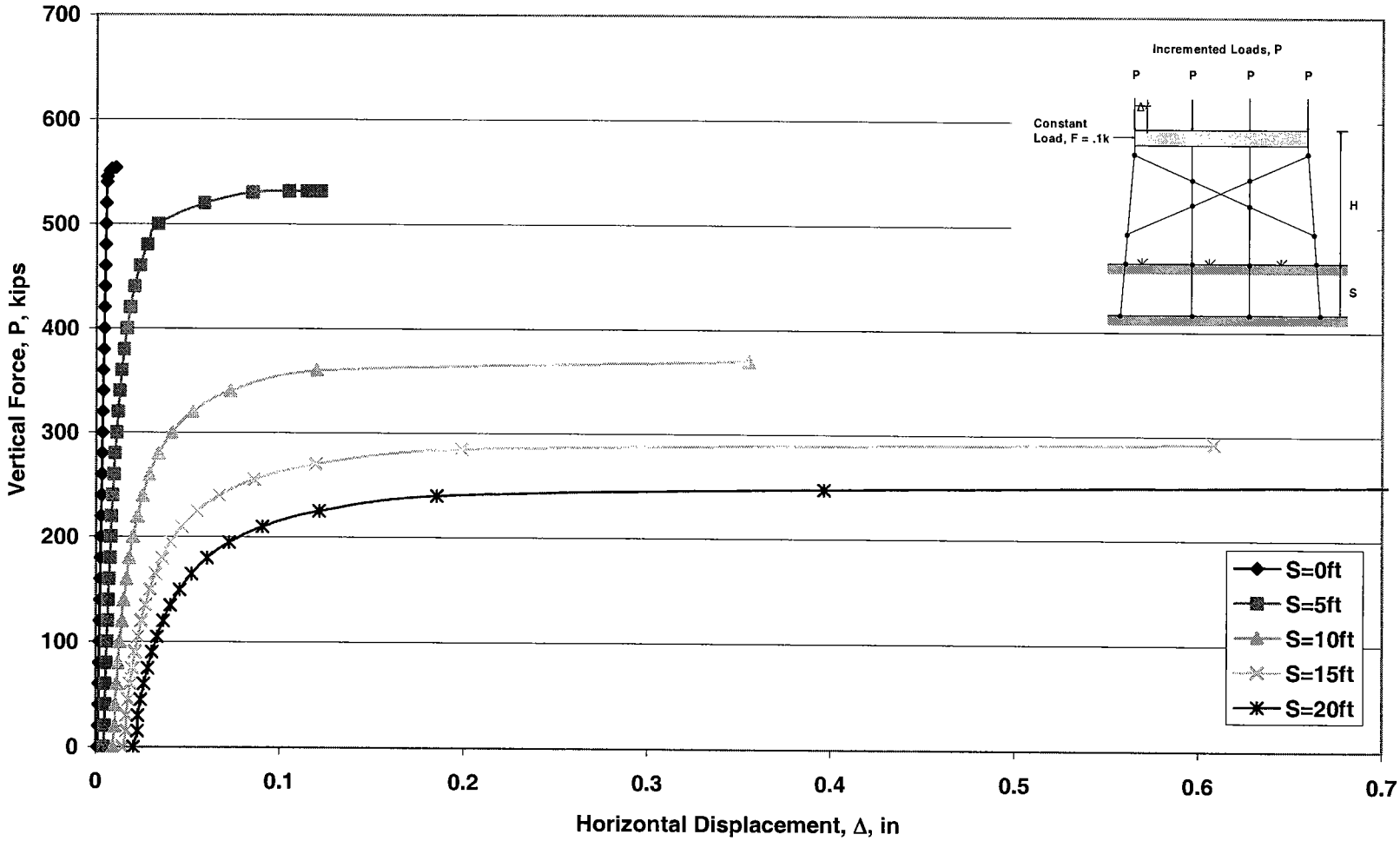

Figure 6.22b. GTSTRUDL Buckling Analysis of One Story X-braced HP12x53 4-Pile Bent Subjected to Scour, H=13ft

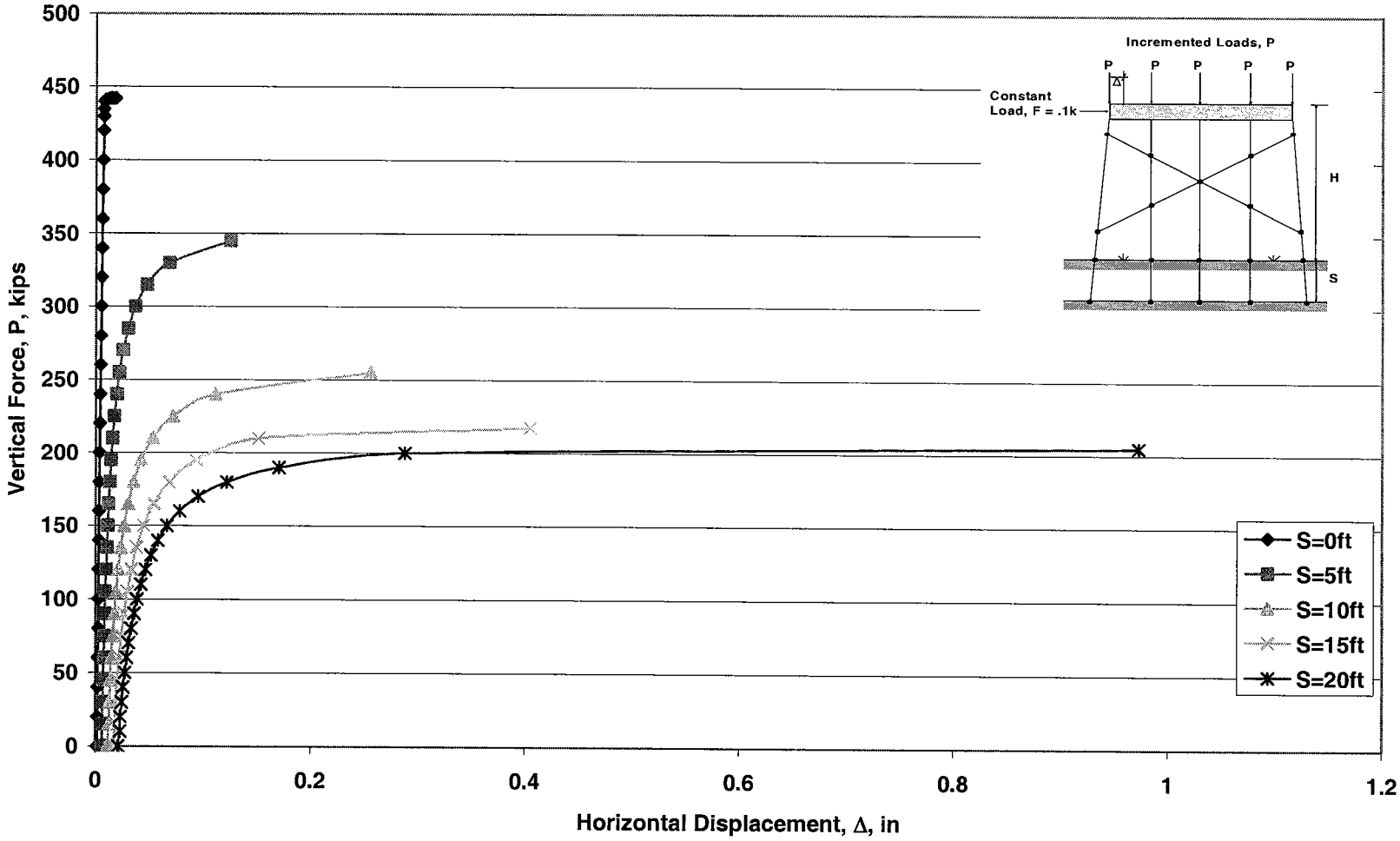

Figure 6.23a. GTSTRUDL Buckling Analysis of One Story X-braced HP10x42 5-Pile Bent Subjected to Scour, H=13ft

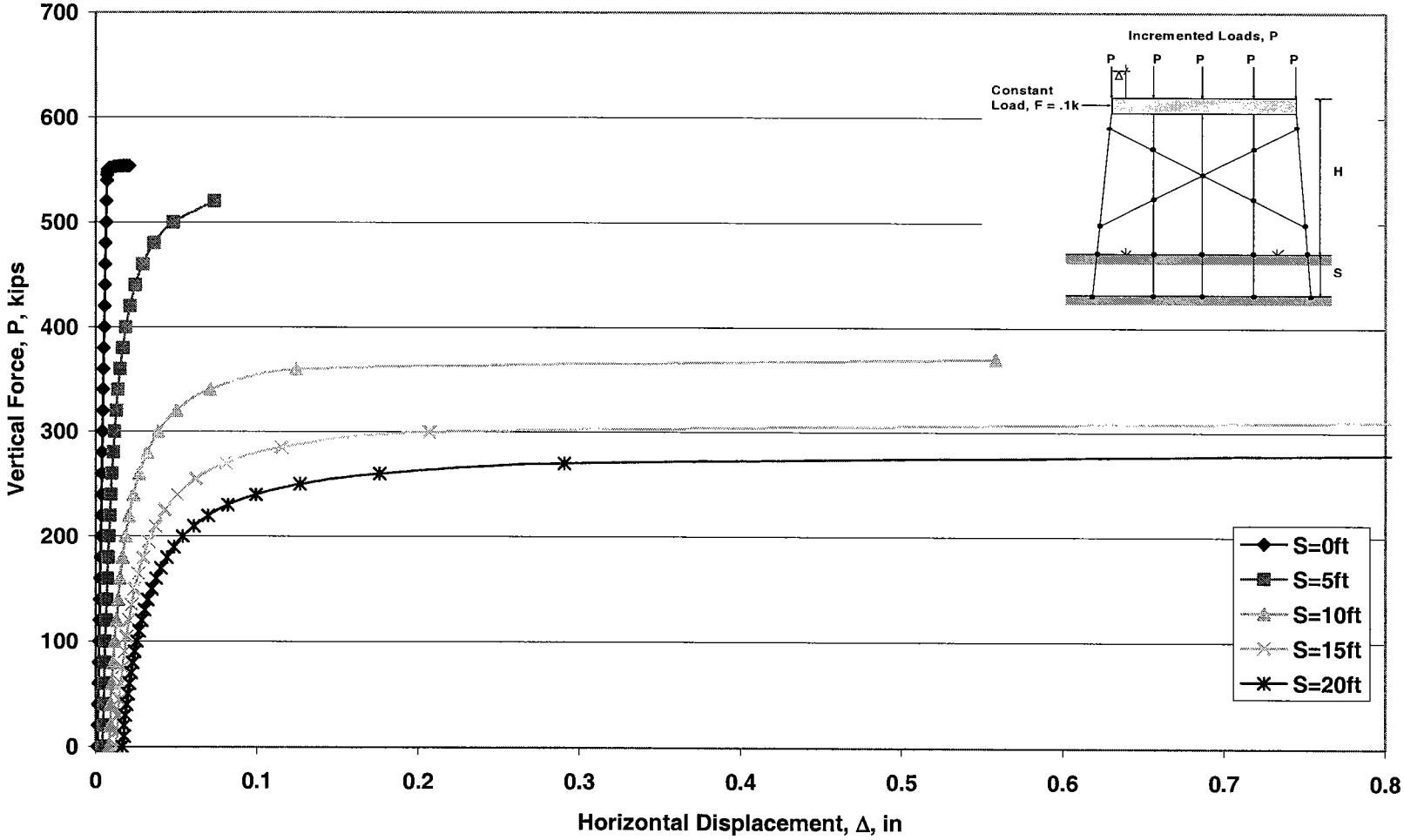

Figure 6.23b. GTSTRUDL Buckling Analysis of One Story X-braced HP12x53 5-Pile Bent Subjected to Scour, H=13ft

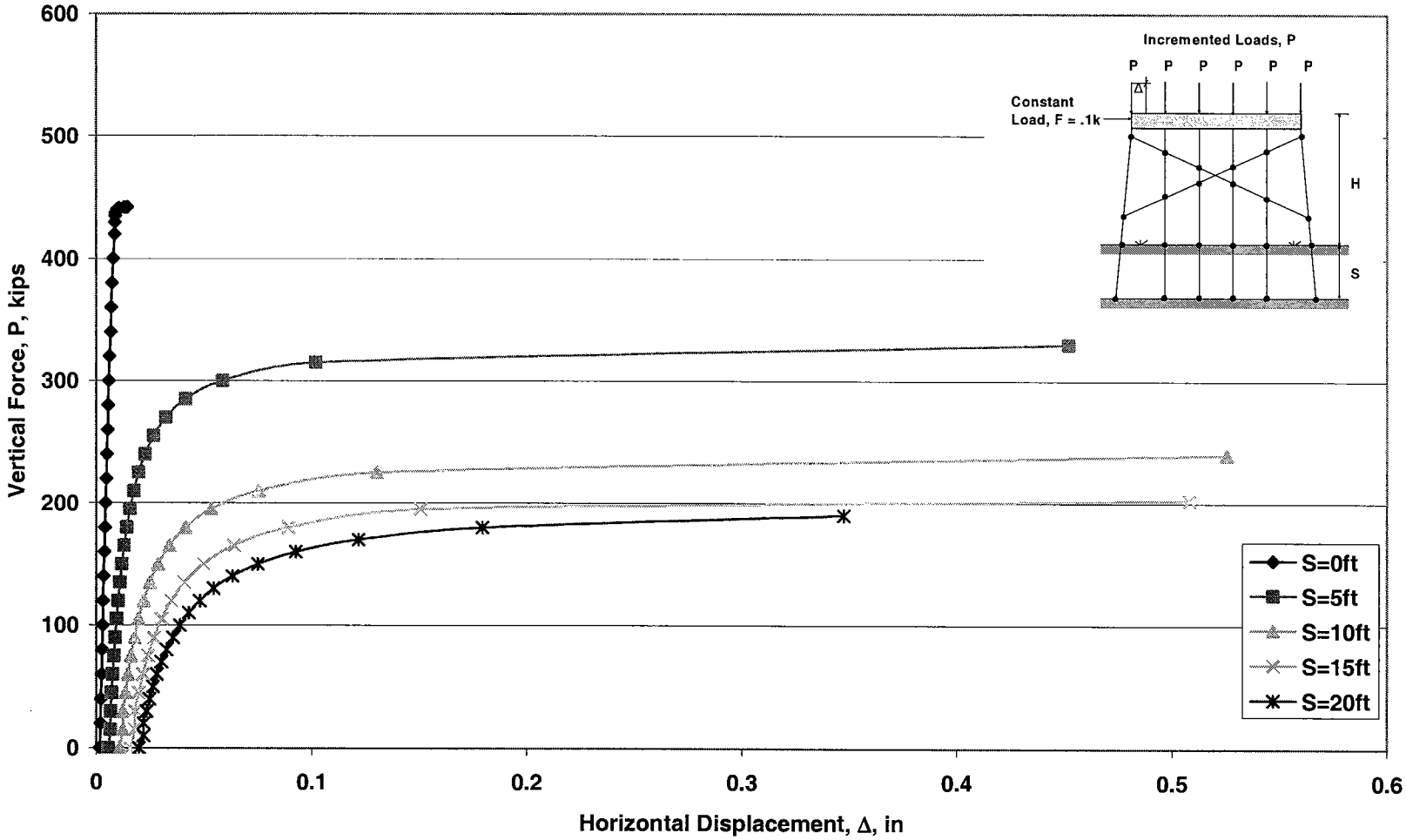

Figure 6.24a. GTSTRUDL Buckling Analysis of One Story Single X-braced HP10x42 6-Pile Bent Subjected to Scour, H=13ft

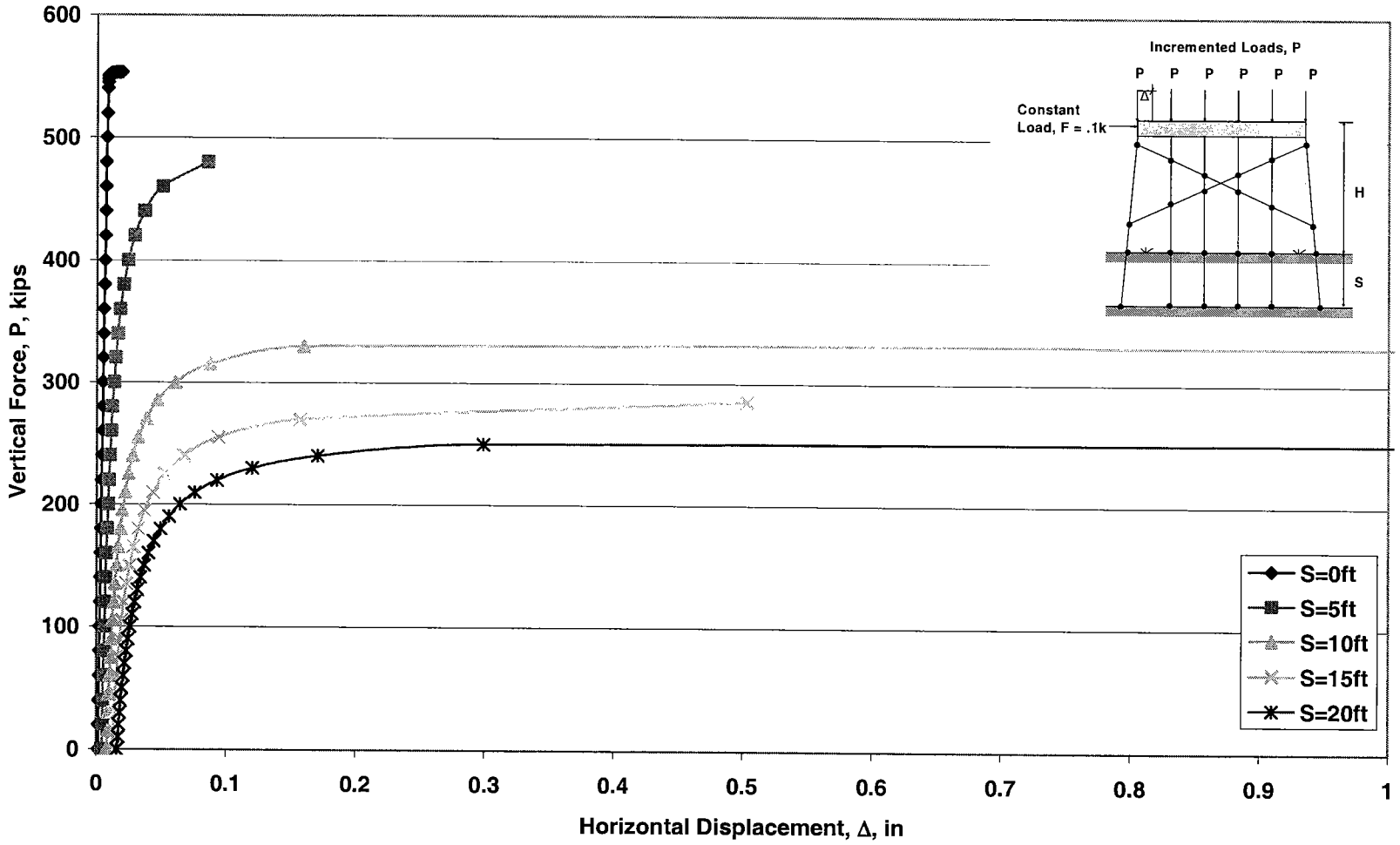

Figure 6.24b. GTSTRUDL Buckling Analysis of One Story Single X-braced HP12x53 6-Pile Bent Subjected to Scour, H=13ft

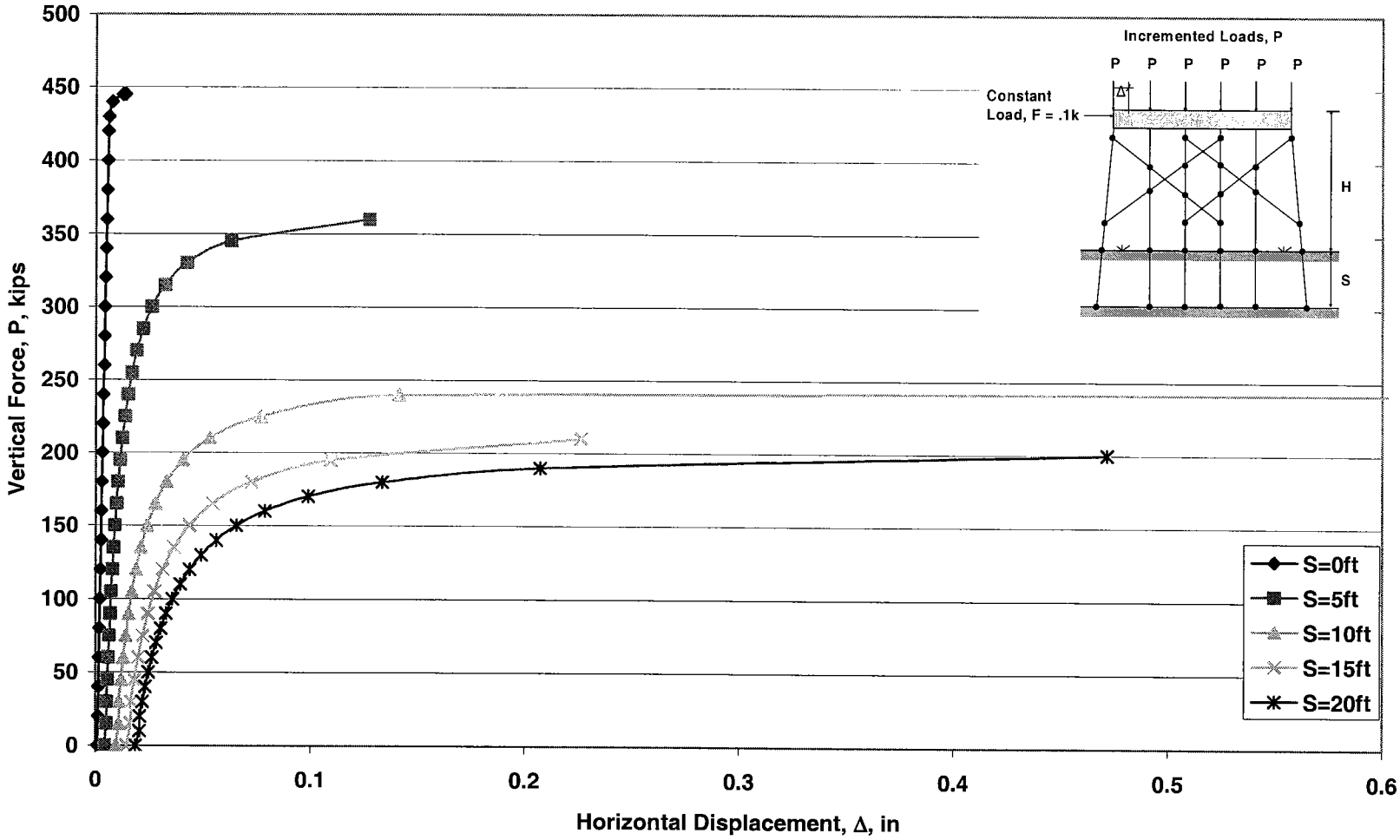

Figure 6.25a. GTSTRUDL Buckling Analysis of One Story Double X-braced HP10x42 6-Pile Bent Subjected to Scour, H=13ft

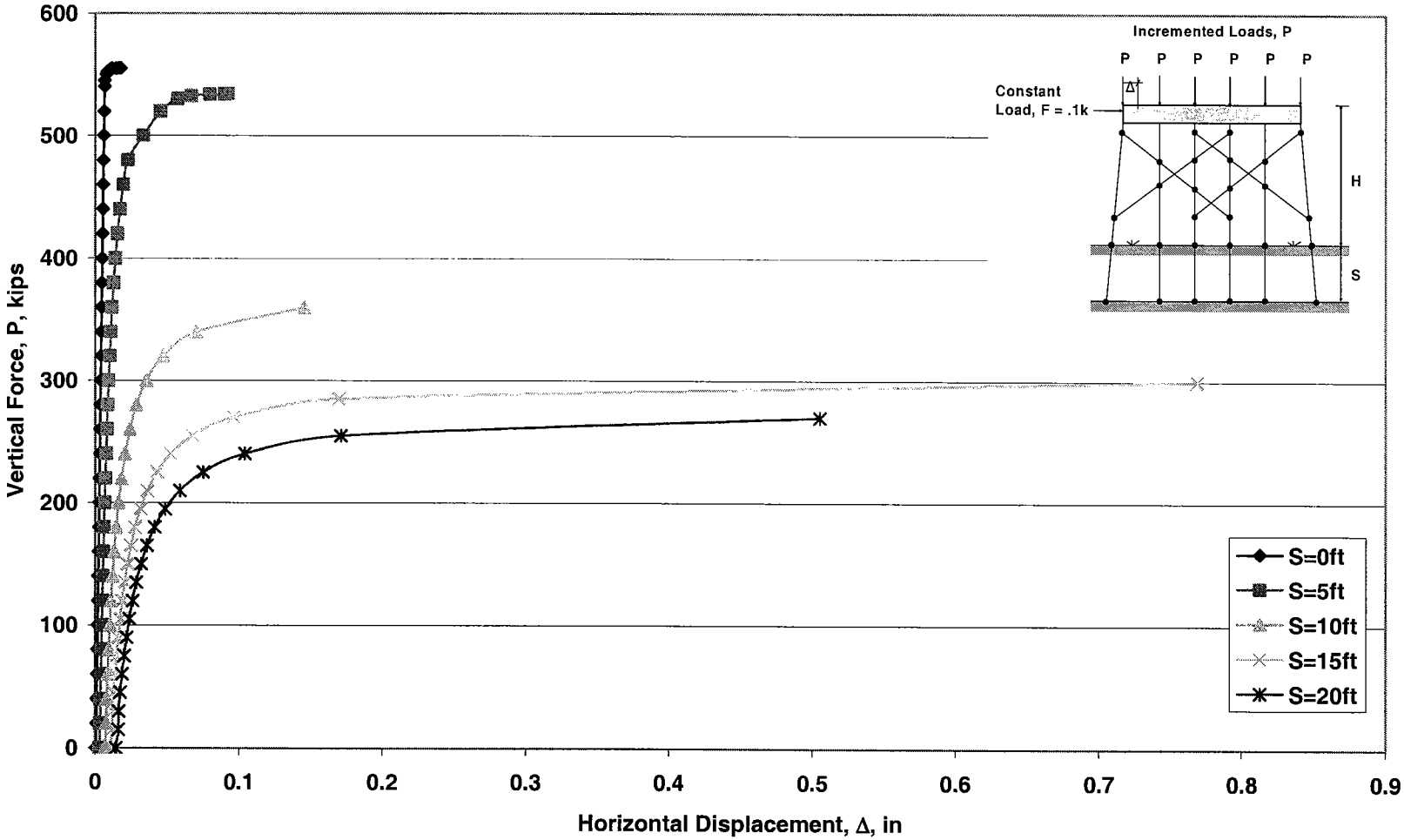

Figure 6.25b. GTSTRUDL Buckling Analysis of One Story Double X-braced HP12x53 6-Pile Bent Subjected to Scour, H=13ft

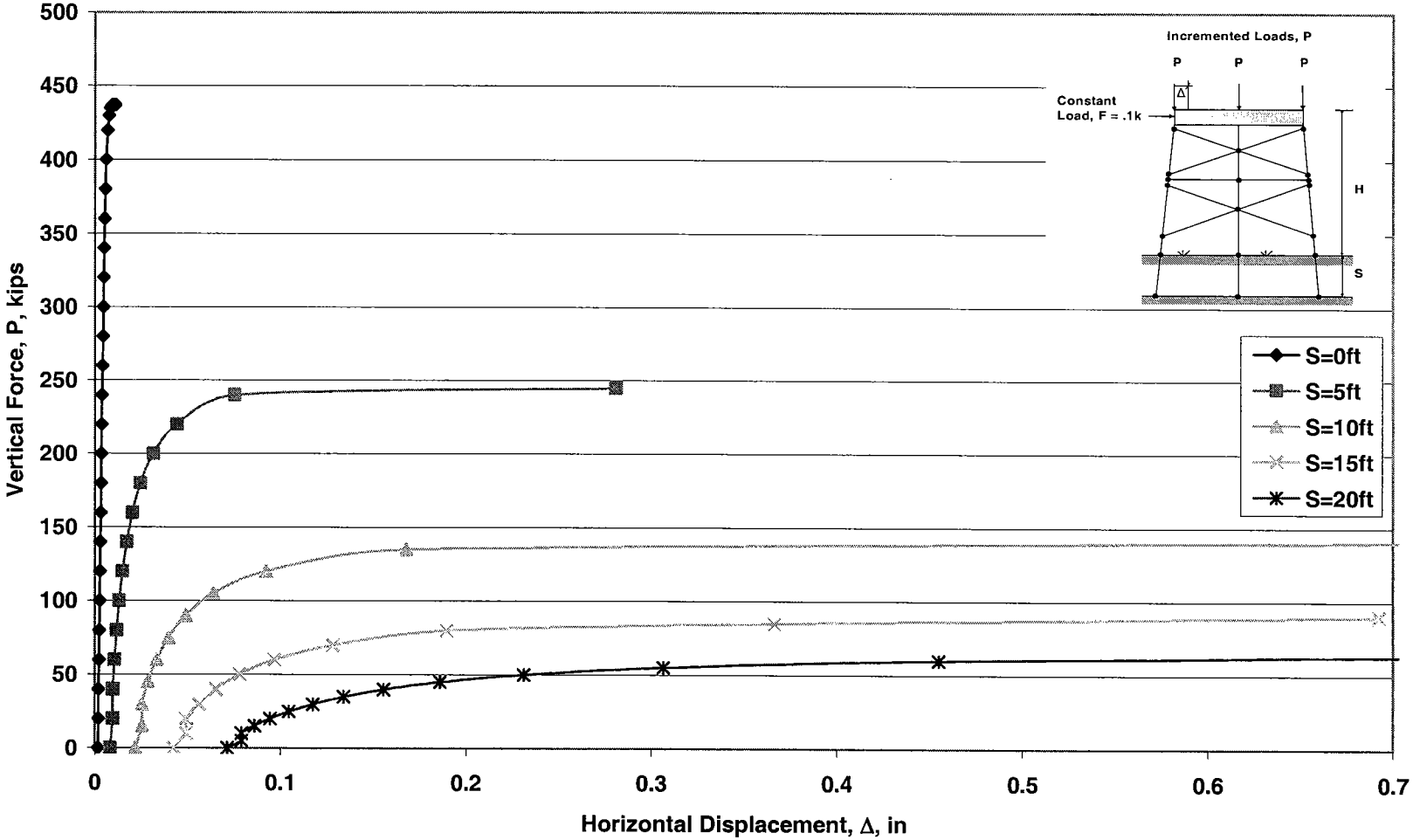

Figure 6.26a. GTSTRUDL Buckling Analysis of Two Story X-braced HP10x42 3-Pile Bent Subjected to Scour, H=25ft

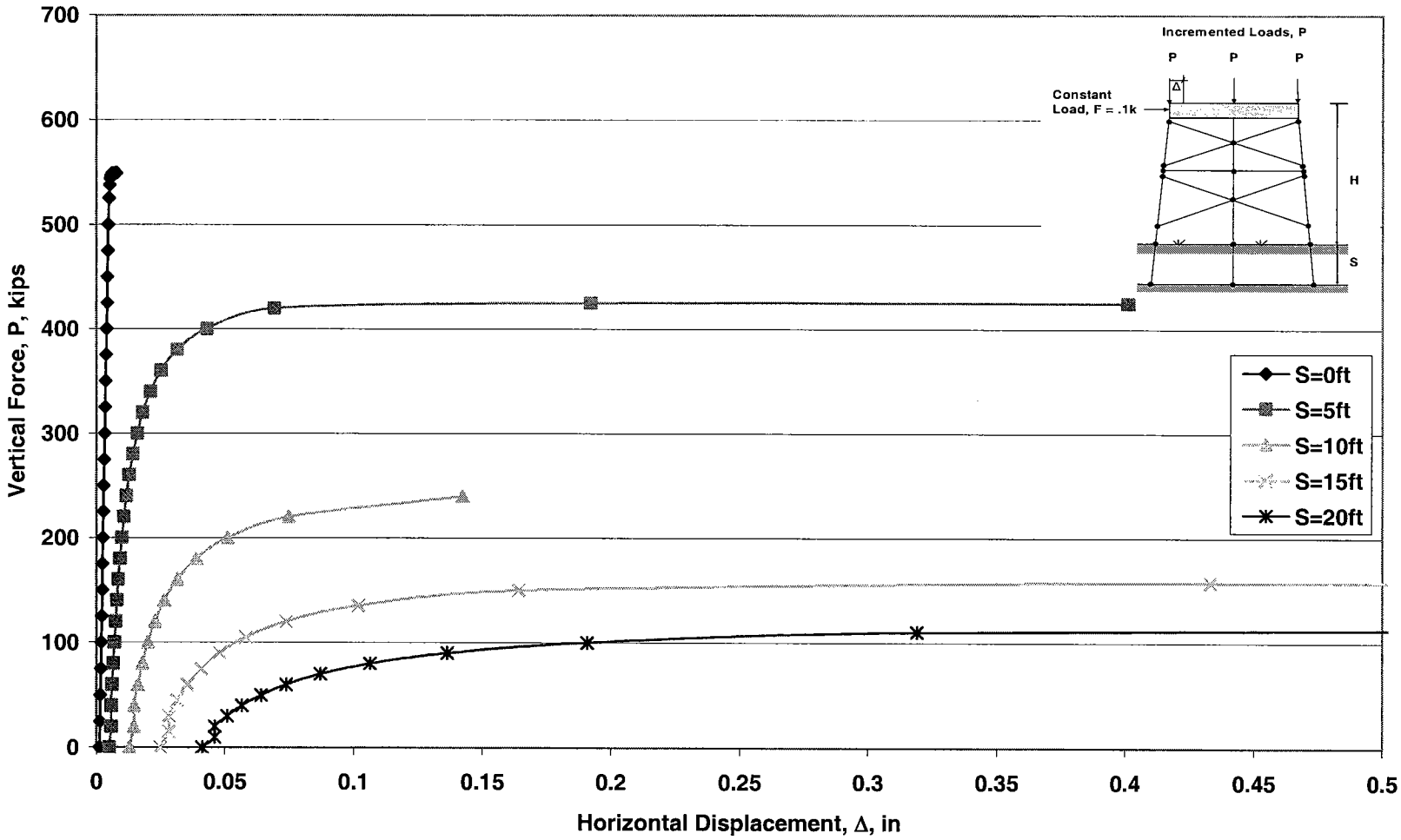

Figure 6.26b. GTSTRUDL Buckling Analysis of Two Story X-braced HP12x53 3-Pile Bent Subjected to Scour, H=25ft

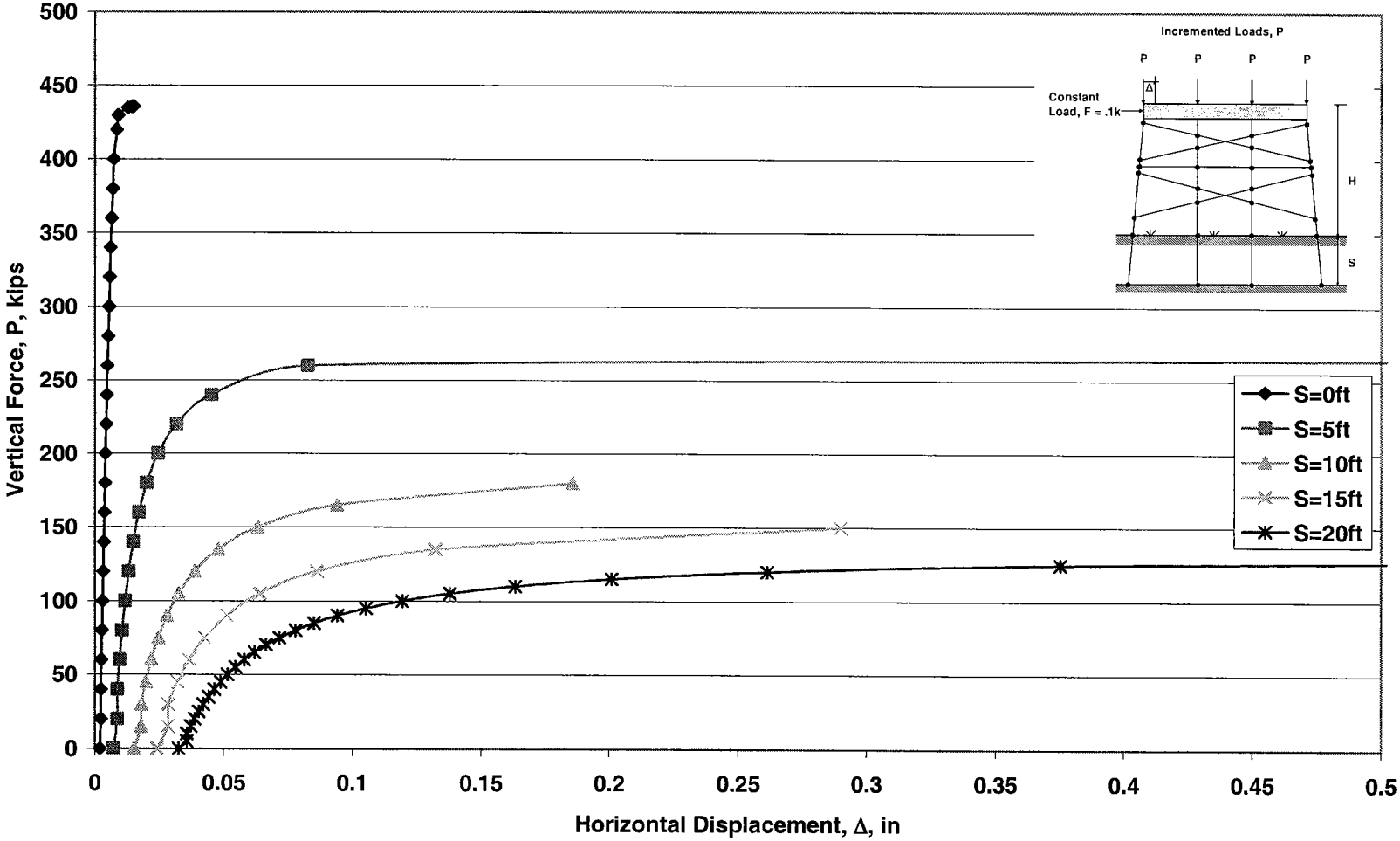

Figure 6.27a. GTSTRUDL Buckling Analysis of Two Story X-braced HP10x42 4-Pile Bent Subjected to Scour, H=25ft

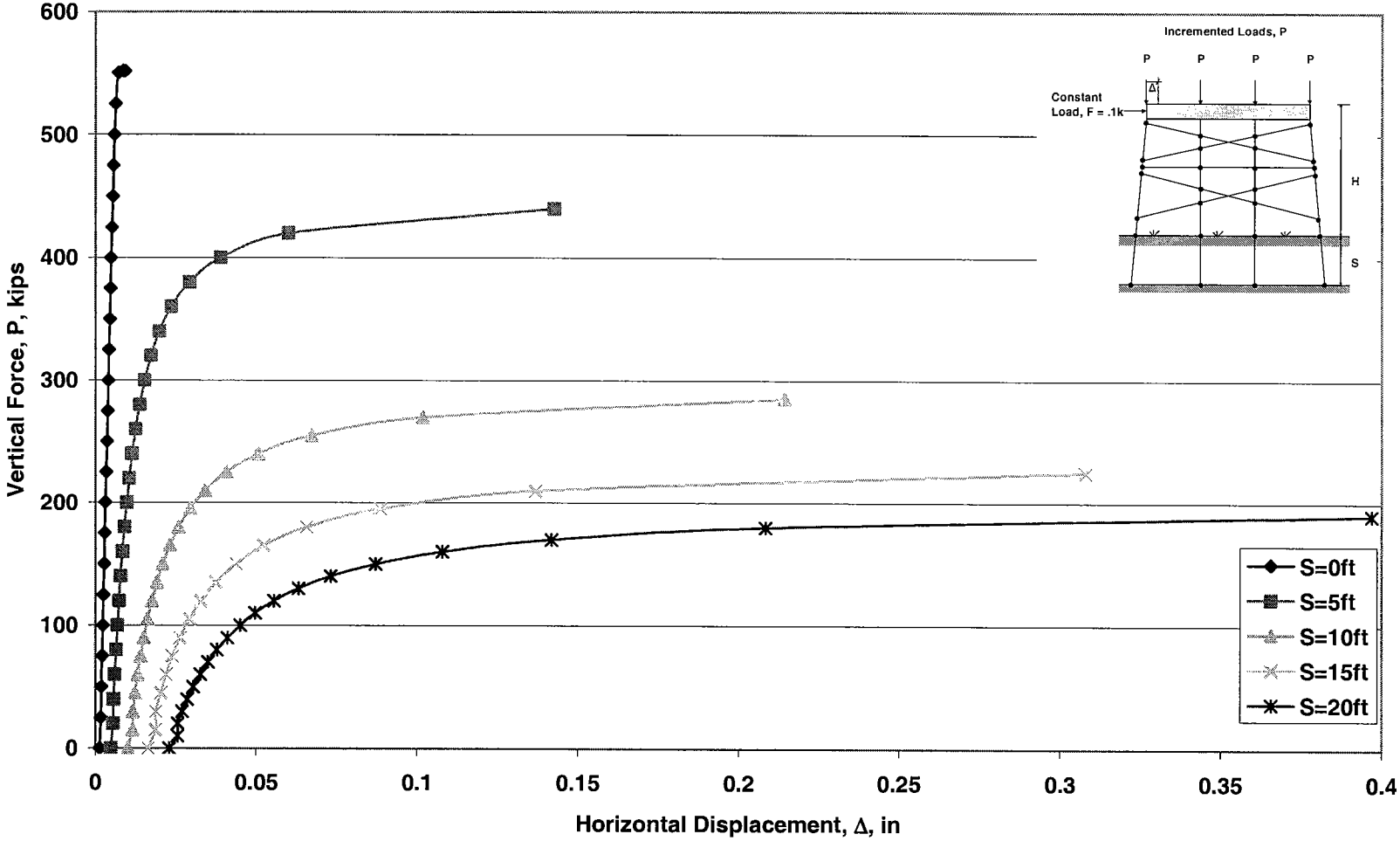

Figure 6.27b. GTSTRUDL Buckling Analysis of Two Story X-braced HP12x53 4-Pile Bent Subjected to Scour, H=25ft

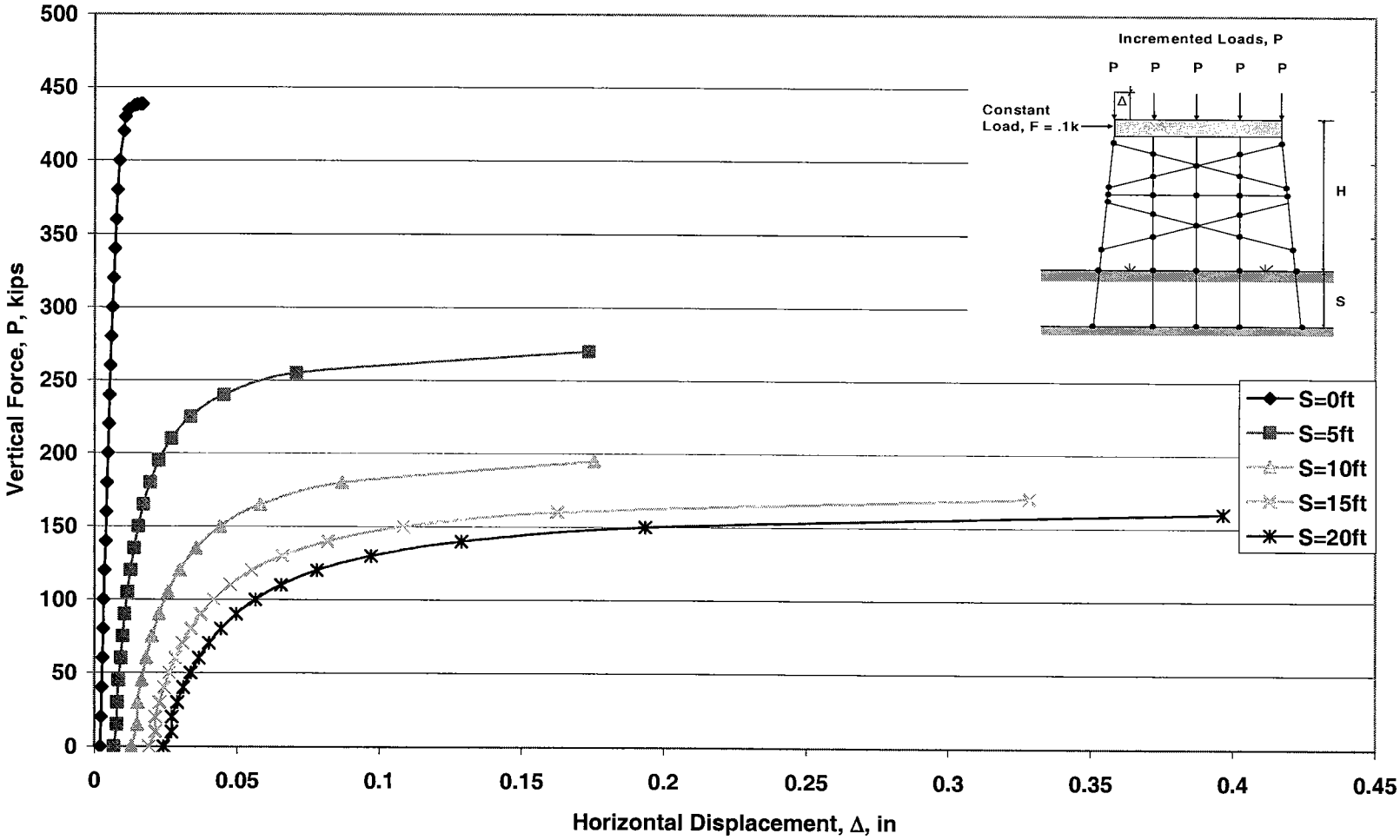

Figure 6.28a. GTSTRUDL Buckling Analysis of Two Story X-braced HP10x42 5-Pile Bent Subjected to Scour, H=25ft

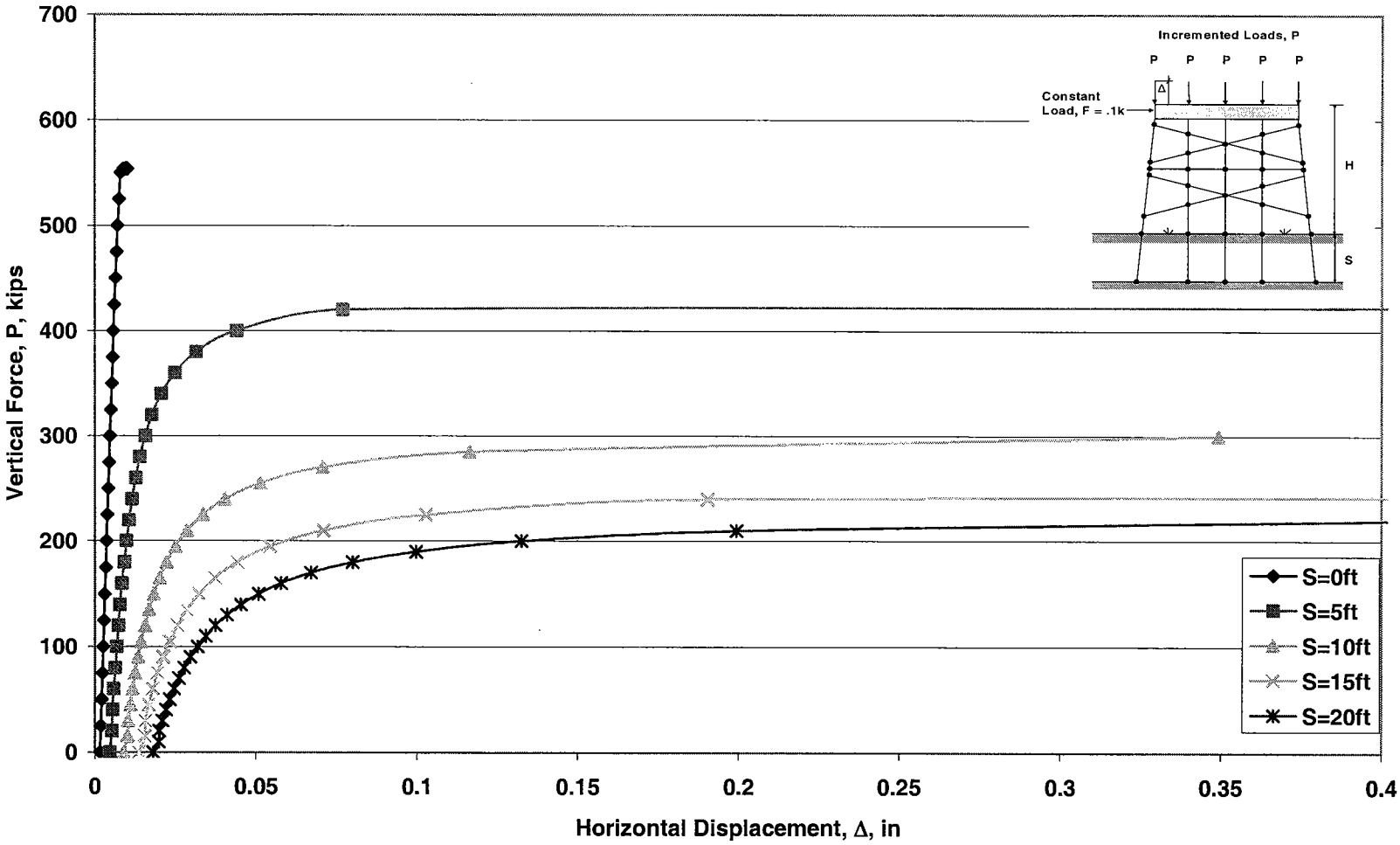

Figure 6.28b. GTSTRUDL Buckling Analysis of Two Story X-braced HP12x53 5-Pile Bent Subjected to Scour, H=25ft

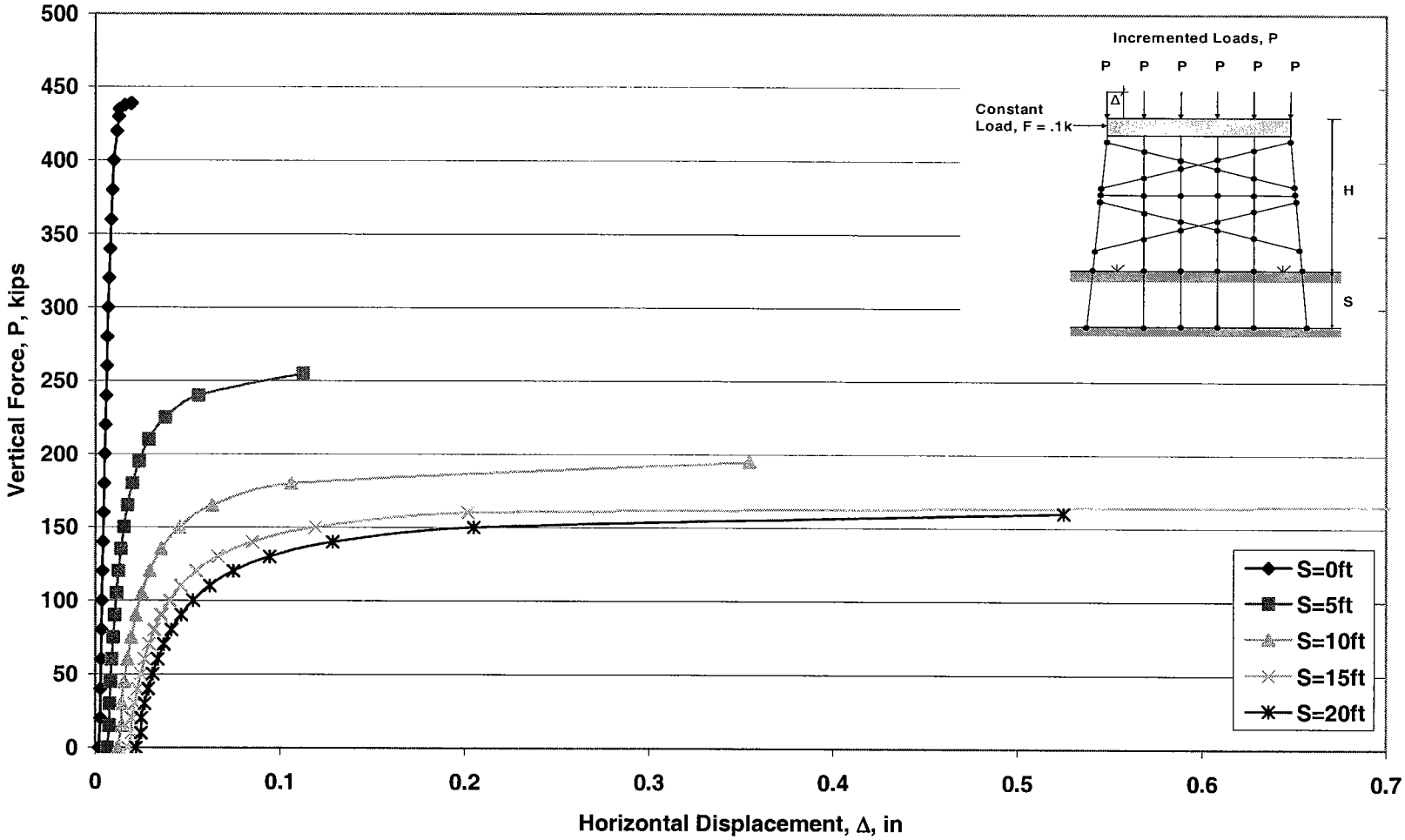

Figure 6.29a. GTSTRUDL Buckling Analysis of Two Story Single X-braced HP10x42 6-Pile Bent Subjected to Scour, H=25ft

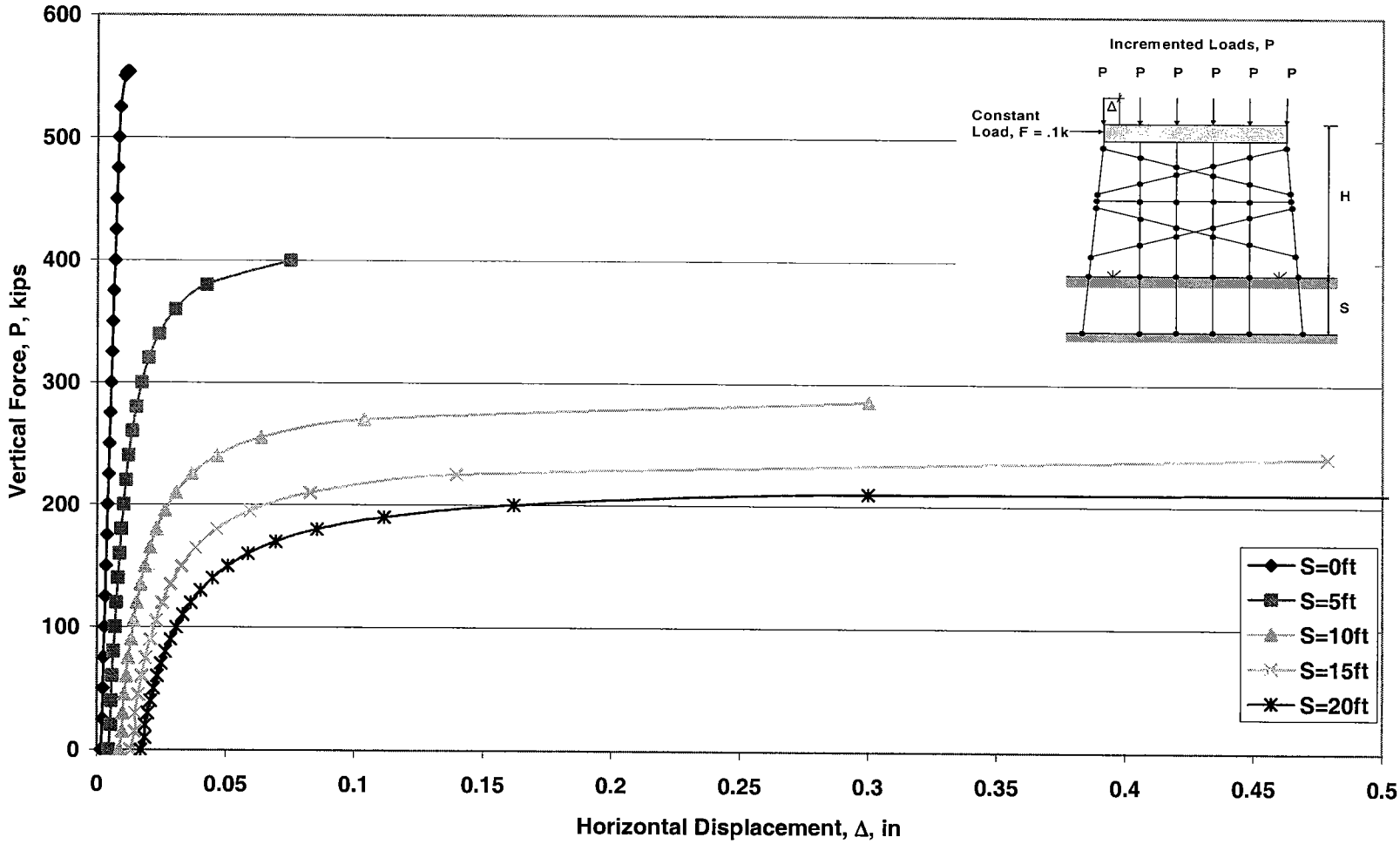

Figure 6.29b. GTSTRUDL Buckling Analysis of Two Story Single X-braced HP12x53 6-Pile Bent Subjected to Scour, H=25ft

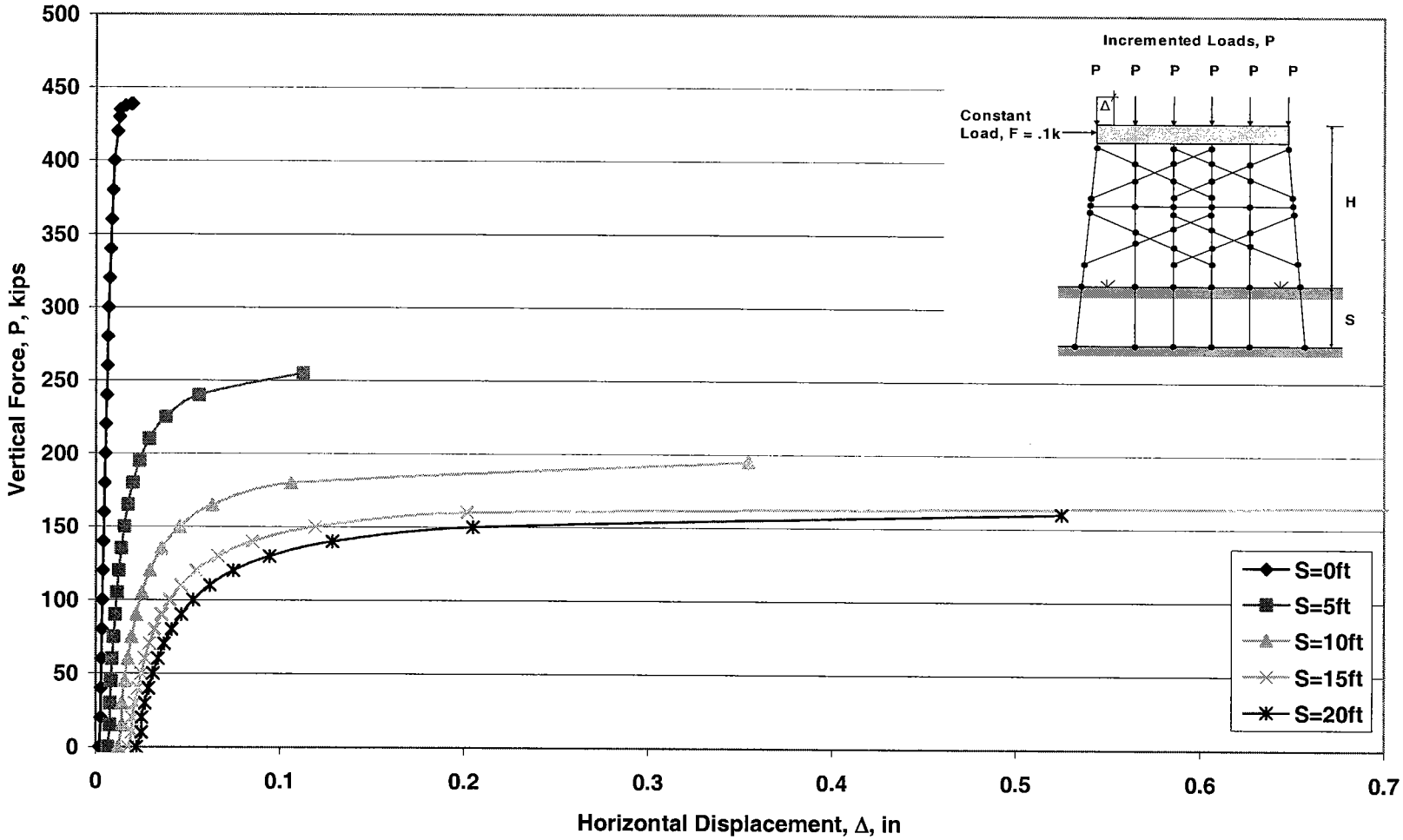

Figure 6.30a. GTSTRUDL Buckling Analysis of Two Story Double X-braced HP10x42 6-Pile Bent Subjected to Scour, H=25ft

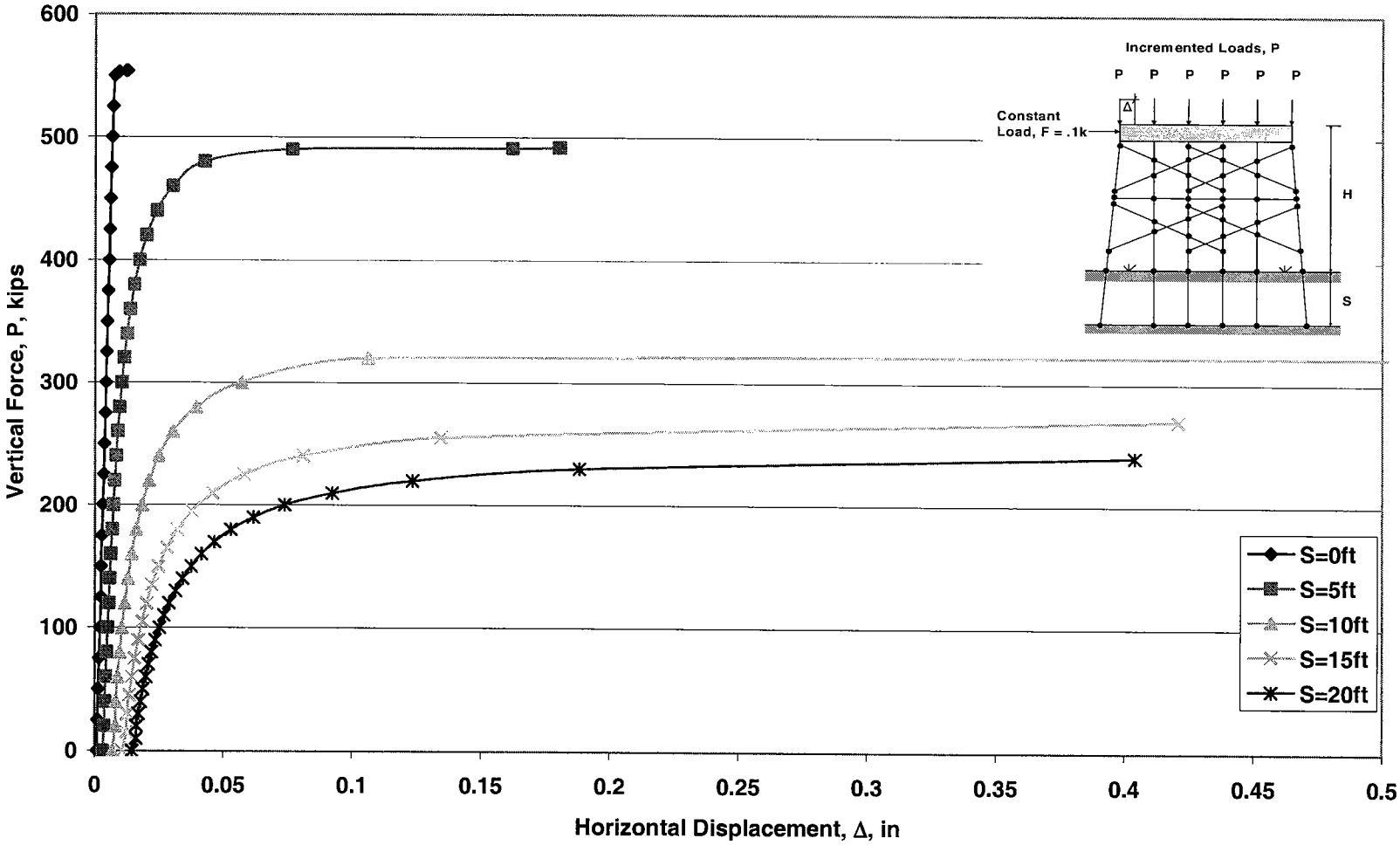

Figure 6.30b. GTSTRUDL Buckling Analysis of Two Story Double X-braced HP12x53 6-Pile Bent Subjected to Scour, H=25ft

CHAPTER 7: COMPARISON OF FB-PIER AND GTSTRUDL PUSHOVER ANALYSIS MODELINGS AND RESULTS FOR NON X-BRACED BENTS

7.1 General

The focus of this chapter is to compare the FB-Pier and GTSTRUDL pushover analysis results for non X-braced bents to develop an accurate modeling of these bents and better understand their predicted behavior. Two different loading conditions were examined using the pushover analysis procedures of FB-Pier and GTSTRUDL on the tallest 5-pile non X-braced bent with H=13ft. For the first loading condition a constant horizontal load of 1 kip was applied to the bent cap and the gravity loads centered over each pile, P_{pile}, were incremented to the point of collapse (see Figure 7.2 for loading details). This modeling was performed to simulate the ultimate pile buckling capacities due to dead loads of the superstructure as well as live loads from traffic for different levels of scour. The 1 kip lateral force has no significance other than to introduce a small initial displacement or imperfection to the piles which often occurs in the form of load eccentricities or crookedness of the piles from formation of the wide flange sections. As the gravity loads are incremented, the initial deflection is magnified only when instability is reached. A similar model was examined with GTSTRUDL in Chapter 6, but with a constant horizontal load of 0.1 kip. For both models the initial lateral displacements are insignificant, but become greatly magnified as the incremented vertical loads approach the pile buckling loads. As the vertical loads are incremented, the lateral stiffness of the piles decreases and eventually results in pushover of the bent. In the second load case the gravity loads centered over each pile remained constant at 100 kip, a typical bridge pile load, while the horizontal force was incremented (see Figure 7.8 for loading details). This model is serving as a preliminary analysis for horizontal forces that develop in the transverse direction of the bent due to the debris raft which may collect

around the pile bent during major flood events. The constant 100 kip forces over each pile are thought to be reasonable approximations for the gravity loads and are therefore unfactored loads. Variations in the magnitude of these constant gravity loads are not presented in this research, but will be analyzed further in the final screening tool.

In addition to varying the bent loading conditions, the end boundary conditions of the piles were also altered for the pushover analysis. Initially, it was conservatively assumed that the piles were attached to the bent cap via pinned connections in the computer models as shown in Figures 7.2-7.11. Along with this assumption, the bents were given fixed connections to the ground for GTSTRUDL whereas a cohesionless soil with a subgrade modulus of 150 lb/in^3 was used as the base condition in the FB-Pier models. For the second modeling of pile boundary conditions, shown in Figures 7.12-7.21 the piles were assumed to have rigid connections to the cap with pinned connections at the base for the GTSTRUDL models and a cohesionless soil having a subgrade modulus of 150 lb/in^3 for the FB-Pier models. The pushover analysis procedures for both FB-Pier and GTSTRUDL were performed for a 5-pile non X-braced bent with H=13ft and scour levels of 0ft, 5ft, 10ft, 15ft, and 20ft. Additionally, the bent cap was modeled using a flexural stiffness equal to I_{gross} and all piles are modeled as unencased steel H sections. After determining the most appropriate bent model, a subsequent analysis will include pushover results for a bent with H=10ft to allow for comparisons when H<13ft. For each modeling the bent height, H, is given as the distance from the top of the bent cap to the ground line before a scour event has occurred.

7.2 FB-Pier Pushover Analysis Results

The FB-Pier pushover analysis results for pile bents with pinned connections at the cap are plotted in Figures 7.2-7.11. When the vertical gravity loads are used as the incremented loads as in Figures 7.2-7.6 with piles pinned at the cap, the ultimate pile buckling capacities, P_{pile}, from FB-Pier range from 160 kips to 110 kips for S=0ft to S=20ft. It is meaningful to note here that for each level of scour the gravity load capacity over each pile remains above 100 kips (the load which was used in the pushover analysis model with constant gravity loads). According to

this analysis bents modeled with pinned connections at the cap would not be at risk of failure for the realistic approximation of gravity loads on the bent (provided the horizontal force remains below 1 kip). The constant 100 kip loads were based on a girder line analysis which approximates the gravity load of the superstructure and is applied to each pile from girders which sit directly above the piles. Additionally, placing a pinned connection between the piles and cap is somewhat conservative, and these bents are not expected to fail when P=100 kip for the levels of scour presented. Alternatively, when the vertical gravity loads remain constant and the horizontal force is incremented at the cap as shown in Figures 7.7-7.11 for piles pinned at the cap, the ultimate horizontal loading in FB-Pier ranges from 7 kips to 2 kips for S=0ft to S=20ft. These curves exhibit linear load-deflection behavior until termination of the pushover analysis.

The FB-Pier pushover analysis results for pile bents with rigid connections at the cap are plotted in Figures 7.12-7.21. When the vertical gravity loads are used as the incremented loads as in Figures 7.12-7.16, the ultimate pile buckling capacities P_{pile}, range from 380 kips to 180 kips for S=0ft to S=20ft respectively. Examining the second pushover loading condition with constant gravity loads and incremented horizontal force as shown in Figures 7.17-7.21, the horizontal loads are bound by 31 kips when S=0ft and 7 kips when S=20ft and also appear to exhibit linear p-delta behavior until failure.

7.3 GTSTRUDL Pushover Analysis Results

The GTSTRUDL pushover analysis results for pile bents with pinned connections at the cap are plotted with the FB-Pier results in Figures 7.2-7.11. When the vertical gravity loads are used as the incremented loads (Figures 7.2-7.6), the ultimate pile buckling capacities, P_{pile}, range from 360 kips to 210.6 kips for S=0ft and S=20ft respectively. When the vertical gravity loads remain constant and the horizontal force at the cap is incremented (Figures 7.7-7.11), the ultimate horizontal loading ranges from 424.8 kips to 18.1 kips for S=0ft and S=20ft respectively.

The GTSTRUDL pushover analysis results for pile bents with rigid connections at the cap are plotted in Figures 7.12-7.21. Values of P_{pile} for the incremented gravity loading condition of Figures 7.12-7.16 range from 400 kips to 200 kips for S=0ft and S=20ft. Examining the second

pushover loading condition with constant gravity loads and an incremented horizontal force as shown in Figures 7.17-7.21, the horizontal load capacities are 453.1 kips when S=0ft and 17.6 kips when S=20ft.

7.4 Comparison of FB-Pier and GTSTRUDL Pushover Analysis Results

As shown by comparison of the p-delta curves for the bents modeled with pinned connections at the cap (Figures 7.2-7.11) to the bents modeled with the rigid connections at the cap (Figures 7.12-7.21), the bents modeled with rigid connections at the cap produce p-delta curves for both FB-Pier and GTSTRUDL that are much more similar for initial loads and displacements. For this fixed-pinned modeling and the load case where vertical gravity loads, P, are incremented and the horizontal force, F, at the cap remains constant (Figures 7.12-7.16), the p-delta curves for both programs track similar paths until a reasonably precise collapse load is achieved. Slight variations of the two curves are expected due to the effects of different base conditions modeled by the two programs. With GTSTRUDL the bents are fully pinned, whereas with FB-Pier the bents are supported by an elastic soil foundation. While the FB-Pier modeling would seem to model the base condition more accurately, there appears to be a significant disadvantage as seen by the pushover analysis results for the case with constant vertical loads and an incremented horizontal load (Figures 7.17-7.21), i.e. the FB-Pier results appear to end prematurely before the structure begins to lay over.

Due to the extreme differences in pushover capacities between FB-Pier and GTSTRUDL shown in Figures 7.7-7.11 and 7.17-7.21 when the vertical forces remain constant and the horizontal force is incremented, a closer look at the stresses developing within the piles was made in order to determine a realistic limit state for this loading. While examining the pile stresses for the GTSTRUDL model, excessively large stresses were found. This revealed that the GTSTRUDL modeling was accounting only for the geometric nonlinearity of the bent and was not taking into account material nonlinearity, since the stresses exceeded the yield strength of the piles by such a large degree. To account for the steel strength/yielding, plastic hinges were placed at both ends of each pile with yield strengths of 36 ksi as all standard ALDOT bents are

constructed using A36 steel piles. The GTSTRUDL pushover analysis was then performed again with the plastic hinges included and the resulting p-delta curves placed in Figures 7.22-7.26. Introducing plastic hinges into the piles for this loading dramatically decreased the ultimate horizontal load, F, on the p-delta curve from 453 kips to 42 kips for S=0ft. It should be noted that the pile stresses during pushover analysis for the load case with incremented vertical loads and a constant horizontal load did not exceed the yield stress of A36 steel prior to failure of the bent. Therefore, the p-delta curves for this loading are unchanged and remain as shown in Figures 7.2-7.6 (for bents pinned at the cap and fixed at the ground) and 7.12-7.16 (for bents fixed at the cap and pinned at the ground).

Although the inclusion of plastic hinges in the GTSTRUDL models significantly reduced the difference between the ultimate horizontal force of the FB-Pier and GTSTRUDL pushover analysis results, a significant difference still remained between the failure loads produced by each program (Figures 7.22-7.26). The resulting pile stresses were therefore examined in the FB-Pier models, and it was found that in most trials the analysis procedure terminated before yield strength of the piles was reached. Upon review of FB-Pier's Help Manual, early termination of the pushover analysis procedure is thought to be the consequence of FB-Pier's failure ratio parameter which is calculated from the bi-axial interaction diagram of each pile. As mentioned in the Literature Review, FB-Pier's Help Manual (6) states that the cross section failure ratio is calculated by taking the M_x-M_y diagram for a constant axial load. This failure ratio is calculated as the vector (P, M_x, M_y) length divided by the point at which the extended vector will touch the failure curve (see Figure 2.20) and terminates the pushover analysis procedure when the ratio exceeds a value of one. This method assumes that the axial load of the cross-section will remain constant and although it is conservative, it is not very realistic (6). In indeterminate structures, all forces interact and for the moments to increase, the axial load must also increase. Therefore, it appears that the pushover analysis results of FB-Pier in fact do terminate prematurely and the results of GTSTRUDL give more realistic approximations to the ultimate horizontal force capacity of the bents. Furthermore, from simply looking at the P-delta curves for the FB-Pier results in Figures 7.22-7.26, something looks incorrect. In most of the figures the curves appear to be

exhibiting linear behavior of the bent (which is highly indeterminate and made of ductile material) and the curve suddenly ends without "laying over". This does not seem realistic or feasible and further supports the notion that FB-Pier's failure ratio criterion is not reasonable for this modeling.

7.5 Material Nonlinearity and Plastic Hinge Parameters

After noticing an increase in stiffness near the end of several of the pile bent p-delta curves for the GTSTRUDL modelings (Figures 7.22-7.26), GTSTRUDL's plastic hinge parameters were examined to better understand the nonlinear stress strain relationship being used during the pushover analysis procedure. As indicated in the GTSTRUDL 27 Release Guide (4), the assumed steel stress-strain curve for plastic hinges is a very sophisticated modeling of the nonlinear material behavior (see Figure 7.62). Most notable is the inclusion of a strain-hardening region in which the ultimate stress is bounded by 1.5FY or 54 ksi, when FY, the yield strength of the steel, is 36 ksi. In order to simplify the modeling and attempt to give a more distinct pushover load for the bents, the default stress-strain curve parameters shown in Figure 7.62 were modified to exhibit an elastic-perfectly plastic, or elastoplastic, relationship with a yield strength of 36 ksi. The resulting pushover analysis p-delta curves are shown in Figures 7.27-7.31 for bents with fixed bases. As expected the p-delta curves for the elastic-perfectly plastic hinges and the hinges with a sophisticated stress-strain modeling behave similarly (elastically) to the point where the curves begin to lay over. However, the curves for bents with elastoplastic hinges level off and reach a failure load at the point where the sophisticated plastic hinge models are just entering the strain-hardening region of the stress strain curve. Additionally, by plotting the p-delta curve resulting from the elastic-perfectly plastic model beside the model exhibiting a sophisticated stress-strain relationship, the reserve capacity developed from strain hardening of the steel is shown. Since the nonlinear behavior during strain hardening is somewhat unpredictable, the elastic-perfectly plastic stress-strain curve will be used in future models in an effort to attain a more distinctive pushover load and to remain conservative and not assume that strain-hardening will occur. For succeeding non X-braced bent models the pushover results of bents modeled with the sophisticated plastic hinges will be plotted along side those with elastoplastic hinges to show

any reserve capacity resulting from strain hardening. However, the actual capacity of the bent will be taken from the model with elastic perfectly plastic hinges. (It may be noted that FB-Pier's default stress-strain curve for steel is elastic perfectly plastic, although bents modeled with FB-Pier behave linearly until premature failure.)

GTSTRUDL also offers a sophisticated method for modeling material/member behavior by its capability to model residual stresses that may be present in steel members as a result of the H-pile formation process. The assumed residual stress distribution of GTSTRUDL for wide flange plastic hinges is shown in Figure 7.63. These residual stresses are accounted for via the ALPHA term in the plastic hinge parameters. According to the GTSTRUDL Release Guide, any positive value for ALPHA is allowed; however, in practice, ALPHA should be 0.5 or less (4). Therefore, the pushover analysis procedures were performed with ALPHA equal 0.5 to account for residual stresses and compared to the pushover analysis data for models with no residual stresses where ALPHA was set equal to 0. The pushover analysis results for these two values of ALPHA are plotted in Figures 7.32-7.36 for bents with fixed bases. The graphs show that the presence of residual stresses in the piles does not affect either the horizontal load capacity or lateral stiffness of the pile bents, and therefore the residual stress term will be set equal to 0 henceforth.

7.6 Pushover Analysis for Bents with Fixed Bases

Figures 7.37-7.41 show a comparison of the pushover analysis results from FB-Pier bent models and GTSTRUDL bents modeled with fixed bases for H=13ft. As a result of the previous study on material nonlinearity, the GTSTRUDL results are shown for bents having both elastoplastic and strain hardening plastic hinges. It is believed that the connection between the ground and the pile lies somewhere between a fully pinned and fully fixed condition. Since GTSTRUDL does not have the capability to model partial fixities, pushover analyses will be performed on bents with alternate models of pile fixities as shown in Figure 7.1. Modeling bents with fixed bases using GTSTRUDL is considered to provide the stiffest, strongest, and least conservative model but may come close to the actual pile end conditions of some existing pile

bent structures. Although FB-Pier's pushover analysis terminates before the bent "lays over" it remains possible to compare the stiffness of the FB-Pier and GTSTRUDL models for initial loads and displacements (note FB-Pier's premature termination is discussed in Section 7.4). The GTSTRUDL pushover loads for the loading conditions shown in these figures (Figures 7.37-7.41) are 60.3 kips, 48.1 kips, 42.7 kips, 39.4 kips, and 37.3 kips for S=0ft, 5ft, 10ft, 15ft, and 20ft respectively, when elastic-perfectly plastic material behavior is assumed. Additionally, each of these figures shows that the bent stiffness for the GTSTRUDL models with fixed bases is approximately twice that of the FB-Pier models which have elastic foundations, and as a result may be too unconservative for future pushover analyses. The pushover loads for bents modeled with fixed bases are listed in Table 7.1 for ease of comparison.

7.7 Pushover Analysis for Bents with Additional Length to Fixity

As mentioned in Chapter 5, alternate methods may be used to assume partial fixities at the top and bottom of bent piles. Previous GTSTRUDL pushover analysis procedures were performed by placing a rigid connection at the cap and either a fully pinned or fully fixed connection at the base. Alternatively, we can examine the case with the top and bottom of the piles fully fixed with an additional length of ℓ_f = 5ft added to the bent height, H, as indicated in Figure 7.1. This additional 5ft was drawn from the previous results of FB-Pier modelings in Chapter 5 where it was concluded from both a buckling analysis and a stiffness analysis that the pile lateral displacements decreased to approximately zero at a depth of 5ft below the ground surface for a very wide range of soil subgrade modulus values (5-500 lb/in^3). As shown in the depiction of this modeling provided in Figures 7.42-7.46, the distance ℓ_f=5ft is added to H + S in order to reach the elevation below the ground line (after scour) where a full fixity may be assumed. Thus, the total bent height after scour is represented by the sum of H+S+5ft for the GTSTRUDL model. The total bent height of the FB-Pier model with an elastic foundation remains as H+S.

The p-delta curves produced by the GTSTRUDL model with an additional length to fixity are compared with the pushover results of the original FB-Pier models which have a total bent

height of H+S in Figures 7.42-7.46 for H=13ft. The corresponding GTSTRUDL pushover loads for bents with effective pile lengths of H+S+5ft when S=0ft, 5ft, 10ft, 15ft, and 20ft are 48.1 kips, 42.7 kips, 39.4 kips, 37.3 kips, 36.5 kips respectively when elastic-perfectly plastic behavior is assumed. These values are also summarized in Table 7.1. Using Figures 7.42-7.46 to compare the stiffness of bents modeled with an additional 5ft to fixity using GTSTRUDL to those modeled with elastic foundations in FB-Pier shows that the stiffness of the GTSTRUDL model is somewhat greater than that of the FB-Pier model for each level of scour. However, the difference in bent stiffness for GTSTRUDL and FB-Pier is much smaller when the GTSTRUDL model incorporates the additional length to fixity instead of the original bent height as in the previous section. This modeling may produce fixity levels quite similar to many actual pile end conditions, since placing full fixities at the cap and base is mostly likely an overly unconservative estimate of pushover failure loads. However, in an effort to remain conservative, the pushover analysis results for bents modeled with pinned connections to the ground in GTSTRUDL should also be evaluated and compared to FB-Pier's modeling of bents with an elastic soil foundation.

7.8 Pushover Analysis for Bents with Pinned Bases

The pushover analysis results for GTSTRUDL bents modeled with pinned bases are compared with the original FB-Pier bent models in Figures 7.47-7.51 for H=13ft. The GTSTRUDL pushover analysis results are shown for bents which exhibit both elastic-perfectly plastic and strain hardening behavior as in the previous sections. When gravity forces above each pile are constant at 100 kips and the horizontal force is incremented, the GTSTRUDL pushover loads are 34.9 kips, 32.9 kips, 30.9 kips, 22.5 kips, and 15.5 kips for S=0ft, 5ft, 10ft, 15ft, and 20ft respectively when elastic-perfectly plastic material behavior is assumed. These capacities are also listed in Table 7.1. Comparing the p-delta curves of bents modeled with pinned bases for GTSTRUDL to those modeled with an elastic foundation in FB-Pier, the stiffness for each modeling is very close. For smaller levels of scour the pinned base models of GTSTRUDL appear to provide slightly conservative stiffness behavior. The stiffness of each model becomes nearly identical for S=15ft, and beyond this value the stiffness of the FB-Pier model is slightly less

than that of GTSTRUDL. Thus, it seems that modeling bents with pinned bases is a close approximation to those modeled with an elastic soil foundation.

Since the GTSTRUDL modeling of bents with pinned bases appears to be the closest approximation to the load deflection behavior predicted with FB-Pier's elastic foundation, a GTSTRUDL pushover analysis for this model was also performed on bents with H=10ft so that p-delta curve comparisons can be made for non X-braced bents with H<13ft. The FB-Pier and GTSTRUDL comparisons of these results are shown in Figures 7.52-7.56. A comparison of the stiffness of the GTSTRUDL models to the FB-Pier models for bents with H=10ft also suggests that modeling the bents with pinned bases produces stiffness behavior that is very close to the FB-Pier bents with elastic foundations. The maximum loads at pushover according to the GTSTRUDL model with elastic-perfectly plastic behavior and H=10ft are 40.6 kips, 33.5 kips, 34.7 kips, 27.0 kips, 19.5 kips for S=0ft, 5ft, 10ft, 15ft, and 20ft respectively. These pushover capacities are summarized in Table 7.2. As expected the pushover loads for bents with H=10ft are slightly larger than those for H=13ft, however, the differences between the two are only minor. Therefore, the pushover analyses for non X-braced bents with H=10ft and 13ft are thought to provide sufficient comparison for the majority of non X-braced bent heights.

7.9 GTSTRUDL Pushover Analysis for Bents with Various Pile Numbers

As noted in Chapter 4, typical bridge pile bents may have 3 to 7 piles (see Section 4.1). Of the 31 Standard bent drawings examined the majority have between 3-6 piles. This section will further evaluate whether non X-braced bents with more piles are less susceptible to scour failure (Figures 7.57a-7.57e) and directly determine the impact of scour on the pushover loads for standard non X-braced ALDOT bents with H=13ft (Figures 7.53-7.56).

To determine if bents with more piles are less susceptible to scour failure, a pushover analysis was performed using GTSTRUDL for scour levels of S=0ft, 5ft, 10ft, 15ft, and 20ft on the non X-braced bents with the results shown in Figures 7.57a-7.57e. For each bent in this study the piles were given rigid connections to the cap and pinned connections to the ground as shown in the corresponding figures. It was concluded in previous sections that this GTSTRUDL

modeling appears to provide very accurate stiffness behavior to FB-Pier bents modeled with an elastic foundation. For S=0ft (Figure 7.57a) stiffness and strength both increase as the number of piles in the bent increases. The pushover loads for these 3, 4, 5, and 6-pile bents (H=13ft) with no scour are 13.2 kips, 27.9 kips, 34.9 kips, and 37.1kips respectively with corresponding increases in stiffness. When S=5ft (Figure 7.57b), however, there is no increase in stiffness between the 5-pile and 6-pile bents, although the 6-pile bent withstands a slightly larger pushover load. As scour increases to 20ft (Figure 7.57e), it appears that the stiffness of the 6-pile bent becomes slightly less than that of the 5-pile bent even though the pushover load of the 6-pile bent remains slightly larger. The pushover capacities of these bents are listed in Table 7.3 for ease of comparison.

To obtain a more direct assessment of the impact that scour has on the pushover load for standard non X-braced ALDOT bents with 3, 4, 5, and 6 piles, Figures 7.58-7.61 show the p-delta curves for each bent with H=13ft and scour of S=0ft, 5ft, 10ft, 15ft, and 20ft. For simplicity this study only considers the placement of the horizontal force at the center of the cap and all bents were conservatively modeled with pinned connections to the ground. The resulting GTSTRUDL pushover analysis curves are used to show the level of scour at which the bents become unstable. This is characterized by a rapid increase in deflection for small increases in loading. As mentioned previously, the maximum lateral forces at failure are summarized in Table 7.3 for each level of scour considered. Unlike the 3-pile non X-braced bent, the 4, 5, and 6-pile non X-braced bents were stable for each level of scour up to 20ft. Scour had a much larger impact on the 3-pile non X-braced bent which lost half of its lateral capacity with the first 5ft of scour and became unstable for $S \geq 15$ft (Figure 7.58).

Table 7.1 Horizontal Failure Loads at Bent Cap in the Transverse Direction for Three GTSTRUDL Pushover Analysis Modelings of the HP10x42 5-Pile Bents Shown in Figure 7.1.

Scour (ft) Original H =13ft	Horizontal Failure Load, F (kips)		
	Bents w/ Fixed Base Fig. 7.1a (see Figs 7.37-7.41)	Bents w/ Fixed Base 5ft below Ground Line Fig. 7.1b (see Figs 7.42-7.46)	Bents w/ Pinned Base Fig. 7.1c (see Figs 7.47-7.51)
0	60.3	48.1	34.9
5	48.1	42.7	32.9
10	42.7	39.4	30.9
15	39.4	37.3	22.5
20	37.3	36.5	15.5

* Note: All bents are modeled with rigid connections to the cap.

Table 7.2 Horizontal Failure Loads at Bent Cap in the Transverse Direction for GTSTRUDL Pushover Analysis Modeling of the HP10x42 5-Pile Bents Shown in Figure 7.1c.

Scour (ft) Original H =10ft	Horizontal Failure Load, F (kips)
	Bents w/ Pinned Base Fig. 7.1c (see Figs 7.52-7.56)
0	40.6
5	33.5
10	34.7
15	27.0
20	19.5

* Note: All bents are modeled with rigid connections to the cap.

Table 7.3. GTSTRUDL Pushover Capacity of Non X-braced Bents with Scour (See Figures 7.58-7.61)

Scour, S (ft) H=13ft	Horizontal Failure Load, F (kips)			
	3-Pile Bent (kips)	4-Pile Bent (kips)	5-Pile Bent (kips)	6-Pile Bent (kips)
0	13.2	27.8	34.9	37.1
5	6.4	24.6	32.9	33.7
10	1.5	20.8	30.9	32.4
15	unstable	14.5	22.5	23.6
20	unstable	9.3	15.5	16.3

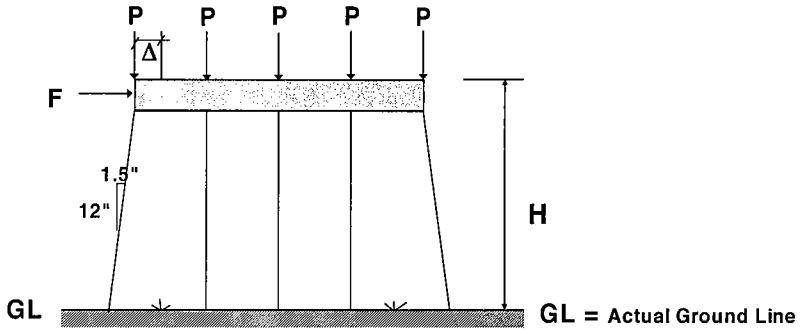

a) Bent Piles Assumed Fixed at GL

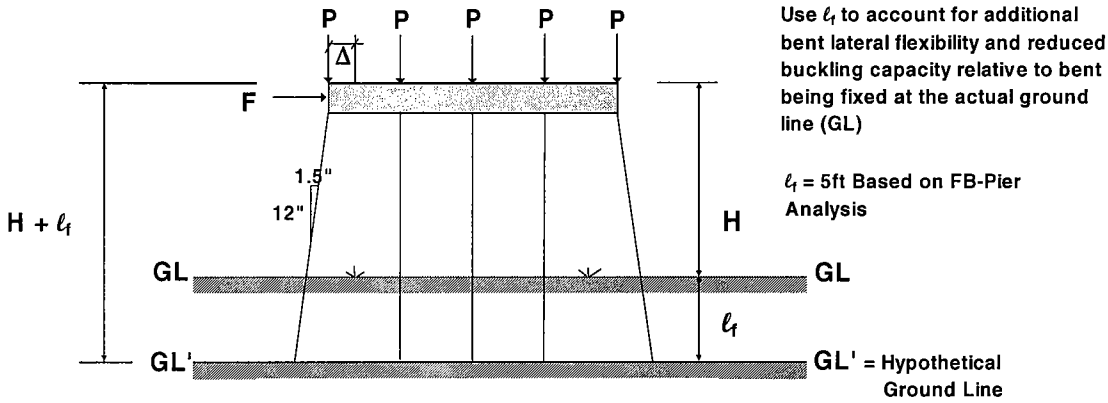

b) Bent Piles Assumed ℓ_f = 5ft Longer and Fixed at GL

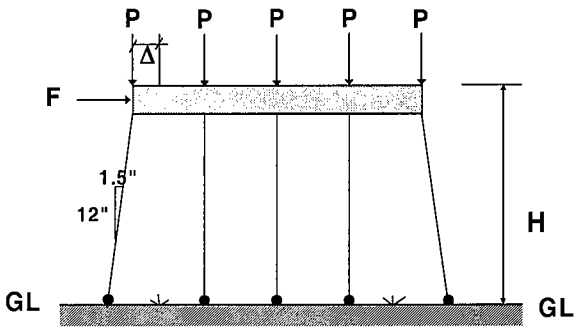

c) Bent Piles Assumed Pinned at GL

Figure 7.1. Alternate Modelings of Bridge Pile Bent

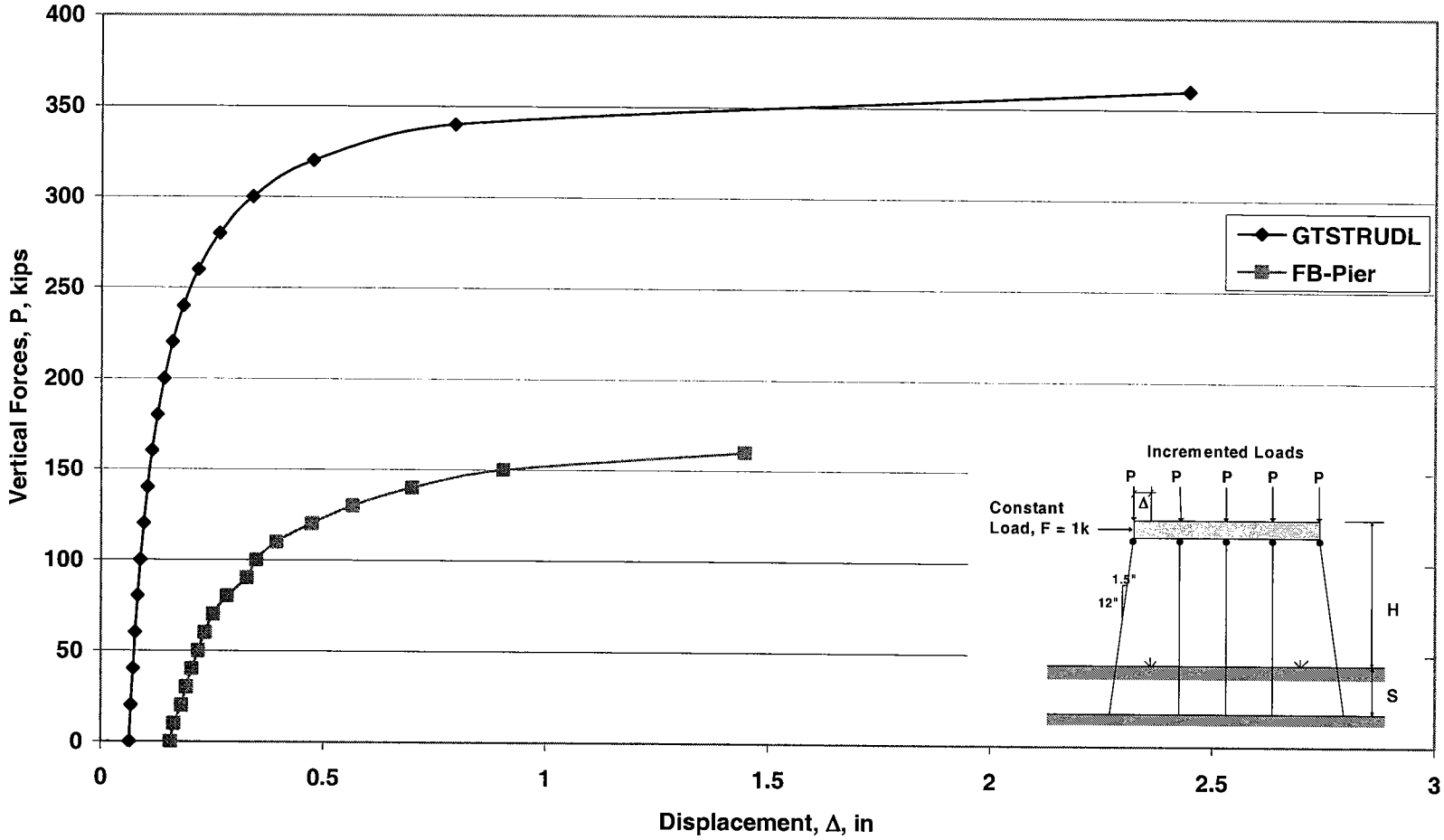

Figure 7.2. Pushover (Buckling) Analysis Comparison for HP10x42 5-Pile Bent, Pinned at Cap, Fixed at Ground (for GTSTRUDL), Soil K_o = 150 lb/in^3 (for FB-Pier), H=13ft, S=0ft

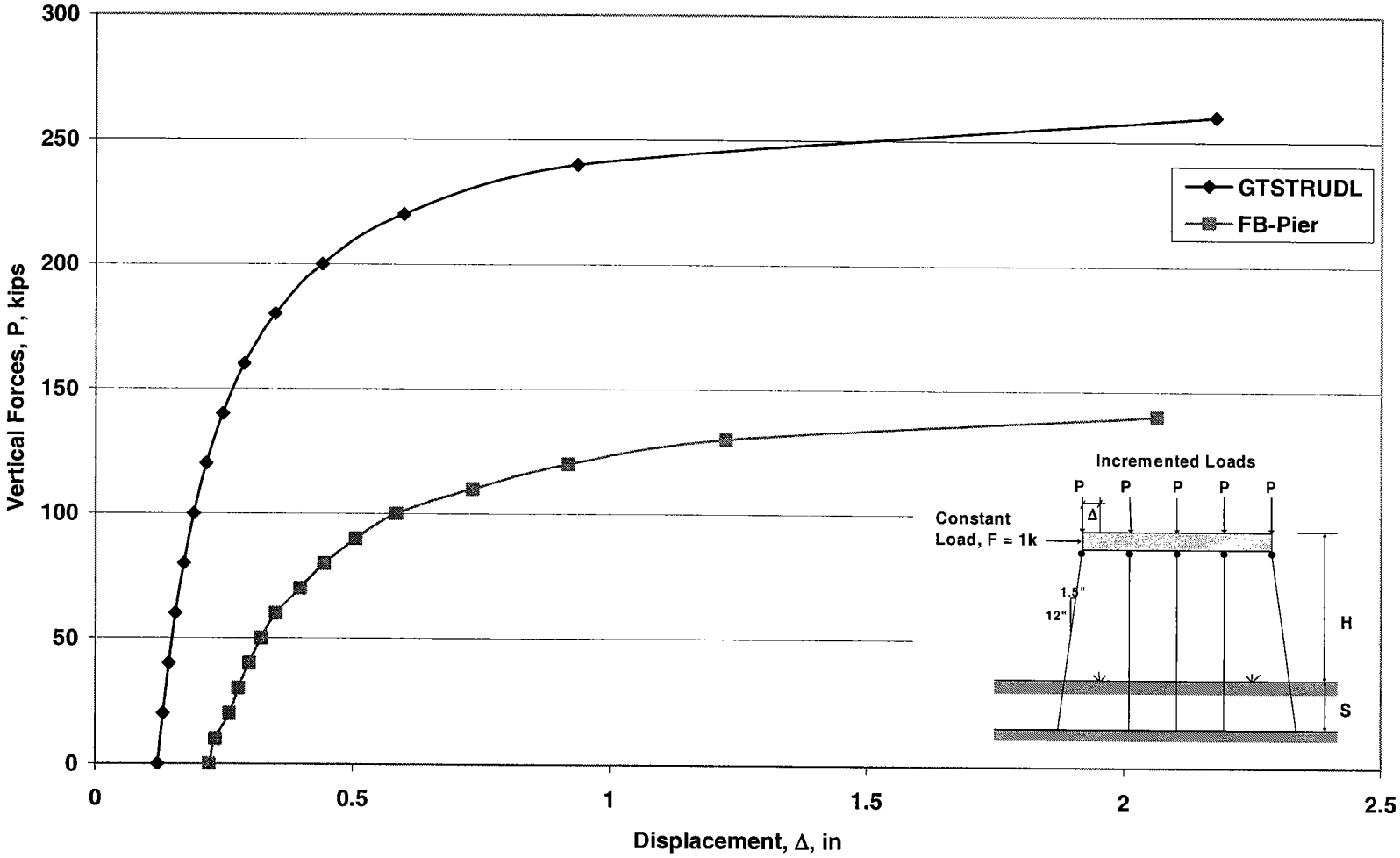

Figure 7.3. Pushover (Buckling) Analysis Comparison for HP10x42 5-Pile Bent, Pinned at Cap, Fixed at Ground (for GTSTRUDL), Soil K_o = 150 lb/in^3 (for FB-Pier), H=13ft, S=5ft

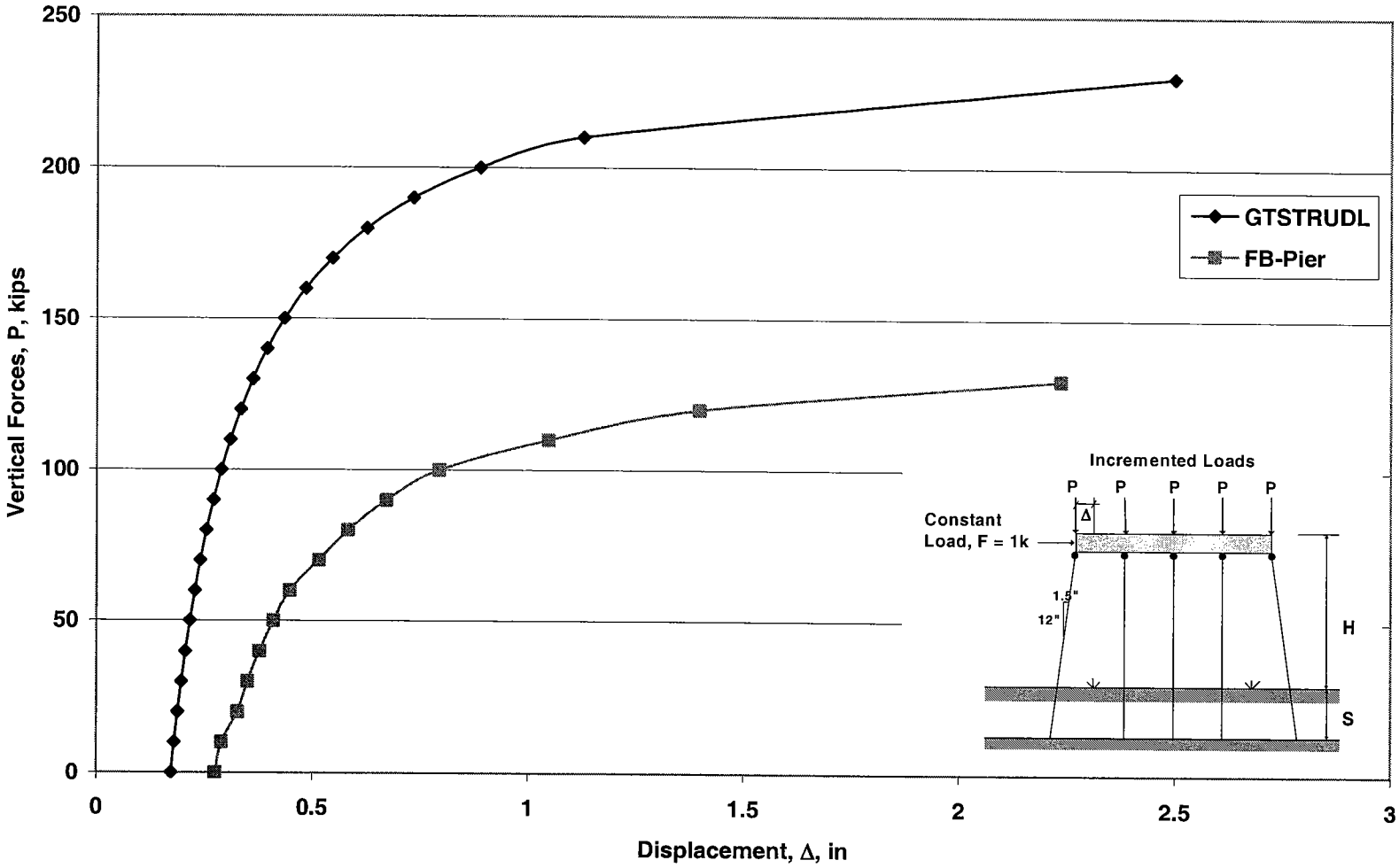

Figure 7.4. Pushover (Buckling) Analysis Comparison for HP10x42 5-Pile Bent, Pinned at Cap, Fixed at Ground (for GTSTRUDL), Soil K_o = 150 lb/in^3 (for FB-Pier), H=13ft, S=10ft

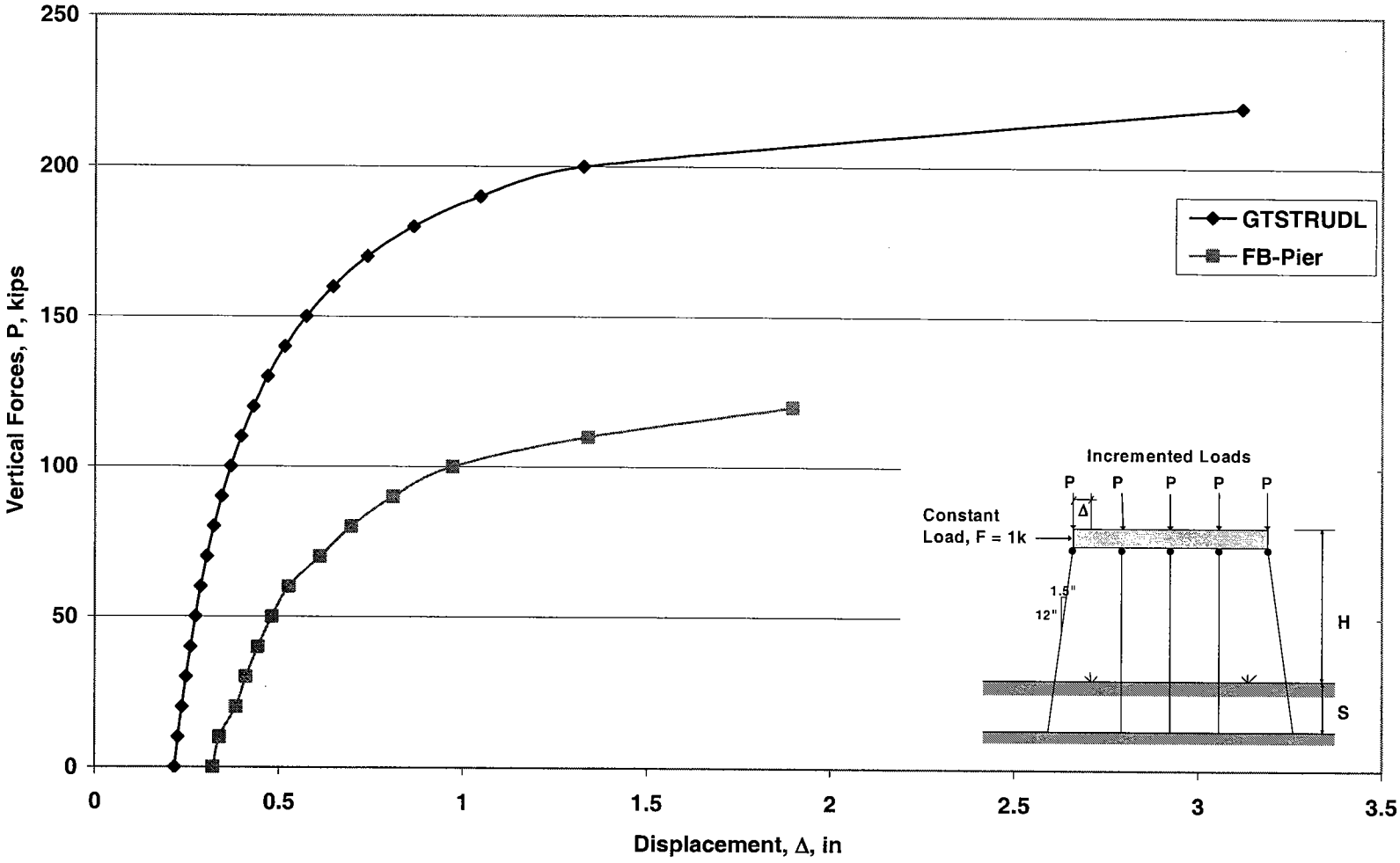

Figure 7.5. Pushover (Buckling) Analysis Comparison for HP10x42 5-Pile Bent, Pinned at Cap, Fixed at Ground (for GTSTRUDL), Soil K_o = 150 lb/in^3 (for FB-Pier), H=13ft, S=15ft

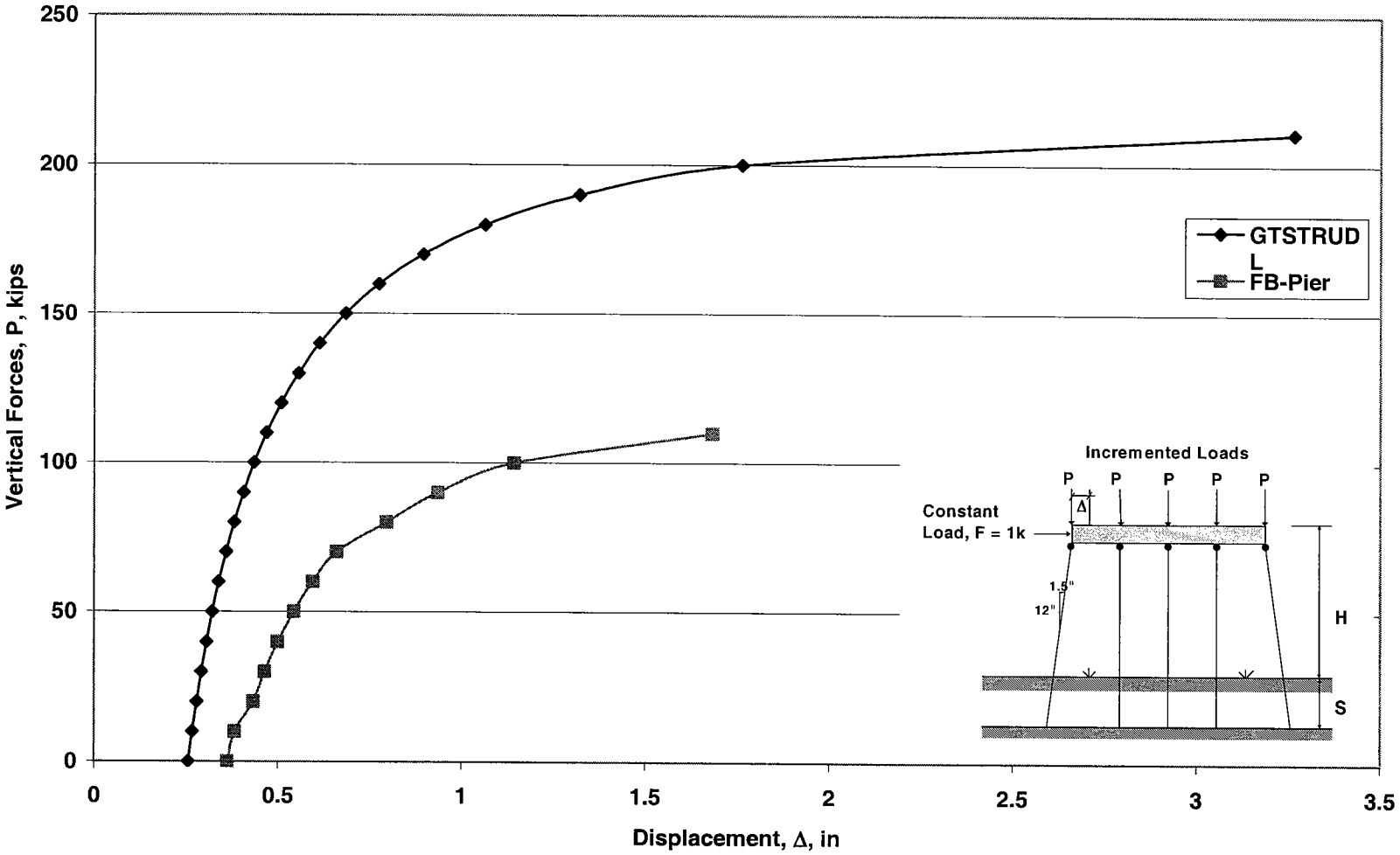

Figure 7.6. Pushover (Buckling) Analysis Comparison for HP10x42 5-Pile Bent, Pinned at Cap, Fixed at Ground (for GTSTRUDL), Soil K_o = 150 lb/in^3 (for FB-Pier), H=13ft, S=20ft

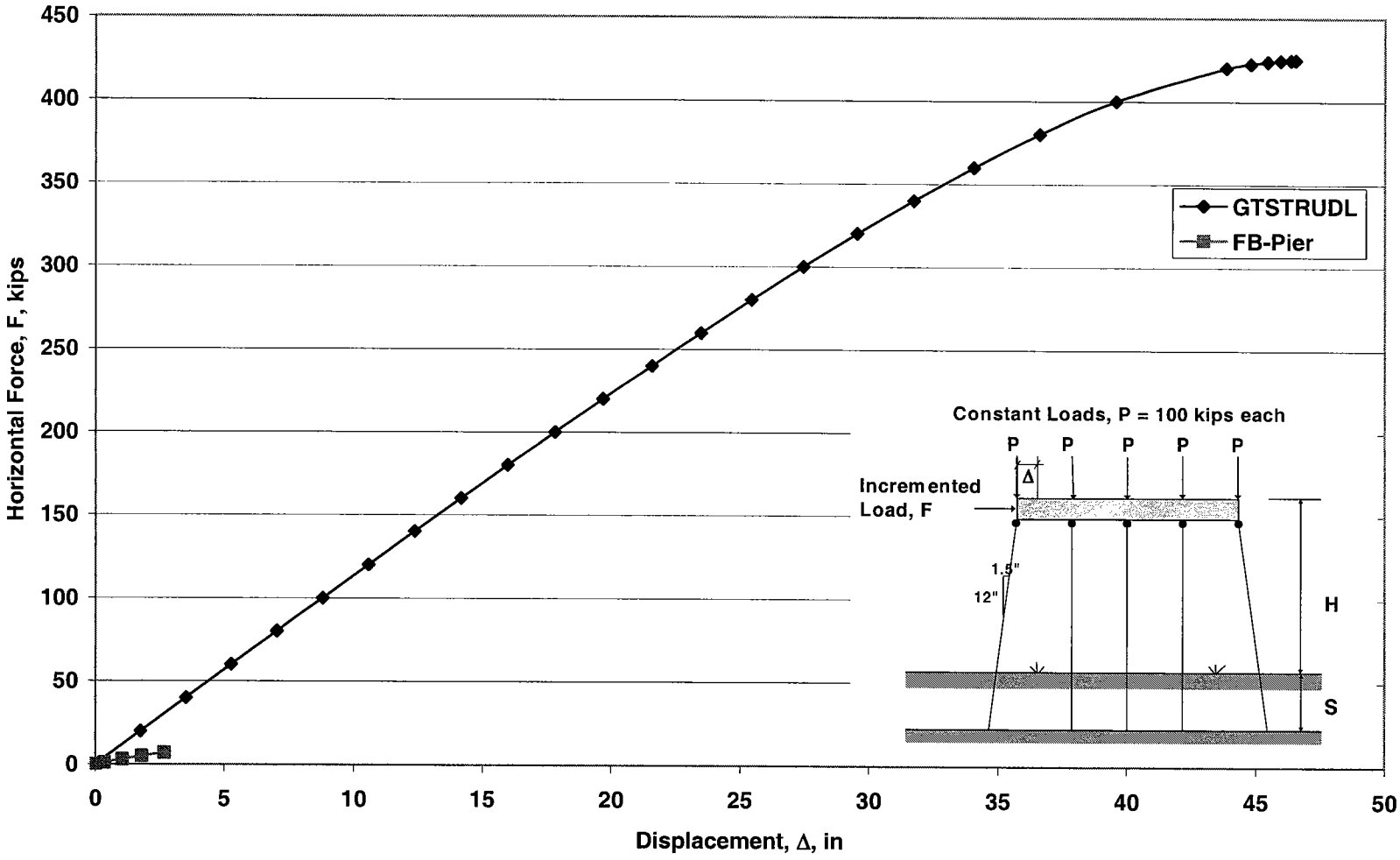

Figure 7.7. Pushover Analysis Comparison for HP10x42 5-Pile Bent, Pinned at Cap, Fixed at Ground (for GTSTRUDL), K_o = 150 lb/in^3 (for FB-Pier), H = 13ft, S=0ft

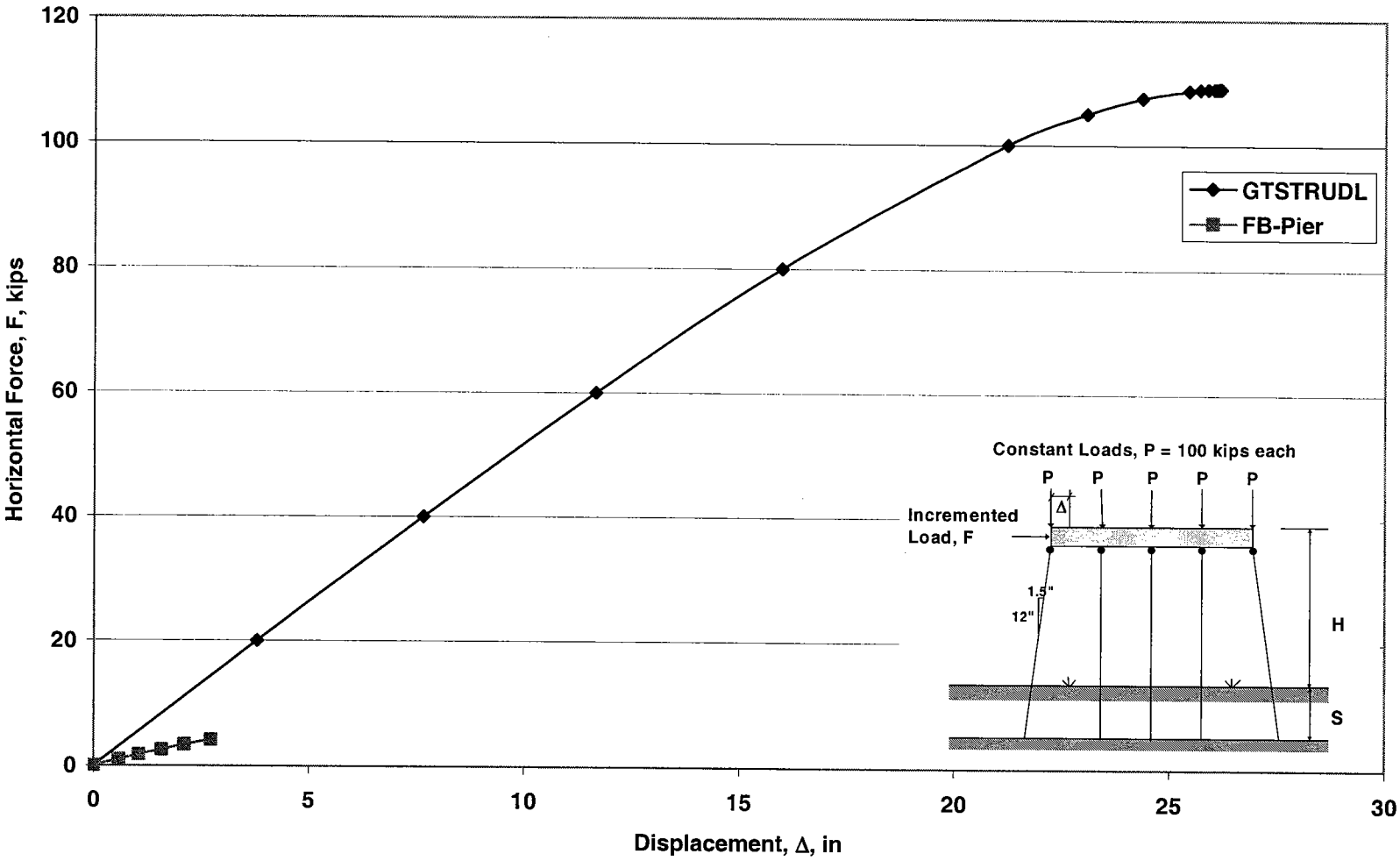

Figure 7.8. Pushover Analysis Comparison for HP10x42 5-Pile Bent, Pinned at Cap, Fixed at Ground (for GTSTRUDL), K_o = 150 lb/in^3 (for FB-Pier), H = 13ft, S=5ft

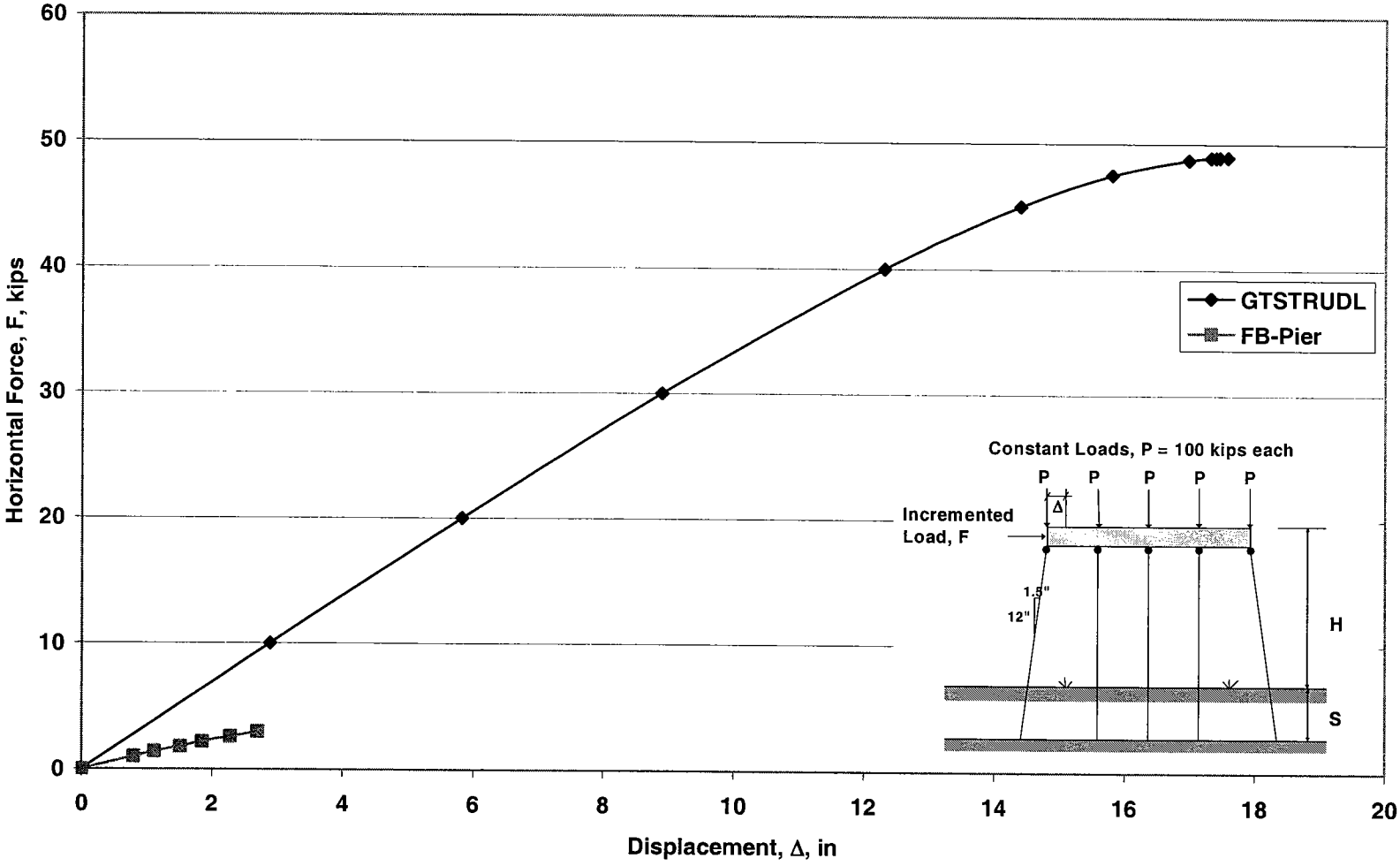

Figure 7.9. Pushover Analysis Comparison for HP10x42 5-Pile Bent, Pinned at Cap, Fixed at Ground (for GTSTRUDL), K_o = 150 lb/in^3 (for FB-Pier), H = 13ft, S=10ft

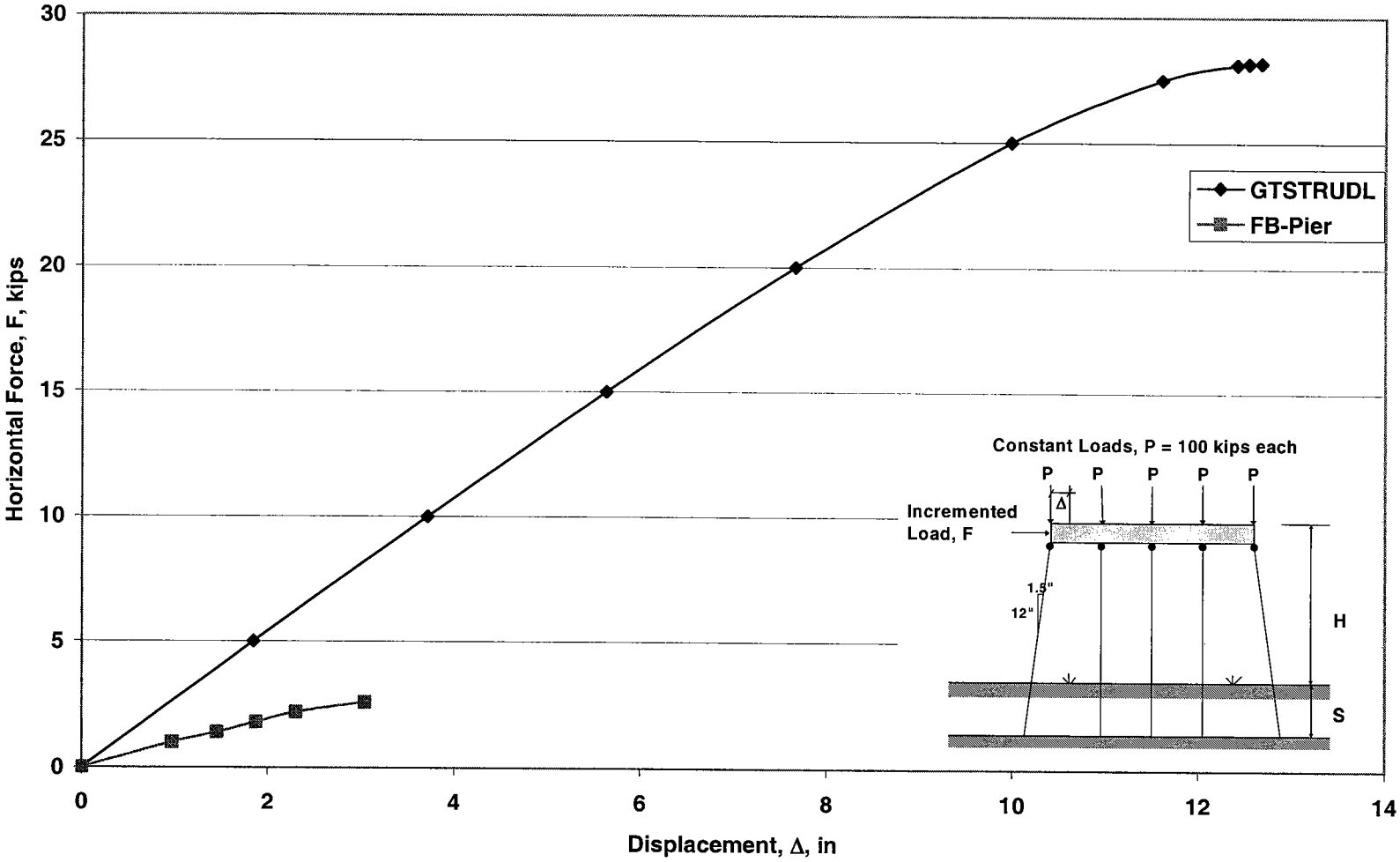

Figure 7.10. Pushover Analysis Comparison for HP10x42 5-Pile Bent, Pinned at Cap, Fixed at Ground (for GTSTRUDL), K_o = 150 lb/in^3 (for FB-Pier), H = 13ft, S=15ft

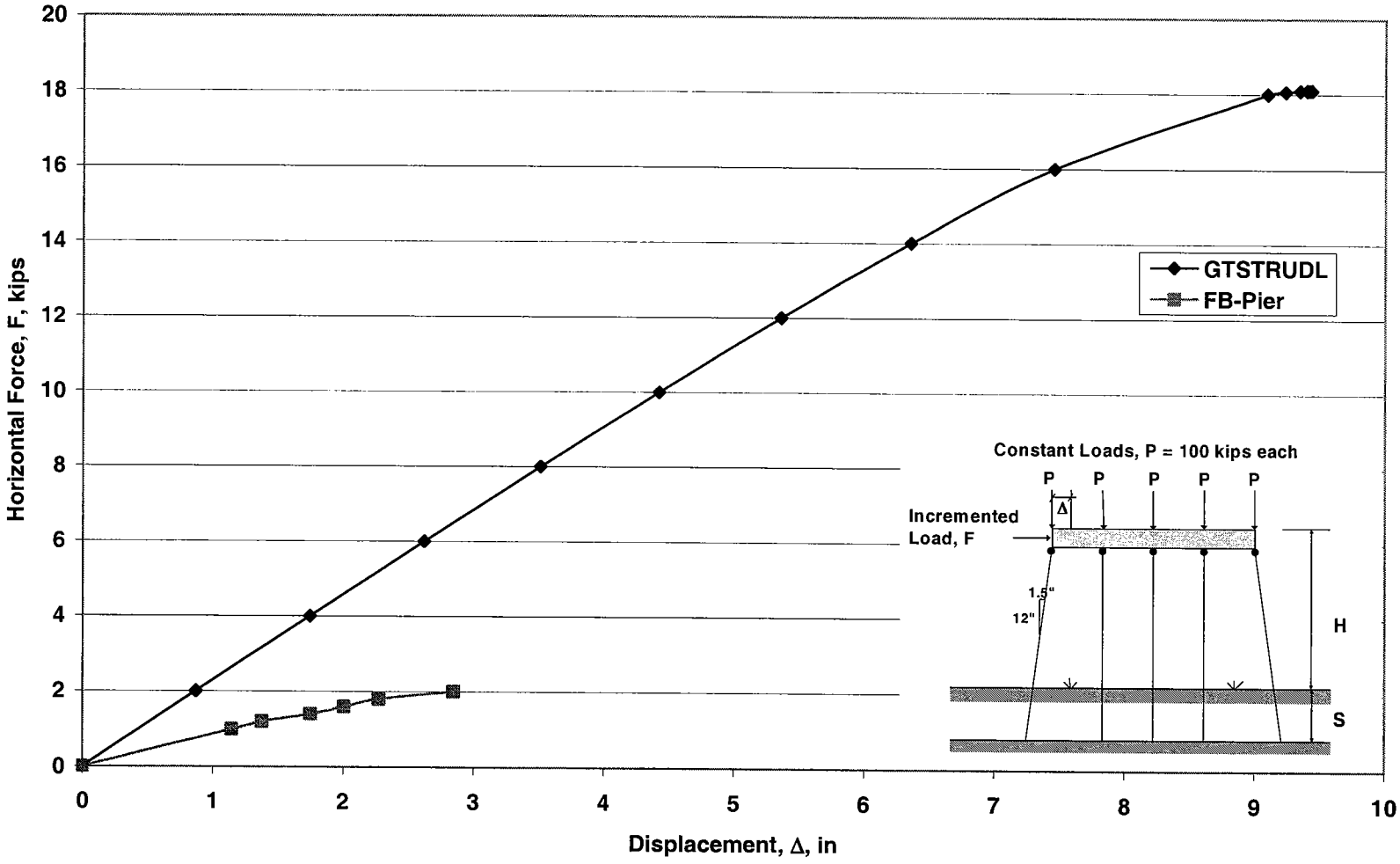

Figure 7.11. Pushover Analysis Comparison for HP10x42 5-Pile Bent, Pinned at Cap, Fixed at Ground (for GTSTRUDL), K_o = 150 lb/in^3 (for FB-Pier), H = 13ft, S=20ft

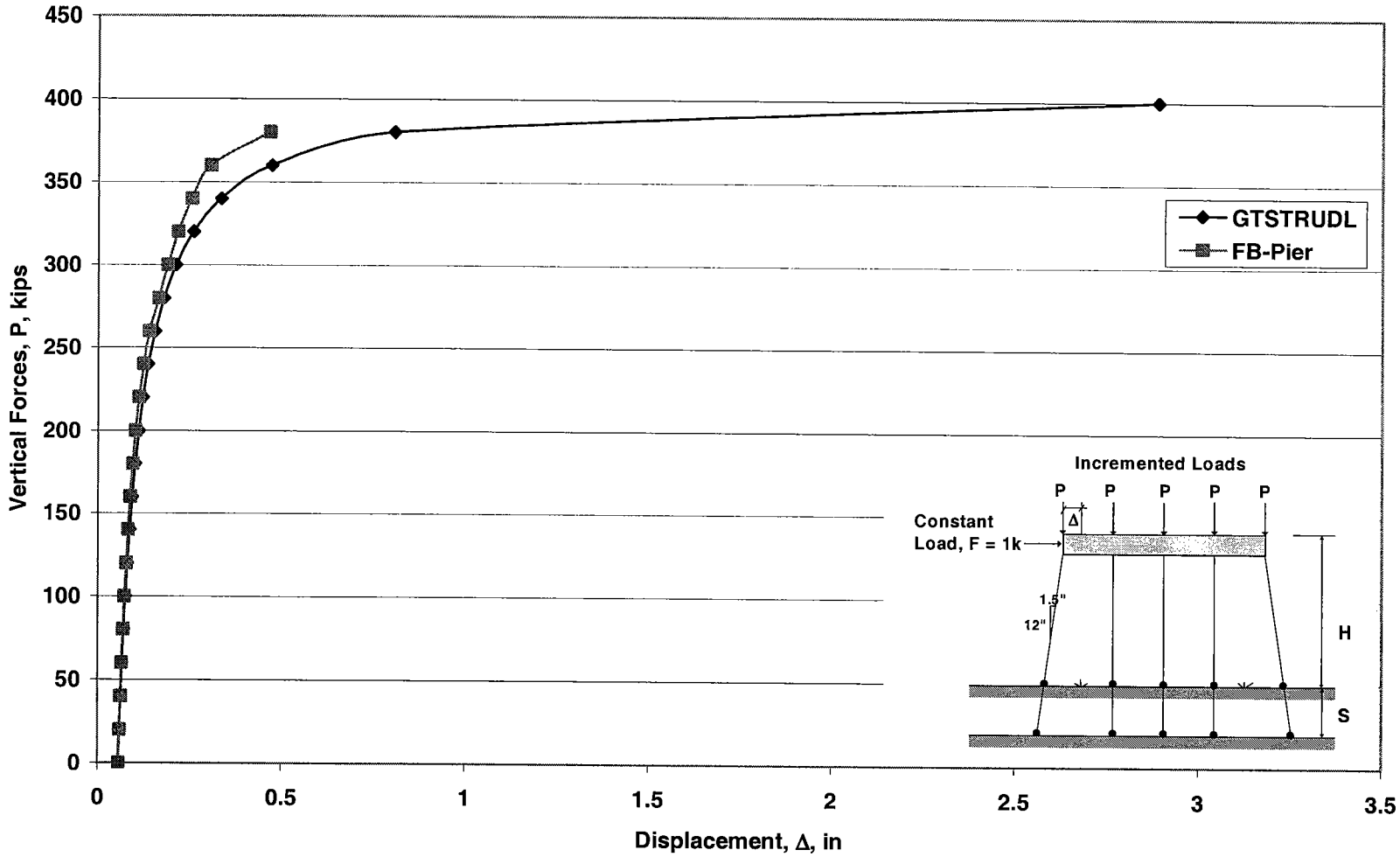

Figure 7.12. Pushover (Buckling) Analysis Comparison for HP10x42 5-Pile Bent, Fixed at Cap, Pinned at Ground (for GTSTRUDL), Soil K_o=150lb/in^3 (for FB-Pier), H=13ft, S=0ft

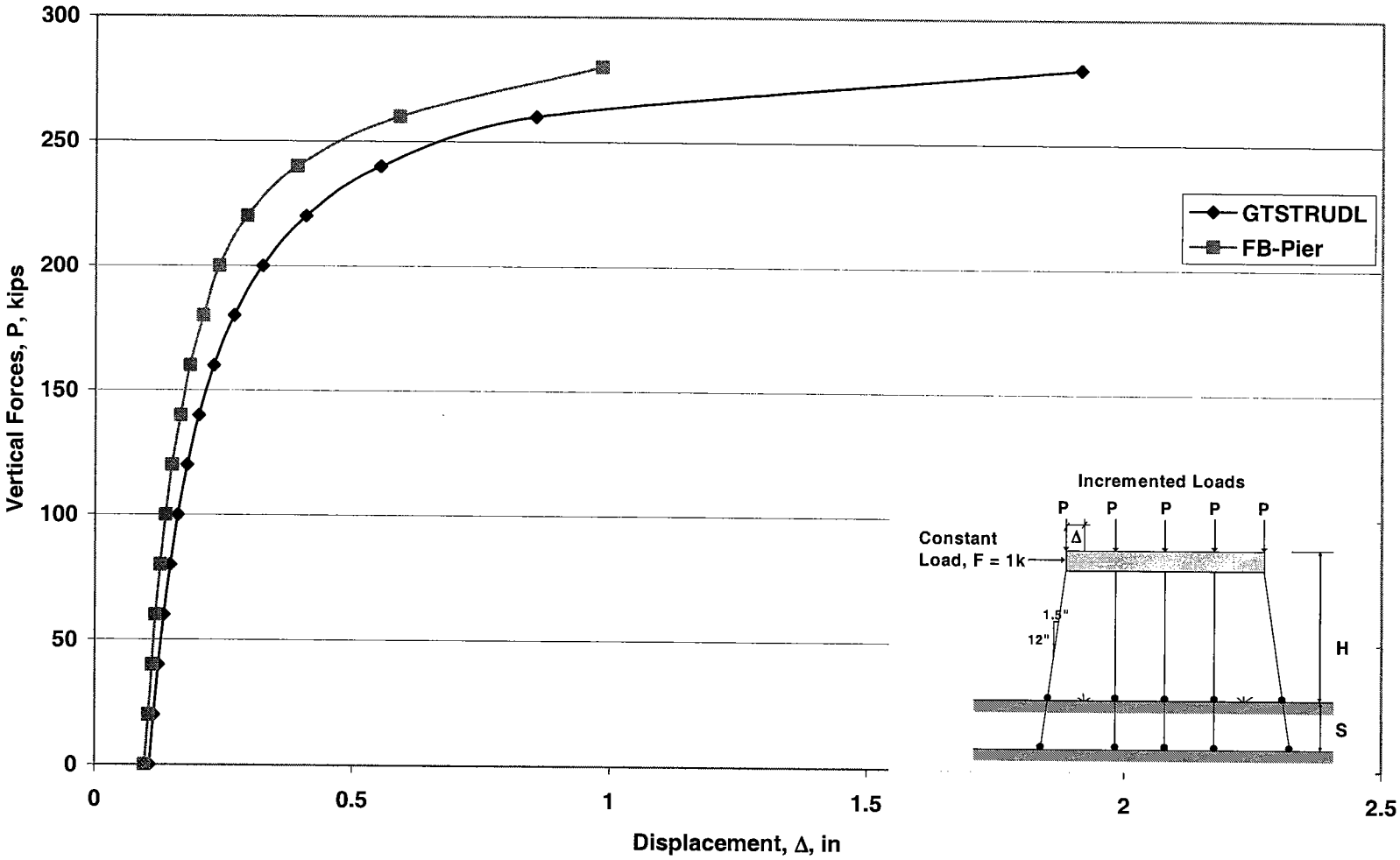

Figure 7.13. Pushover (Buckling) Analysis Comparison for HP10x42 5-Pile Bent, Fixed at Cap, Pinned at Ground (for GTSTRUDL), Soil K_o=150lb/in^3 (for FB-Pier), H=13ft, S=5ft

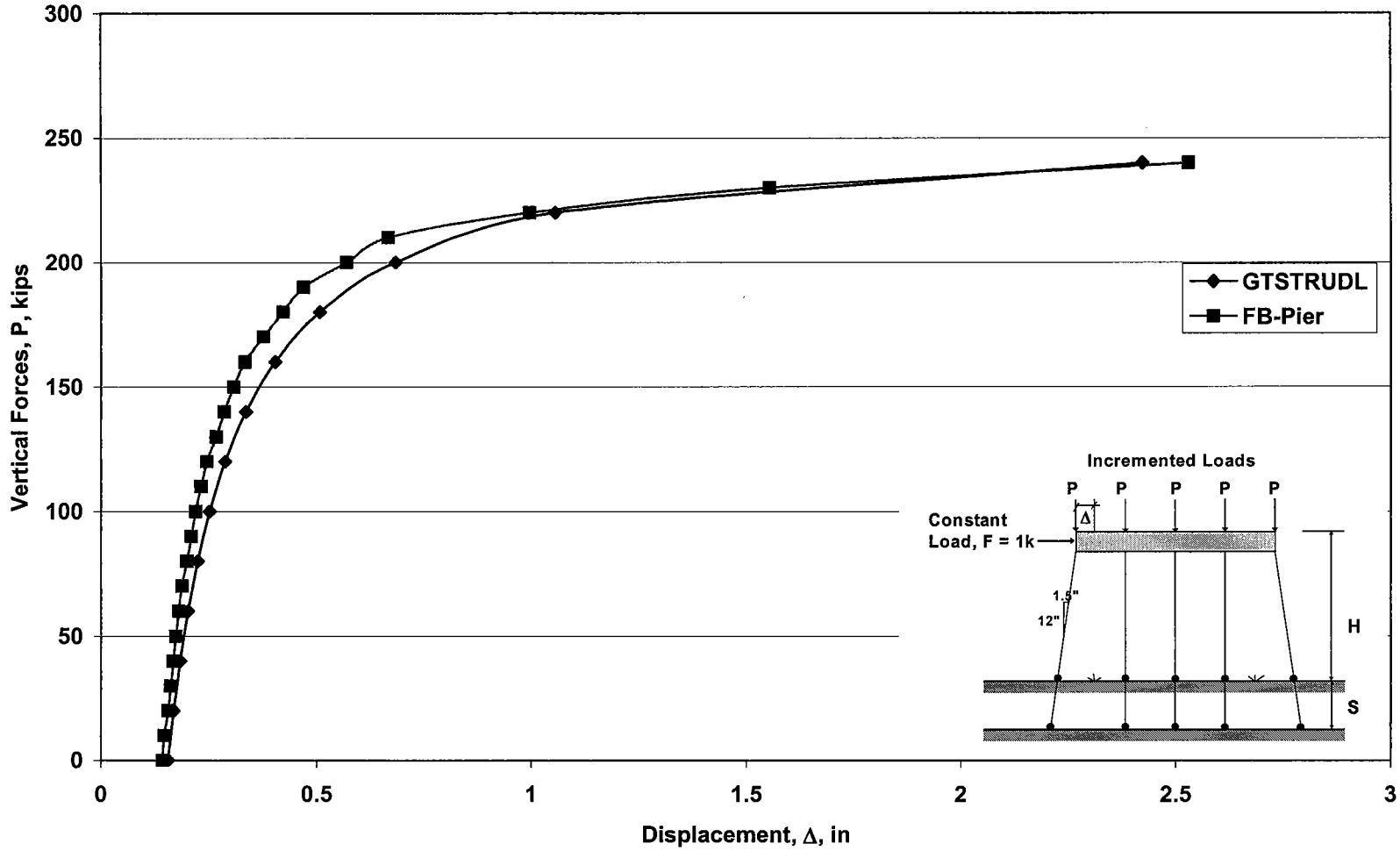

Figure 7.14. Pushover (Buckling) Analysis Comparison for HP10x42 5-Pile Bent, Fixed at Cap, Pinned at Ground (for GTSTRUDL), Soil K_o=150lb/in^3 (for FB-Pier), H=13ft, S=10ft

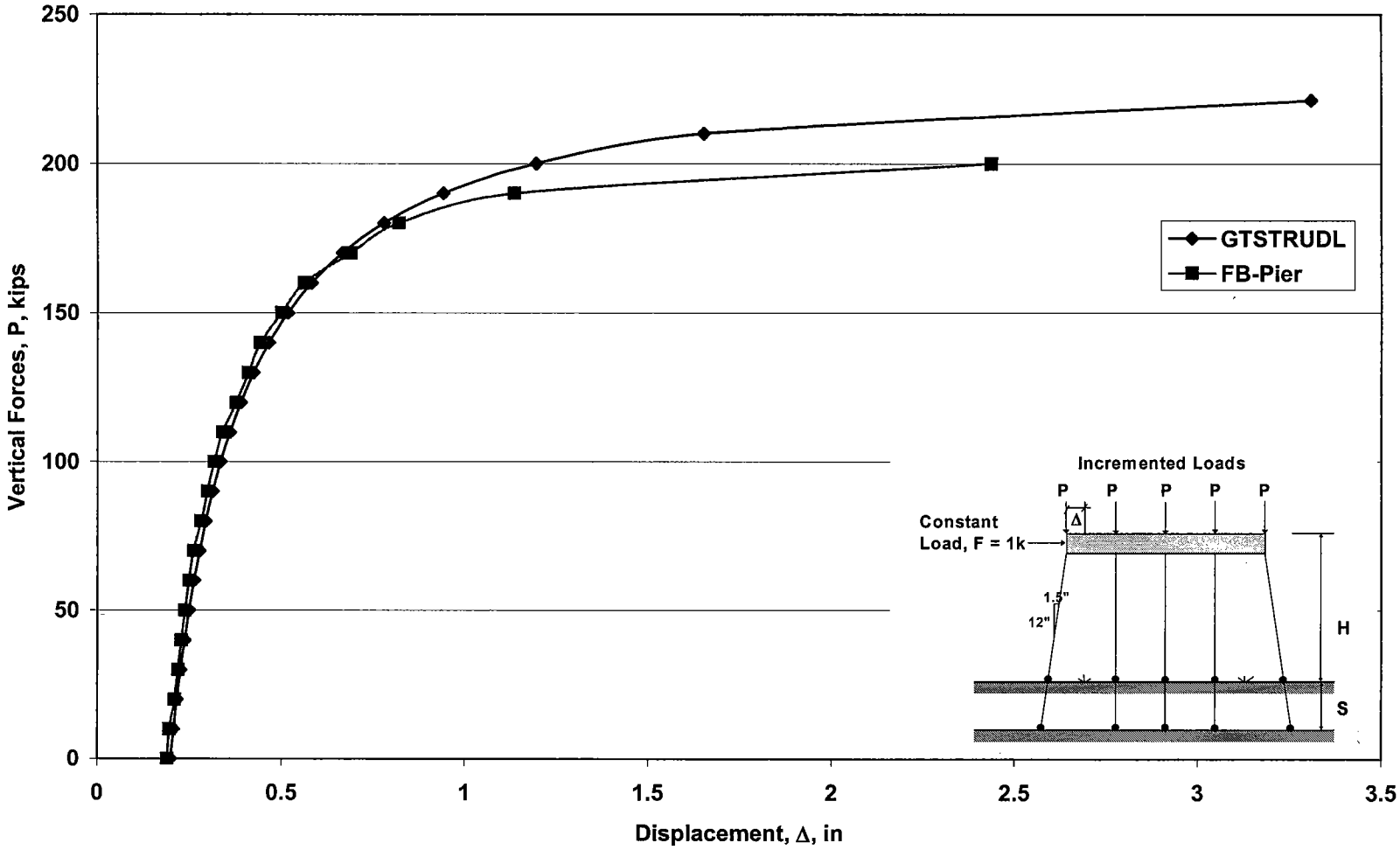

Figure 7.15. Pushover (Buckling) Analysis Comparison for HP10x42 5-Pile Bent, Fixed at Cap, Pinned at Ground (for GTSTRUDL), Soil K_o=150lb/in^3 (for FB-Pier), H=13ft, S=15ft

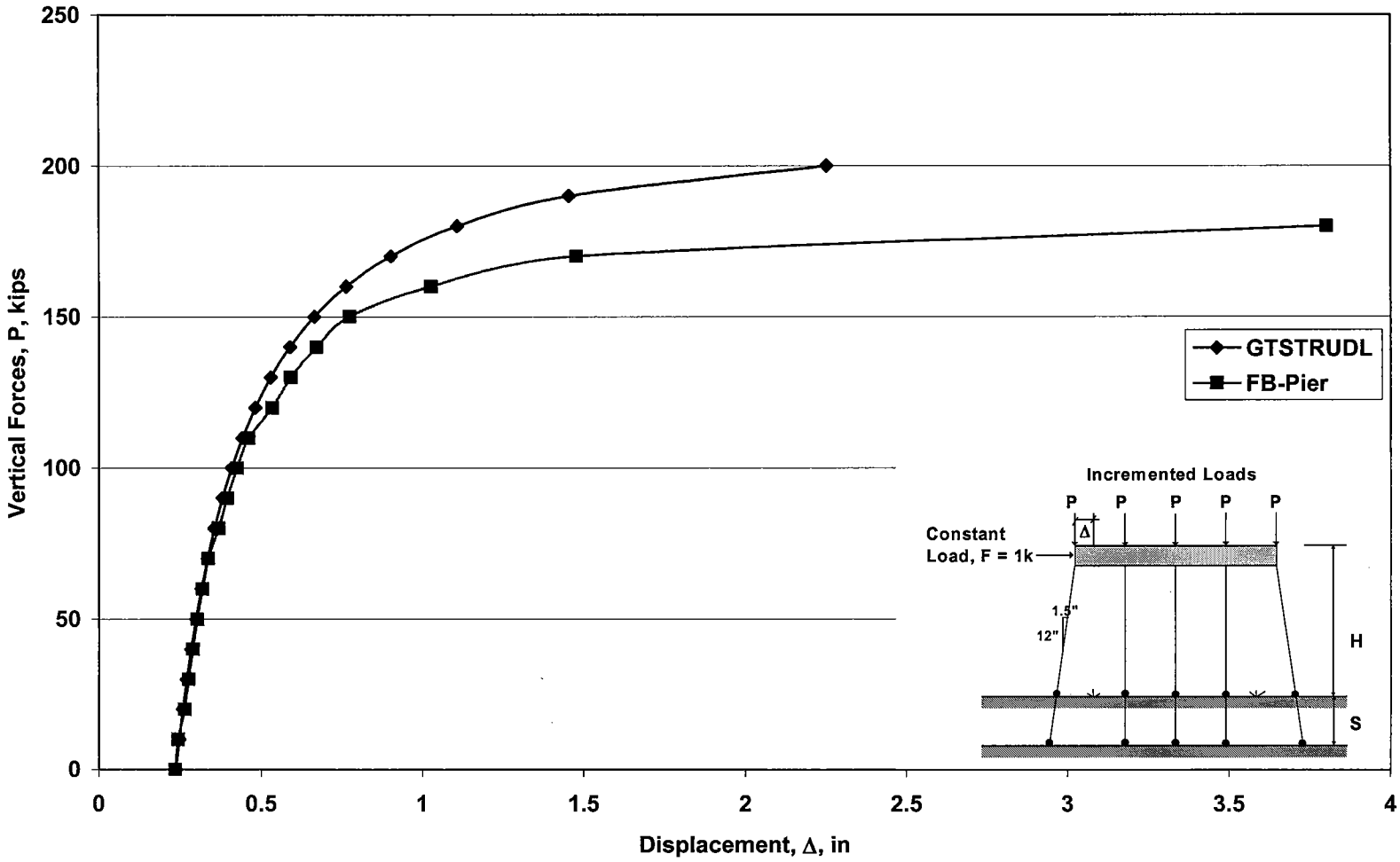

Figure 7.16. Pushover (Buckling) Analysis Comparison for HP10x42 5-Pile Bent, Fixed at Cap, Pinned at Ground (for GTSTRUDL), Soil K_o=150lb/in^3 (for FB-Pier), H=13ft, S=20ft

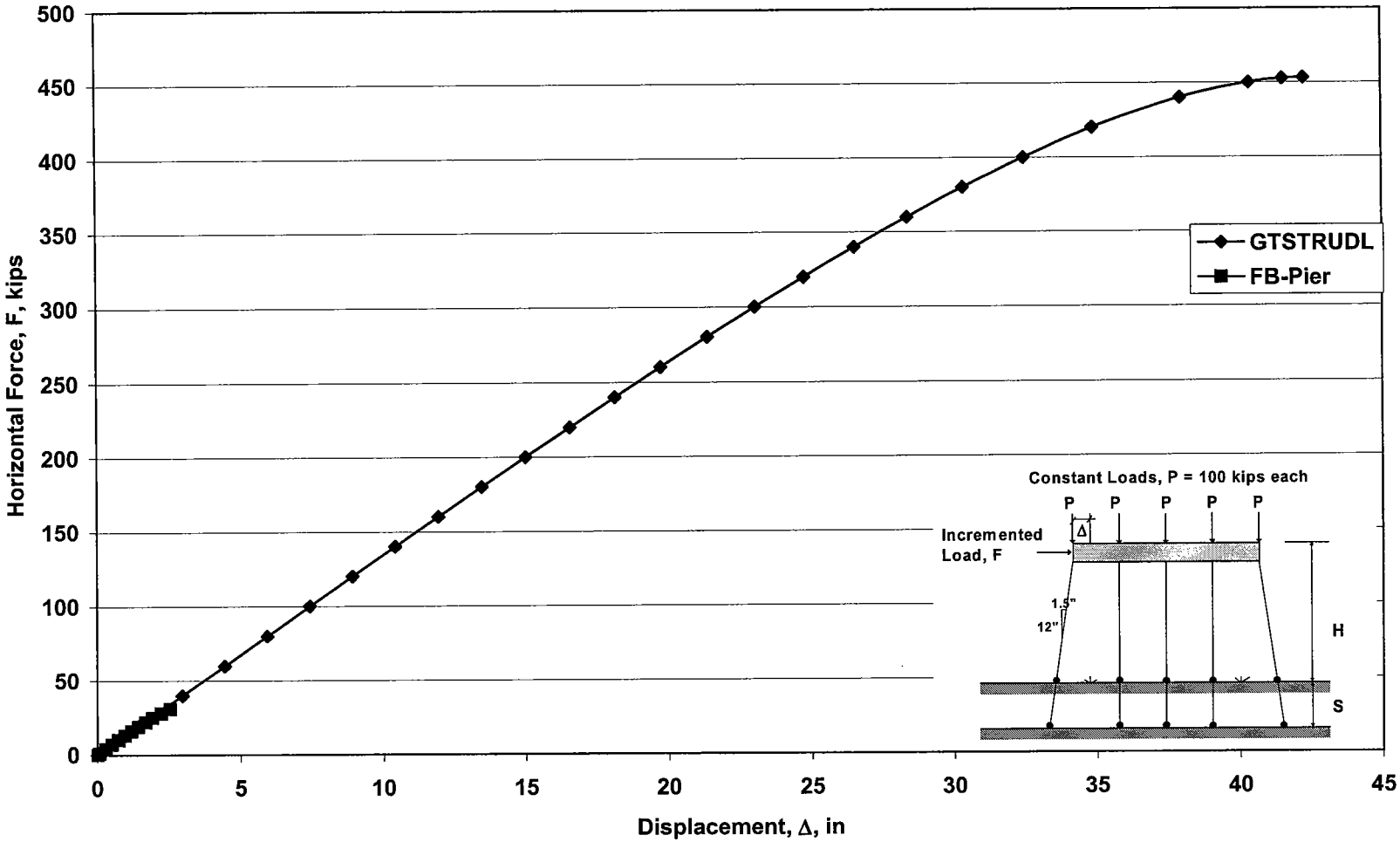

Figure 7.17. Pushover Analysis Comparison for HP10x42 5-Pile Bent, Fixed at Cap, Pinned at Ground (for GTSTRUDL), K_o = 150 lb/in^3 (for FB-Pier), H = 13ft, S=0ft

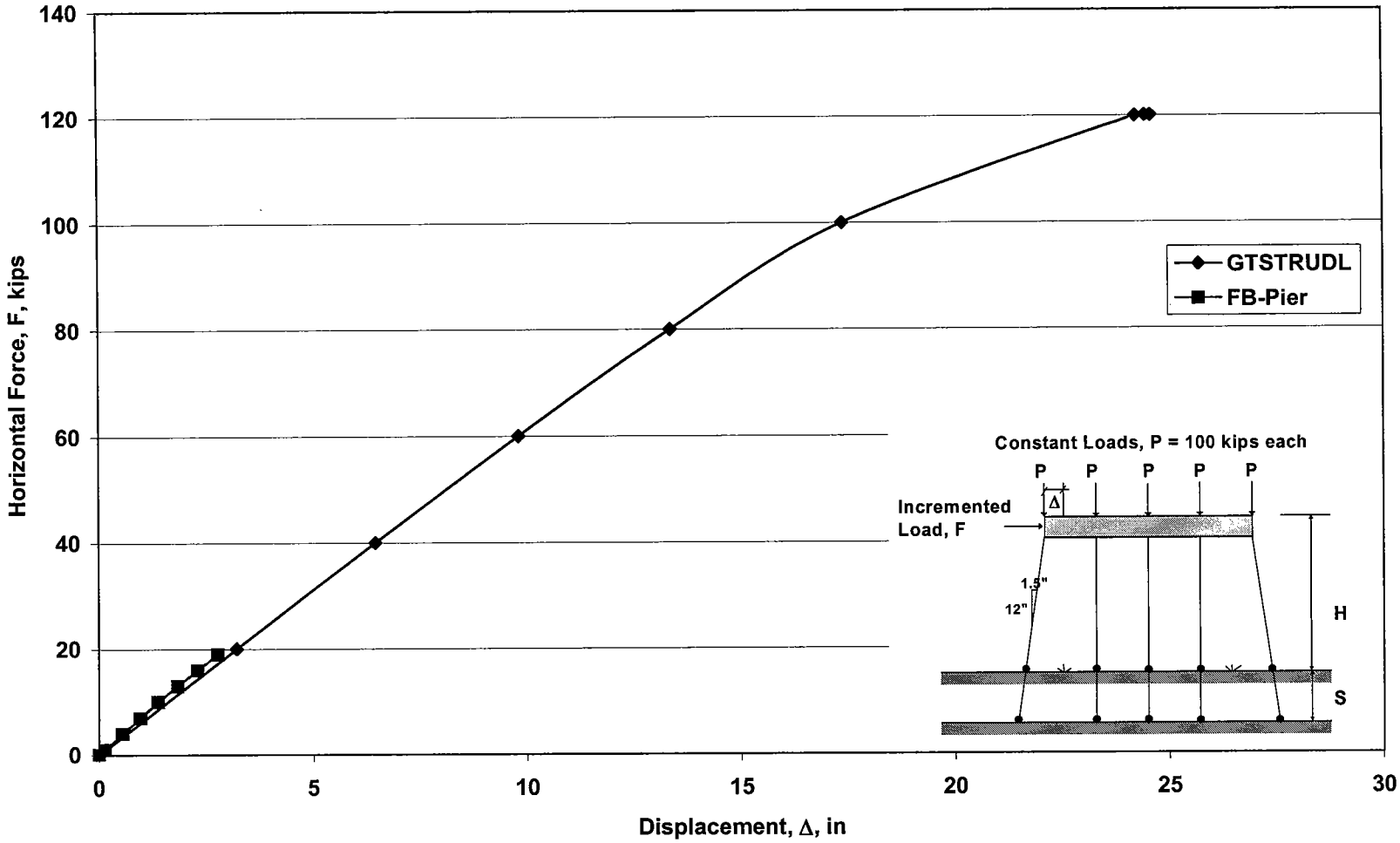

Figure 7.18. Pushover Analysis Comparison for HP10x42 5-Pile Bent, Fixed at Cap, Pinned at Ground (for GTSTRUDL), K_o = 150 lb/in^3 (for FB-Pier), H = 13ft, S=5ft

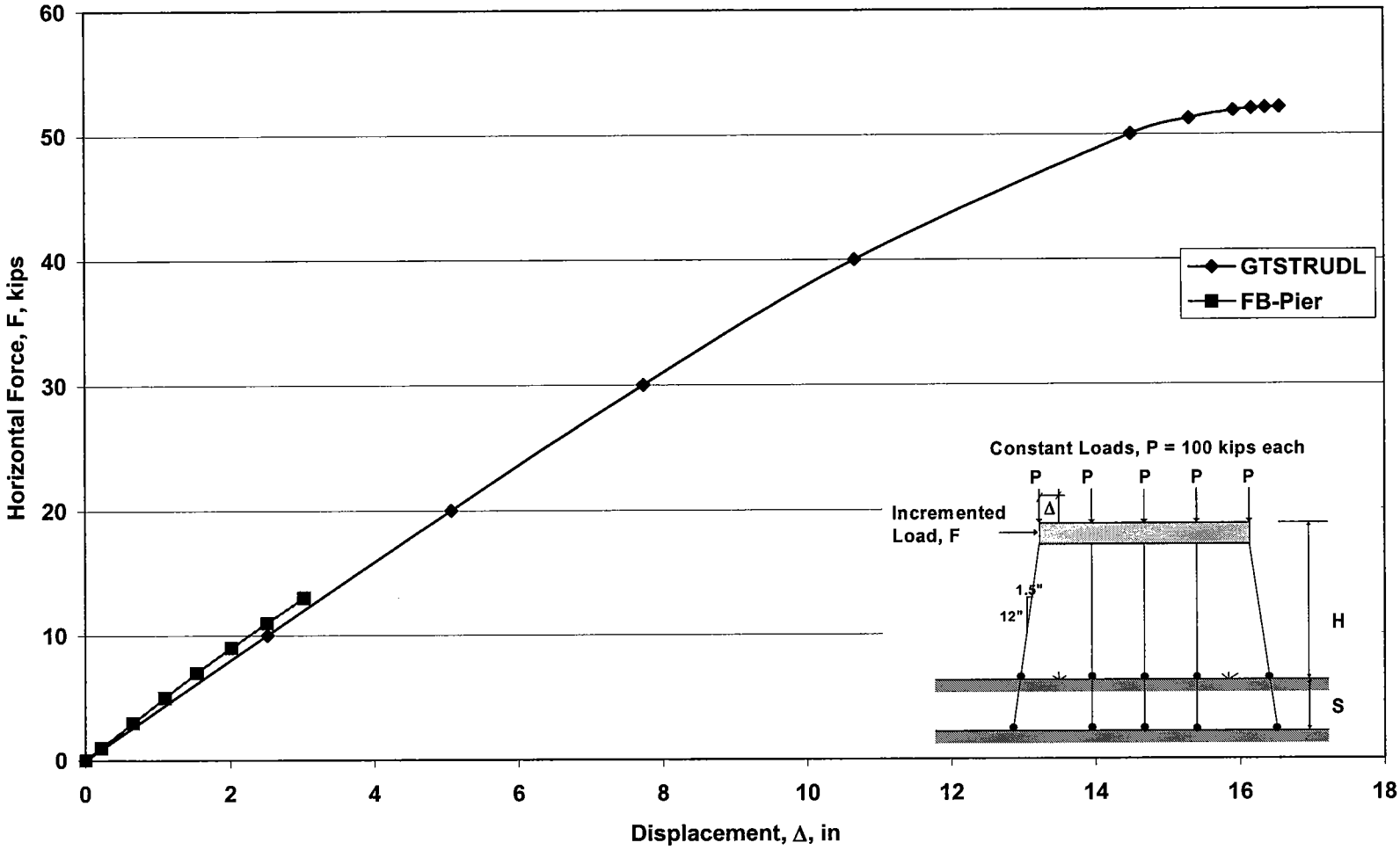

Figure 7.19. Pushover Analysis Comparison for HP10x42 5-Pile Bent, Fixed at Cap, Pinned at Ground (for GTSTRUDL), K_o = 150 lb/in^3 (for FB-Pier), H = 13ft, S=10ft

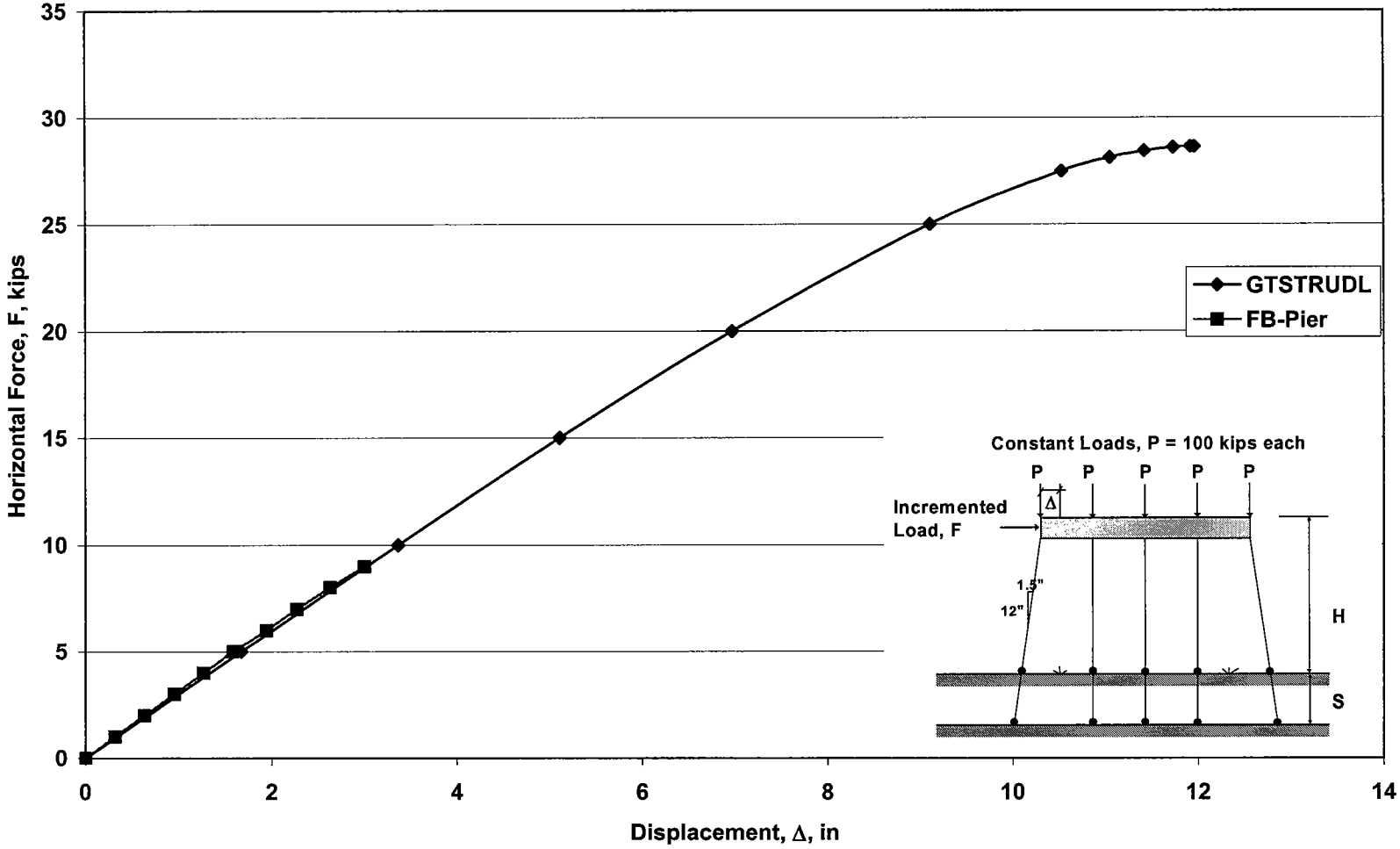

Figure 7.20. Pushover Analysis Comparison for HP10x42 5-Pile Bent, Fixed at Cap, Pinned at Ground (for GTSTRUDL), K_o = 150 lb/in^3 (for FB-Pier), H = 13ft, S=15ft

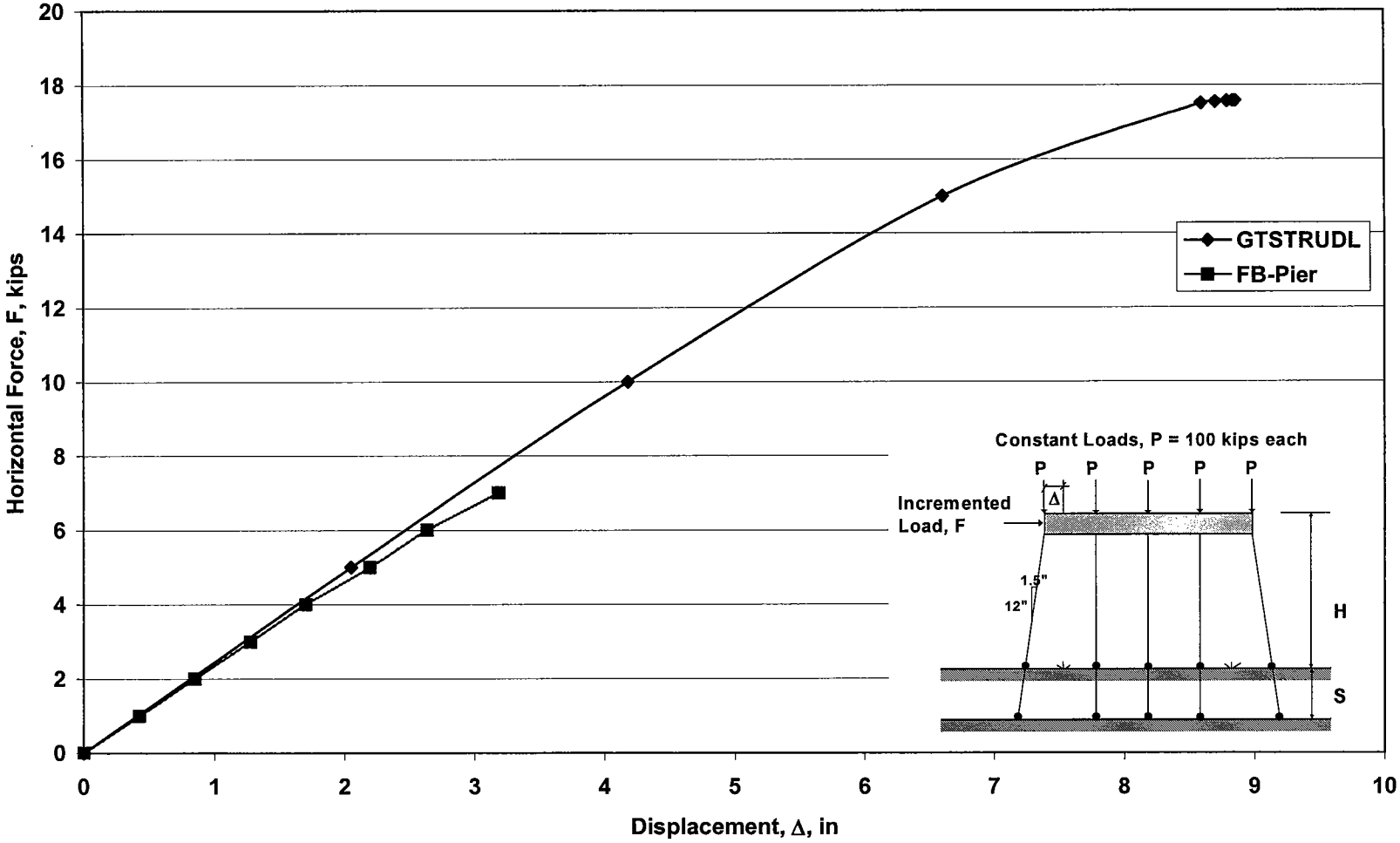

Figure 7.21. Pushover Analysis Comparison for HP10x42 5-Pile Bent, Fixed at Cap, Pinned at Ground (for GTSTRUDL), K_o = 150 lb/in^3 (for FB-Pier), H = 13ft, S=20ft

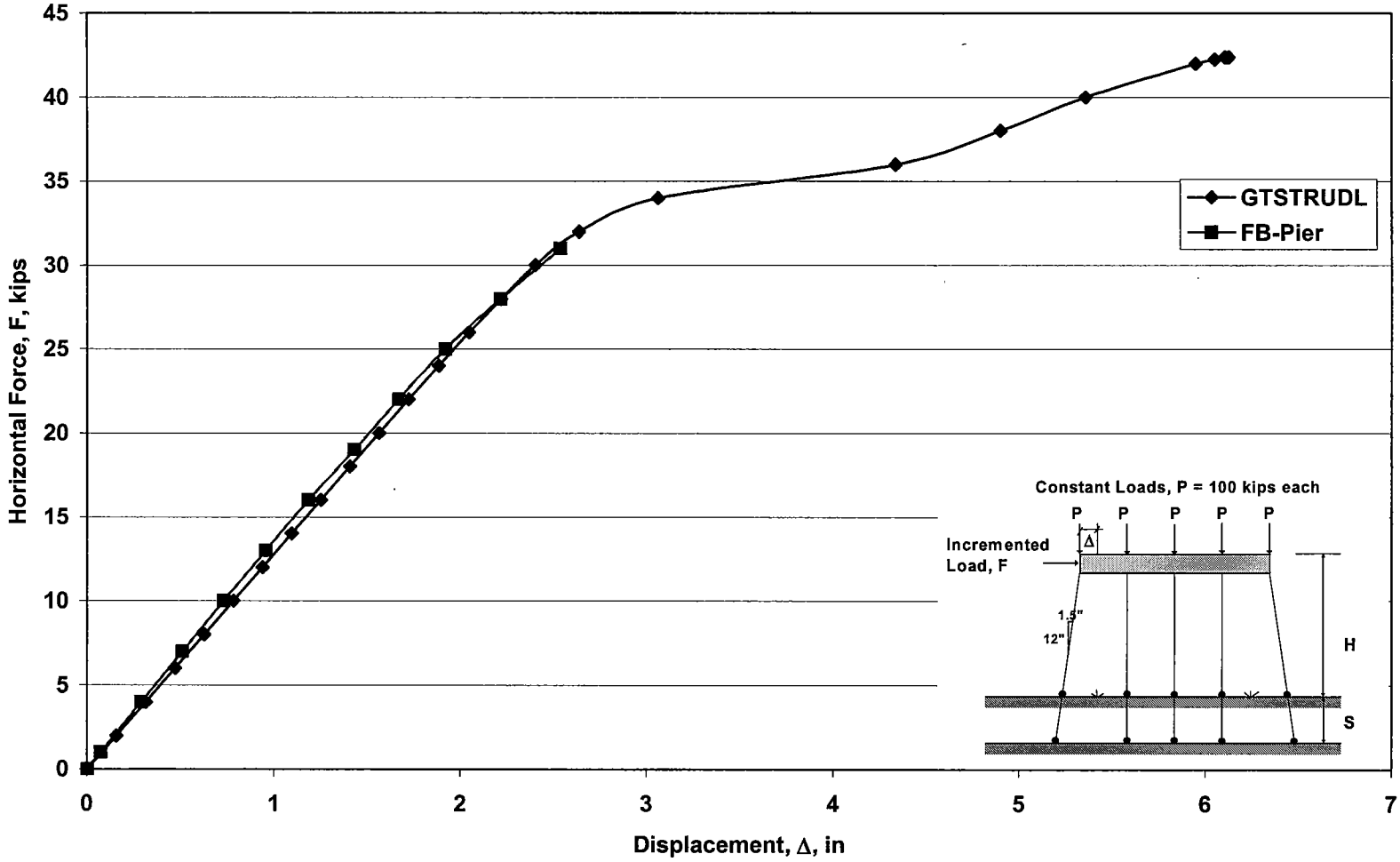

Figure 7.22. Pushover Analysis Comparison for HP10x42 5-Pile Bent with Plastic Hinges for GTSTRUDL, Fixed at Cap, Pinned at Ground (for GTSTRUDL), K_o = 150 lb/in^3 (for FB-Pier), H = 13ft, S=0ft

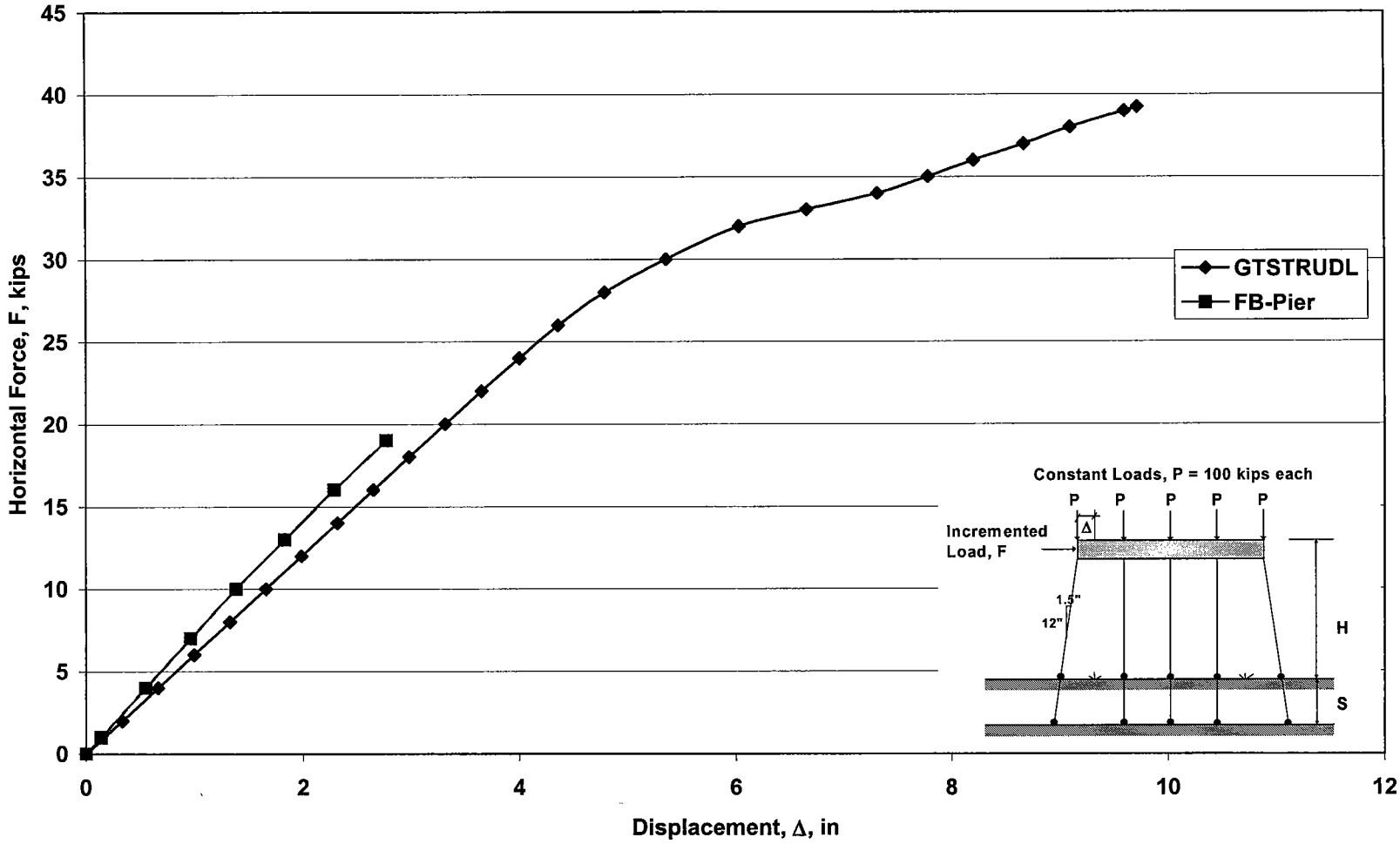

Figure 7.23. Pushover Analysis Comparison for HP10x42 5-Pile Bent with Plastic Hinges for GTSTRUDL, Fixed at Cap, Pinned at Ground (for GTSTRUDL), K_o = 150 lb/in^3 (for FB-Pier), H = 13ft, S=5ft

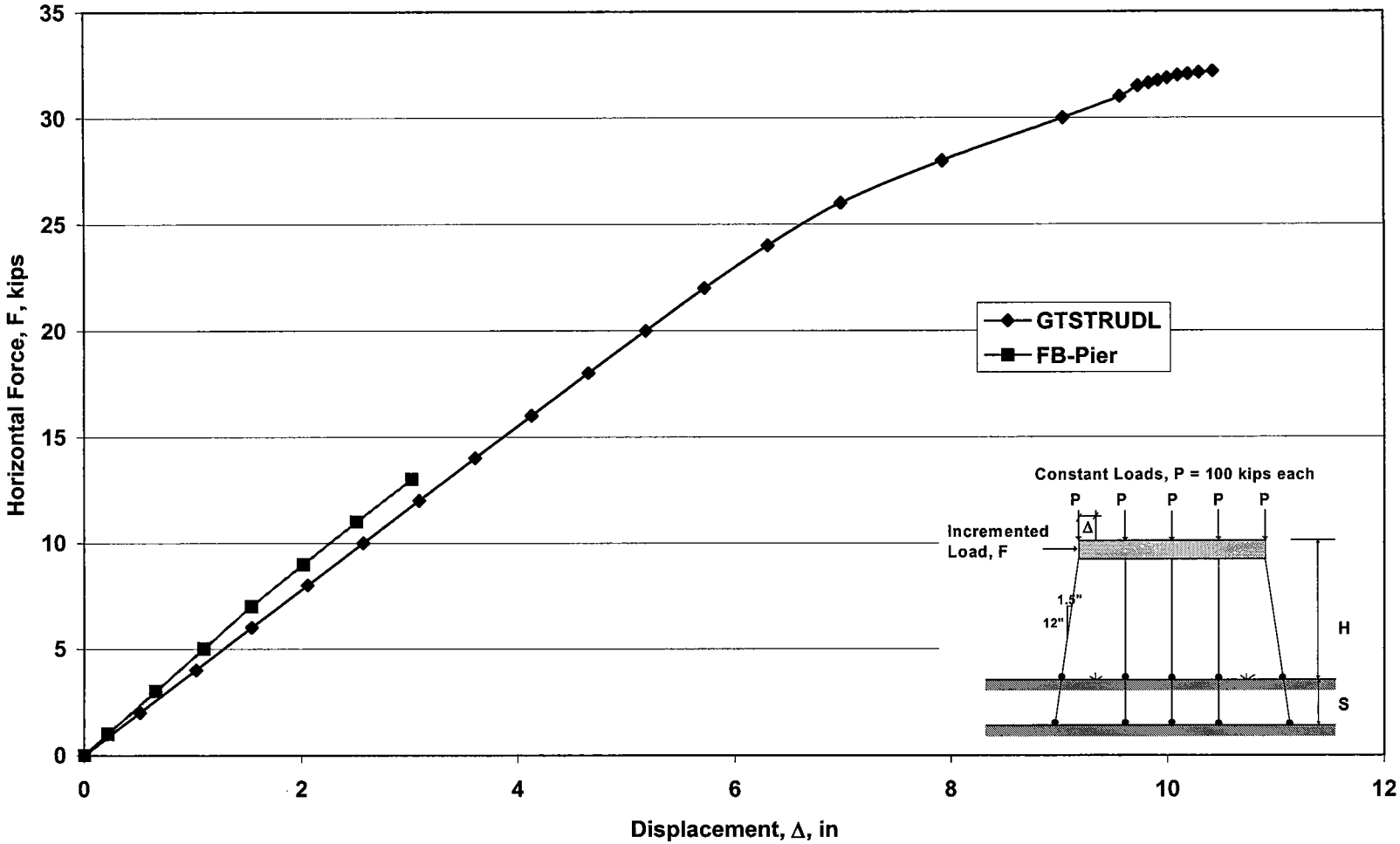

Figure 7.24. Pushover Analysis Comparison for HP10x42 5-Pile Bent with Plastic Hinges for GTSTRUDL, Fixed at Cap, Pinned at Ground (for GTSTRUDL), K_o = 150 lb/in^3 (for FB-Pier), H = 13ft, S=10ft

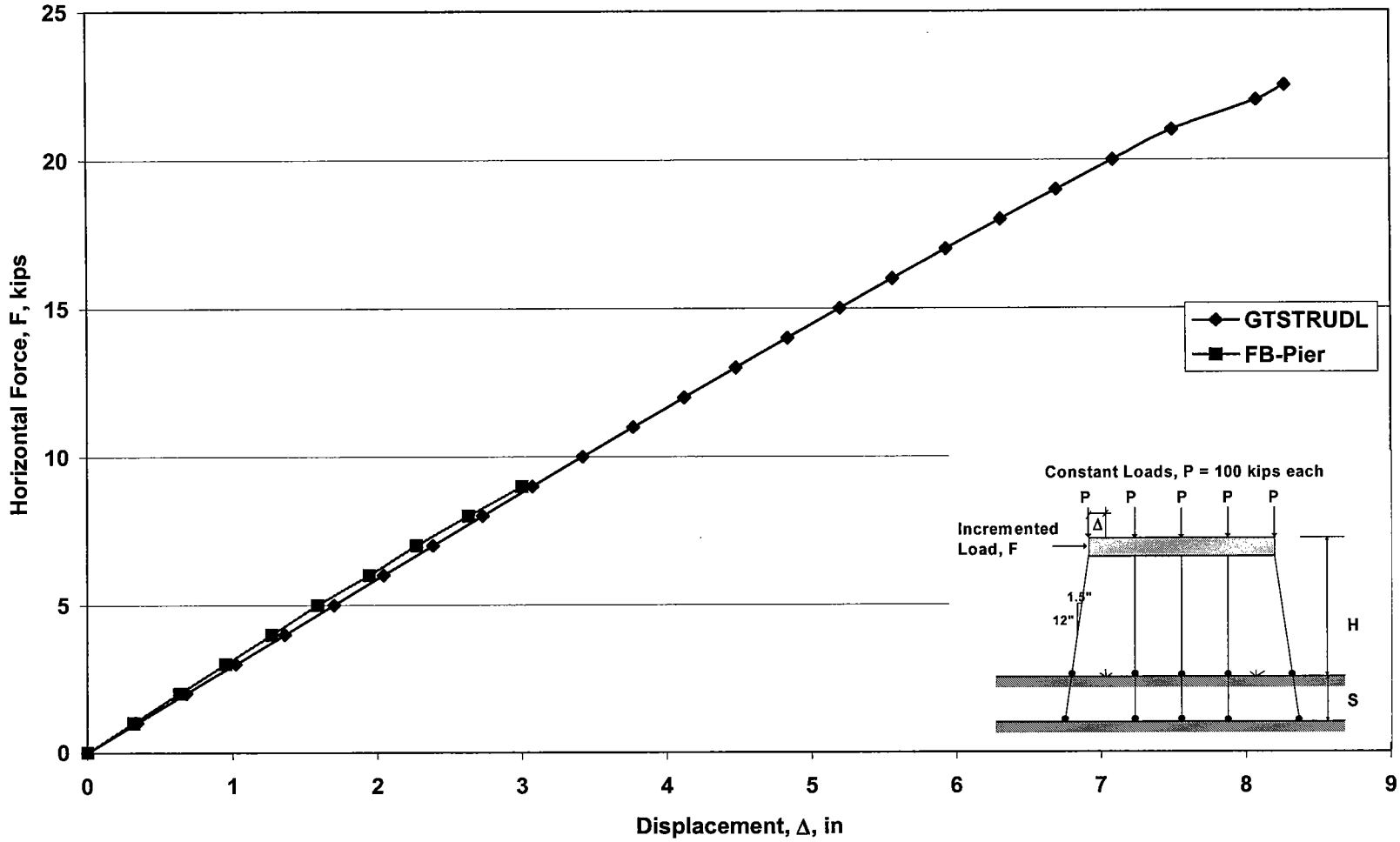

Figure 7.25. Pushover Analysis Comparison for HP10x42 5-Pile Bent with Plastic Hinges for GTSTRUDL, Fixed at Cap, Pinned at Ground (for GTSTRUDL), K_o = 150 lb/in^3 (for FB-Pier), H = 13ft, S=15ft

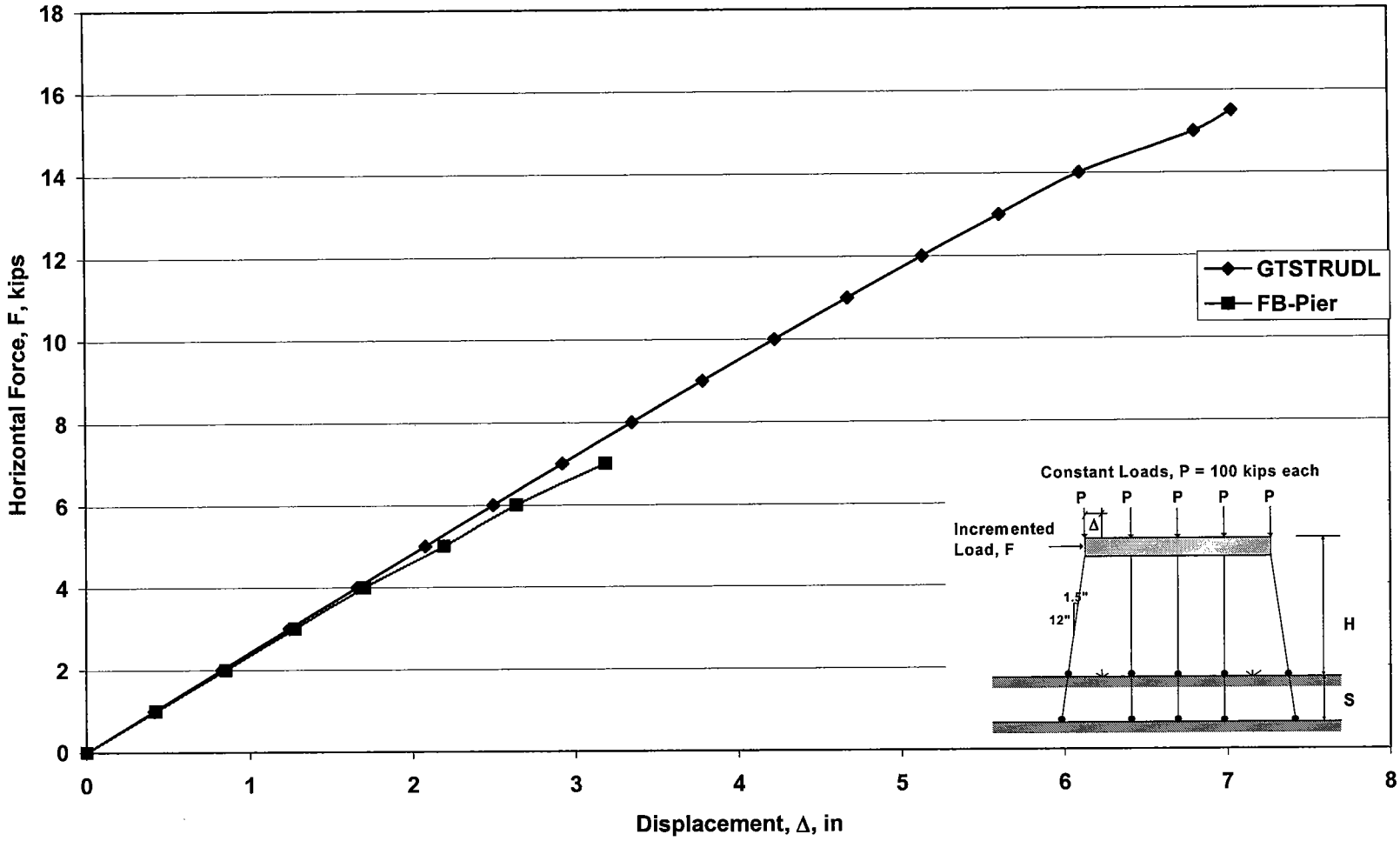

Figure 7.26. Pushover Analysis Comparison for HP10x42 5-Pile Bent with Plastic Hinges for GTSTRUDL, Fixed at Cap, Pinned at Ground (for GTSTRUDL), K_o = 150 lb/in^3 (for FB-Pier), H = 13ft, S=20ft

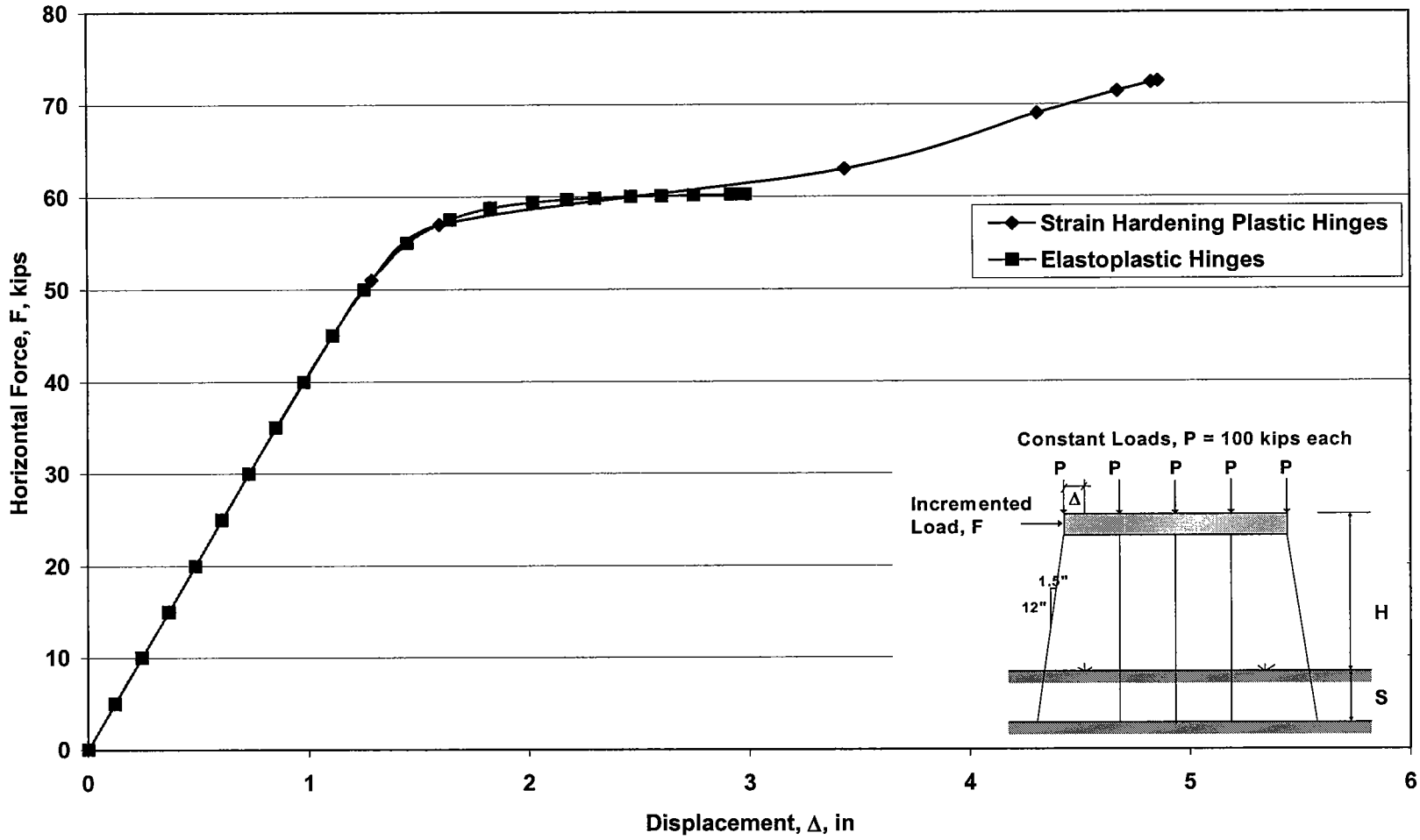

Figure 7.27. Effect of Stress-Strain Relationship in GTSTRUDL Pushover Analysis for HP10x42 5-Pile Bent, Fixed at Cap, Fixed at Ground, H=13ft, S=0ft

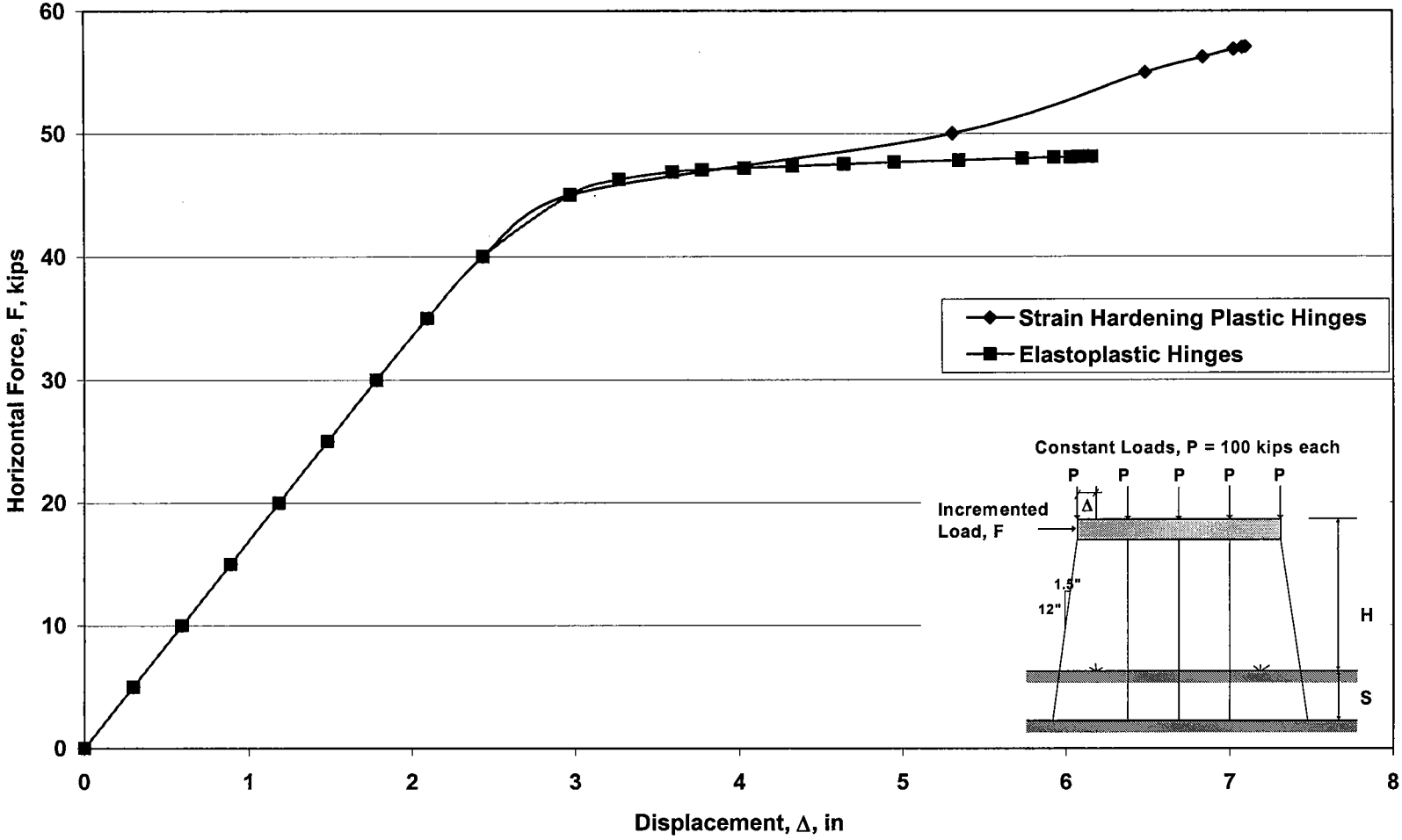

Figure 7.28. Effect of Stress-Strain Relationship in GTSTRUDL Pushover Analysis for HP10x42 5-Pile Bent, Fixed at Cap, Fixed at Ground, H=13ft, S=5ft

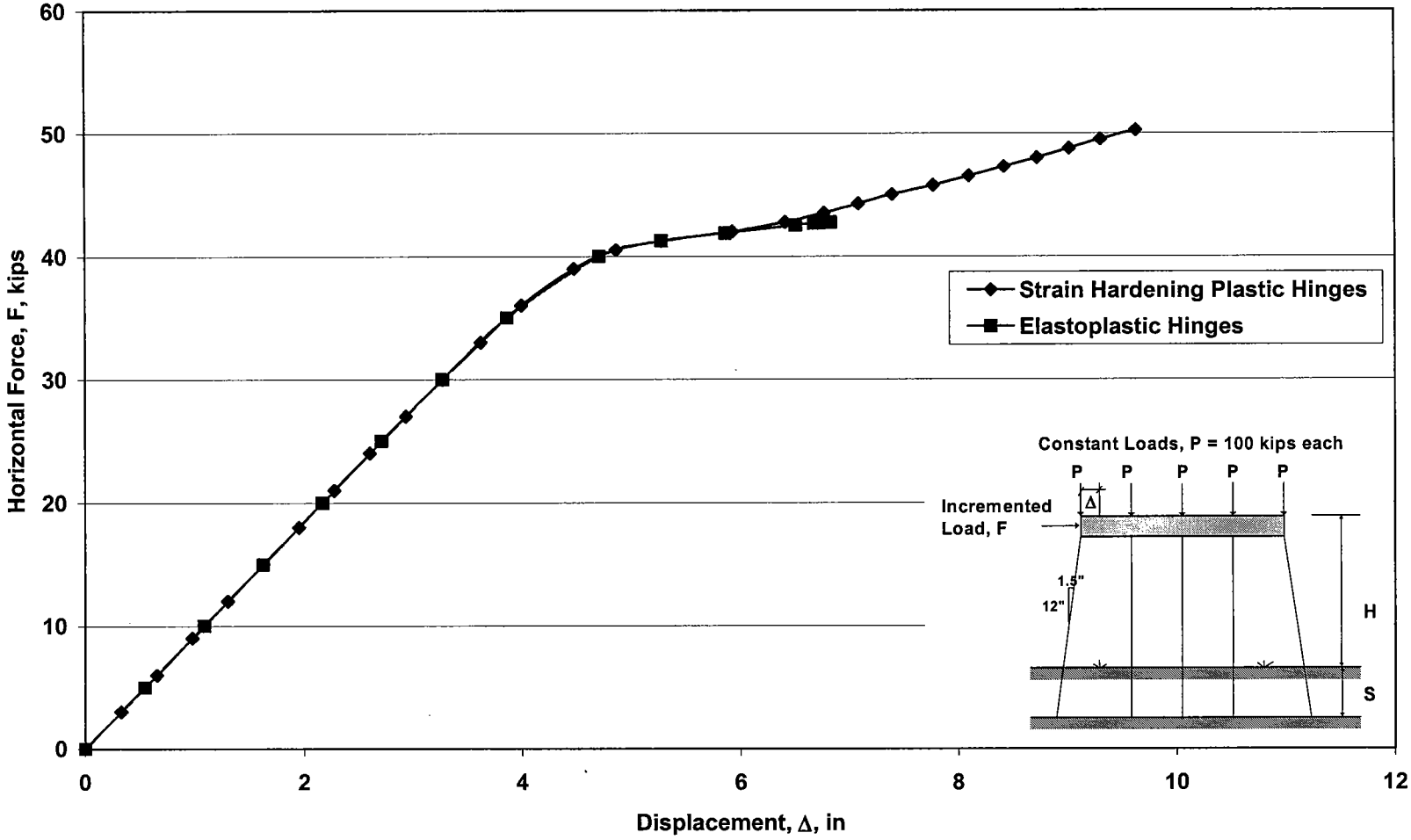

Figure 7.29. Effect of Stress-Strain Relationship in GTSTRUDL Pushover Analysis for HP10x42 5-Pile Bent, Fixed at Cap, Fixed at Ground, H=13ft, S=10ft

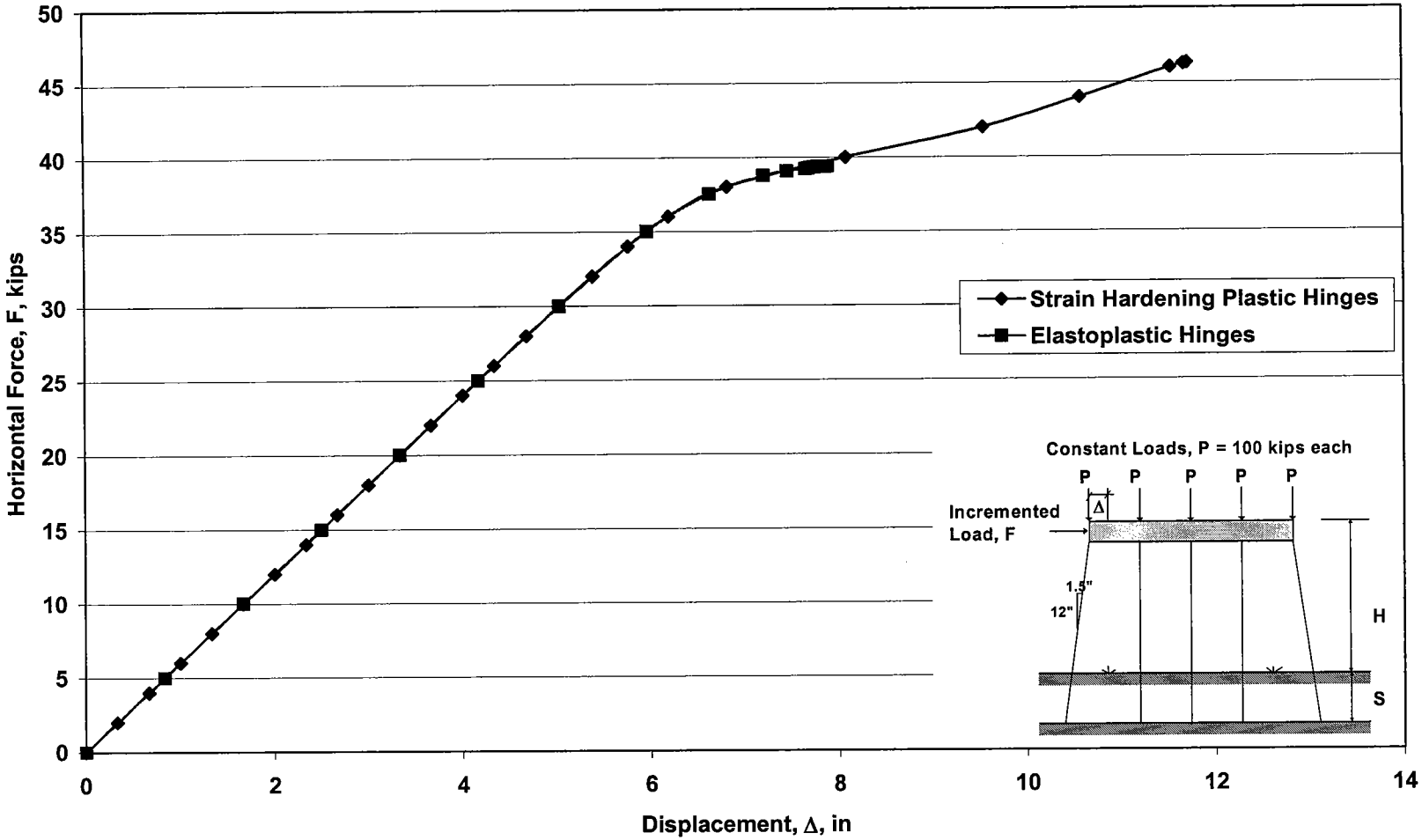

Figure 7.30. Effect of Stress-Strain Relationship in GTSTRUDL Pushover Analysis for HP10x42 5-Pile Bent, Fixed at Cap, Fixed at Ground, H=13ft, S=15ft

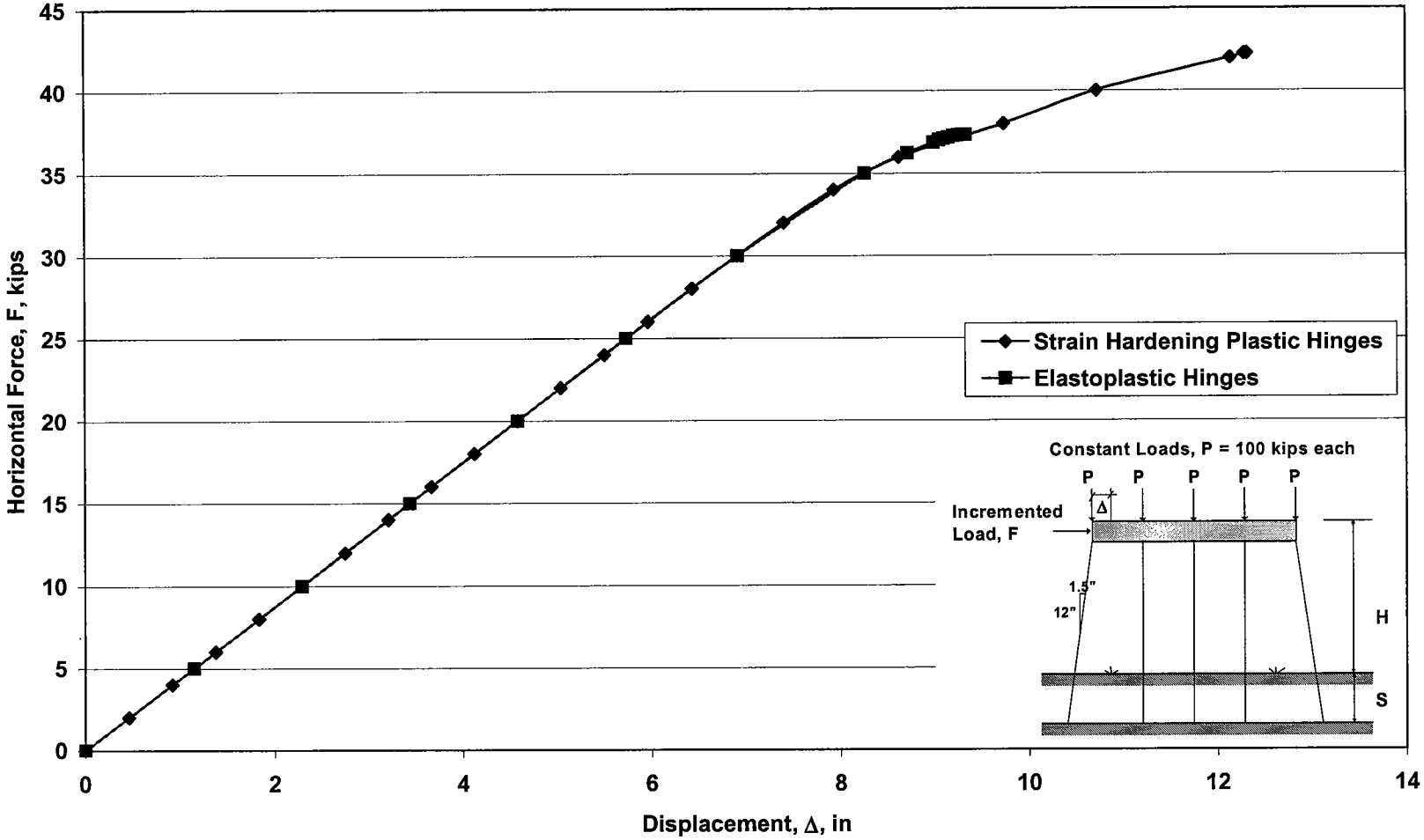

Figure 7.31. Effect of Stress-Strain Relationship in GTSTRUDL Pushover Analysis for HP10x42 5-Pile Bent, Fixed at Cap, Fixed at Ground, H=13ft, S=20ft

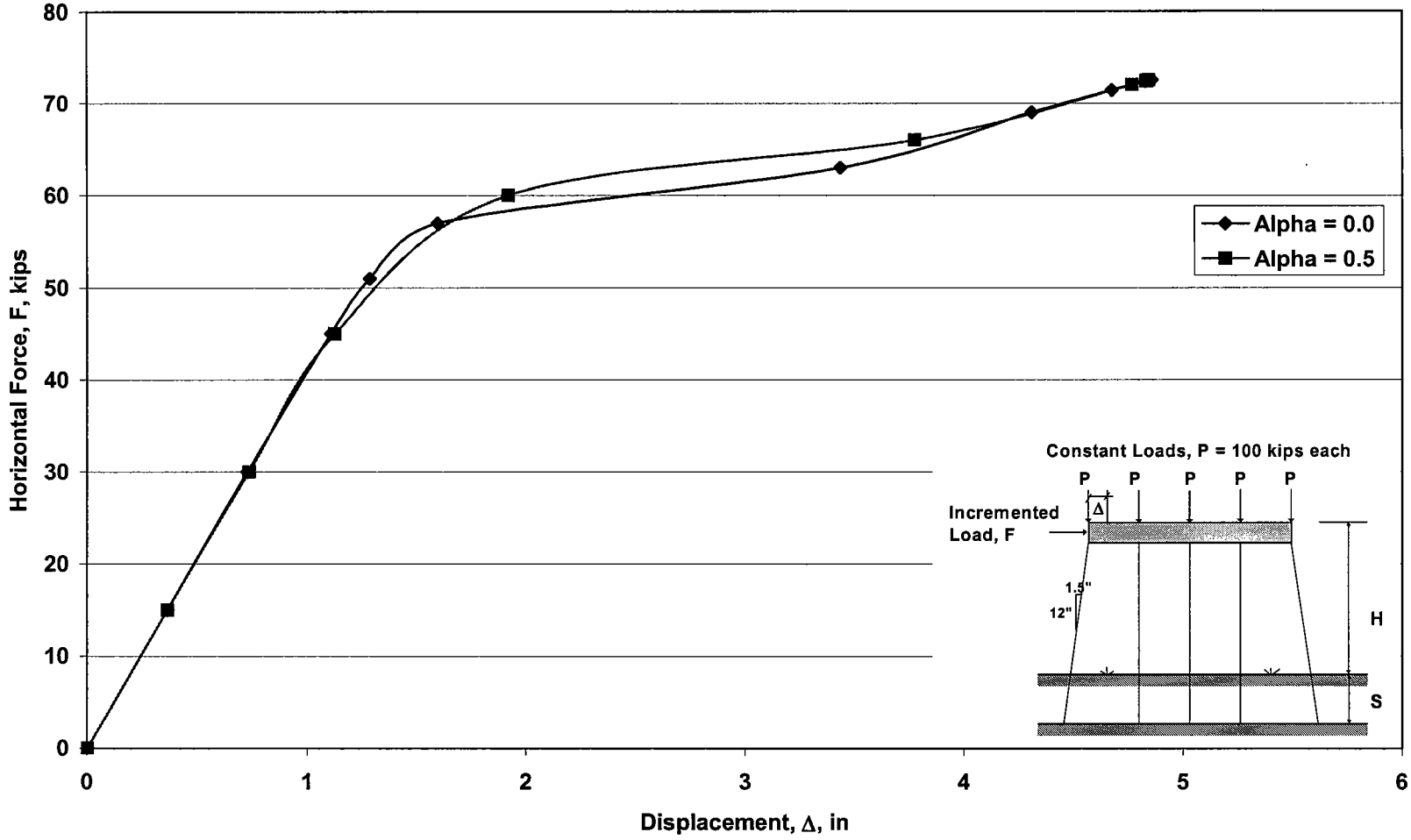

Figure 7.32. Effect of Residual Stresses in Piles for GTSTRUDL Pushover Analysis for HP10x42 5-Pile Bent, Fixed at Cap, Fixed at Ground, H=13ft, S=0ft

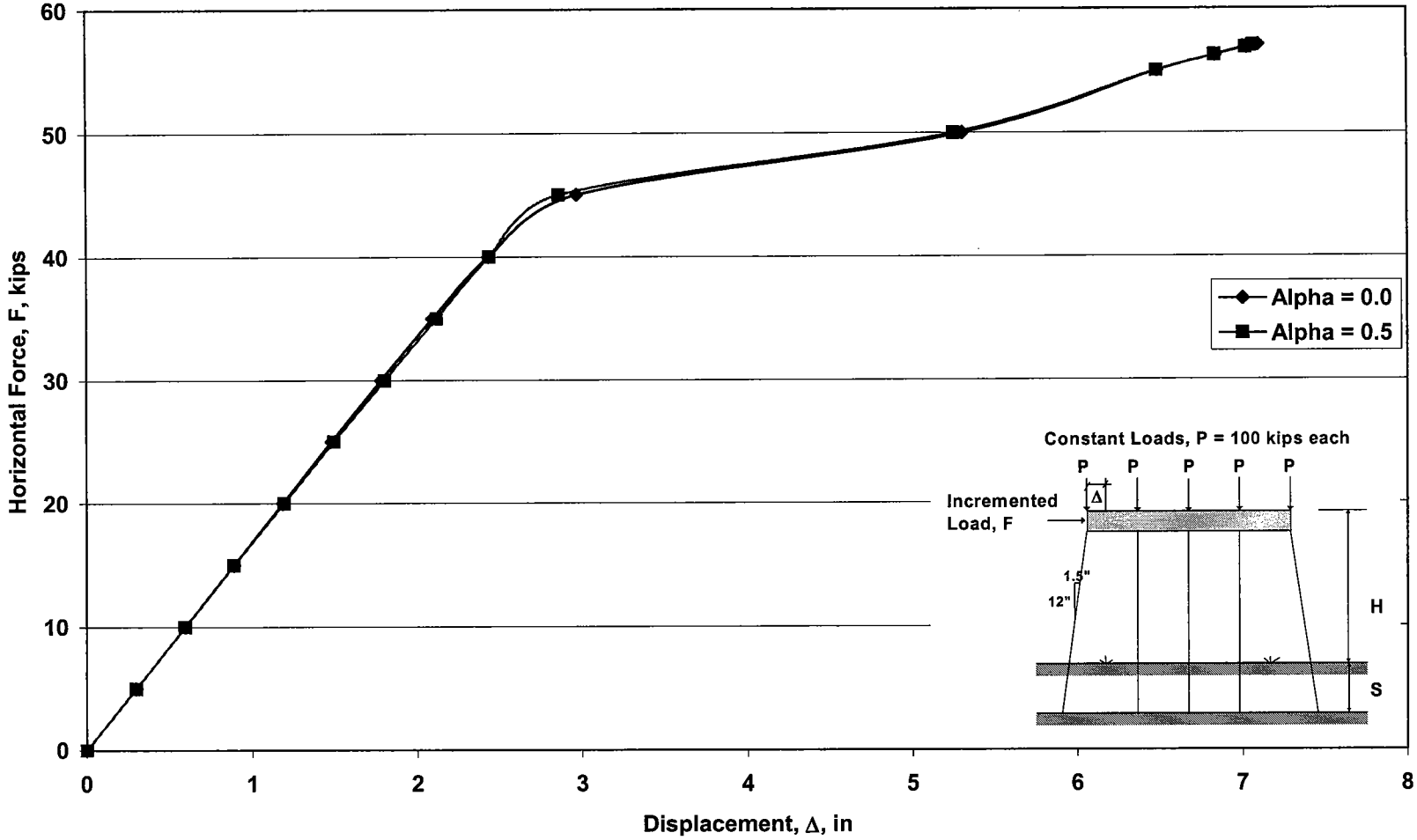

Figure 7.33. Effect of Residual Stresses in Piles for GTSTRUDL Pushover Analysis for HP10x42 5-Pile Bent, Fixed at Cap, Fixed at Ground, H=13ft, S=5ft

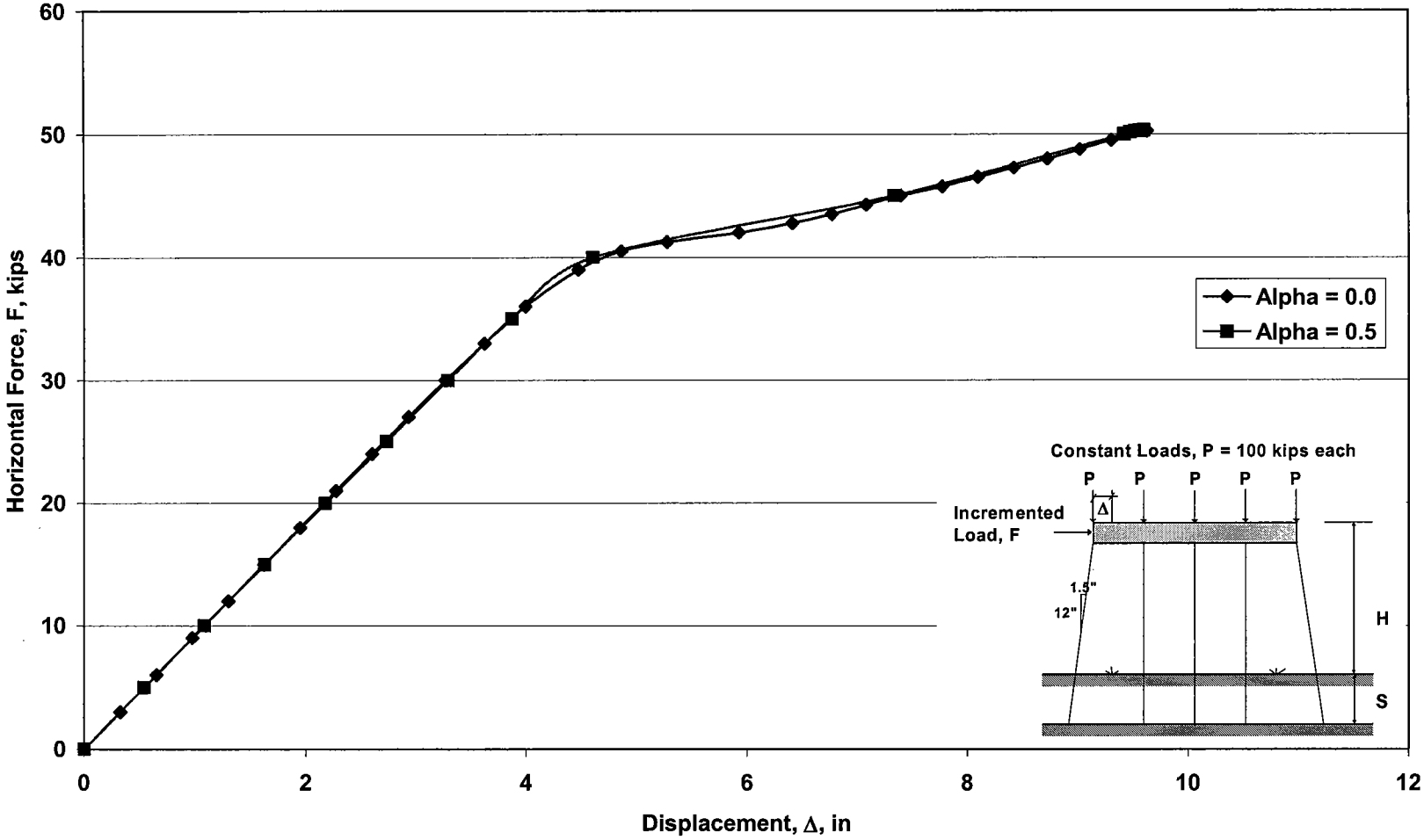

Figure 7.34. Effect of Residual Stresses in Piles for GTSTRUDL Pushover Analysis for HP10x42 5-Pile Bent, Fixed at Cap, Fixed at Ground, H=13ft, S=10ft

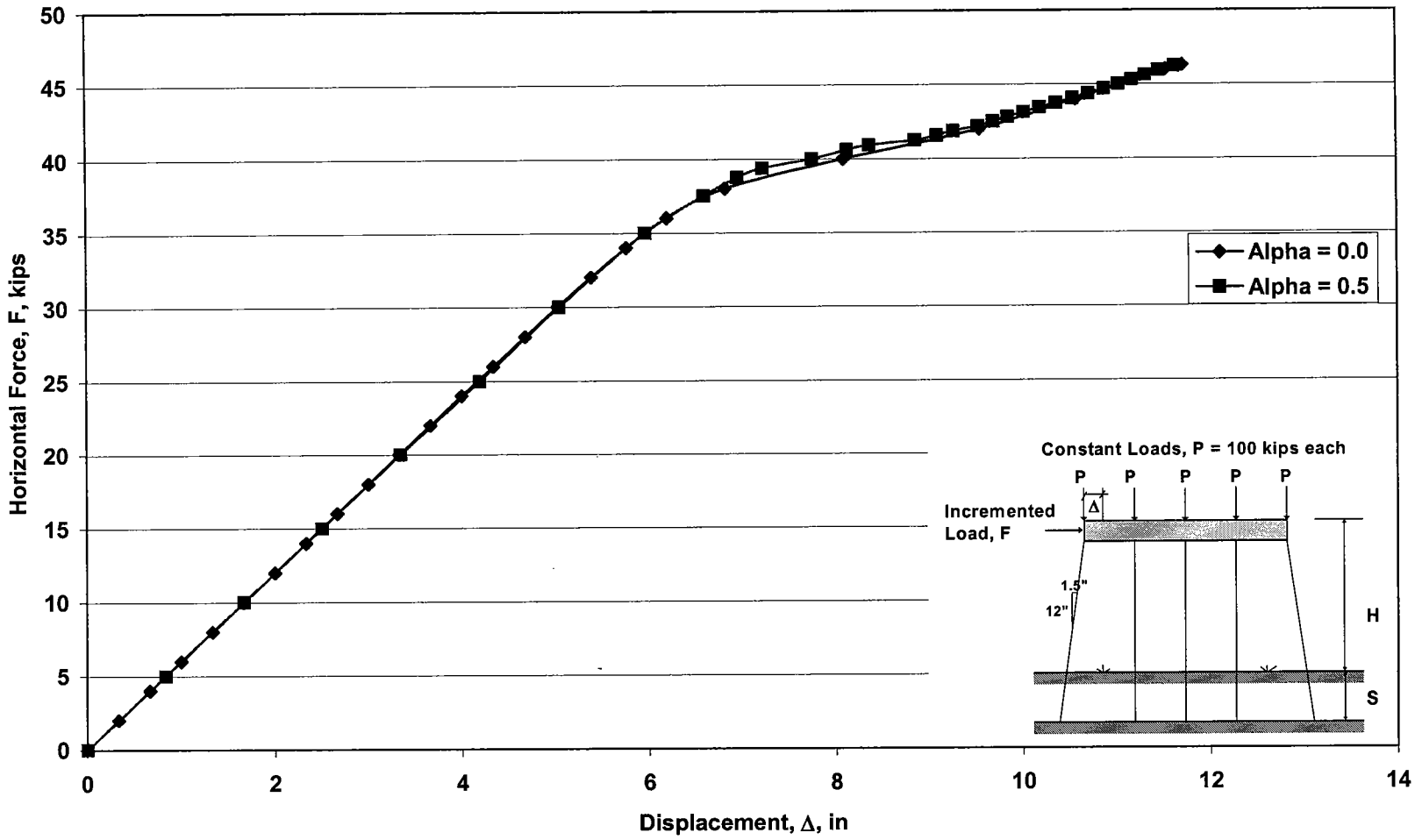

Figure 7.35. Effect of Residual Stresses in Piles for GTSTRUDL Pushover Analysis for HP10x42 5-Pile Bent, Fixed at Cap, Fixed at Ground, H=13ft, S=15ft

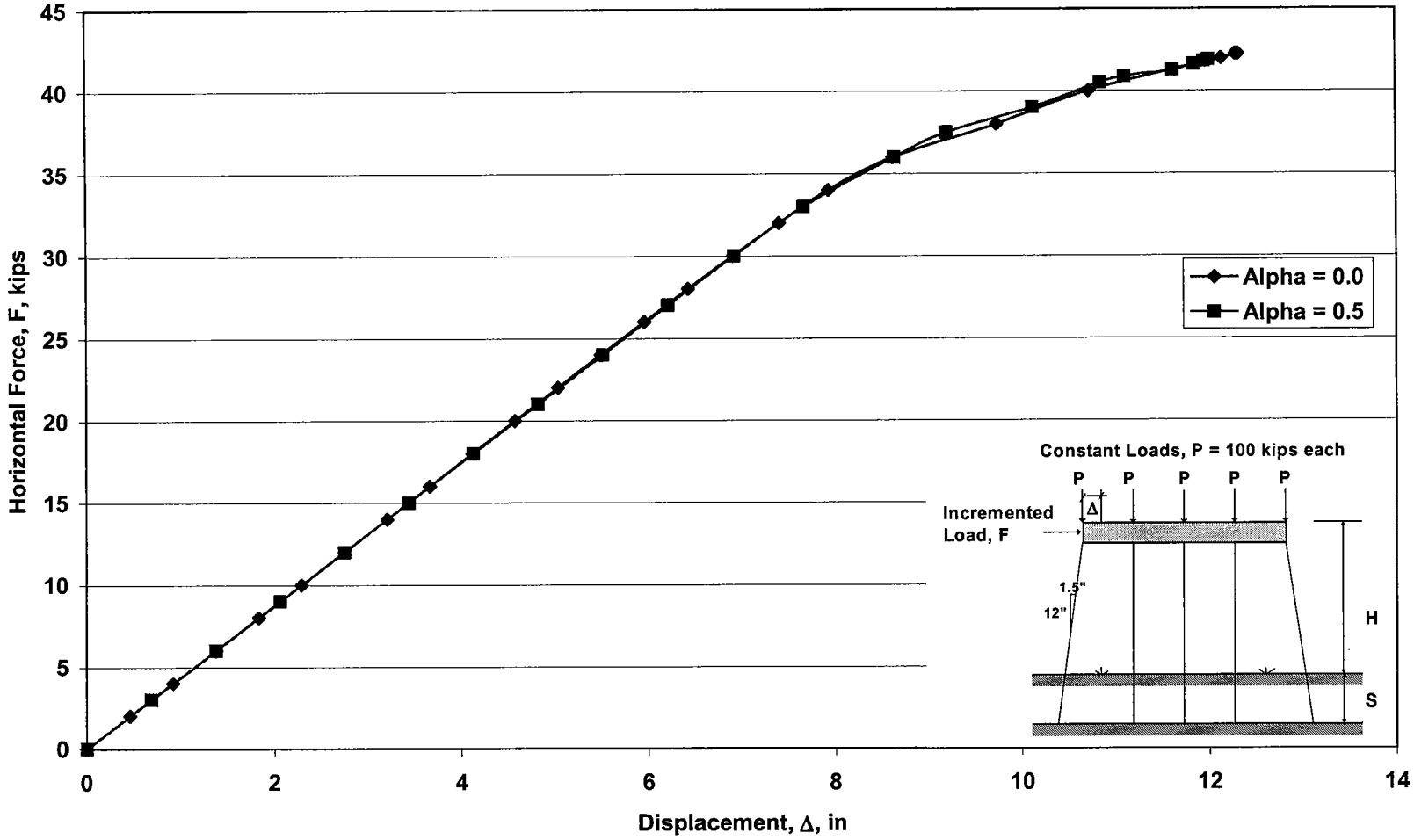

Figure 7.36. Effect of Residual Stresses in Piles for GTSTRUDL Pushover Analysis for HP10x42 5-Pile Bent, Fixed at Cap, Fixed at Ground, H=13ft, S=20ft

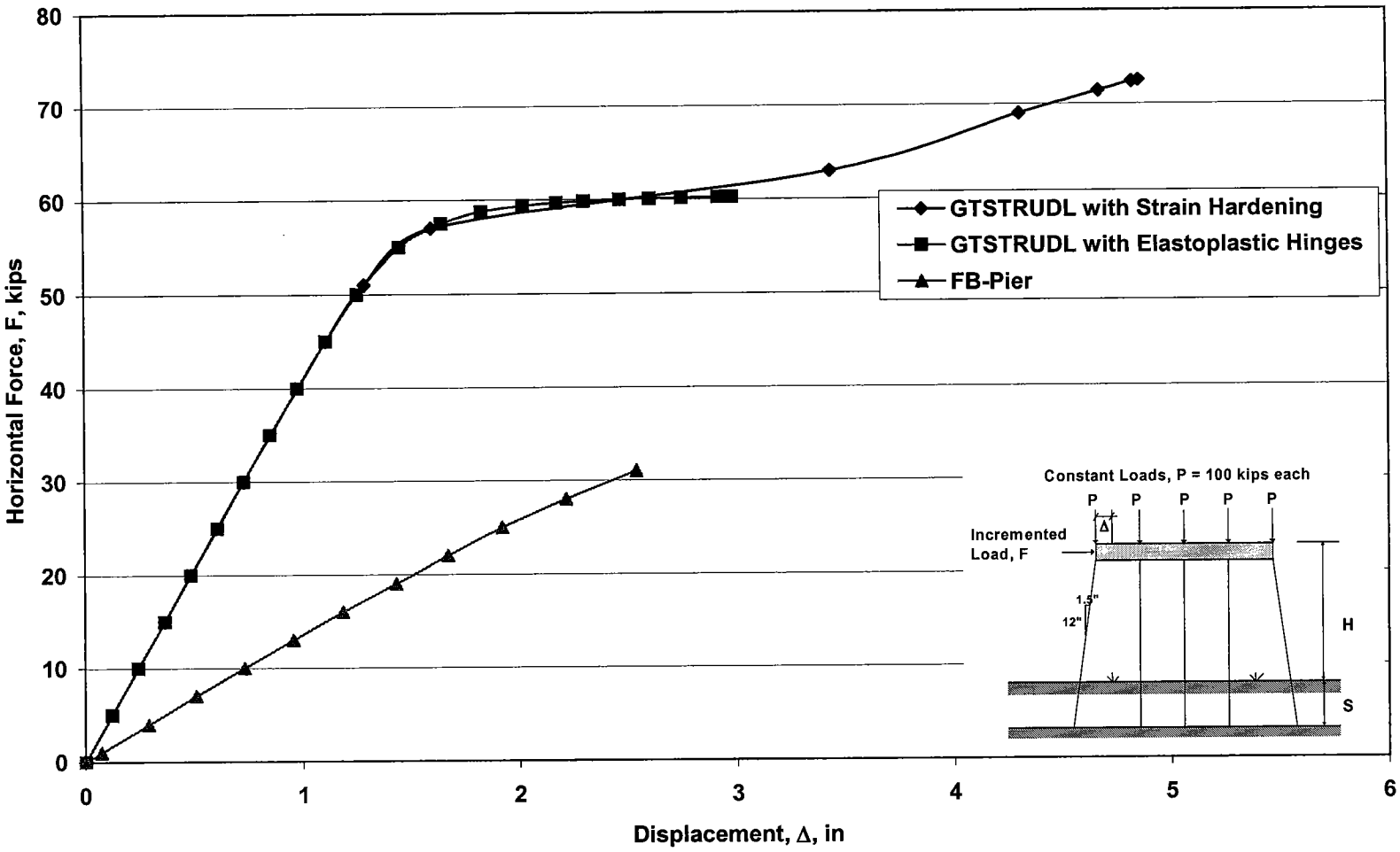

Figure 7.37. Pushover Analysis Comparison for HP10x42 5-Pile Bent, Fixed at Cap, Fixed at Ground (for GTSTRUDL), Soil K_o=150lb/in^3 (for FB-Pier), H=13ft, S=0ft

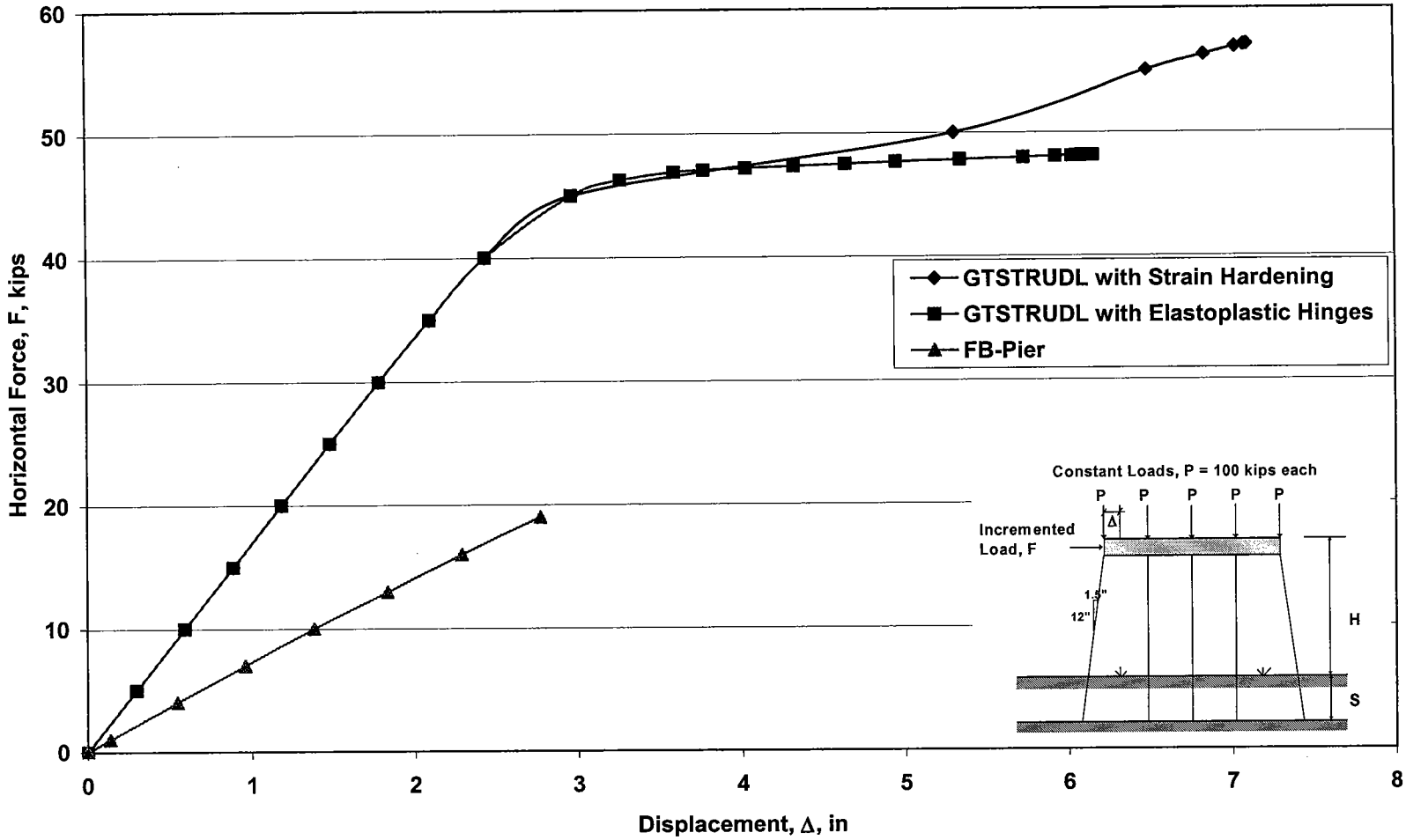

Figure 7.38. Pushover Analysis Comparison for HP10x42 5-Pile Bent, Fixed at Cap, Fixed at Ground (for GTSTRUDL), Soil K_o=150lb/in^3 (for FB-Pier), H=13ft, S=5ft

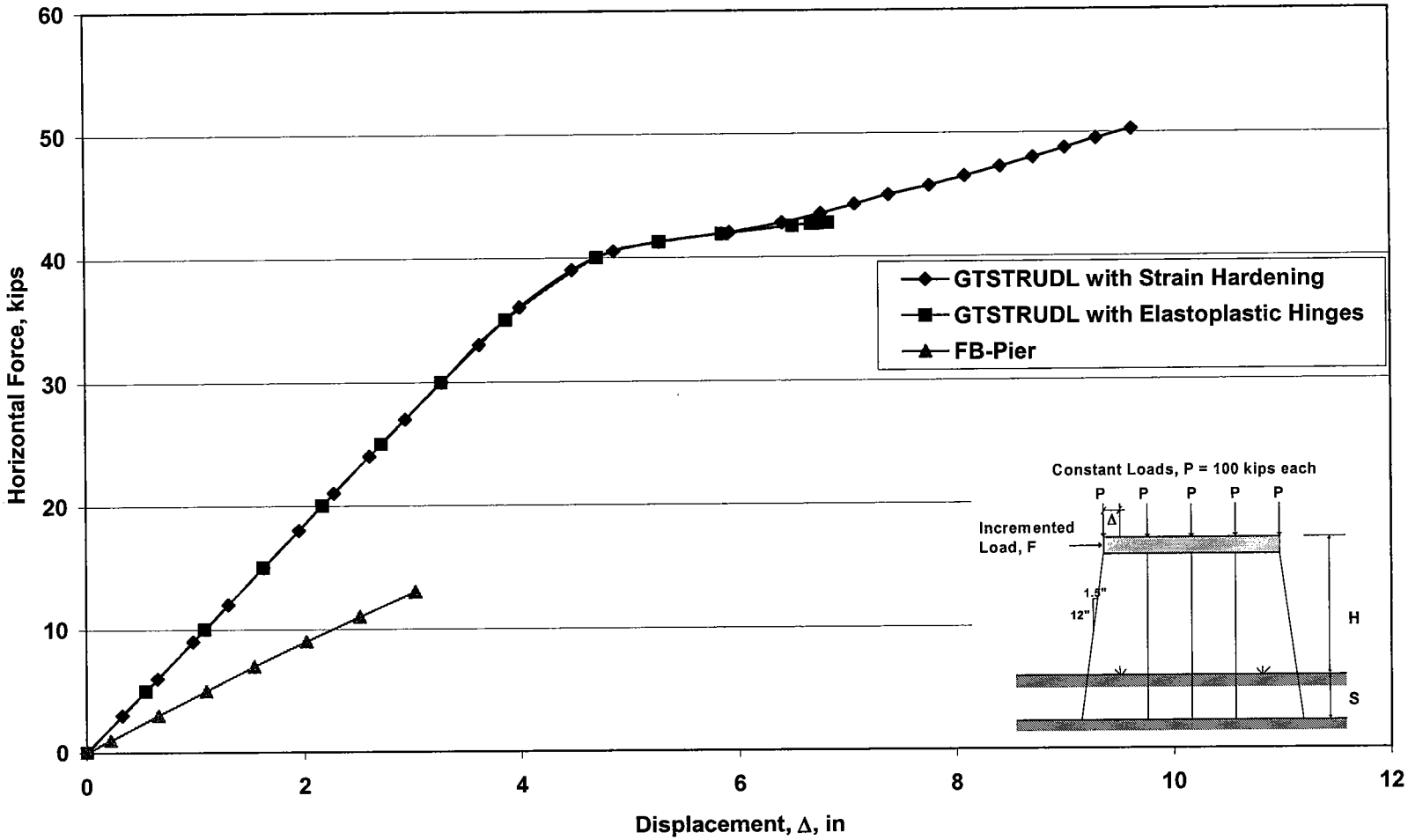

Figure 7.39. Pushover Analysis Comparison for HP10x42 5-Pile Bent, Fixed at Cap, Fixed at Ground (for GTSTRUDL), Soil K_o=150lb/in^3 (for FB-Pier), H=13ft, S=10ft

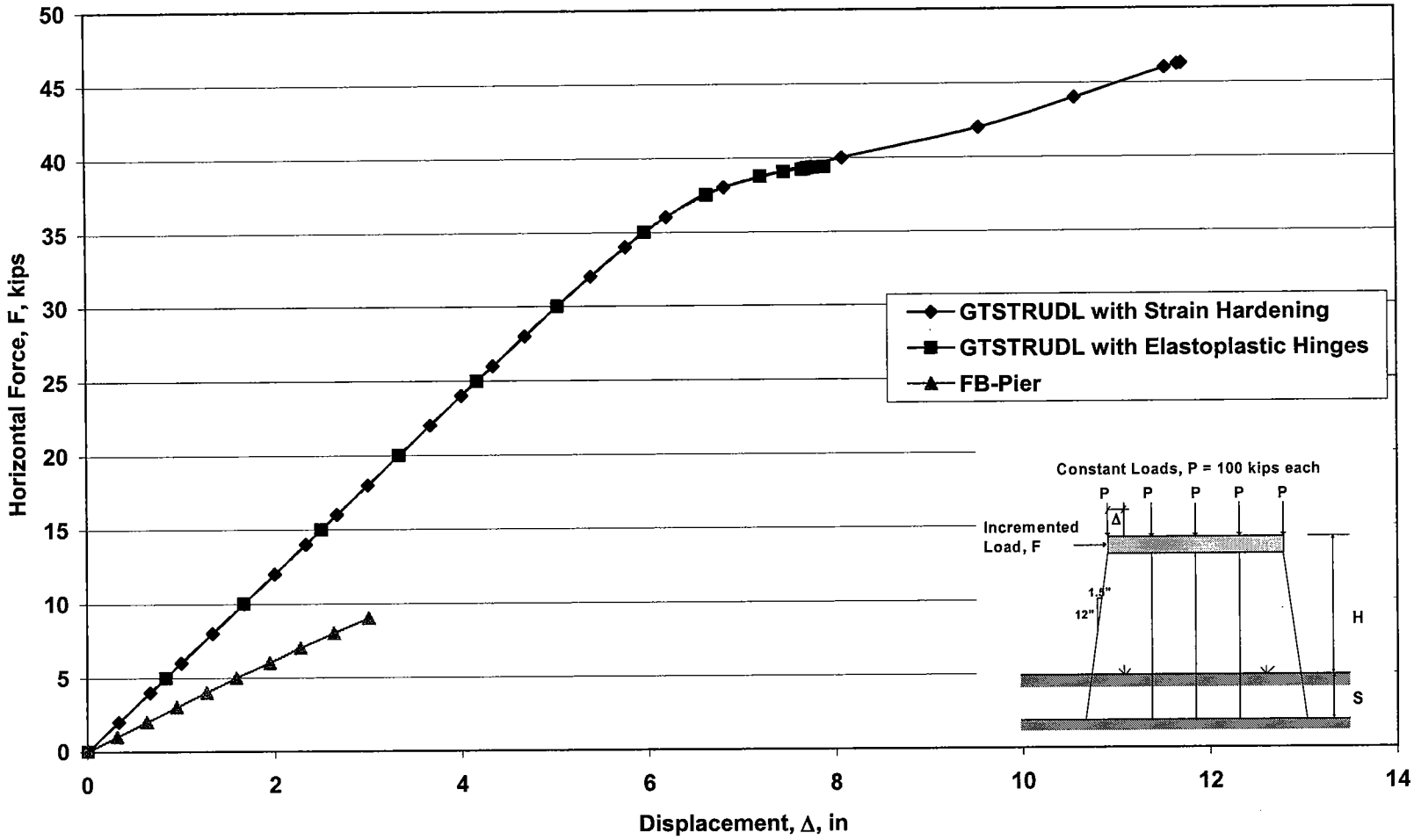

Figure 7.40. Pushover Analysis Comparison for HP10x42 5-Pile Bent, Fixed at Cap, Fixed at Ground (for GTSTRUDL), Soil K_o=150lb/in^3 (for FB-Pier), H=13ft, S=15ft

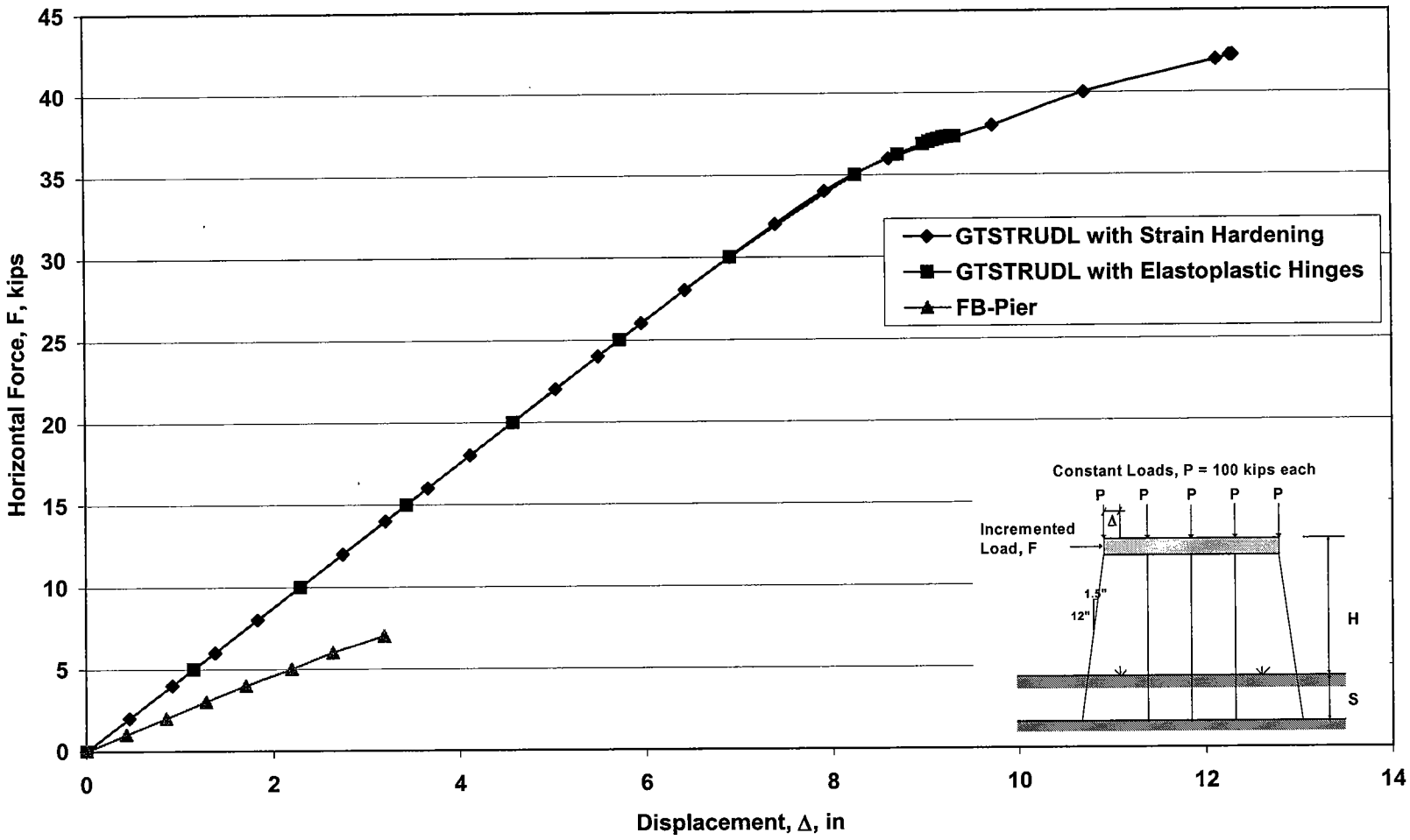

Figure 7.41. Pushover Analysis Comparison for HP10x42 5-Pile Bent, Fixed at Cap, Fixed at Ground (for GTSTRUDL), Soil K_o=150lb/in^3 (for FB-Pier), H=13ft, S=20ft

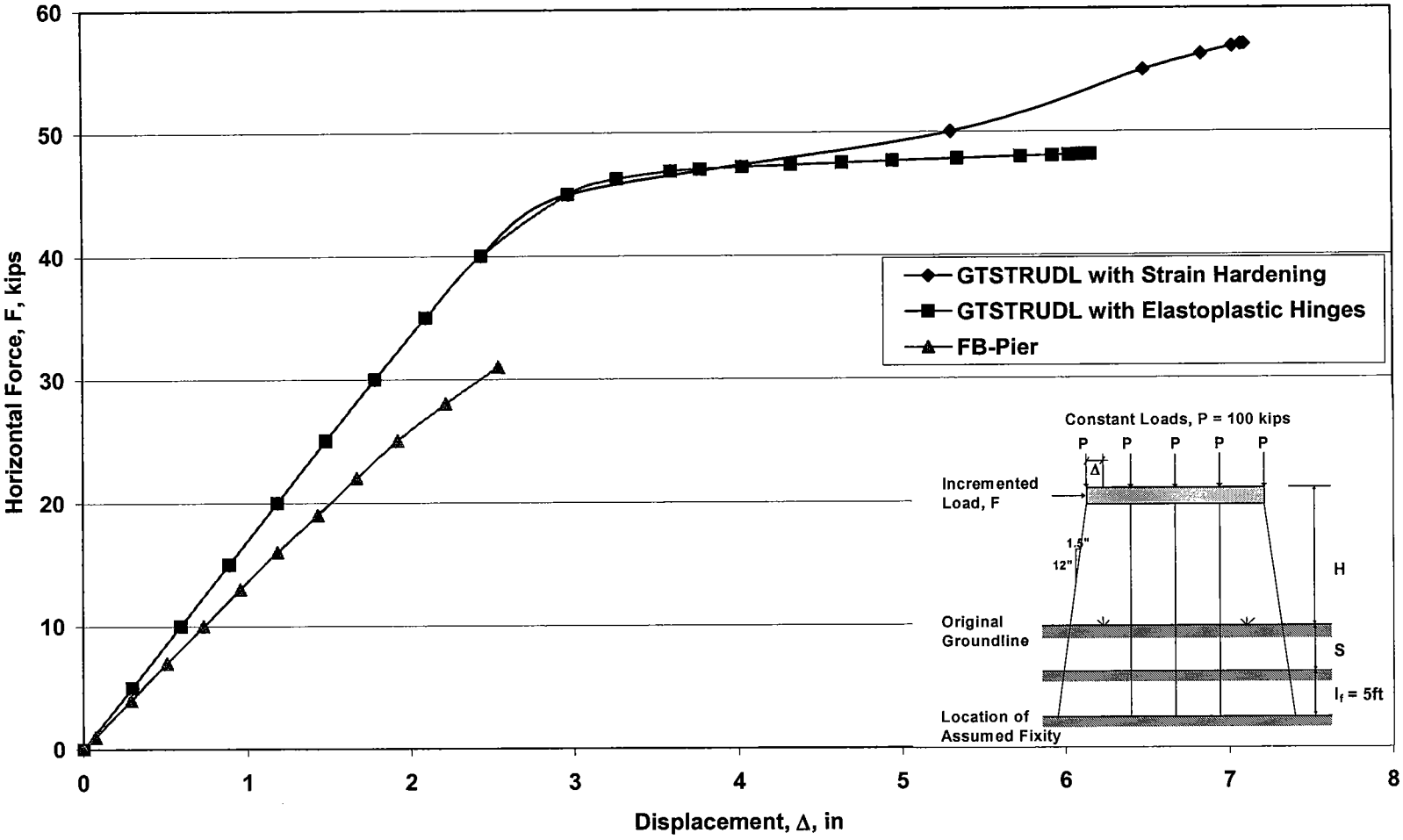

Figure 7.42. Pushover Analysis Comparison for HP10x42 5-Pile Bent, Fixed at Cap, Fixed at Assumed Fixity Length Below Ground l_f = 5ft (for GTSTRUDL), Soil K_o=150lb/in^3 (for FB-Pier), H=13ft, S=0ft

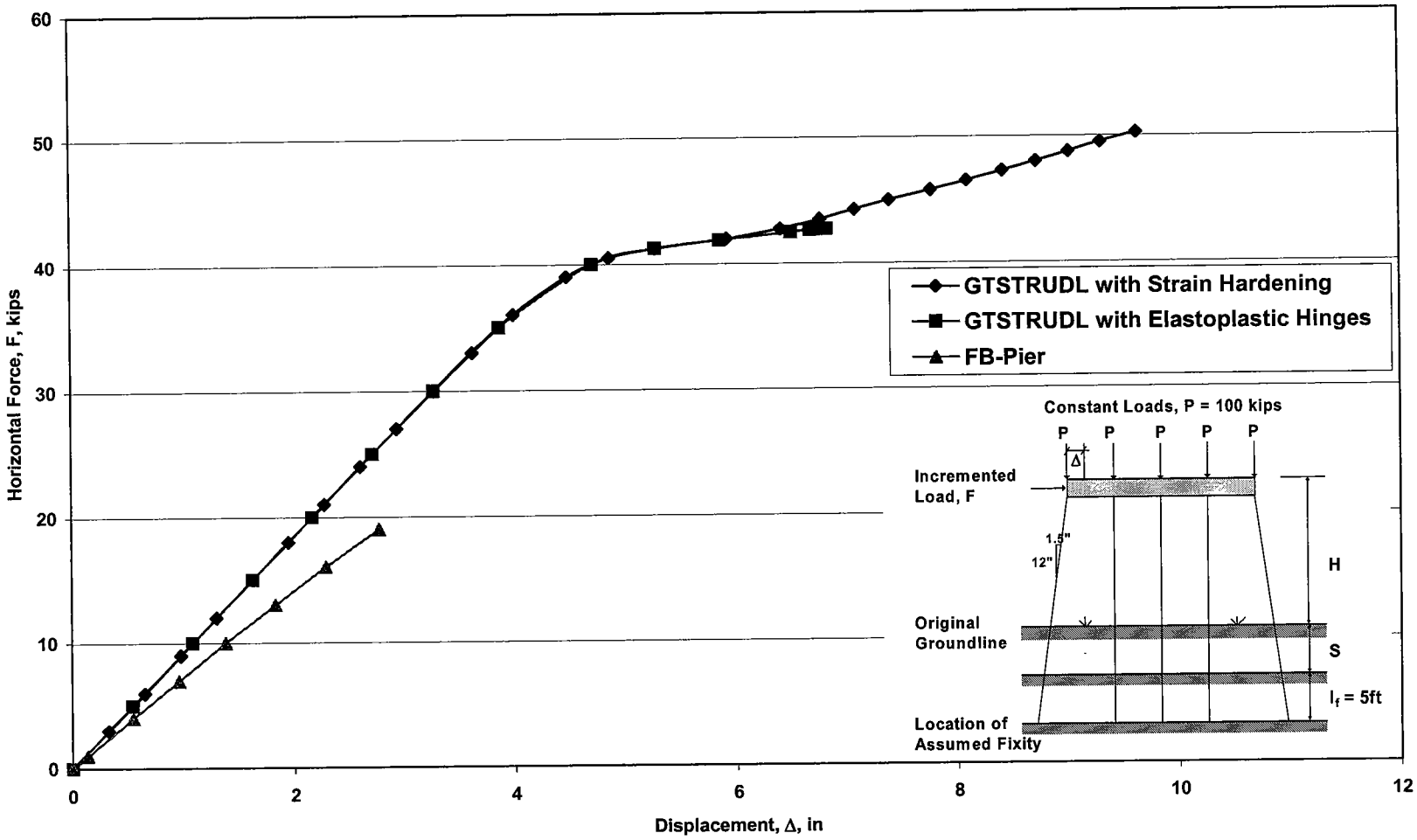

Figure 7.43. Pushover Analysis Comparison for HP10x42 5-Pile Bent, Fixed at Cap, Fixed at Assumed Fixity Length Below Ground l_f = 5ft (for GTSTRUDL), Soil K_o=150lb/in^3 (for FB-Pier), H=13ft, S=5ft

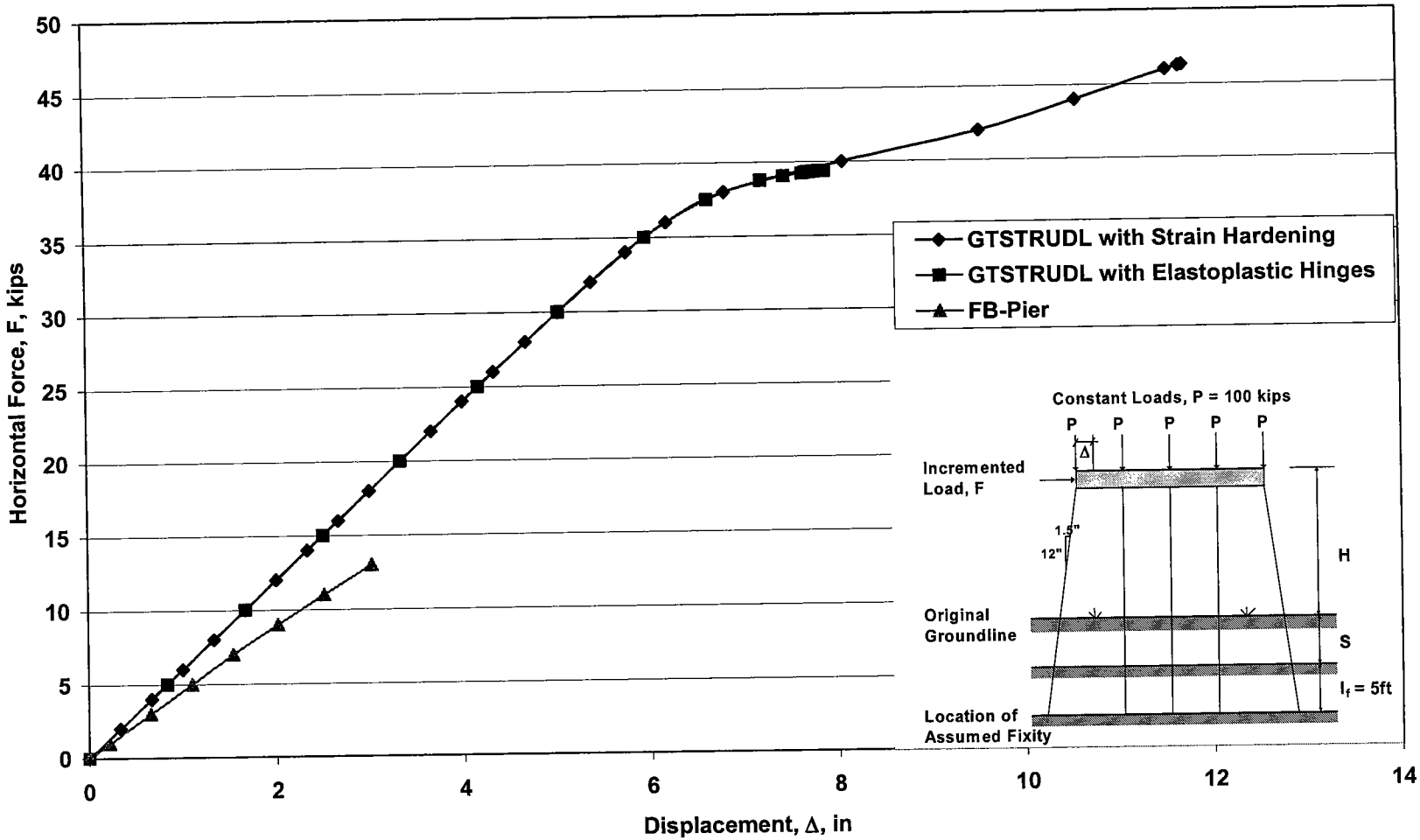

Figure 7.44. Pushover Analysis Comparison for HP10x42 5-Pile Bent, Fixed at Cap, Fixed at Assumed Fixity Length Below Ground l_f = 5ft (for GTSTRUDL), Soil K_o=150lb/in^3 (for FB-Pier), H=13ft, S=10ft

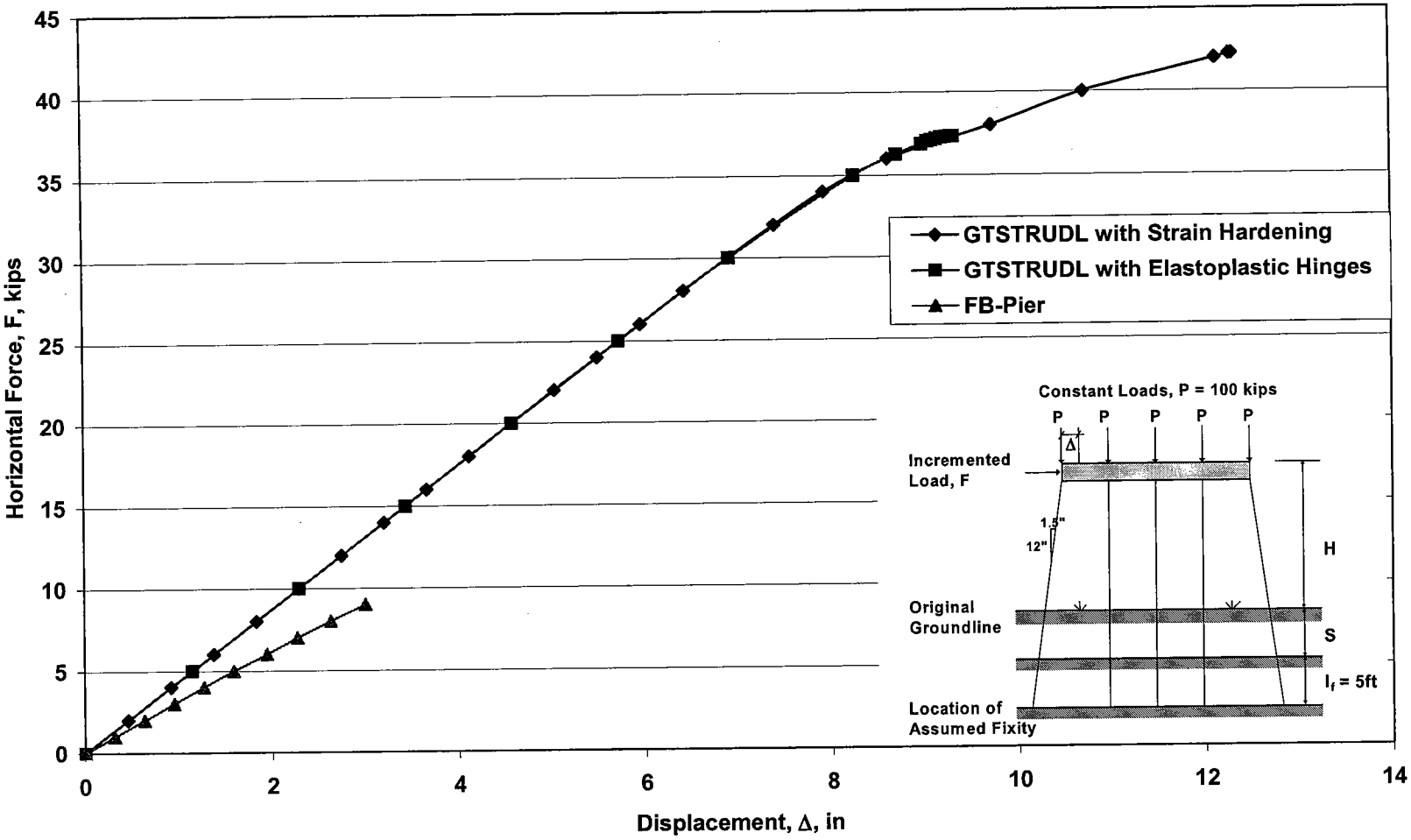

Figure 7.45. Pushover Analysis Comparison for HP10x42 5-Pile Bent, Fixed at Cap, Fixed at Assumed Fixity Length Below Ground l_f = 5ft (for GTSTRUDL), Soil K_o=150lb/in^3 (for FB-Pier), H=13ft, S=15ft

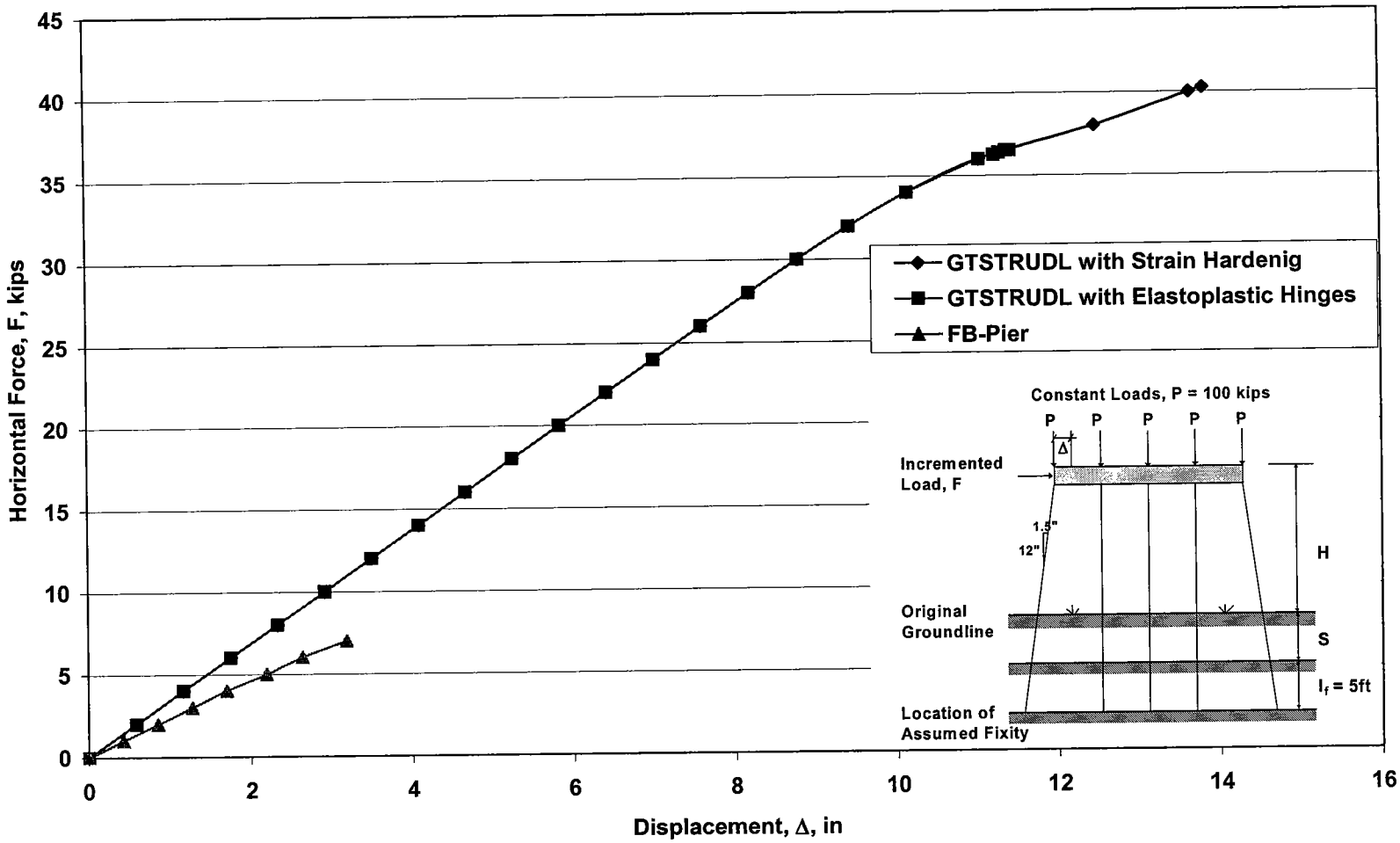

Figure 7.46. Pushover Analysis Comparison for HP10x42 5-Pile Bent, Fixed at Cap, Fixed at Assumed Fixity Length Below Ground l_f = 5ft (for GTSTRUDL), Soil K_o=150lb/in^3 (for FB-Pier), H=13ft, S=20ft

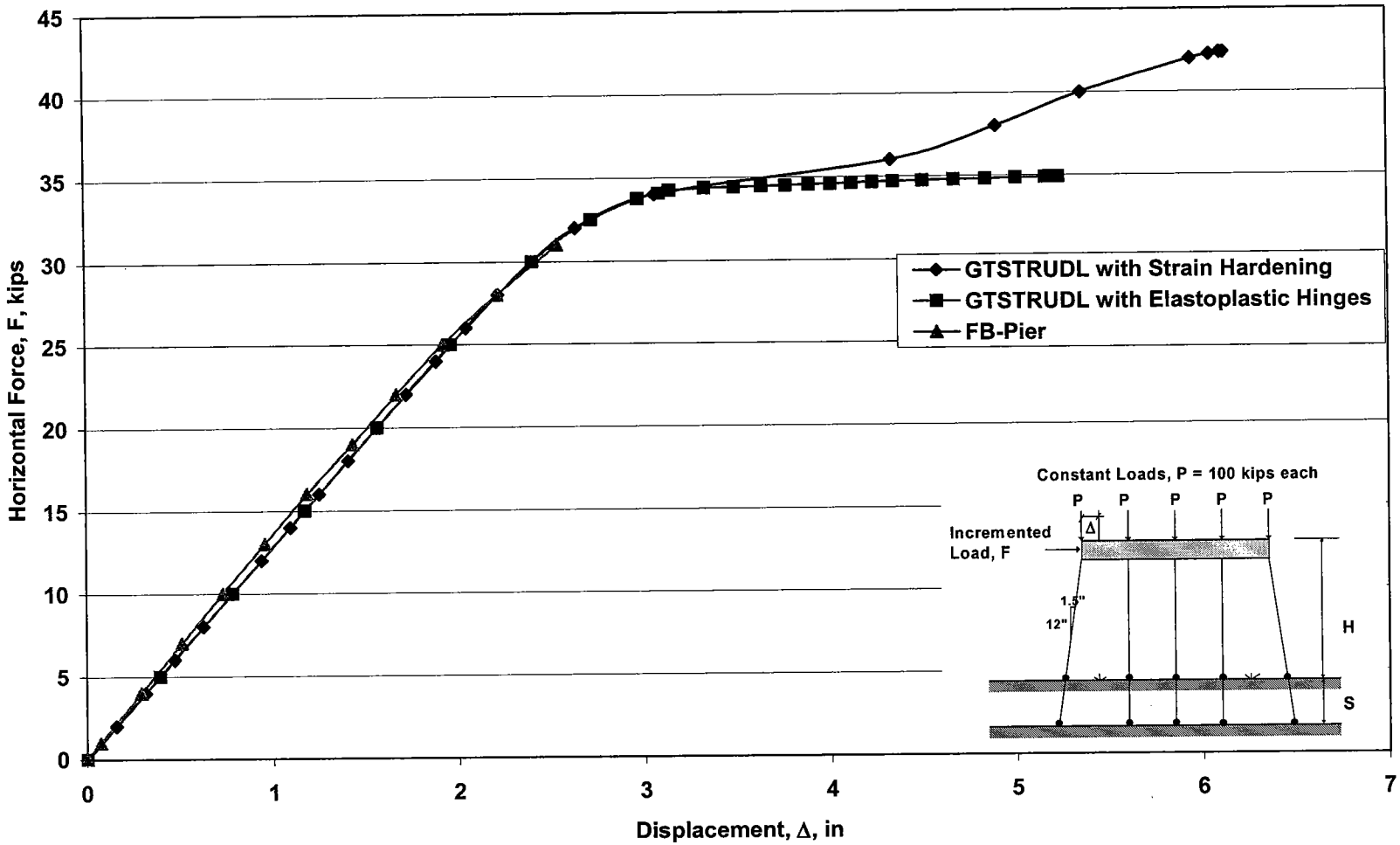

Figure 7.47. Pushover Analysis Comparison for HP10x42 5-Pile Bent, Fixed at Cap, Pinned at Ground (for GTSTRUDL), Soil K_o=150lb/in^3 (for FB-Pier), H=13ft, S=0ft

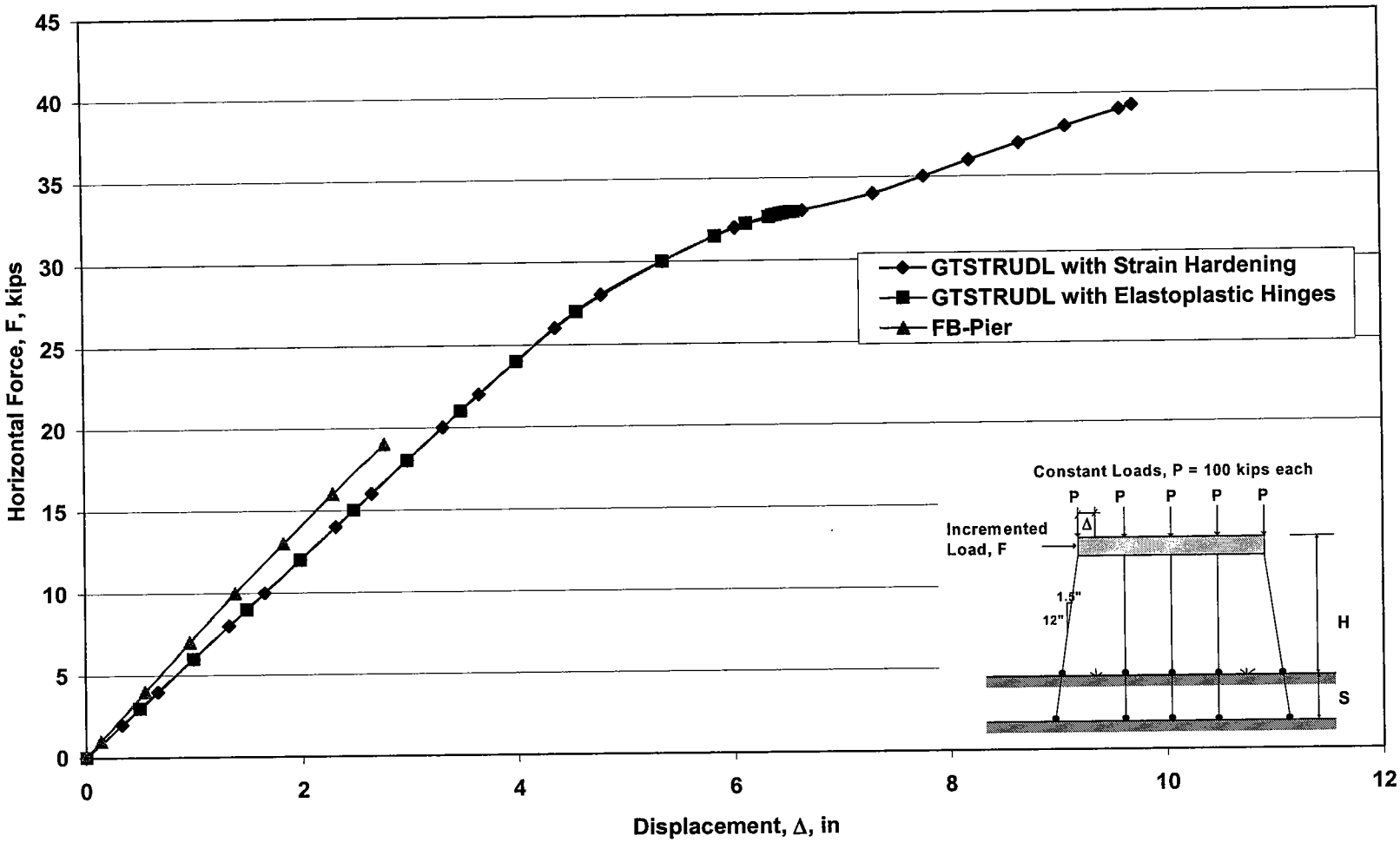

Figure 7.48. Pushover Analysis Comparison for HP10x42 5-Pile Bent, Fixed at Cap, Pinned at Ground (for GTSTRUDL), Soil K_o=150lb/in^3 (for FB-Pier), H=13ft, S=5ft

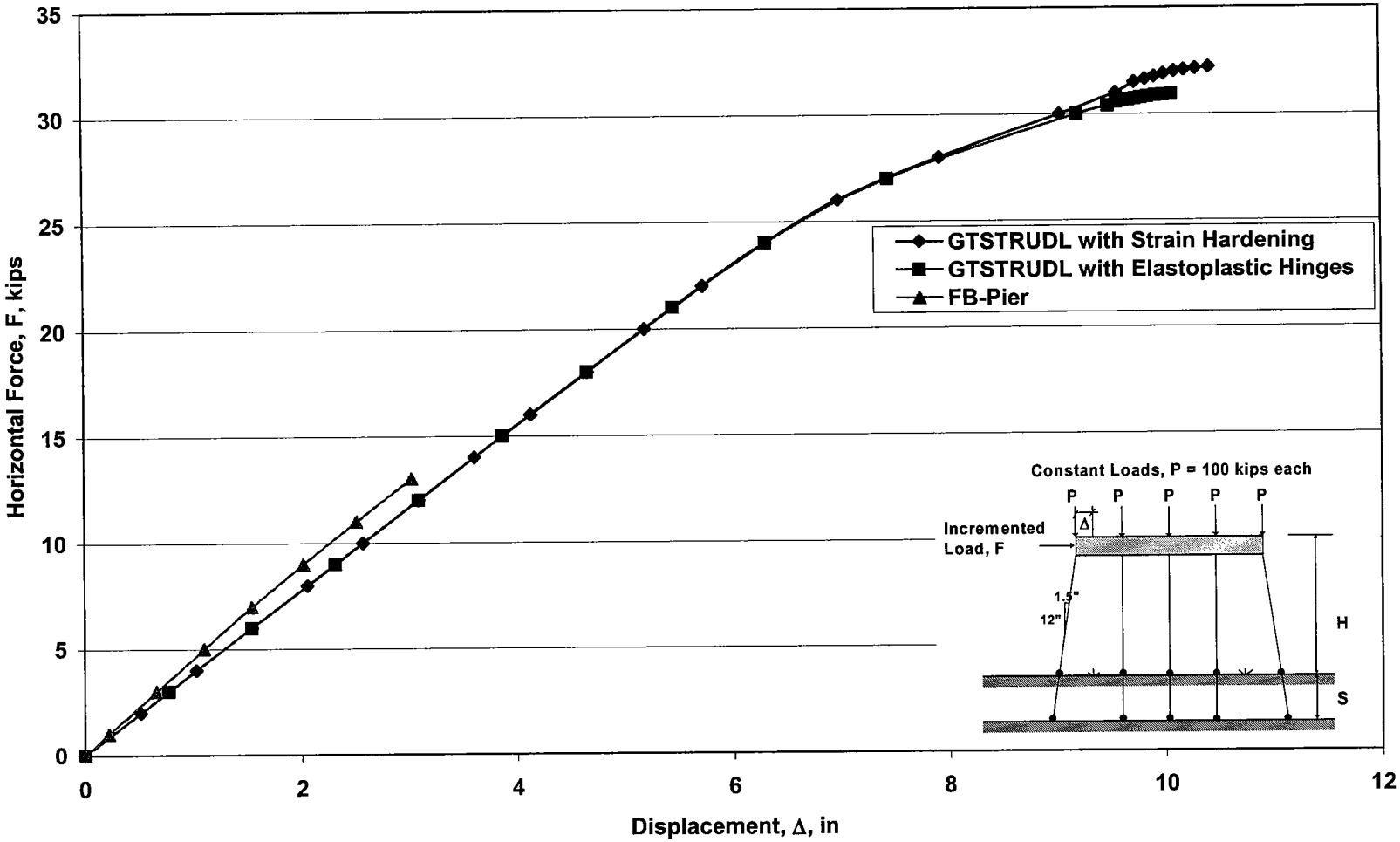

Figure 7.49. Pushover Analysis Comparison for HP10x42 5-Pile Bent, Fixed at Cap, Pinned at Ground (for GTSTRUDL), Soil K_o=150lb/in^3 (for FB-Pier), H=13ft, S=10ft

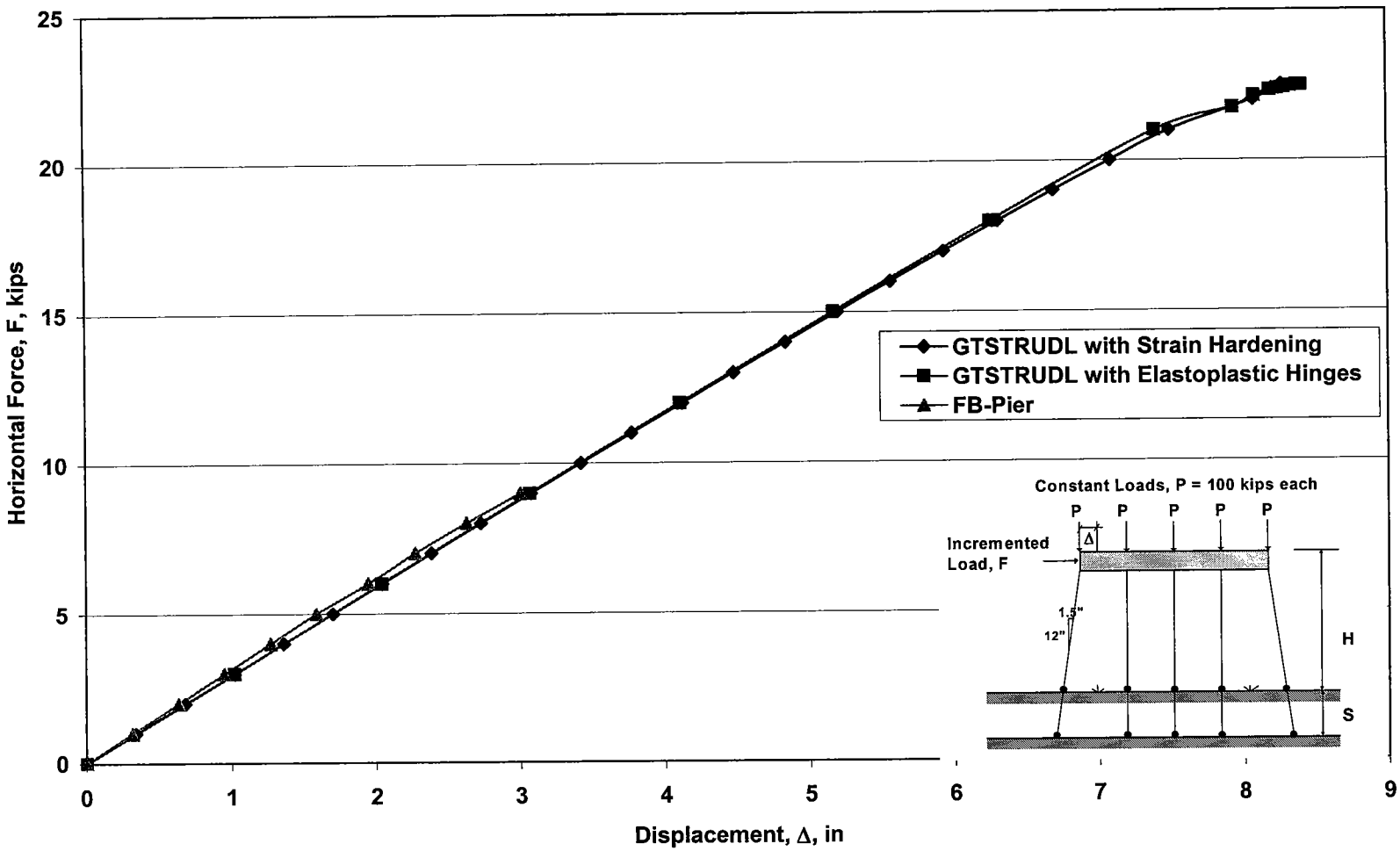

Figure 7.50. Pushover Analysis Comparison for HP10x42 5-Pile Bent, Fixed at Cap, Pinned at Ground (for GTSTRUDL), Soil K_o=150lb/in^3 (for FB-Pier), H=13ft, S=15ft

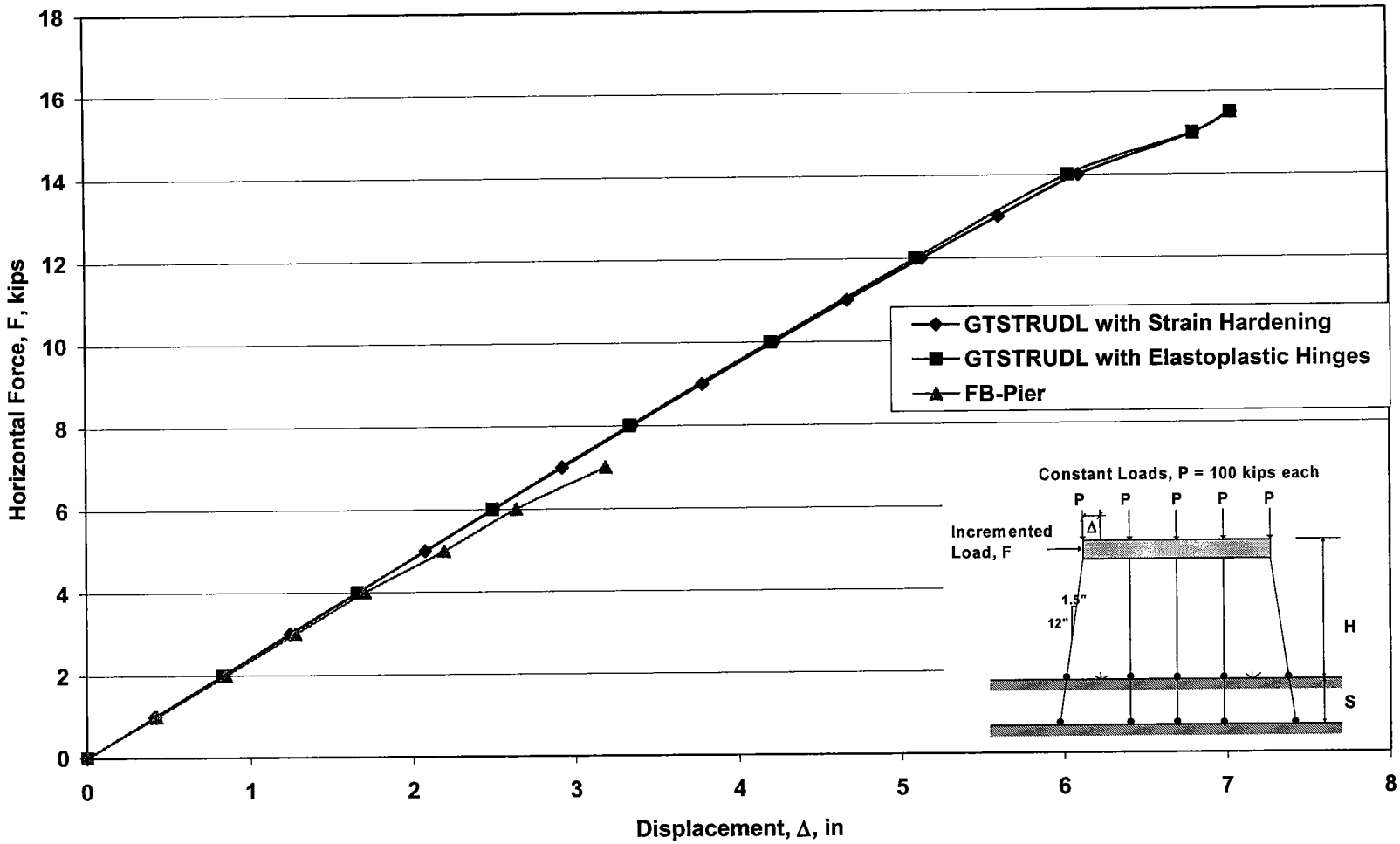

Figure 7.51. Pushover Analysis Comparison for HP10x42 5-Pile Bent, Fixed at Cap, Pinned at Ground (for GTSTRUDL), Soil K_o=150lb/in^3 (for FB-Pier), H=13ft, S=20ft

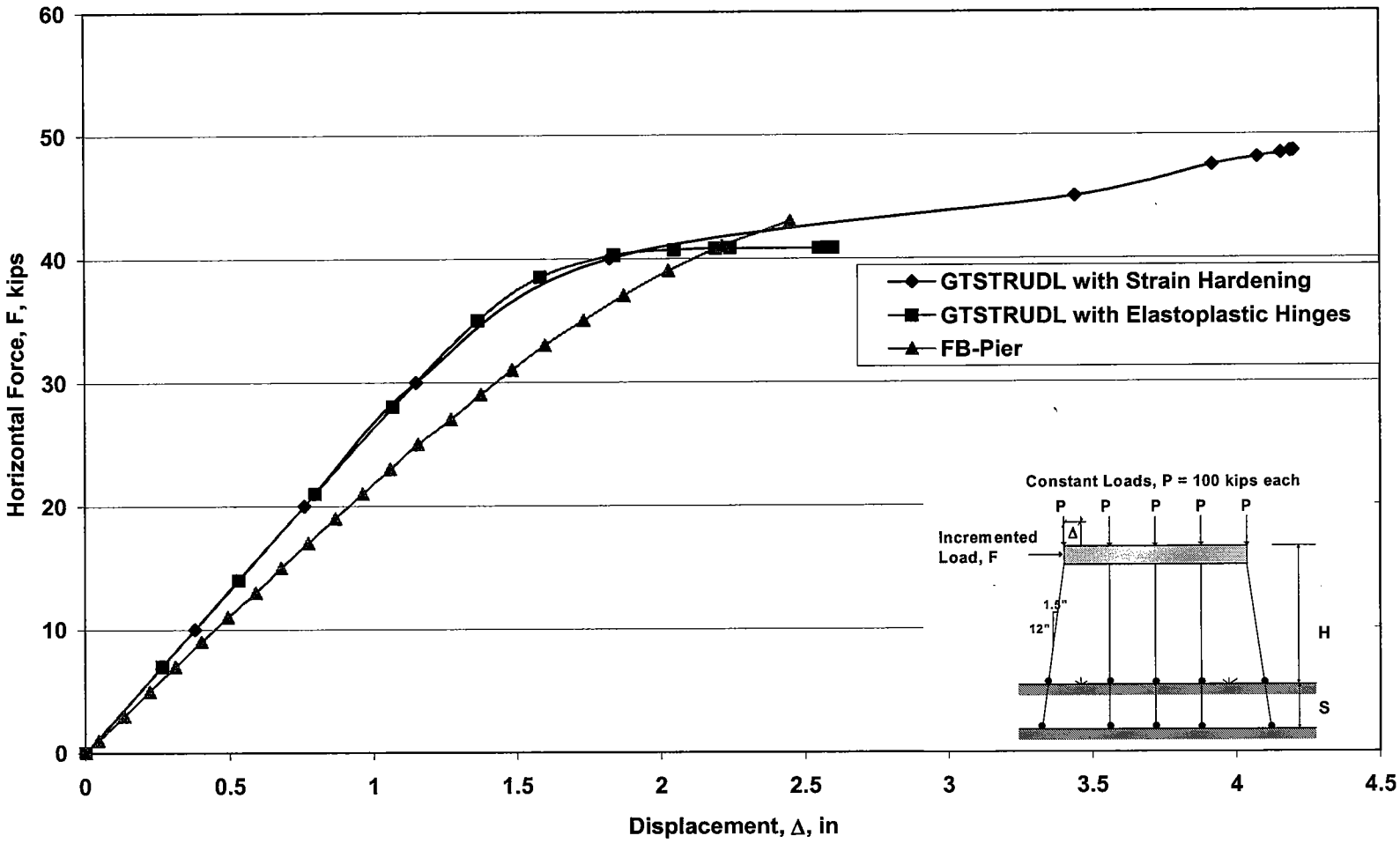

Figure 7.52. Pushover Analysis Comparison for HP10x42 5-Pile Bent, Fixed at Cap, Pinned at Ground (for GTSTRUDL), Soil K_o=150lb/in^3 (for FB-Pier), H=10ft, S=0ft

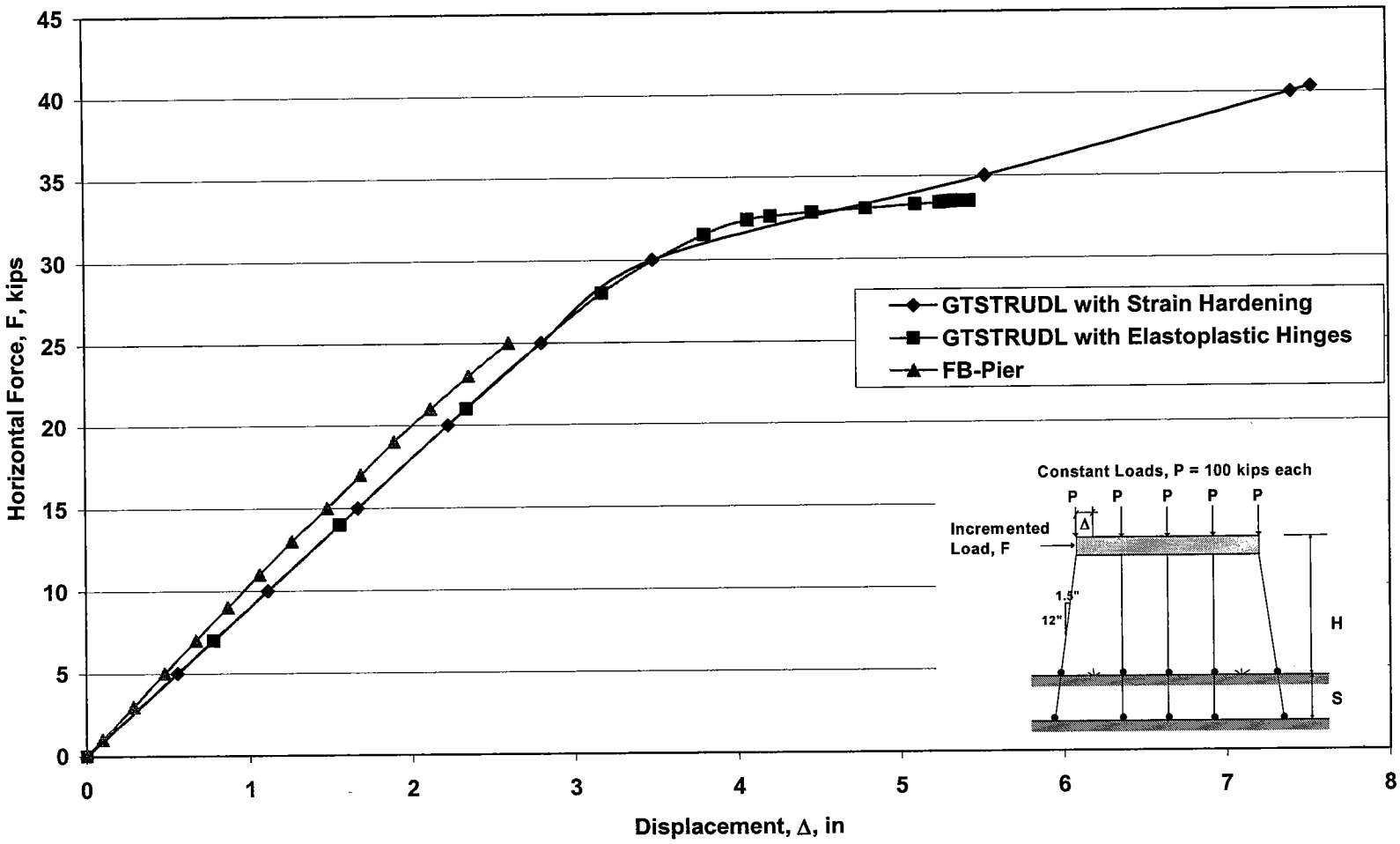

Figure 7.53. Pushover Analysis Comparison for HP10x42 5-Pile Bent, Fixed at Cap, Pinned at Ground (for GTSTRUDL), Soil K_o=150lb/in^3 (for FB-Pier), H=10ft, S=5ft

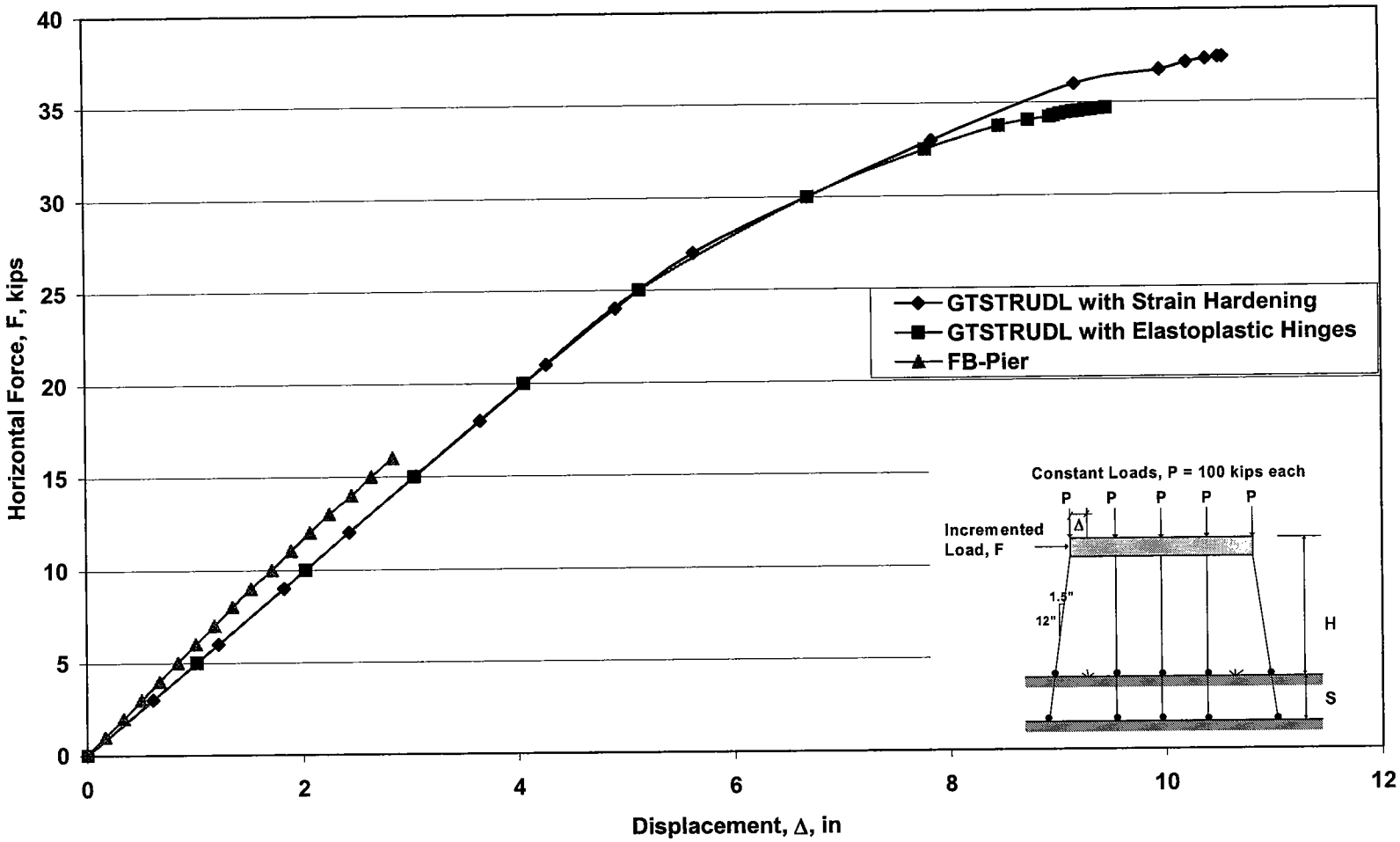

Figure 7.54. Pushover Analysis Comparison for HP10x42 5-Pile Bent, Fixed at Cap, Pinned at Ground (for GTSTRUDL), Soil K_o=150lb/in^3 (for FB-Pier), H=10ft, S=10ft

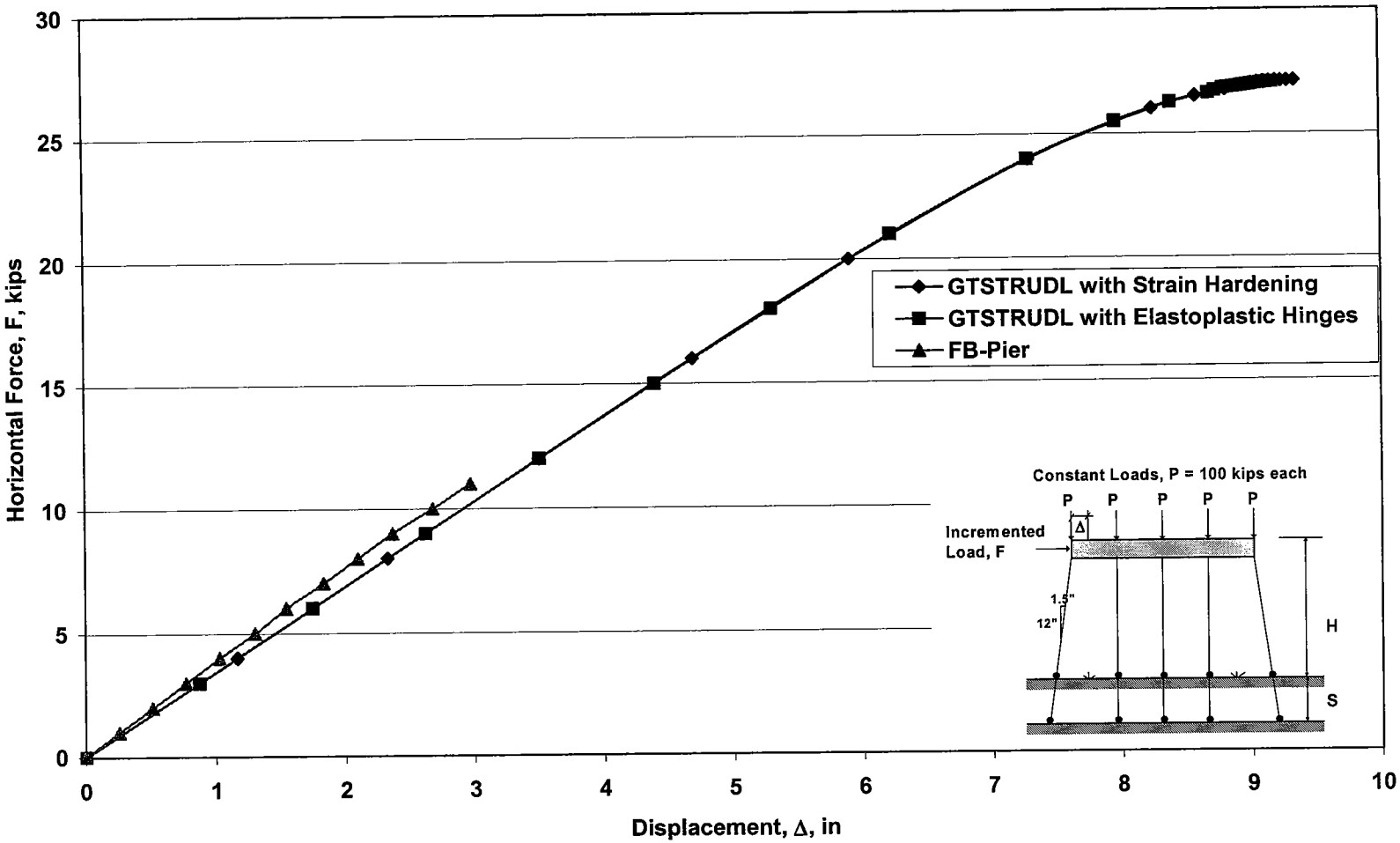

Figure 7.55. Pushover Analysis Comparison for HP10x42 5-Pile Bent, Fixed at Cap, Pinned at Ground (for GTSTRUDL), Soil K_o=150lb/in^3 (for FB-Pier), H=10ft, S=15ft

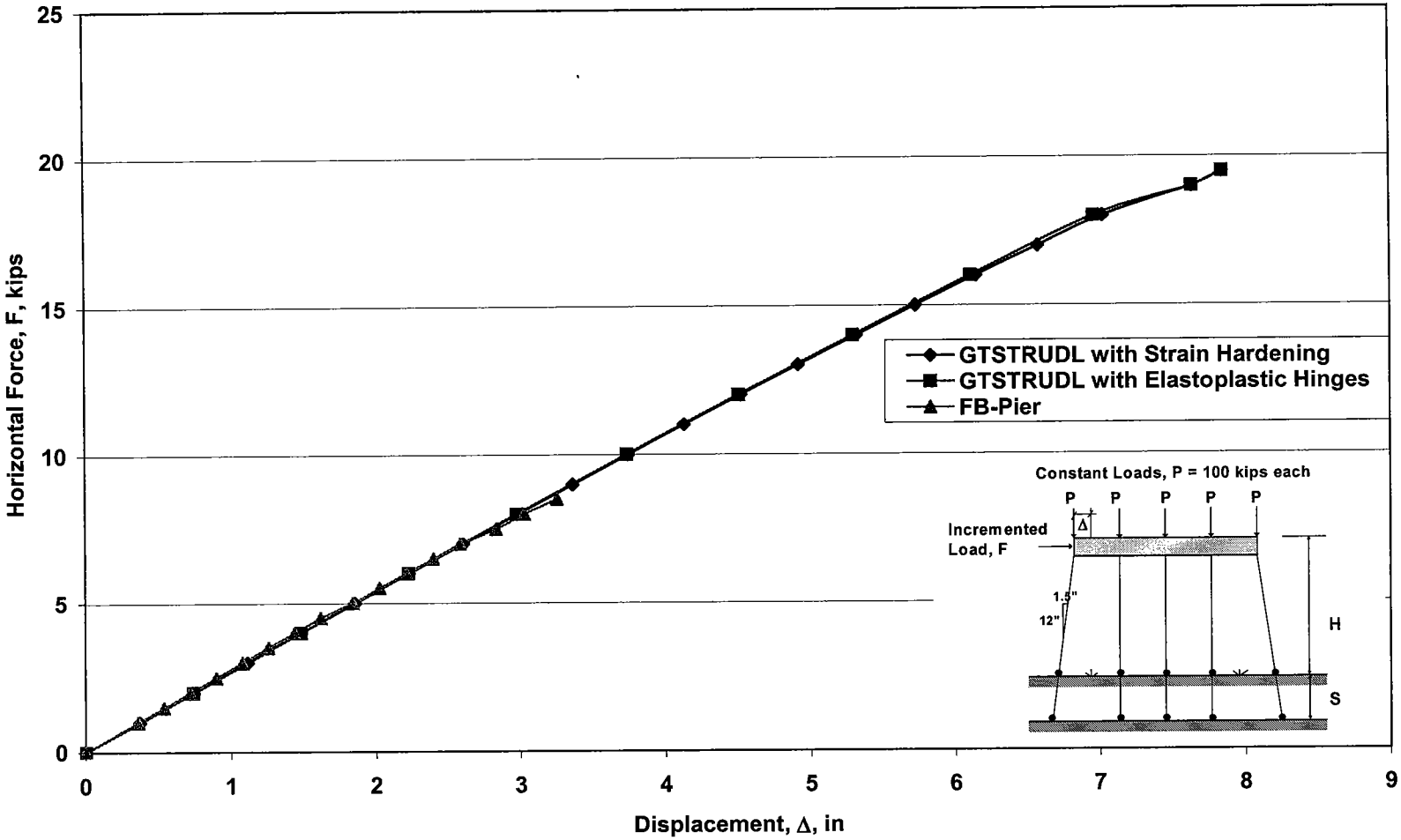

Figure 7.56. Pushover Analysis Comparison for HP10x42 5-Pile Bent, Fixed at Cap, Pinned at Ground (for GTSTRUDL), Soil K_o=150lb/in^3 (for FB-Pier), H=10ft, S=20ft

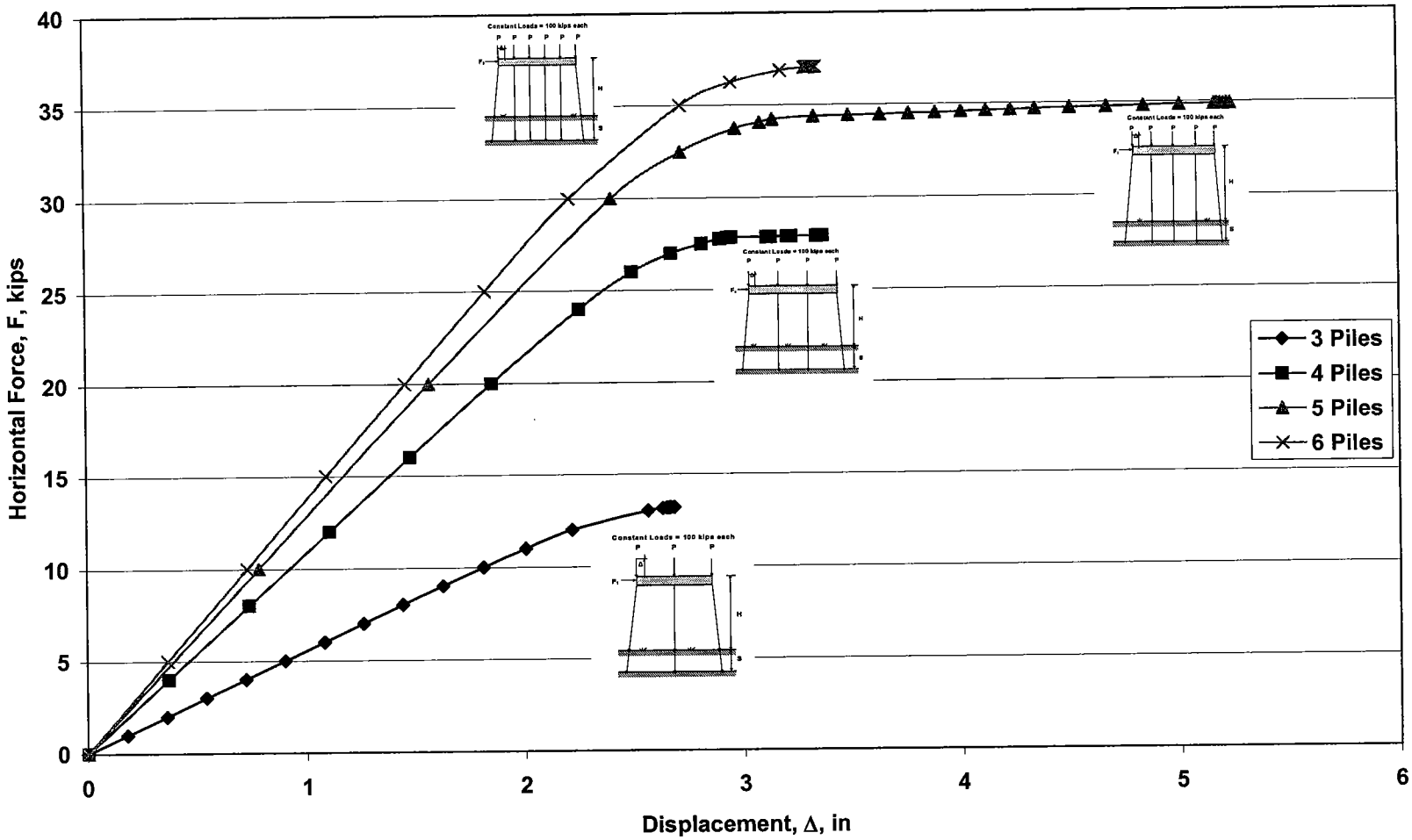

Figure 7.57a. GTSTRUDL Pushover Analysis of HP10x42 Non X-Braced Pile Bents with Different Numbers of Piles, Fixed at Cap, Pinned at Ground, H=13ft, S=0ft

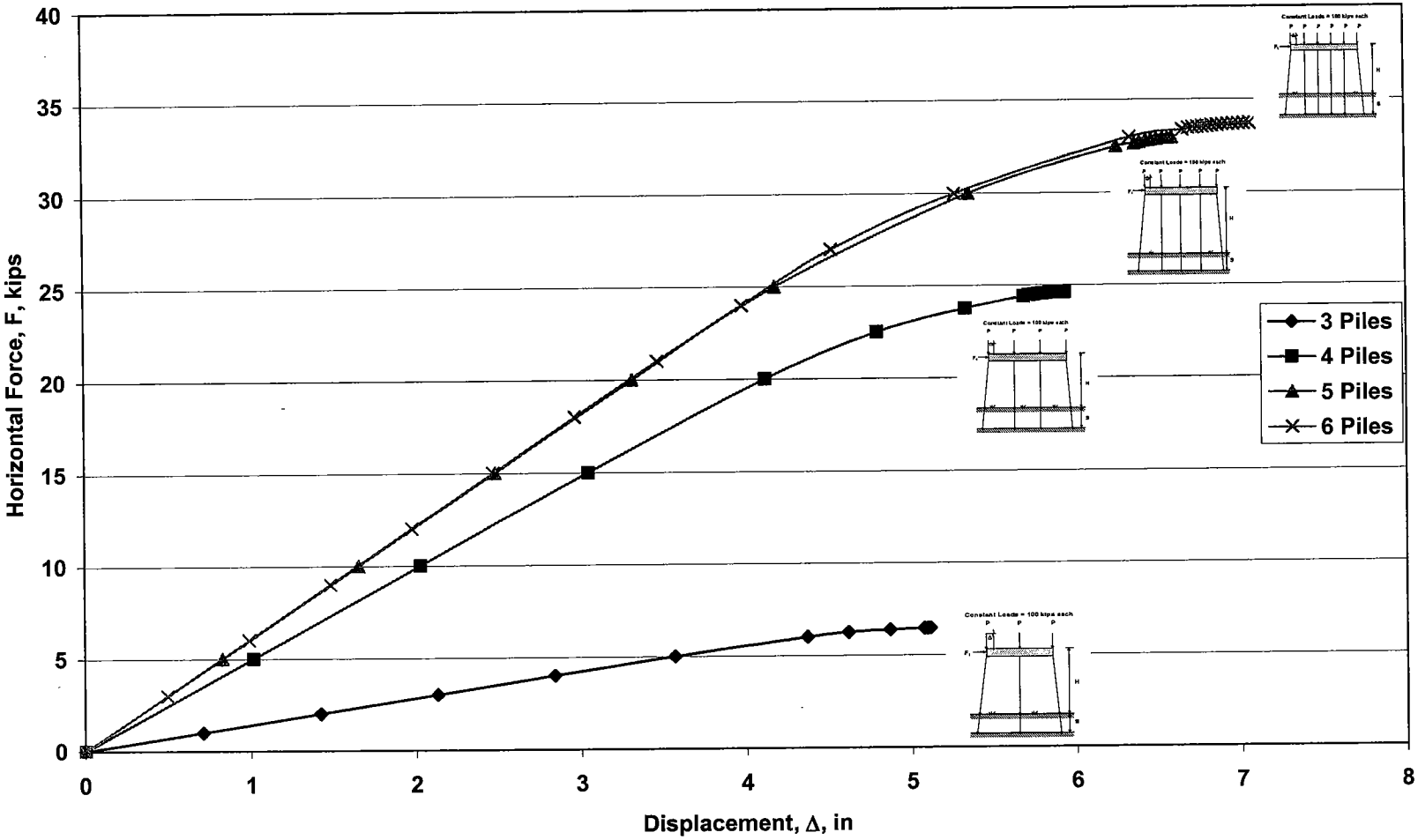

Figure 7.57b. GTSTRUDL Pushover Analysis of HP10x42 Non X-Braced Pile Bents with Different Numbers of Piles, Fixed at Cap, Pinned at Ground, H=13ft, S=5ft

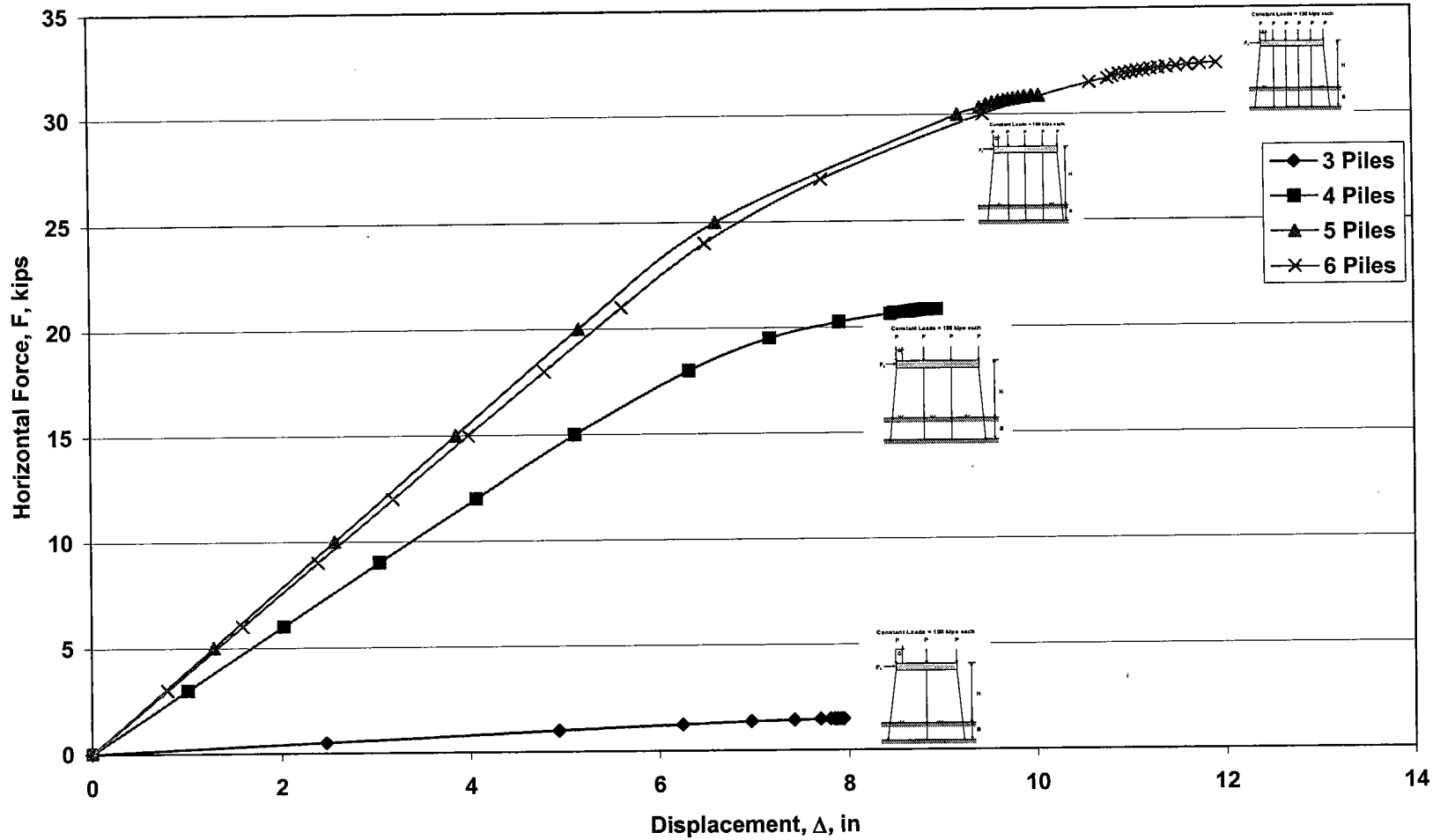

Figure 7.57c. GTSTRUDL Pushover Analysis of HP10x42 Non X-Braced Pile Bents with Different Numbers of Piles, Fixed at Cap, Pinned at Ground, H=13ft, S=10ft

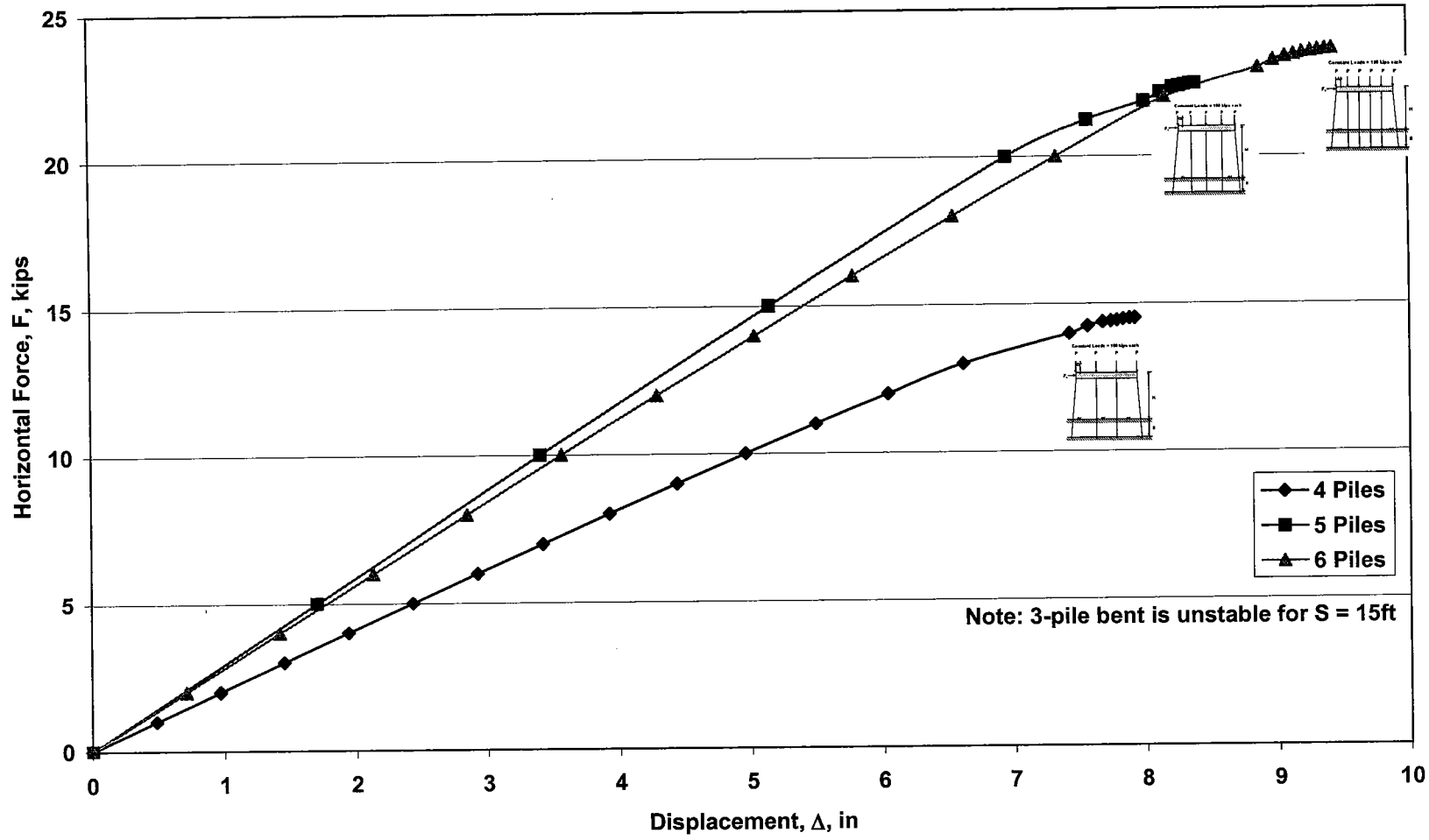

Figure 7.57d. GTSTRUDL Pushover Analysis of HP10x42 Non X-Braced Pile Bents with Different Numbers of Piles, Fixed at Cap, Pinned at Ground, H=13ft, S=15ft

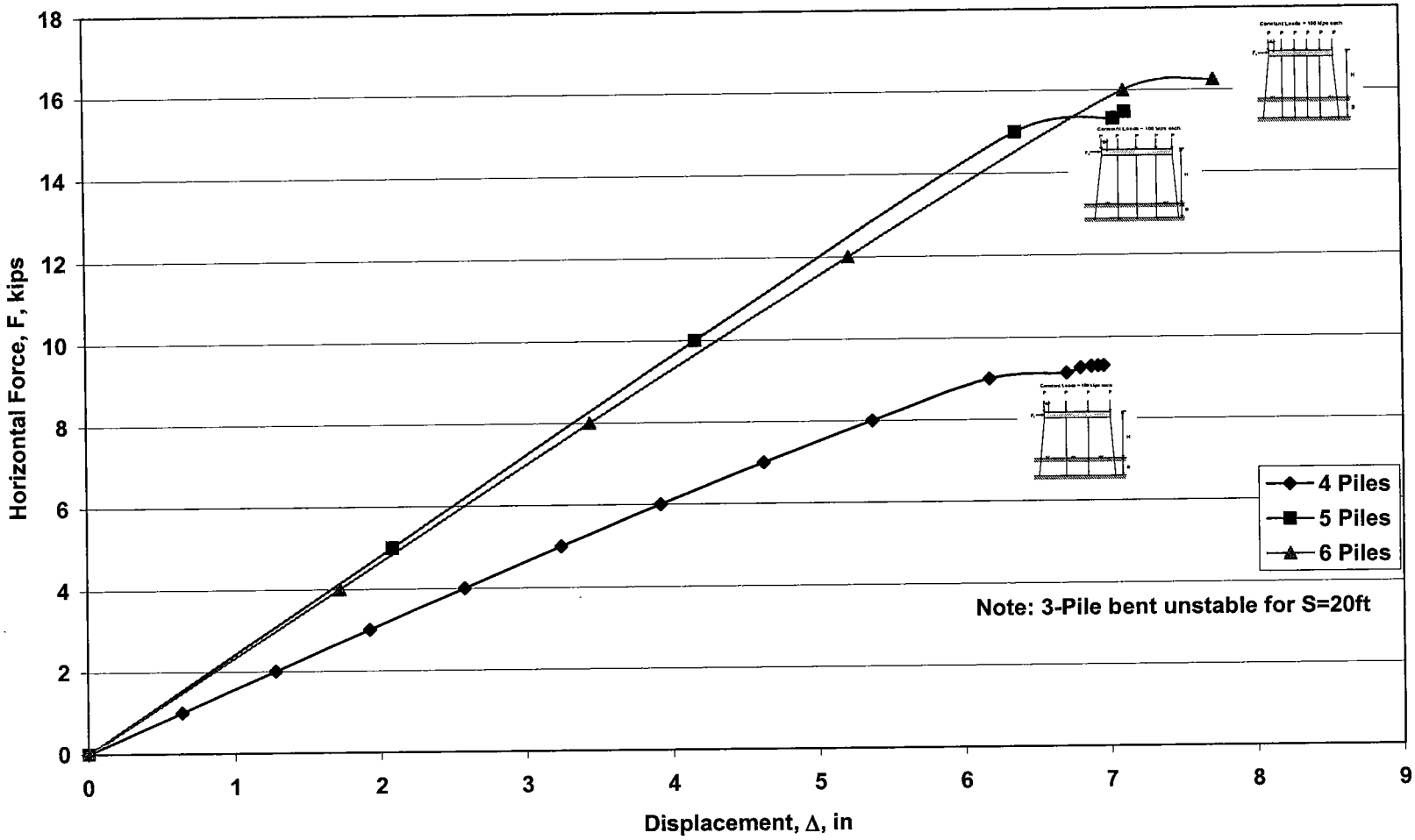

Figure 7.57e. GTSTRUDL Pushover Analysis of HP10x42 Non X-Braced Pile Bents with Different Numbers of Piles, Fixed at Cap, Pinned at Ground, H=13ft, S=20ft

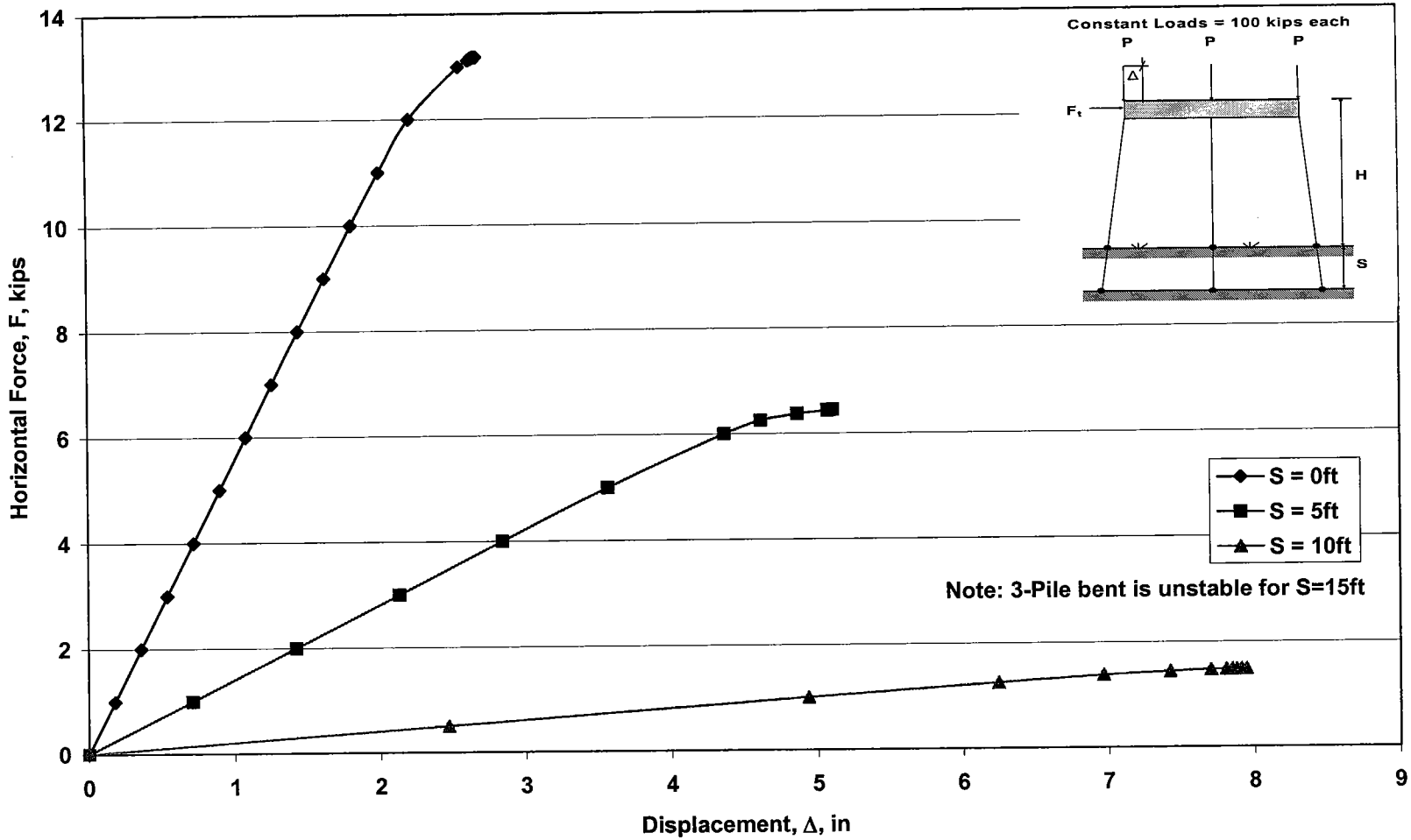

Figure 7.58. GTSTRUDL Pushover Analysis For HP 10x42 3-Pile Non X-braced Bents Subjected to Scour, H = 13ft

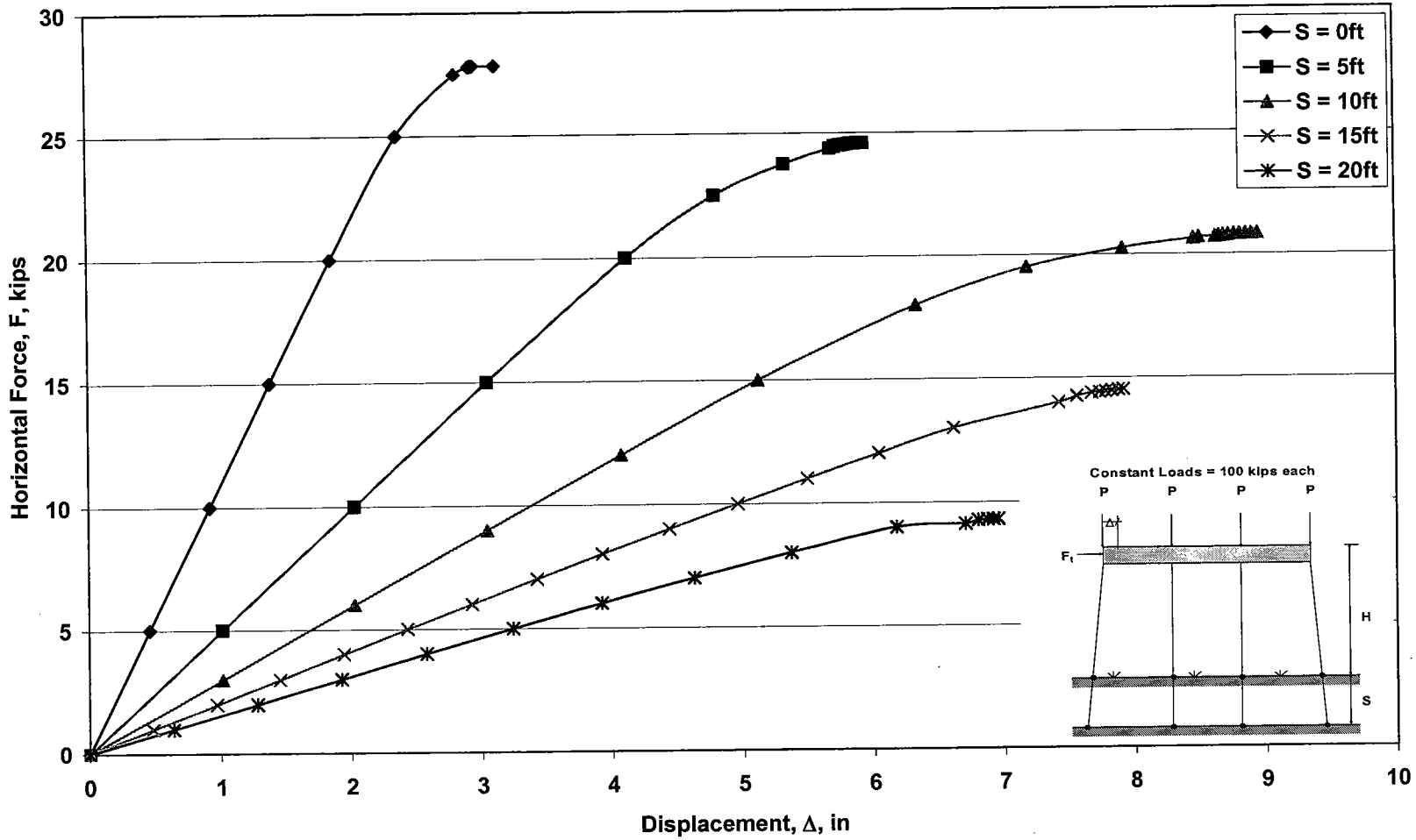

Figure 7.59. GTSTRUDL Pushover Analysis For HP 10x42 4-Pile Non X-braced Bents Subjected to Scour, H = 13ft

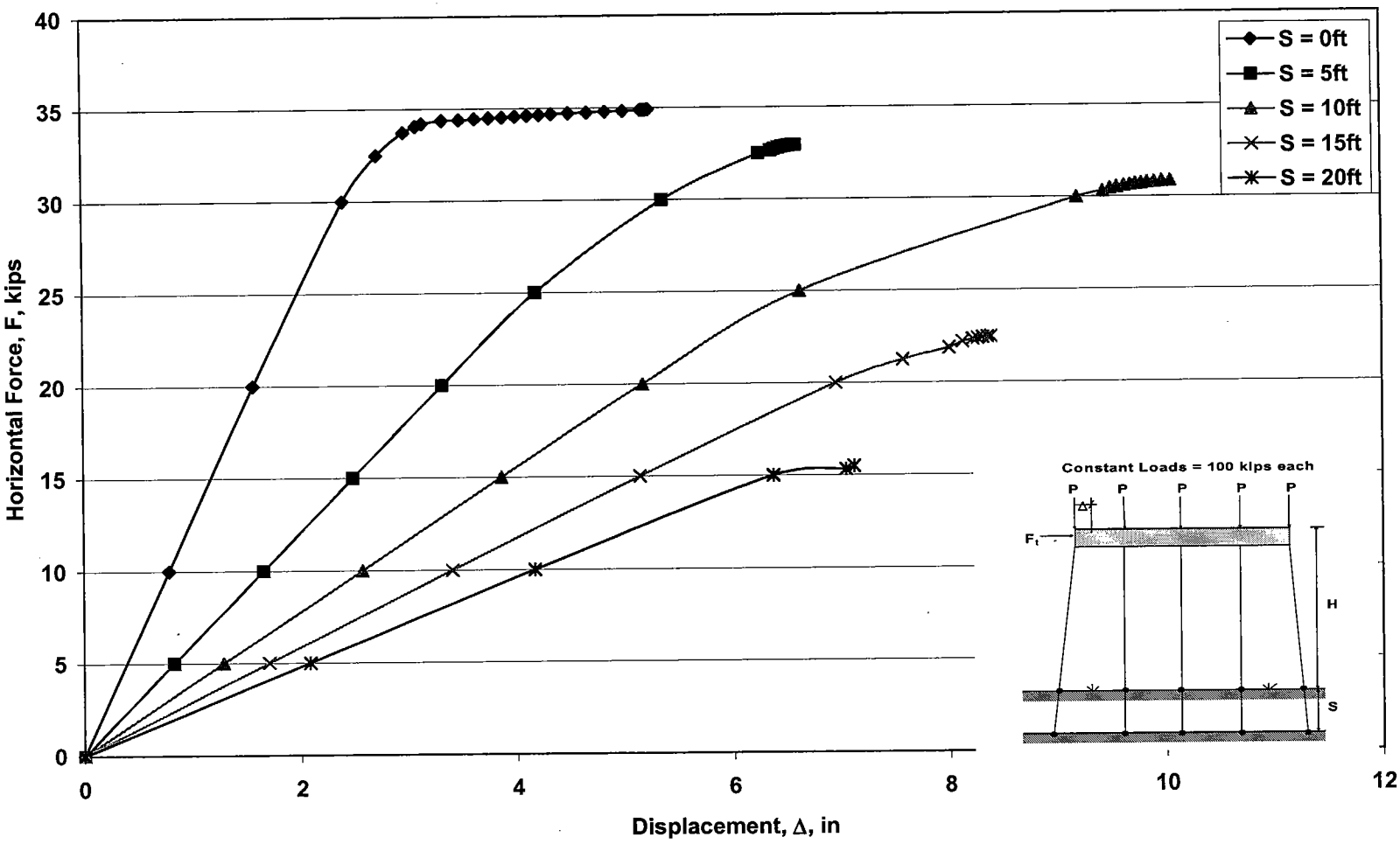

Figure 7.60. GTSTRUDL Pushover Analysis For HP 10x42 5-Pile Non X-braced Bents Subjected to Scour, H = 13ft

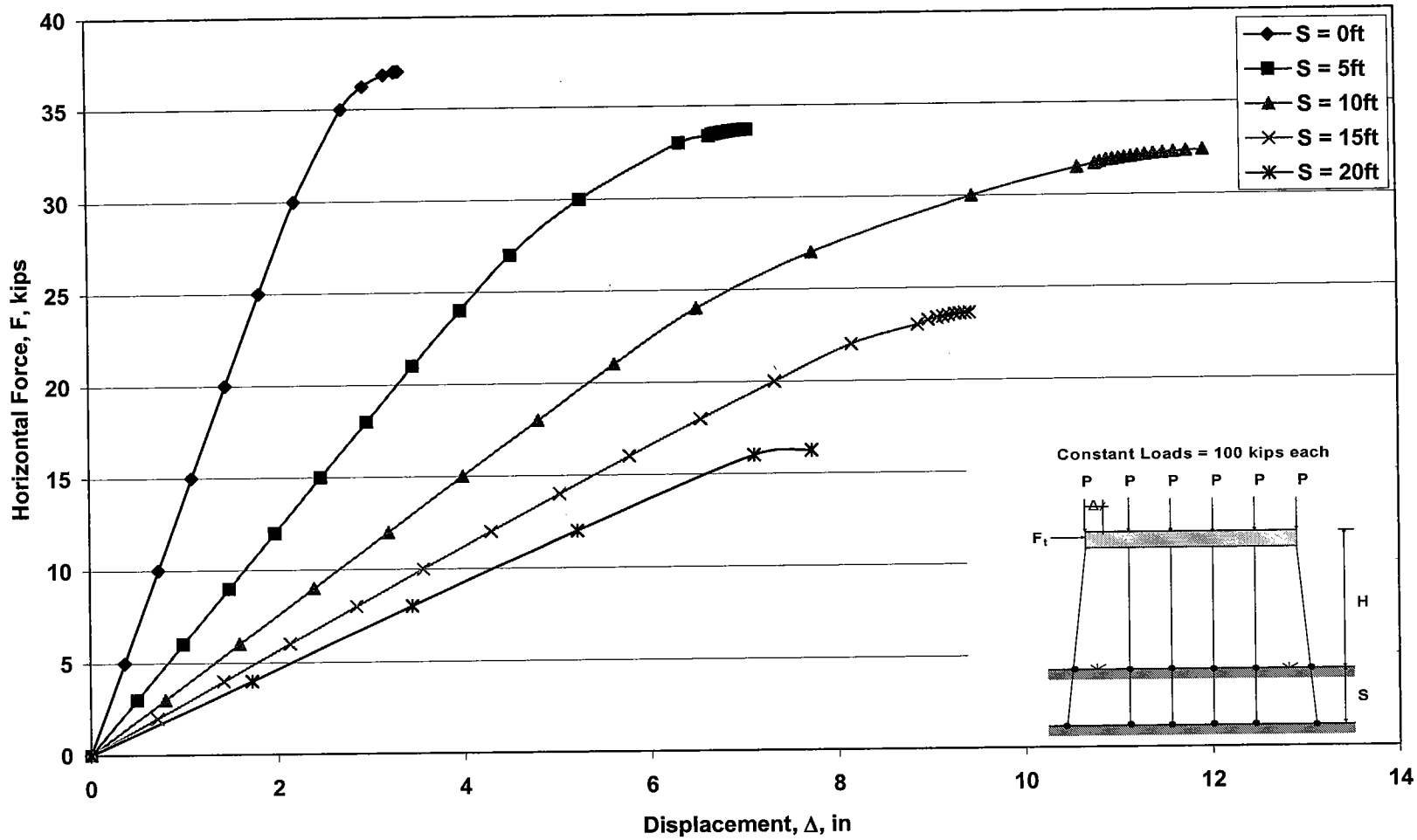

Figure 7.61. GTSTRUDL Pushover Analysis For HP-10x42 6 Pile Non X-braced Bents Subjected to Scour, H = 13ft

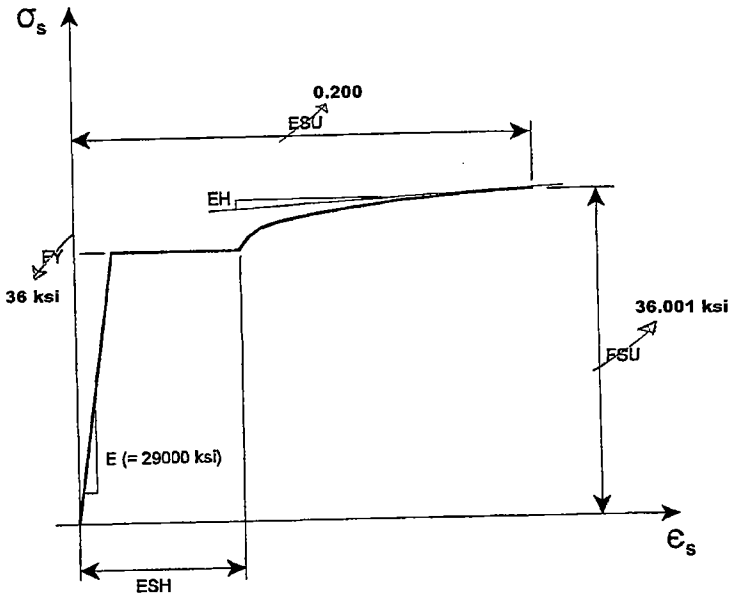

Figure 7.62. GTSTRUDL Stress Strain Curve and Nonlinear Plastic Hinge Parameters (4)

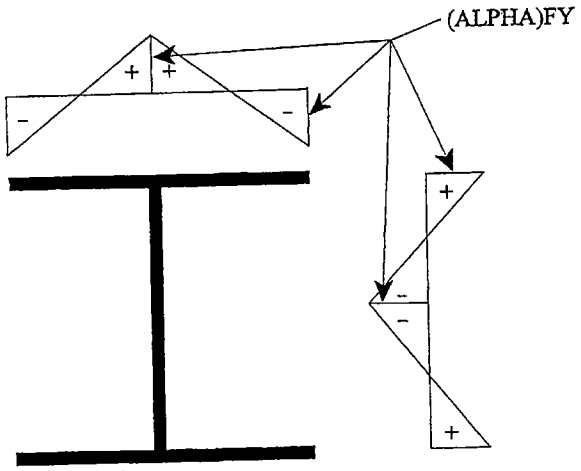

Figure 7.63. GTSTRUDL Assumed Residual Stress Distribution (4)

CHAPTER 8: PUSHOVER ANALYSIS OF X-BRACED PILE BENTS

8.1 General

Pile bents that incorporate X-bracing may be classified as one or two story bents. Typically, pile bents with heights, H, between 13 and 19ft are designed as one story bents whereas bents with heights ranging from 20 to 25ft are constructed as two story bents (where H is taken as the distance from the original ground line to the top of the bent cap). Standard dimensions of common ALDOT pile bents are as shown in Figure 4.1. For purposes of modeling the pushover behavior and buckling capacity of X-braced bents, two extreme cases were examined by modeling the shortest single story X-braced pile bent at H=13ft and the tallest two story pile bent at H=25ft.

8.2 FB-Pier X-braced Pile Bent Models

It appears from experimentation with the FB-Pier program as well as through communication with ALDOT engineers and FB-Pier support staff that X-bracing cannot be added to pile bents in the transverse direction with FB-Pier. Many bridge designers have previously thought that buckling of pile bents in the longitudinal direction (directed along the length of the bridge deck) would be the controlling failure mode due to the lack of lean-on support (during construction before the bridge superstructure is completely in place), and the lack of X-bracing in this direction. However, this appears to be a significant oversight. After construction of the bridge superstructure and its positive connection to the bridge bents and end abutments, the roadway prevents swaying of the bridge pile bents in the longitudinal direction of the bridge. Translation of the bent caps is thereby restricted and longitudinal sidesway is prevented. This being the case, transverse buckling of the bent piles should be the controlling buckling mode. There are additional factors that contribute to buckling failure in the transverse direction.

Significant river loads imposed by debris rafts often act on the bents in the transverse direction, and flood water loads in conjunction with gravity loads may cause pushover of the bent in the transverse direction or buckling of the bent piles about their weak axes. Thus it is thought that the controlling buckling mode will be in the transverse direction, and due to the inability of FB-Pier to model pile bents with transverse X-bracing, no FB-Pier models or corresponding pushover analysis results are presented in this chapter. However, FB-Pier modeling and evaluation of non X-braced bents, such as those sometimes used when $H \leq 13$ft, have been made and the results reported in Chapter 7.

8.3 GTSTRUDL X-braced Pile Bent Models

Unlike FB-Pier, GTSTRUDL is capable of modeling bents with transverse X-bracing and quite an extensive study of the X-braced member behavior is examined in this chapter. Because the standard X-brace members are small angles (4"x3 ½" x 5/16"), the braces themselves are very susceptible to buckling and for this reason, two separate models for the one and two story pile bent classifications were initially considered. One case models the X-bracing as tension and/or compression members in which the angles can support both tensile and compressive forces. The bent X-bracing will behave in this manner to the point where the axial compressive forces in the X-bracing become large enough to buckle the angle members. Once this point is reached, the buckled X-brace members will maintain the Euler buckling load, but they will provide no further contribution to additional lateral stiffness. Since these members may be neglected from this stage forward, any remaining resistance to loading is achieved via only the X-braced members in tension. Therefore, the second case to be considered models the X-bracing as tension only members which essentially act as cables. For all X-braced bent models the X-braced members are pin connected to the piles so that the X-bracing carries no bending moments.

In an effort to simplify the models the X-bracing is pinned to the battered piles only. This is thought to be a reasonable model since GTSTRUDL does not check to see if the X-members have buckled during its structural analysis. However, this makes it necessary to keep track of the

axial forces that are developed in the X-bracing and determine the load increment during the pushover analysis where the Euler buckling load of the brace is exceeded. The following calculation was made to estimate the buckling capacity of the 4"x3 ½" x 5/16" angle members between adjacent piles of a bent. Typical pile spacing ranges from 7-9ft with the majority falling between 7 and 8ft. As a result, an effective unbraced length was approximated as l = 100in (the brace length corresponding to a 7'-6" pile spacing).

For the L 4"x3 ½" x 5/16" bracing members:

$A = 2.25in^2$

$r_z = 0.730in$

$I_{min} = Ar_z^2 = 2.25\ (0.730)^2 = 1.20in^4$

$$P_{cr} = \frac{\pi^2 \cdot E \cdot I_{min}}{\lambda^2}$$

$$P_{cr} = \frac{\pi^2 \cdot 29{,}000 \cdot 1.20}{100^2} = 34.3^k$$

$P_y = A\sigma_y$

For A36 steel,

$P_y = 2.25x36 = 81.0^k$

$\therefore P_{cr} < P_y/2$ and buckling of the X-member between piles is elastic

Thus, the maximum compressive axial force that can be applied to the X-brace members without them undergoing elastic buckling or yielding is approximately 34.3 kips. This was the value taken as the upper limit of what a bracing member in compression could support.

8.4 GTSTRUDL Pushover Analysis Results of X-braced Bents

Results of the GTSTRUDL pushover analysis for the 5-pile bents modeled with tension and compression X-bracing as well as tension only X-bracing are plotted in Figure 8.1 for the one story HP10x42 pile bent with H=13ft and Figure 8.2 for the two story pile bent with H=25ft. For the one story X-braced bent shown in Figure 8.1 the maximum pushover load was determined to be approximately 110kips when X-members support tension and compression forces. However,

if X-members are only allowed to resist tensile forces, the pushover load only reaches approximately 81kips. To determine the actual pushover capacity of the bent, the axial forces in the X-members must be examined. Table 8.1 provides a summary of axial forces developed in the compression members of the bent X-bracing for the horizontal load increments used during the pushover analysis procedure. It should be noted for the two story bents, that the axial force developed in the horizontal strut is not significant, since the force in this member is relatively small and the member consists of two 4x3 ½ x 5/16 angle members which are connected to each other via battens to prevent buckling.

Examination of the axial forces within the X-bracing of the one story bents modeling tension and compression X-members (Table 8.1a), shows that the 34.3 kips Euler buckling load for the 4"x3 ½" x 5/16" angle is exceeded when the horizontal force on the bent cap is between 70-80kips for the one story bent with H=13ft. Therefore, the bent should exhibit the load/deflection behavior plotted in Figure 8.1 (for the tension and compression model) until the horizontal force reaches approximately 75kips. From this point on, it is assumed that the X-braced member in compression has buckled and bracing resistance for any additional horizontal force is provided solely from the bracing tension member. The level of additional load which can be resisted via the tension bracing members can then be determined from the model with tension only X-members also plotted in Figure 8.1. Although with this method it is difficult to determine the deflection behavior of the bent beyond the load where the X-member in compression has buckled, the ultimate lateral load capacity is conservatively estimated as the pushover load for the bent modeled with tension only X-bracing (81kips).

This same analysis can be applied to the two story bent pushover analysis of Figure 8.2. When modeled with tension and compression X-members, the pushover load for the two story bent (H=25ft) was found to be approximately 89 kips. Axial forces of the X-members of the two story bent are provided in Table 8.1b and show that the Euler buckling load for the 4"x3 ½" x 5/16" angle is exceeded for both compression members when the horizontal force nears 70kips. Similar to the previous analysis, it is thought that the bent will exhibit the load/deflection behavior of the tension and compression model below 70kips. Beyond this force the strength gain is only

achieved through additional tension via the bracing member in tension to an approximate pushover load of 81kips.

To provide a more accurate modeling of the load-deflection behavior of the pile bents after the X-members in compression have buckled, an alternate model was conceived to force the X-bracing compression members to fail when their buckling load is reached. To do this, axial plastic hinges were placed in the compression members of the X-bracing. Since the area of the angle members is known ($2.25in^2$) as well as the axial force at which they will buckle (34.3 kips from previous calculation), a yield strength for the plastic hinges can be computed ($15.2kip/in^2$). Once this yield stress is reached, the axial force at yielding remains equal to the Euler buckling load for the X-bracing compression members. Therefore, from an analysis stand point, the axial plastic hinges prevent the axial forces in the compression member from going beyond the elastic buckling load, but will allow the angle member to continue to support or resist its buckling load.

Due to the fact that GTSTRUDL only allows specific cross section shapes to have plastic hinges, a slight modification had to be made to the X-braced pile bent models. According to Table 2.5.2-1 of the GTSTRUDL Reference Manual (4), plastic hinges may only be placed in cross sections of the following shapes: wide flange, tees, channels, pipes, structural tube, R-C circular, and R-C rectangles. To account for this, a channel section with a cross sectional area nearly equal to the 4"x3 ½" x 5/16" angle was used in place of the X-members. Although a channel section was used, any shape having a similar cross sectional area could be used. Since the X-members are pin-connected at their respective ends, they only carry an axial force and are prevented from developing bending stresses. This means that the entire cross section will become plastic at precisely the same time and, therefore, as long as the area is nearly equal to a 4"x3 ½" x 5/16" angle, the shape is not significant.

Using the Manual of Steel Construction, the replacement member for the 4"x3 ½" x 5/16" angle is determined to be a C4x7.25 channel having an area of $2.13in^2$, since this is the closest area to that of the actual angle member. In order to keep the bucking load of the X-members at the previously calculated Euler buckling load of 34.3 kips, the slightly smaller area of the channel members was accounted for by setting the yield stress of the plastic hinges in the X-bracing

compression members to 16.1kip/in^2. Although the X-members are modeled as being pinned to the battered piles only, the buckling load assumes that the X-bracing will buckle over an effective length of 100in (the brace length corresponding to a 7'-6" pile spacing). Thus, the actual buckling mode of the X-members is represented by buckling of the X-members between each intermediate pile.

Results of the GTSTRUDL pushover analysis containing the new channel X-members with plastic hinges are plotted in Figures 8.3 and 8.4 along with the p-delta curves for the bents previously modeled with tension and compression members and tension only members for a comparison of behavior. In Figures 8.3 and 8.4 the p-delta curves for the X-bracing with axial plastic hinges further supports what was expected from the previous tension and compression and tension only models of the X-bracing. The load-deflection behavior for the X-bracing with plastic hinges is initially identical to that for the X-bracing modeled with tension and compression members. It was determined in Table 8.1a that the buckling load of the X-members was reached when the horizontal force at the cap was between 70-80 kips. As expected, Figure 8.3 diverts from the tension and compression model when the horizontal force approaches 75kips. For larger values of the horizontal force, the bent stiffness is reduced and the changes in slope for the new curve appear to be identical to that modeled by the tension only X-members. This also was expected since any additional load resistance gained after the X-member has buckled is accomplished via the bracing tension members.

Likewise, in the two story bent the X-members reach their buckling load when the horizontal force at the cap is approximately 70kips (Table 8.1b). Figure 8.4 shows identical elastic load-deflection behavior between the tension and compression X-bracing model and the X-bracing model with plastic hinges until the horizontal force surpasses 70kips. Beyond this load the p-delta curve exhibits changes in slope very similar to the tension only X-braced model.

Previously it had been expected that the ultimate capacities of the pile bents would be equal to the capacity given by the bents with tension only X-members. Figures 8.3 and 8.4, however, reveal that the capacity can be significantly greater than that of the tension only X-bracing models. The single story bent with axial plastic hinges in the compression X-member

gives an ultimate pushover capacity of approximately 105 kips compared to the capacity of 81kips for the tension only model as shown in Figure 8.3. The difference is less significant for the two story bent of Figure 8.4 which shows an ultimate capacity of approximately 85kips in contrast to 81kips for the tension only model.

An additional modification to the pile bent models was evaluated to determine if the previous models with X-bracing pinned to the end piles only was an oversimplification. The pushover analysis for bents modeled with the X-bracing pin-connected to each intermediate pile was performed and the results are presented in Figures 8.5 and 8.6. When compared with the p-delta curves of Figures 8.3 and 8.4, the p-delta curves for bents modeled with X-members pinned to each intermediate pile reveal a considerable increase in stiffness and pushover capacity. By pinning the X-members to each pile the pushover capacity for the single story bents having X-members with plastic hinges increases from 105 kips to 118 kips. Similarly, the lateral load capacity for the two story pile bent is increased from 85 kips to 115 kips. Aside from the general increases in stiffness of the pile bents, all other aspects of the p-delta curves remain unchanged. For instance, the p-delta curve for the bent with plastic hinges in the compression X-members is initially identical to that for the bent modeling X-bracing with tension and compression members. Beyond the horizontal force at which the compression X-members reach their buckling load the curves exhibit similar changes in slope as the bent modeled with tension only X-bracing. Since the X-bracing is typically welded to each pile during construction of the bent, all future pushover analysis models of X-bracing will be pinned to each intermediate pile as this seems more realistic.

8.5 GTSTRUDL Pushover Analysis for X-braced Bents with Fixed Bases

As with the non X-braced bents in Chapter 7, pushover analyses were performed on the X-braced pile bents for different base condition fixities and scour levels 0-20ft. The p-delta curves for a one story HP10x42 5-pile bent with original H=13ft are plotted in Figure 8.7. Previous research has suggested that the addition of a horizontal strut near the base of the X-bracing may provide significant increases in stiffness and lateral load capacity in the event of scour due to improved truss action of X-bracing, thus, Figure 8.8 shows the pushover analysis for the single

story bent with the new strut included. This strut is treated similar to the horizontal strut which divides the upper and lower stories of the two story bents. In other words, it is composed of two 4x3 ½ x 5/16 angle members that are welded to one another by battens to prevent buckling of the angles. The load-deflection behavior will be compared for both models (with and without the strut) to determine the impact of the proposed addition to the X-bracing.

For the single story bent without the proposed strut (Figure 8.7) the lateral load capacity, F, is 117.4 kips when no scour is present. Significant reduction in lateral load capacity and stiffness occurs as scour is introduced. For S=5ft, 10ft, 15ft and 20ft the capacities, F, are 68.8kips, 50.4kips, 42.4kips, and 26.1kips respectively. Each of the p-delta curves lay over clearly with the exception of the curve for S=20ft. When scour becomes this severe, the bent deflects linearly until capacity is achieved. This behavior may be explained by a quick loss of capacity due to instability of such a tall structure with large unbraced pile lengths below the X-bracing. For p-delta curves of bents with the proposed strut (Figure 8.8) the horizontal load capacities for S=0ft, 5ft, 10ft, 15ft, and 20ft are F=170.9kips, 78.7kips, 52.7kips, 42.7kips, and 30.9kips respectively. The additional stiffness of the bent provided by the proposed horizontal strut is relatively small, and the increase in horizontal load capacity is only significant when $S \leq 5ft$.

P-delta curves for the two story HP 10x42 pile bent with H=25ft are plotted in Figures 8.9 and 8.10 where the latter includes the new horizontal strut. From Figure 8.9 the ultimate horizontal load capacities for S=0ft, 5ft, 10ft, 15ft, and 20ft are F=115.0kips, 64.4kips, 45.8kips, 37.4kips, and 33.2kips respectively. Pushover analysis results for the two story bent with the extra horizontal strut placed just below the lower X-bracing (Figure 8.10) give capacities F=190.0kips, 128.2kips, 81.8kips, 61.0kips, and 49.3kips for the same range of scour. In contrast to the single story bent, inclusion of the horizontal strut in the two story bent increases the horizontal loading capacity significantly for each value of S. Additionally, because the two story X-bracing serves to more evenly distribute the lateral and vertical loads, this bent is slightly more stable at S=20ft than the single story bent. This is evident by observing the corresponding p-delta curves in Figure 8.7 - 8.10. Unlike the curves for S=20ft in Figures 8.7 and 8.8 which

deflect linearly to failure, the curves for S=20ft in Figures 8.9 and 8.10 for the two story bent are clearly laying over when capacity is reached. The results of this analysis show that for each level of scour the addition of the proposed lower strut only has a significant impact on the one story bent when $S \leq 5$ft, but greatly improves the load capacity of the two story bents for each level of scour.

8.6 GTSTRUDL Pushover Analysis for X-braced Bents with Pinned Bases

In the previous bent models of Section 8.3, fixed connections to the ground were assumed; however, this is an exaggeration of the actual level of fixity as mentioned in previous chapters. Therefore, as was considered for the non X-braced bents, the case with pinned connections at the base should also be evaluated. The behavior of these bents can then be compared to those with fixed bases as well as those with an additional length to fixity to gain a better understanding of how the bent would behave with partial fixities at the pile ends.

The pushover analysis results for the single story X-braced bents with pinned connections at the ground are shown in Figures 8.11 and 8.12 for bents with and without the proposed lower strut. As seen in Figure 8.11 the lateral load capacities of the typical single story bent for S=0ft, 5ft, 10ft, 15ft, and 20ft are F=64.4kips, 35.1kips, 28.9kips, 28.2kips, and 20.6kips. In general, the values for horizontal load capacity for these bents are nearly half of the capacities observed if the base is fixed (except for $S \geq 15$ft). Similar to the fixed base models, when S=20ft the load-deflection behavior of the bent appears to be linear until failure occurs. This is explained as the consequence of a rapid loss in capacity due to instability associated with the bent's height. Figure 8.12 shows the p-delta curves for the single story X-braced bent with the proposed horizontal strut. For S=0ft, 5ft, 10ft, 15ft, and 20ft the lateral load capacities are F=88.1kips, 37.2kips, 27.6kips, 26.3kips, and 22.5kips respectively. The horizontal strut has similar effect whether the base of the bent is pinned or fixed. It only provides a considerable increase in capacity when S<5ft. Additionally, when the strut is included, the unbraced length of the piles is decreased and the p-delta curve for S=20ft appears to lay over slightly. This shows that the

unbraced length of the piles below the X-bracing is responsible to some extent for the tendency of the curve to lay over.

P-delta curves for the two story X-braced bents are shown in Figures 8.13 and 8.14. The two story bent without the lower horizontal strut (Figure 8.13) gives horizontal load capacities of F=56.2kips, 27.8kips, 21.0kips, 18.3kips, and 12.8kips when S=0ft, 5ft, 10ft, 15ft, and 20ft. These lateral capacity values are also roughly half the capacity values of the fixed base bents. For the two story bent modeled with the proposed lower horizontal strut (Figure 8.14) the capacities are F=148.6kips, 59.9kips, 37.8kips, 28.7kips, and 16.3kips when S=0ft, 5ft, 10ft, 15ft, and 20ft. These capacities are significantly larger compared to the capacities without the strut. When no scour is present, the increase in capacity due to the strut is nearly threefold. For ease of comparison, the horizontal load capacities for bents with fixed and pinned bases are given in Table 8.2 for single story X-braced bents and Table 8.3 for two story X-braced bents. It appears from this analysis of bents with pinned bases that the proposed lower strut has a considerable impact on one story bents when S<5ft and two story bents for all levels of scour.

8.7 GTSTRUDL Pushover Analysis for X-braced Bents with Additional Length to Fixity

Pushover analysis was also performed for X-braced bents with an additional length to fixity of 5ft to allow for a comparison of relative fixities similar to that considered for the non X-braced bents in Chapter 7. The results of this analysis for the single story X-braced bents are plotted in Figure 8.15 for typical bent construction and Figure 8.16 for bents with the proposed horizontal strut. Results of the two story X-braced bents with additional 5ft to fixity are shown in Figure 8.17 for typical bents and Figure 8.18 for bents with the proposed strut. The addition of 5ft to the bent height has the same effect of adding 5ft of scour. Therefore, the p-delta curves for bents with the additional 5ft length to fixity as shown in Figures 8.15-8.18 are identical to curves corresponding to S+5ft in Figures 8.7-8.10. Scour was incremented by intervals of 5ft until the pushover analysis could no longer be performed due to structural instability of the bents. This occurred as scour levels approached S=20ft for the X-braced bents with additional 5ft to fixity.

For ease of comparison, the horizontal load capacities at the bent cap for pile bents modeled with fixed bases, pinned bases, and an additional length to fixity are given in Table 8.2 for single story X-braced bents and Table 8.3 for two story X-braced bents. It can be seen in both of these tables that the bents modeled with pinned bases and bents modeled with an additional length to fixity 5ft below the ground line give fairly comparable results. Also, the pinned base modeling gives lower and thus more conservative failure results. Based on these comparisons, the unencased bent piles should be modeled as pinned at the ground line in future analyses.

8.8 GTSTRUDL Pushover Analysis for Bents with Various Pile Numbers

In Chapter 4 it was noted that the number of piles in typical ALDOT bridge pile bents varies from 3-7 piles (see Section 4.1). Of the 31 standard bent drawings examined 2 have 3 piles, 10 have 4 piles, 8 have 5 piles, 10 have 6 piles, and only 1 has 7 piles. Since the majority of bents have between 3-6 piles, these bents will be studied in this section to compare the effects of adding X-bracing to non X-braced bents (Figures 8.19a-8.22e), determine whether X-braced bents with more piles are less susceptible to scour failure (Figures 8.23a-8.24e), and directly determine the impact of scour on the pushover load for standard ALDOT X-braced bents (Figures 8.25-8.34). Further examination of the standard bent drawings revealed that X-braced bents with 3-5 piles are always constructed with a single X-bracing layout as shown previously in this chapter. X-braced bents having 6 or more piles on the other hand, may be configured so that they contain a single X-braced or double X-braced layout per story.

Figures 8.19a-8.22e compare pushover data for X-braced and non X-braced bents in order to directly asses strength gains as a result of adding X-bracing. This comparison is made for 3, 4, 5, and 6-pile bents with scour levels of 0ft, 5ft, 10ft, 15ft, and 20ft. Reviewing these figures, the addition of X-bracing to pile bents is shown to significantly increase bent pushover capacity only when S<5ft. Bent stiffness, on the other hand, remains considerably greater for the X-braced bents when $S \leq 10$ft. P-delta curves for the 3-pile bents are shown in Figures 8.19a, b, and c for S=0ft, 5ft, and 10ft (the 3-pile non X-braced bent becomes unstable when $S \geq 15$ft). When no scour is present Figure 8.19a shows pushover loads of 13.2 kips for the non X-braced

bent and 43.7 kips for the X-braced bent. For S=5ft Figure 8.19b gives a pushover capacity of 6.4 kips for the non X-braced bent and 16.2 for the X-braced bent. Finally, for S=10ft Figure 8.19c shows pushover capacities of 1.5 kips for the non X-braced bent and 7.0 kips when X-braced. For better comparison a summary of these pushover capacities is shown in the second column of Tables 8.4a and 8.4b, where the data in Table 8.4a has been repeated from Section 7.9.

As shown in Tables 8.4a and 8.4b, the strength gain which results from adding X-bracing is almost entirely lost after the first 5ft of scour with exception of the 3-pile bent. (For the 3-pile bent at S=5ft, the strength of the X-braced bent remains 2.5 times larger than the strength of the non X-braced bent.) Despite this rapid loss of strength with scour, the stiffness gained from adding X-bracing does not fully diminish with the first 5ft of scour. As shown in Figures 8.20d, 8.21d, and 8.22d for the 4, 5, and 6-pile bents, the stiffness of the X-braced bent becomes very similar to that of the non X-braced as S approaches 15ft. For bents with various pile numbers the corresponding columns of Tables 8.4a and 8.4b reveal that X-bracing increases the strength of each bent by approximately 30 kips when S=0ft, but only slight increases in strength are seen for $S \geq 5$ft. When double X-bracing is used in the 6-pile bent, stiffness is increased and strength improves by 15 kips beyond the strength of the single X-braced bent for S=0ft (see Figure 8.22a). However, the strength gain created by the double X-bracing is also significantly diminished after the first 5ft of scour. This is evident in that the 6-pile non X-braced, single X-braced, and double X-braced bents provide similar pushover capacities for $S \geq 5$ft.

In a few instances, the capacity of the non X-braced bent actually exceeded the capacity of the X-braced bent (namely the 5 and 6-pile bents at S=10ft). This is thought to be a result of beam action on the battered piles caused by the X-bracing. When H=13ft and S=10ft, the X-bracing frames into the battered piles very near mid height. With a transverse force applied in this critical section, or mid height, the battered pile buckles with slightly less effort, i.e. when the force in the compression X-member is smaller. Thus, for H=13ft and S=10ft a one story X-braced bent will fail at slightly smaller transverse cap loads than a non X-braced bent.

In order to determine if bents with more piles are less susceptible to scour failure a pushover analysis was performed for scour levels of S=0ft, 5ft, 10ft, 15ft, and 20ft on one story and two story X-braced bents having 3-6 piles (see Figures 8.23a-8.24e). The pushover results for the one story X-braced bents (H=13ft) are provided in Figures 8.23a-8.23e for S=0ft, 5ft, 10ft, 15ft, and 20ft. When S=0ft, pushover loads for the one story bents with 3, 4, 5, and 6 piles are 43.7 kips, 55.1 kips, 64.4 kips, 70.0 kips (single X-braced), and 85.7 kips (double X-braced). Although lateral strength increased with the addition of each pile, stiffness does not show the same direct proportionality. As shown in Figure 8.23a the stiffness actually decreases slightly as more piles are added to the bent when S=0ft, an exception being the 6-pile bent with double X-bracing. The double X-bracing layout commonly seen in bents with 6 or more piles significantly increases stiffness and pushover load if no scour is present. At the onset of scour (Figures 8.23b-e), bents having more piles show greater stiffness than those with fewer piles. However, as scour increases to 20ft the stiffness of the single X-braced 6-pile bent becomes identical to that of the 5-pile bent, although it maintains a slightly larger pushover capacity. Additionally, the double X-bracing in the 6-pile bent does not have nearly as great an effect on stiffness or capacity when S=20ft.

The two story bent pushover analysis results are shown in Figures 8.24a-8.24e as well as Table 8.4c for S=0ft, 5ft, 10ft, 15ft, and 20ft. The pushover forces applied to the 3, 4, 5, and 6-pile bents (H=25ft) are 45.9 kips, 49.7 kips, 57.1 kips, 61.7 kips (single X-braced), and 79.9 kips (double X-braced) respectively when S=0ft. P-delta curves for the two story bents reveal similar stiffness behavior as the one story bents. While stiffness decreases for bents with more piles when S=0ft, lateral strength continues to increase with the addition of piles. As observed for the one story bents, the stiffness of the double X-braced 6-pile two story bent remains substantially larger than the single X-braced bent when S=0ft. Also, the pushover capacity of each bent is reduced by approximately half with the first 5ft of scour, an exception being the 3-pile bent. When S=5ft, the capacity of the two story 3-pile X-braced bent is reduced by only 1/3 of the capacity at S=0ft. As scour is incremented (Figures 8.24b-e), the two story bents having more piles show greater stiffness than those with fewer numbers of piles, and the double X-bracing in the 6-pile

two story bent has a somewhat greater impact on stiffness and lateral strength than seen in the double X-braced one story bent.

To obtain a more direct assessment of the impact that scour has on the pushover load for each ALDOT standard X-braced bent studied in this section, Figures 8.25-8.34 show the p-delta curves for each bent with scours of S=0ft, 5ft, 10ft, 15ft, and 20ft. These figures may be used to determine the level of scour at which the bents become unstable, which is characterized by a rapid increase in deflection for small increases in loading. For simplicity this study only considers the placement of the horizontal force at the center of the cap and all bents were conservatively modeled with pinned connections to the ground.

Figures 8.25-8.29 show the pushover results for one story X-braced bents with 3-6 piles and H=13ft. The respective lateral load capacities have been summarized in Table 8.4b. As stated previously, this table reveals for each bent that the largest decrease in capacity occurs within the first 5ft of scour. Scour of 5ft reduces the pushover capacity of the 4, 5, and 6-pile bents by at least half and nearly 2/3 for the 3-pile bent. Similar to the non X-braced bents, the 3-pile one story X-braced bent is greatly affected by scour and nearly becomes unstable for S=15ft. Furthermore, at each scour level greater than 5ft, the one story 6-pile bents provide nearly the same capacity regardless of whether single X-bracing or double X-bracing is used (see columns 5 and 6 of Table 8.4b).

The pushover analysis results of the two story X-braced bents with 3-6 piles and H=25ft are given in Figures 8.30-8.34 as well as Table 8.4c. With the exception of the 3-pile bent each of the two story bents were stable at scour levels of 20ft. Additionally, at least half the lateral load capacity is lost with the first 5ft of scour. The 6-pile bents show only small strength gains due to the double X-bracing when $S \geq 5ft$.

Table 8.1. Horizontal Force at Bent Cap and Resulting Axial Forces In Compression Member of X-bracing for HP10x42 Pile Bents, X-bracing Modeled with Tension and Compression Members

Horizontal Force (kips) At Bent Cap	Axial Force (kips) In Compression Member
40	-19.3
50	-23.9
60	-28.5
70	-33.2
80	-37.8

a) Single Story (H=13ft)

Horizontal Force (kips) At Bent Cap	Axial Force (kips)	
	Compression Member in Top Story	Compression Member In Lower Story
40	-20.5	-20.5
50	-25.5	-25.4
60	-30.4	-30.2
70	-34.8	-35.3
80	-39.0	-40.4

b) Two Story (H=25ft)

Table 8.2 Horizontal Failure Loads at Bent Cap in the Transverse Direction for GTSTRUDL Pushover Analysis Modelings of HP10x42 Single Story X-braced 5-Pile Bent

Scour, S (ft) H=13ft	Horizontal Failure Load, F (kips)					
	Bents w/ Fixed Base (See Fig. 8.7-8.8)		Bents w/ Pinned Base (See Fig. 8.11-8.12)		Bents w/ Fixed Base (Plus 5ft to fixity) (See Fig. 8.15-8.16)	
		w/ strut		w/ strut		w/ strut
0	117.4	170.9	64.4	88.1	68.8	78.7
5	68.8	78.7	35.1	37.2	50.4	52.7
10	50.4	52.7	28.9	27.6	42.4	42.7
15	42.4	42.7	28.2	26.3	26.1	30.9
20	26.1	30.9	20.6	22.5	unstable	unstable

Table 8.3 Horizontal Failure Loads at Bent Cap in the Transverse Direction for GTSTRUDL Pushover Analysis Modelings of HP10x42 Two Story X-braced 5-Pile Bent

Scour, S (ft) H=25ft	Horizontal Failure Load, F (kips)					
	Bents w/ Fixed Base (See Fig. 8.9-8.10)		Bents w/ Pinned Base (See Fig. 8.13-8.14)		Bents w/ Fixed Base (plus 5ft to fixity) (See Fig. 8.17-8.18)	
		w/ strut		w/ strut		w/ strut
0	115.0	190.0	56.2	148.6	64.4	128.2
5	64.4	128.2	27.8	59.9	45.8	81.8
10	45.8	81.8	21.0	37.8	37.4	61.0
15	37.4	61.0	18.3	28.7	33.2	49.3
20	33.2	49.3	12.8	16.3	unstable	unstable

Table 8.4a. Pushover Capacity of Non X-braced Bents with Scour (See Figures 7.53-7.56)

Scour, S (ft) H=13ft	3-Pile Bent (kips)	4-Pile Bent (kips)	5-Pile Bent (kips)	6-Pile Bent (kips)
0	13.2	27.8	34.9	37.1
5	6.4	24.6	32.9	33.7
10	1.5	20.8	30.9	32.4
15	unstable	14.5	22.5	23.6
20	unstable	9.3	15.5	16.3

Table 8.4b. Pushover Capacity of One Story X-braced Bents with Scour (See Figures 8.25-8.29)

Scour, S (ft) H=13ft	3-Pile Bent (kips)	4-Pile Bent (kips)	5-Pile Bent (kips)	6-Pile Bents (kips)	
				Single X-braced	Double X-braced
0	43.7	55.1	64.4	70.0	85.7
5	16.2	28.1	35.1	37.7	39.8
10	7.0	21.0	28.9	30.2	31.4
15	1.2	17.4	28.2	30.2	30.4
20	unstable	11.3	20.6	23.0	23.4

Table 8.4c. Pushover Capacity of Two Story X-braced Bents with Scour (See Figures 8.30-8.34)

Scour, S (ft) H=25ft	3-Pile Bent (kips)	4-Pile Bent (kips)	5-Pile Bent (kips)	6-Pile Bents (kips)	
				Single X-braced	Double X-braced
0	45.9	49.7	57.1	61.7	79.9
5	15.3	22.3	28.2	31.0	34.8
10	4.8	13.9	21.1	23.3	26.7
15	unstable	9.3	18.4	20.7	24.8
20	unstable	5.0	13.2	15.7	18.6

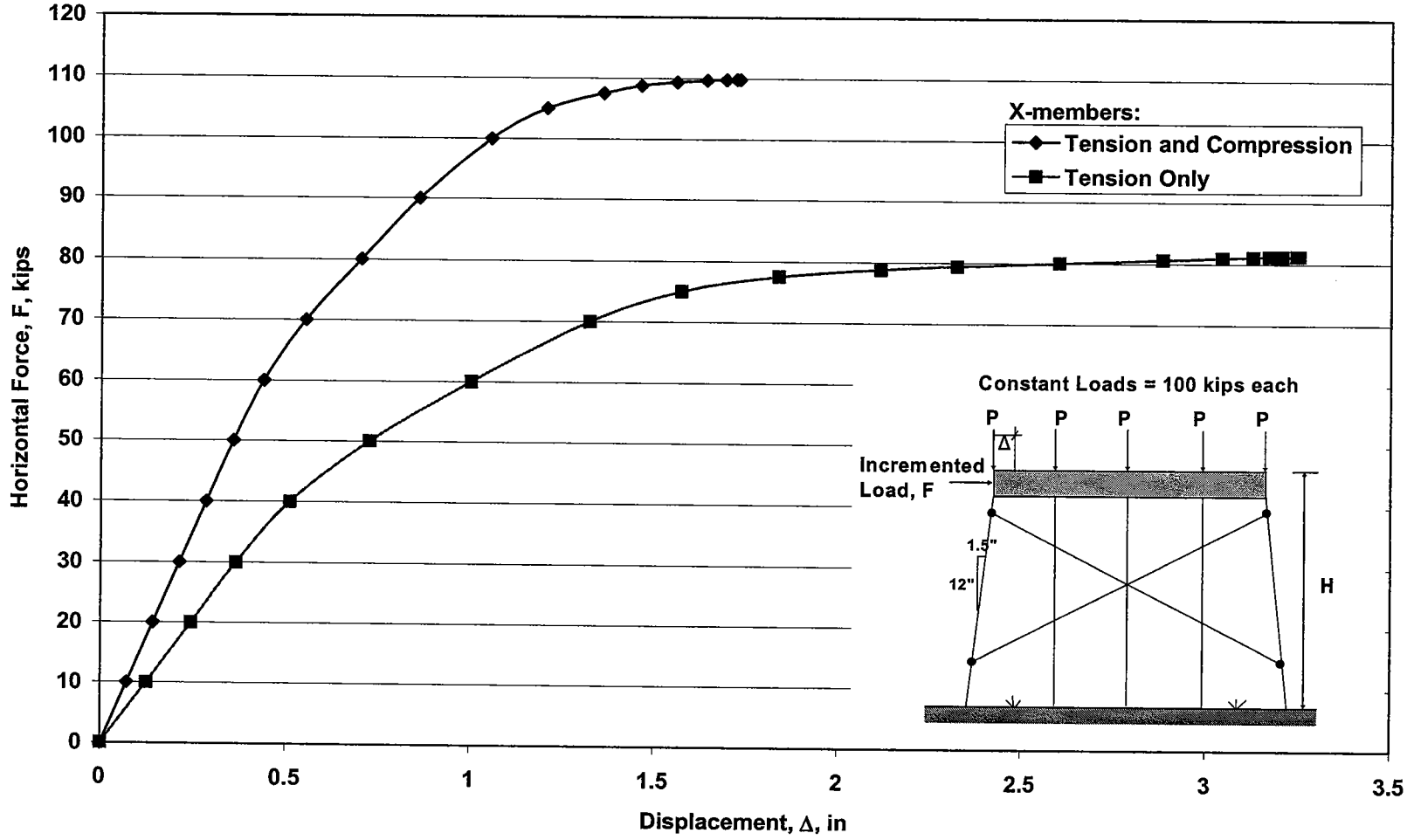

Figure 8.1. GTSTRUDL Pushover Analysis for Single Story X-braced HP10x42 5-Pile Bent with Alternate Models of X-bracing, X-bracing Pinned to End Piles Only, Piles Fixed at Ground, H=13 ft

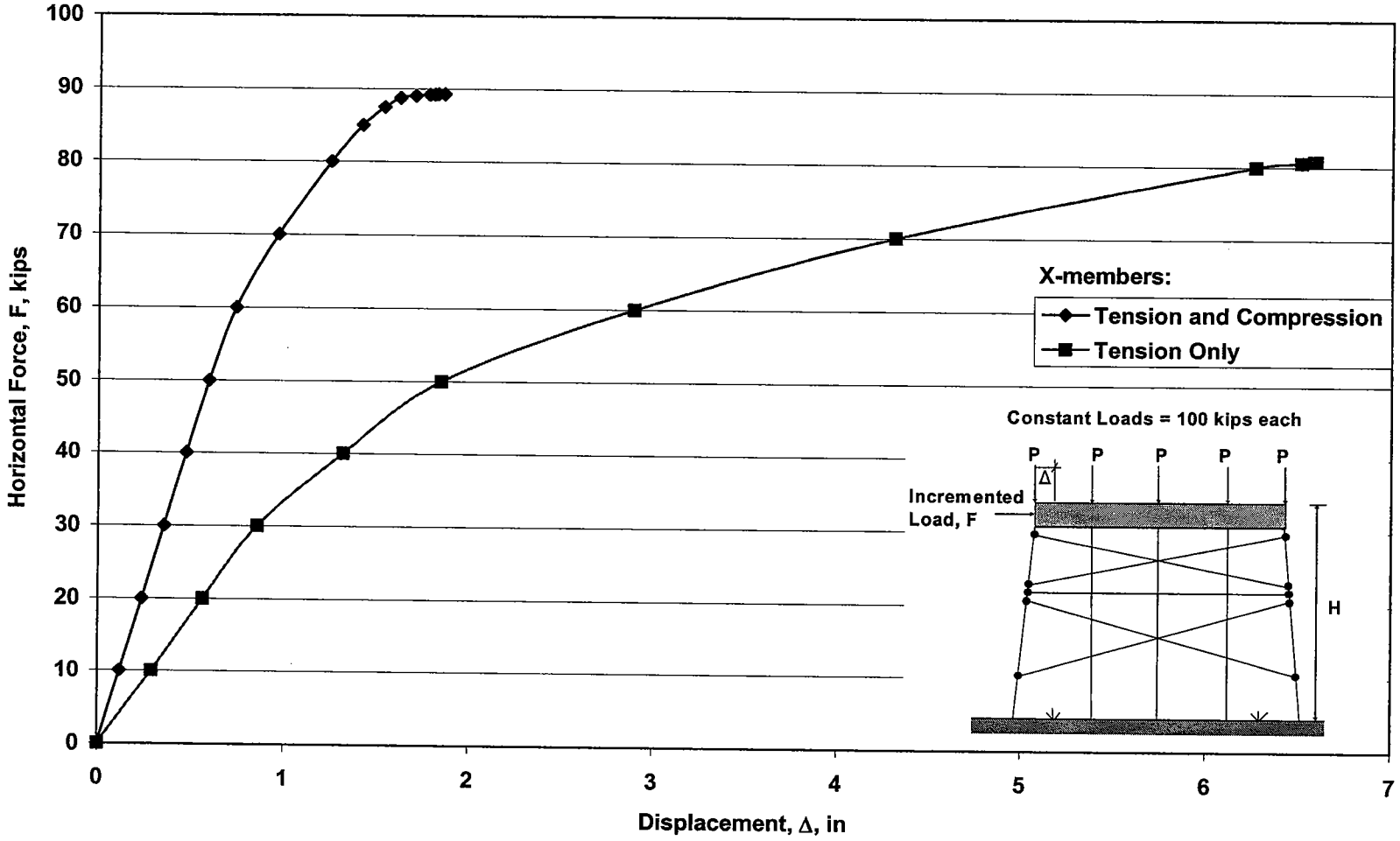

Figure 8.2. GTSTRUDL Pushover Analysis for Two Story X-braced HP10x42 5-Pile Bent with Alternate Models of X-bracing, X-bracing Pinned to End Piles Only, Piles Fixed at Ground, H=25 ft

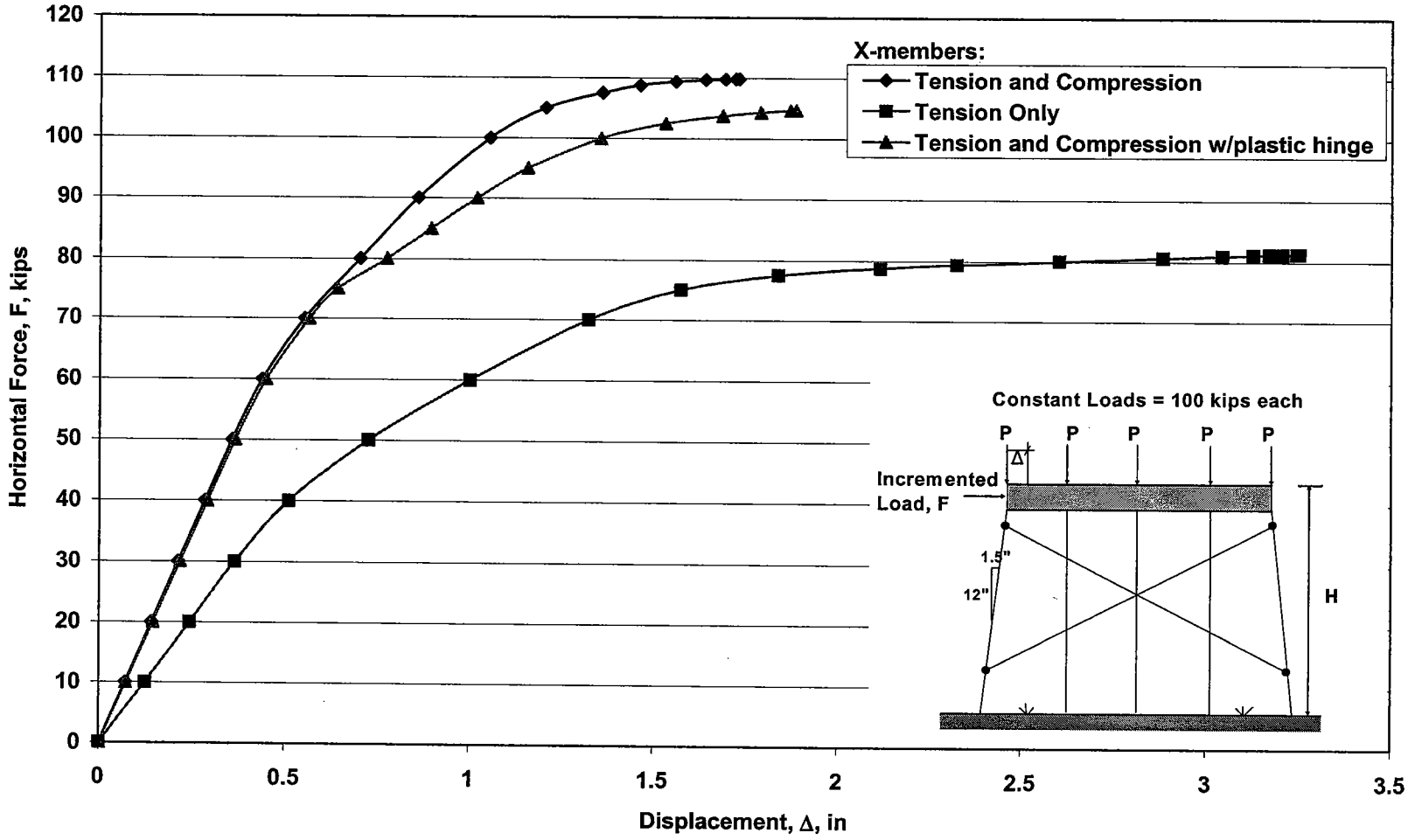

Figure 8.3. GTSTRUDL Pushover Analysis for Single Story X-braced HP10x42 5-Pile Bent with Alternate Models of X-bracing, X-bracing Pinned to End Piles Only, Piles Fixed to Ground, H=13 ft

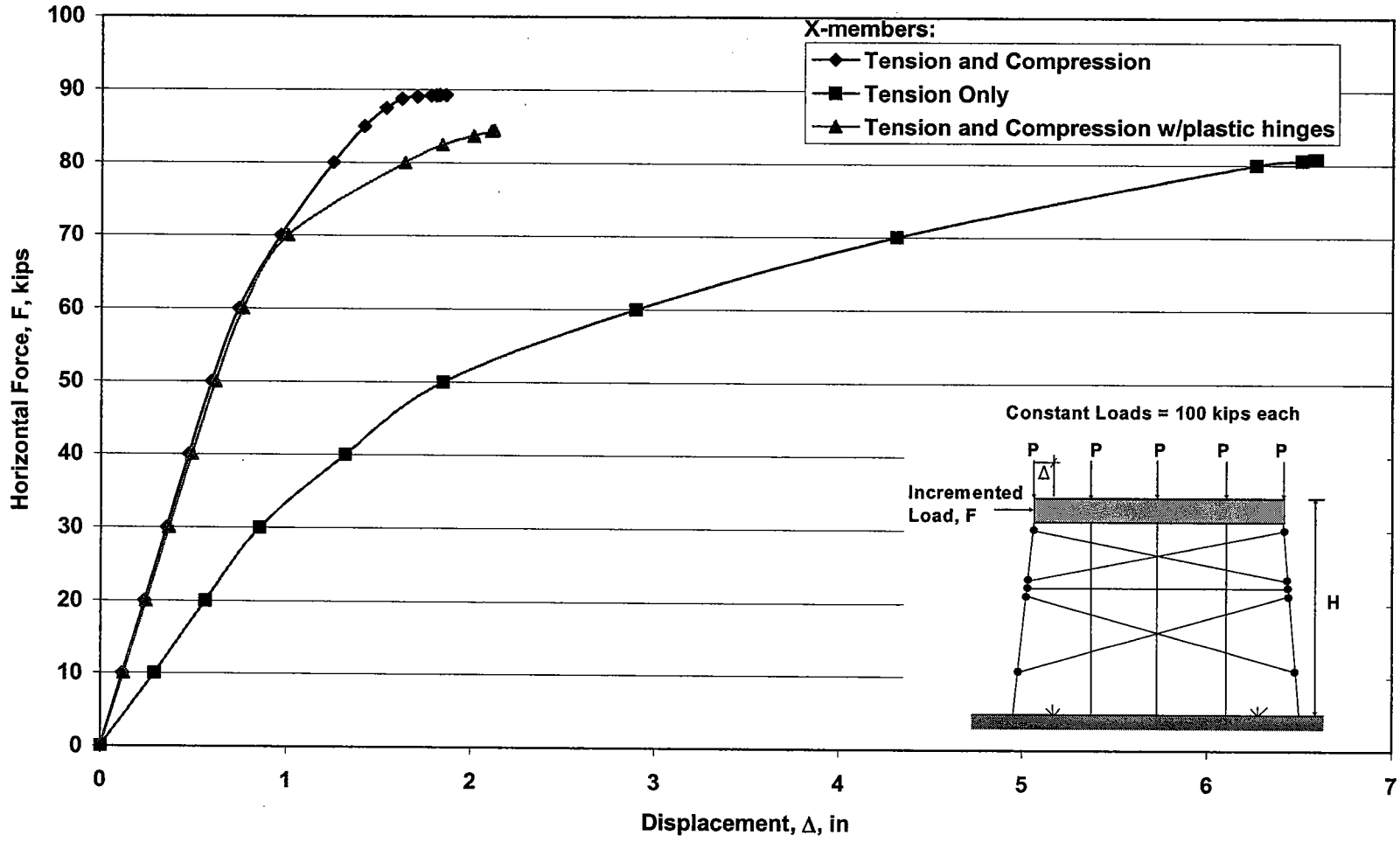

Figure 8.4. GTSTRUDL Pushover Analysis for Two Story X-braced HP10x42 5-Pile Bent with Alternate Models of X-bracing, X-bracing Pinned to End Piles Only, Piles Fixed to Ground, H=25 ft

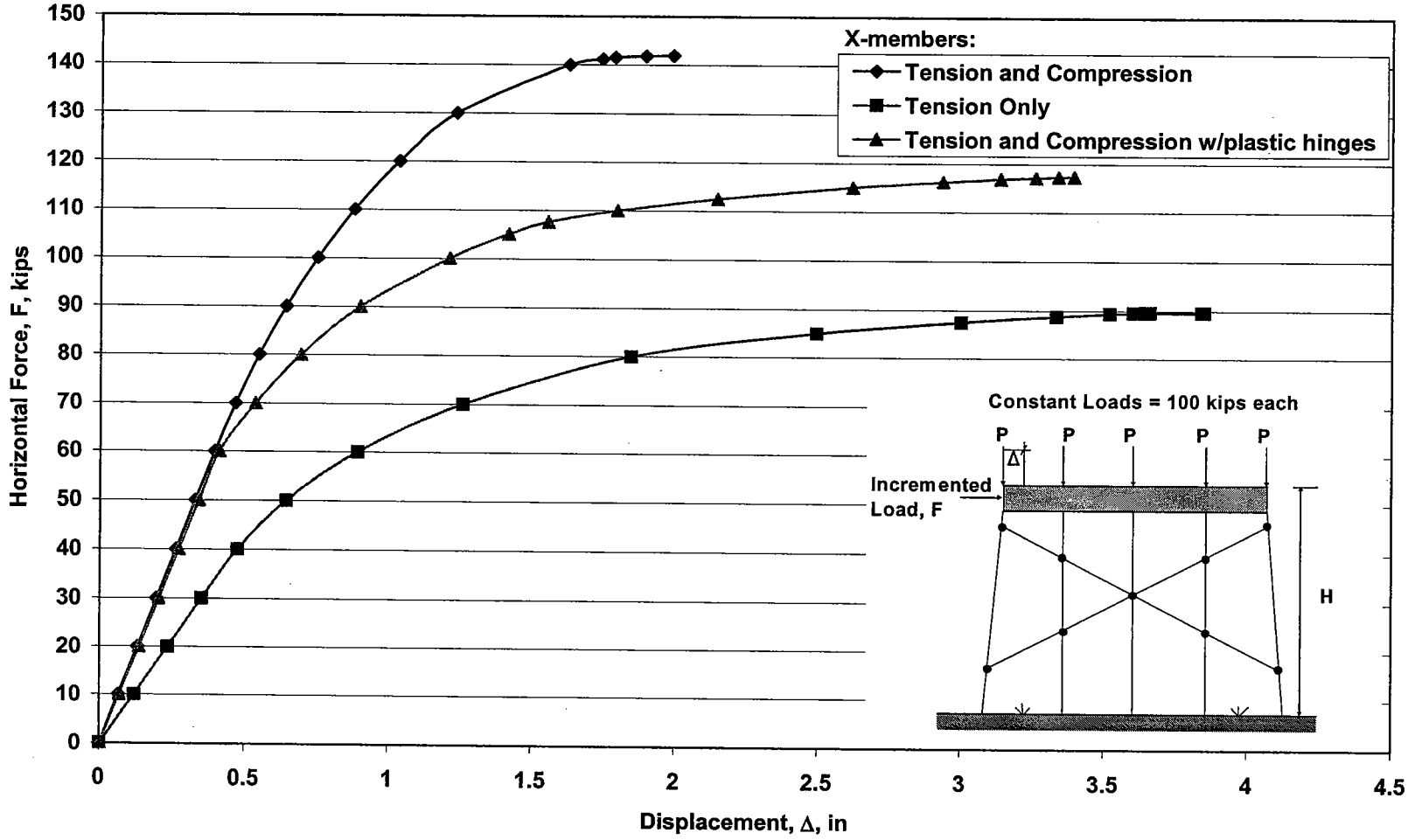

Figure 8.5. GTSTRUDL Pushover Analysis for Single Story X-braced HP10x42 5-Pile Bent with Alternate Models of X-bracing, X-bracing Pinned to All Intermediate Piles, Piles Fixed to Ground, H=13 ft

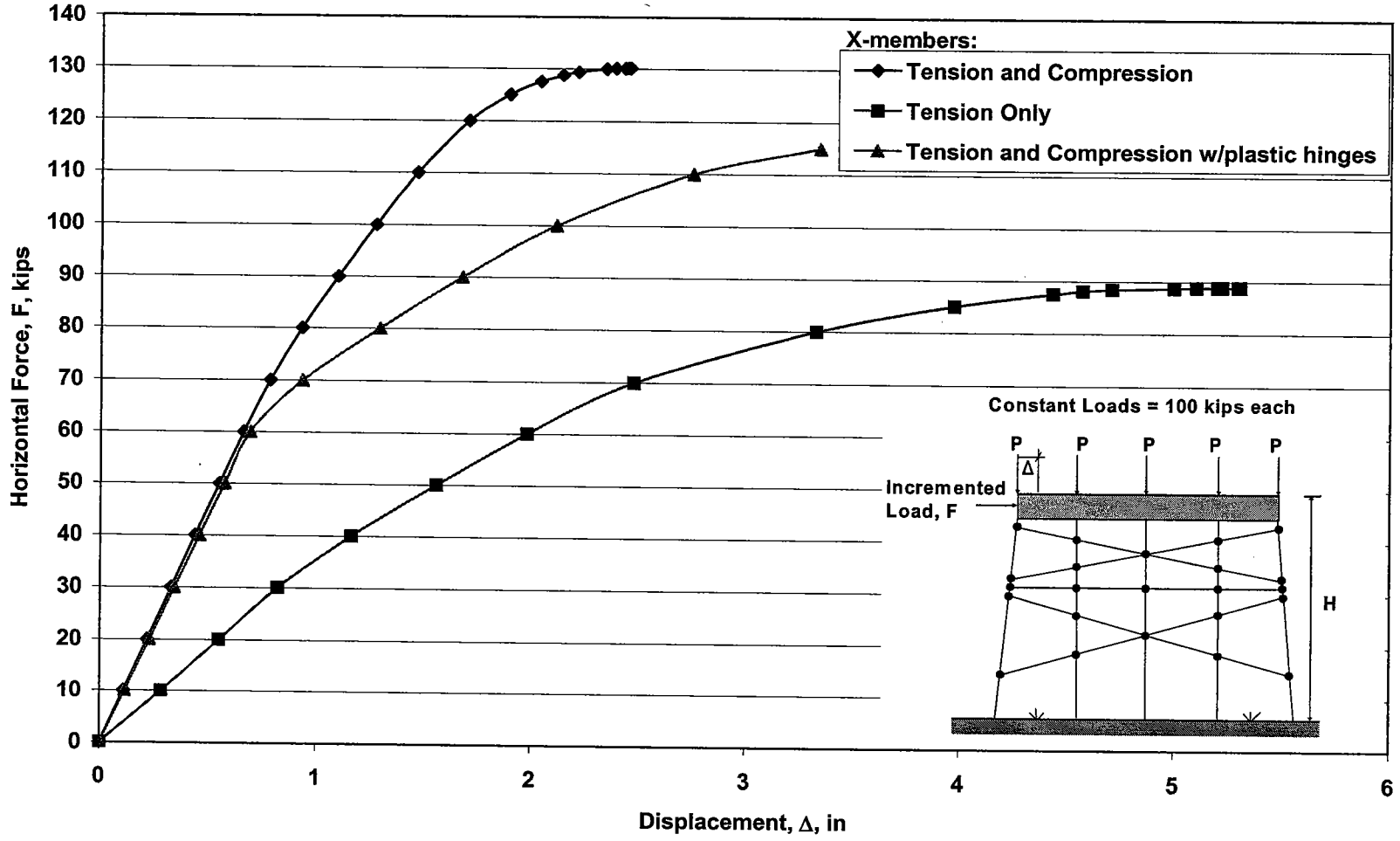

Figure 8.6. GTSTRUDL Pushover Analysis for Two Story X-braced HP10x42 5-Pile Bent with Alternate Models of X-bracing, X-bracing Pinned to All Intermediate Piles, Piles Fixed to Ground, H=25 ft

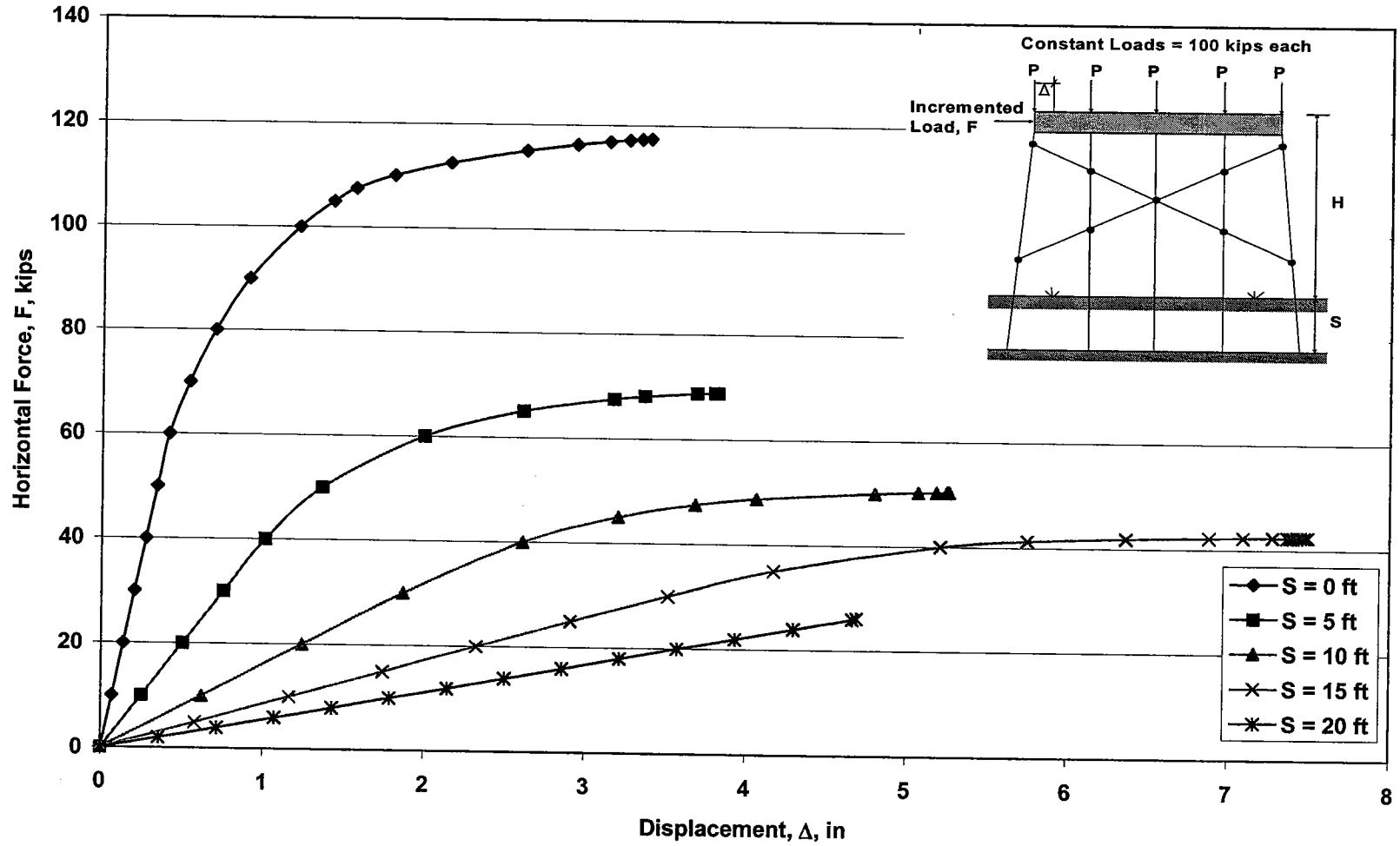

Figure 8.7. GTSTRUDL Pushover Analysis for One Story X-braced HP10x42 5-Pile Bent Subjected to Scour, Piles Fixed at Ground, H = 13ft

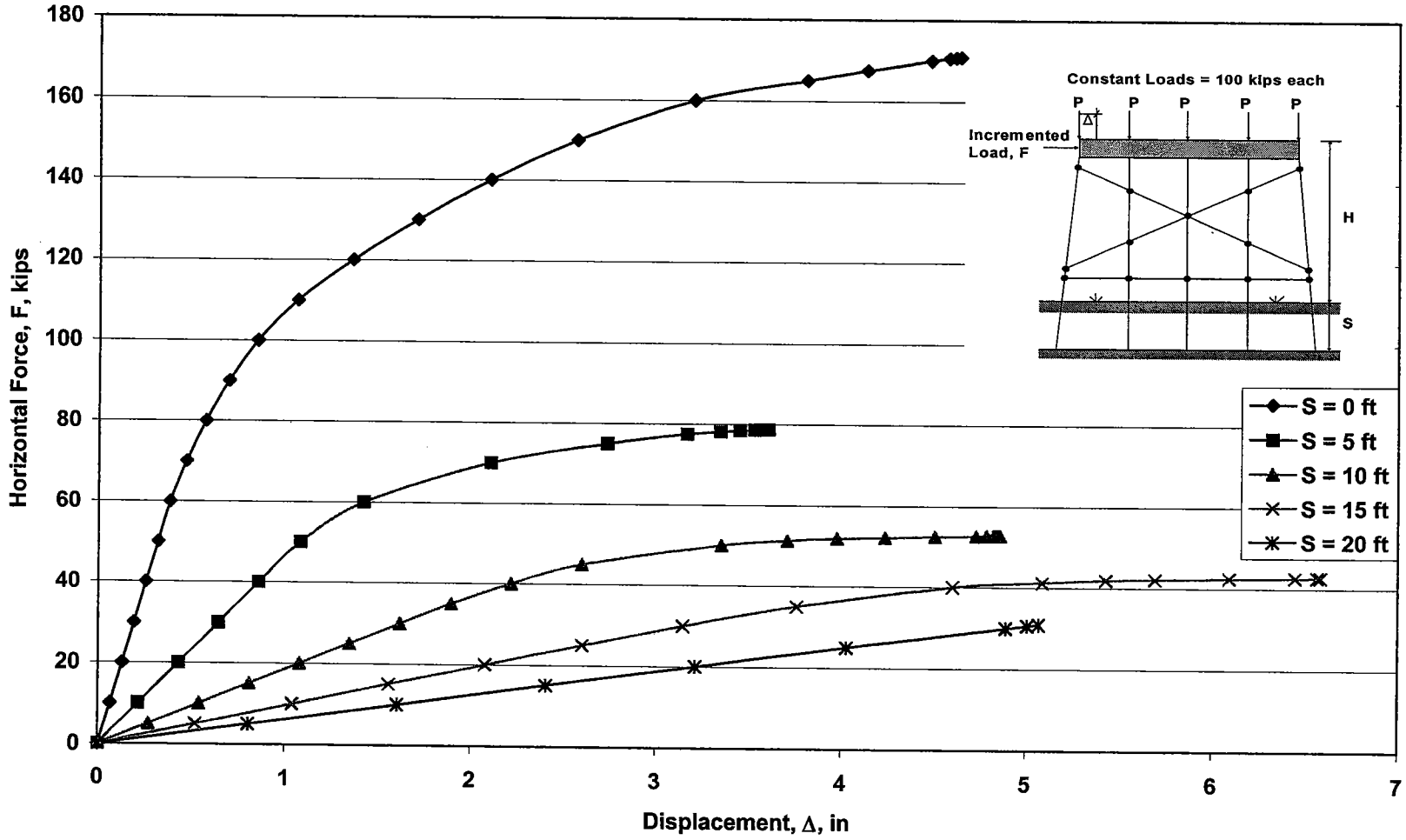

Figure 8.8. GTSTRUDL Pushover Analysis for One Story X-braced HP10x42 5-Pile Bent (with Proposed Lower Horizontal Member in X-Bracing) Subjected to Scour, Piles Fixed at Ground, H = 13 ft

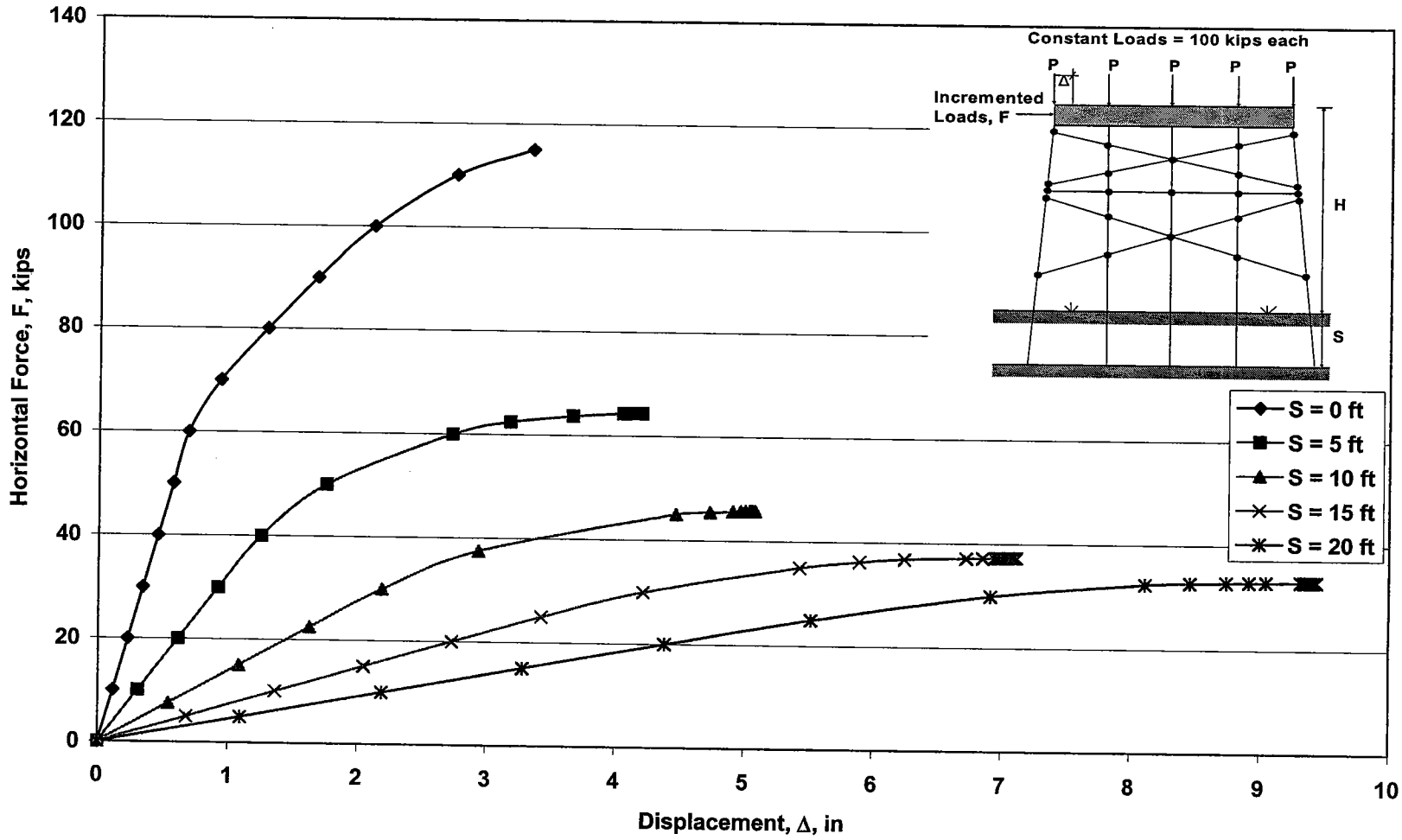

Figure 8.9. GTSTRUDL Pushover Analysis for Two Story X-braced HP10x42 5-Pile Bent Subjected to Scour, Piles Fixed at Ground, H = 25ft

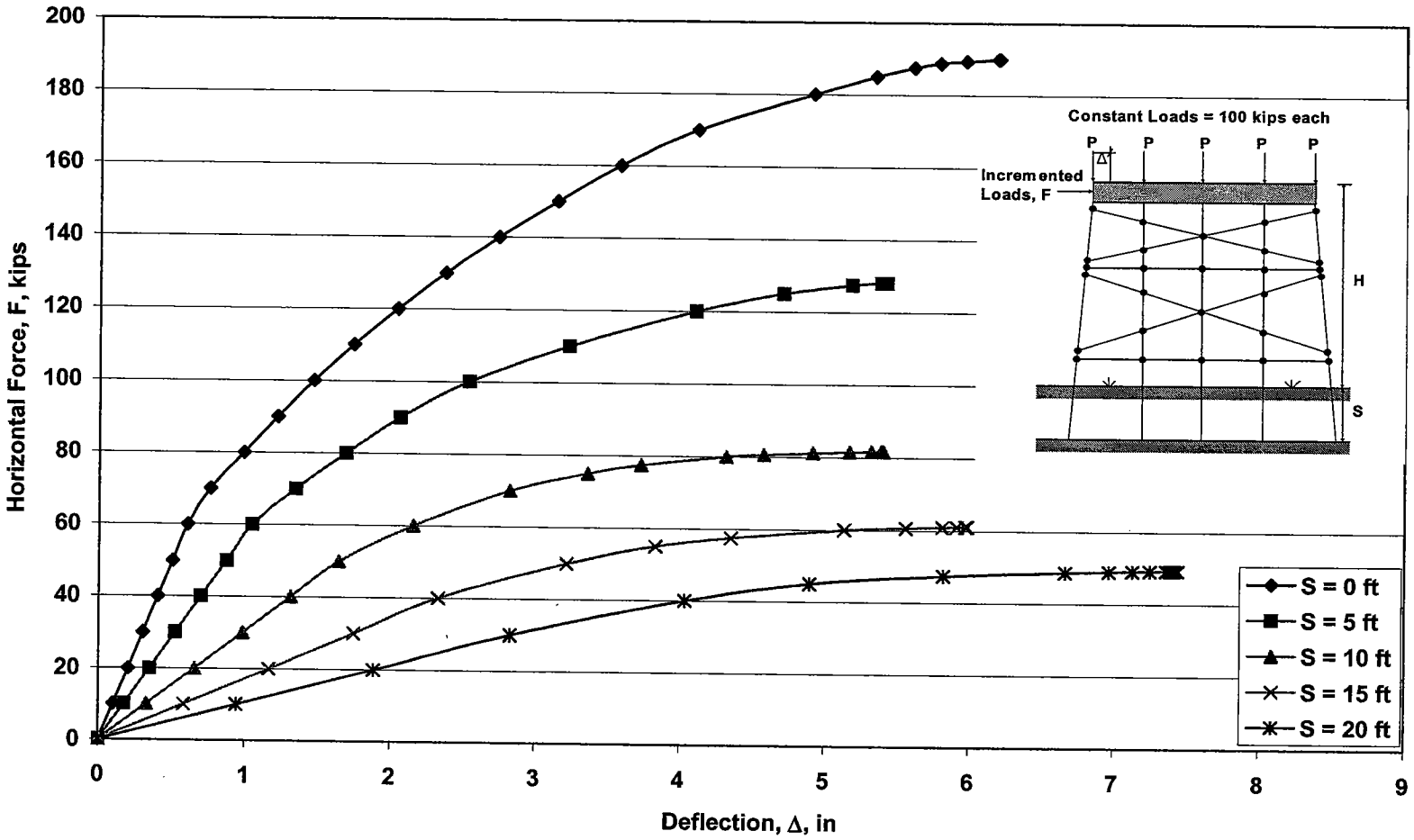

Figure 8.10. GTSTRUDL Pushover Analysis for Two Story HP10x42 5-Pile Bent, (with Proposed Lower Horizontal Member in X-Bracing) Subjected to Scour, Piles Fixed at Ground, H = 25 ft

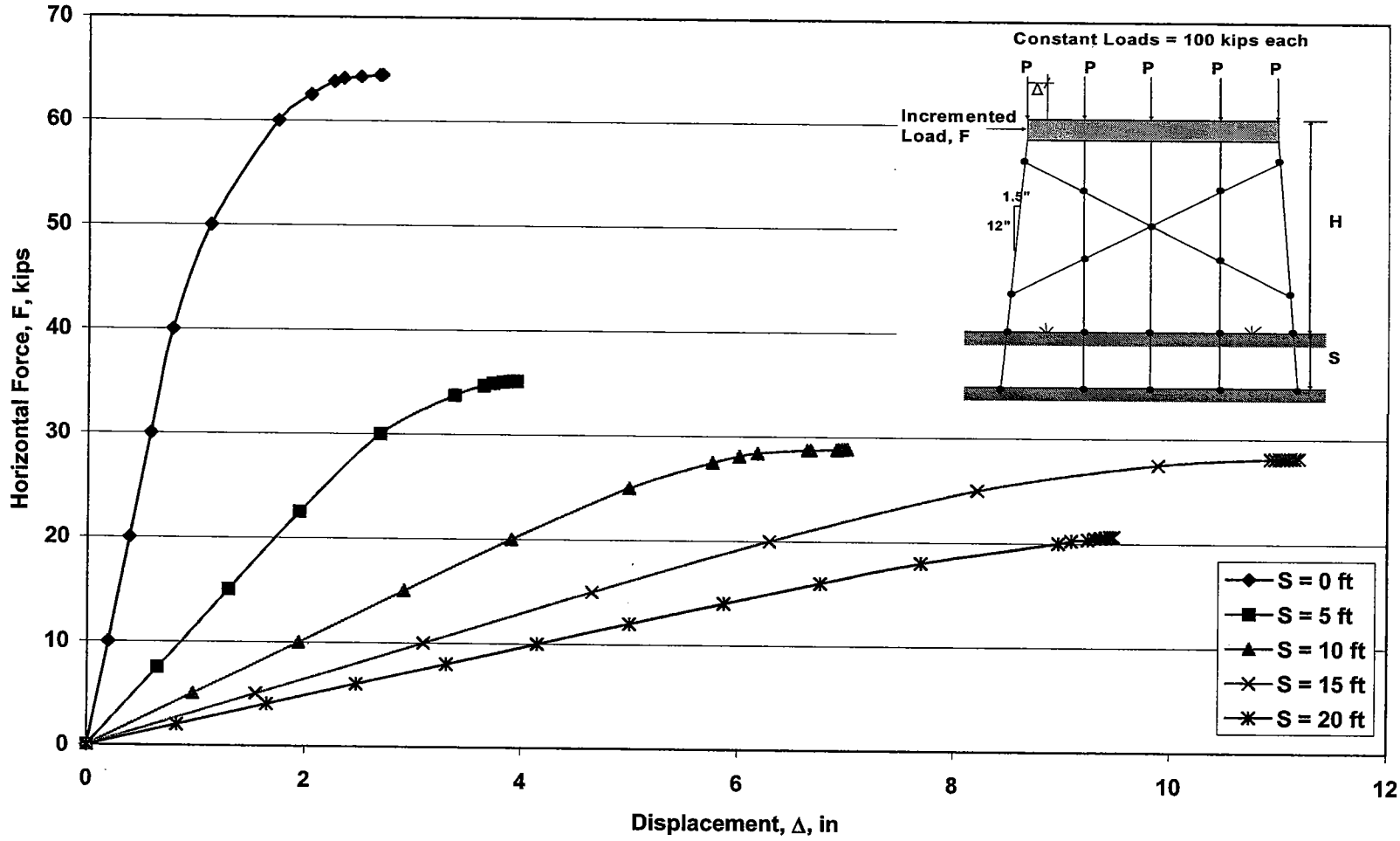

Figure 8.11. GTSTRUDL Pushover Analysis for One Story X-braced HP10x42 5-Pile Bent Subjected to Scour, Piles Pinned to Ground, H = 13ft

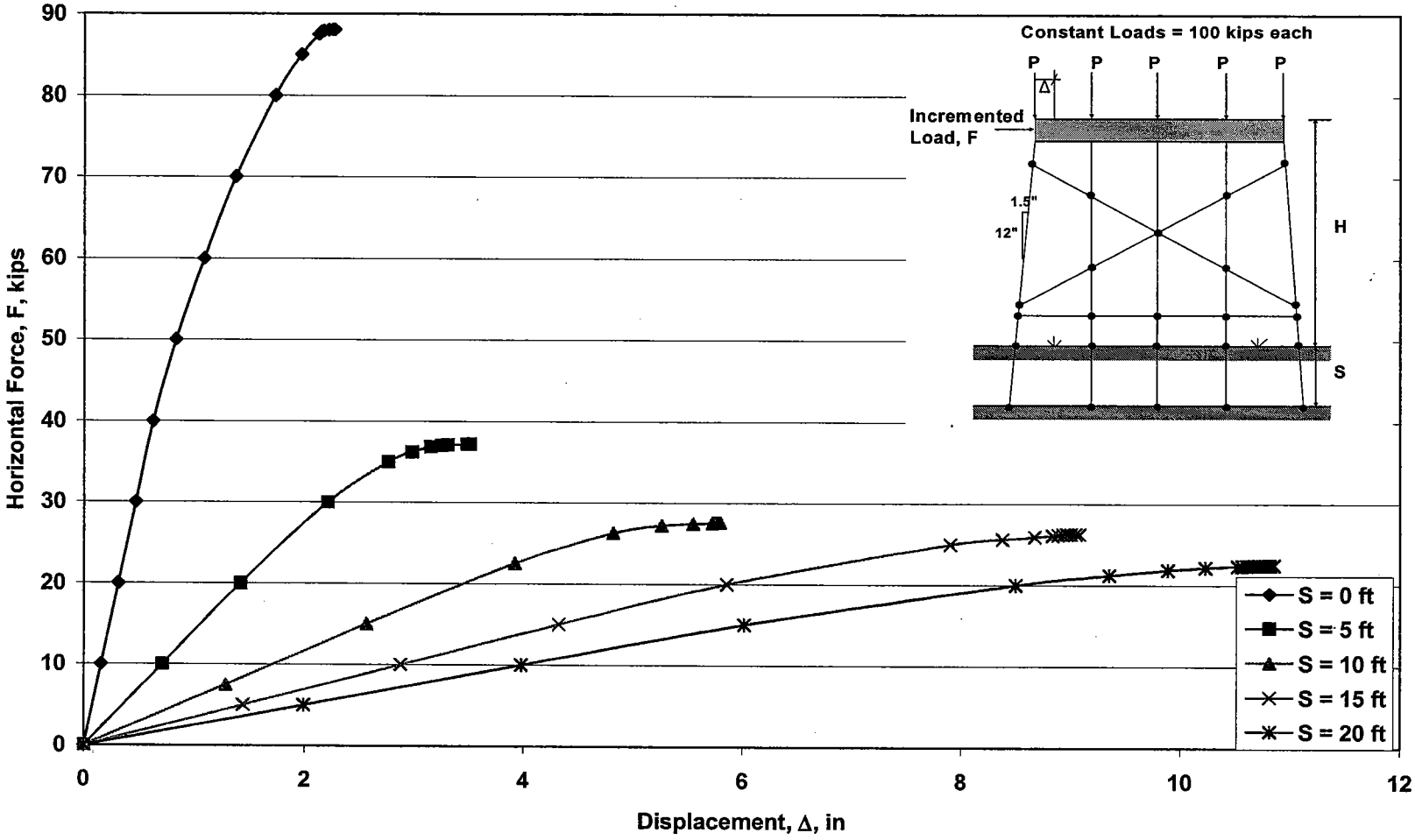

Figure 8.12. GTSTRUDL Pushover Analysis for One Story HP10x42 5-Pile Bent (with Proposed Lower Horizontal Member in X-Bracing) Subjected to Scour, Piles Pinned at Ground, H = 13 ft

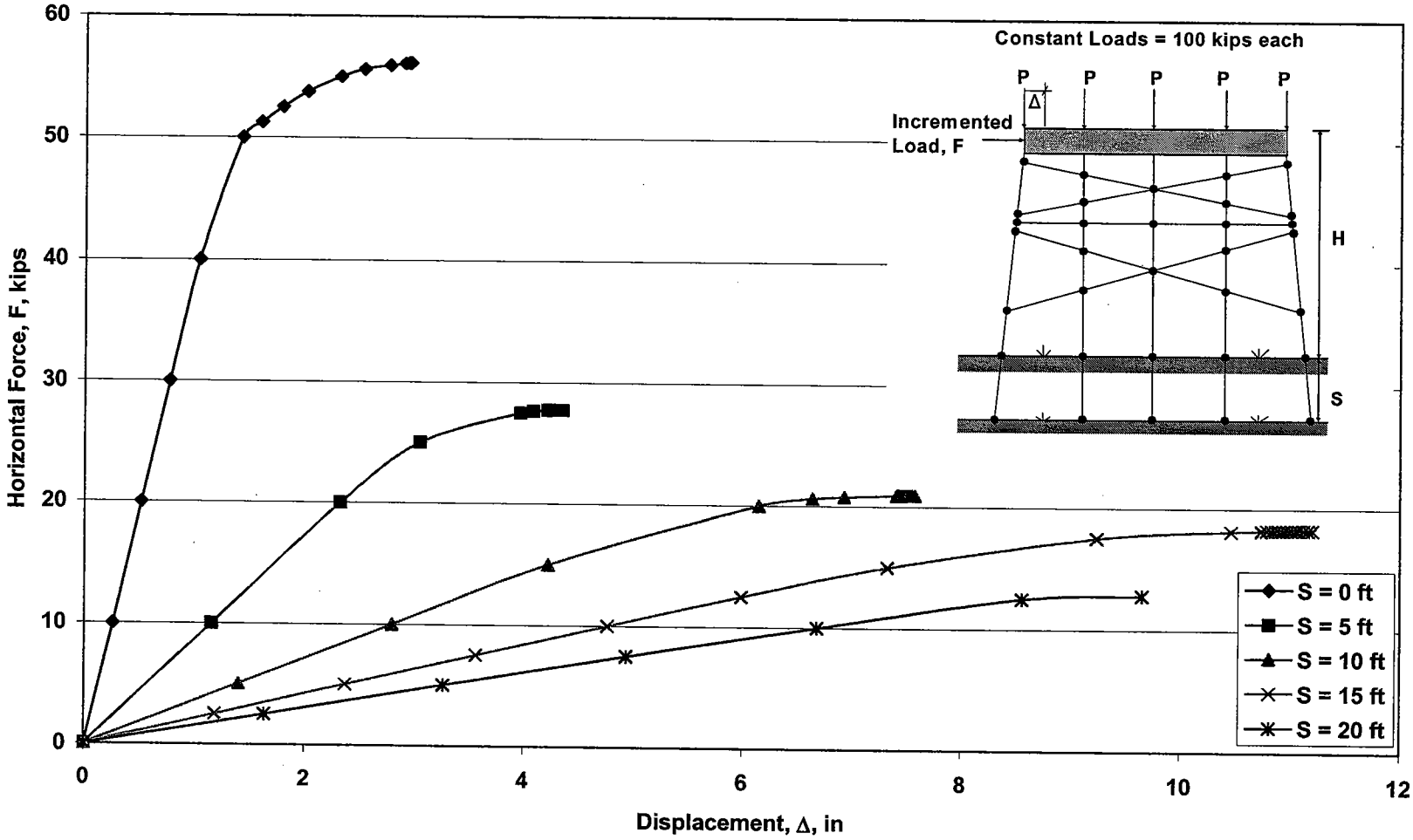

Figure 8.13. GTSTRUDL Pushover Analysis for Two Story X-braced HP10x42 5-Pile Bent Subjected to Scour, Piles Pinned at Ground, H = 25ft

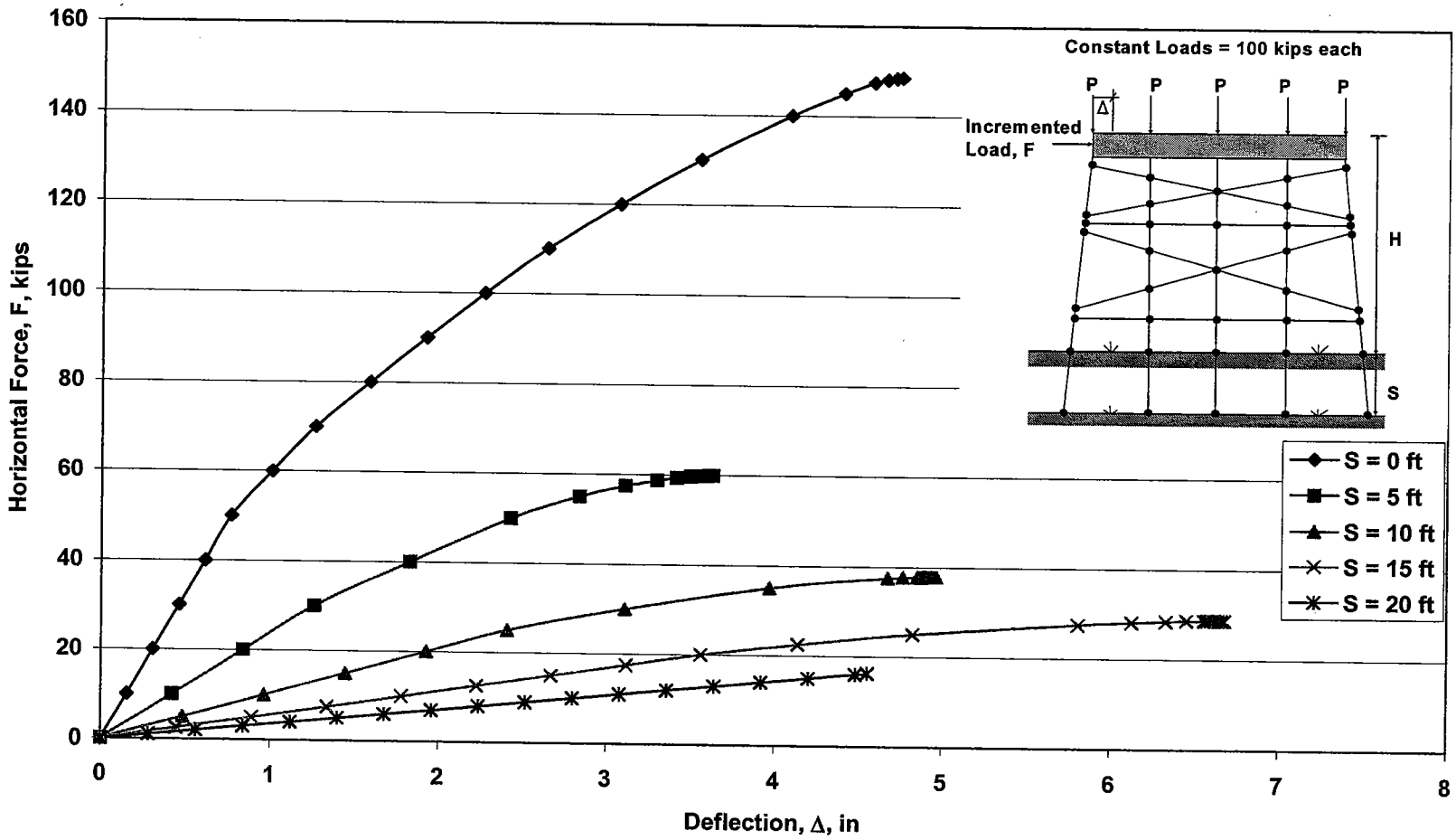

Figure 8.14. GTSTRUDL Pushover Analysis for Two Story HP10x42 5-Pile Bent (with Proposed Lower Horizontal Member in X-Bracing) Subjected to Scour, Piles Pinned at Grounnd, H = 25 ft

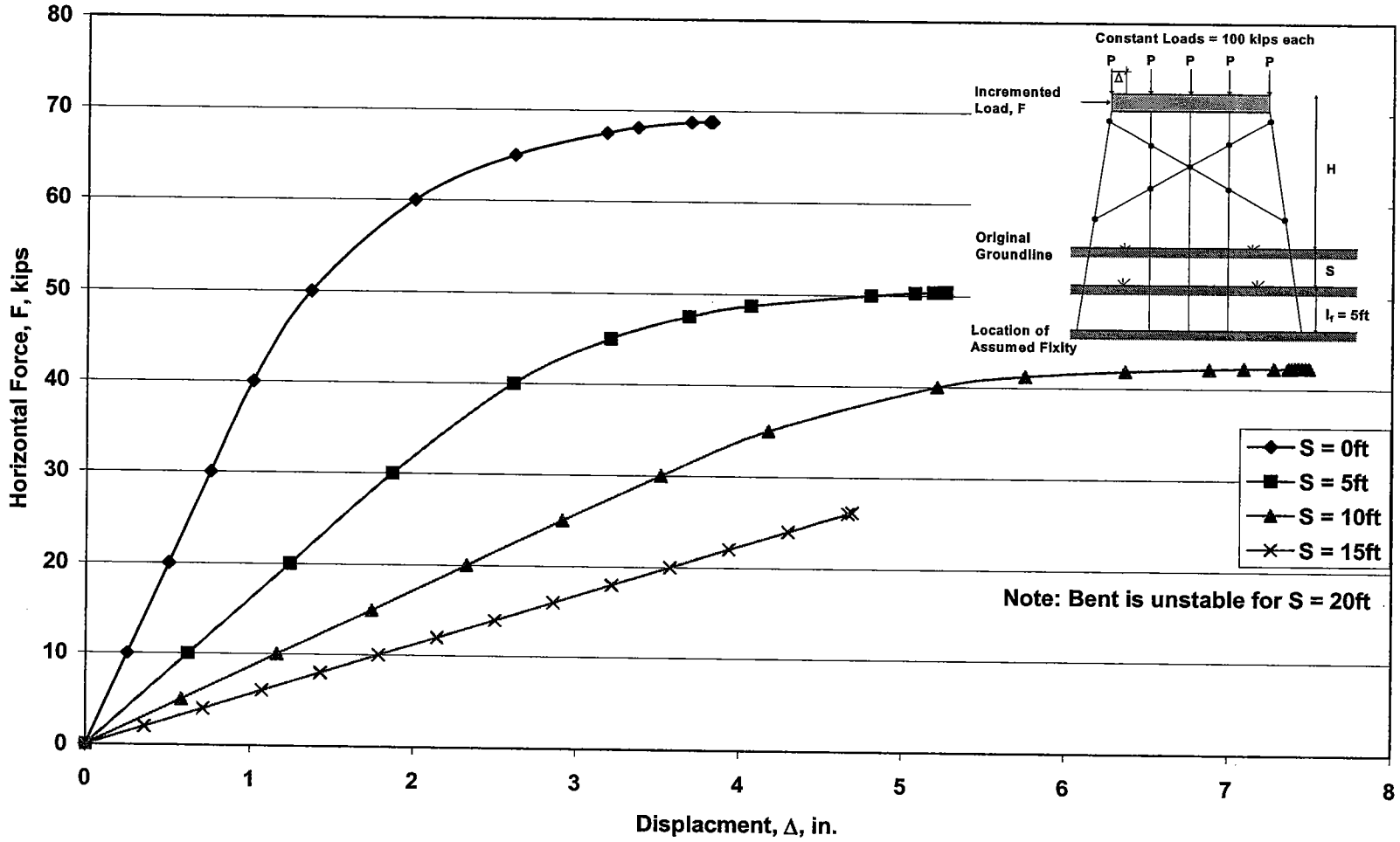

Figure 8.15. GTSTRUDL Pushover Analysis for One Story X-braced HP10x42 5-Pile Bent Subjected to Scour, Piles Assumed Fixed at l_f = 5ft Below Ground line, H = 13ft

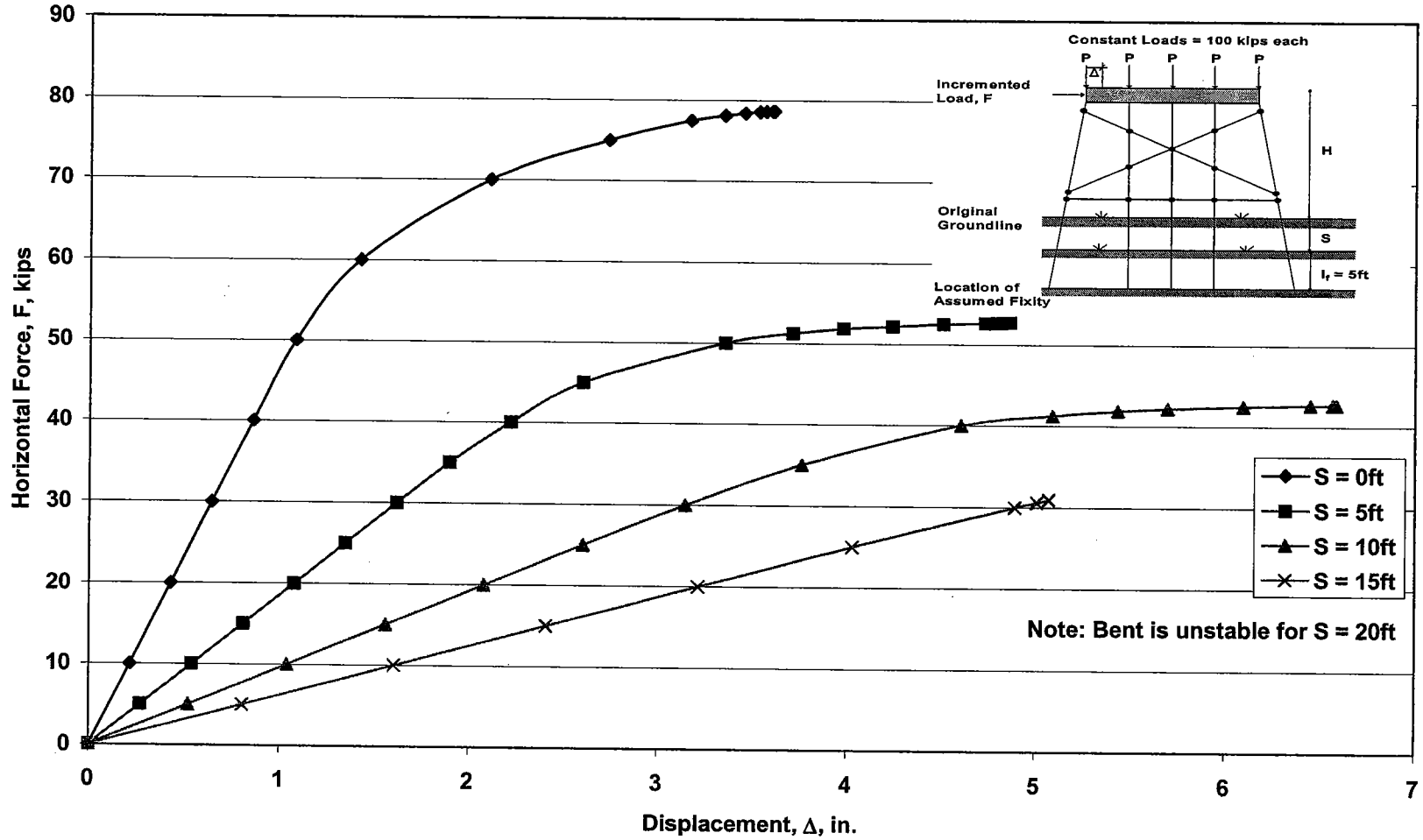

Figure 8.16. GTSTRUDL Pushover Analysis for One Story HP 10x42 5-Pile Bent (with Proposed Lower Horizontal Member in X-Bracing) Subjected to Scour, Piles Assumed Fixed at l_f = 5ft Below Ground line, H = 13 ft

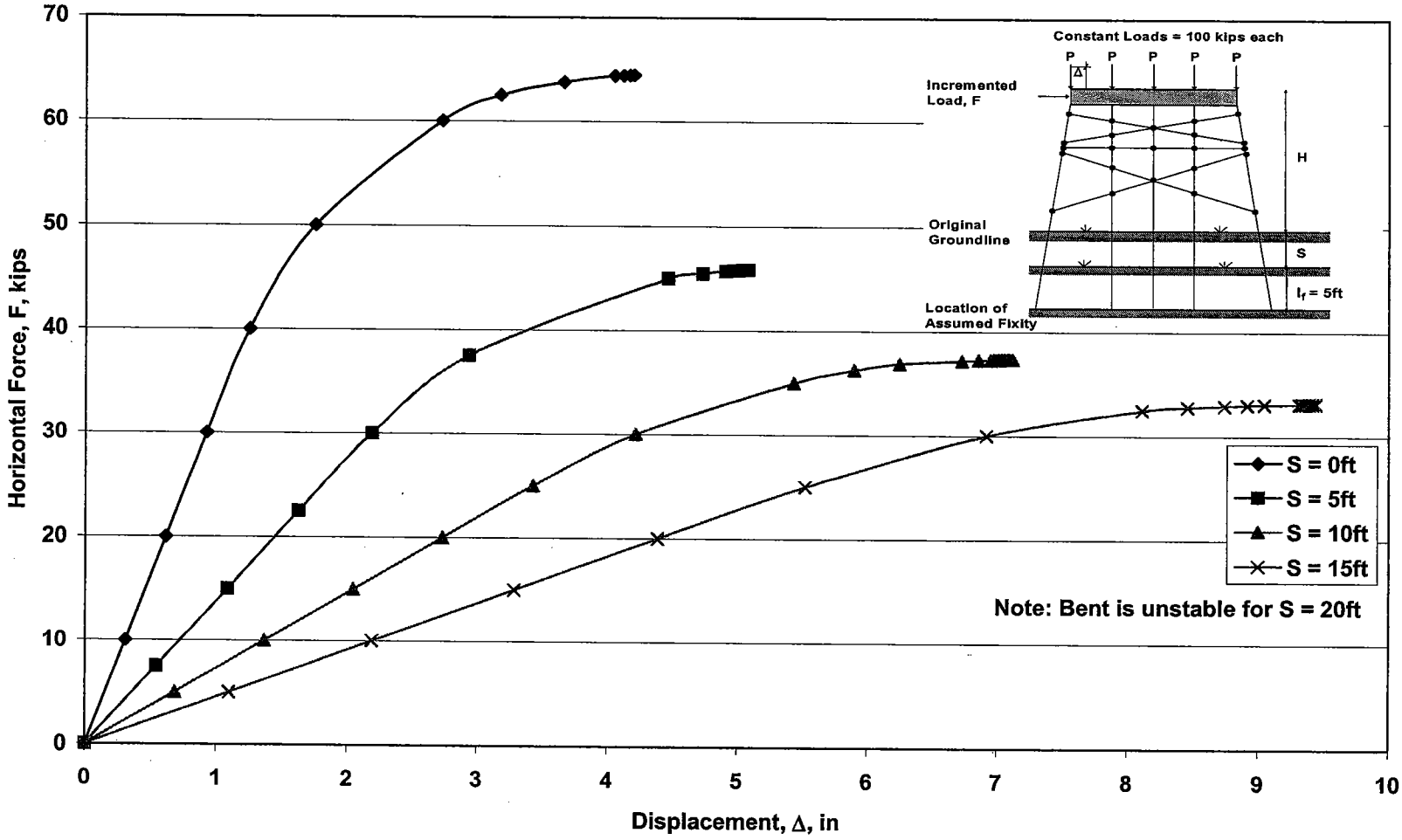

Figure 8.17. GTSTRUDL Pushover Analysis for Two Story X-braced HP10x42 5-Pile Bent Subjected to Scour, Piles Assumed Fixed at l_f = 5ft Below Ground line, H = 25ft

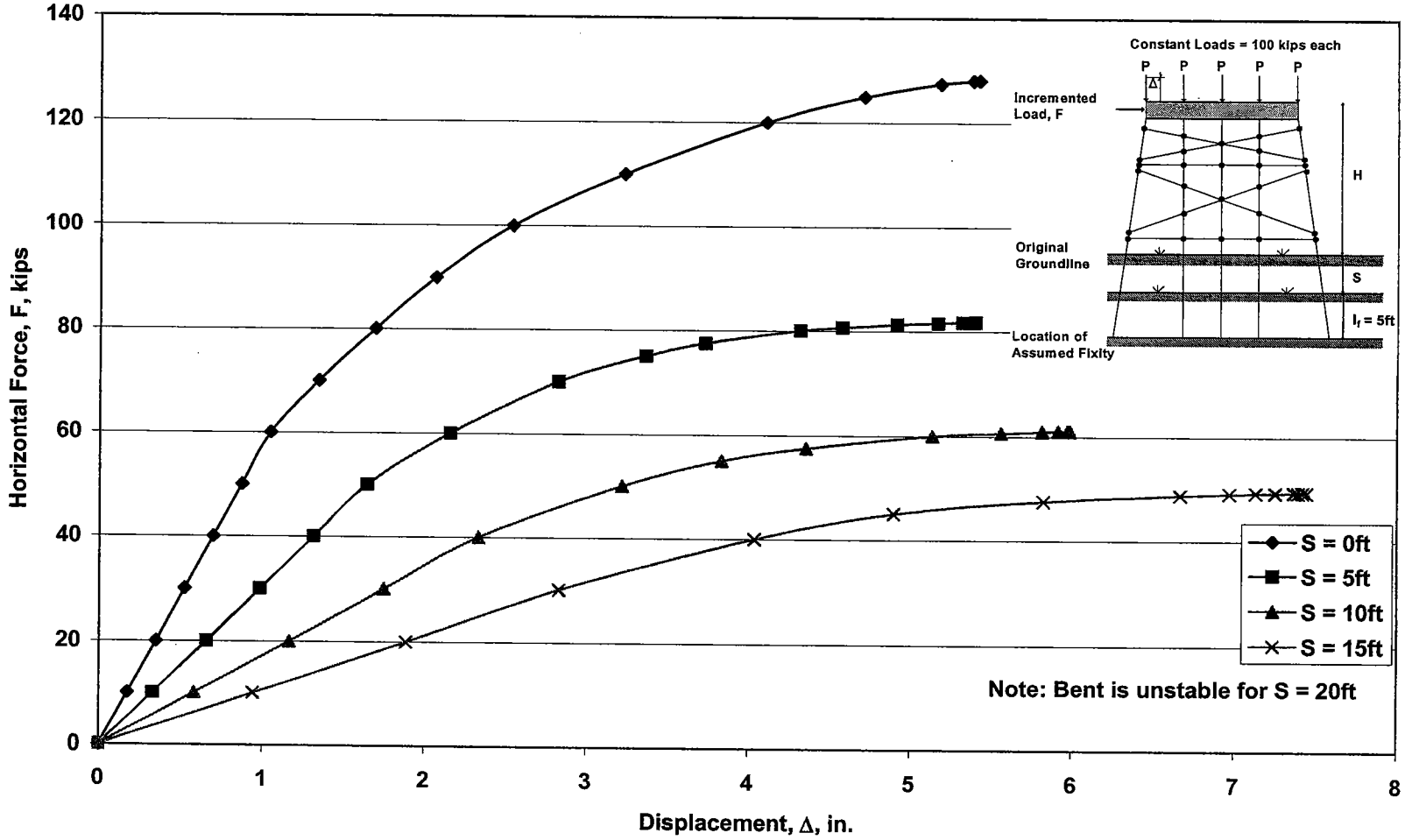

Figure 8.18. GTSTRUDL Pushover Analysis for Two Story HP 10x42 5-Pile Bent (with Proposed Lower Horizontal Member in X-Bracing) Subjected to Scour, Piles Assumed Fixed at l_f = 5ft Below Ground line, H = 25 ft

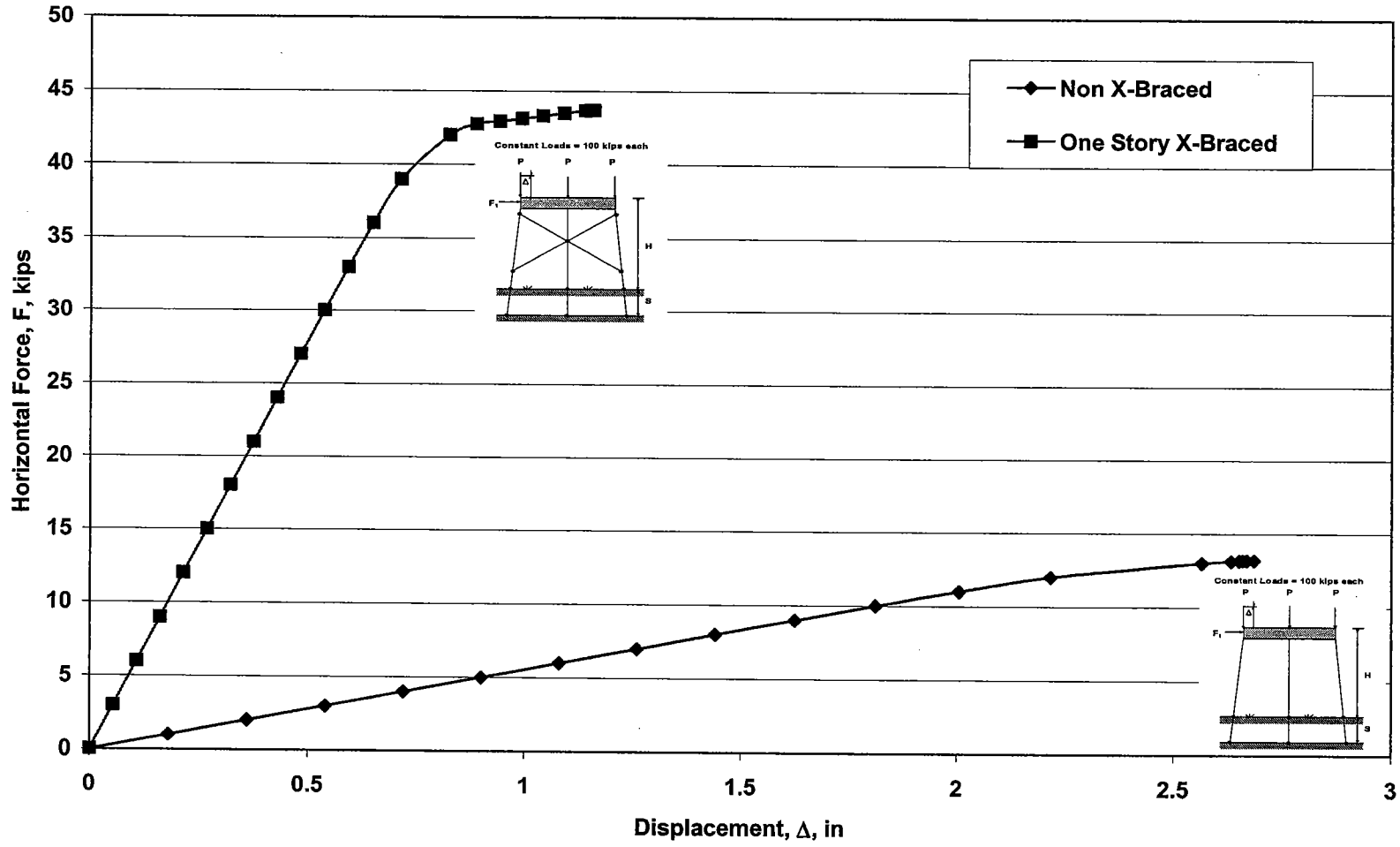

Figure 8.19a. GTSTRUDL Pushover Analysis for HP10x42 3-Pile Bents, Bents Pinned at Ground, H=13ft, S=0ft

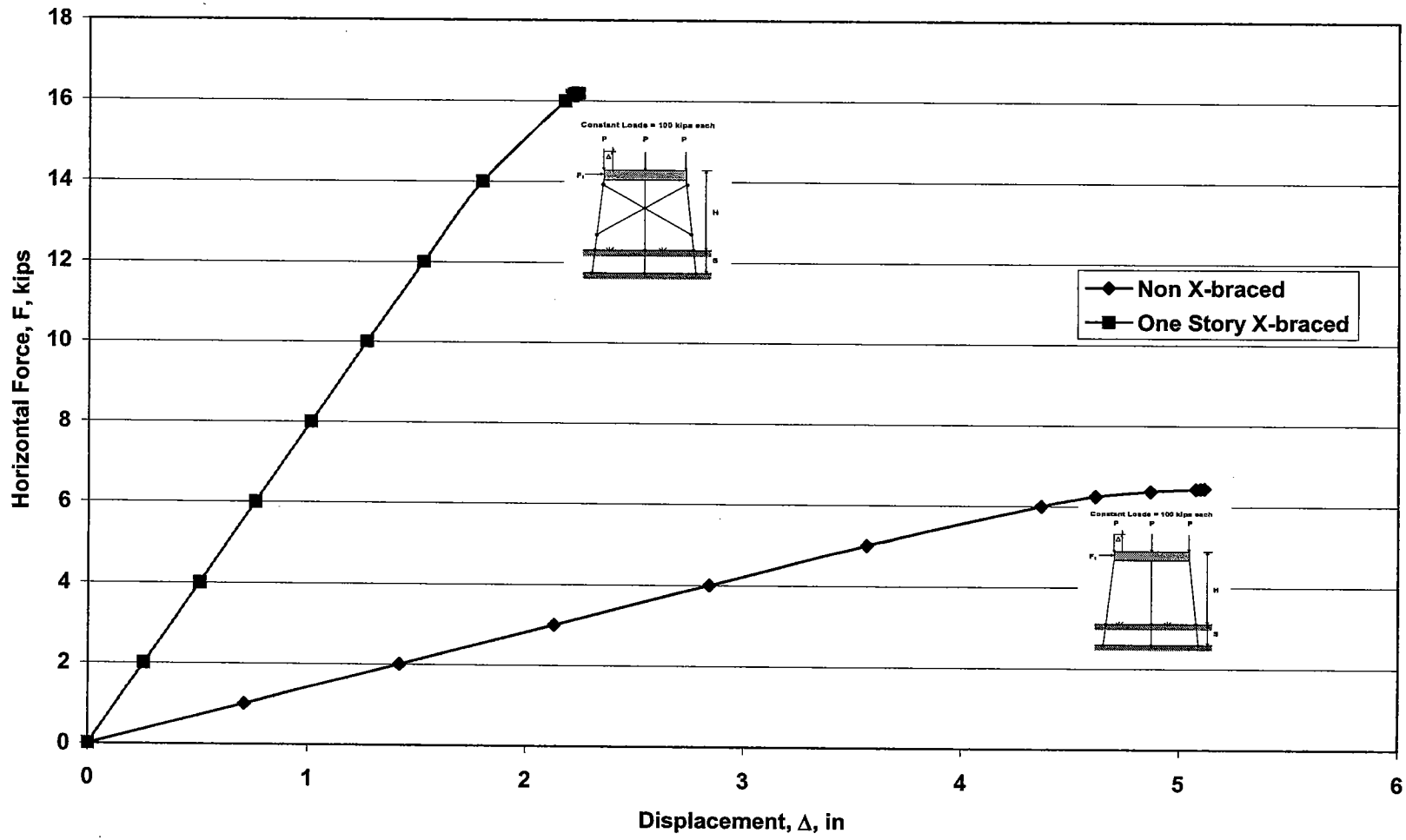

Figure 8.19b. GTSTRUDL Pushover Analysis for HP10x42 3-Pile Bents, Bents Pinned at Ground, H=13ft, S=5ft

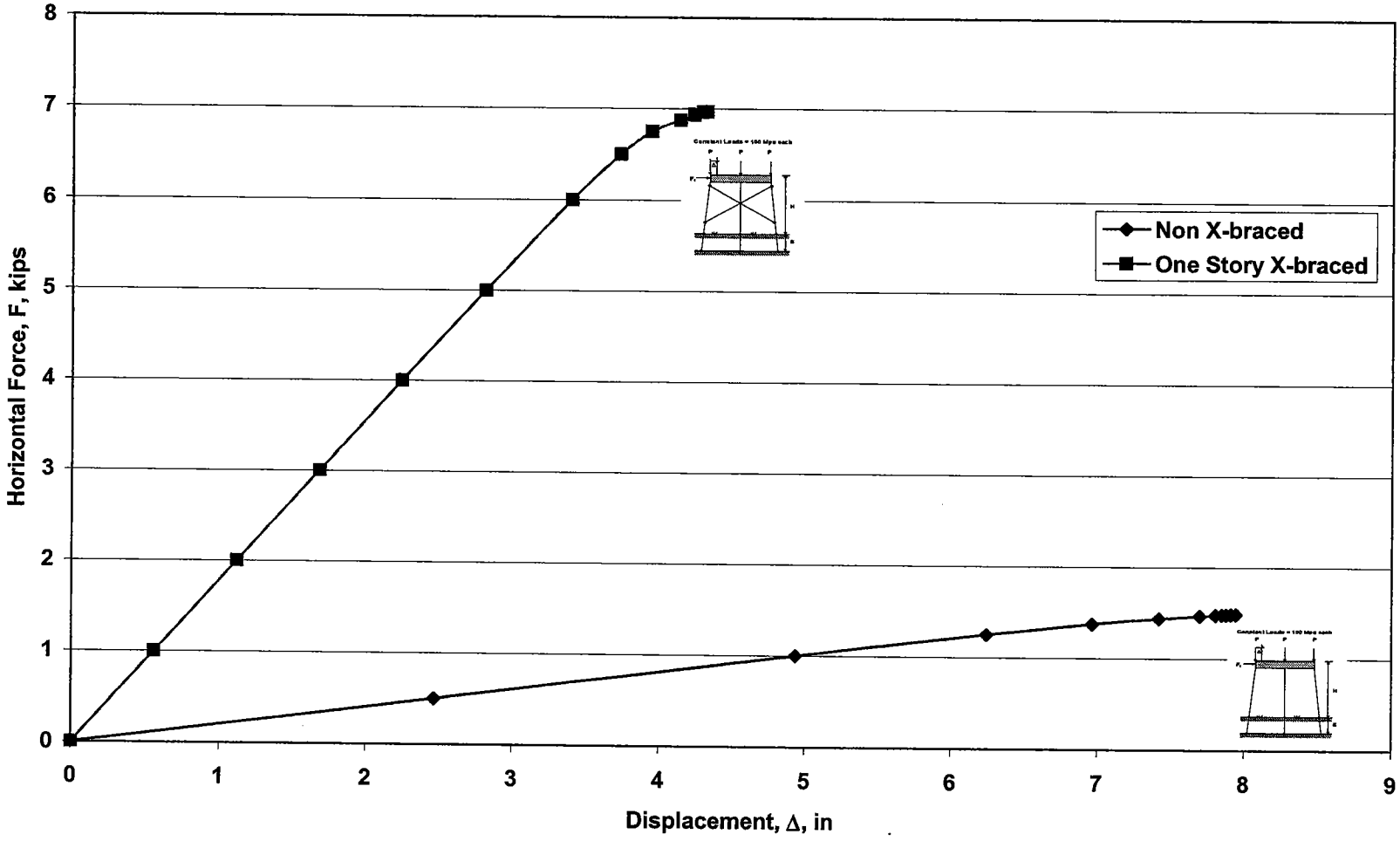

Figure 8.19c. GTSTRUDL Pushover Analysis for HP10x42 3-Pile Bents, Bents Pinned at Ground, H=13ft, S=10ft

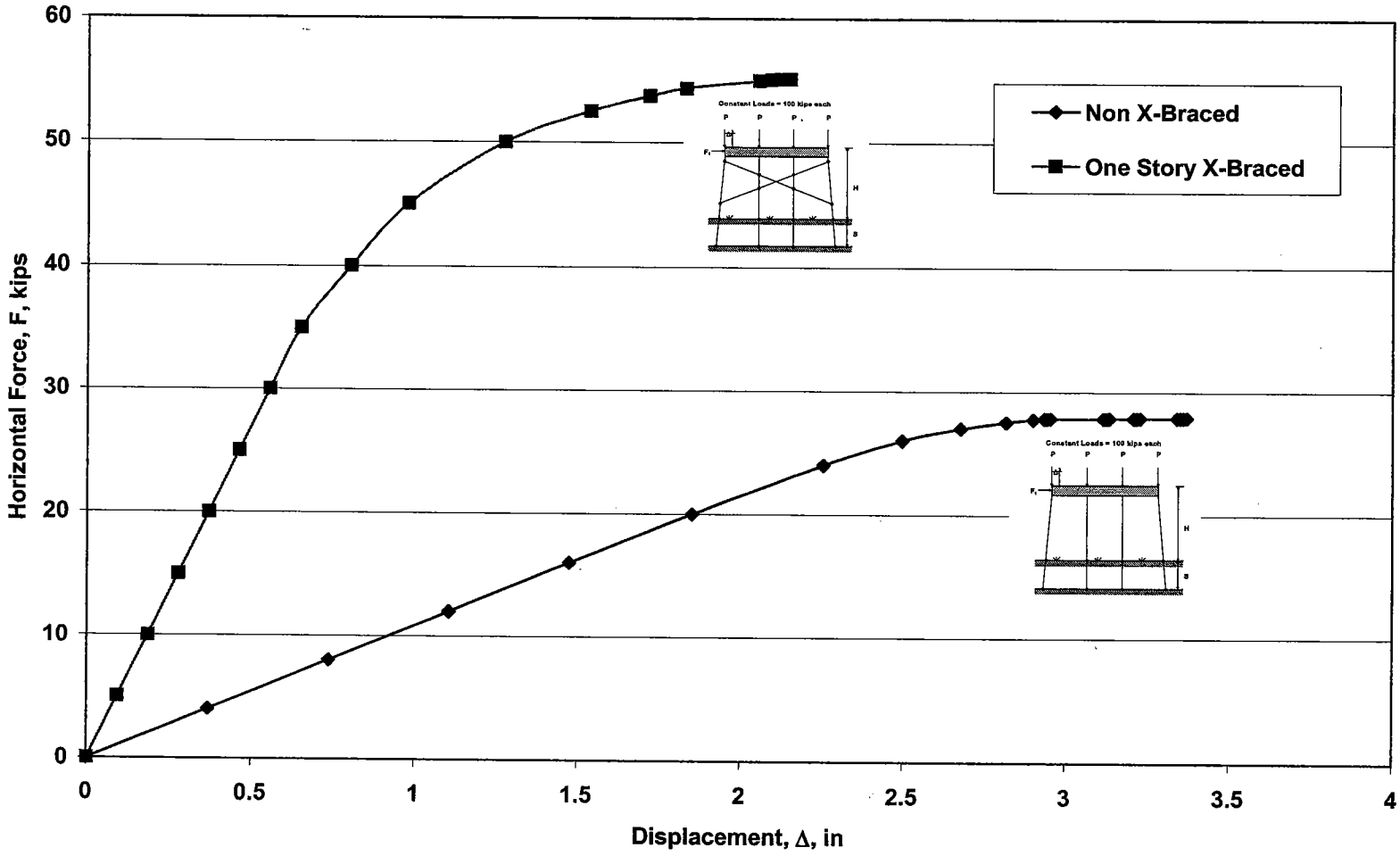

Figure 8.20a. GTSTRUDL Pushover Analysis for HP10x42 4-Pile Bents, Bents Pinned at Ground, H=13ft, S=0ft

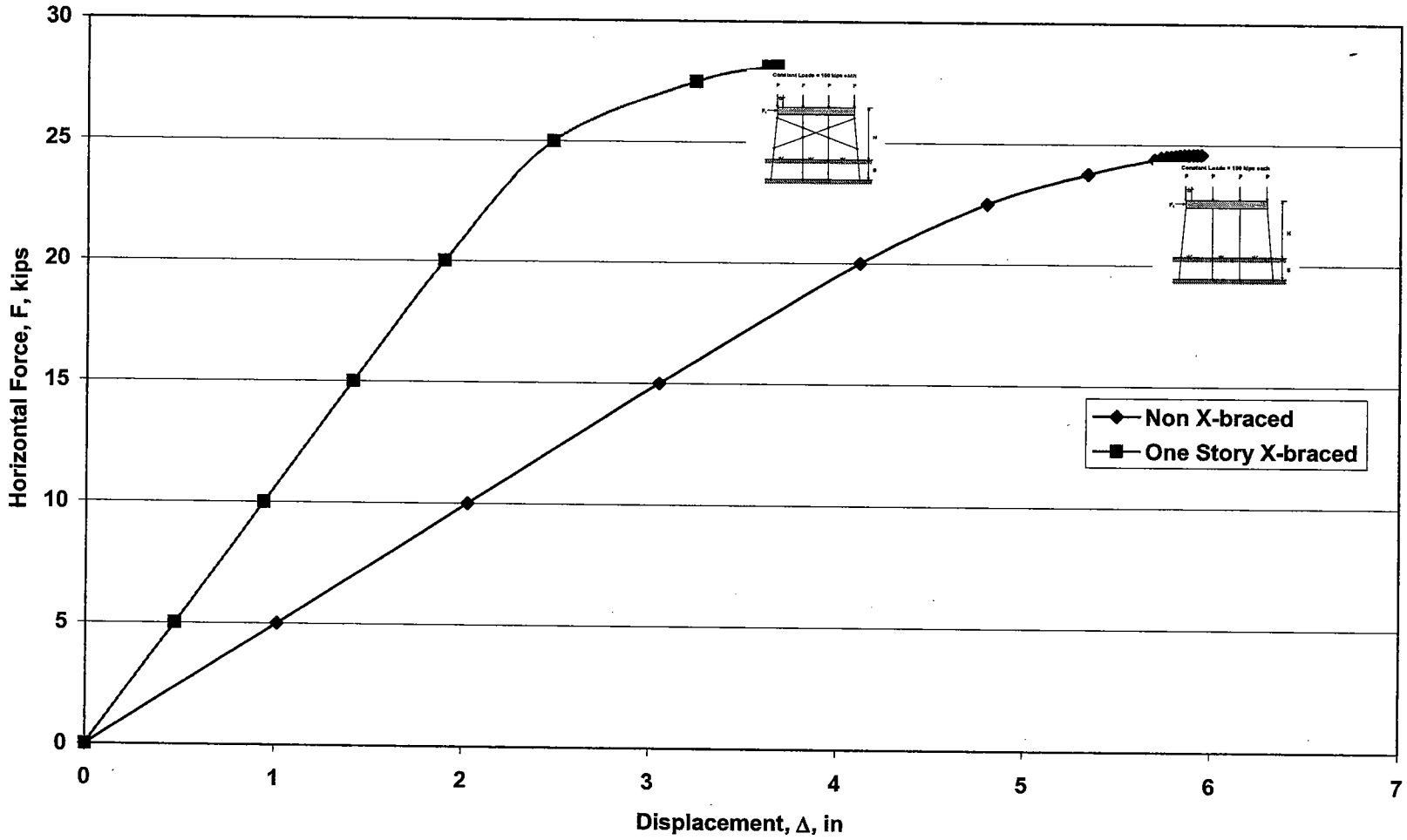

Figure 8.20b. GTSTRUDL Pushover Analysis for HP10x42 4-Pile Bents, Bents Pinned at Ground, H=13ft, S=5ft

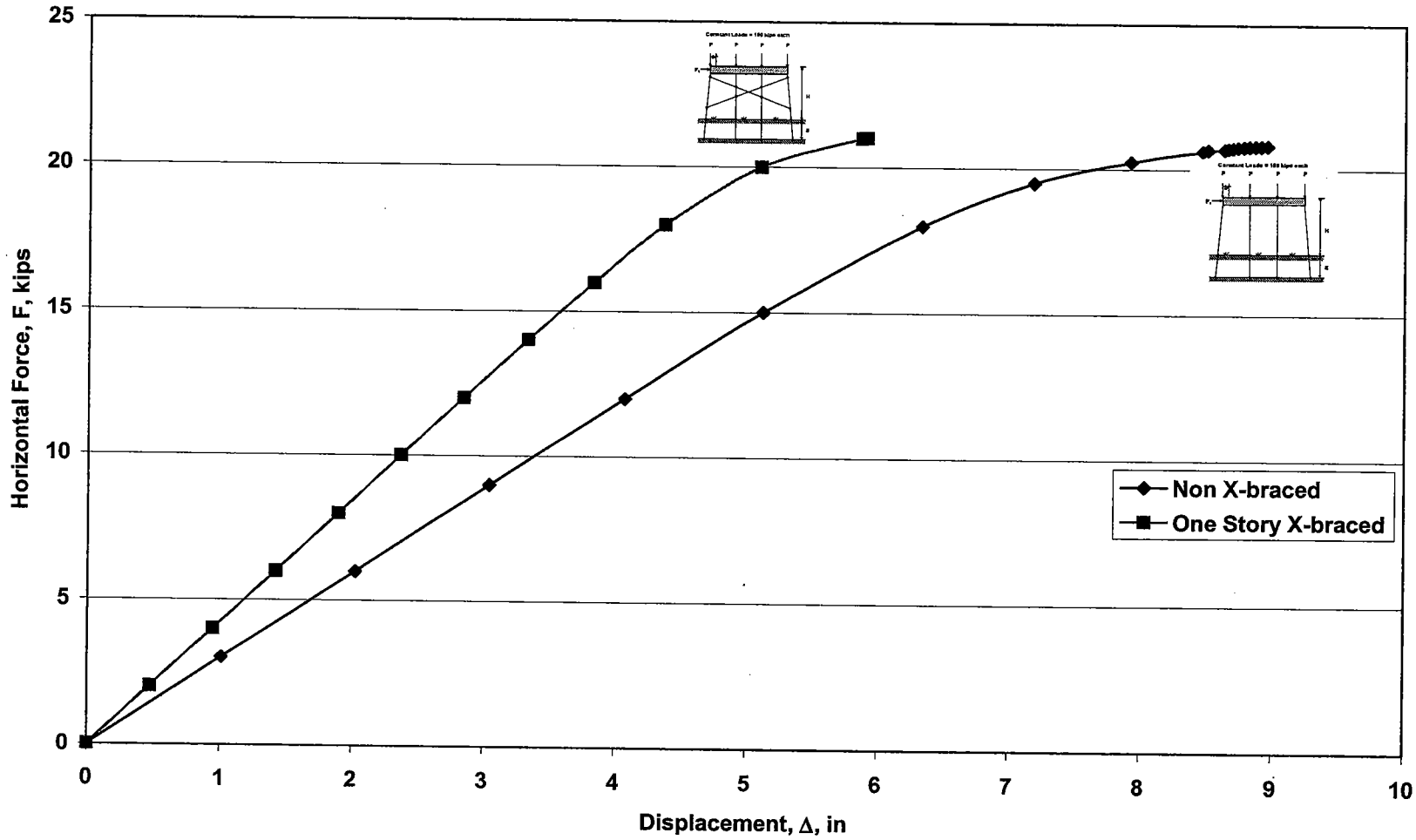

Figure 8.20c. GTSTRUDL Pushover Analysis for HP10x42 4-Pile Bents, Bents Pinned at Ground, H=13ft, S=10ft

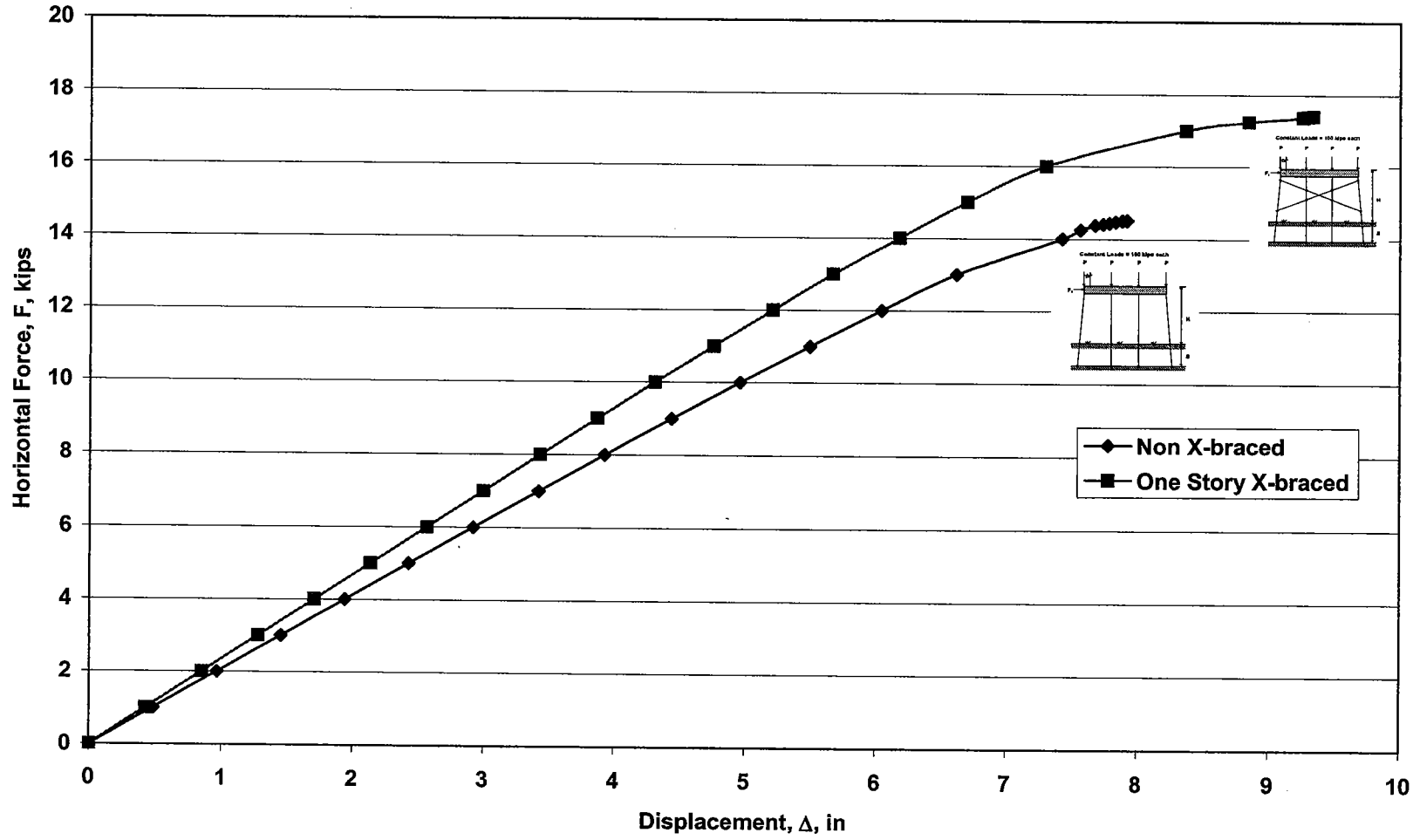

Figure 8.20d. GTSTRUDL Pushover Analysis for HP10x42 4-Pile Bents, Bents Pinned at Ground, H=13ft, S=15ft

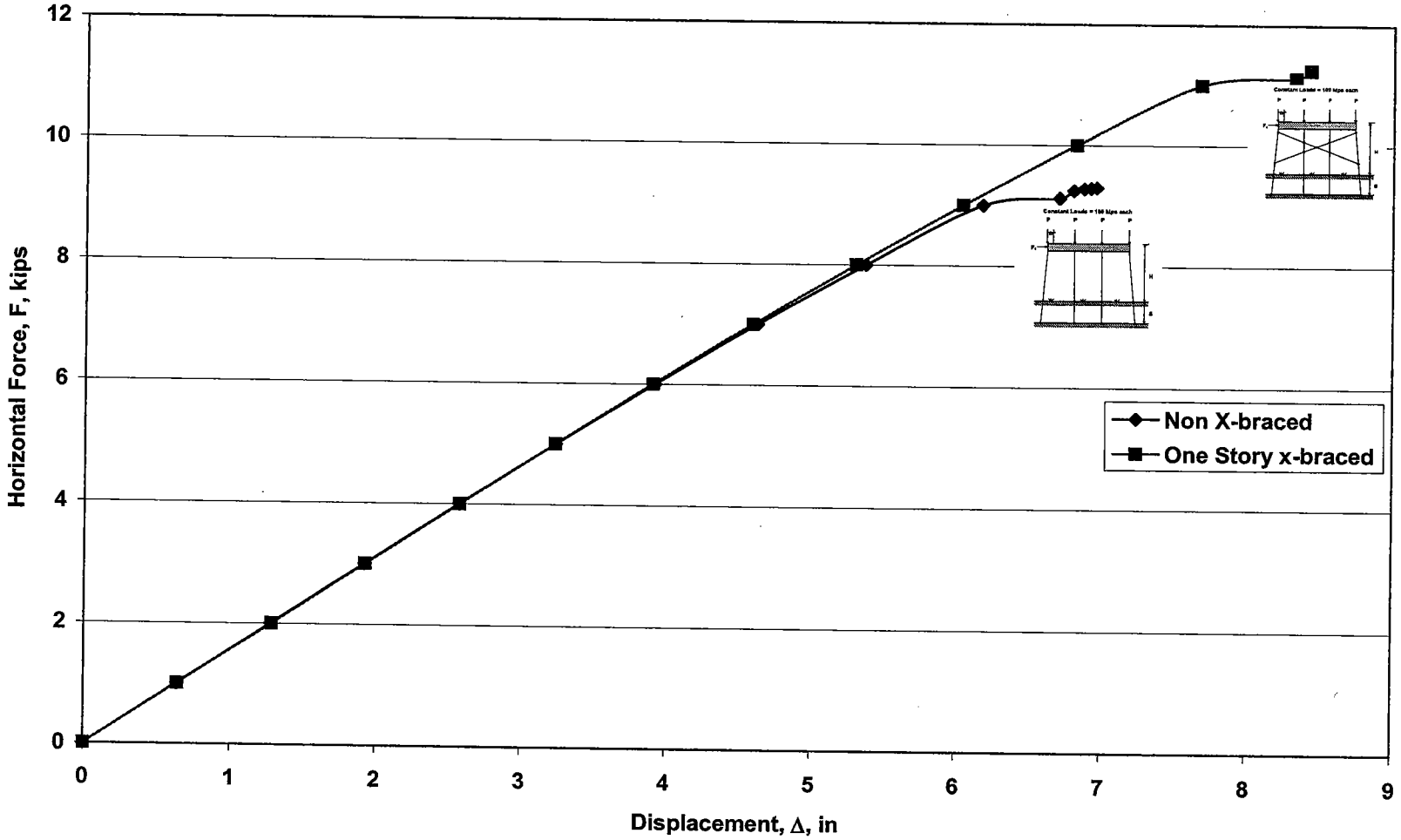

Figure 8.20e. GTSTRUDL Pushover Analysis for HP10x42 4-Pile Bents, Bents Pinned at Ground, H=13ft, S=20ft

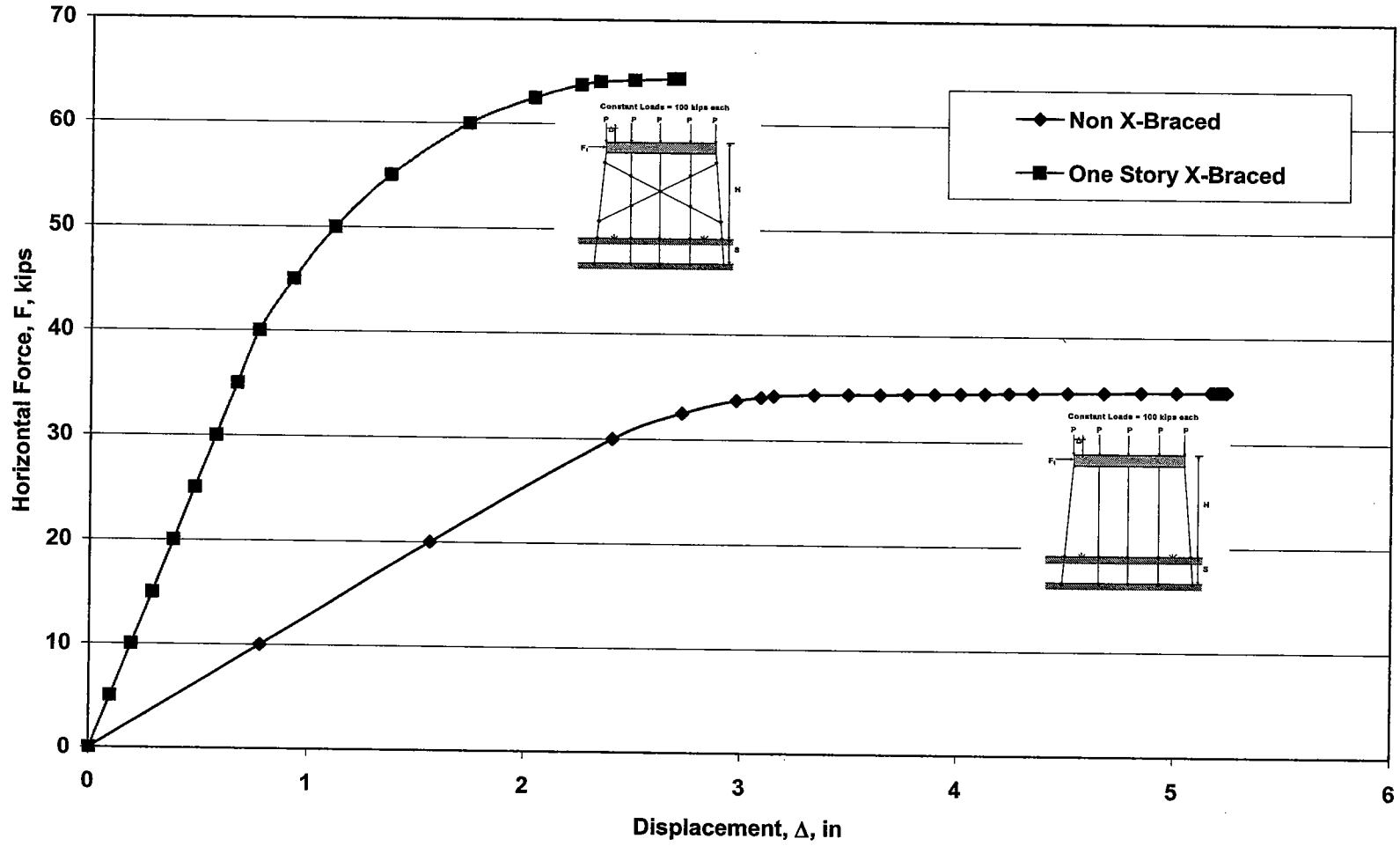

Figure 8.21a. GTSTRUDL Pushover Analysis for HP10x42 5-Pile Bents, Bents Pinned at Ground, H=13ft, S=0ft

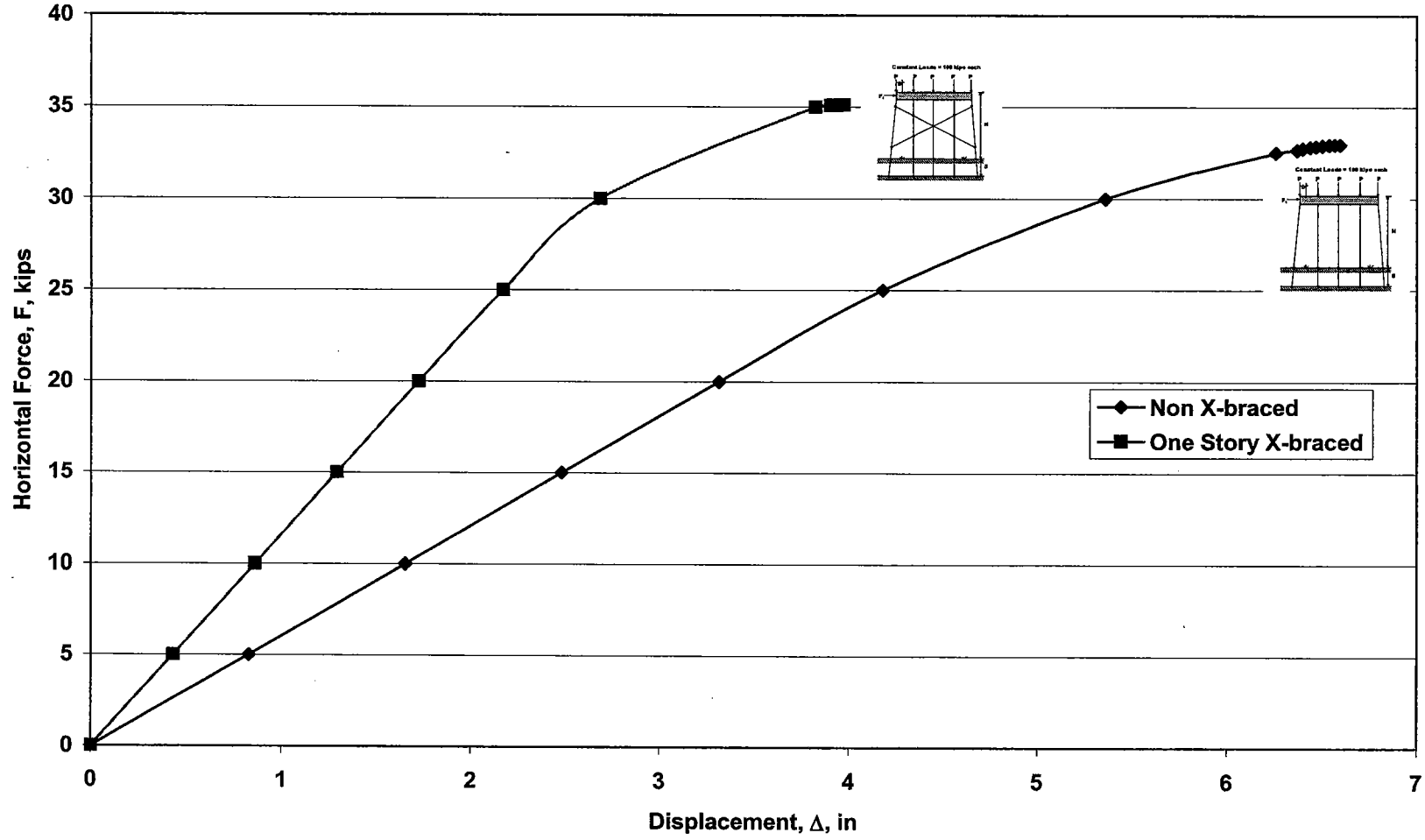

Figure 8.21b. GTSTRUDL Pushover Analysis for HP10x42 5-Pile Bents, Bents Pinned at Ground, H=13ft, S=5ft

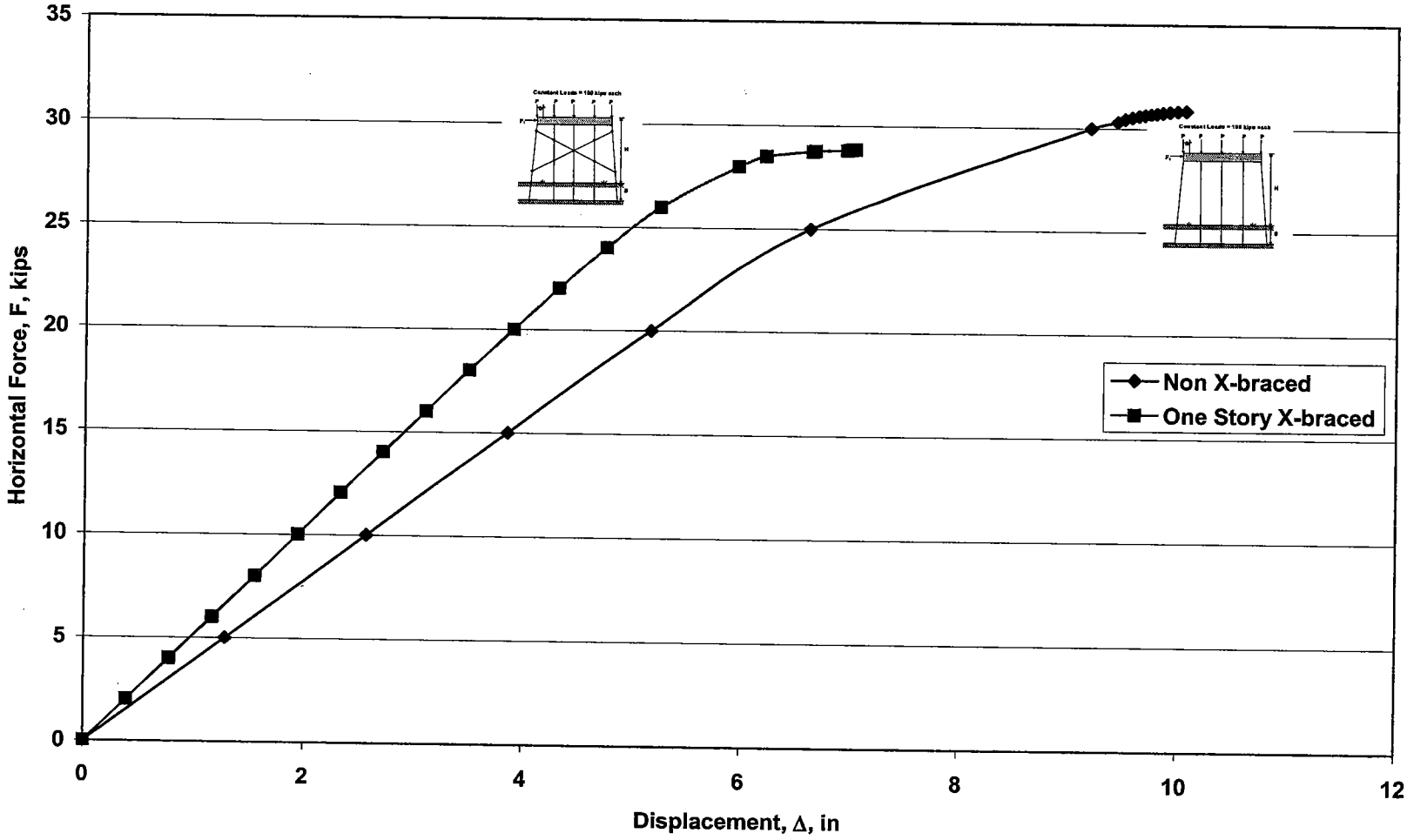

Figure 8.21c. GTSTRUDL Pushover Analysis for HP10x42 5-Pile Bents, Bents Pinned at Ground, H=13ft, S=10ft

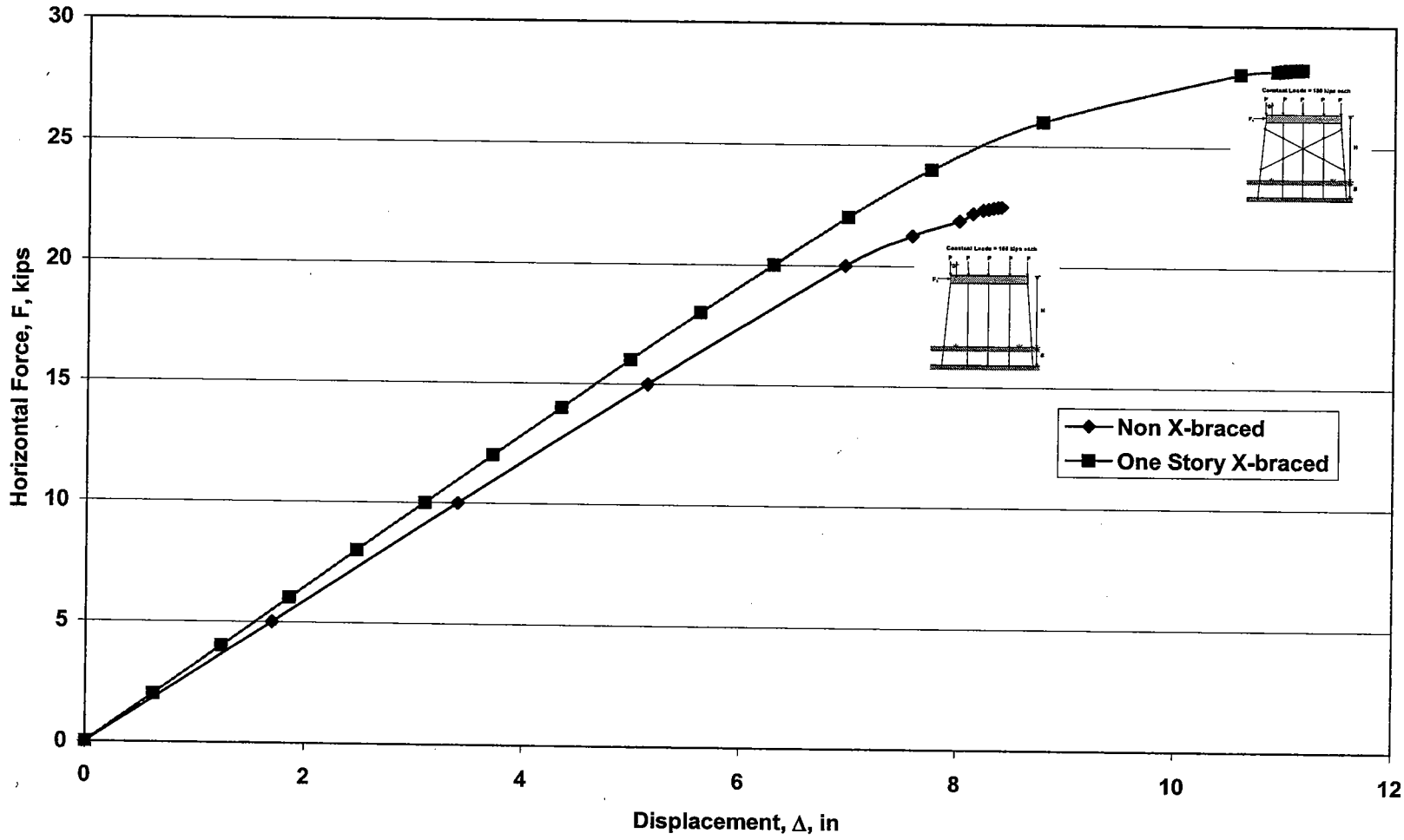

Figure 8.21d. GTSTRUDL Pushover Analysis for HP10x42 5-Pile Bents, Bents Pinned at Ground, H=13ft, S=15ft

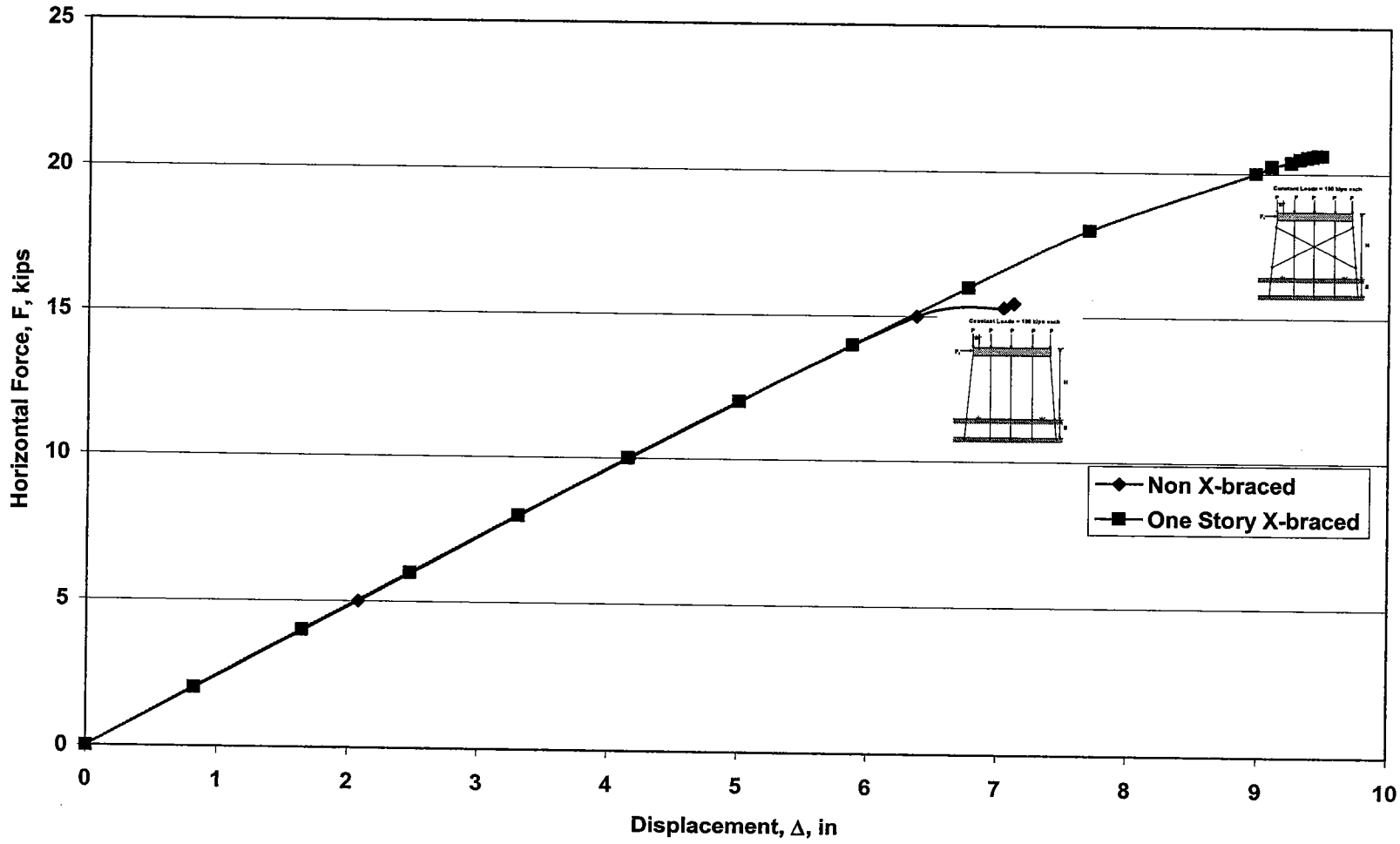

Figure 8.21e. GTSTRUDL Pushover Analysis for HP10x42 5-Pile Bents, Bents Pinned at Ground, H=13ft, S=20ft

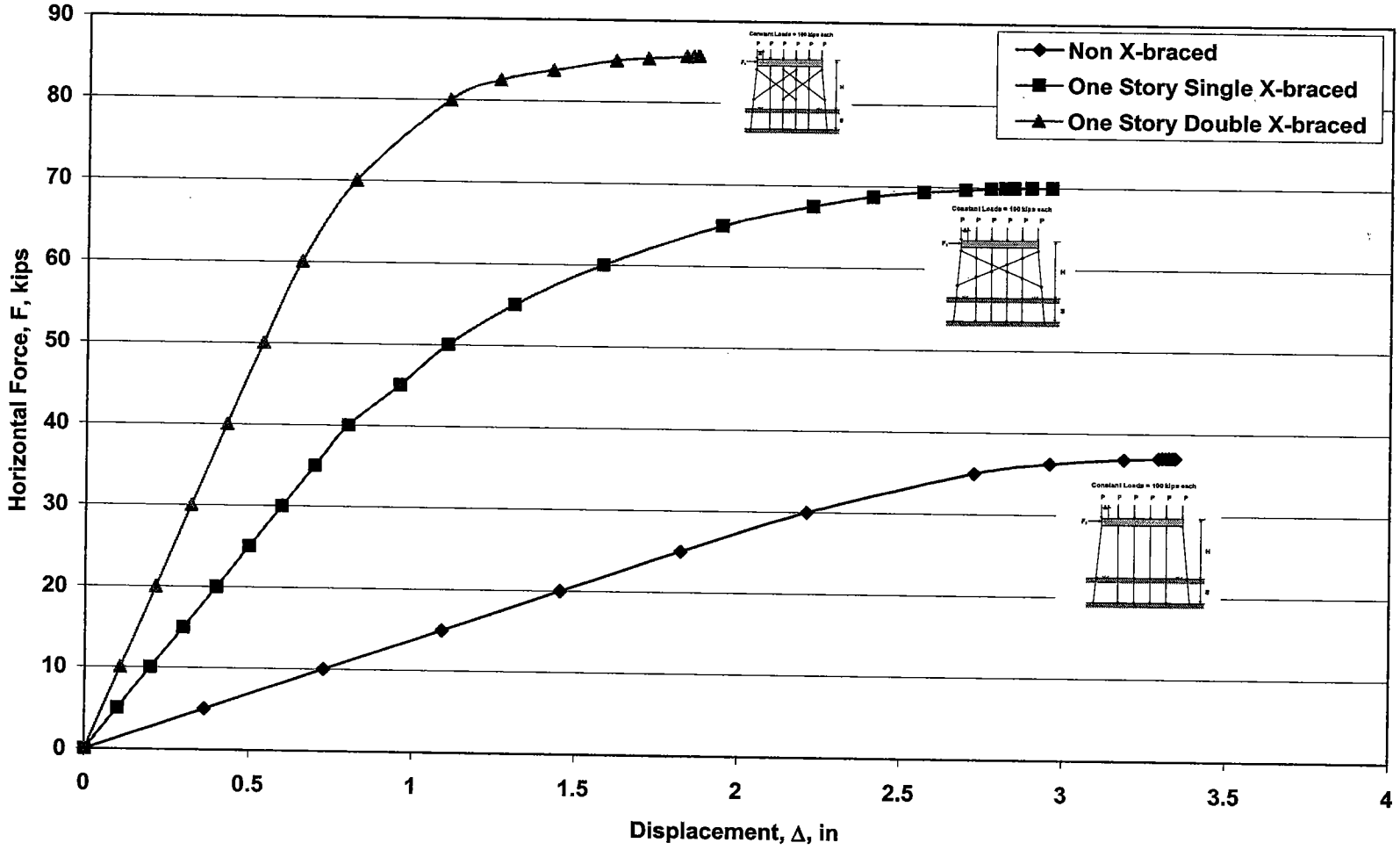

Figure 8.22a. GTSTRUDL Pushover Analysis for HP10x42 6-Pile Bents, Bents Pinned at Ground, H=13ft, S=0ft

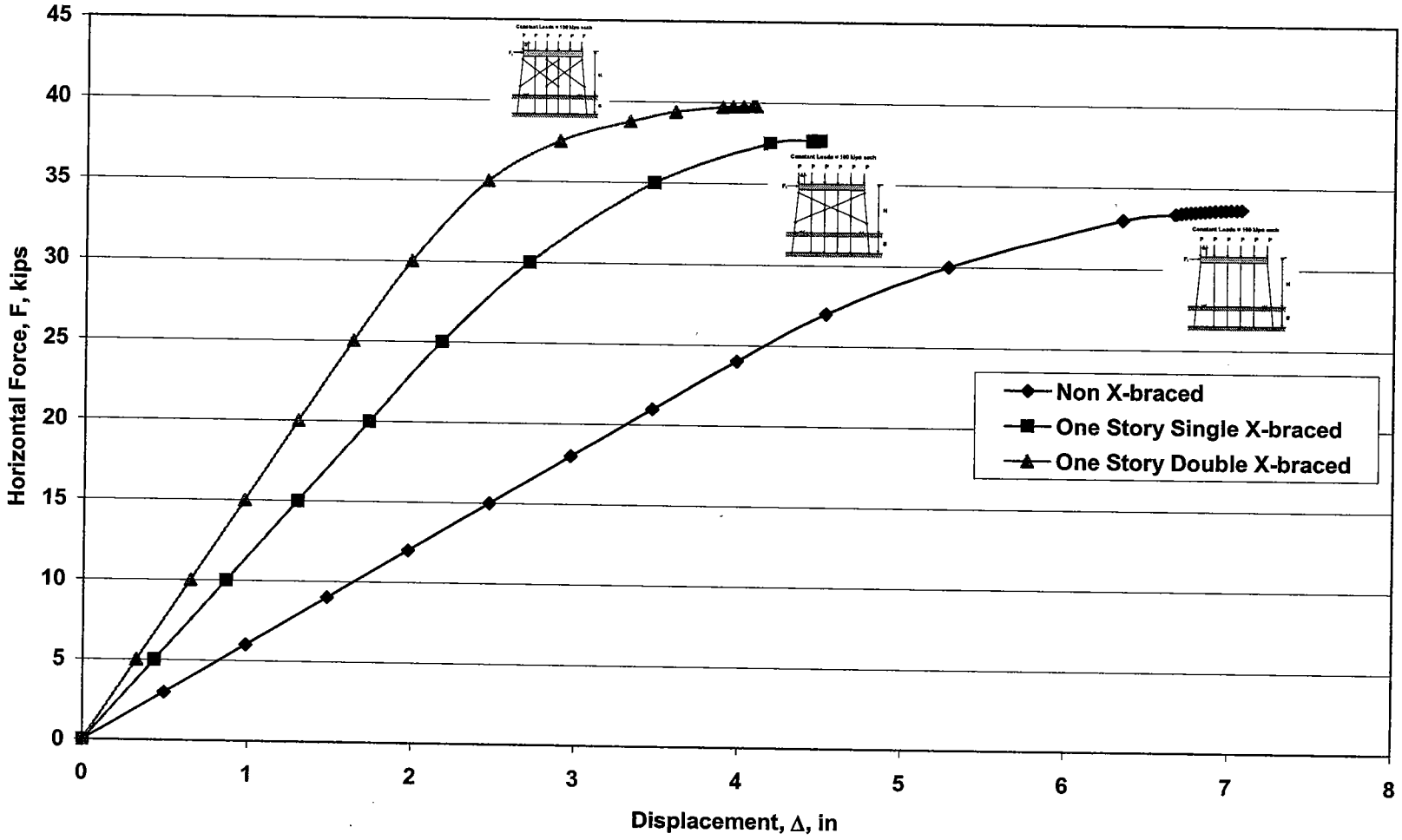

Figure 8.22b. GTSTRUDL Pushover Analysis for HP10x42 6-Pile Bents, Bents Pinned at Ground, H=13ft, S=5ft

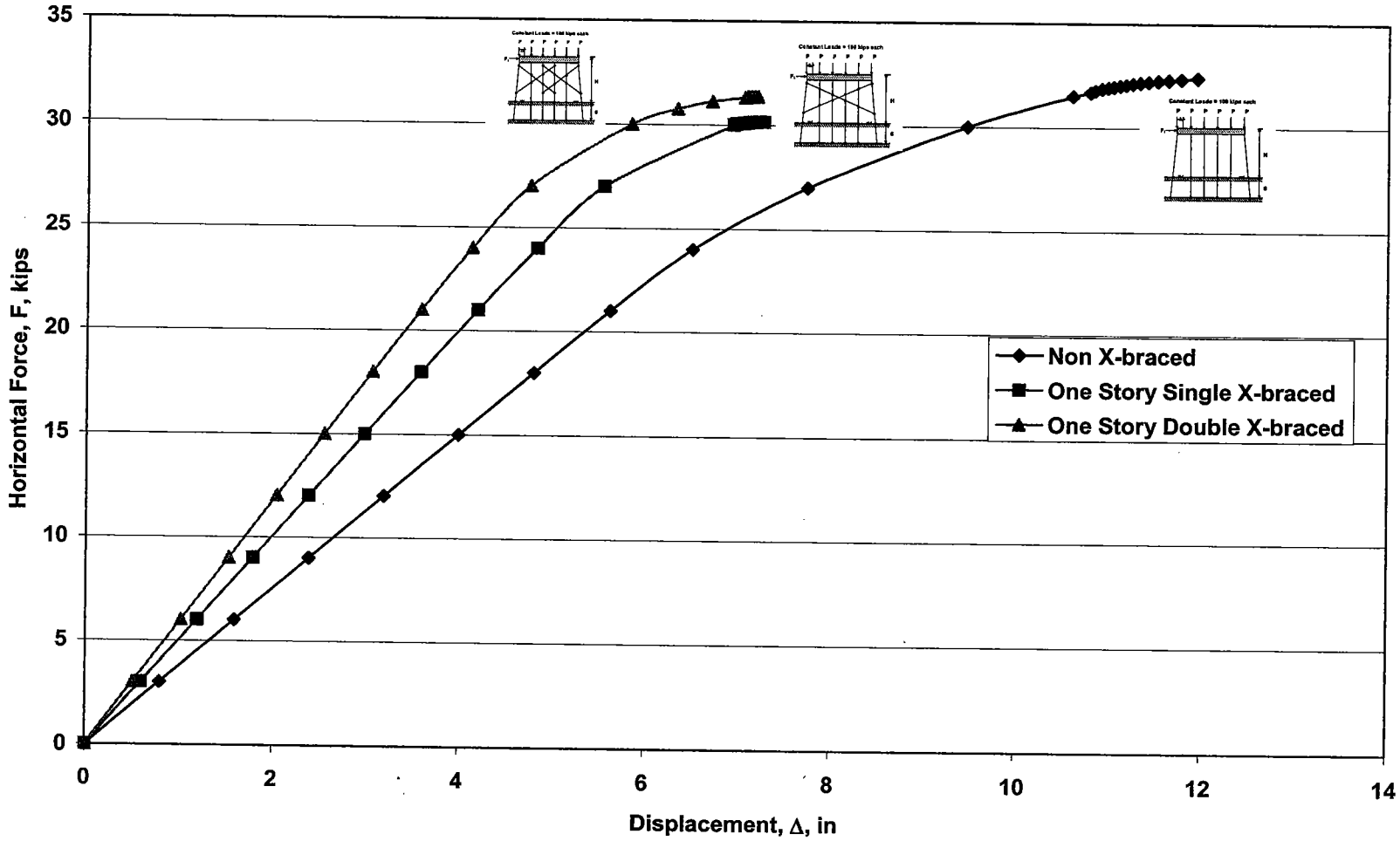

Figure 8.22c. GTSTRUDL Pushover Analysis for HP10x42 6-Pile Bents, Bents Pinned at Ground, H=13ft, S=10ft

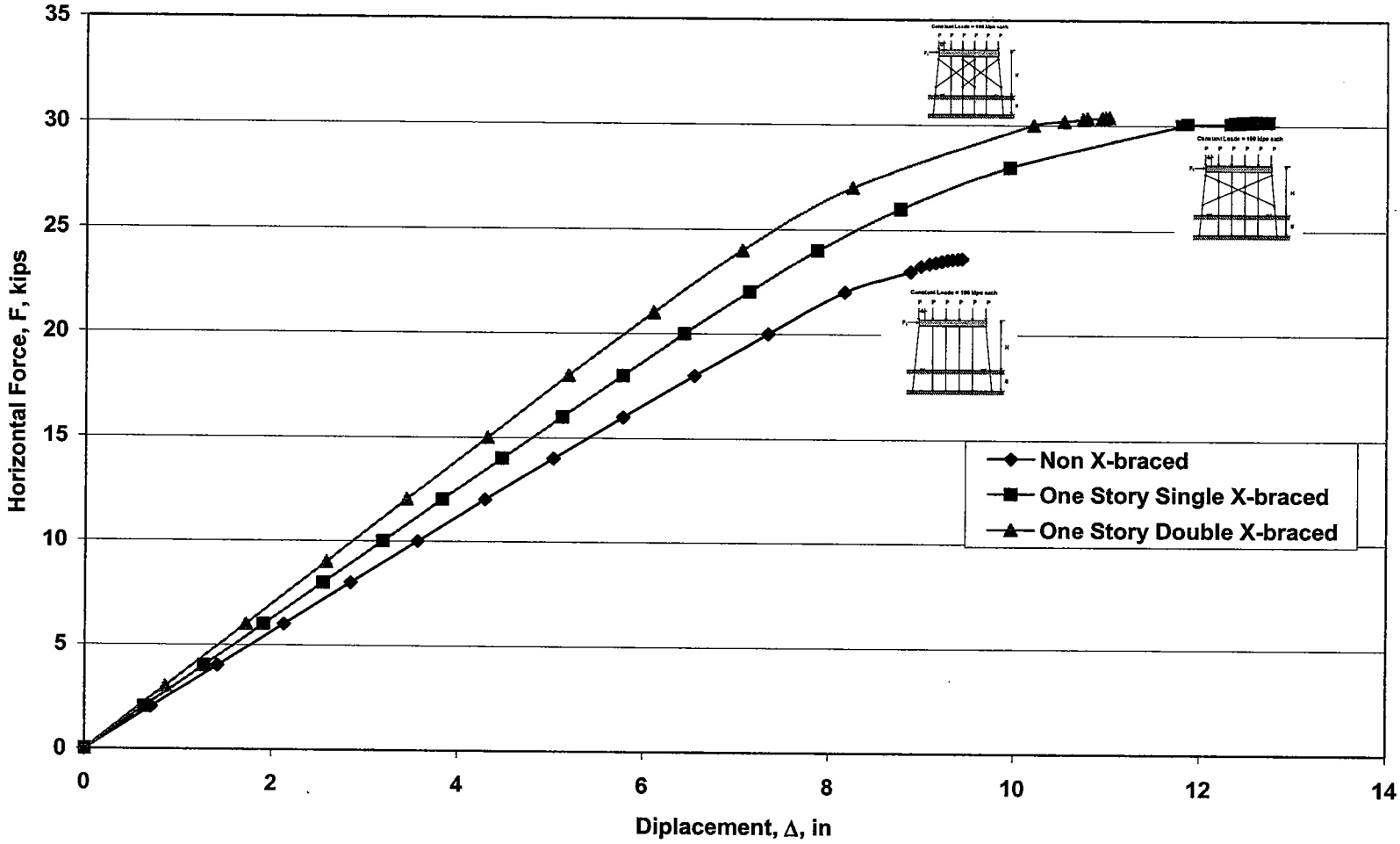

Figure 8.22d. GTSTRUDL Pushover Analysis for HP10x42 6-Pile Bents, Bents Pinned at Ground, H=13ft, S=15ft

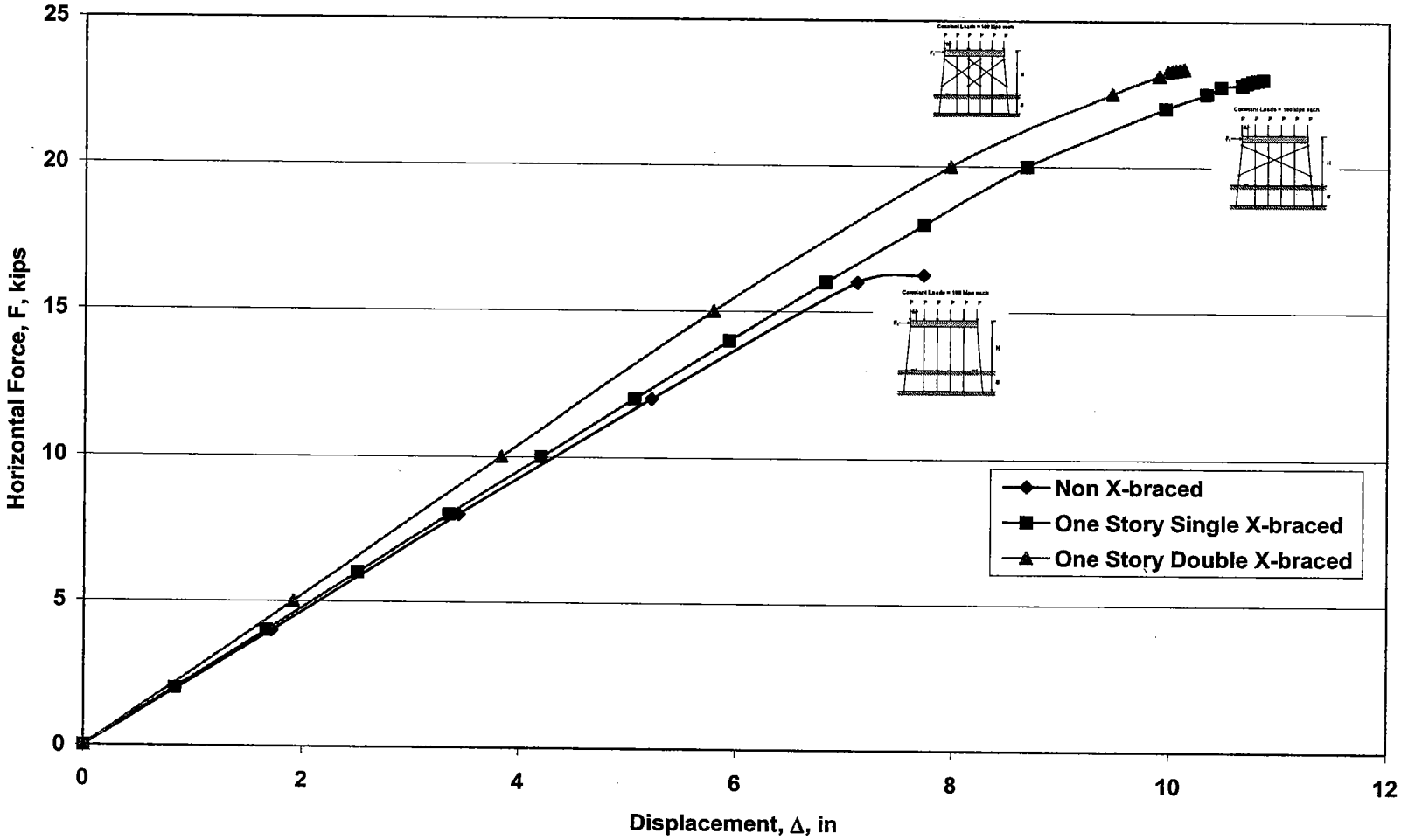

Figure 8.22e. GTSTRUDL Pushover Analysis for HP10x42 6-Pile Bents, Bents Pinned at Ground, H=13ft, S=20ft

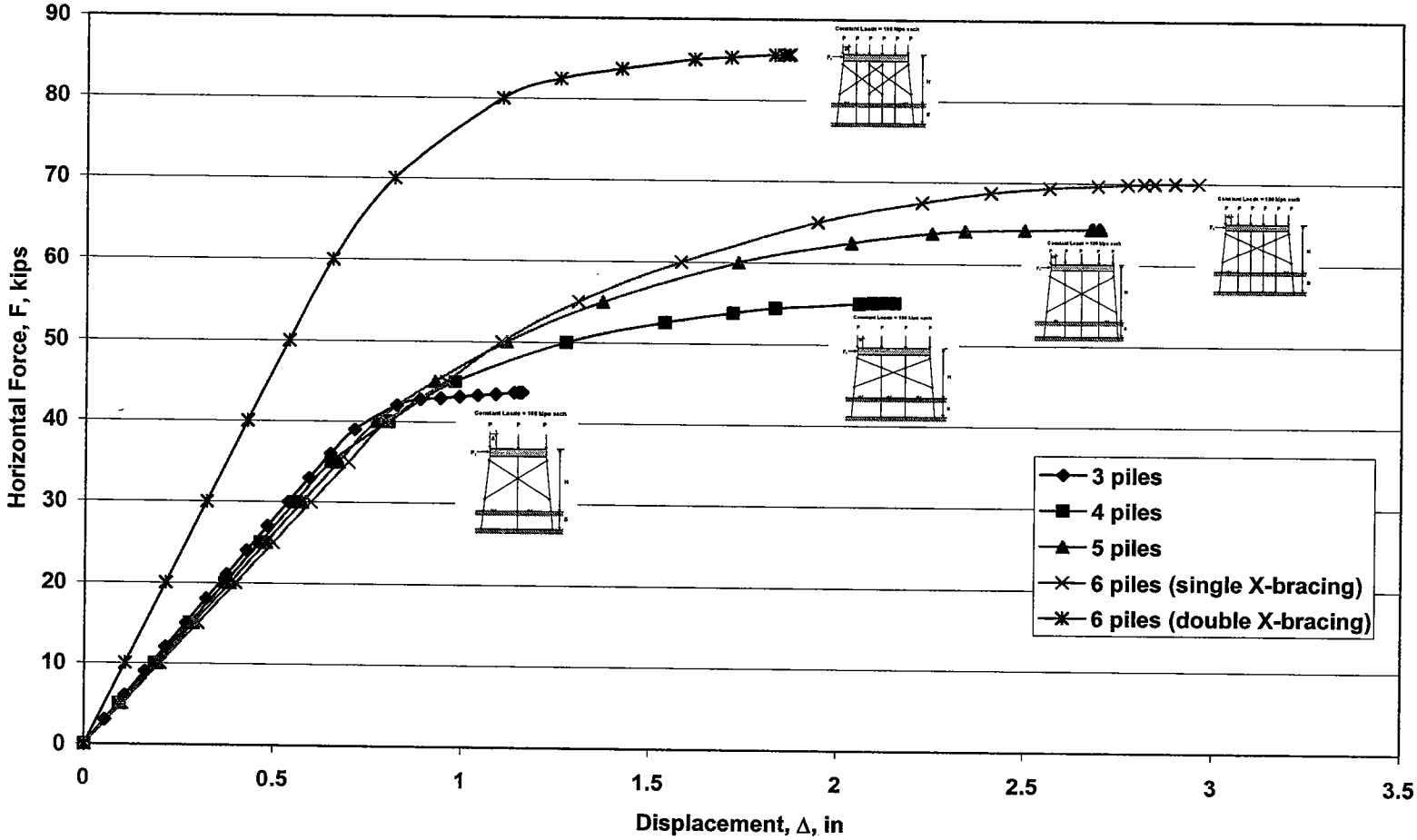

Figure 8.23a. GTSTRUDL Pushover Analysis for HP10x42 One Story X-Braced Pile Bents With Different Numbers of Piles, Bents Pinned at Base, H=13ft, S=0ft

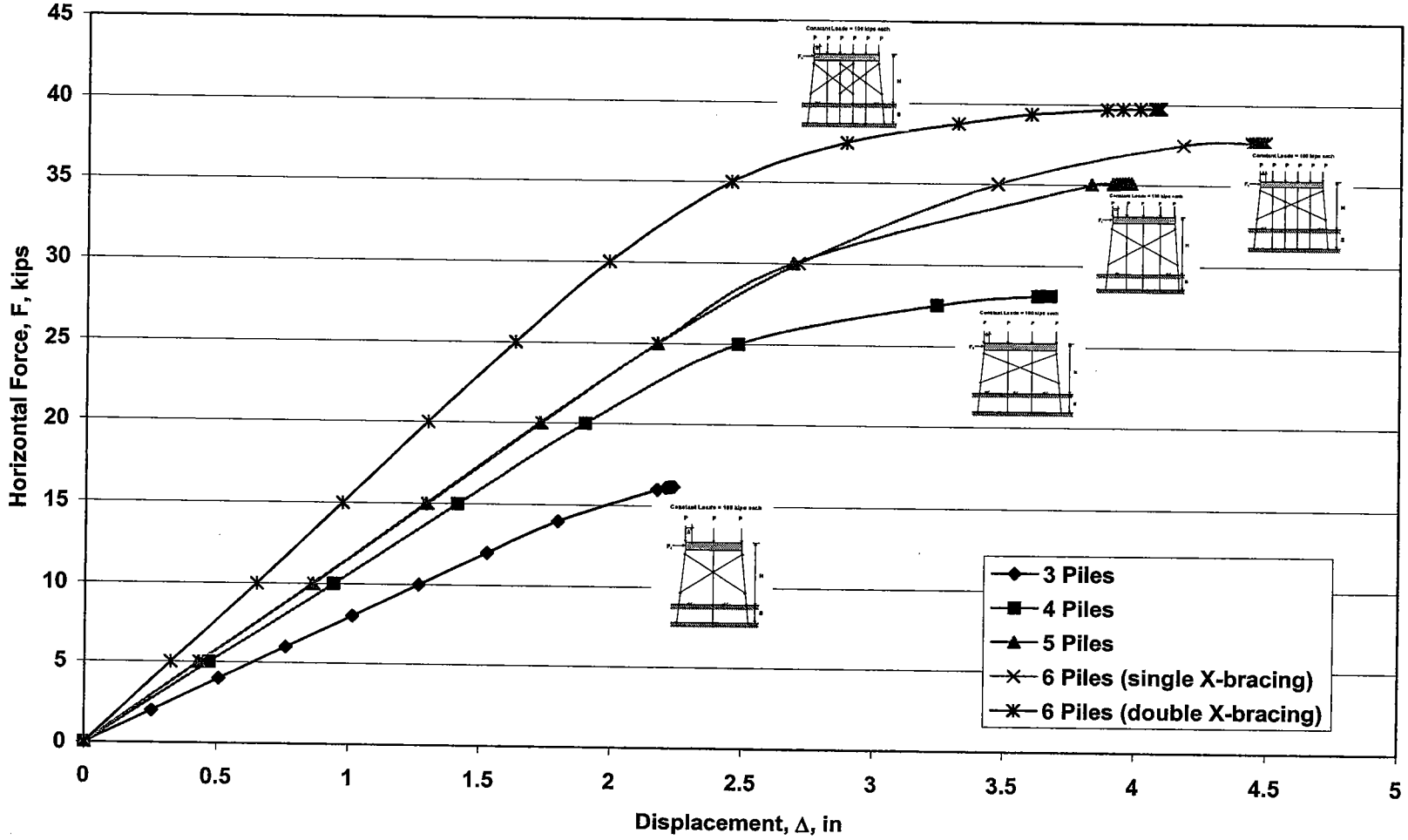

Figure 8.23b. GTSTRUDL Pushover Analysis for HP10x42 One Story X-Braced Pile Bents With Different Numbers of Piles, Bents Pinned at Base, H=13ft, S=5ft

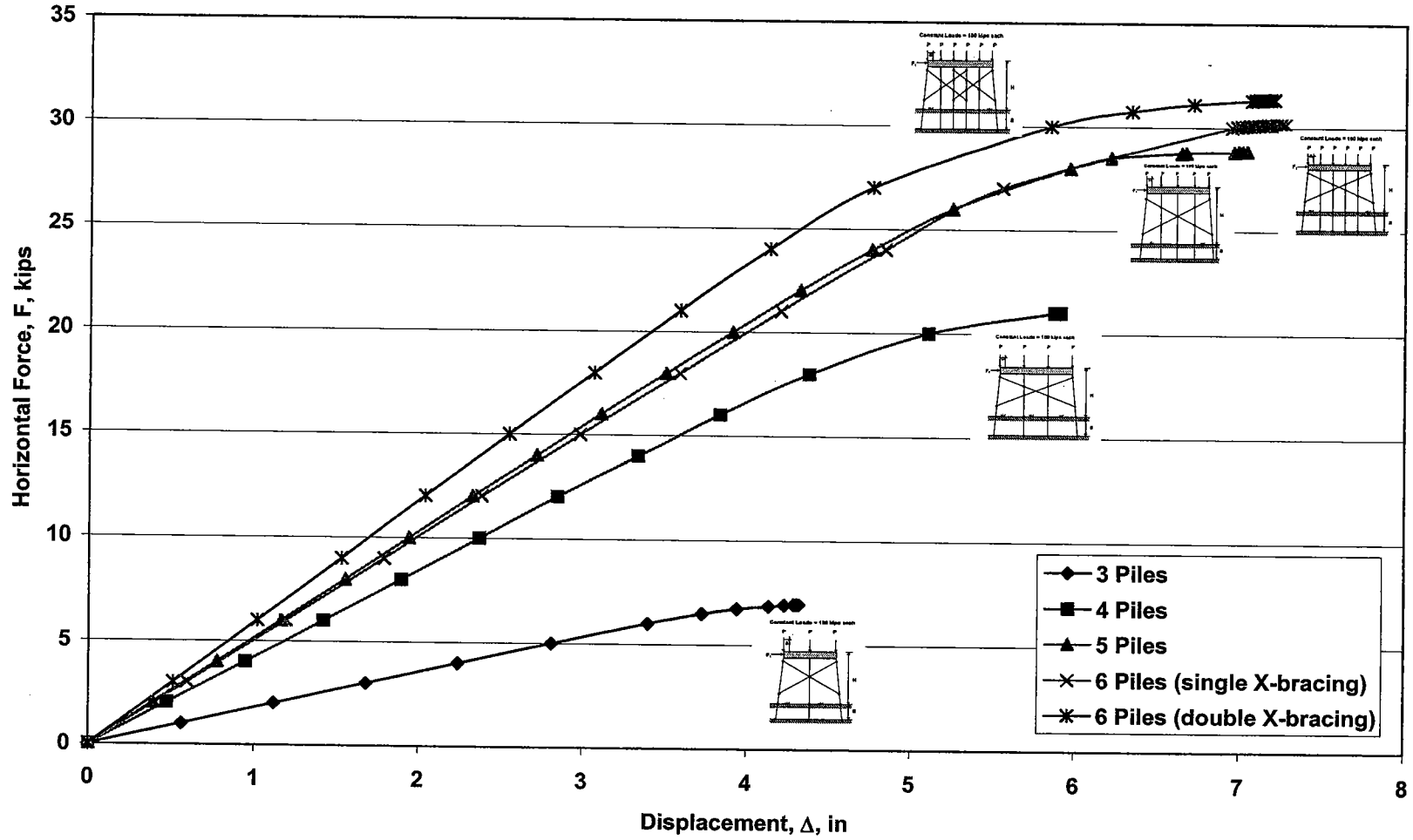

Figure 8.23c. GTSTRUDL Pushover Analysis for HP10x42 One Story X-Braced Pile Bents With Different Numbers of Piles, Bents Pinned at Base, H=13ft, S=10ft

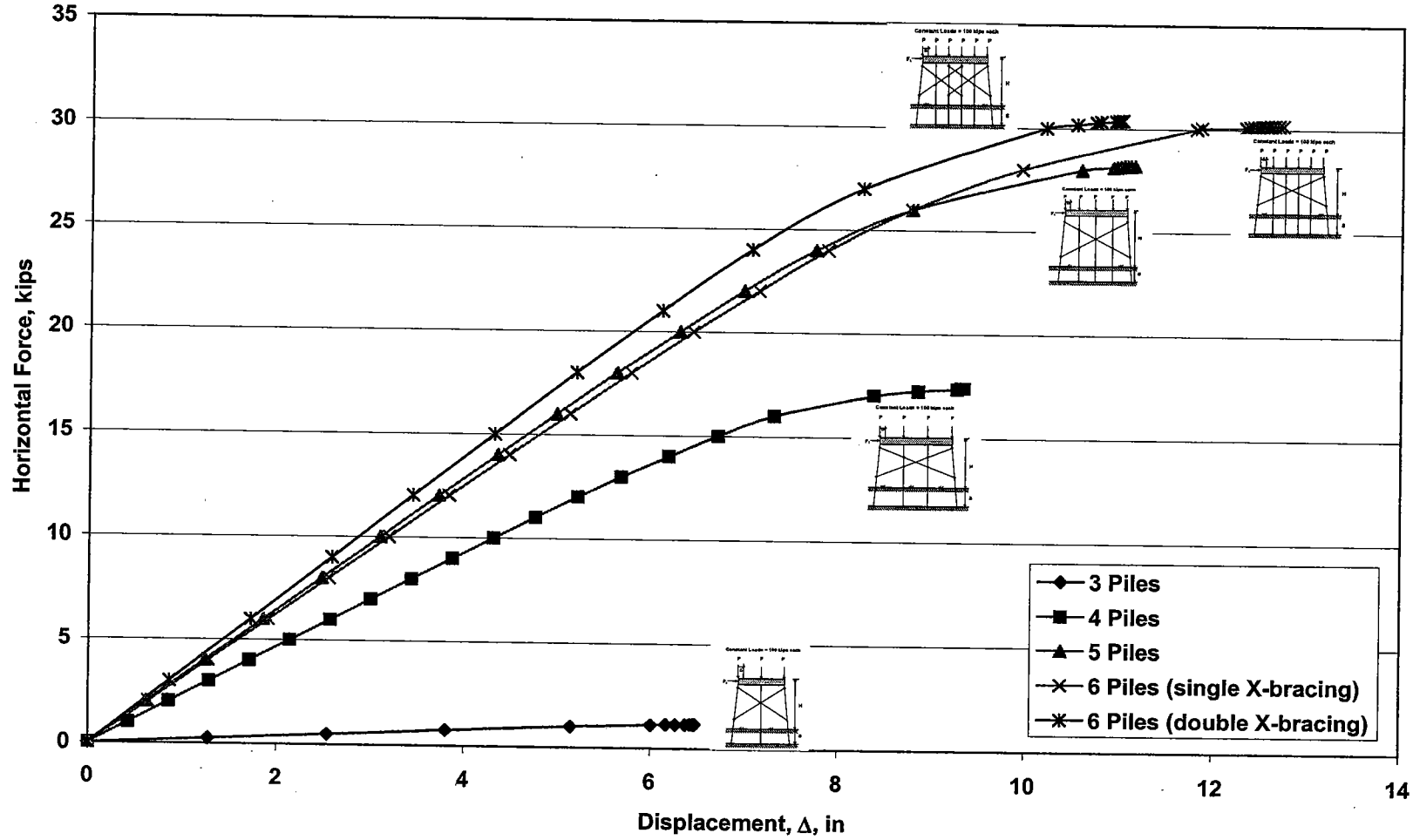

Figure 8.23d. GTSTRUDL Pushover Analysis for HP10x42 One Story X-Braced Pile Bents With Different Numbers of Piles, Bents Pinned at Base, H=13ft, S=15ft

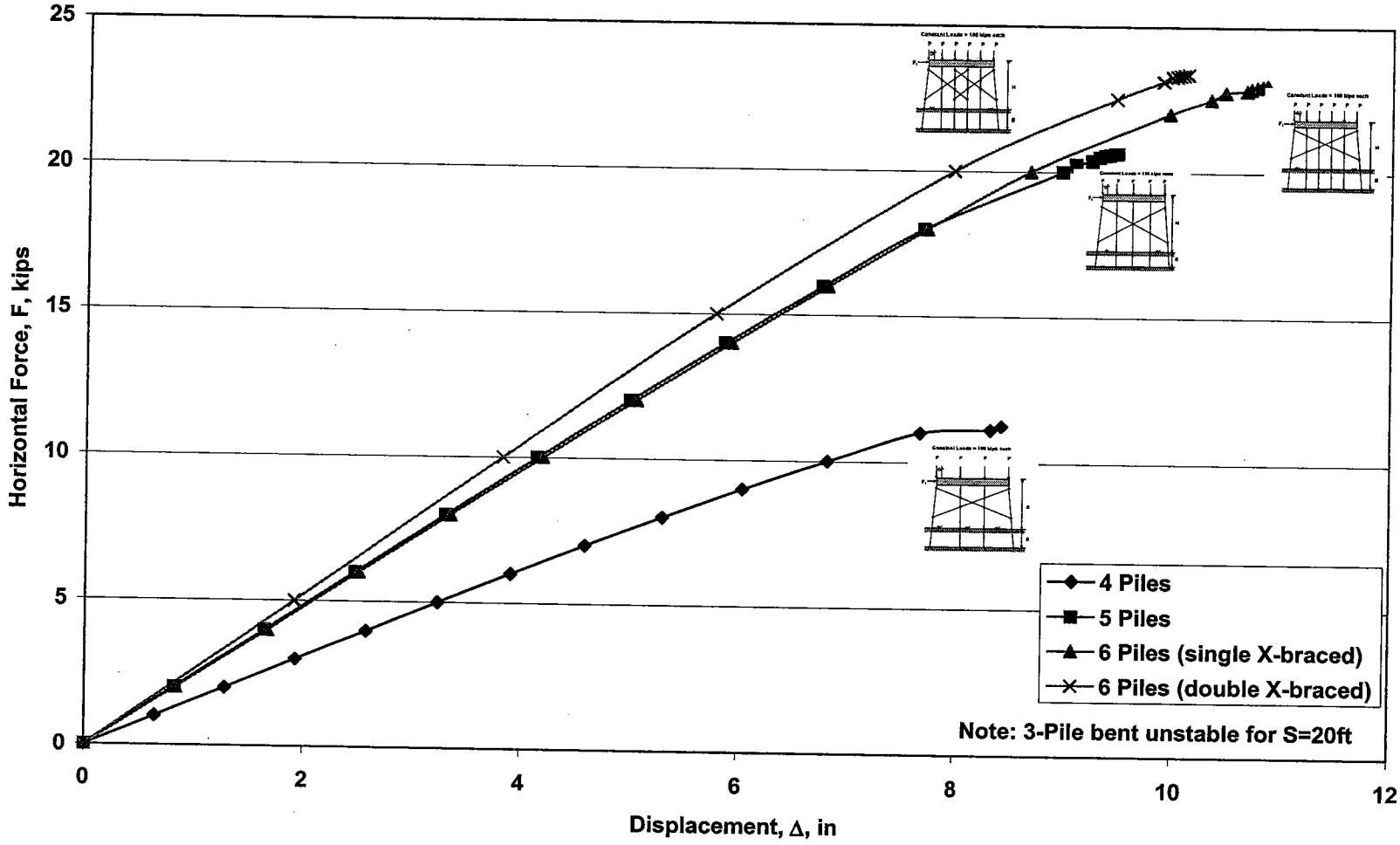

Figure 8.23e. GTSTRUDL Pushover Analysis for HP10x42 One Story X-Braced Pile Bents With Different Numbers of Piles, Bents Pinned at Base, H=13ft, S=20ft

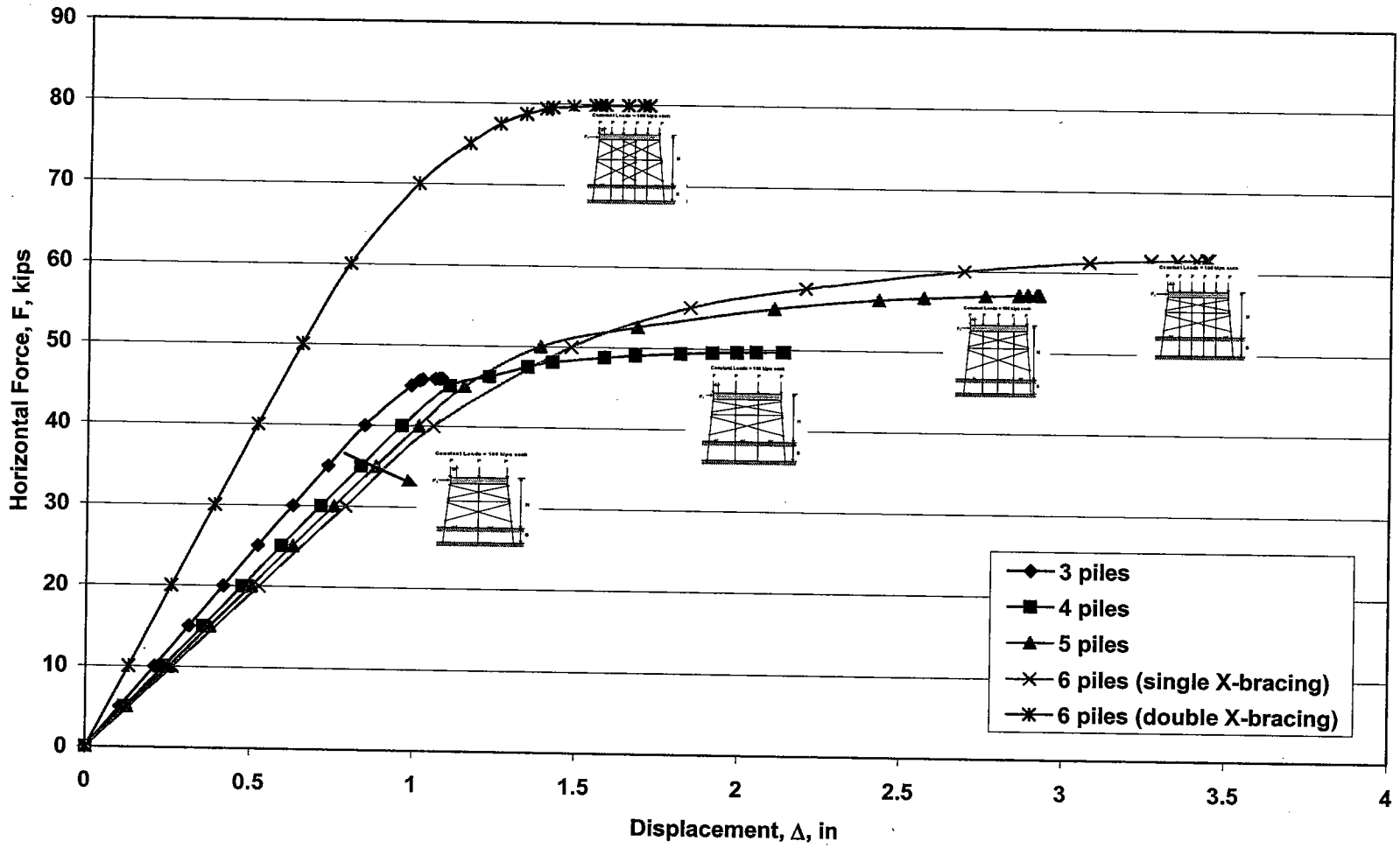

Figure 8.24a. GTSTRUDL Pushover Analysis for HP10x42 Two Story X-Braced Pile Bents With Different Numbers of Piles, Pinned at Base, H=25ft, S=0ft

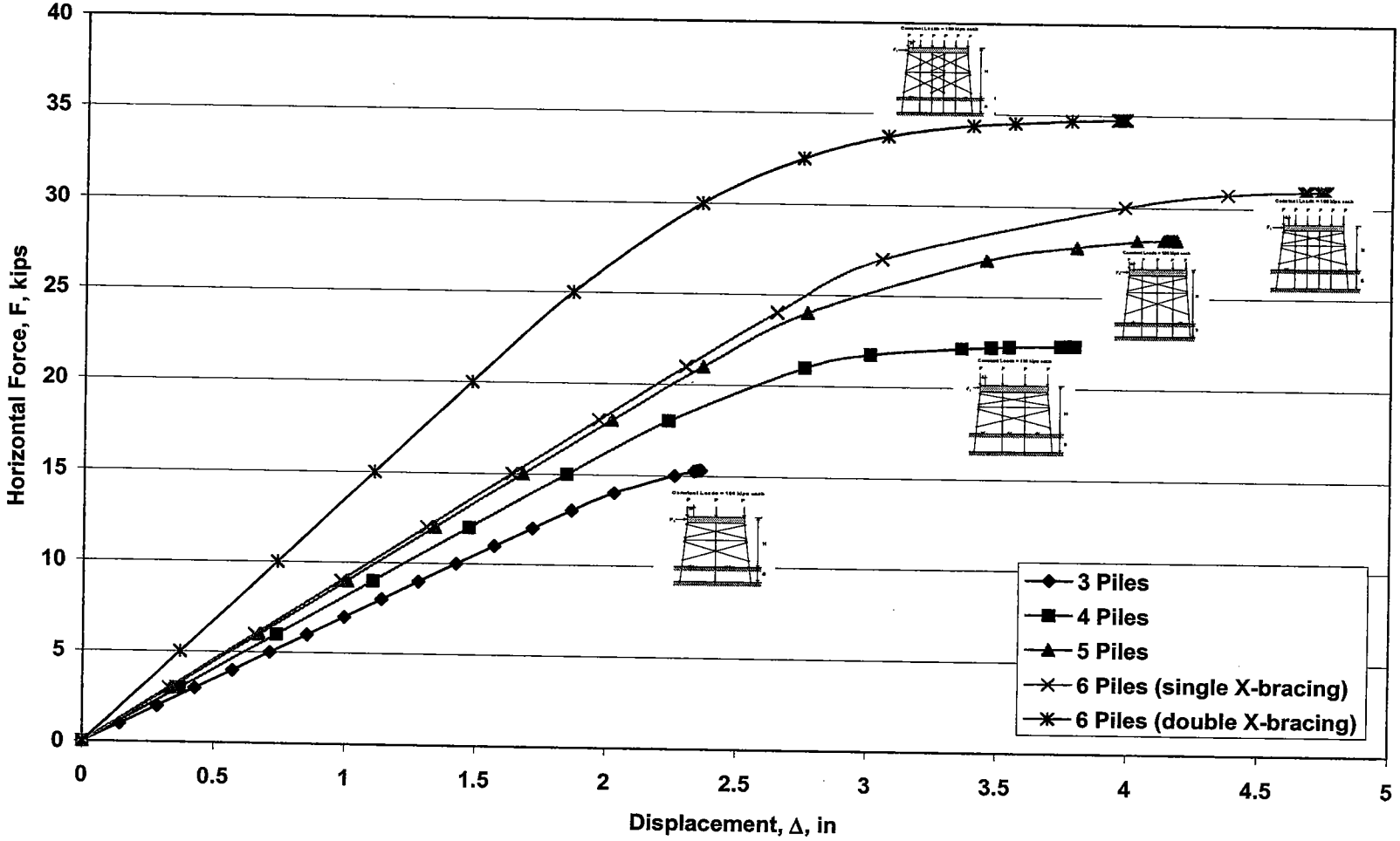

Figure 8.24b. GTSTRUDL Pushover Analysis for HP10x42 Two Story X-Braced Pile Bents With Different Numbers of Piles, Pinned at Base, H=25ft, S=5ft

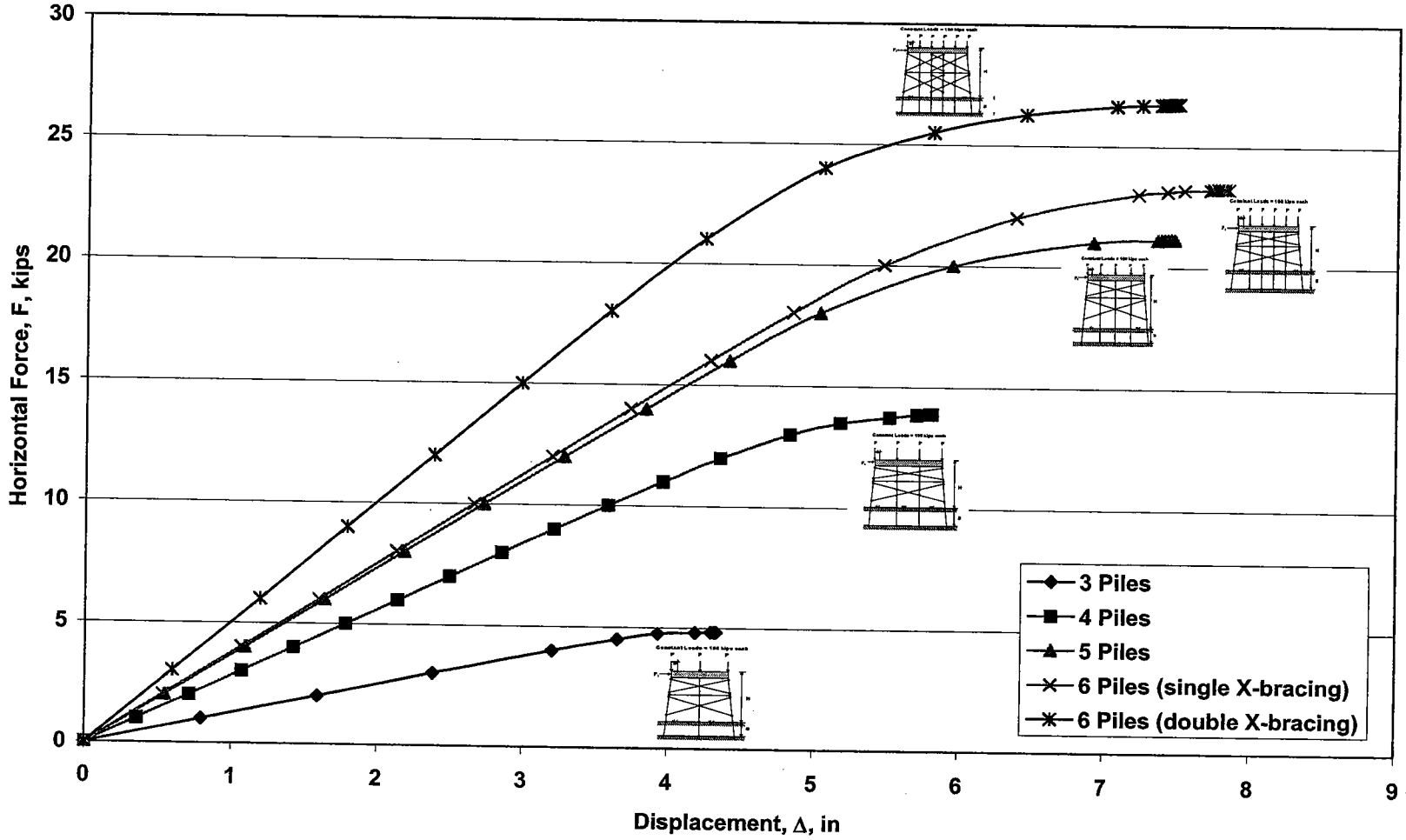

Figure 8.24c. GTSTRUDL Pushover Analysis for HP10x42 Two Story X-Braced Pile Bents With Different Numbers of Piles, Pinned at Base, H=25ft, S=10ft

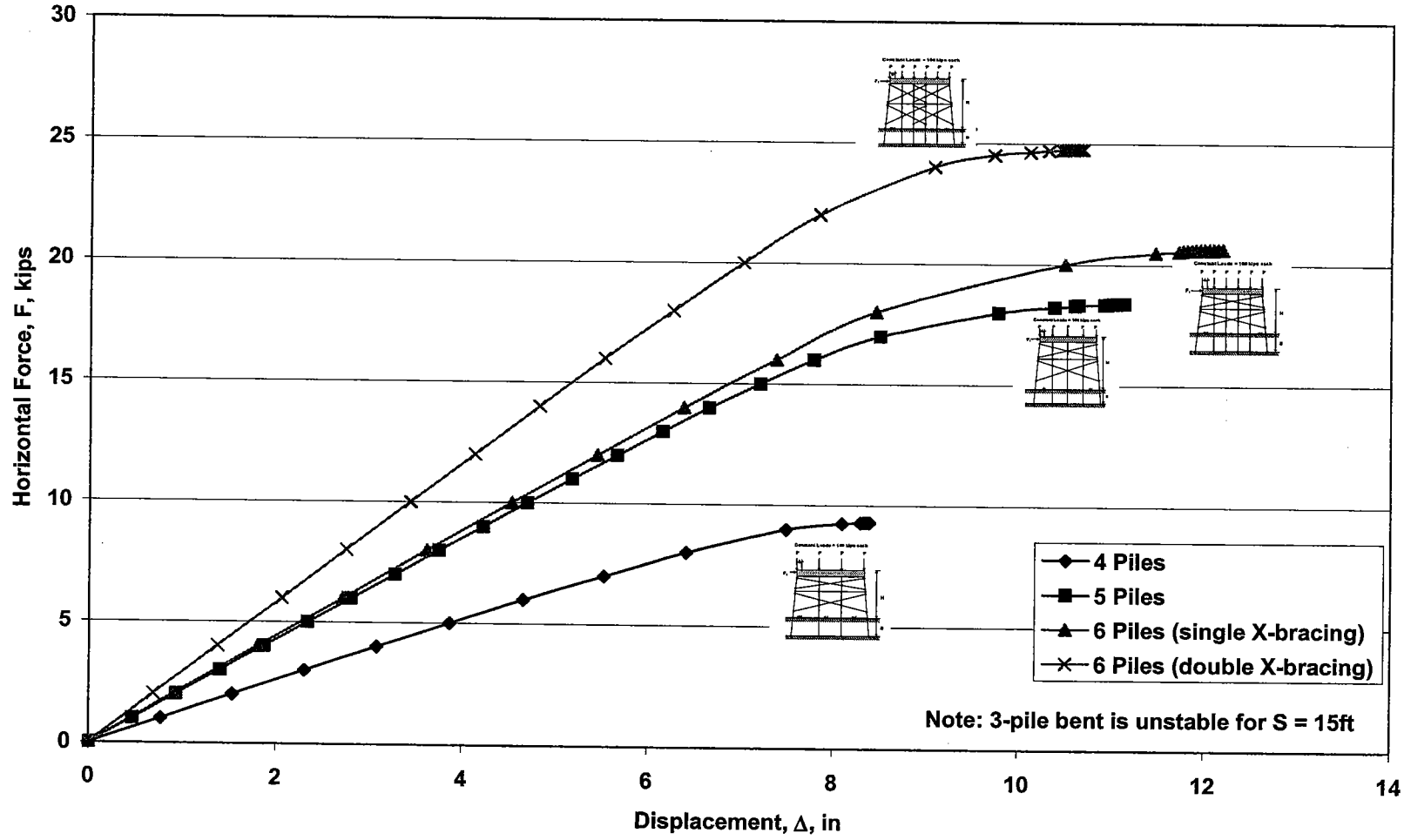

Figure 8.24d. GTSTRUDL Pushover Analysis for HP10x42 Two Story X-Braced Pile Bents With Different Numbers of Piles, Pinned at Base, H=25ft, S=15ft

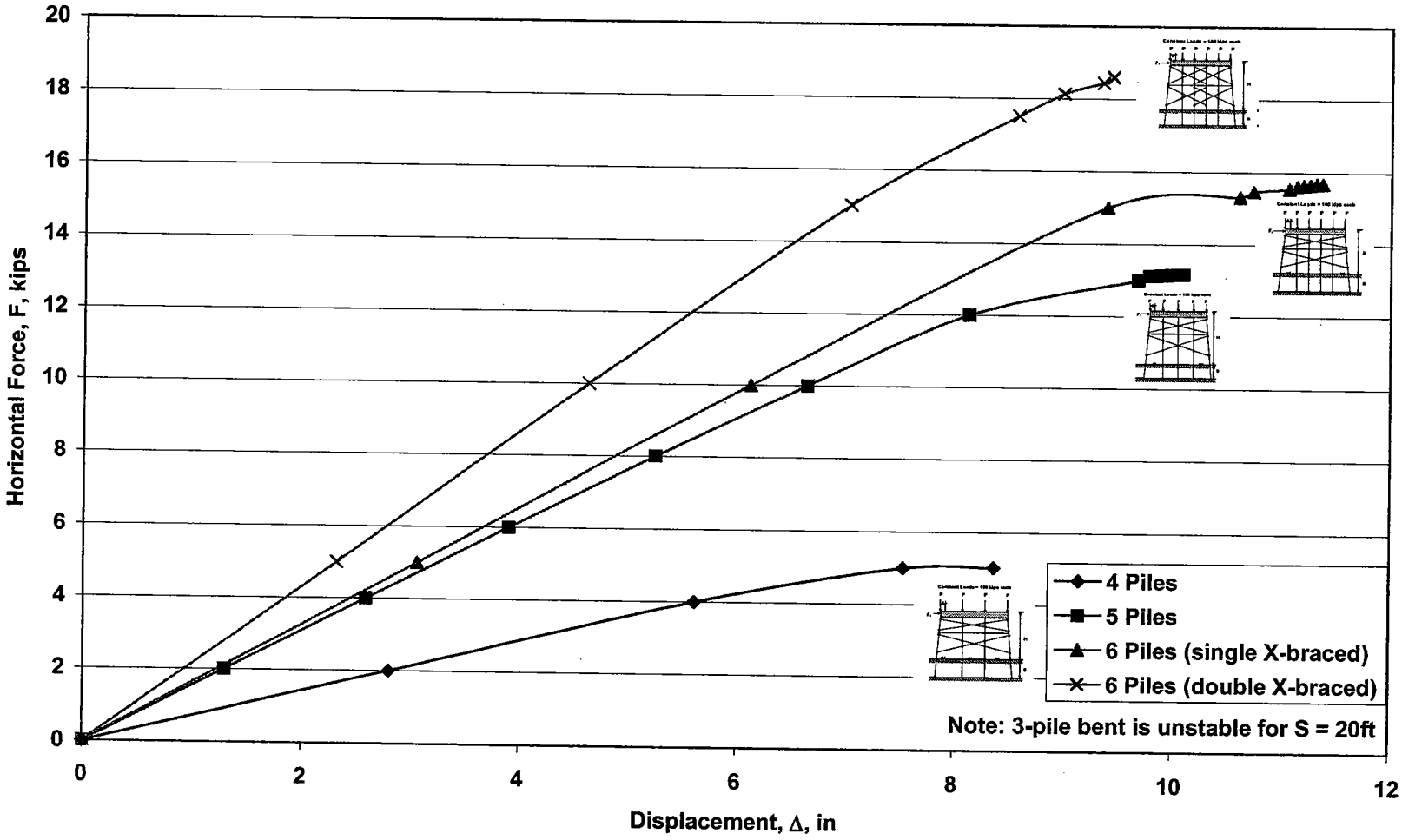

Figure 8.24e. GTSTRUDL Pushover Analysis for HP10x42 Two Story X-Braced Pile Bents With Different Numbers of Piles, Pinned at Base, H=25ft, S=20ft

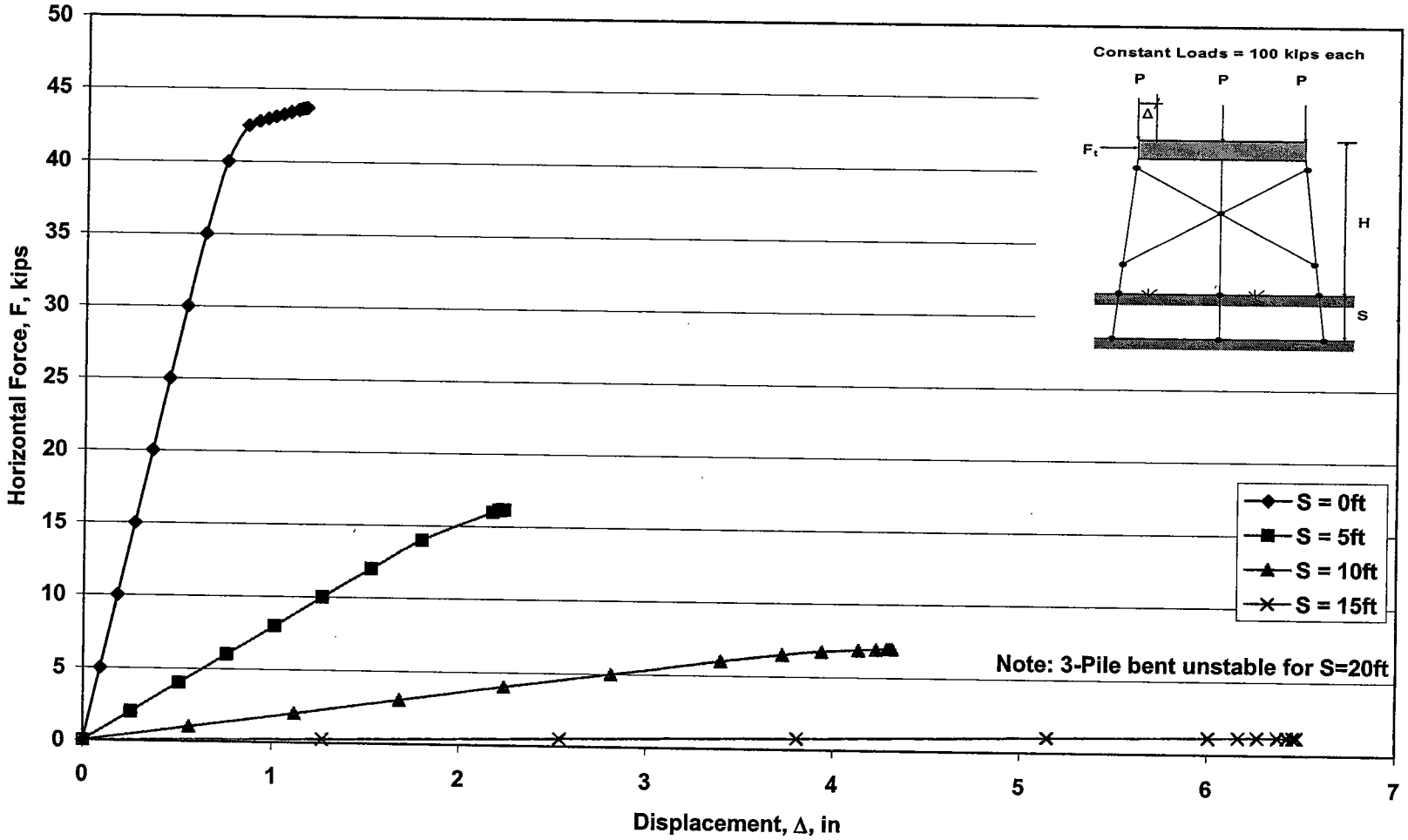

Figure 8.25. GTSTRUDL Pushover Analysis For HP 10x42 3-Pile One Story X-braced Bents Subjected to Scour, H = 13ft

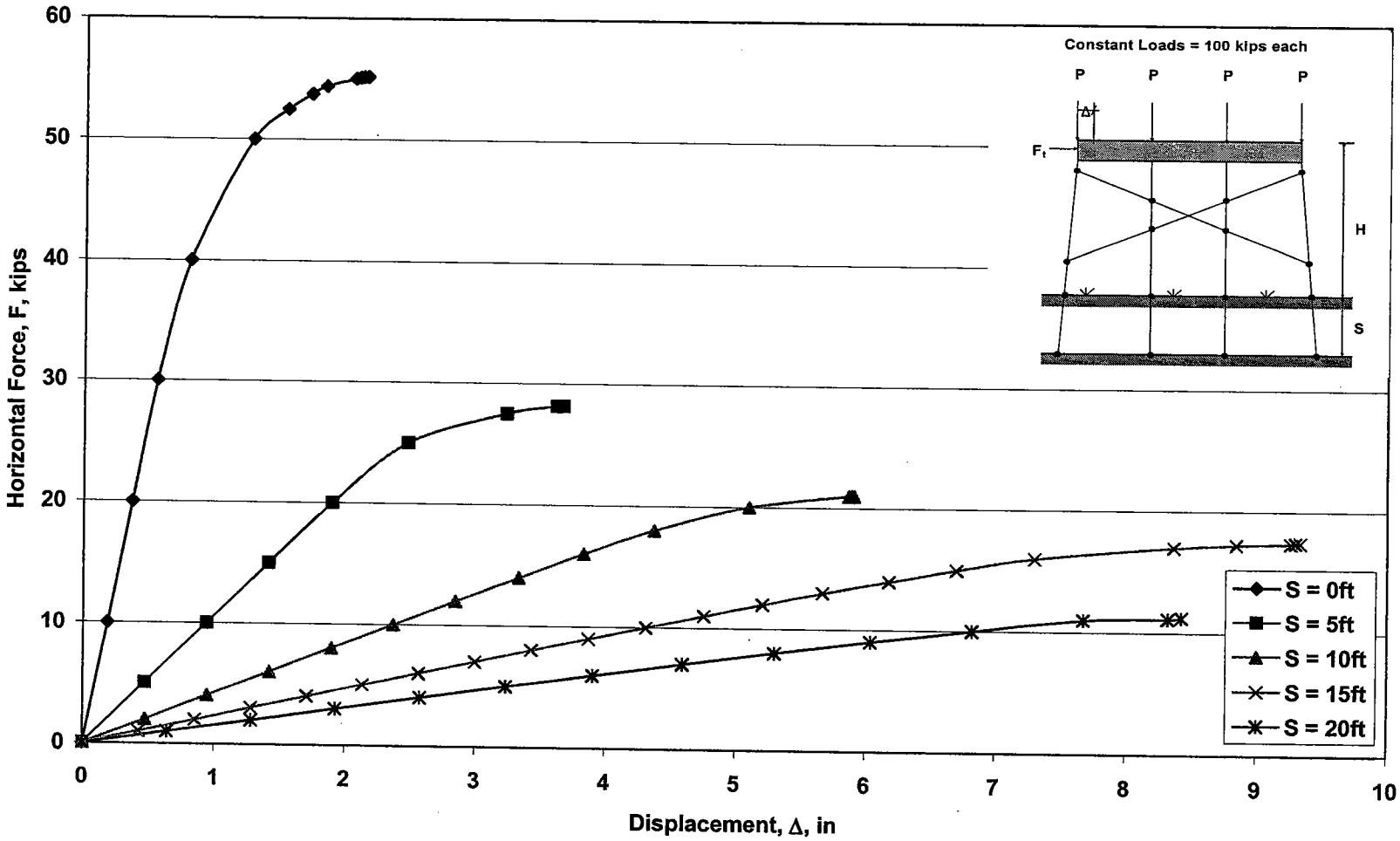

Figure 8.26. GTSTRUDL Pushover Analysis For HP 10x42 4-Pile One Story X-braced Bents Subjected to Scour, H = 13ft

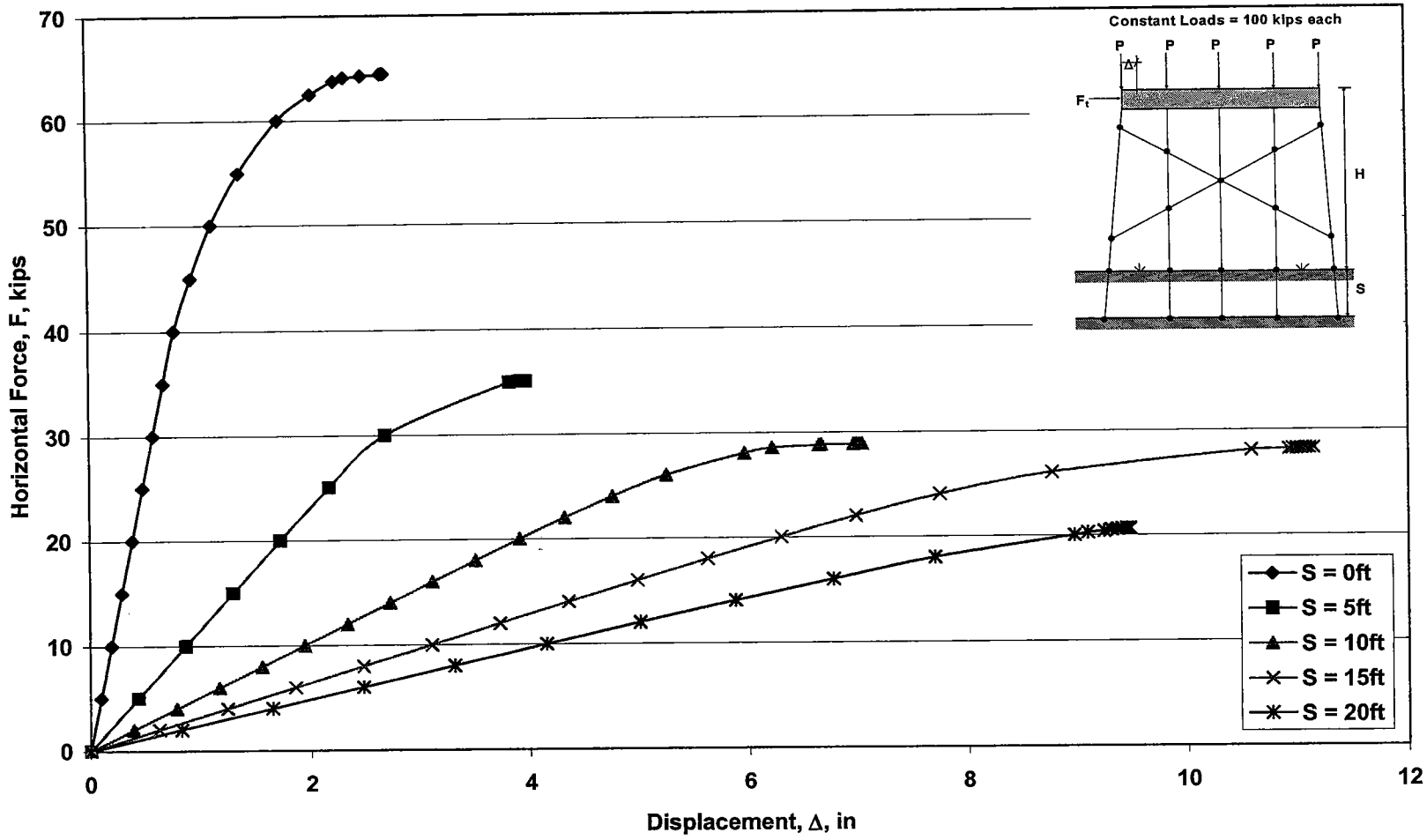

Figure 8.27. GTSTRUDL Pushover Analysis For HP 10x42 5-Pile One Story X-braced Bents Subjected to Scour, H = 13ft

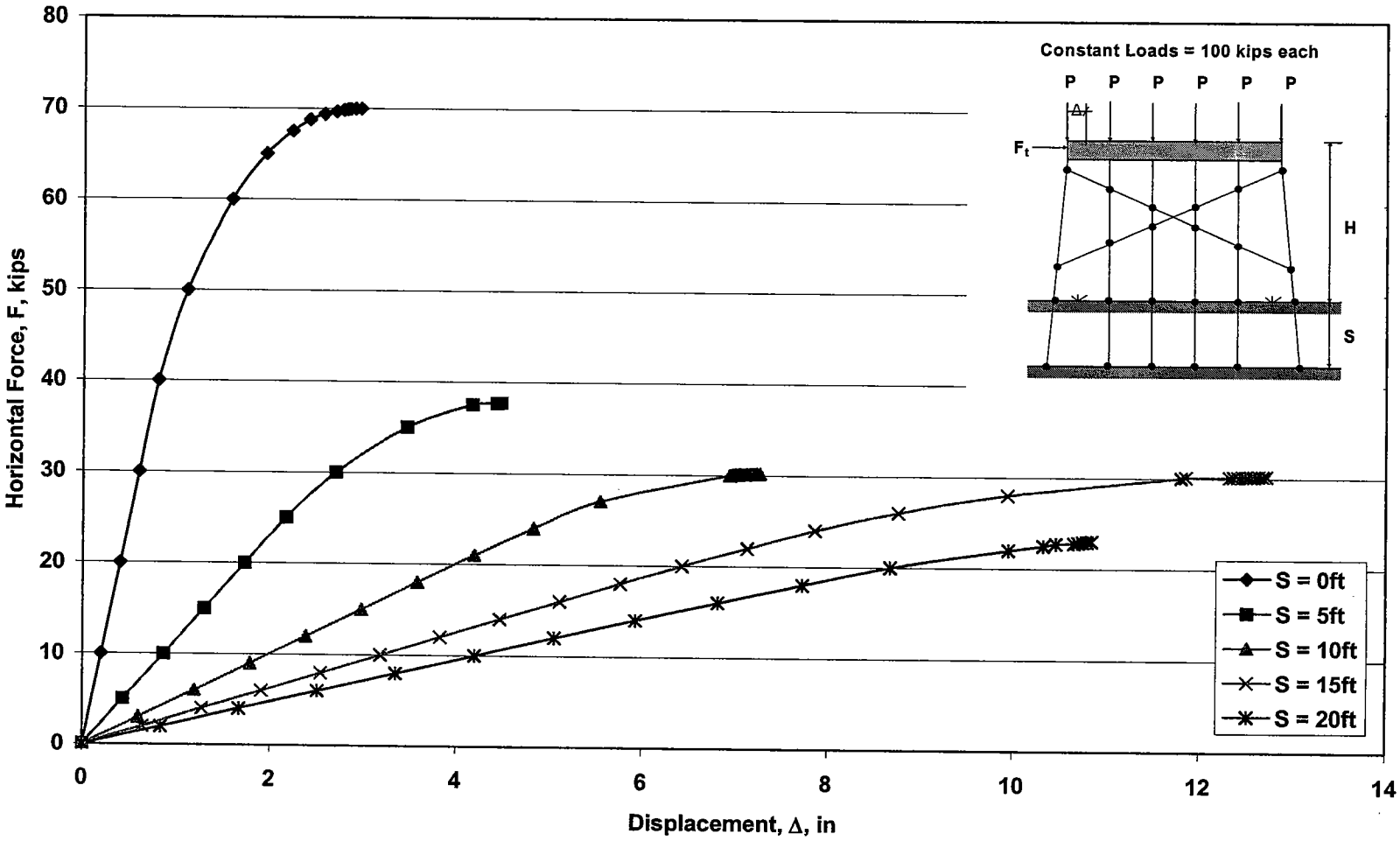

Figure 8.28. GTSTRUDL Pushover Analysis For HP 10x42 6-Pile One Story Single X-braced Bents Subjected to Scour, H = 13ft

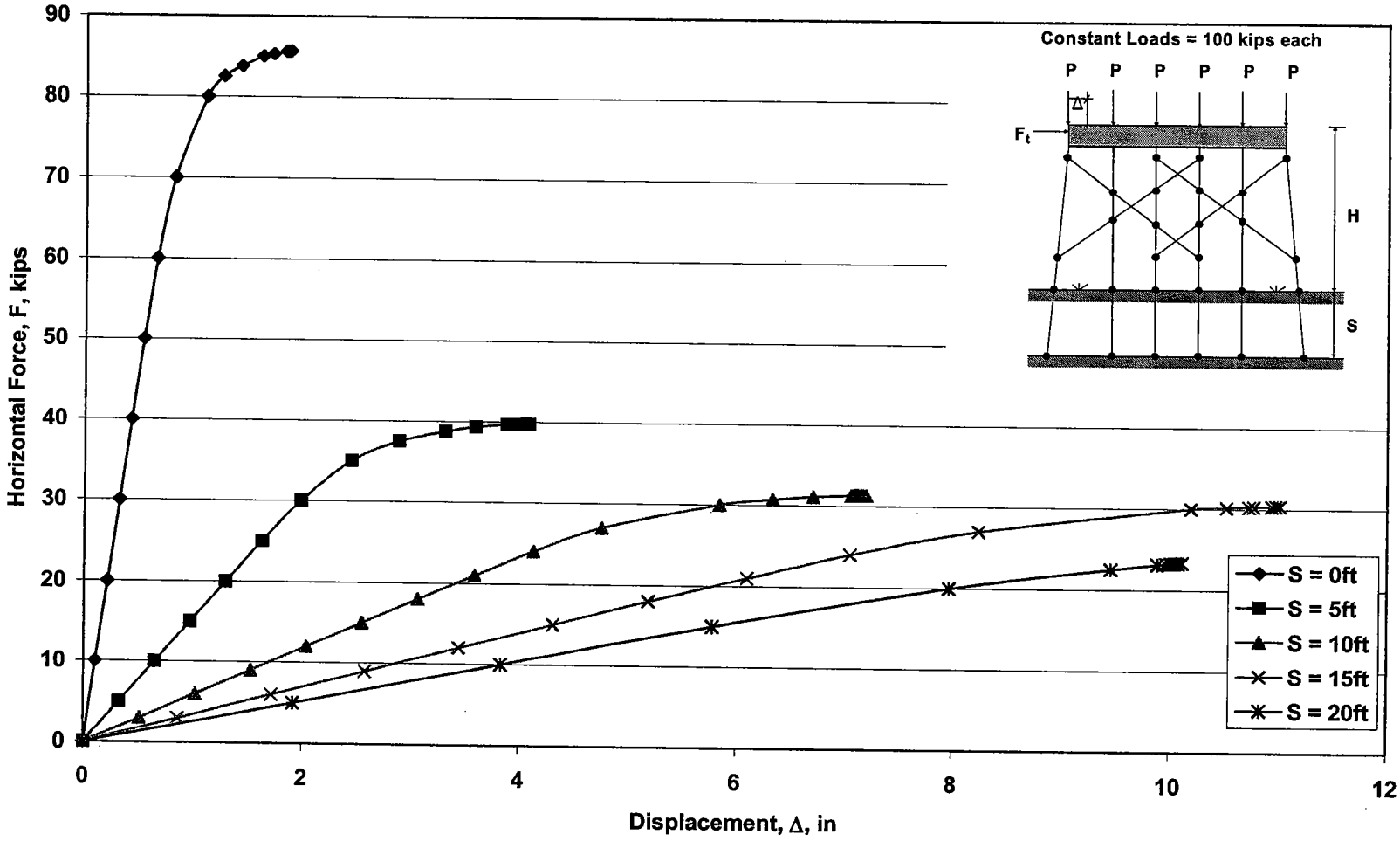

Figure 8.29. GTSTRUDL Pushover Analysis For HP 10x42 6-Pile One Story Double X-braced Bents Subjected to Scour, H = 13ft

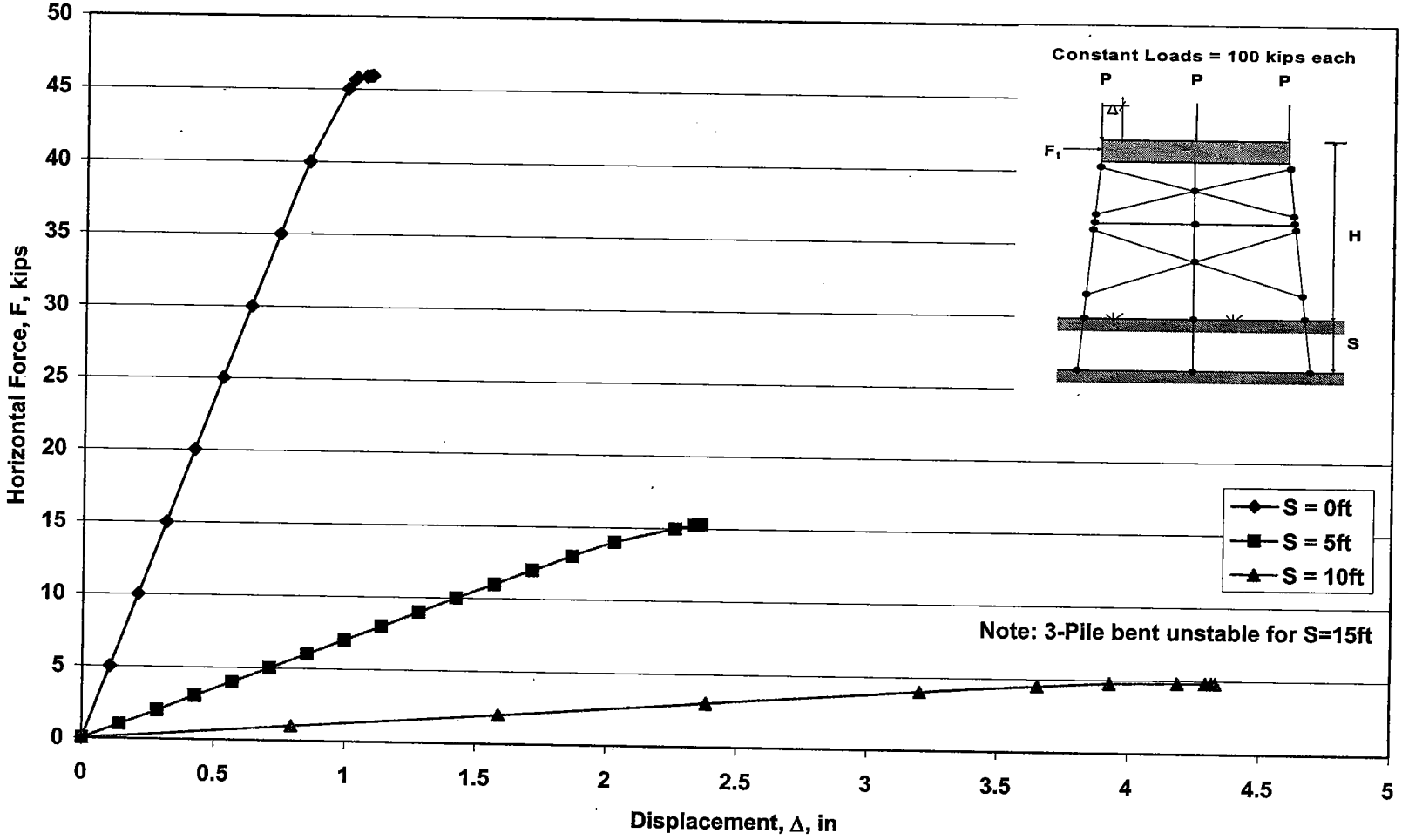

Figure 8.30. GTSTRUDL Pushover Analysis For HP 10x42 3-Pile Two Story X-braced Bents Subjected to Scour, H = 25ft

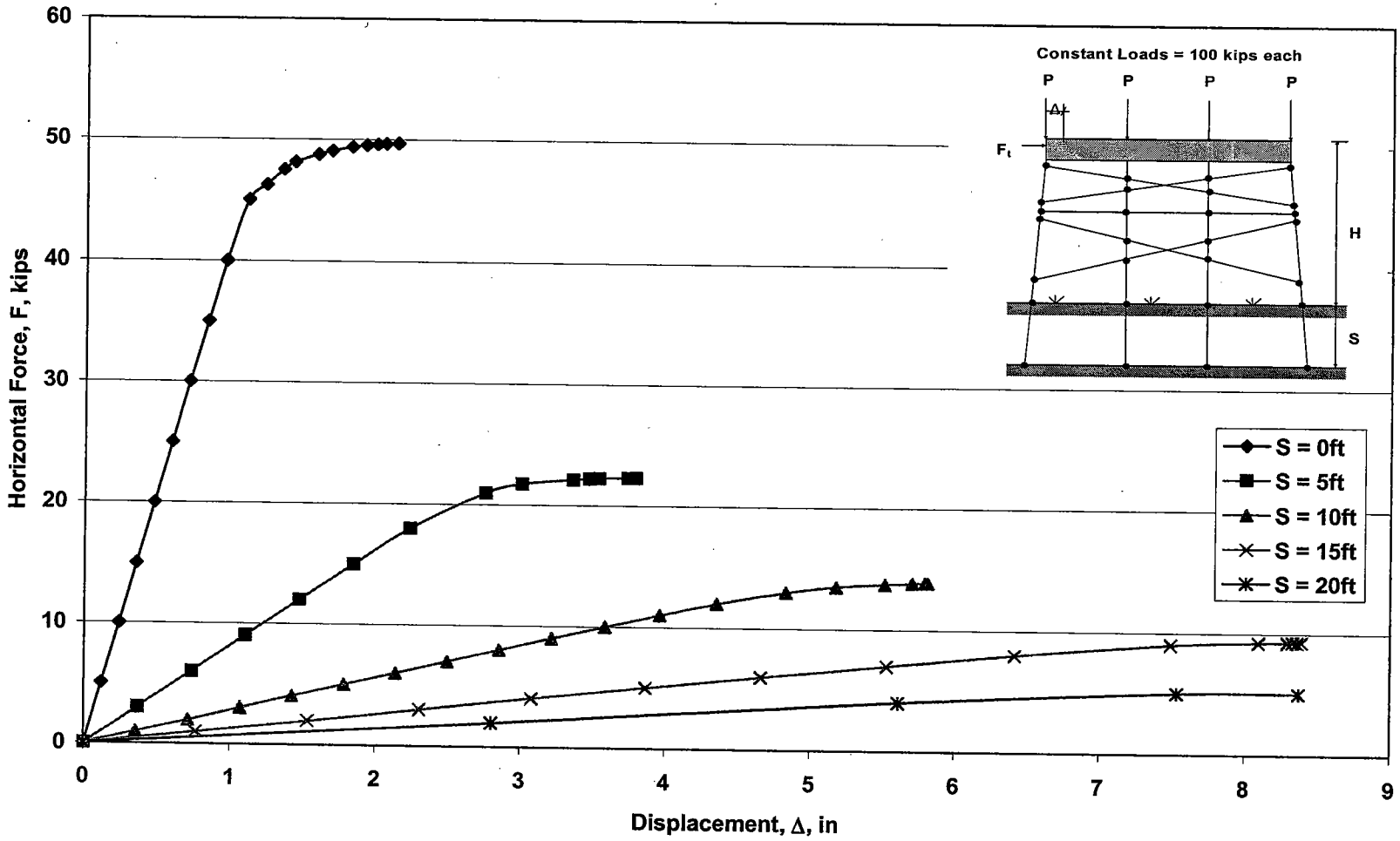

Figure 8.31. GTSTRUDL Pushover Analysis For HP 10x42 4-Pile Two Story X-braced Bents Subjected to Scour, H = 25ft

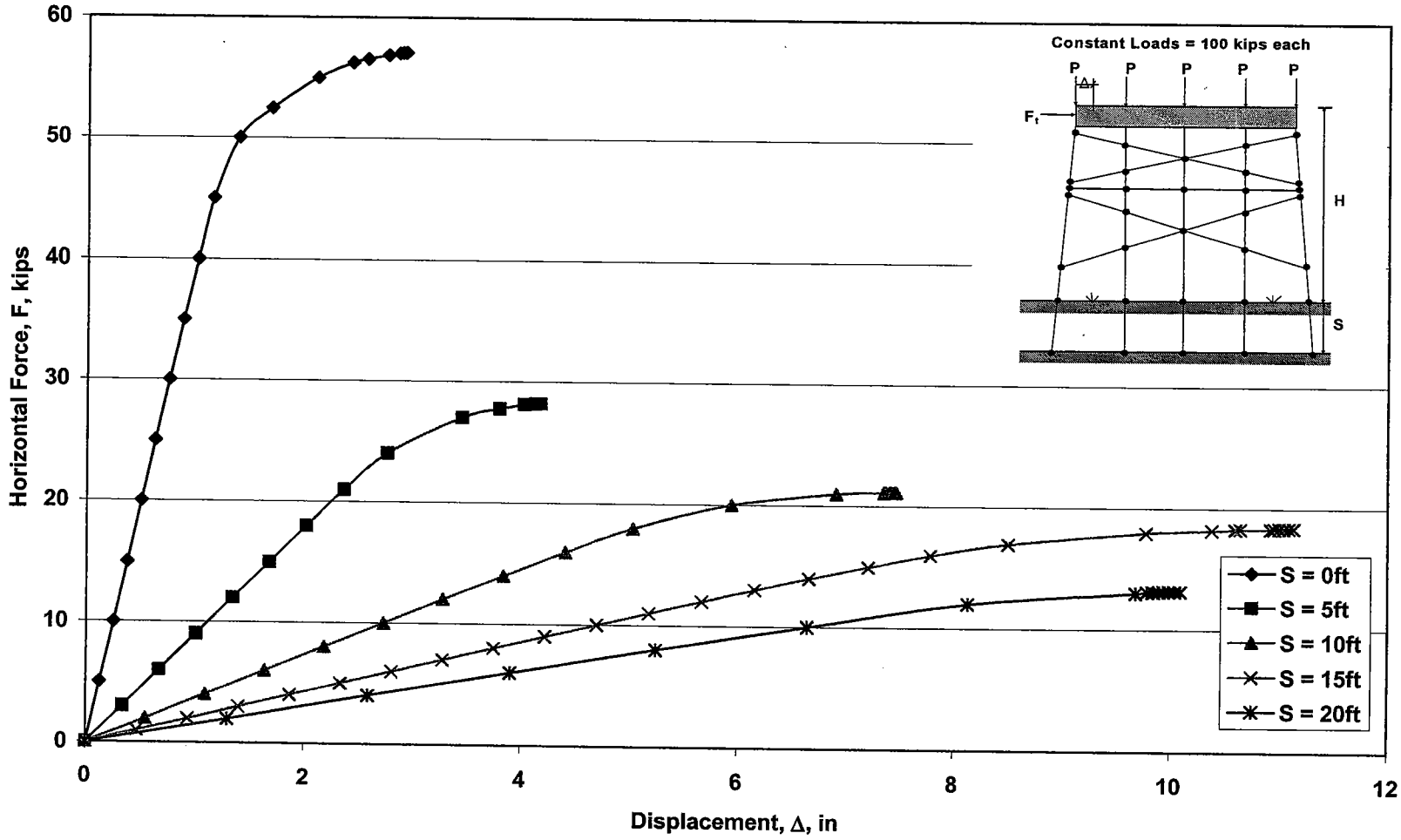

Figure 8.32. GTSTRUDL Pushover Analysis For HP 10x42 5-Pile Two Story X-braced Bents Subjected to Scour, H = 25ft

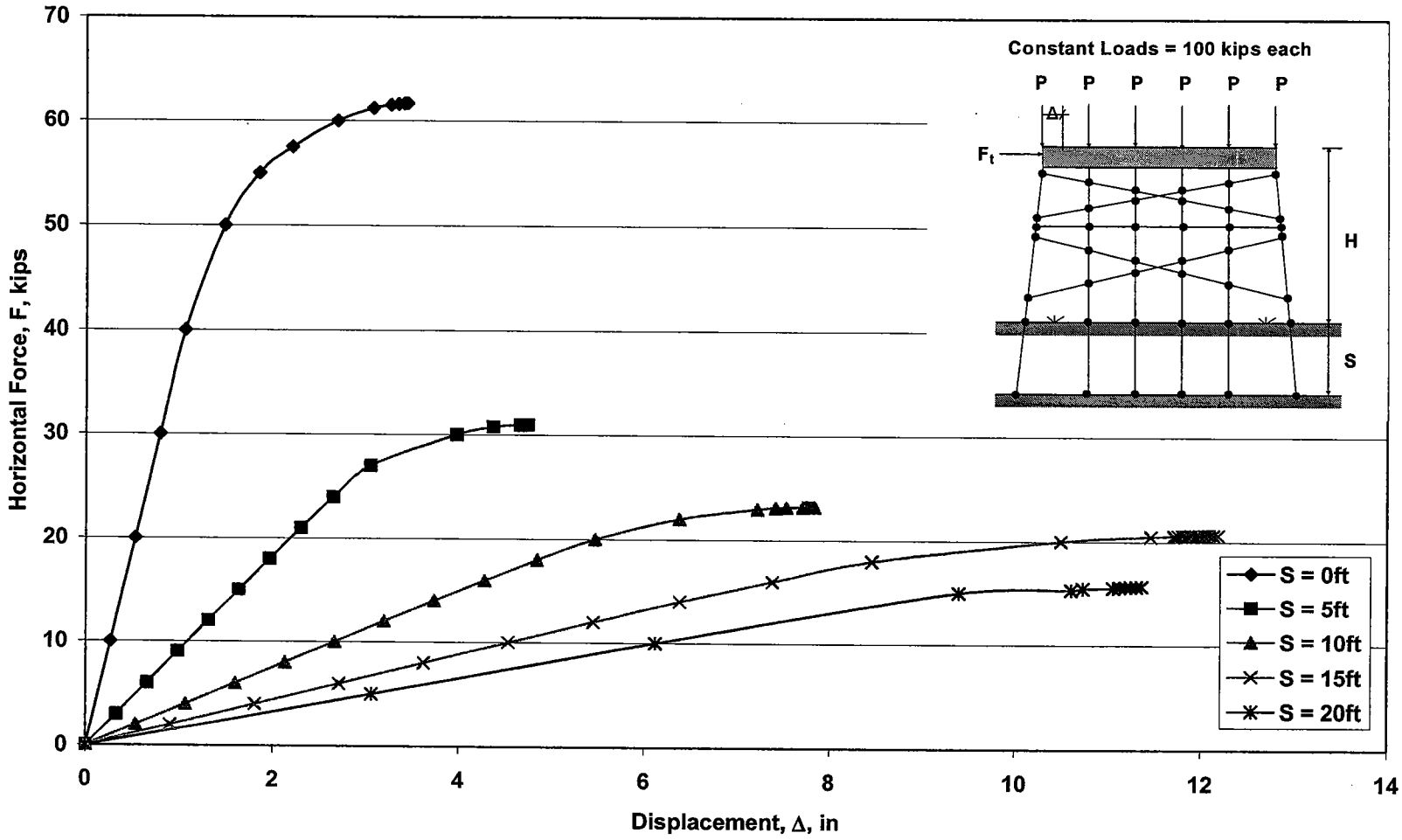

Figure 8.33. GTSTRUDL Pushover Analysis For HP 10x42 6-Pile Two Story Single X-braced Bents Subjected to Scour, H = 25ft

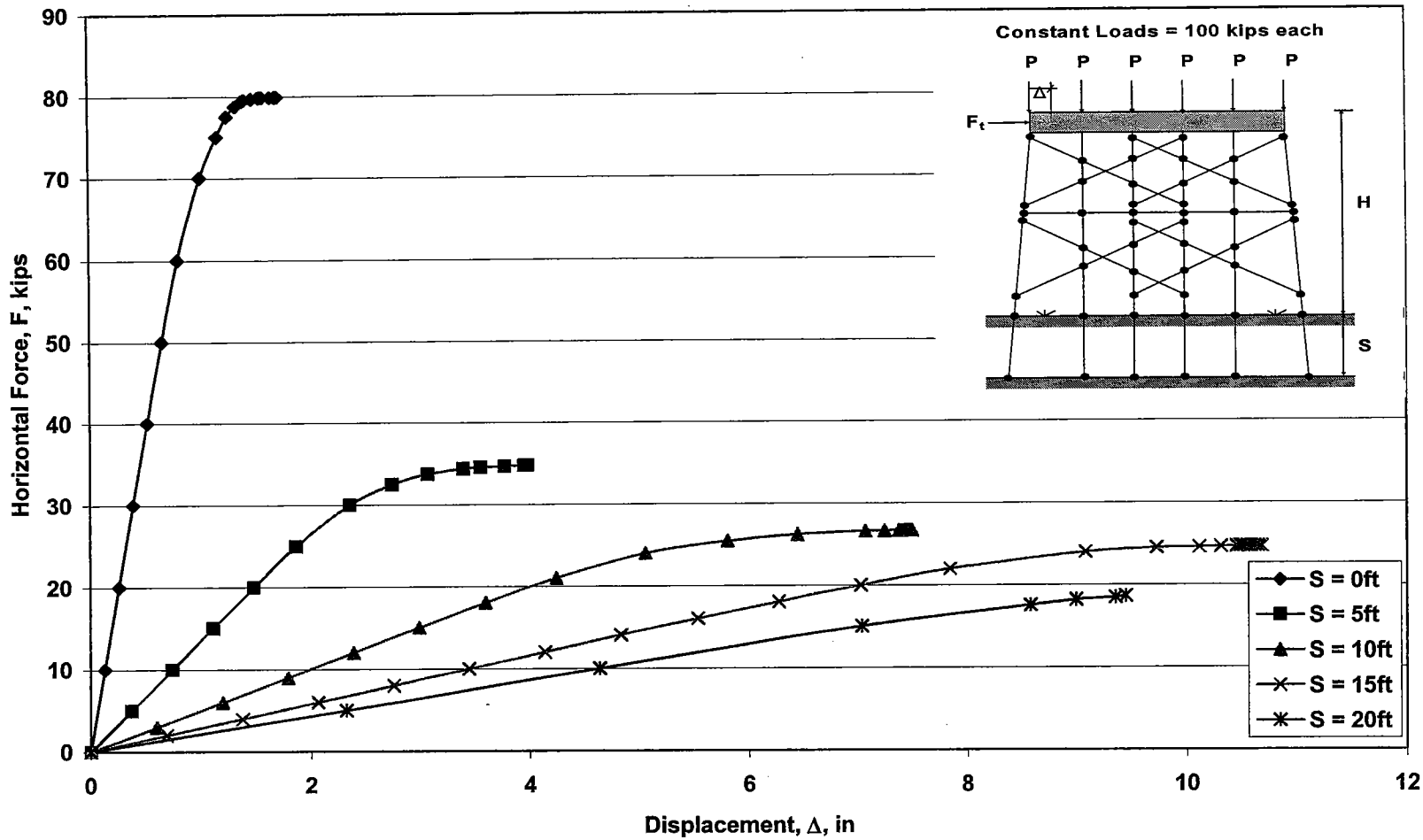

Figure 8.34. GTSTRUDL Pushover Analysis For HP 10x42 6-Pile Two Story Double X-braced Bents Subjected to Scour, H = 25ft

CHAPTER 9: CONCLUSIONS AND RECOMMENDATIONS

9.1 General

During major flood/scour events, it appears that buckling of bridge pile bents in the transverse direction governs the bridge failure load from a structural stability viewpoint. Although ALDOT pile bent standards show pile bents X-braced in the transverse direction, when bent heights are less than 13ft, the X-bracing is usually omitted and replaced with a concrete encasement of the pile from 3 feet below the ground line to the underside of the bent cap. When this is done, the steel H-pile and encasement are not interlocked to act compositely and only a very light steel spiral (No. 2 bar at 12 in. pitch) is used in the encasement. Due to the lack of composite action between the concrete encasement and steel H-pile, the encasement may spall off during extreme flooding events as debris gathers around the end piles. Water currents may act on these debris rafts and impose large transverse forces on the bents. When forces are applied in the transverse direction of a pile bent, the piles are oriented so that they bend and may buckle about their weak axes. This, in combination with the fact that sidesway buckling is prevented by the superstructure in the longitudinal direction (after the expansion joints are closed), leads to the conclusion that buckling in the transverse direction and/or frame action in this direction governs the bridge failure load.

FB-Pier allows a sophisticated modeling of the pile-soil system of a pile bent and appears to be widely used by state highway agencies. However, its modeling of nonlinear behavior is not as sophisticated as the nonlinear analysis capabilities of GTSTRUDL. GTSTRUDL's pushover analysis procedure on the other hand, does not allow sophisticated modeling of soil foundations. According to H. Granholm, elastic buckling capacities of piles are quite insensitive to the properties of the soil. Thus, it appears that the GTSTRUDL modeling and pushover analysis procedure may provide an easier modeling and more accurate failure load estimation than FB-

Pier. Checking this via comparative modeling and analyses was one of the goals of this research. The most appropriate computer program and bent modeling were investigated so that these may be utilized in ALDOT's final bridge bent "screening tool" and for bents requiring an individual evaluation.

The second impetus and purpose of this research was to determine if the bent end batter piles provide sufficient lateral support to prevent sidesway bucking of non X-braced bents in the transverse direction after a major scour event has occurred. By developing accurate computer models and examining the failure mode of these bents, more precise buckling equations and pushover capacities can be incorporated into ALDOT's final "screening tool" to determine which of its bridge bents are safe during an extreme flooding event and which bents require additional evaluation.

9.2 Conclusions

The extent of this research was limited to computer modeling and analysis as no laboratory or field tests were performed. The pushover and buckling analysis was for the most part limited to the tallest non X-braced bents at 13ft, the potentially shortest one story X-braced bents at 13ft, and the tallest two story bents at 25ft. It is believed that these bents provide an adequate sampling for comparative modeling and analysis of bents in the transverse direction with FB-Pier and GTSTRUDL. Additionally, all piles in the non X-braced bent models were conservatively modeled as unencased H-sections due to the lack of composite action between the concrete encasement and the steel H-pile.

Based on the work conducted in this research, the following conclusions can be drawn from the FB-Pier modeling and analysis.

1. The soil subgrade modulus, K_o, does not appear to have much of an effect on lateral pile/bent displacements and capacities during pushover.
2. When a pile approaches its buckling capacity and begins to deflect laterally, the lateral displacements along the pile's axis approach zero at a distance of 5 ft

below the ground line. This is true for nearly any subgrade modulus value as long as K_o>5 lb/in^3 which should be the case for all existing bent structures.

3. If sidesway is prevented for a bent, the equation $P_e \approx \frac{2\pi^2 EI}{L^2}$ provides a close approximation to the elastic buckling capacity of piles with 50% rotational fixities at each end (even when a parabolic distribution of inelastic buckling loads is assumed as illustrated in Figure 5.17).

4. Of the methods listed in Table 5.2 to determine the non sidesway buckling loads of individual piles, FB-Pier's analysis (which includes material and geometric nonlinearity) appears to provide the most accurate buckling load, P_{max}^{pile}, since piles will buckle inelastically for pile lengths, $L \leq$ 35.74ft when sidesway is prevented. Where elastic buckling occurs, the average FB-Pier buckling load (for piles pinned and fixed at the top) is most similar (although slightly smaller) to that given by $P_e \approx \frac{2\pi^2 EI}{L^2}$ which assumes 50% fixities at both pile ends. Therefore this equation provides reasonable elastic buckling capacities for piles of X-braced bents not susceptible to sidesway buckling.

5. If sidesway is prevented and sufficient scour occurs for elastic buckling to control, it appears that buckling loads given by the approximate equation $P_e \approx \frac{2\pi^2 EI}{L^2}$ are more conservative than both $P_e \approx \frac{3\pi^2 EI}{l^2}$ (where the effective length, l, includes an additional 5ft to the assumed fixity below the ground line), and Granholm's Equation (where P_e is the average buckling capacity of piles with a pinned and fixed top).

6. Both material and geometric nonlinearity (incorporated in pushover analysis) are critical in the determination of pile and/or pile bent buckling loads. FB-Pier (and GTSTRUDL) considers two forms of geometric nonlinearity during pushover

analysis. These exist in the form of secondary effects due to bending displacements along the axis of an axial loaded member (p-y effects) as well as lateral translation of one end of an axial loaded member with respect to the other end (p-delta effects).

7. A significant oversight exists in FB-Pier in that it does not allow for modeling of X-braced bents since X-members cannot be added to computer models of the bents in the transverse direction.

Based on the work conducted in this research, the following conclusions can be drawn from GTSTRUDL modeling and analysis.

1. For typical levels of scour, i.e. S=0ft-20ft, all non X-braced bents constructed with the standard end pile batter of 1.5" in 12" will be susceptible to failure by sidesway buckling as noted in Figures 6.9-6.16 where $k_{eq}<k_{ideal}$.
2. Using a larger end pile batter equal to 2.0" in 12" only slightly decreases bent flexibility and does not increase bent stiffness enough to prevent sidesway for typical levels of scour. Therefore, increasing the batter for bents constructed in the future does not appear to offer significant advantages.
3. Sidesway is not greatly affected by the flexural strength of the bent cap, and it does not appear that increasing the flexural strength of the cap via strengthening measures would increase the stiffness of the bent enough to prevent sidesway for expected levels of scour.
4. The buckling analysis results in Section 6.6 reveal that 4, 5, and 6-pile bents should have adequate buckling capacity to support typical bent pile gravity loads (approximately 100 kips from a girder-line analysis) even for extreme levels of scour (when lateral loads are minimal). The 3-pile bents, however, may not have adequate buckling capacity for large levels of scour and may require additional support near the foundation to prevent scour from occurring and keep buckling capacity above 100 kips.

5. The pushover analysis results of the X-braced bents reveal that for scour levels exceeding 5ft, nearly all of the additional pushover capacity gained by adding X-bracing is lost (see Table 8.4), although the additional stiffness provided from the X-bracing is lost more gradually as scour is increased.
6. The addition of a horizontal strut in the lower portion of one story X-braced bents (H=13ft) does not appear to offer significant improvements in pushover capacity when $S \geq 5$ft. The addition of this lower strut does however increase the pushover capacity of the two story X-braced bent (H=25ft) for each level of scour.
7. Although elastic-perfectly plastic material was used to determine the capacities of the steel piles in this research, GTSTRUDL offers a very sophisticated model of the stress-strain relationship of steel. This provides an estimate of the additional capacity gained from strain hardening to be observed. However, it is not recommended that strain hardening be used in the determination of pushover capacities since this phenomenon will only occur after large deformations/strain have taken place, thus, instability has already occurred.

The following conclusions are provided from comparisons of the FB-Pier and GTSTRUDL pushover analysis procedures and results as well as their respective ease of modeling.

1. Modeling bents with FB-Pier is very straightforward. The tabbed dialogue boxes within the program direct the user through the modeling process by showing the required input for a specific type of problem. Tabs not required for a certain problem type are crossed out and cannot be selected. Nonlinear analysis of the bent is easily specified as well as nonlinear material behavior of the piles (the default σ–ε curve for steel is elastic-perfectly plastic). Additionally, only two parameters are required to execute the pushover analysis procedure, the loading rate and number of loading increments. The pushover failure load is determined from interaction diagrams of each element and the analysis appears to terminate before material failure occurs.

2. Modeling bents with GTSTRUDL is somewhat more complicated than with FB-Pier since the software is designed for more general modeling applications. The user must calculate joint coordinates (and find X-member/pile intersections if X-braced) of the structure which can be much more time consuming for complicated models. For the pushover analysis procedure nonlinear geometry of the members must be specified and plastic hinges must be inserted to account for nonlinear material behavior (elastic-perfectly plastic behavior must be specifically specified). These nonlinear parameters cannot be defined using GTSTRUDL's graphical interface (GTMENU) and must be accounted for by inserting them directly into the input file as shown in Chapter 6. GTSTRUDL's pushover analysis procedure is much more sophisticated than FB-Pier's and, as a result, makes use of many more parameters, such as the back-up loading rate and various convergence tolerance values to more accurately locate the failure load. The failure load is determined directly from the p-delta curve using the Newton-Raphson tangent stiffness method which corresponds to a rapid reduction in structural stiffness.

3. Pushover analysis is a nonlinear analysis which considers both geometric and material nonlinearities, and thus it implicitly checks for possible buckling failure of a bent due to inadequate strength or stiffness. Both programs account for geometric nonlinearity in the form of p-delta effects due to lateral translations of one end of an axial loaded member with respect to the other end as well as p-y effects from displacements along a member's axis due to bending.

4. After running the pushover analysis of both programs on non X-braced bents modeled with different pile end conditions, it was determined that GTSTRUDL bents modeled with piles fixed to the cap and pinned to the ground produce p-delta curves initially very similar to FB-Pier bents modeled with piles fixed to the cap and elastic foundations at the ground.

5. When the pushover analysis was performed on non X-braced bents with the transverse load incremented, the resulting FB-Pier p-delta curves terminate very early without laying over. Furthermore, the steel piles do not reach the yield stress before the analysis ends for this loading which may explain why the p-delta curves exhibit linear behavior through failure. This is believed to be the result of FB-Pier's failure ratio (demand/capacity) which is determined from the interaction diagram of each element as discussed in the Literature Review.

6. When the pushover analysis procedure was executed on non X-braced bents with the gravity loads incremented (buckling analysis), the resulting p-delta curves for both programs are very similar (provided that the GTSTRUDL bents are modeled with piles fixed at the cap and pinned at the ground). This appears to be due in part to the fact that the pile stresses did not reach yielding at capacity for either program using this loading.

7. Although modeling bents with GTSTRUDL is slightly more complicated than FB-Pier, the pushover analysis output is much more convenient and user friendly than that of FB-Pier. After running the pushover analysis command in GTSTRUDL each load increment is listed sequentially and the joint deflections for each load can be shown in tabular form. This makes graphing the p-delta curves in a spreadsheet fairly simple. FB-Pier, on the other hand, creates one large output file which requires the user to search through a large amount of data and find the cap deflections for each load increment. This becomes somewhat more time consuming when many small load factors are used.

9.3 Recommendations

Based on the previous conclusions the following recommendations are given for use in the development and formation of a screening tool that will help to determine which ALDOT bridge bents are at risk of failure after an extreme scour event.

1. GTSTRUDL appears to offer the most suitable bridge pile bent modeling and pushover analysis procedure for use in a bridge bent screening tool since the pushover analysis procedure is much more sophisticated and many of FB-Pier's pushover analysis results terminate before the bents lay over. Additionally, GTSTRUDL has the ability to model bents with X-bracing in the transverse direction unlike FB-Pier.

2. When modeling pile bents with GTSTRUDL, the bents should be modeled with piles having fixed connections to the cap and pinned connections to the ground. In general, this appears to produce p-delta curves with bent stiffness very similar to FB-Pier's bents having elastic foundations. This should also provide conservative results, since the level of fixity at the base of existing bents is expected to be somewhat greater than a pinned connection.

3. Since it was determined that all non X-braced bents are susceptible to sidesway for typical scour levels, the individual pile buckling capacity of these bents should be calculated from the elastic buckling equation $P_{CR} = \frac{0.5\pi^2 EI}{L^2}$, where the coefficient has been reduced by half to account for 50% rotational fixities at pile ends. This buckling equation should also be used in the case of X-braced bents that have experienced enough scour to make them susceptible to sidesway buckling below the X-bracing which can occur for large levels of scour.

4. For X-braced bents which prevent sidesway buckling, the individual pile buckling capacity may be calculated from the elastic buckling equation $P_{CR} = \frac{2\pi^2 EI}{L^2}$, where the coefficient has been reduced by half to account for 50% rotational fixities at pile ends. For the non sidesway pile buckling mode in X-braced bents, it is assumed that X-members do not provide intermediate support for the piles. It is likely that the small angle members will buckle simultaneously with the piles rather than create a point of inflection.

5. The pushover analysis results for X-braced bents with and without the proposed lower horizontal strut appear to be somewhat inconclusive. The extra member does not greatly affect the pushover capacities of the one story bent (H=13ft), but significantly increases the capacity of the two story bent (H=25ft) for nearly each level of scour. Therefore, unless the final screening tool finds that the two story bents are highly susceptible to pushover failure, the inclusion of this lower strut in future bents is not warranted.

6. It is recommended that additional pushover analyses be performed to verify adequate load carrying capacity of pile bents. The buckling analysis results provided herein give the buckling capacity after much of the lateral load produced in a flood subsides (recall these results were obtained in Chapter 6 by incrementing the gravity loads and assuming a very small constant lateral force of 0.1 kip at the cap). Although typical bent pile gravity loads are well below the buckling capacity for the 4, 5, and 6-pile bents at each level of scour, it is very likely that some bents may be at greater risk of failure during a flooding event which may impose large constant gravity loads simultaneously with large transverse water loads. Therefore, a range of typical gravity loads (i.e. P = 100k, 120k, 140k and 160 kips from a girder line analysis of typical dead loads and HS20 AASHTO live loads) should be placed above each pile with the horizontal load incremented until failure is reached. If the actual applied lateral force is less than the capacity predicted by the pushover analysis ($F_{t\,max\ applied} < F_{t\,push\text{-}over\ load}$), the bent will have adequate load carrying capacity and should be safe from buckling.

7. The pushover analysis results provided in this research were obtained by placing the incremented transverse "pushover" force at the centerline of the bent cap. However, the actual location of this force is dependant on the size/depth of the debris raft and the height of the water surface during the extreme flooding event.

Therefore, these parameters should be taken into consideration in future bent models and ALDOT's final bridge bent screening tool.

8. The appropriate safety factors should be determined from ALDOT and applied to the bent pushover capacities in the final screening tool since the GTSTRUDL failure loads are the result of a rapid reduction in stiffness due to instability or yielding of the piles.

REFERENCES

1. Granholm, Hjalmer. 1929. "On the Elastic Stability of Piles Surrounded by a Supporting Medium." *Ingeniors Vetenskaps Akademien Handlingar Nr89*. Stockholm, Sweden. pp 1-56.

2. Yura, J.A. and Todd A. Helwig, 1997. "Bracing for Stability." Notes from Seminar Sponsored by Stability Research Council and AISC.

3. Ramey, G.E., and D.A. Brown. November 2003. "Stability of Highway Bridges Subject to Scour – Phase I." Alabama Department of Transportations Project 930-585, Final Report.

4. GTSTRUDL Reference Manual, Vol. 3. February 2002.

5. Bowles, Joseph E. 1998. *Foundation Analysis and Design*. 4th Edition. New York, New York: McGraw-Hill.

6. FB-Pier Version 3. 2000. Computer Software Help Topics Menu.

7. Chajes, Alexander. 1974. *Principles of Structural Stability Theory*. Englewood Cliffs, New Jersey: Prentice-Hall, Inc.

8. BSI Newsletter. Spring 2005. "Technical Corner – Interaction Diagrams". Bridge Software Institute.